MOLECULAR AND SUBCELLULAR CARDIOLOGY

Effects of Structure and Function

ADVANCES IN EXPERIMENTAL MEDICINE AND BIOLOGY

Recent Volumes in this Series

Volume 375
DIET AND CANCER: Molecular Mechanisms of Interactions
Edited under the auspices of the American Institute for Cancer Research

Volume 376
GLYCOIMMUNOLOGY
Edited by Azita Alavi and John S. Axford

Volume 377
TISSUE RENIN–ANGIOTENSIN SYSTEMS: Current Concepts of Local Regulators in Reproductive and Endocrine Organs
Edited by Amal K. Mukhopadhyay and Mohan K. Raizada

Volume 378
DENDRITIC CELLS IN FUNDAMENTAL AND CLINICAL IMMUNOLOGY, Volume 2
Edited by Jacques Banchereau and Daniel Schmitt

Volume 379
SUBTILISIN ENZYMES: Practical Protein Engineering
Edited by Richard Bott and Christian Betzel

Volume 380
CORONA- AND RELATED VIRUSES: Current Concepts in Molecular Biology and Pathogenesis
Edited by Pierre J. Talbot and Gary A. Levy

Volume 381
CONTROL OF THE CARDIOVASCULAR AND RESPIRATORY SYSTEMS IN HEALTH AND DISEASE
Edited by C. Tissa Kappagoda and Marc P. Kaufman

Volume 382
MOLECULAR AND SUBCELLULAR CARDIOLOGY: Effects of Structure and Function
Edited by Samuel Sideman and Rafael Beyar

Volume 383
IMMUNOBIOLOGY OF PROTEINS AND PEPTIDES VIII: Manipulation or Modulation of the Immune Response
Edited by M. Zouhair Atassi and Garvin S. Bixler, Jr.

MOLECULAR AND SUBCELLULAR CARDIOLOGY

Effects of Structure and Function

Edited by

Samuel Sideman and Rafael Beyar

Technion–Israel Institute of Technology
Haifa, Israel

SPRINGER SCIENCE+BUSINESS MEDIA, LLC

Library of Congress Cataloging-in-Publication Data

Molecular and subcellular cardiology : effects of structure and function / edited by Samuel Sideman and Rafael Beyar.
p. cm. -- (Advances in experimental medicine and biology ; v. 382)
Includes bibliographical references and index.
ISBN 978-1-4613-5772-8 ISBN 978-1-4615-1893-8 (eBook)
DOI 10.1007/978-1-4615-1893-8
1. Heart--Molecular aspects. I. Sideman, S. II. Beyar, Rafael. III. Series.
QP114.M65M62 1995
612.1'7--dc20 95-25128
CIP

Proceedings of the Ninth Goldberg Workshop on Molecular and Subcellular Cardiology: Effects on Structure and Function, held December 4–8, 1994, in Haifa, Israel

ISBN 978-1-4613-5772-8

Originally published by Plenum Press, New York in 1995
Softcover reprint of the hardcover 1st edition 1995

10 9 8 7 6 5 4 3 2 1

To

Our families—for their love and encouragement

Our sponsors—for their trust and support

Our colleagues—for their vision and stimulation

Our students—for their enthusiasm and imagination

The 9th Goldberg Workshop
Molecular and Subcellular Cardiology: Effects of Structure and Function

December 4–8, 1994
Haifa, Israel

Organizing Committee

Professor J. Bassingthwaighte
Director, Center of Biomedical Engineering, University of Washington, Seattle, WA, USA

Professor R. Beyar, Co-Chairman
Department of Biomedical Engineering, Technion-Israel Institute of Technology, Haifa Israel

Professor S. Sideman, Chairman
Chair, Department of Biomedical Engineering, Technion-Israel Institute of Technology, Haifa Israel

Professor E.L. Ritman
Biodynamics Laboratory, Mayo Medical School, Roshester, MN, USA

Scientific Advisory Committee

Professor H.A. Fozzard
The University of Chicago, 5841 Maryland Avenue, MC 6094, Chicago, IL USA

Professor M. Gotsman
Director, Cardiology Department, Hadassah Medical Organization, Jerusalem, Israel

Professor Eduardo Marban
Department of Cardiology, Johns Hopkins University School of Medicine, 725 N. Wolf Street, Baltimore, MD USA

Professor R. Reneman
Department of Physiology, University of Limburg, Rijksuniv, Limburg, The Netherlands

Professor S.V. Vatner
Primate Research Center, 1 Pine Hill Drive, Southboro, MA USA

Professor M. L. Weisfeldt, Chairman
Chair, Department of Medicine, Columbia Presbyterian Medical Center, New York, NY, USA

Professor W. Welkowitz
Department of Biomedical Engineering, Rutgers University, Piscataway, NJ, USA

The 9th Goldberg Workshop on
MOLECULAR AND SUBCELLULAR CARDIOLOGY:
EFFECTS OF STRUCTURE AND FUNCTION

Sponsored by

THE TECHNION–ISRAEL INSTITUTE OF TECHNOLOGY
THE ISRAEL CARDIOLOGY SOCIETY
MR. JULIUS SILVER, NEW YORK, USA
MR. HENRY (DECEASED) AND VIOLA GOLDBERG, NEW YORK, USA

Supported by

MR. ARTHUR GOLDBERG, NEW JERSEY, USA

PREFACE

The Henry Goldberg Workshops were set up to address the following goals: (1) To foster interdisciplinary interaction between scientists and cardiologists, identify missing links, and catalyze new ideas. (2) To relate basic microscale phenomena to the global, clinically manifested cardiac function. (3) To relate conceptual modeling and quantitative analysis to experimental and clinical data. (4) To encourage international cooperation so as to disperse medical and technological knowhow and lead to better understanding of the cardiac system.

The first Henry Goldberg Workshop, held in Haifa in 1984, introduced the concept of interaction between cardiac mechanics, electrical activation, perfusion, and metabolism, emphasizing imaging in the clinical environment. The second Workshop, in 1985, discussed the same parameters with a slant towards the control aspects. The third Goldberg Workshop, held in the USA at Rutgers University in 1986, highlighted the transformation of the microscale activation phenomena to macroscale activity and performance, relating electrophysiology, energy metabolism, and cardiac mechanics. The fourth Goldberg Workshop, in 1987, continued the effort to elucidate the interactions among the various parameters affecting cardiac performance, with emphasis on the ischemic heart. The fifth Workshop, held in Cambridge, UK, in 1988, dwelt on the effects of inhomogeneity of the cardiac muscle on its performance in health and disease. The sixth Workshop highlighted the role of new modern imaging techniques, that allow us to gain more insight into local and global cardiac performance in cardiac research and clinical practice. The seventh Workshop explored the electrophysiology, microcirculation, and microlevel transport phenomena that affect the cardiac system in health and disease. The eighth Workshop explored the interactive phenomena in the cardiac system. The present ninth Goldberg Workshop aims to highlight some of the basic molecular and subcellular interactions that affect the activation and performance of the heart.

These gatherings of outstanding scientists from all over the world are a testimonial to international cooperation and highlight the pleasure of joining hands in the pursuit of the secrets of the cardiac system.

It is with great pleasure that we acknowledge here those who have helped make these workshops a reality. Particular thanks go to our new sponsor, Mr. Arthur Goldberg, whose support provided for the continuation of these Goldberg Workshops, and to Mrs. Viola Goldberg and the late Mr. Henry Goldberg, for their generosity and kindness, which made these Goldberg Workshops significant milestones in cardiac research. Special thanks are due to Mr. Julius Silver and Ms. Dinny Winslow (Silver) of New York, for their personal support and continued friendship, which inspired and shaped our goals and made it all possible. Thanks are also due to the Women's Division of the American Society for the Technion, who encouraged us with their unshakable trust and provided the means to start the Heart System Research Center. Personal thanks go to the Scientific Advisory Committee and the Organizing Committee. Last, we acknowledge with pleasure and many thanks the secretarial and editorial work of Ms. Deborah E. Shapiro, who made this book what it is.

Samuel Sideman
Rafael Beyar

WELCOME

Medicine and engineering are two great ancient professions which are dedicated to the improvement of human conditions. Both are crucial in man's struggle for survival. Both originate from practice and not from theory, having preceded science by hundreds of centuries, but they were enormously enriched by the penetration and permeation of science. Medicine helps us to cope with our well being. Engineering helps us cope with the environment by providing food, shelter, and improving the standard of living. These two professions have made us the only animal that does not fit naturally into an evolutionary niche; we make our own unique physical, mental, and cultural environment. Dissecting medicine and engineering by scientific tools of analysis uncovers the simplicity behind the complexity. The greater the decomposition down to the cell, the molecular, the atomic level, the greater the potential for reassembling, creating, synthesizing novel and important healing solutions and products. It is Science that weaves medicine and engineering together. This is why you find them both on the Technion campus. This is what the Julius Silver Institute of Biomedical Engineering is doing on our campus: fusing together medicine and engineering, both permeated by science, creating a synergystic amalgam of enormous potential to the improvement of the human condition. In this spirit of scientific progress, I wish you all successful deliberations.

Prof. Z. Tadmor
President, Technion–IIT

INTRODUCTORY REMARKS

I come here as Chairman of the Israel Cardiac Society, as well as one of the original members of a group of physicians and scientists who have been meeting at the Henry Goldberg Workshop for the last 10 years. The present meeting is a natural outcome of our 1992 meeting at the National Institutes of Health in Washington and represents a move into the field of molecular cardiology. Macrophysical forces and their interactions require a clear understanding of the subcellular milieu.

Cardiology has changed in the last 50 years. In the 40s diagnosis and management were made by the stethoscope and cardiac catheterization. Open heart surgery was introduced in the 50s, followed by noninvasive imaging techniques (echo-doppler, nuclear scanning, fast CT, and MRI), coronary artery bypass grafting, percutaneous revascularization of narrowed and obstructed coronary arteries, and now invasive electrophysiology and ablation of arrhythmias. In parallel there has been the development of modern molecular biology, which help us to understand the autocrine and paracrine functions of the cells.

Cardiac research covers a wide range of topics. Biomedical engineering looks at quantitative aspects of cardiac physiology and its building-blocks of molecular biology. It varies from the examination of stress, strain, pressures, work, and functions of the ventricle and the great arteries, to the dynamics of the biochemistry of the cell. It will deal with receptors, transmembrane signaling, internal vesicles and their function, the activation of DNA, manufacture of RNA, and the functions of the endosome and the sarcoplasmic reticulum. Quantitative biochemistry of protein synthesis and turnover will be studied. We will then understand the quantitative dynamics of receptors, the density of the Golgi apparatus, manufacture of smooth and coarse endoplasmic reticulum, and cell multiplication. There is need to create a balance between the clinician on the one hand, who will deliver services to patients, and the molecular biologist on the other, who will have to investigate the profound micromolecular changes in disease. In addition, mathematicians and biophysicists will develop models of interactions between the different subcellular events in the cells.

Claude Lenfant, the Director of the new National Heart Lung and Blood Institute (NHLBI) in the USA, has described two major directions of research in the clinical area that require solutions by well-controlled double-blind trials: one is thrombolysis and acute myocardial infarction and the other involves lipid lowering in atherosclerotic disease. Both have great impact on large populations and on the practice of medicine. NHLBI funds these large, controlled epidemiological research trials. On the other hand, the modern technological explosion has opened new avenues of research in molecular biology. Scientists can now manipulate receptors, turn on DNA and RNA, and understand embryogenesis.

New knowledge requires rapid peer review and quick dissemination. Small special research seminars like the Henry Goldberg Workshop create a dialogue between the scientist and the physician, and are excellent vehicles for the transfer of up-to-date wisdom.

My own field of interest is atherosclerosis. Its pathogenesis is gradually being uncovered. Our knowledge of low-density lipoprotein metabolism has undergone a quantum transformation. How do LDLs enter the subendothelium and what controls their

transit between the blood and the subendothelial matrix? How do the cytokines operate and modify LDLs and induce oxidation? How do oxidized LDLs stimulate the secretion of monocyte chemotactic protein and what other chemotactic proteins are secreted by the endothelial cells? What is their rate of turnover and how quickly do monocytes enter and leave the subendothelial space? Are the monocytes normal or abnormal? How do they change and become macrophages, and how does the macrophage manufacture its scavenger receptor to ingest the oxidized LDL? Where are high-density lipoproteins formed, how do they react with the interstitial and intracellular cholesterol, and at what rate is cholesterol removed? Do HDLs prevent LDL oxidation or only remove cholesterol? Does HDL interact with scavenger macrophages? How are macrophages converted into foam cells, how do the latter disintegrate, and why is the cholesterol that is liberated more damaging than ordinary or oxidized cholesterol imbibed in the cell? What are the dynamics of the cell adhesion molecules? Once the atheromatous plaque develops, what is the rate of fibrosis and calcification? What precipitates rupture of a soft plaque (the soft cholesterol core, weakening of the endothelial cap, infiltration with macrophages and lymphocytes, and the secretion of proteases and collagenases) and what is the role of coronary artery spasm? Once the cap has ruptured and the subendothelium is exposed, at what rate is the clotting mechanism stimulated? We now understand the biochemistry of the platelet and its intercellular interactions, but at what rate are the receptor glycoproteins produced? Spontaneous thrombolysis occurs once the clot forms, but what are the dynamics of the process? Once the artery is occluded, clot changes into fibrous tissue, but what determines its rate of formation and what changes in flow determine the final remodeling of the coronary artery? Today, it is possible to develop antibodies to platelet receptor proteins. Can the pharmacological use of these new substances alter the genesis and breakdown of the thrombi? What is the nature of cell multiplication in restenosis after balloon angioplasty? Why does the muscle myocyte multiply and migrate into the subintima? How does it change its phenotypic profile, and what are the pertinent growth factors? Do the oncologist and the cardiologist have a common basis in studying cell multiplication? The paracrine function of the endothelial cells must be considered as well. At what rate are endothelin derived relaxing factor (EDRF), atraial natriuretic protein (ANP), and the various growth factors and attachment molecules secreted? What are the mechanisms of muscular hypertrophy and embryogenesis and abnormalities of the development of the heart? A great deal of experimental and theoretical work is still needed before we can have correct answers to these and many other related problems!

Professors Sideman and Beyar have created a microcosm of academic excellence at the Technion and their department of bioengineering is an island of medico-engineering-scientific knowledge, and an ingenious center for quantitative analytical cardiac physiology. We are living in a period of great medical advances and changes. The future is bright and we have to expand existing and establish new centers of excellence. The Julius Silver Center for Biomedical Engineering at the Technion has a long tradition for quality, productivity, and excellence, while the Henry Goldberg Workshops have provided the opportunity to meet with peers from the whole world.

This meeting concentrates on modeling and molecular biology and has brought together some of the leading researchers in the field. I look forward to a most challenging meeting, and I wish us all fruitful and productive deliberations.

Professor Mervyn S. Gotsman, MD, FRCP, FACC
Director, Cardiology Department, Hadassah University Hospital
President, Israel Cardiac Society

CONTENTS

Molecular Mechanisms of Sarcolemar Excitability

Intracellular Calcium and Muscle Function – SR and Filaments

Molecular Manifestations of Cell Adaptation

MOLECULAR MECHANISMS OF MEMBRANE EXCITABILITY

CHAPTER 1

ION CHANNELS AND PUMPS IN CARDIAC FUNCTION

Harry A. Fozzard[1] and Gregory Lipkind[2]

ABSTRACT

Ion channels and pumps are intrinsic membrane proteins that regulate the membrane potential and transport of ions and substrates, controlling excitation and excitation–contraction coupling. Several have been cloned and an example of our progress in structure–function correlation is the identification of the pore region of the Na channel.

INTRODUCTION

The surface membrane isolates the cell's cytoplasm from the external environment, so that the cell can provide the special conditions required for its multiple metabolic processes. This membrane is also depolarized during excitation through change in its ion permeability properties. Membranes are composed of phospholipid and other lipids to form a hydrophobic barrier typically 30 – 40 Å thick. Although the impermeability of the basic membrane is essential, there must be some means for entry and exit of solutes and for regulation of cell volume. These functions are achieved by intrinsic membrane proteins. Ion channels are intrinsic membrane proteins that are responsible for excitation and for excitation–contraction coupling. Pumps are also intrinsic membrane proteins that regulate ion concentrations. Intrinsic membrane proteins differ from the better–studied soluble proteins, and the structures of membrane proteins have been harder to determine.

A number of membrane ion channels and pumps have been cloned and their primary sequences determined, allowing inference about their three dimensional structures. They have multiple segments of 18–24 hydrophobic amino acids that span the lipid bilayer,

[1]Departments of Pharmacological & Physiological Sciences and Medicine, and [2]Department of Biochemistry and Molecular Biology, The University of Chicago. MC6094, 5841 S. Maryland Av, Chicago, IL 60637, USA.

Molecular and Subcellular Cardiology: Effects of Structure and Function
Edited by S. Sideman and R. Beyar, Plenum Press, New York, 1995

forming a path across the membrane for ions and substrates. Function of ion channels has been characterized biophysically in exquisite detail by the patch clamp method of studying simple molecular events, allowing elegant structure–function correlation. Pumps typically appear to have 10–14 transmembrane segments often with two homologous domains. The inside regions may contain regulatory or catalytic nucleotide binding sites. The transmembrane components are presumed to comprise the pathway for the transported substrates such as ions or small molecules. The 12–transmembrane segment motif composed of two 6–segment domains is also seen for Cl channels and for the enzyme adenylyl cyclase.

Heart cells combine properties of nerves to coordinate rapid events with properties of muscle to contract and generate force or shorten. Excitability, their nerve–like function, is found in their action potential, which provides an orchestrating signal to the muscle. Heart muscle has Na and Ca channels, K channels, and Cl channels that generate its action potential. Ion channels have four essential components: an ion pore, some selectivity function, gates, and some gating sensor. Voltage–gated channels typically have a more–or–less symmetrical four subunit structure. The principal molecules for Na and Ca channels, the α and $\alpha 1$ subunits respectively, contain four highly homologous sets of six α–helices covalently linked to form the functional channel. The fourth α–helix of each molecule or each homologous domain of the voltage gated channels has a charged residue at each third position, so that there are 4–8 charges spanning the membrane electric field. This structure functions as the channel's voltage sensor. Because of the delicate balance among the components of the cardiac electrical system, many genetic abnormalities of ion channels are lethal, but, subtler ion channel abnormalities are now being found that predispose to dysfunction. For further description, see Catterall [1]. In order to illustrate the relationship between structure and function of an ion channel, we have studied the effect of point mutations in cloned Na channels and their effect on interaction with guanidinium toxins, which block the channel by binding in the outer part of the pore [2]. We then used this information to generate a molecular model of the pore [3].

METHODS

Modelling was made in the Insight and Discover graphical environments (Biosym Technologies, Inc., San Diego). Molecular mechanics energetic calculations utilized the force field cvff (consistent valence force field), where hydrogen bonds are modelled as electrostatic interactions. For energy minimization the steepest descents and conjugate gradients were used. First an optimal conformation was determined for the critical stretches of residues from each domain that line the channel vestibule. Secondary protein structure was based on guidelines derived from X–ray structural analysis of soluble proteins [4]. Use of soluble protein structural data was justified by the impression that the vestibule is on the extracellular surface of the protein and therefore it was a surface in contact with water. Second, interaction of tetrodotoxin (TTX) and saxitoxin (STX) was allowed with peptides from the four domains. Experimental data used in the modelling were derived from toxin analog studies [5], and from Na channel mutation studies [6, 7].

RESULTS

The key concept in this model is the idea that in order to achieve their high binding affinity the TTX and STX molecules fit snugly into the vestibule, interacting with multiple residues on the vestibule surfaces. TTX and STX are quite rigid cyclic structures, with

minimal opportunity to adjust their structures to the contours of the channel's interactive surface. The modelling strategy was to determine a probable secondary structure for the individual pore (P) segments that would form a part of the toxin binding pocket and allow the residues identified as important for toxin interaction to face the inside of the pocket. Then these P–segment secondary structures were aligned to form the full binding pocket. Finally, energetic interactions were allowed between toxins and the constructed binding site. In β strands, sequential residues face opposite to each other and every other residue faces the same way. The P segments are composed of residues with a propensity for forming β structures with reverse turns, forming β hairpins. The importance of turns is that adjacent residues can face the same direction. Energetically stable β hairpins could be formed that allowed the residues identified by Terlau *et al.* [6] and others to be on the same face of the structure (Fig. 1).

The crucial parts of the TTX and STX molecules are identified as the guanidinium groups and two hydroxyl groups. Competition between these toxins for the same site in the Na channel pore means that they share common sites. They show remarkable similarities: if the TTX guanidinium group is aligned with the 7,8,9 guanidinium group of STX, then the two hydroxyls of TTX at C9 and C10 align in space with the two hydroxyls of STX at C12. The guanidinium groups are positively charged at physiological pH, with the charge distributed between the three nitrogens.

In the mutation experiments of Terlau *et al.* [6], TTX block was affected primarily by residues on P segments from domains I and II. The modelled β hairpins of these two domains were sequentially docked onto the TTX molecule and found to form optimal interactions with carboxyls D384 and E387 of domain I and carboxyls E942 and E945 of domain II: D384, E387, and E942 forming salt bridges with the guanidinium group and E945 forming two hydrogen bonds to the hydroxyls (Fig. 2). (Note that in order to describe mutations we use the single letter code for the amino acid and the Na channel numbering sequence for the rat brain channel.) The two hairpins were aligned in an antiparallel fashion for this interaction. Because of its steric similarity to TTX, STX also formed optimal and nearly identical energetic interactions with P segments of domains I and II, without

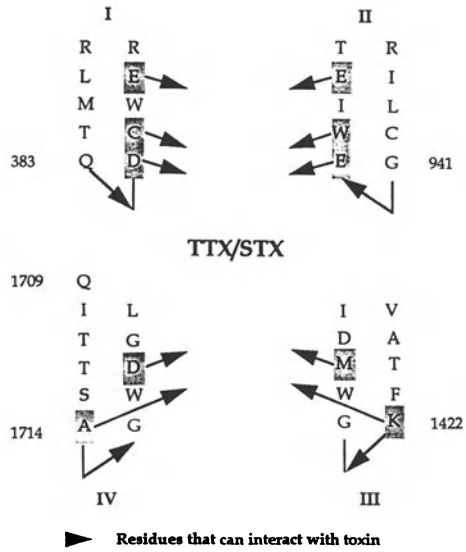

Figure 1. Alignment of four peptide segments to form a toxin binding pocket.

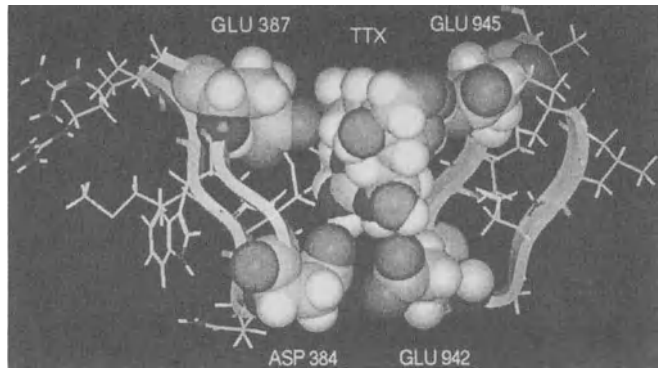

Figure 2. Model of the interaction of TTX with β hairpin peptides of domains I and II of the Na channel.

relocation of the two β hairpins. Terlau *et al.* [6] also showed that STX has an important interaction with a carboxyl on domain IV, which is less important for TTX. Addition of the domain IV β hairpin to the TTX site model by antiparallel alignment with domain I placed it in position for D1717 to form a salt bridge with the second guanidinium group of STX. Finally, addition of the domain III β hairpin in the space between those of domains IV and II, also in an antiparallel relation, placed its two important residues in position to face the pocket. This strategy of wrapping the relevant P segments around the toxin molecules resulted in the formation of a pocket with all of the reactive sites in optimal positions and interacting with effective energy. The potential energy of interaction of STX was less than TTX (higher affinity) because of the additional reactive site on domain IV.

All these amino acid residues in the P segments are conserved between the brain and cardiac isoforms of the Na channels, so these toxin binding interactions are the same. However, the nerve channel has high affinity for TTX and STX and the cardiac Na channel has a 1000-fold lower affinity. Consequently, the difference in toxin affinity between the isoforms was not explained by these interactions. There are two residue differences between the isoforms: the cardiac isoform has a cysteine in position 385 in place of a phenylalanine, and an arginine in position 388 in place of an asparagine. The structure of the binding pocket and the β hairpins lining it defined rather precisely the location of residue 385 and its relationship to the toxin molecules. If residue 385 is a cysteine there is only a modest

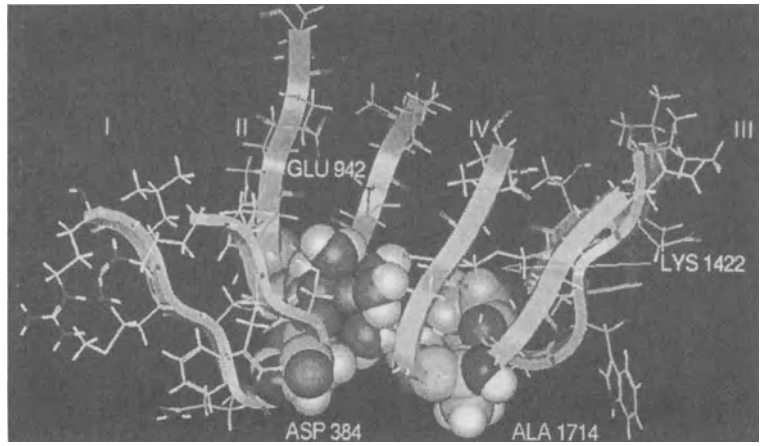

Figure 3. Model of the Na channel vestibule with interaction of Asp384 and Glu942 with a hydrated Na ion.

van der Waals attractive force between it and the toxin molecule. If, on the other hand, this residue is phenylalanine (or tyrosine as in skeletal muscle) containing an aromatic ring, then the ring is located optimally for substantial nonbonded and hydrophobic interaction with the toxin hydrophobic face. Without realignment the decrease in interaction energy from the substitution was calculated to be about −5 kcal/mole, consistent with the effect of these mutations on binding affinity.

Removal of toxin from the modelled binding pocket revealed a funnel-like structure, composed of the four C-terminal sides of the β hairpins, which is a candidate for the structure of the outer vestibule. Its outer margins are about 15 Å between backbone carbons, and it is about 12 Å deep. The inner opening is an asymmetrical slit about 5 x 3 Å, ringed by the residues D384, E942 (Fig. 3), K1422, and A1714, which is surprisingly the right size and shape to be the selectivity filter predicted by Hille [8]. Na in solution can be modelled as an ion of approximately 1.02 Å diameter with six coordinating water molecules and a less well defined outer shell, which are bound with a total energy of −105 kcal/mole. Insertion of such a model of Na into the narrow ring allowed it to coordinate with the two carboxyls D384 and E942 with sufficient energy to offset the energy of the bound waters and effectively dehydrate the ion. The K ion, with diameter of 1.33 Å and a hydration energy of −85 kcal/mol, fitted less well into the coordination site. Ca, with diameter 1.00 Å and hydration energy of −397 kcal/mole could interact with the two carboxyls, but with insufficient energy to displace its water molecules. These two carboxyls were altered by Terlau *et al.* [6] in their study of the toxin binding site, and the mutants showed drastic reduction in single channel conductance. These results support the idea that two carboxyls in the selectivity ring may be optimally placed to dehydrate Na but less optimal for dehydration of K. Ca could still bind to the two carboxyls and block the channel, but they are insufficient to dehydrate Ca completely.

DISCUSSION

An impressive structural similarity can be found between the Na channel α-subunit and the Ca channel α1-subunit [9]. These primary pore-forming subunits are about the same size, and each contains four homologous domains of six transmembrane segments, so they have the same topology. The S5–S6 loops of each contain a very homologous P segment. Functionally, the Ca channel can support large Na or Li currents when divalent ions are absent, and low concentrations of divalent ions block the monovalent currents. Finally, both channel-types are blocked by a general class of peptide toxins called conotoxins. Consequently, a similar shape and structure for the external vestibule and selectivity regions would not be surprising. Examination of the residue comparison led Heinemann *et al.* [10] to suggest that the selectivity ring of the Ca channel was composed of four carboxyls. In the Na channel they made the mutations K1422E and A1714E and created a channel that would conduct Ca and Ba as well as Na, very much like the Ca channel. With this impressive transmutation of a Na channel into one with permeation properties like Ca channels by the single point mutation K1422E, the possibility arose that three carboxyls in the narrow region were sufficient to bind Ca, blocking Na permeation and permitting Ca to permeate. Investigators [11] have systematically mutated one or more of the residues in this presumptive selectivity ring, greatly altering Ca block of Ba current or Li current. Ba currents required the three carboxyls of domains I, II, and III, but not that of domain IV. On the other hand, monovalent currents were preserved after neutralization of two of the carboxyls. These experiments strongly suggest analogies between the Na and Ca channel vestibule/selectivity regions, with some major differences.

CONCLUSIONS

Cloning of ion channels has provided a spectacular opportunity to resolve the structural basis for their transduction process. We have used structural and mutation data to construct a detailed model of the Na channel vestibule/pore. The model can predict mutation results. It also provides a model for the selectivity property of the channel.

DISCUSSION

Dr. Gotsman: One comment: I am flabbergasted!

Dr. Morad: Water going through is critical for your model. How are you going to consider the energy of hydration? Have you thought how the data from deuterium oxide or heavy water would work in this situation?

Dr. Fozzard: If heavy water is hydrating the sodium ion there is a slightly different energy of hydration. Therefore we would expect the speed of interaction to be different and so we would expect a different permeation rate. We could make a prediction based upon what the physicists tell us about heavy water.

Dr. Morad: Which way did it go when you made that prediction?

Dr. Fozzard: It would be slower. But the challenge of doing experiments with deuterium water is fairly formidable. Actually, if I am to use heavy water I am more interested in gating because there are some fascinating things we can learn about gating with heavy water. From my perspective, the sort of experiment that Dr. Marban's lab has done and our lab has done on block by divalent ions would be a particularly fascinating one to use to test this model. We have not tried that for the simple reason that interaction of ions in solution with charged residues implies that we know something of the dielectric constant in this vestibule. To be perfectly honest, we do not. The standard for protein modeling is to say that protein has a dielectric constant of about 10. This is arbitrary. My guess is that the dielectric constant changes as the ion moves into that vestibule because you can only pack about 20 waters into that vestibule. So we are down into a sort of quasi-molecular system. We are trying to work with our friends at Champaign, Urbana who have two Cray computers to work with, to put water in and figure out what the water is doing in the vestibule. I believe we will be able to look at divalent interaction, which I hope will be very helpful.

Dr. J. Bassingthwaighte: I am a little confused about the water. You noted that the binding of the hydrated sodium had an energy which was equivalent to the dehydration energy required to dehydrate the sodium, and then in your beautiful picture, sodium ions came through with water on it. Does that rehydrate it then, as it exits?

Dr. H. Fozzard: We are forced to accept the idea that the sodium ion is hydrated in the bulk solution before it goes in the channel. At least in the model, we simply have put 6-waters on sodium, which is geometrically convenient for sodium, although there is an outer ring too that we don't model here. So we just took that inner ring. In order to go through, it has been assumed biophysically that we have to dehydrate the ion, although that may not be 100% true, but the hydration energy is something like 100 kcal/mole and that is a lot. It requires a huge amount of energy for each ion. As you know, classically, that was a big problem. How on earth can we have 10^6 sodium ions going through per second and yet have each one of them require 100 kcal/mole? The only possible suggestion was that the channel could substitute and interact with the ion in place of the water. In our model we propose the idea that the two carboxyls, which of course have four oxygens on them, interact with the ion and substitute for water. As a result of that, four of the

waters are displaced. But the energy of interaction of the two carboxyls with sodium, in that selectivity ring, is equal to the 100 kcal/mole. The two waters on the bottom and top just happen to be fellow travellers. Energetically, they are not held in place. That is of course hypothetical.

Dr. E. Marban: We find that many of the residues that you have pointing away from the lumen, when mutated to cystene or to other amino acids for that matter, very palpably alter the pore phenotype, in a way that is inconsistent with the kind of β–strand architecture that would have one side chain pointing into the lumen and the next one pointing into the protein, unless the channels are so distorted that they are not like they were before they were mutated, which is always the bugger–boo of site–directed mutagenesis. Art Karlin [Akabas *et al.*, *Science.* 258:307–310, 1992] has seen the same kind of problem in a nicotinic acetylcholine receptor in a structure which he would like to have β–barrel like with serial cystene mutagenesis in the pore region. The way he tries to reconcile it is by saying, it could be a β–barrel, but if so, its plane of orientation is orthogonal to the lumen, so both residues have some access to the lumen. But the lining of the lumen is really the backbone itself. That to me is a very unsatisfying explanation because, if it is possible, one can never reject it. It seems you might be able to reject it purely on energetic constraints. I do not think you can pack that many orthogonally placed residues, if you had them in all four domains, is that right?

Dr. H. Fozzard: In our model, we absolutely can not have direct interaction of the alternate residues in the β–strand. In the β turn region, of course, we can. As you say, one of the crucial problems with this is that when you change one residue in a molecule that spatially alters interactions with others, we can have allosteric effects. We only argue, like you, that as long as the channel keeps functioning, we have maintained some kind of integrity to this pore region, however much we have done otherwise. In our case, we have this vestibule, but it is surrounded by a lot of protein and we do not know what its structure is. In order to provide the rigidity of the residues in our system, we put forward the β–hairpin, because that has a strong interaction across the hairpin to hold things in place. It could be that that region is much more disordered, such as a random coil, which is actually what we think is going on in the K channel, and that some of these alternate residues are not as rigidly directed away as we have shown them. We will only know that as we examine your data and other data, to add to this model and use it as a test. If it performs its function as a model, we may prove it wrong with your help.

Dr. M. Lab: There are channels in the membrane which distort with stretch and open. Recently there has been interest in mechanosensitivity of some of the other channels, i.e. the KATP channel and the L–type calcium channel. These channels pass more current when the membrane is stretched. Do you understand enough about your particular model and intramolecular structure of the hairpins, to suggest that this channel has the facility to be mechanosensitive as well? In other words, as the molecules are distorted, they can pass more sodium.

Dr. H. Fozzard: This model locates 40 residues out of the total of 2000, and we do not know where the other 1,960 are. I suspect that this molecule is not well suited for the function of mechanotransduction. Part of the requirement for selectivity in this sense is that we must have rigidity in the selectivity region so that the protein around it has somehow to hold these residues exactly in the right place for the carboxyls to be where they need to be, to distinguish between sodium and potassium. This is a pretty tricky job, as you can understand, since they are only different by about 1/4 Å. However, another well studied model channel is the gramicidin model where the walls can move as a function of the interaction with the lipid around it. It would not be difficult to get a channel like the gramicidin channel to be mechanosensitive, so that things that happen in the membrane could easily influence it. Of course we can always imagine a cytoskeletal interaction from some other part of the molecule where the gates are functioning and that would be another way of getting mechanosensitivity. We are nowhere near the inactivation gate, but this selectivity ring is at least a candidate for the activation gate.

Dr. G. Kessler-Icekson: Computations are certainly a very powerful tool in the study of structure and function of nucleus in the cell. Is there any evidence for naturally occurring mutations in the sodium channel that affect function, or are linked with a disease.

Dr. H. Fozzard: Yes. Hyperkalemic periodic paralysis and similar associated skeletal muscle diseases are the result of genetically determined single-residue mutations in the skeletal muscle sodium channel. If we count the one in the horse, there are 13 different ones now, mostly affecting the inactivation behavior of the channel. Quite fascinating, because it really does offer a chance to compare the structure to the pathophysiology of those relatively rare muscle diseases. The other advantage, the sort of pseudo-naturally occurring point mutations that we exploit, is isoform differences between sodium channels in different tissues. There are now 17 different isoforms of the sodium channel, at last count, that have been cloned. The naturally occurring differences between isoforms is also a tremendous source of ideas about what is going on. As far as I know, there is no basis for saying that there is a naturally occurring point mutation in the cardiac channel, but then it might be lethal.

REFERENCES

1. Catterall WA: Cellular and molecular biology of voltage-gated sodium channels. *Physiol Rev.* 1992;72:S15-S48.
2. Satin J, Kyle JW, Chen M, Bell P, Cribbs LL, Fozzard HA, Rogart RB: A mutant of TTX-resistant cardiac sodium channels with TTX-sensitive properties. *Science.* 1992;256:1202-1205.
3. Lipkind GM, Fozzard HA: A structural model of the tetrodotoxin and saxitoxin binding site of the Na+ channel. *Biophys J.* 1994;66:1-13.
4. Creighton TE: *Proteins. Structures and Molecular Properties,* 2nd ed. New York: W.H.Freeman and Company; 1991.
5. Kao CY: Structure-activity relations of tetrodotoxin, saxitoxin and analogues. *Ann NY Acad Sci.* 1986;479:52-67.
6. Terlau H, Heinemann SH, Stuhmer W, Pusch M, Conti F, Imoto K, Numa S: Mapping the site of block by tetrodotoxin and saxitoxin of sodium channel-II. *FEBS Lett.* 1991;293:93-96.
7. Backx P, Yue D, Lawrence J, Marban E, Tomaselli G: Molecular localization of an ion-binding site within the pore of mammalian sodium channels. *Science.* 1992;257:248-251.
8. Hille B: The permeability of the sodium channel to organic cations in myelinated nerve. *J Gen Physiol.* 1971;58:599-619.
9. Mikami A, Imoto K, Tanabe T, Niidome T, Mori Y, Takeshima H, Narumiya S, Numa S: Primary structure and function expression of the cardiac dihydropyridine-sensitive calcium channel. *Nature.* 1989;340:230-233.
10. Heinemann SH, Terlau H, Stuhmer W, Imoto K, Numa S: Calcium channel characteristics conferred on the sodium channel by single mutations. *Nature.* 1992;356:441-443.
11. Yang J, Alienor PT, Slather WA, Hang J, Tsien RW: Molecular determinants of Ca2+ selectivity and ion permeation in L-type Ca2+ channels. *Nature.* 1993;366:158-161.

CHAPTER 2

MOLECULAR MECHANISMS OF K^+ CHANNEL BLOCKADE: 4-AMINOPYRIDINE INTERACTION WITH A CLONED CARDIAC TRANSIENT K^+ (Kv1.4) CHANNEL

Randall L. Rasmusson,[1] Ying Zhang,[2] Donald L. Campbell,[2] Mary B. Comer,[2] Robert C. Castellino,[3] Shuguang Liu,[4] Michael J. Morales,[2] and Harold C. Strauss[4]

ABSTRACT

We studied the blocking effects of 4-aminopyridine (4-AP) on a Kv1.4 K^+ channel. A permanently charged 4-AP derivative only produced block when applied intracellularly. 4-AP block accumulated from pulse to pulse indicating trapping of 4-AP in deactivated channels. For long trains of depolarizing pulses, 4-AP block increased with *decreasing* pulse duration. This increase took many pulses (>10) to accumulate and was relieved by two to three subsequent pulses of 500 msec duration. We conclude that the time- and voltage-dependence of 4-AP block can *not* be accounted for solely by either simple pure open channel or pure closed channel blocking schemes. We propose that the data can be explained by a model in which 4-AP binding is most stable when the channel has a symmetric arrangement in the binding regions.

INTRODUCTION

Many antiarrhythmic drugs block voltage gated K^+ channels, although their mechanisms of action vary significantly [1-4]. The effects of a particular blocker on a K^+ channel are presumably determined by molecular interactions between the blocking compound and specific regions of the channel. For those K^+ channel blocking compounds for which sidedness has been determined, the site of action is intracellular, and near the permeation pathway. One notable exception to this generalization is TEA^+, which has a

Departments of [1]Biomedical Engineering, [2]Pharmacology, [3]Cell Biology, and [4]Medicine Duke University, Durham, NC 27710, USA.

Molecular and Subcellular Cardiology: Effects of Structure and Function
Edited by S. Sideman and R. Beyar, Plenum Press, New York, 1995

high affinity extracellular binding site at the mouth of the permeation pathway in some K^+ channel types [5].

The mechanism of block may not always be determined by the particular K^+ channel blocker, but may be more dependent upon the target channel. For example, 4–AP appears to block in the cationic form and the site of action has been demonstrated to be on the cytoplasmic side of the membrane [6–9]. However, its mechanism of action varies significantly. Open–state [10, 11], closed–state [12–15], trapping [8] and mixed [16] mechanisms of block have all been reported. Segmental exchange mutagenesis studies between Kv2.1 and Kv3.1 channels have shown that 4–AP binding is localized to the cytoplasmic halves of membrane spanning domains S5 and S6 [17] thought to be located near the intracellular vestibule of the channel pore [18]. In addition, studies of gating currents recorded from Shaker K^+ channels have implicated 4–AP interactions with movement of the S4 voltage sensor. Recently, studies of block of native ferret [14] and human [19] cardiac I_{to} channels by 4–AP have described closed–state block which may also imply interactions with the voltage sensor [14].

In order to further elucidate the molecular basis of coupling between 4–AP and activation in cardiac K^+ channels, this study examines the mechanism of block of FK1 channels [20] by 4–AP. FK1 is a transient "I_{to}–like" voltage–gated potassium channel isolated from a ferret ventricular cDNA library and is a member of the Kv1.4 subfamily, which includes the closely related channels RCK4 [21] and HK1 [22]. Both FK1 and a fast inactivation deletion mutant of FK1 (ΔNco, [20]) were employed to assess state–dependent interactions of 4–AP. The blocking effects of 4–AP on this ferret ventricular Kv1.4 K^+ clone show some similarities to the mechanism of block of Kv2.1 and Kv3.1 delayed rectifier–like channels [17, 23], such as an ability to become trapped within the channel, but also shows significant differences in time– and voltage–dependence. Our study examines the physical implications of the time dependent open–state block and closed–state/trapping block as it relates to the known tetrameric structure of this class of channels.

METHODS

Preparation of cRNA. Construction of the FK1 cDNA clone, pBSMC1–12, and its inactivation mutant, ΔNco, has been previously described [20]. ΔNco is a deletion mutant in which amino acids 2–146 have been removed. This deletion removes fast inactivation without significantly altering activation or permeability characteristics [20].

Electrophysiological Techniques. Oocytes were obtained from anesthetized mature female *Xenopus laevis* using an enzymatic dispersion technique described in detail elsewhere [20]. Stage V–VI oocytes were injected with 50 nL of cRNA and incubated at 18°C for 24–72 hr in an antibiotic containing Barth's solution as described elsewhere [20]. Methods of ferret ventricular cell isolation are described elsewhere [14]. Voltage clamp techniques for oocytes and single ferret ventricular myocytes are standard and described in detail elsewhere [14, 20, 24]. For analysis of the active form and "sidedness" of 4–AP block, the permanently charged 4–AP derivative 4–aminopyridine–methiodide (4–APMI) was used [6]. The effects of extracellular 4–APMI were analyzed using the standard two microelectrode voltage–clamp technique, while the effects of intracellular 4–APMI were determined by applying it to the exposed intracellular surface of torn off "inside out" macropatches as previously described [24].

RESULTS

We have previously shown that 4-AP blocks the native transient K^+ current, I_{to}, in ferret right ventricular myocytes in a time- and voltage-dependent manner [14]. Characterization of the association and dissociation kinetics and voltage dependence of 4-AP binding led Campbell *et al.* [14] to propose a closed-state binding model. However, due to experimental limitations Campbell *et al.* [14] could not rule out the possibility that low affinity open-state block occurred at a rate which was slow relative to fast inactivation. To examine the possibility of a slow component of open-state binding and to further address potential interactions with the activation process we studied 4-AP block of the cloned FK1 channel and an NH_2-terminal deletion mutant, ΔNco [20], that lacked fast inactivation. Application of 4-AP to native ferret I_{to} and to FK1 both produced a "cross-over" of current records consistent with delayed unblocking of 4-AP bound closed channels (Fig. 1). However, significant differences in the kinetic behavior of the I_{to} and FK1 in the presence of 4-AP were noted.

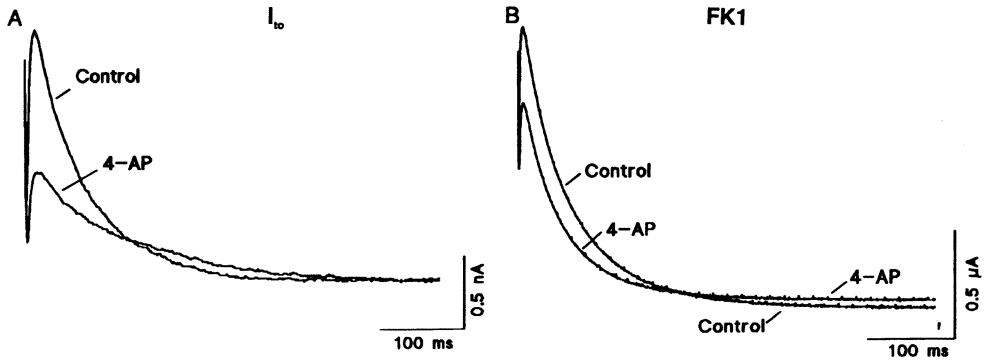

Figure 1. **A:** 4-AP (0.25 mM) causes the native myocyte I_{to} current waveform to crossover the current recorded in control solution. Although peak currents were reduced by 4-AP, late currents were larger in the presence of 4-AP. Holding potential -90 mV; test potential + 50 mV. **B:** 4-AP (1.0 mM) also caused a crossover in the current waveforms of FK1 expressed in oocytes. Holding potential -90 mV; test potential + 50 mV (adapted from [24] with permission).

To further elucidate the mechanism of block of the cloned channel by 4-AP we examined the effects of a permanently charged membrane impermeant 4-AP analogue, 4-APMI, on ΔNco. External application of 10 mM 4-APMI failed to produce any significant block of ΔNco at +50 mV (Fig. 2A). However, in the same oocyte, subsequent application of 10 mM external 4-AP led to a rapid reduction and ultimate block of the current. In contrast, when 10 mM 4-APMI was applied to the exposed intracellular face of a torn off ("inside out") macropatch, internal 4-APMI produced a rapid and reversible block (Fig. 2B). These results confirm that the cationic form of 4-AP is producing block, and that the binding site responsible for this block is only accessible from the intracellular side of the membrane (e.g. [6, 25, 26]).

Figure 2A also shows that 10 mM 4-AP also altered the kinetic behavior of ΔNco, producing an inactivation-like behavior during the depolarizing pulse that was indicative of open-channel block. Steady-state equilibration of lower concentrations of 4-AP (0.1-0.2 mM) still produced this inactivation-like behavior in ΔNco, albeit more slowly and to

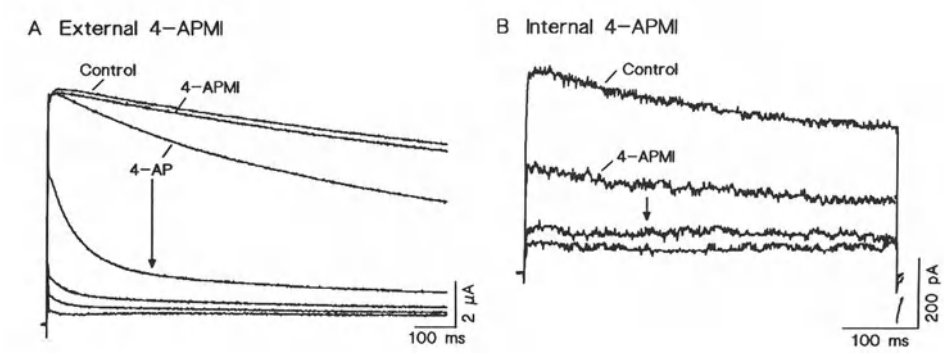

Figure 2. Effects of external and internal application of 10 mM 4–APMI on ΔNco channels. **A:** 10 mM extracellular 4–APMI failed to block ΔNco channels. After obtaining the control pulse, 10 mM 4–APMI was applied for nearly 5 min. The trace labelled "4–APMI" is the final recording obtained at the end of this ~5 min exposure. The traces labelled "4–AP" are subsequent consecutive traces obtained after switching to perfusion of 10 mM 4–AP. HP = –90 mV, 1 second pulses to +50 mV at 0.1 Hz. **B:** 10 mM internal 4–APMI produces a rapid reversible block of ΔNco channels recorded in a torn off ("inside out") macropatch.

a lesser degree. Inactivation like behavior in the presence of 0.2 mM 4–AP is clearly evident in the top traces of Fig. 3B. However, several other factors indicate that open–channel block does not completely describe the mechanism of 4–AP action. Block of Kv1.4 channels accumulates from pulse to pulse [11, 24], indicating that 4–AP can become trapped within the channel. The transient nature of open–channel block of ΔNco suggests that the amount of 4–AP bound to the channel at the end of the pulse is not 100% trapped during the process of deactivation. Otherwise, successive pulses would already be at equilibrium and would therefore not show time–dependent inactivation–like behavior. Furthermore the degree of trapping can be modulated by the deactivation potential [24].

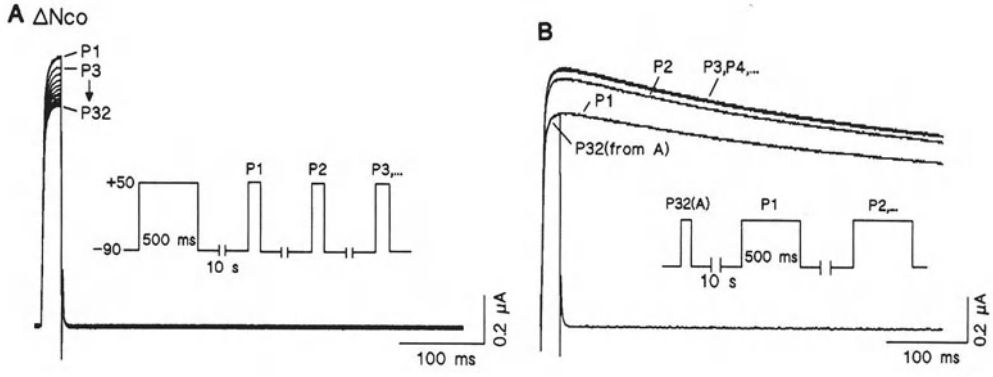

Figure 3. **A:** Development of 4–AP block of FK1 by a long train of brief pulses. An oocyte expressing ΔNco was pulsed at 0.1 Hz to + 50 mV for 500 msec from a holding potential of –90 mV in the presence of 0.2 mM 4–AP until steady–state current was achieved. Pulse width was then reduced to 25 msec and the oocyte was pulsed continuously at 0.1 Hz to +50 mV until a new steady–state was reached. **B:** Relief of brief–pulse duration block by long pulses in ΔNco. Following attainment of steady–state block using 25 msec duration pulses in panel A, pulse duration was abruptly changed to 500 msec and the reduction in current was reversed (adapted from [24] with permission).

The ability of 4–AP trapping to be modulated by the voltage range of deactivation suggests the possibility that deactivation may remove some or all of the open–state block. To test this possibility the following voltage clamp protocol was applied to ΔNco in the presence of 1 mM 4–AP. First, from a holding potential of –90 mV a series of short (25 msec) voltage clamp pulses to +50 mV were applied at a frequency of 0.1 Hz (schematic in Fig. 3A) which resulted in a reduction in peak current. Such pulse–length–dependent behavior was not observed in control solution for ΔNco (data not shown). After steady–state block had been reached (16–32 pulses, depending upon oocyte) the pulse duration was then changed to 500 msec (schematic in Fig. 3B) causing the peak current height to rapidly *increase* back to the original steady–state value within 3 pulses (Fig. 3B). This is consistent with relatively high affinity binding to a short lived state which occurs during deactivation. However, the rapid unbinding of 4–AP associated with long duration pulses suggests that unbinding of 4–AP from the deactivated state occurs as a result of a prolonged depolarizing pulse. This would account for the difference between the time course of the ΔNco currents between the first and subsequent 500 msec pulses illustrated in Fig. 3B. These results therefore indicate that pulse duration modulates the ratio of open–channel to closed–channel block.

DISCUSSION

Evidence for Closed, Open and Partially Deactivated Channel Block

The data from this and previous studies indicate that 4–AP blocks Kv1.4 and its fast inactivation deletion mutant ΔNco in a very complex time– and voltage–dependent manner. Although high concentrations (10 mM) of 4–AP can cause block of resting ΔNco channels, the rate at which 4–AP associates with the resting channel is so slow (min) as to be negligible [24]. Evidence for open–channel block of Kv1.4 channels by 4–AP has included (1) induction of block by channel activation [11, 24], (2) induction of apparent fast inactivation–like behavior in ΔNco, and (3) development of block during a prepulse which displayed voltage–dependence near the threshold of activation [24]. Evidence in support of a state dependent trapping mechanism included the observations that (1) block accumulated from pulse to pulse following initial exposure to 4–AP (Fig. 2A, [11, 24]), (2) trapping type block of a subsequent pulse (10 sec later) was sensitive to the deactivation potential of the preceding pulse [24], and (3) block was enhanced by a long series of brief depolarizing pulses (Fig. 3, [24]).

Channel Blocking Models

Open–Channel Blocking Models Fail to Predict the time– and voltage dependence of 4–AP trapping. A simple pure open–channel blocking mechanism similar to the one proposed by Yao and Tseng [11], shown as Model A in Fig. 4, can account for the time–dependent development of open–channel block and competition with N–type inactivation but fails to describe the trapping behavior which we observed. The addition of a mechanism by which drug bound to the open channel can become trapped in a deactivating channel can further account for trapping as shown in Model B (where T denotes closed channels in which drug is trapped). However, both of these models fail to predict (i) the increase in block observed with short–duration pulses (Fig. 3) and (ii) the dependence of trapping behavior on activation/deactivation potential reported by Rasmusson *et al.* [24].

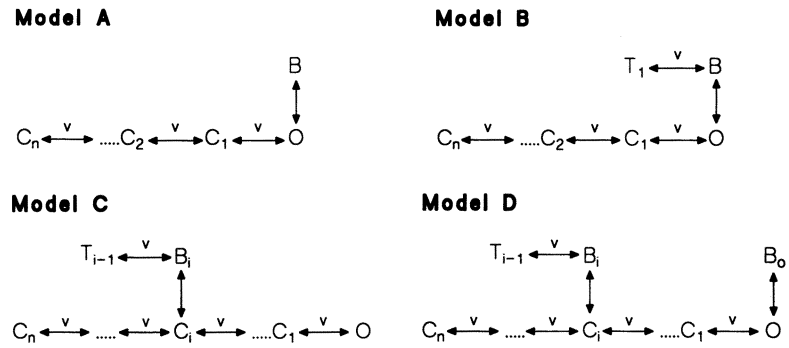

Figure 4. Comparison of models for blocking mechanisms. C_x denotes one of several closed states, O denotes open channels, v denotes voltage sensitive transitions, B denotes drug bound channels from which drug may freely associate and dissociate, and T denotes a closed state in which drug is "trapped".

Pure closed-state blocking models fail to predict the time- and voltage dependence of open-channel blockade. We can also consider binding to a single closed state as shown by Model C. Such a model can account for some of the observations, such as the ability of short pulses to accumulate block (Fig. 3) and the sensitivity of trapping to deactivation potential [22]. These observations are suggestive of binding and trapping to a closed state in which the channel has the highest probability of occupancy in the potential range −30 to −50 mV (i.e., the potential range where deactivation kinetics are slowest). However, Model C fails to predict the observed time-dependent *increase* in block during a sustained depolarization (e.g., Fig. 2A, Top trace Fig. 3A).

Since binding to neither a single open nor a single closed conformational state alone can explain all of the observed data, we must consider binding to multiple states. Model A can account for some of the time-dependent block observed during sustained depolarizations, and Model C can account for the observed phenomena, such as accumulated block during a sustained series of short pulses. Therefore, drug binding in these two models are complementary: each one can account for the set of experimental observations that the other fails to explain. In addition, the two models involve interactions with different, although not necessarily completely exclusive, channel states. To account for all of our data, Models A and C can be combined to form a minimal two state binding model (Model D).

Open channel block and deactivated state trapping are separated by a lower affinity conformation. As shown in Model D, there is no direct communication between the blocked open state and the blocked or trapped closed states. If communication between these two blocked states was identical to the intervening opening and closing transitions of the unblocked channel, the general behavior of Model D would approximate that of Model B but with a lower threshold for the onset of block. In addition, it would not produce the time-dependent block observed upon depolarization illustrated in Fig. 2A. In other words, 4-AP bound to the open state and 4-AP trapped in the closed channel are separated by transitions through lower affinity conformations associated with activation and deactivation. Although the lack of communication between B_i and B_o in Model D probably represents an oversimplification, the following qualitative observation remains: activation and deactivation pass through a transition-state which has a *lower affinity* for 4-AP than binding to the open state or the partially activated/deactivated state.

Such bi-stable binding is consistent with a proposed physical model in which the affinity of 4-AP to the FK1 channel is highest when the channel has a symmetric arrange-

ment of voltage sensors (i.e., four subunits in a fully activated or deactivated conformation), while the affinity is lower for conformations with asymmetric arrangements (i.e., transition states). Using the terminology of the Tytgat and Hess [27] model of cloned rat brain RCK1 K^+ channel activation, each channel subunit can reside in either a permissive or non–permissive state corresponding to the activated conformation of that particular subunit. When all four subunits are in a permissive conformation, the intracellular vestibule region is formed and the channel is in the open state. In this conformation, 4–AP interacts with four symmetric open channel subunits. Similarly, when all four subunits are in a non–permissive conformation and the intracellular vestibule region has not yet returned to the closed or resting configuration, the channel is again in a symmetric but deactivated state. 4–AP can therefore again interact with four symmetric subunits. As shown in the schematic of Fig. 5B, unbinding from intermediate states during activation and deactivation results in such a model because asymmetric arrangements will have binding energies which are 75, 50, 25, and 0% of the binding energy of the two symmetric arrangements and will result in a much faster dissociation rate during these transition states. Presumably movement of 4–AP from one binding site to another within the channel is also possible. In contrast to the predictions of the Kirsch and Drewe [23] (K–D) model where 4–AP will have no effect on gating currents (based on observations of Kv2.1 and Kv3.1 [17, 23]), our model predicts that at least some fraction of the gating currents will be altered. Removal of the slow component of gating currents by 4–AP in *Shaker* B channels has recently been observed by McCormack *et al.* [28], indicating some interaction between 4–AP and the voltage sensor in at least one K^+ channel clone.

Tetrapentylammonium also dissociates quickly from deactivating channels (on the time scale of hundreds of μsec; [29, 30]), indicating that changes in channel conformation related to deactivation alter the affinity for this compound as well. This is consistent with a symmetric subunit requirement similar to the energy additivity model of TEA^+ binding to open K^+ channels proposed by Heginbotham and MacKinnon [31]. Thus, both quaternary ammoniums and 4–AP may involve simultaneous interactions with four separate channel subunits.

Is there one binding site for 4–AP which shifts position within the channel during transitions associated with activation, as the cartoon presented in Fig. 5 suggests, or are there two distinct sites for which access changes in response to changes in channel conformation? Clearly, the affinity of one conformation can be different than the affinity of another. In addition, the affinity of quaternary ammonium compounds can be altered by mutations in the H5 region which are presumably quite physically distant from the actual binding site of the drug [32]. Thus, it is possible that a single binding site may move within the channel during activation and deactivation but may be modulated by neighboring residues which differ with activation state and that significant insights into the mechanisms of activation and inactivation coupling can be gained by comparing the structures of channels which display different modes of 4–AP block.

The study of Kirsch and Drewe [23] indicates that for 4–AP binding to Kv2.1 and Kv3.1 channels, differs substantially from that of FK1 (Kv1.4). In particular, the K–D model used to describe 4–AP block of Kv2.1 and Kv3.1 channels is inconsistent with our data from Kv1.4 channels because of the lack of a direct correspondence between open–channel block developed during a pulse and trapping during a subsequent pulse. In contrast, activation and deactivation of Kv1.4 appears to involve conformational changes through intermediate states which have a lower affinity for 4–AP than the affinity of either the fully activated or deactivated channel. This suggests a coupling of 4–AP binding to the voltage sensor in Kv1.4 channels which is distinct from Kv2.1 and Kv3.1 channels.

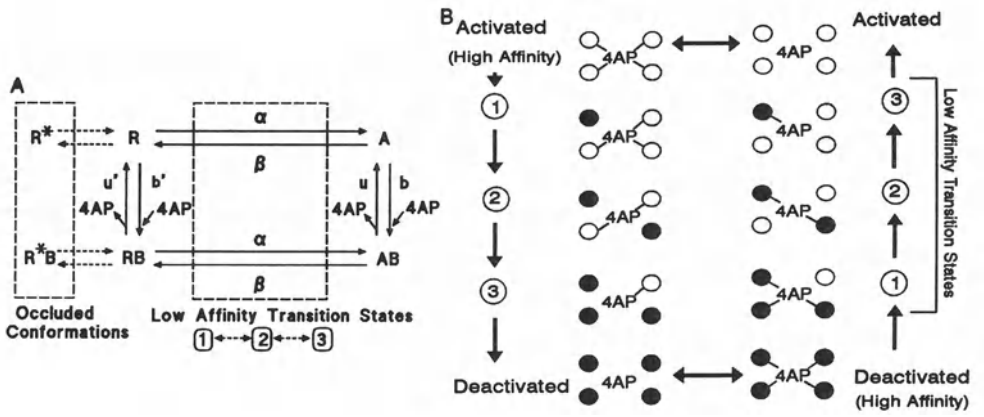

Figure 5. **A:** Block of ΔNco by 4–AP differs from block of Kv2.1 and Kv3.1. The four state model proposed to describe block and unblock of Kv2.1 and Kv3.1 channels [23] is shown with solid lines in the center of the figure. The dashed arrows indicate additional transitions and the dashed boxes indicate regions for which the ΔNco (Kv1.4) data suggest the involvement of additional states which were not explicitly included in the K–D model. The two qualitative differences are: 1) A relatively short–lived high affinity deactivated state (R) which can transition to an occluded conformation (R^*) that does not allow drug binding or unbinding, and 2) Lower affinity transition states which are associated with the activation and deactivation pathways (1, 2, 3) and may be responsible for generating the "bi–stable" nature of 4–AP block of Kv1.4 channels (see panel B). **B:** Proposed physical basis for bi–stable block and lower affinity transition states. For this physical model, we propose that the regions of each subunit involved in binding 4–AP shift in response to changes in the activation state of each subunit. Hollow circles denote subunits which are in the permissive state. Four subunits in a permissive state correspond to the activated state of the channel. Solid circles denote subunits which are in the non–permissive state. Four subunits in a non–permissive state correspond to the resting state of the channel. Both the resting and activated states have four coordinated bonds with which to bind 4–AP. In the upper left hand corner, the conformation corresponds to 4–AP bound to the open channel with a symmetric arrangement of bonds (denoted by short lines) interacting with 4–AP. In response to a deactivating clamp pulse, the channel would proceed from an activated to a deactivated state (downward along the left column) as subunits move from the permissive to non–permissive conformations. As a result of the deactivation, 4–AP which was bound to the permissive subunits will interact with 3, 2 and 1 subunits, with a corresponding decrease in free energy and an increased K_{off}. Similarly, 4–AP bound to the deactivated (or resting channel, bottom right hand corner) loses its symmetric arrangement of bonds during the process of activation. Potentially, bound 4–AP can move between the two binding sites without exiting the channel.

In addition, trapping was described in the K–D model by a slow access time. Physically, these slow kinetics may be due to steric occlusion of the binding site [14, 15, 23, 24]. We needed to explicitly include this putative stericly hindered resting state (designated R^*) due to the nature of 4–AP binding to the deactivated conformation. The need to explicitly include this mechanism was suggested by our previous trapping results [24] in which block was maximal for a deactivation potential of −50 to −40 mV. At this potential three factors coincide: 1) deactivation is complete, 2) deactivation has its slowest time course, and 3) the steady–state inactivation relationship for FK1 predicts that the intracellular channel vestibule is open [20, 24]. To explain trapping in our model, we propose that 4–AP binds to a partially deactivated channel in which the intracellular vestibule is not closed; upon vestibular closing 4–AP then becomes trapped. As a result, access, but not necessarily affinity, is reduced.

Much evidence has accumulated to demonstrate the formation of an intracellular vestibule coupled to activation in response to a depolarizing step [17, 19, 24, 33]. Formation or opening of such a vestibule may be responsible for the final step which

precedes channel opening in many models of various voltage gated channels [28, 33, 34]. The similarities and differences between binding of 4–AP and quaternary amines suggest that opening and closing of the intracellular vestibule is a critical event in activation and deactivation. The similarity between steady–state inactivation in FK1 and development of block during a pre–pulse by 4–AP in ΔNco suggests that the process of opening of the intracellular vestibule, which permits access to the open–state binding site for 4–AP, is related to formation of the inactivation ball receptor. The ability of 4–AP to bind to the deactivated state of the FK1 channel suggests that closure of this intracellular vestibule follows channel deactivation and that at least some of the voltage sensitive conformational changes of the channel can precede closure of the internal mouth of the pore.

CONCLUSION

The complex time dependent behavior of 4–AP binding to Kv1.4 can be explained by a model in which (i) 4–AP binding is most stable when the channel has a symmetric arrangement in the drug binding domain (i.e., four subunits in a fully activated or deactivated conformation), (ii) 4–AP has a lower affinity for asymmetric subunit arrangements (i.e., transition states), and (iii) the 4–AP binding site(s) is occluded by conformational changes in the intracellular channel vestibule region associated with channel deactivation.

Acknowledgements

We thank Dr. Gerry Oxford for the generous gift of 4–APMI and A. Crews and D. Lamson for technical assistance. Supported in part by NIH grants HL–19216, 52874 and 17670 to HCS and a Whitaker Foundation Research Grant to RLR.

DISCUSSION

Dr. H. Fozzard Is a closed–state blockade a desirable action for antiarrhythmic therapy?

Dr. H. Strauss: One would predict minimal antiarrhythmic efficacy for a compound that has similar association and dissociation kinetics to that of 4–AP. The reason for this is that the drug's net effect on repolarization is likely to be maximal at slow heart rates and minimal at fast heart rates. This would predispose the heart toward Tosades de pointes and confer relatively little antiarrhythmic protection during tachycardia when one would like to achieve maximal antiarrhythmic effect.

Dr. E. Marban: Could you comment on the mechanisms of 4–AP blockade of different K^+ channels as most of the experiments have been implemented in more than one cell type. With these potassium channel blockers, can you extrapolate your results to vascular smooth muscle from these experiments? Do the same mechanisms hold in both types of cells?

Dr. H. Strauss: Unfortunately, the response to 4–AP varies widely amongst different currents in different cell types. On the other hand, evidence is becoming available to indicate which α–subunits exist in vascular smooth muscle. Making the unverified assumption that the α– and β–subunits, and regulatory enzymes that modulate the degree of phosphorylation of these functioning K^+ currents are comparable, then one would predict that drug interaction with the same potassium channels in the vascular smooth muscle and heart would be similar. What will still be different is the fact that differences in action potentials between vascular smooth muscle and cardiac cells will result in

kinetic differences in the currents between these two types of cells yielding different pharmacological responses. But if you analyze, in a comparable manner the kinetics of association/dissociation, I believe that the patterns of interaction will be comparable even though patterns of blockade in an unclamped cell might differ.

Dr. H. Fozzard: The neurologists have, from time to time, used 4–AP to treat patients with multiple sclerosis. Is there any information about what effect this has had on the heart or on the cardiac electrical system?

Dr. H. Strauss: We have not yet analyzed the literature exhaustively to address this question. However, the concentrations that are employed to analyze its effects here are in the millimolar range, perhaps that is in excess of that required to achieve blockade in those patients. It is something worth exploring, certainly.

Dr. Y. Rudy: What species did you use? Do you feel that this species could be generalized to other species as well?

Dr. H. Strauss: It turns out that the ferret ventricular myocyte that we have used has a transient outward current whose functional properties bear a striking similarity to that observed in the human ventricular myocyte. Further, FK1 clone that we have isolated from the ferret has the highest degree of sequence homology to that of the human HK1. In terms of 4–AP blocking properties on the transient outward current, there are some species differences reported in the literature. Part of the difference may have to do with the fact that overlapping multiple voltage–dependent K^+ channel currents with varying affinity for 4–AP may have complicated the interpretation of the blocking properties of 4–AP on the transient outward current in other species possibly exaggerating potential differences.

Dr. M. Lab: The transient outward current seems to be specific to the site from where the cells are isolated. Is that right? I am referring to Antzelovitch's work, epicardium vs endocardium [Litovsky and Anzelovitch. *Circ Res.* 1988;62:116–126]

Dr. H. Strauss: Furukawa *et al.* [*Circ Res.* 1989;67:1287] and Liu *et al.* [*Circ Res.* 1993;72:671] have demonstrated the relative absence of transient outward current in papillary muscle and endocardial layer of cat and dog ventricle. Comparable differences in Kv4.2 mRNA expression have been noted in rat ventricular muscle [Dixson JE & McKimmon D. *Circ Res.* 1994;75:252]. We have not done an extensive analysis of transient outward current expression in the ferret heart so I cannot address the question in this species.

REFERENCES

1. Hondeghem LM, Snyders LM. Class III antiarrhythmic agents have a lot of potential but a long way to go. Reduced effectiveness and dangers of reverse use dependence. *Circulation.* 1990;81:686–690.
2. Snyders DJ, Knoth KM, Roberds SL, Tamkun MM. Time–, voltage–, and state–dependent block by quinidine of a cloned human cardiac potassium channel. *Mol Pharmacol.* 1992;41:322–330.
3. Campbell DL, Rasmusson RL, Comer MB, Strauss HC. The cardiac calcium–independent transient outward potassium current: kinetics, molecular properties, and role in ventricular repolarization. In: Zipes DP, Jalife J, eds. *Cardiac Electrophysiology. From Cell to Bedside.* Philadelphia: Saunders; 1994;83–96.
4. Rasmusson RL, Campbell DL, Qu Y, Strauss HC. Conformation–dependent drug binding to cardiac potassium channels. In: Brown AM, Catterall WA, Kaczorowski GJ, Spooner PM, Strauss, HC, eds. *Ion Channels in the Cardiovascular System. Function and Dysfunction.* Armonk/New York; Futura Publishing; 1994;387–414.
5. Hille B. *Ionic Channels of Excitable Membranes.* Sunderland/MA; Sinauer Associates; 1992.

6. Kirsch GE, Narahashi T. Site of action and active forms of aminopyridines in squid axon membranes. *J Pharmacol Exp Therap.* 1983;226:174–179.
7. Oxford GS, Wagoner PK. The inactivating K^+ current in GH_3 pituitary cells and its modification by chemical reagents. *J Physiol (Lond).* 1989;410:587–612.
8. Choquet D, Korn H. Mechanism of 4–aminopyridine action on voltage gated potassium channels in lymphocytes. *J Gen Physiol.* 1992;99:217–240.
9. Hirsh JK, Quandt FN. Aminopyridine block of potassium channels in mouse neuroblastoma cells. *J Pharmacol Exp Therap.* 1993;267:604–611.
10. Hice RE, Swanson R, Folander K, Nelson D. Aminopyridines alter inactivation rates of transient potassium channels. *Biophys J.* 1992;61:A376.
11. Yao J–A, Tseng G–N. Modulation of 4–AP block of a mammalian A–type K channel clone by channel gating and membrane voltage. *Biophys J.* 1994;67:130–142.
12. Yeh JZ, Oxford GS, Wu CH, Narahashi T. Dynamics of aminopryidine block of potassium channels in squid axon membrane. *J Gen Physiol.* 1976;68:519–535.
13. Kehl SJ. 4–aminopyridine causes a voltage–dependent block of the transient outward K^+ current in rat melanotrophs. *J Physiol (Lond).* 1990;431:515–528.
14. Campbell DL, Rasmusson RL, Qu Y, Strauss HC. The calcium–independent transient outward potassium current in isolated ferret right ventricular myocytes. II. Closed state "reverse use–dependent" block by 4–aminopyridine. *J Gen Physiol.* 1993;101:601–626.
15. Castle NA, Slawsky MT. Characterization of 4–aminopyridine block of the transient outward K^+ current in adult rat ventricular myocytes. *J Pharmacol Exp Therap.* 1993;264:1450–1459.
16. Thompson S. Aminopyridine block of transient potassium current. *J Gen Physiol.* 1982;80:1–18.
17. Kirsch GE, Shieh C–C, Drewe JA, Vener DF, Brown AM. Segmental changes define 4–aminopyridine binding and the inner mouth of K^+ pores. *Neuron* 1993;11:503–512.
18. Slesinger PA, Jan YN, Jan LY. The S4–S5 loop contributes to the ion–selective pore of potassium channels. *Neuron.* 1993;11:739–749.
19. Li, GR, Feng, J, Wang, Z, Fermini, B, and Nattel, S. Mechanism of 4–aminopyridine resistant transient outward current in human atrial myocytes. *Circulation.* 1994;90:I–145.
20. Comer MB, Campbell DC, Rasmusson RL, Lamson DR, Morales MJ, Zhang Y, Strauss HC. Cloning and characterization of an I_{to}–like channel from ferret ventricle. *Am J Physiol (Heart Circ Physiol 36).* 1994;267:H1383–H1395.
21. Stühmer W, Ruppersberg JP, Schröter KH, Sakmann B, Stocker M, Giese KP, Perschke A, Baumann A, Pongs O. Molecular basis of functional diversity of voltage–gated potassium channels in mammalian brain. *EMBO J.* 1989;8:3235–3244.
22. Tamkun MM, Knoth KM, Walbridge JA, Kroemer H, Roden DM, Glover, DM. Molecular cloning and characterization of two voltage–gated K^+ channel cDNAs expressed in rat heart. *FASEB J.* 1991;5:331–337.
23. Kirsch GE, Drewe JA. Gating–dependent mechanism of 4–aminopyridine block in two related K^+ channels. *J Gen Physiol.* 1993;102:797–816.
24. Rasmusson, RL, Zhang, Y, Campbell, DL, Comer MB, Castellino RC, Liu S, and Strauss, HC. Bi–stable block of a cloned cardiac transient K^+ channel (Kv1.4) by 4–aminopyridine. *J Physiol (Lond).* 1995; in press.
25. Howe JR, Ritchie JM. On the active form of 4–aminopyridine: Block of K^+ currents in rabbit schwann cells. *J Physiol (Lond).* 1991;433:183–205.
26. Stephens GJ, Garratt JC, Robertson B, Owen DG. On the mechanism of 4–aminopyridine action on the cloned mouse brain potassium channel mKv1.1. *J Physiol (Lond).* 1994;477.2:187–196.
27. Tytgat J, Hess, P. Evidence for cooperative interactions in potassium channel gating. *Nature.* 1992;359:420–423.
28. McCormack K, Joiner WJ, Heinemann SH. A characterization of the activating structural rearrangements in voltage–dependent *Shaker* K^+ channels. *Neuron.* 1994;12:301–315.
29. Armstrong CM. Inactivation of the potassium conductance and related phenomena caused by quaternary ammonium ion injected in squid axons. *J Gen Physiol.* 1969;54:553–575.
30. Taglialatela M, VanDongen AMJ, Drewe JA, Joho RH, Brown AM, Kirsch GE. Patterns of internal and external tetraethylammonium block in four homologous K^+ channels. *Mol Pharmacol.* 1991;40:299–307.
31. Heginbotham L, MacKinnon R. The aromatic binding site for tetraethyl–ammonium ion on potassium channels. *Neuron.* 1992;8:483–491.

32. Yellen G, Jurman ME, Abramson T, MacKinnon R. Mutations affecting internal TEA blockade identify the probable pore forming region of a K^+ channel. *Science (Wash DC).* 1991;251:939–942.
33. Zimmerberg J, Bezanilla F, Parsegian VA. Solute inaccessible aqueous volume changes during opening of the potassium channel of the squid giant axon. *Biophys J.* 1990;57:1049–1064.
34. Zagotta WN, Aldrich RW. Voltage-dependent gating of Shaker A-type potassium channels in Drosophila muscle. *J Gen Physiol.* 1990;95:29–60.

CHAPTER 3

Na^+, K^+-ATPase and Heart Excitability

David Lichtstein[1]

ABSTRACT

The Na^+, K^+-activated adenosine triphosphatase (ATPase) is present in the membrane of eukaryotic cells and represent a major pathway for Na^+ and K^+ transport across the plasma membrane. Cardiac glycosides, such as digoxin or ouabain, inhibit this enzyme activity by binding to a specific receptor on the membrane. Studies conducted in this and other laboratories have proven the existence of digitalis-like compounds in animal and human tissues which may serve as regulators, *in vivo*, of the Na^+, K^+-pump activity. The levels of digitalis-like compounds in the plasma are increased in hypertension and other illnesses. A possible link at the cellular and molecular level between these compounds and etiology of arrhythmias, an important cause of morbidity and mortality in patients with various diseases of the heart, can be postulated: Na^+, K^+-ATPase activity contributes directly and indirectly to the electrical membrane potential of cardiac cells. The inhibition of this pump by the endogenous digitalis-like compounds, in discrete areas of the heart, can induce changes of the membrane potential of these cells. These changes may cause an increase in excitability of the particular cells and contribute to the generation of arrhythmias.

INTRODUCTION

Na^+,K^+-ATPase and Its Regulators

Na^+, K^+-adenosine triphosphatase (Na^+, K^+-ATPase, Na^+, K^+-pump, E.C.3.6.1.3) activity is considered to represent the enzymatic activity associated with the cellular Na^+, K^+-pump. The system hydrolyses ATP in the presence of Mg^{++} and the free energy of hydrolysis is used to transport potassium into the cell and sodium out of the cell, against their electrochemical gradients. An enormous amount of data on this enzymatic system has accumulated in the last 30 years (for review see [1-2]) and several possible models for its

[1]Department of Physiology, Hebrew University - Hadassah Medical School, Jerusalem, Israel.

Molecular and Subcellular Cardiology: Effects of Structure and Function
Edited by S. Sideman and R. Beyar, Plenum Press, New York, 1995

action have been presented. It has been recently demonstrated that several isozymes exist for the catalytic subunit of the enzyme and the distribution of the isozymes in various tissues and differences in their function is being explored [3]. The maintenance of Na^+ and K^+ transmembranal gradients is one of the requirements of several transport processes in the living cell. Furthermore, the activity of the Na^+, K^+–ATPase has been shown to be involved in the specialized function of several tissues including heart muscle, neurons and kidney (for review see [2–3]). The mechanism by which the activity of the Na^+, K^+–pump is regulated is therefore an issue of a major importance.

Regulation of Na^+, K^+–ATPase Activity at the Digitalis Binding Site

Digitalis (cardiac glycosides), such as ouabain or digoxin, bind specifically to Na^+, K^+–ATPase preparations and this interaction results in the inhibition of the enzyme activity and Na^+ and K^+ transport (for review see [4]). There have been numerous studies on the interaction of these cardiac glycosides with particular preparations of Na^+, K^+–ATPase obtained from a wide variety of tissues and species. It was shown that ouabain inhibits the enzyme activity by binding to the outer side of the cell membrane and the inhibition process was analyzed at the molecular level [5, 6].

ENDOGENOUS DIGITALIS–LIKE COMPOUNDS

The cardiac glycosides are extracted from the dried leaf of the common purple foxglove, Digitalis purpura, and the seeds and leaves of some other plants [7]. In the animal kingdom, structurally related compounds with cardiotonic activity have been shown until recently to exist only in the poison glands of bufonid toads [8] and in the skin of several species of amphibia [9, 10]. The existence of a specific binding site for digitalis and the variety of pharmacological effects of these compounds raised the possibility of the existence of an unknown "digitalis–like" compound which regulates the activity of the Na^+, K^+–ATPase through this binding site. Such an approach was very fruitful in the study of opiates and resulted in the discovery of the enkephalins [11]. In recent years evidence have been presented that extracts from mammalian brain [12–15], heart [16, 17], adrenal [18, 19], plasma [21–23], hemofiltrate [24], urine [25–27], and CSF [28–29] contain a digitalis–like activity. All these endogenous compounds have the common feature of interacting with the ouabain binding site on the Na^+,K^+–ATPase and inhibit its activity and, like digitalis, increase the force of contraction of heart muscle. For a thorough description of the field see recent reviews [30–32].

Several substances have been proposed as digitalis–like compounds. These include unsaturated fatty acids [33–35], hydroxy unsaturated fatty acids [36] lysophosphatidylcholines [37–38], dihydroxyeicosatrienic acid [39], dopamine [40], dehydroepiandrosterone sulfate [41], lignan [42] and ascorbic acid [43]. However, none of these compounds appear to be the natural ligand of the digitalis receptor of the Na^+, K^+–ATPase because of their limited specificity and affinity (for review see [30–32].

Hamlyn and coworkers [44] have recently demonstrated the presence of the plant cardiac glycoside ouabain (Fig. 1) in human plasma of mildly volume–expanded patients. They have also demonstrated that ouabain is present in many internal organs and that the adrenal gland is the probable source of the endogenous ouabain. Goto and coworkers [45] have, on the other hand, demonstrated that digoxin (Fig. 1) is a normal constituent of human urine. Finally, we have recently identified two new steroids 19–norbufalin, and 19–norbufalin peptide derivative (Fig. 1) from human cataractous eye lens nuclei [46]. These

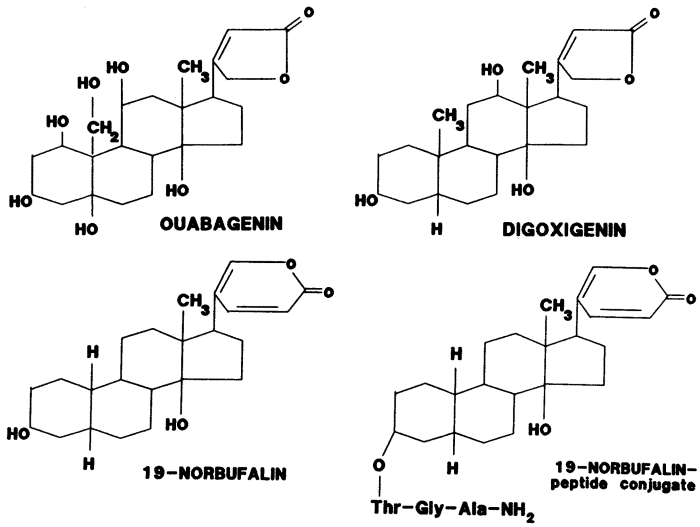

Figure 1. Chemical structures of digitalis-like compounds identified in human tissues.

steroids resemble the structure of ouabain and digoxin but differ mainly by having a six member lactone ring. These observations imply that the synthesis of five and six member cyclic unsaturated lactone steroids is not restricted to plants but can occur in mammalian tissues as well. This, as yet, has not been demonstrated.

DIGITALIS-LIKE COMPOUNDS IN CARDIAC ARRHYTHMIAS - POSSIBLE INVOLVEMENT

An arrhythmia is an abnormality of rate, regularity, or site of origin of the cardiac impulse or a disturbance in conduction that causes an alteration in the normal sequence of activation of the atria and ventricles. Clinically, ventricular arrhythmias are classified as benign, potentially malignant, or malignant based on the risk of their causing sudden death [47]. Two main mechanisms for the development of cardiac arrhythmias have been postulated: 1) Arrhythmias due to abnormalities of impulse generation. 2) Arrhythmias caused by abnormalities of impulse conduction [47, 48]. The first mechanism includes altered normal automaticity in one of the cardiac pace makers [49] and abnormal generation of impulses [50]. The second mechanism includes slow or fast conductions of action potentials which cause re-entrant reexcitation of the ventricle. All these mechanisms are subjects of ongoing experimental investigations. Detailed description and classification of arrhythmias are well documented. For review see [47, 48, 50].

Cardiac arrhythmias are an important cause of morbidity and mortality in patients with various diseases of the heart. Their prevalence and severity is dependent on the underlying cardiac pathology and the influence of various extra-cardiac factors, i.e. electrolyte imbalance, cardiac active drugs, autonomic neuronal control and various humoral agents. Most notorious of these humoral agents are the catecholamines and many studies have shown correlation between increased plasma levels of catecholamines and frequency of arrhythmic episodes [51].

We postulate that the endogenous steroidal digitalis-like compounds (ouabain, digoxin, and the 19-norbufalins) may be involved in the etiology of cardiac arrhythmias.

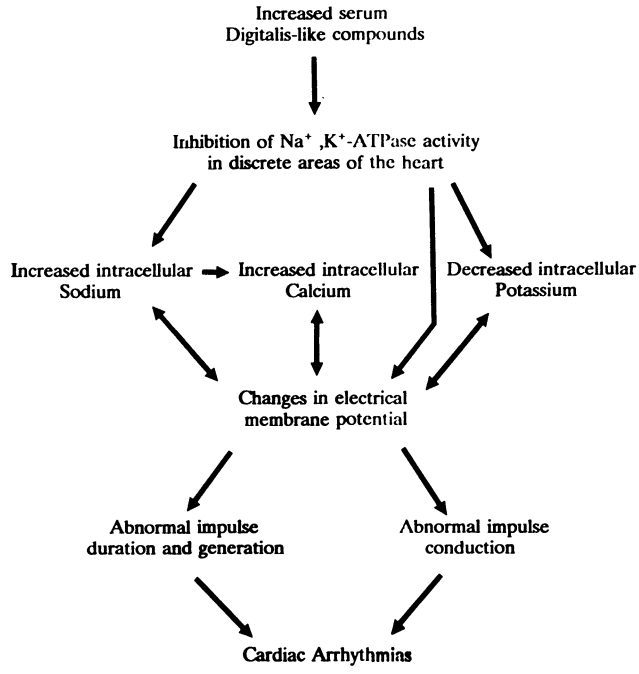

Figure 2. Suggested effect of increased digitalis-like compounds on cardiac excitability and arrhythmias.

The rational for this hypothesis is straight forward (Fig. 2): The Na^+, K^+-ATPase activity contributes directly (being electrogenic pump) and indirectly (being responsible for the ionic gradients across the cell membrane) to the electrical membrane potential of cardiac cells. As mentioned above, several isozymes exist for the catalytic subunit of the enzyme. These isozymes differ in their sensitivity to digitalis [3]. Thus, the presence of digitalis or the endogenous digitalis-like compounds will differently affect distinct cells according to the particular isozyme present in these cells. The inhibition of the pump by the endogenous digitalis-like compounds in discrete area of the cardiac muscle will induce, therefore, changes in the electrical membrane potential of the cells. Such changes may be an important causes of increased excitability of the particular cells and contribute to the generation of arrhythmias in one of the pathways described above.

CONCLUSION

The increased levels of digitalis-like compounds in the plasma in hypertension and other illnesses suggest a link between these compounds and the etiology of arrhythmias involving local mediation of the Na^+,K^+-ATPase activity in the heart. Two lines of research may confirm or refute this hypothesis: 1) The determination of serum digitalis-like compounds in humans afflicted with cardiac arrhythmias in comparison to the levels in healthy individuals. 2) The evaluation of the effect of local application of digitalis to different areas of the heart on commencement of cardiac arrhythmias.

DISCUSSION

Dr. A. Shainberg: Does digoxin treatment increase the probability of cataract formation?

Dr. D. Lichtstein: I do not think that anyone has done this study. We are in the middle of doing that, so I do not have an answer yet.

Dr. J. Solarao: Can you use any of the subunits of the Na^+, K^+–ATPases in the purification protocol to pull these factors out, for example, or even use the synaptosomes. You have a naturally occurring high affinity ligand.

Dr. D. Lichtstein: We never tried it; others did. The synaptosomes would not be such a good preparation because the density of the pumps is not high enough. A purified ATPase, on the other hand, can be used. I know that other groups have tried it.

Dr. E. Marban: The peptide conjugate of 19–norbufalin seems potentially very important. The finding of ouabain in human plasma has been somewhat disappointing. After all, we have cheap digitalis. But if there were something novel that the body makes, and this peptide conjugate might be such a candidate, maybe it would imply a very important regulatory role. Do you have any ideas about how it is made, and whether it is active as a Na^+, K^+–ATPase inhibitor, or is it present in other tissues in disease states?

Dr. D. Lichtstein: The peptide derivative of 19–norbufalin is very active as a Na^+, K^+–ATPase inhibitor. At present, we do not know the site of its specific production. As far as the uniqueness of this particular compound, it is not only that it has the peptide moiety, although I agree with you that it might be very important, but that it is 19–nor steroid. If you look in the literature, you will see that 19–nor steroids such as 19–nor–testosterone, or 19–nor–progesterone, are very different from their parent 19 steroids. Sometimes they are much more potent than the parent steroid. This study, as far as we know, is the first demonstration of 19–nor–digitalis. We did some molecular modeling of this compound as compared to ouabain or digitalis and found that it differs very significantly in its 3D structure. We think that this may be a unique structure and an interesting compound.

Dr. H.E.D.J. ter Keurs: What is the IC 50 of the inhibitory effect of 19–norbufalin on the Na^+, K^+–ATPase?

Dr. D. Lichtstein: It obviously depends on the condition that you do the assay. But in the condition that you have an effect of ouabain, say an 10 nM IC 50, you will have it by 19–norbufalin by around 1 nM. It is at least 10 times more potent than ouabain, in any system that we have tested so far.

Dr. H.E.D.J. ter Keurs: This is interesting with respect to its effect on the heart because if one uses digitalis–like compounds in the treatment of a patient, one aims for a level of 1 nM.

Dr. M. Morad: Has anybody looked at the effect of this compound on the Na^+, K^+–ATPase from an electrophysiological point of view rather than just putting it on the frog heart and showing that frog heart tension goes up? There are a number of steps before that happens. Was it easy to measure the Na^+, K^+–ATPase activity at a physiological tissue and add this compound and show if it inhibits or not?

Dr. D. Lichtstein: If you ask if we did some physiological studies *in vivo* or *in vitro*, the answer is no. The reason is that in order to do these experiments one obviously would need sufficient

quantity of the compound. We are in the process of organic synthesis of our compound so that these experiments can be done.

Dr. M. Morad: If you can put it on a frog heart, you can certainly put it on a frog myocyte.

Dr. D. Lichtstein: Yes, but you should be aware of the stage of purification. You can use crude extract in any experimental system. That is not the problem. But then, at a low level of purity you can not say whether it is one compound or more affecting it. I believe the goal is to synthesize the 19-nor bufalin and use the synthetic material, after proving that it fits exactly to the characteristics that I showed you here. The synthetic material will then be used in different experimental systems. The characterization of the effect of an extract, unless you have a really purified material, will have problems of interpretation.

REFERENCES

1. Skou JC, Norby JG, Maunsbach AB, Esmann M. *The Na^+, K^+-pump, Parts A and B.* New York: Alan R. Liss Inc.; 1988.
2. Apell HJ. Electrogenic properties of the Na,K pump. *J Membr Biol.* 1989;110:103-114.
3. Urayama O, Shutt H, Sweadner KJ. Identification of three Isozyme proteins of the catalytic subunit of the Na^+, K^+-ATPase in rat brain. *J Biol Chem.* 1989;264:8271-8280.
4. Hoffman BF, Bigger JT, Jr. Digitalis and allied cardiac glycosides. In: Goodman Gilman A, Rall TW, Nies AS Taylor P, eds. *The Pharmacologic basis of Therapeutics.* 8th edition. New York: Pergamon Press, 1990; 814-839.
5. Lindenmayer GE. Mechanism of action of digitalis glycoside at the subcellular level. *Pharmacol Ther.* 1976;2:843-861.
6. Lee KS, Klaus W. The subcellular basis for the mechanism of inotropic action of cardiac glycosides. *Pharm Rev.* 1972;23:193-250.
7. Briggs MH, Brotherton J. Plant Steroids, In: Briggs MH, Bretherton J, eds. *Steroid Biochemistry and Pharmacology.* London: Academic Press, 1970; 265-296.
8. Meyer K, Kinde H. Collection of toad venoms and chemistry of the toad venom steroids. In: Bucherl W, Buckley E, eds. *Venomous Animal and their Venoms.* Vol. 2. New York: Academic Press, 1971; 521-552.
9. Flier JS. Ouabain-like activity in toad skin and its implications for endogenous regulation of ion transport. *Nature.* 1978;274:285-286.
10. Flier JS, Edwards MW, Daly JW, Myers CW. Widespread occurrence in frogs and toads of skin compounds interacting with the ouabain site of Na^+, K^+-ATPase. *Science.* 1980;208:503-505.
11. Hughs J, Smith TW, Kosterlitz HW, Fothergill LA, Morgan BA, Morris HR. Identification of two related pentapeptides from brain with potent opiate agonist activity. *Nature.* 1975;258:577-579.
12. Fishman M. Endogenous digitalis-like activity in mammalian brain. *Proc Natl Acad Sci USA.* 1979;76:4661-4663.
13. Haupert GT Jr, Sancho JM. Sodium transport inhibitor from bovine hypothalamus. *Proc Natl Acad Sci USA.* 1979;76:4658-4660.
14. Lichtstein D, Samuelov S. Endogenous 'ouabain like' activity in rat brain. *Biochem Biophys Res Comm.* 1980;96:1518-1523.
15. Akagawa K, Hava N, Tsukada Y, Partial purification and properties of the inhibitors of Na^+, K^+-ATPase and ouabain binding in bovine central nervous system. *J Neurochem.* 1984;42:775-780.
16. De Pover A, Castaneda-Hernandez G, Godfraind T. Water versus acid extraction of digitalis-like factor from guinea pig heart. *Biochem Pharmacol.* 1982;31:267-271.
17. Khatter JC, Agbanyo M, Navaratnam S. Endogenous inotropic substance from heart tissue has digitalis-like properties. *Life Sci.* 1990;48:387-396.
18. Tamura M, Lam TT, Inagami T. Isolation and characterization of a specific endogenous Na^+, K^+-ATPase inhibitor from bovine adrenal. *Biochemistry.* 1988;27:4244-4253.
19. Doris PA, Stocco DM. An endogenous digitalis-like factor derived from the adrenal gland: Studies of adrenal tissue from various sources. *Endocrinol.* 1989;125:2573-2579.
20. Kramer HJ. Natriuretic hormone - a circulating inhibitor of sodium and potassium-activated adenosine triphosphatase. *Klin Wochenschr.* 1981;59:1225-1230.

21. Gruber KA, Rudel LL, Bullock BC. Increased circulating levels of an endogenous digoxin-like factor in hypertensive monkeys. *Hypertension*. 1982;4:348-354.
22. Gonick HC, Kramer HJ, Paul W, Lu E. Circulating inhibitor of sodium-potassium activated adenosine triphosphatase after expansion of extracellular fluid volume in rats. *Clin Sci Mol Med.* 1977;53:329.
23. Montali U, Balzan S, Ghione S. Purification of endogenous digitalis-like factor(s) from cord blood of neonate by immunoaffinity chromatography. *Biochem Int.* 1991;25:835-859.
24. Kuske R, Moreth K, Renner D, Wizemann V, Schoner W. Sodium pump inhibitor in the serum of patients with essential hypertension and its partial purification from hemofiltrate. *Klin Wochenschr.* 1987;65(Suppl VIII):53.
25. Licht A, Stein S, McGregor CW, Bourgoinie JJ, Bricker N. Progress in isolation and purification of an inhibitor of sodium transport obtained from dog urine. *Kidney Int.* 1982;21:339-344.
26. Clarkson EM, De Wardener HE. Observation on a low molecular weight natriuretic and Na^+, K^+-ATPase inhibitory material in urine. *Clin Exp Hypert Part A.* 1985;A7:673-683.
27. Cloix JF, Crabos M, Grichois ML, Meyer P. An endogenous digitalis-like compound extracted from human urine: biochemical and chemical studies. *Can J Physiol Pharmacol.*. 1987;65:1522-1527.
28. Lichtstein D, Minc D, Bourrit A, Deutsch J, Karlish SJD, Belmaker H, Rimon R, Palo J. Evidence for the presence of a ouabain-like compound in human cerebrospinal fluid. *Brain Res.* 1985;325:13-19.
29. Halperin JA. digitalis-like properties of an inhibitor of the Na^+/K^+ pump in human cerebrospinal fluid. *J Neurol Sci.* 1989;90:217-230.
30. Buckalew VM Jr, Paschal-McCormick C. Endogenous digitalis-like factors: Current status. *Am J Nephrol.* 1989;9:329-342.
31. Goto A, Yamada K, Sugimoto T. Endogenous digitalis: Reality or myth? *Life Sci.* 1991;48:2109-2118.
32. Haber E, Haupert GT. The search for hypothalamic Na^+, K^+-ATPase inhibitor. *Hypertension.* 1987;9:315-324.
33. Bidard JN, Rossi B, Renaud JF, Lazdunski M. A search for an 'ouabain-like' substance from the electric organ of *Electrophorus electricus* which led to arachidonic acid and related fatty acids. *Biochem Biophy Acta.* 1984;769:245-252.
34. Kelly RA, O'Hara DS, Mitch WE, Smith TW. Identification of NaK-ATPase inhibitors in human plasma as nonesterified fatty acids and lysophospholipids. *J Biol Chem.* 1986;261: 11704-11711.
35. Tal DM, Yanuck MD, van Hall G, Karlish SJD. Identification of Na^+/K^+-ATPase inhibitors in bovine plasma as fatty acids and hydrocarbons. *Biochim Biophys Acta.* 1989;985:55-59.
36. Lichtstein D, Samuelov S, Gati I, Felix AM, Gabriel TF, Deutsch J. Identification of 11,13-dihidroxy-14-octadecaenoic acid as a circulating Na^+, K^+-ATPase inhibitor. *J Endocrinol.* 1991;128:71-78.
37. Rauch AL, Buckalew VM Jr. Plasma volume expansion increase Lysophosphatidylcholine and digitalis-like activity in rat plasma. *Life Sci.* 1988;42:1189-1197.
38. Tamura M, Harris TM, Higashimori K, Sweetman BJ, Blair IA, Inagami T. Lysophosphatidylcholines containing polyunsaturated fatty acids were found as Na^+, K^+-ATPase inhibitors in acutely volume-expanded hog. *Biochemistry.* 1987;26:2797-2806.
39. Schwartzman ML, Balazy M, Masferrer J, Abraham NG, McGiff JH, Murphy RC. 12(R)-Hydroxyicosatetraenoic acid: A cytochrome P450-dependent arachidonate metabolite that inhibits Na^+, K^+-ATPase in the cornea. *Proc Natl Acad Sci USA.* 1987;84:8125-8129.
40. Clarkson EM, De Wardener HE. Observation on a low molecular weight natriuretic and Na^+, K^+-ATPase inhibitory material in urine. *Clin Exp Hypert Part A.* 1985;A7:673-683.
41. Vasdev S, Longerich L, Johnson E, Brent D, Gault MH. Dehydroepiandrosterone sulphate as a digitalis-like factor in plasma of healthy human adults. *Res Commun Chem Pathol Pharmacol.* 1985;49:387-399.
42. Fagoo M, Braquet P, Robin JP, Esanu A, Godfraind T. Evidence that mammalian lignans show endogenous digitalis-like activities. *Biochem Biophys Res Commun.* 1986;134: 1064-1070.
43. Ng YC, Akera T, Han CS, Braselton WE, Kennedy RH, Temma K, Brody TM, Sato PH. Ascorbic acid: an endogenous inhibitor of isolated Na^+, K^+-ATPase. *Biochem Pharmacol.* 1985;34:2525-2530.
44. Hamlyn JM, Blaustein MP, Bova S, DuCharme DW, Harris DW, Mandel F, Mathews WR Ludens JH. Identification and characterization of ouabain-like compound from human plasma. *Proc Natl Acad Sci USA.* 1991;88:6259-6263.

45. Goto A, Ishiguro T, Yamada K, Ishii M, Yoshioka M, Eguchi C, Shimura M, Sugimoto T. Isolation of a urinary digitalis-like factor indistinguishable from digoxin. *Biochem Biophys Res Commun.* 1990;173:1093-1101.
46. Lichtstein D, Gati I, Samuelov S, Berson D, Rozenman Y, Landau L, Deutsch J. Identification of digitalis-like compounds in human cataractous lenses. *Eur J Biochem.* 1993;216:261-268.
47. Bigger JT, Hoffman BF. Antiarrhythmic drugs. In: Goodman Gilman A, Rall WT, Nies AS, Taylor P, eds. *The Pharmacological Basis of Therapeutics.* New York: Pergamon Press, 1990; 840-873.
48. Bigger JT. Electrical properties of cardiac muscle and possible causes of cardiac arrhythmias. In: Dreifus LS, Likoff W, eds. *Cardiovascular Arrhythmias.* New York: Grune and Stratton, 1973; 13-34.
49. Bigger JT, Reiffel JA. Sick sinus syndrome. *Ann Rev Med.* 1979;30:91-118.
50. Cranefield PF, Aronson RS. *The Role of Triggered Activity and Other Mechanisms.* New York: Futura Press, 1988.
51. Moss AJ. Prediction and prevention of sudden cardiac death. *Ann Rev Med.* 1980;31:1-12.

CHAPTER 4

EXCITATION–CONTRACTION COUPLING IN VENTRICULAR MYOCYTES: EFFECTS OF ANGIOTENSIN II

William H. Barry,[1] Hiroshi Matsui,[1] John H.B. Bridge,[1,2] and Kenneth W. Spitzer[2]

ABSTRACT

The effects of the vasoactive peptide angiotensin II (AII) on contractility and excitation–contraction coupling in isolated adult rabbit ventricular myocytes were investigated. In most ventricular myocytes, AII (10^{-8} M) induced a significant increase in fractional shortening which was not associated with an increase in the calcium transient measured with indo–1. AII did increase the intracellular pH by approximately 0.2 5 pH units coincident with the positive inotropic effect. Effects of AII on pH and contractility were blocked by inhibitors of Na^+/H^+ exchange. AII also increased the rate of pH_i recovery from intracellular acidosis at pH_i values above 6.9. AII was shown not to affect the L–type inward calcium current. However, in an occasional cell, AII was observed to cause a slight increase in the calcium transient. We hypothesize that this response may reflect an increase of calcium influx on the sodium calcium exchanger, as a consequence of an increase in subsarcolemmal sodium concentration resulting from enhanced Na^+– H^+ exchange.

INTRODUCTION

The clinical benefit of angiotensin converting enzymes (ACE) inhibitors in patients after myocardial infarction is well established [1]. This has been generally assumed to be due to reduction in left ventricular afterload. However, recent studies have shown that left ventricular diastolic dysfunction during ischemia of isolated rabbit hearts can be reduced by ACE inhibition [2] and that angiotensin II (AII) directly exacerbates ischemic dysfunction in isolated hearts [3]. These studies indicate that the local cardiac renin–angiotensin system [4] may produce significant amounts of AII, and that this AII could have direct myocardial effects of pathophysiologic significance. We therefore sought to examine the direct effects of AII on excitation contraction–coupling in isolated ventricular myocytes.

---

[1]The Division of Cardiology and [2]The Nora Eccles Harrison Cardiovascular Research Training Institute, University of Utah Medical School, Salt Lake City, UT 84132, USA.

Molecular and Subcellular Cardiology: Effects of Structure and Function
Edited by S. Sideman and R. Beyar, Plenum Press, New York, 1995

METHODS

Isolated adult rabbit or guinea pig ventricular myocytes were prepared by retrograde aortic perfusion with collagenase as described previously [5, 6]. Isolated myocytes were stimulated to contract by means of an extracellular electrode, and shortening quantitated with a video motion detector system as previously described [6].

Intracellular calcium and intracellular pH were measured with the fluorescent probes indo-1, and SNARF-1. Isolated myocytes were loaded by exposing them to the AM forms of the dyes, as previously described [7, 8]. In some experiments, a transient intracellular acidosis was produced by exposure to subsequent washout of 10 mM NH_4Cl [5]. These experiments were done in HEPES-buffered HCO_3 - CO_2 free solutions to inhibit the Na^+ - independent Cl^- - HCO_3^- exchange [9] and Na^+ - HCO_3^- co-transport [10].

The effects of exposure to AII on calcium currents were measured with conventional whole cell patch clamp techniques. The ability of reverse Na^+ - Ca^{2+} exchange to trigger release of calcium from the sarcoplasmic reticulum was investigated in ventricular myocytes dialyzed with various concentrations of Na^+ in the presence and absence of the Na^+-Ca^{2+} exchanger inhibitor peptide XIP [11]. To investigate the contribution of I_{Ca} to excitation-contraction coupling, we used a rapid perfusion system that allowed us to rapidly expose cells to the calcium channel blocker nifedipine between voltage clamp pulses. Thus it was possible to establish the significance of a block of I_{Ca} before depletion of sarcoplasmic reticulum calcium had occurred [11].

Contractility studies were performed at 37°C, and voltage clamp studies at room temperature (23°C). The pH of cell bathing solutions was 7.4.

RESULTS

We first examined the effects of AII on shortening and calcium transients. As shown in Fig. 1, exposure of isolated rabbit ventricular myocytes to high extracellular calcium concentration of 3.6 mM or to 10^{-8} M AII caused a similar increase in shortening of isolated ventricular myocytes. However, AII in this experiment did not increase the calcium transient to a degree comparable to that observed after exposure to high calcium. Average results for 10 cells are shown in Table 1.

Table 1. Measurements of Cell Shortening and $[Ca^{2+}]_i$ in Isolated Rabbit Myocytes.

		0.9 mM Ca^{2+}	3.6 mM Ca^{2+}	Angiotensin II
Systolic Cell Position	(% of baseline)	100	269 ± 30*	362 ± 51*
Diastolic Cell Position	(% of baseline)	0	83 ± 24*	182 ± 38*
Systolic F400:500 Ratio	(% of baseline)	100	156 ± 5*	93 ± 14
Diastolic F400:500 Ratio	(% of baseline)	0	28 ± 7*	0.8 ± 14

Systolic and diastolic cell position: the baseline diastolic cell position was assigned a value of zero and the peak systolic cell position was assigned a value of 100. The baseline diastolic $[Ca^{2+}]_i$ -sensitive F400:500 nm ratio signal was assigned a value of zero and the peak systolic F400:500 nm ratio signal was assigned a value of 100. Calibration experiments performed under baseline conditions showed a diastolic $[Ca^{2+}]_i$ level of 174 ± 30 nM and a peak systolic $[Ca^{2+}]_i$ level of 817 ± 134 nM. * = $p < 0.05$ versus baseline. (From [12], with permission of the authors and the Physiological Society, UK.)

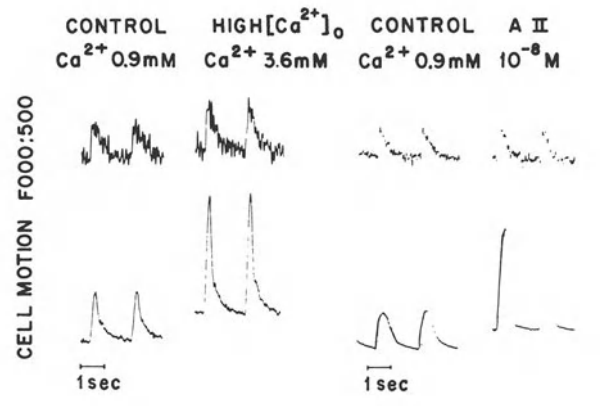

Figure 1. Examples of steady state effects on $[Ca^{2+}]_i$ (indo 400/500 nm fluorescence ratio), **upper traces**, and motion, **lower traces**, of altering superfusate Ca^{2+} and exposure to AII in isolated paced rabbit myocytes. In these experiments, $[Ca^{2+}]_i$ transients were recorded only briefly during control conditions, and then again after 3 min exposure to AII or 3.6 mM Ca, to decrease dye bleaching. Control end-diastolic $[Ca^{2+}]_i$ and cell position were assigned a value of 0, and peak systolic $[Ca^{2+}]_i$ and cell position were assigned a value of 100. Changes in $[Ca^{2+}]_i$ and motion after exposure to AII or high Ca^{2+} were measured on this scale. A different cell was used for determination of effects of AII and Ca^{2+} in each experiment (from [12], with permission of the authors and the Physiological Society, UK).

Figure 2 demonstrates simultaneous measurement of intracellular pH and contraction during exposure to AII, illustrating that a positive inotropic effect observed after exposure to AII is associated with an increase in the intracellular pH. This increase in pH was

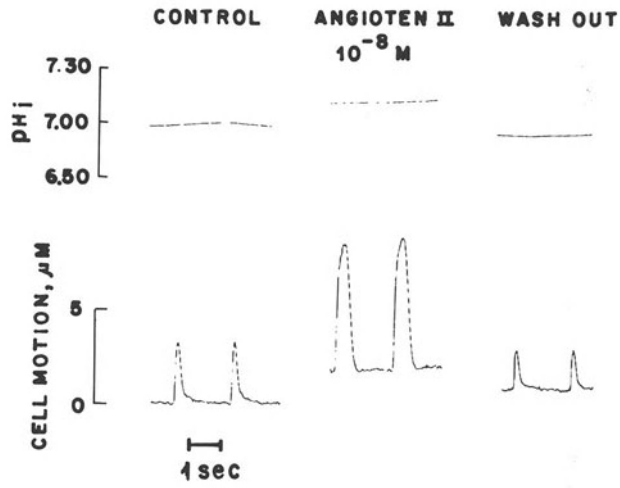

Figure 2. Example of effects of exposure to 10^{-8} M AII in an isolated paced rabbit myocyte loaded with the pH-sensitive fluorescence SNARF 1. Superfusion of the myocyte with AII resulted in a change in the calibrated fluorescence signal indicative of an increase in pH_i (**upper traces**) within 3 min. Intracellular alkalinization caused by AII was coincident with an increase in contractility evident as a simultaneous increase in amplitude of cell shortening (**lower traces**). The pH signal was filtered at 0.1 Hz (from [12], with permission of the authors and the Physiological Society, UK).

inhibited with EIPA or amiloride. Voltage clamp experiments revealed that the calcium current was unaffected by 10^{-8} M AII, but was increased by 30% within 2 min after exposure to 3.6 mM $CaCl_2$.

These results demonstrate that a positive inotropic effect can be induced by AII in isolated rabbit ventricular myocytes in the absence of an increase of cytosolic calcium, and without an effect on these inward calcium current. These observations are consistent with findings in intact perfused rabbit hearts, in which a positive inotropic effect of AII was observed without alteration of the indo-1 fluorescence ratio [12] and suggest that the positive inotropic effect of AII is due in large part to an intracellular alkalosis with a resulting sensitization of the contractile elements to calcium [5].

In order to investigate more directly whether stimulation of $Na^+ - H^+$ exchange was involved in this effect of AII in the isolated ventricular rabbit myocytes, we investigated the influence of AII on the rate of recovery from an intracellular acidosis caused by washout of NH_4Cl. The results are shown in Fig. 3.

Figure 3A illustrates the effects of AII on recovery of intracellular pH after exposure to, and washout of, ammonium chloride. There was an enhanced rate of recovery of intracellular pH in the presence of 100 nM AII. Figure 3B shows average results from five cells: There is a statistically significant stimulation of the rate of recovery of intracellular pH in cells exposed to AII between pH 6.9 and 7.0. These results indicate that AII enhances $Na^+ - H^+$ exchange in these myocytes, and that this is the cause of the intracellular alkalosis.

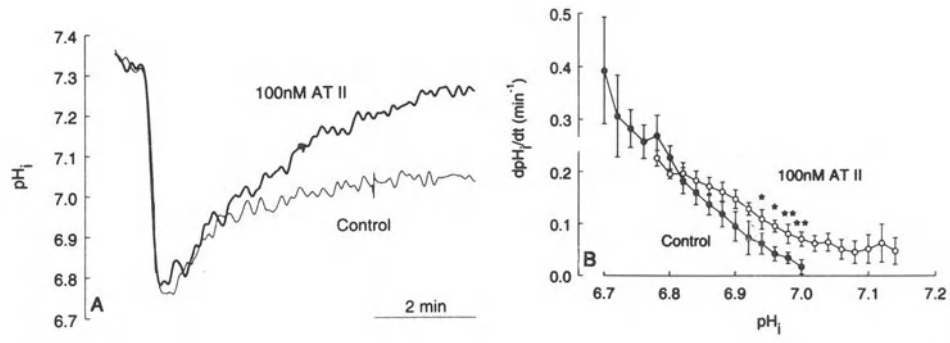

Figure 3. A: Effect of AII on pH_i recovery from intracellular acidosis elicited by rapid removal of 10.0 mM NH_4Cl (pH_o 7.4). AII (100 nM) increased the rate of pH_i recovery from acidosis. **B:** Average effect of AII (100 nM) on pH_i recovery from intracellular acidosis. Results from five cells are shown. Plotted is the relationship between the rate of pH_i recovery (dpH_i/dt) and the pH_i at which it occurred. * $p < 0.05$; ** $P < 0.01$ (from Matsui *et al.*, *Cardiovasc Res.* 1995;in press, with permission of the BMJ Publishing Group and authors).

The above findings are consistent with the hypotheses that AII induces a positive inotropic effect in adult rabbit ventricular myocytes primarily by increasing sodium hydrogen exchange, and causing an intracellular alkalosis. Consistent with this conclusion in the result shown in Fig. 4, in which simultaneous exposure to amiloride and AII inhibited the positive inotropic effect of AII.

As mentioned, the most typically observed effect of AII on the calcium transient was to cause no change. However, in some cells, an increase in the calcium transient could

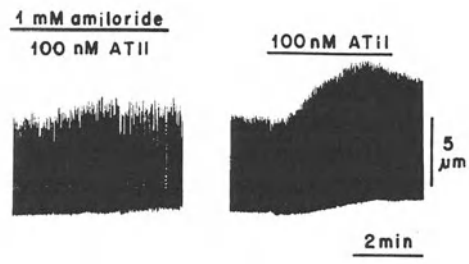

Figure 4. Effect of amiloride on AII–induced increase in cell shortening. **Left:** The response of cell shortening to AII (100 nM) following a 7 min preincubation period in 1.0 mM amiloride. **Right:** The cell was then bathed in amiloride–free solution for 9 min before reapplying AII. Amiloride suppressed the increase in cell shortening elicited by AII. Pacing cycle length = 2 sec (from Matsui *et al.*, *Cardiovasc Res.* 1995;in press, with permission of the BMJ Publishing Group and authors).

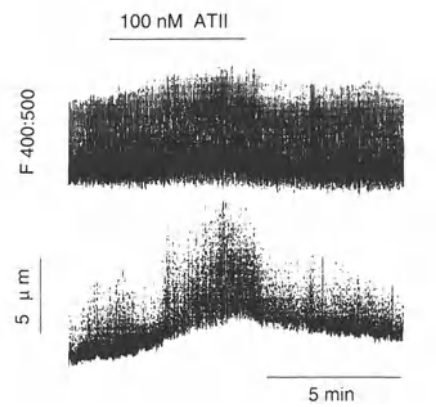

Figure 5. Effect onf Ca^{2+} transient. The indo–1 fluorescence ratio (400/500 nm) **(top)**, increased in amplitude slightly during the increased amplitude of shortening **(bottom)** induced by exposure to 100 nM AII.

be observed. An example is shown in Fig. 5 in which a small but distinct increase in the calcium transient was produced during exposure to AII.

Thus, although the majority of the positive inotropic effect of this vasoactive peptide appears to be due to stimulation of $Na^+ - H^+$ exchange, and sensitization of the contractile elements due to an intracellular alkalosis, an additional component of the inotropic effect may be due to a very small and inconsistent increase in the cytosolic calcium transient as well.

It is difficult to be certain what factors could account for this occasional apparent increase in the $[Ca^{2+}]_i$ transient after exposure to AII. Possibilities include an effect on I_{Ca} (not supported by our voltage clamp data), an effect of intracellular alkalosis on indo–1 fluorescence (not supported by the inconsistency of the observation), or an effect of enhanced Na^+ influx. Recent work from our laboratory [10, 13, 14] has demonstrated that Ca^{2+} influx on the Na^+/Ca^{2+} exchanger can trigger SR Ca^{2+} release and induce contraction. An example of this effect and its sensitivity to intracellular $[Na^+]$ in isolated guinea pig ventricular myocytes are shown in Fig. 6.

Although we have at present no direct experimental evidence to support this hypothesis, it is possible that an increase in subsarcolemmal Na^+ resulting from enhanced

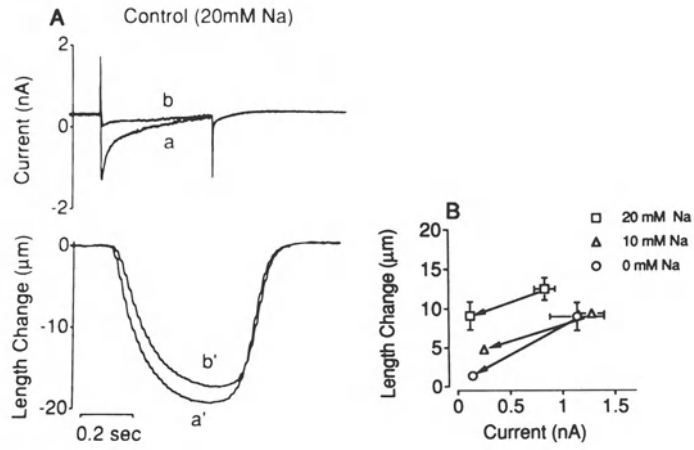

Figure 6. A: Curves showing currents and shortening measured when the cell was dialyzed with 20 mmol/L sodium. a, L-type calcium currents. a indicates current measured during depolarization from –40 to +10 mV; b, current measured after the cell was abruptly superfused with 20 m mol/L nifedipine. a', cell shortening measured at the same time as current a; b', shortening measured at the same time as current b. Shortening in the presence of nifedipine (b') could be almost completely inhibited by dialyzing the cell with the Na^+–Ca^{2+} exchanger inhibitor, XIP (not shown). **B:** Loss of shortening vs loss of calcium current when cells were treated with 20 mmol/L nifedipine. Results were obtained from cells dialyzed with 0, 10, or 20 mmol/L sodium. The dependence on $[Na^+]_i$ of the ability of Ca^{2+} influx via Na^+–Ca^{2+} exchange to trigger contraction is apparent (from [11], with permission of the authors and the American Heart Association).

$Na^+ - H^+$ exchange, as well as an intracellular alkalosis, could increase the influx of Ca^{2+} on the $Na^+ - Ca^{2+}$ exchanger and thus increase the Ca^{2+} transient.

DISCUSSION

The effects of AII on excitation–contraction coupling in isolated ventricular myocytes appear to be predominantly mediated by an intracellular alkalosis produced by stimulation of $Na^+ - H^+$ exchange. AII binding to cardiac receptors can result in stimulation of phospholipid hydrolysis [15, 16] and the resulting activation of protein kinase C (PKC) may contribute to the stimulation of sodium hydrogen exchange. Consistent with this hypothesis is our previous report [12] that stimulation of PKC by exposure to phorbol ester increases pH_i and contractility in paced adult rabbit ventricular myocytes. Another vasoactive peptide, endothelin, also appears to increase pH_i and stimulate contractility as the result of stimulation of $Na^+ - H^+$ exchange as well [17].

The present findings, and previously reported studies in intact ventricular myocardium [12], indicate that AII can induce a prominent positive inotropic effect in myocytes in the absence of any change in the calcium transient, as quantitated by indo-1 fluorescence. However, it is intriguing that in an occasionally cell, an increase in calcium can be observed during exposure to AII (see Fig. 5). This inconsistent effect of vasoactive peptide on cytosolic calcium transients has also been reported in studies of the effects of endothelin on adult rat ventricular myocytes [17]. The factors which could contribute to this occasional increase in the calcium transient are not clear at the present time. However, it has been argued that there is a subsarcolemmal sodium diffusion barrier, in which sodium concentration can be markedly increased transiently by sodium influx [18–20]. In addition,

recent work [11, 13, 14, 21] has suggested that calcium influx via $Na^+ - Ca^{2+}$ exchange can also serve as a trigger to release calcium from a sarcoplasmic reticulum. This process would be expected to be markedly enhanced when intracellular sodium concentration is elevated. Thus, it is possible that enhanced $Na^+ - H^+$ exchange, with a resulting increase in sodium influx, in some cells is able to cause a rise in subsarcolemmal sodium concentration sufficient to enhanced trigger release of calcium from the SR, even when the calcium current is not measurably enhanced. Further experiments are needed to address this issue.

Inhibitors of $Na^+ - H^+$ exchange have been demonstrated to improve myocardial function after ischemia/reperfusion in the intact heart [22–24]. Experimental evidence suggests that this is due to reduced Na^+ loading and that thus reduced Ca^{2+} loading via $Na^+ - Ca^{2+}$exchange [22]. Other studies have suggested that alkalosis may enhance myocyte injury during ATP depletion [25]. Our results suggest that in the presence of mild acidosis, early in or during recovery from ischemia, AII stimulates $Na^+ - H^+$ exchange. Thus, the beneficial effect noted previously of ACE inhibitors to preserve myocardial function preserving following ischemia – reperfusion may result in part from the ability to prevent an AII induced elevation of intracellular Na^+ (and thus Ca^{2+}) or from altered pH_i. Our results suggest that the direct myocardial effects of AII may also be of importance in physiology and pathophysiology.

DISCUSSION

Dr. J. Janicki: What role do the Angiontensin II receptors play in your observations?

Dr. W.H. Barry: We think the AT–I receptor is involved. We have obtained some Losartan from Merck and are planning to do experiments on the effect of AT–I receptor blockade, but I do not have any data yet.

Dr. J. Janicki: We have done some experiments with Angiotensin II infusion into rats and we have been able to completely prevent myocyte necrosis that one would normally see with elevated levels of angiotensin when using losartan.

Dr. W.H. Barry: In the intact heart results are complicated by the possible effects of Angiotensin II on the vascular system of course, mainly vasoconstriction. It is interesting that in these isolated myocyte models of ischemic injury, where delivery and washout of substrate are obviously not an issue, we still see a potentially deleterious effect of Angiotensin II exposure.

Dr. B. O'Rourke: Did you see a different positive inotropic effect with Angiontensin II in different buffer solutions?

Dr. W.H. Barry: The contractility experiments with Angiontensin II were primarily done in bicarbonate buffer media. The voltage clamp experiments were done primarily in Hepes buffer medium. We have found a positive inotropic effect in both Hepes and bicarbonate buffer medium, but we have not really compared the magnitude of the effects sufficiently to allow any comment about it.

Dr. Gania Kessler-Icekson: What is the dose dependency of this effect? 100 nM is a relatively high concentration of Angiontensin II.

Dr. W.H. Barry: A concentration of 100 nM is on the plateau of the dose response curve. Around 10 nM is the threshold of the inotropic effect.

Dr. M. Morad: Did you always see the increase in baseline tension with an increase in inotropic state or did you see sometimes inotropy without an increase in baseline tension?

Dr. W.H. Barry: We almost always saw an increase in the baseline tension (a decrease in resting length) during the positive inotropic effect of Angiotensin II.

Dr. M. Morad: Is that also based on pH change?

Dr. W.H. Barry: Yes, but it can also be seen following elevations in extracellular calcium. For example, if you stop pacing, cells continue to relax and lengthen for a while until they reach a new resting length. If you then expose them to BDM, which inhibits calcium-induced force, you see further relaxation. Thus, these isolated myocytes do have a measurable resting tone.

Dr. M. Morad: Is it related to the inotropic state, or is it an additional effect?

Dr. W.H. Barry: Based on our results, I believe that an intervention that either elevates diastolic calcium slightly, or increases sensitivity of the contractile elements to calcium, such as intracellular alkalosis, will cause a decrease in resting length of these cells.

Dr. M. Morad: A number of us have done experiments on SR Ca^{2+} release induced by Ca^{2+} influx via Na^{+}/Ca^{2+} exchange in rat and guinea pig, and we do not get any effect of intracellular sodium. I believe there is still a problem as to whether you have completely blocked the calcium channel and whether you have overloaded the intracellular SR stores. Once the stores are highly loaded, anything will trigger them to release.

REFERENCES

1. Pfeffer MA, Braunwald E, Moye LA, Basta L, Brown EJ, Cuddy TE, Davis BR, Geltman EM, Goldman S, Flaker GC, Klein M, Lamas GA, Packer M, Rouleau J, Rouleau JL, Rutherford J, Wertheimer JH, Hawkins CM. Effect of captopril on mortality and morbidity in patients with left ventricular dysfunction after myocardial infarction. *New Engl J Med.* 1992;327:669–691.
2. Eberlie FR, Apstein CS, Mgoy S, Lorell BH. Exacerbation of left ventricular ischemic diastolic dysfunction by pressure-overload hypertrophy. Modification by specific inhibition of cardiac angiotensin converting enzyme. *Circ Res.* 1992;70:931–943.
3. Mochizuki T, Eberli RF, Apstein CS, Lorell BH. Exacerbation of ischemic dysfunction by angiotensin II in red cell–perfused rabbit hearts. *J Clin Invest.* 1992;89:490–498.
4. Baker KM, Booz GW, Dostal DE. Cardiac actions of angiotensin II: role of an intracardiac renin–angiotensin system. *Ann Rev Physiol.* 1992;5:227–241.
5. Kohmoto O, Spitzer KW, Movsesian MA, Barry WH. Effects of intracellular acidosis on $[Ca^{2+}]_i$ transients, transsarcolemmal Ca^{2+} fluxes, and contraction in ventricular myocytes. *Circ Res.* 1990;66:622–632.
6. Ikenouchi H, Kohmoto O, McMilliam M, Barry WH. Contributions of $[Ca^{2+}]_i$, $[Pi]_i$, and pH_i to altered diastolic myocytes tone during partial metabolic inhibition. *J Clin Invest* .1991; 88:55–61.
7. Kohmoto O, Ikenouchi H, Hirata Y, Momomura S, Serizawa T, Barry WH. Variable effects of endothelin-1 on $[Ca^{2+}]_i$ transients, pH_i and contraction in ventricular myocytes. *Am J Physiol.* 1993;265:H793–H800.
8. Peeters GA, Hlady V, Bridge JHB, Barry WH. Simultaneous measurement of calcium transients and motion in cultured heart cells. *Am J Physiol.* 1987;253:H1400–H1408.
9. Xu P, Spitzer KW. Na-independent Cl^{-} – HCO_3– exchange mediates recovery of pH_i from alkalosis in guinea pig ventricular myocytes. *Am J Physiol.* 1994;267:H85–H91.
10. Lagadic-Gossmann D, Buckler KJ, Vaughan-Jones RD. Role of bicarbonate in pH recovery from intracellular acidosis in the guinea pig ventricular myocyte. *J Physiol.* 1992;458:361–384.
11. Kohmoto O, Levi AJ, Bridge JHB. Relation between reverse sodium–calcium exchange and sarcoplasmic reticulum calcium release in guinea pig ventricular cells. *Circ Res.* 1994;74:550–554.
12. Ikenouchi H, Barry WH, Bridge JHB, Weinberg EO, Apstein CS, Lorell BH. Effects of angiotensin

II on intracellular Ca^{2+} and pH in isolated beating rabbit hearts and myocytes loaded with the indicator indo 1. *J Physiol (Lond).* 1994;480:203–215.

13. Levi AJ, Spitzer KW, Kohmoto O, Bridge JHB. Depolarization–induced Ca entry via Na–Ca exchange triggers SR release in guinea pig cardiac myocytes. *Am J Physiol.* 1994;266:H1422–H1433.
14. Lipp P, Niggli E. Sodium current–induced calcium signals in isolated guinea–pig ventricular myocytes. *J Physiol (Lond).* 1994;474:439–446.
15. Baker KM, Singer HA. Identification and characterization of guinea pig angiotensin II ventricular and atrial receptors: coupling to inositol phosphate production. *Circ Res.* 1988;62:896–904.
16. Ishihata A, Endoh M. Pharmacological characteristics of the positive inotropic effect of angiotensin II in the rabbit myocardium. *Br J Pharmacol.* 1993;108:999–1005.
17. Kelly RA, Eid H, Kramer BK, O'Neill M, Liang BT, Reers M, Smith TW. Endothelin enhances the contractile responsiveness of adult rat ventricular myocytes to calcium by a pertusis–toxin–sersitiua pathway. *J Clin Invest.* 1990;86:1164–1171.
18. Leblanc N, Hume JR. Sodium current–induced release of calcium from cardiac sarcoplasmic reticulum. *Science.* 1990;248:372–376.
19. Lederer WJ, Niggli E, Hadley RW. Sodium–calcium exchange in excitable cells: fuzzy space. *Science.* 1990;248:283.
20. Carmeliet E. A fuzzy subsarcolemmal space for intracellular Na^+ in cardiac cells? *Cardiovasc Res.* 1992;26:433–442.
21. Nuss BH, Houser SR. Sodium–calcium exchange mediated contractions in feline ventricular myocytes. *Am J Physiol.* 1992;263:H1165–H1169.
22. Murphy E, Perlman M, London RE, Steenbergen C. Amiloride delays the ischemia–induced rise in cytosolic free calcium. *Circ Res.* 1991;68:1250–1258.
23. Scholz W, Albus U, Linz W, Martorana P, Lang HJ, Scholkens BA. Effects of Na^+/H^+ exchange inhibitors in cardiac ischemia. *J Mol Cell Cardiol.* 1992;24:733–741.
24. Moffat MP, Karmazyn M. Protective effects of the potent Na/H exchange inhibitor methylisobutyl amiloride against post–ischemic contractile dysfunction in rat and guinea–pig hearts. *J Mol Cell. Cardiol.* 1993;25:959–971.
25. Bond JM, Chacon E, Herman B, Lemasters JJ. Intracellular pH and Ca^{2+} homeostasis in the pH paradox of reperfusion injury to neonatal rat cardiac myocytes. *Am J Physiol.* 1993;34:C129–C137.
26. Matsui H, Barry WH, Livsey C, Spitzer KW. Angiotensin II stimulates Na^+/Ca^{++} exchange in adult rabbit ventricular myocytes. *Cardiovasc Res.* 1995; in press.

CHAPTER 5

PROSPECTS FOR GENETIC MANIPULATION OF CARDIAC EXCITABILITY

John H. Lawrence, David C. Johns, Nipavan Chiamvimonvat, H. Bradley Nuss, and Eduardo Marban[1]

ABSTRACT

Despite impressive advances in the therapy of a number of types of heart disease in the last two decades, sudden cardiac death remains a public health problem of staggering dimensions. Current treatment options include antiarrhythmic drugs that have higher than desired failure rates and implantable defibrillators that incur significant costs to the patient and society. The development of therapies that better suppress the cardiac arrhythmias responsible for sudden cardiac death requires a broad and comprehensive understanding of the basic mechanisms underlying electrical instability in the heart. This study explores the scientific basis for a molecular genetic approach to modify cardiac excitability and thereby to create animal models of sudden cardiac death. The availability of such models will open up new avenues of research in arrhythmogenesis and facilitate the development of novel antiarrhythmic agents.

INTRODUCTION

About half a million people per year die suddenly of cardiac arrhythmias in the U.S.A. [1]. Despite impressive advances in the therapy of a number of types of heart disease in the last two decades, sudden cardiac death remains a public health problem of staggering dimensions. The pathophysiology underlying sudden cardiac death is most often a rapid ventricular arrhythmia that compromises contractility and produces hypotension, global myocardial ischemia and death [2]. The initiation of this lethal arrhythmia is, in most cases, dependent on a susceptible myocardium that is rendered hyperexcitable by various conditions, including heart failure, hypertrophy, coronary artery disease and the long QT syndrome [3].

---

[1]Division of Cardiology, Department of Medicine, The Johns Hopkins University, Baltimore, MD 21205, U.S.A.

Molecular and Subcellular Cardiology: Effects of Structure and Function
Edited by S. Sideman and R. Beyar, Plenum Press, New York, 1995

This study explores the prospects for targeting sudden cardiac death by introducing molecular genetic techniques to the study of its basic biological mechanisms. The primary goal is to modify the electrical substrate of the mammalian heart *in vitro* and *in vivo* by heterologous expression of ion channel genes that alter myocardial excitability. In particular, recombinant adenoviruses will be engineered that encode ion channels engineered so as to alter cardiac excitability. For example, overexpression of an inactivation-defective potassium channel would shorten the action potential and abbreviate excitation, while an inactivation-defective sodium channel would tend to prolong the action potential plateau.

This presentation is limited to discussion of the rationale, relevant background work, and prospects for viral gene transfer of ion channels.

APPROACHES TO GENE TRANSFER

The identification of genes involved in normal cardiac development [4] and a number of genetically determined cardiac disorders, including the identification of a series of missense mutations in cardiac β-myosin heavy chain in patients with familial hypertrophic cardiomyopathy [5], has prompted a search for techniques to introduce foreign genes into the heart. Recent advances in two areas of molecular biology render plausible the idea of genetically altering cardiac excitability to produce new animal models. The first set of breakthroughs has been in the area of carrier-mediated heterologous gene transfer. The surprising observation by Wolff and colleagues [6] that plasmid DNA could be introduced locally into striated muscle by direct intramuscular injection has stimulated new approaches to somatic gene therapy of cardiovascular disease. Recently, the efficient expression of adenovirally transduced genes has been demonstrated in postmitotic tissues, including cardiac myocytes [7–9], skeletal muscle [10, 11], the respiratory tract [12–14], and neurons [15].

Recombinant replication-deficient type 5 human adenovirus vectors have been employed by many laboratories to transfer reporter genes (usually β-galactosidase or luciferase) to a variety of cell types *in vitro*. These reporter genes have also been expressed *in vivo* by local injection or exposure of recombinant adenovirus to skeletal muscle [16], airway epithelium [17], brain [15] and vascular endothelium [18]. Intravenous [7] or intraperitoneal [19] injection of these vectors has also produced successful gene transfer to remote tissues, with tissue-specific expression presumably influenced by the selection of promoter sequences. Recombinant adenovirus-mediated expression of functional α1-antitrypsin [12] (a secretory protein), the LDL receptor [20] (a membrane protein), and the cystic fibrosis transmembrane conductance regulator [13] (CFTR; a channel protein) has also been demonstrated. These results portend successful transfer and expression of ion channel genes to myocardial cells following peripheral injection of recombinant adenovirus.

Other prototypes for gene therapy involve recombinant myoblasts [21, 22], transgenic animals [23–25], and targeted recombination ("gene knockout") in mouse embryonic stem cells [26]. To date, none of these approaches have been used to achieve heterologous expression (or targeting) of an ion channel gene in the heart.

The second area of critical recent advances has been in the cloning and expression of the genes that encode ion channels. These are the proteins that make cells excitable and that, by being present in a given combination, shape the particular excitability characteristic of a given cell type [27]. A large number of ion channel genes have now been isolated, and in many cases the cDNA has been successfully used to express specific channels in cells where they are not normally present. Studies in which defined regions of the DNA are mutated prior to expression have led to a fairly sophisticated understanding of how these

channels function; for example, we can now genetically engineer sodium channels that are inactivation-defective and therefore continue to open during maintained depolarization [28-30].

RESULTS AND DISCUSSION

Rationale for Targeting the Action Potential to Modify Cardiac Excitability

When excitable cells are stimulated, they give rise to a tissue-specific electrical response known as the action potential. This response is the characteristic change in transmembrane potential that occurs as the net effect of stimulation of the cell's distinctive complement of membrane currents [31]. The action potential of ventricular cells has a rapid upstroke followed by a characteristic "plateau", during which depolarization is maintained for several tens or hundreds of milliseconds prior to repolarization [27].

The plateau reflects the balance of two opposing processes: inward currents, which favor depolarization, and outward currents, which favor hyperpolarization of the surface membrane. Under normal ionic conditions, L-type calcium channels make up the dominant inward current during the plateau [32], while potassium channels generate the outward currents. Although the opening of sodium channels underlies the sharp action potential upstroke, the vast majority of sodium channels normally inactivate within 10-20 msec and thus do not contribute to the maintenance of the plateau. If non-inactivating sodium channels could be expressed in heart cells, the balance would be tilted towards maintained depolarization and lengthening of the plateau. This prediction is supported by the observation that toxins that interfere with sodium channel inactivation prolong the action potential [33]. Alternatively, if the native potassium current were supplemented by additional outward current, repolarization would be hastened and the action potential would shorten. Support for the potential role of such currents in arrhythmogenesis comes from recent genetic analyses of patients with the long QT syndrome, a clinical disorder characterized by prolonged action potentials, ventricular arrhythmias and sudden cardiac death. This phenotype is genetically heterogeneous, with localization of 3 candidate genes to different chromosomes (3,7, and 11) [34]. Each locus maps near known (but different) ion channel genes or modulators of ion channel function [34]. It appears that changes in the net balance of plateau phase ionic currents, rather than a change in one particular ionic current, are responsible for development of arrhythmias in these patients.

In order to modify the cardiac action potential by heterologous gene transfer, one might predict that it would be necessary to achieve intense widespread expression of a specific ion channel gene or a gene encoding a modulator of channel function. However, owing to the high membrane impedance during the plateau and the electrical coupling of adjacent cardiac cells, high levels of expression may not be necessary. Classical experiments by Weidmann have shown that small currents can markedly alter the plateau of the cardiac action potential [35]; i.e., the plateau exhibits a high input impedance. Contemporary experiments in guinea pig ventricular myocytes have revealed that the membrane conductance during the plateau is approximately 1 nS [36, 37]. A single 20 pS channel would produce a 2% change in conductance; 50 such channels could double the ionic current flowing across the membrane during the plateau. Since myocytes are coupled electrically, not all cells need be modified to effect depolarization of cardiac tissue. Thus, a low density of supplemental inward or outward current during the plateau would be capable of modulating the action potential duration.

Rationale for Using Recombinant Adenovirus

The most efficient gene transfer schemes now available involve viral carriers. In hematopoietic systems, retroviruses are effective vehicles. However, they are inefficient at delivering genes to heart as they depend on DNA replication for integration of genes into the host cell genome and would not be capable of integrating into the post-mitotic cardiomyocyte. A recent report has shown that intravenous administration of a recombinant adenovirus results in long-term gene transfer throughout mouse skeletal and cardiac muscles and demonstrates that the adenoviral vector is capable of transferring genes to nondividing cells, albeit with fairly low efficiency [7]. Adenoviruses are DNA viruses consisting of linear double-stranded DNA molecules of approximately 36 kB [38]. For several reasons, they have recently become popular vectors for heterologous gene expression: the viral particle is relatively stable, can transform a variety of post-mitotic cell types, and efficiently penetrates targeted cells (approaching 100% in many cell lines); the viral genome does not undergo spontaneous rearrangement at a high rate; and gene inserts are generally maintained through multiple rounds of viral replication [39]. The major advantages of recombinant adenovirus vectors for this work include their ability to multiply to high titers and their capacity for achieving high levels of expression of foreign genes. Deletion of the early gene regions E1A and E1B produces a replication-deficient virus that can infect cells, but does not readily replicate. Supplemental deletion of sequences in the E3 region further inhibits viral replication and late-gene expression. Since the most DNA that can be packaged in adenovirions is approximately 105% of the wild-type genome, these deletions free up space for gene inserts as large as 8.3 kB [40]. The main drawback to using recombinant adenovirus is related to the large size of its genomic DNA which prevents the use of simple restriction digests for subcloning the desired insert; rather, a homologous recombination step in permissive cells is required. A second concern is that longterm *in vivo* expression, especially in adult animals, appears to be limited by an immune response. However, preliminary reports from several laboratories reveal that this immune response is inhibited by cyclosporine and other groups are working to modify the adenoviral genome to reduce its immunogenicity.

Adenoviral-Mediated Expression in Cardiomyocytes Following Intravascular Injection

Although we and others have shown that intravascular delivery of recombinant adenovirus results in expression of its gene insert in the heart, it is not yet established how much of the expression is in myocytes versus endothelial cells. *In vivo* adenovirus-mediated gene transfer via the pulmonary artery in sheep produces β-galactosidase activity not only in the endothelium, but also in lung parenchyma [14]. Adenovirus injected directly into a rabbit coronary artery produced dense β-galactosidase activity throughout a cross section of myocardium suggesting that the virus exits at the capillary level and is capable of reaching every cardiocyte [41]. The ability to modify the electrical substrate of the heart, even if only in a small region, would represent a major step toward ultimate gene therapy for cardiac arrhythmias.

CONCLUSIONS

Sudden cardiac death is a common and devastating manifestation of heart disease. Survivors of cardiac arrest have a one-year recurrence rate as high as 30% if untreated [42]. Identification of patients who are at the greatest risk for these arrhythmias is possible

only for a subset of patients with structural heart disease. Current treatment options include antiarrhythmic drugs that have high failure rates and implantable defibrillators that incur significant costs to the patient and society [43, 44]. Because of its cataclysmic nature, sudden cardiac death is preferably prevented than treated. The development of therapies that better suppress the cardiac arrhythmias responsible for sudden cardiac death requires a broad and comprehensive understanding of the basic mechanisms underlying electrical instability in the heart. To this end, we are in the process of engineering novel animal models for sudden cardiac death. Molecular genetic approaches involving recombinant adenoviruses will be used to modify the electrical substrate in the heart such that it becomes arrhythmogenic. Important data regarding the efficiency of gene transfer and the best delivery routes for gene transfer to cardiomyocytes will be directly available through this research program. Although the gene transfer strategies described will initially be employed to create animal models of disease, they may ultimately be modifiable to allow specific human gene therapy for lethal cardiac arrhythmias.

DISCUSSION

Dr. H. ter Keurs: These are very interesting possibilities to explain arrhythmias in patients with heart failure. It occurs to me that you might consider another possibility as well, and that is related to increased calcium entry as a result of prolongation of the action potential. In that case I would surmise that it could generate overload of the sarcoplasmic reticulum and therefore induce triggered propagated contractions and therefore initiate triggered arrhythmias, or one beat of a triggered arrhythmia which may initiate reentry.

Dr. E. Marban: That is a good point. There are two general categories of triggered arrhythmias, one of which is related to early after depolarizations and prolongation of the action potential. The other one is classically associated with digitalis toxicity and delayed after depolarizations. But it is important to recognize, as you so correctly point out, that they are not mutually exclusive and that prolongation of the action potential, by virtue of loading up the calcium stores, will also predispose to the delayed after depolarizations and the calcium overload mediated arrhythmias. I do not have any evidence for or against a role for calcium overload in heart failure arrhythmias, but it is conceptually entirely possible that it would be playing a role here.

Dr. M. Morad: I am concerned about the significance of suppression of transient outward current in heart failure. The major prlongation of the action potential, as you described, is always around -30 mV. This was also described in the Euckelmann studies and repeated by others in various myopathies and hypertrophies [Beuckelmann et al., *Circulation*, 1992;85:1046; Thollon, *Canad J Physiol & Pharm.* 1989;67:1471]. The action potential always prolongs specifically in this zone which predisposes the heart to after-depolarizations, as you have elegantly shown. A rather recent paper [Studer *et al. Circ Res.* 1994;75:443] and another paper by us [Hatem *et al., Circ Res.* 1994;74:253] on this issue, suggest an overexpression of sodium-calcium exchanger in heart failure and myopathy. This would produce a large inward current in the area in which action potential prolongation is seen and causes these problems. I wonder whether that may not be the real culprit! The calcium ATPase measurement shows that the pump has been down regluated [Hasenfuss, *Circ Res.* 1994;75:434] and its job is being carried out by the exchanger now. My question is: How do you reconcile the idea that the action potential prolongation occurs at regions well below -10, -20 mV, where as you remember I_{to} is turned off?

Dr. E. Marban: The right experiment has not been done. First of all the action potential recordings have all been done under incredibly unphysiological conditions where calcium is highly buffered. We are now in the process of repeating these experiments under more realistic ionic conditions

where, first of all, we might be able to calculate what the reversal potential of sodium–calcium exchange might be and actually keep it in the equation. Another consideration is that some species, including the dog, have a calcium-activated component of I_{to} and that obviously would not be active during recordings in which there is 10 mm EGTA in the pipette. But the other aspect that more directly addresses your concern is that, even though the striking repolarization delay occurs late, there are very important differences in the initial plateau potential that would of course then determine the rest of the history of repolarization. What has not been done is the kind of experiment which would really get at that, which is to do an action potential clamp and then release it at about 0 mV, keeping everything else equal. I would agree with you. I think if I_{to} were the only difference and you did an action potential clamp, that is you forced a failing heart cell to mimic a normal heart cell during the initial trajectory of depolarization, and then released it, it would probably be completely normal, unless there is another abnormality, e.g., sodium–calcium exchange.

Dr. M. Morad: This is very critical because you, together with Dr. Wier, did elegant experiments with Cesium, which is probably the best model of Torsades du pointes. If Cesium blocks only the inward rectifier, it does not have much of an effect on the other currents.

Dr. E. Marban: That is a good point.

Dr. W.H. Barry: As you know, the rapid delayed rectifier $I_{k,r}$ seems to be very poorly expressed in humans, and this accounts for some of these long action potentials in dissociated myocytes. I wonder if you had an opportunity to examine $I_{k,r}$ in your dog myocytes and if there is any abnormality in those cells associated with heart failure and also if the Q–T interval is prolonged in those animals, which may reflect the prolonged action potential duration.

Dr. E. Marban: I will answer the second point first. The Q–T is prolonged by about 15%. The isolated action potentials are prolonged by about 40%. There is a difference there. Maybe it is due to the fact that the action potential recordings were done with buffered calcium, for example. Maybe it is due to the fact that the Q–T reflects a conducted action potential whereas in the cells, obviously, you are getting a membrane action potential so you take the loading term out of it. In humans, interestingly, with heart failure, there is not much of a difference in Q–T, but there is a big difference in Q–T dispersion and patients who have increased Q–T dispersion and heart failure are at a higher risk for sudden cardiac death than patients that do not. So it may be that, in patients, we do not see the Q–T increase because they are on so many drugs, or because it is not very manifest due to compensatory mechanisms *in vivo*. But the dispersion nevertheless predisposes them to arrhythmias. The role of the rapid component of the delayed rectifier, $I_{k,r}$, is undoubtedly important when it exists. But, again, the right experiments have not been done, either in the published human data or in our dog data yet. We have all dialyzed the cells with rather large pipettes to enable high fidelity membrane current recordings in the same cells that you study action potentials. The down side is that this $I_{k,r}$ component dialyzes out pretty quickly. I cannot be sure that human cells have very little $I_{k,r}$ as has been quoted, because as far as I can tell nobody has done it with a perforated patch in which you would get much less rundown. Likewise, we have not done any such recordings yet in the dog model. Important cautions here are in terms of the mechanism; we have not yet taken into account the possible roles of sodium–calcium exchange, nor of $I_{k,r}$, both of which would be very susceptible to the conditions of the experiments.

REFERENCES

1. Shen W–K, Hammill SC. Survivors of acute myocardial infarction: who is at risk for sudden cardiac death? *Mayo Clin Proc.* 1991;66:950–962.
2. Bardy GH, Olson WH. Clinical characteristics of spontaneous-onset sustained ventricular tachycardia and ventricular fibrillation in survivors of cardiac arrest, in Zipes DP, Jalife J (eds): *Cardiac Electrophysiology: From Cell to Bedside.* Philadelphia, W.B. Saunders Co., 1990, pp 778–790.

3. Myerburg RJ, Castellanos A. Cardiac arrest and sudden cardiac death, in Braunwald E (ed): *Heart Disease: A Textbook of Cardiovascular Medicine*. Philadelphia, WB Saunders Co, 1988, pp 742–777.
4. Chien KR. Molecular advances in cardiovascular biology. *Science*. 1993;260:916–917.
5. Geisterfer–Lowrance AA, Kass S, Tanigawa G, Vosberg HP, McKenna W, Seidman CE, Seidman JG. A molecular basis for familial hypertrophic cardiomyopathy: a beta cardiac myosin heavy chain gene missense mutation. *Cell*. 1990;62:999–1006.
6. Wolff JA, Malone RW, Williams P, Chong W, Acsadi G, Jani A, Felgner PL. Direct gene transfer into mouse muscle in vivo. *Science*. 1990;247:1465–1468.
7. Stratford–Perricaudet LD, Makeh I, Perricaudet LD, Briand P. Widespread long–term gene transfer to mouse skeletal muscles and heart. *J Clin Invest*. 1992;90:626–630.
8. Guzman RJ, Lemarchand P, Crystal RG, Epstein SE, Finkel T. Efficient gene transfer into myocardium by direct injection of adenovirus vectors. *Circ Res*. 1993;73:1202–1207.
9. Kass–Eisler A, Falck–Pedersen E, Alvira M, Rivera J, Buttrick PM, Wittenberg BA, Cipriani L, Leinwand LA. Quantitative determination of adenovirus–mediated gene delivery to rat cardiac myocytes in vitro and in vivo. *Proc Natl Acad Sci USA*. 1993;90:11498–11502.
10. Ragot T, Vincent N, Chafey P, Vigne E, Gilgenkrantz H, Couton D, Cartaud J, Briand P, Kaplan J–C, Perricaudet M, Kahn A. Efficient adenovirus–mediated transfer of a human minidystrophin gene to skeletal muscle of *mdx* mice. *Nature*. 1993;361:647–650.
11. Vincent N, Ragot T, Gilgenkrantz H, Couton D, Chafey P, Gregoire A, Briand P, Kaplan JC, Kahn A, Perricaudet M. Long–term correction of mouse dystrophic degeneration by adenovirus–mediated transfer of a minidystrophin gene. *Nat Genet*. 1993;5:130–134.
12. Rosenfeld MA, Siegfried W, Yoshimura K, Yoneyama K, Fukayama M, Stier LE, Pääkko PK, Gilardi P, Stratford–Perricaudet LD, Perricaudet M, Jallat S, Pavirani A, Lecocq J–P, Crystal RG. Adenovirus–mediated transfer of a recombinant α–1–antitrypsin gene to the lung epithelium in vivo. *Science*. 1991;252:431–434.
13. Zabner J, Couture LA, Gregory RJ, Graham SM, Smith AE, Welsh MJ. Adenovirus–mediated gene transfer transiently corrects the chloride transport defect in nasal epithelia of patients with cystic fibrosis. *Cell*. 1993;75:207–216.
14. Lemarchand P, Jones M, Danel C, Yamada I, Mastrangeli A, Crystal RG. In vivo adenovirus–mediated gene transfer to lungs via pulmonary artery. *J Applied Physiol*. 1994;76:2840–2845.
15. Le Gal La Salle G, Robert JJ, Berrard S, Ridoux V, Stratford–Perricaudet LD, Perricaudet M, Mallet J. An adenovirus vector for gene transfer into neurons and glia in the brain. *Science*. 1993;259:988–990.
16. Quantin B, Perricaudet LD, Tajbakhsh S, Mandel J–L. Adenovirus as an expression vector in muscle cells *in vivo*. *Proc Natl Acad Sci*. 1992;89:2581–2584.
17. Mastrangeli A, Danel C, Rosenfeld MA, Stratford–Perricaudet L, Perricaudet LD, Pavirani A, Lecocq J–P, Crystal RG. Diversity of airway epithelial cell targets for in vivo recombinant adenovirus–mediated gene transfer. *J Clin Invest*. 1993;91:225–234.
18. Lemarchand P, Jones M, Yamada I, Crystal RG. In vivo gene transfer and expression in normal uninjured blood vessels using replication–deficient recombinant adenovirus vectors. *Circ Res*. 1993;72:1132–1138.
19. Mittal SK, McDermott MR, Johnson DC, Prevec L, Graham FL. Monitoring foreign gene expression by a human adenovirus–based vector using the firefly luciferase gene as a reporter. *Virus Res*. 1993;28:67–90.
20. Herz J, Gerard RD. Adenovirus–mediated transfer of low density lipoprotein receptor gene acutely accelerates cholesterol clearance in normal mice. *Proc Natl Acad Sci*. 1993;90:2812–2816.
21. Dhawan J, Pan LC, Pavlath GK, Travis MA, Lanctot AM, Blau HM. Systemic delivery of human growth hormone by injection of genetically engineered myoblasts. *Science*. 1991;254:1509–1512.
22. Barr E, Leiden JM. Systemic delivery of recombinant proteins by genetically modified myoblasts. *Science*. 1991;254:1507–1509.
23. Overbeek PA, Lai SP, Van Quill KR, Westphal H. Tissue–specific expression in transgenic mice of a fused gene containing RSV terminal sequences. *Science*. 1986;231:1574–1577.
24. Jackson T, Allard MF, Sreenan CM, Doss LK, Bishop SP, Swain JL. The c–*myc* proto–oncogene regulates cardiac development in transgenic mice. *Mol Cell Biol*. 1990;10:3709–3716.
25. Field LJ. Transgenic mice in cardiovascular research. *Annu Rev Physiol*. 1993;55:97–114.
26. Charron J, Malynn BA, Fisher P, Stewart V, Jeanotte L, Goff SP, Robertson EJ, Alt FW. Embryonic lethality in mice homozygous for targeted disruption of the N–myc gene. *Genes Dev*. 1992;6:2248–2257.

27. Noble D. Ionic mechanisms in normal cardiac activity, in Zipes DP, Jalife J (eds): *Cardiac Electrophysiology*. Philadelphia, WB Saunders Co, 1990, pp 163–171.
28. Stühmer W, Conti F, Suzuki H, Wang X, Noda M, Yahagi N, Kubo H, Numa S. Structural parts involved in activation and inactivation of the sodium channel. *Nature*. 1989;339:597–603.
29. West JW, Patton DE, Scheuer T, Wang Y, Goldin AL, Catterall WA. A cluster of hydrophobic amino acid residues required for fast Na^+–channel inactivation. *Proc Natl Acad Sci*. 1992;89:10910–10914.
30. Lawrence JH, Nuss HB, Xu RH, Marban E, Tomaselli GF. Mechanism of antiarrhythmic drug binding: insights from lidocaine block of inactivation–deficient mutant sodium channels. *Clin Res*. 1993;41:143A(Abstract).
31. Hille B. *Ionic channels of excitable membranes*. Sunderland, Massachusetts, Sinauer Associates, Inc., 1992, .
32. Rose WC, Balke CW, Wier WG, Marban E. Macroscopic and unitary properties of physiological ion flux through L–type calcium channels in guinea–pig ventricular myocytes. *J Physiol*. 1992;456:267–284.
33. Strichartz G, Rando T, Wang GK. An integrated view of the molecular toxinology of sodium channel gating in excitable cells. *Ann Rev Neurosci*. 1987;10:237–267.
34. Jiang C, Atkinson D, Towbin JA, Splawski I, Lehmann MH, Li H, Timothy K, Taggart RT, Schwartz PJ, Vincent GM, Moss AJ, Keating MT. Two long QT syndrome loci map to chromosomes 3 and 7 with evidence for further heterogeneity. *Nature Genetics*. 1994;8:141–147.
35. Weidmann S. Effect of current flow on the membrane potential of cardiac muscle. *J Physiol*. 1951;115:227–236.
36. Nichols CG, Ripoll C, Lederer WJ. ATP–sensitive potassium channel modulation of the guinea pig ventricular action potential and contraction. *Circ Res*. 1991;68:280–287.
37. Backx PB, Marban E. Background potassium current active during the plateau of the action potential in guinea pig ventricular myocytes. *Circ Res*. 1993;72:890–900.
38. Graham FL, Prevec L. Manipulation of adenovirus vectors, in Murray EJ (ed): *Methods in Molecular Biology, Vol. 7: Gene Transfer and Expression Protocols*. Clifton, N.J., The Humana Press, Inc., 1991, pp 109–128.
39. Berkner KL. Expression of heterologous sequences in adenoviral vectors. *Curr Topics Micro Immunol*. 1992;158:39–66.
40. Bett AJ, Haddara W, Prevec L, Graham FL. An efficient and flexible system for construction of adenovirus vectors with insertions or deletions in early regions 1 and 3. *Proceedings of the National Academy of Sciences of the United States of America*. 1994;91:8802–8806.
41. Barr E, Tripathy SK, Kozarsky K, Wilson JM, Carroll JD, Leiden JM. Efficient catheter–mediated gene transfer into the heart using replication–defective adenovirus. *Circ*. 1993;88:I–475(Abstract).
42. Baum RS, Alvarez H, Cobb LA. Survival after resuscitation from out–of–hospital ventricular fibrillation. *Circ*. 1974;50:1231–1235.
43. Poole JE, Mathisen TL, Kudenchuk PJ, McAnulty JH, Swerdlow CD, Bardy GH. Long–term outcome in patients who survive out of hospital ventricular fibrillation and undergo electrophysiologic studies: evaluation by electrophysiologic subgroups. *J Am Coll Cardiol*. 1990;16:657–665.
44. Winkle RA, Hardwin R, Ruder MA, Gaudiani VA, Smith NA, Buch WS, Schmidt P, Shipman T. Long–term outcome with the automatic implantable cardioverter–defibrillator. *J Am Coll Cardiol*. 1989;13:1353–1361.

CHAPTER 6

INTEGRATIVE MODELS AND RESPONSES IN CARDIAC ISCHEMIA

Simon Horner and Max J. Lab[1]

ABSTRACT

This chapter considers the study of electrophysiological changes during ischemia and incorporates mechanoelectric feedback, i.e., mechanical changes affecting electrophysiology. It considers these interactions in the cell, through multicell systems, the intact heart and the intact organism.

INTRODUCTION

Myocardial ischemia is important in both a clinical and physiological sense. There are several excellent reviews on electrophysiological changes during ischemia [1, 2]. Sudden cardiac death is a major cause of mortality throughout the western world, in the United States of America it kills approximately 1000 people per day [3] and comprises almost 50% of all cardiovascular deaths [3]. These are usually caused by ischemic heart disease with thrombus being present in the coronary arteries of 95% of those dying suddenly [4]. Most of those dying of a myocardial infarction do so within one hour of the onset of infarction, of ventricular fibrillation [5]. Half of all patients suffering a myocardial infarction die before reaching hospital [6]. These deaths are thought to be caused by arrhythmia [7]. Of those that do reach hospital approximately 20% experience a clinically significant arrhythmia [8, 9]. Thus the events associated with early ischemia that affect the electrophysiology of the myocardium are of considerable importance and these electrophysiological events have been the subject of intense scrutiny [2]. There is consequently a considerable drive to understand the mechanism of the responses to acute myocardial ischemia. There is also a great deal of observational clinical data concerning

[1]British Heart Foundation Cardiac Arrhythmia Research Group, Department of Physiology, Charing Cross and Westminster Medical School, London W6 8RF, United Kingdom.

Molecular and Subcellular Cardiology: Effects of Structure and Function
Edited by S. Sideman and R. Beyar, Plenum Press, New York, 1995

the final events in the organism as a whole. However, in order to understand the need for models we should first consider the experimental data.

Modelling implies a representation of the object or phenomenon of interest. To this extent many experimental paradigms are models of the clinical situation [10]. Experiments involving *in situ* heart models have the advantage of an intact autonomic nervous system. An important experimental consideration is the size of the heart, as a reentry circuit must be larger than the product of the action potential duration and the conduction velocity. The variation in conduction velocity and effective refractory period is not as great as the variation in the size of the heart from animal to animal. Consequently, the smaller hearts of the guinea pig and rabbit may spontaneously come out of ventricular fibrillation whereas this is not seen in the larger heart of the pig. The models of ischemia in man are limited in the duration of the ischemia that may be used. One way around this is to use specimens excised at surgery but which suffer from the same limitations as other isolated preparations. Other experimental problems include the high degree of collaterals seen in some experimental preparations, such as guinea pig, so that it is impossible to make localized areas of the myocardium ischemic.

ELECTROPHYSIOLOGICAL FEATURES OF ISCHEMIA

Basic Changes

The experimental data on electrophysiological changes during ischemia are now considered to illustrate the need for an integrated approach.

Ischemia raises extracellular potassium [11, 12]. This is the principle but not entire cause of the cellular depolarization found in ischemia [13]. Other factors such as hypoxia, intracellular acidosis, intracellular calcium accumulation [14] and amphipathic lipid accumulation [15] also contribute. The depolarization of the resting membrane potential causes more of the sodium channels to be in an inactivated state and this reduces the subsequent inward sodium current and slows Vmax of the upstroke of the action potential [16, 17]. Hypoxia, an increase in intracellular calcium and acidosis also slow V_{max}. This in turn reduces conduction velocity [18]. Approximately 10% of the reduction in conduction velocity is contributed to by the reduction in cell to cell coupling which increases the intracellular electrical resistance and by the collapse of the microvasculature increasing the extracellular electrical resistance to conduction [19]. The increase in extracellular potassium decreases the amplitude of the action potential [11, 20], and the duration of the action potential [21].

The action potential duration increases in the first minute or so after acute myocardial ischemia [22], then reduces over the next few minutes before rising again for the next 10–30 mins (see diagrammatic depiction, Fig. 1). Thereafter there is a steady decline. The effective refractory period changes roughly in parallel. It decreases initially and then increases again as post repolarization refractoriness occurs [16, 23]. The last may be due to a delay in recovery of V_{max} [24]. Intracellular ATP reduces and this opens KATP channels which further reduces the action potential duration [25].

Mechanoelectric feedback, the influence of mechanical changes on electrophysiological properties [26] increases during the first 10 min (Fig. 1) of coronary artery occlusion [27]. As seen, cellular contractile function reduces rapidly and the reasons are not entirely clear [28]. They are most likely related to changes in calcium cycling, phosphate accumulation, and reduction in action potential duration. This contractile failure may also affect electrophysiological properties by the same mechanisms used by mechanoelectric feedback.

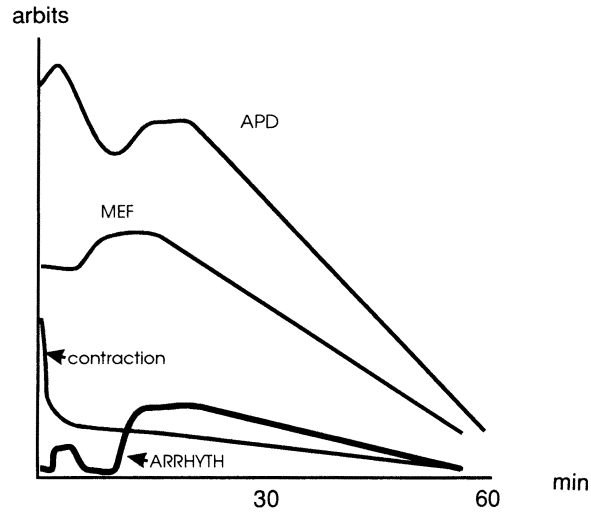

Figure 1. Diagram indicating electromechanical parameters changing over the first hour of experimental regional ischemia in intact heart *in situ*. Upper curve depicts electrophysiological changes such as conduction velocity and action potential duration, APD. These show an initial increase, decrease, increase then decrease towards zero [22]. The next curve shows the mechanical influence on action potential duration, MEF– mechanoelectric feedback. It shows a peak which overlaps in time with the second peak in the upper graph. The "contraction" curve shows a rapid decline, within a minute of the onset of regional ischemia. The lowest curve indicates incidences of electrical alternans and arrhythmias, showing two peaks roughly corresponding with those seen in the top line.

These features apply to all the affected cells, but underlying the genesis of an arrhythmia is often a discontinuity of electrophysiological properties in a multicellular preparation. Interestingly, the incidence of arrhythmia parallels, in time, some of the other electrophysiological changes (Fig. 1).

Important Multicellular Features, and Heterogeneity

A different aspect of the relevance of time is the change in electrophysiological properties with time after myocardial infarction. There is a period of increased conduction velocity during the first few minutes of ischemia [2], and it parallels action potential duration changes. The action potential duration goes through a sequence of an initial increase then decrease in duration. After 7 mins of ischemia it increases up to 15 mins then subsequently decreases until the myocardium becomes inexcitable [22] (Fig. 1).

In a multicellular preparation potassium diffuses away from the area of ischemia through the extracellular fluid so that there is a gradient of potassium at the periphery of the infarct. There is a corresponding gradient of electrophysiological properties in the myocardium [12]. The larger the area of ischemia or infarction the greater the likelihood of arrhythmia. Conduction velocity is slowed leading to delayed activation and conduction block [29]. There is a differential response to ischemia in the epicardium and endocardium [30, 31] which may be explained by the differential expression of membrane currents in the endocardium and epicardium [32]. The transient outward current is however species dependent and may be different in man.

Anisotropy of conduction in the myocardium is preserved during ischemia with both longitudinal and transverse conduction being depressed by approximately the same amount [18].

Whole Organism Integrative Features

The autonomic nervous system exerts a considerable influence over arrhythmias during acute myocardial ischemia [33]. There are also local changes in sympathetic stimulation of the myocardium, with noradrenaline in the infarcting tissue rising to very high levels. These features are absent in isolated preparations or single cell preparations, and the influences difficult if not impossible to asses. Conversely, we can not measure transmembrane currents in intact preparations. There is therefore a need for the integration of single cell results into the situation in the heart as a whole. The need for integration is, moreover, not dependent primarily on the presence ischemia in one region and not another, but is heightened by ischemia together with certain additional features. For example, the extracellular build up of potassium and the end products of metabolism which diffuse down an extracellular concentration gradient. Such features are present in the intact preparation but not the single cell preparation.

Integration in Multidimensional Media

The argument for integration becomes stronger when one considers other dimensions which affect the physiology of the myocardium. A physiological dimension related to the electrophysiology of the myocardium has been already alluded to: mechanoelectric feedback [26]. The mechanical activity is different in the part of the ventricular wall affected by ischemia [34] and through mechanoelectric feedback this may contribute to the electro–physiological changes seen [27]. That is, the feedback contributes to electrophysiological heterogeneity.

Additional dimensions are supplied by the coronary arteries. Collateral branches of adjacent coronary arteries may supply a variable amount of blood to the otherwise ischemic segment of myocardium following coronary artery occlusion. No one experimental model ideally summarizes the situation in man increasing the amount of integration necessary.

Time is a dimension necessitating integration of experimental results in two ways. Firstly, through the temporally dependent features of the electrophysiology of the myocardium per se. Secondly because of the time course of change in myocardial electrophysiology due to ischemia. Thus the degree of collateral flow in the experimental model under study is an important issue, the porcine model has very few collateral branches and has been likened to a sudden coronary artery occlusion in a previously fit human whereas the canine model has relatively more and is similar to the situation seen in chronic ischemic heart disease in man.

The variation in monophasic action potential with beat to beat interval is altered by ischemia with a flattened restitution curve (time course of electrophysiological recovery), the plateau of the curve also being depressed [22]. Consequently the electrophysiological properties of the ischemic myocardium and the dispersion between these properties and those of the normal myocardium will depend on the immediate beat to beat interval and the previous recent history of beat to beat intervals.

Alternans of electrophysiological properties is also frequently seen in ischemia [35] as is alternans of intracellular calcium [36]. Alternans increases with heart rate, and due to its regional nature, it increases dispersion. This may be related to the observation that the incidence of alternans in ischemia parallels that of arrhythmia, as in Fig. 1.

Some of these features may be related to autonomic changes and require an intact preparation and incorporation in any integrative model responding to ischemia.

Extension of the Time Domain in Ischemia

Coronary reperfusion is now in the forefront of therapy. The possibility of thrombolysis within hours of an acute episode of ischemia [37] is becoming a reality in the western world, and reperfusion after an episode of ischemia, with it's manifestations has to be considered. The above electromechanical sequence of changes occurs with a fixed coronary artery occlusion whereas in reality reperfusion and reocclusion may occur so that changing coronary flow with time adds another dimension to the picture. During reperfusion there are rapid changes in the electrophysiology of the myocardium associated with arrhythmias [38, 39]. On reocclusion, preconditioning [40] takes place. Experimental models using coronary artery ties are therefore limited since the artery is continuously tied. Coronary artery tie models are also limited in that the sympathetic nerves follow the artery and will be tied, models that mimic thrombus such as using angioplasty balloons may be better.

ARRHYTHMIA

The integration of all these individual features aims to provide a better understanding of the physiology of the myocardium and the genesis and subsequent form of arrhythmias. The observed incidence of experimental and some clinical arrhythmias follows two initial early peaks of unknown mechanism as pointed out in Fig. 1. One occurs within 5–10 mins and another at 20–30 mins so that the temporal dimension is important in the context of arrhythmia. Most arrhythmias in acute myocardial ischemia are thought to be due to "reentry" [41]. A reduction in the refractory period and conduction velocity and increase in dispersion of the refractory period in the myocardium all predispose to reentry arrhythmias. The establishment of a block in some areas, but not in others, is facilitated by an increased dispersion of refractory periods, as is seen in ischemia, so that in some areas the myocardium is inexcitable whereas it is excitable in others [42]. The time taken for conduction from the myocardium that has been normally depolarized to that proximal to the block must be adequate for the latter to repolarize. Reentry is thus favored by long lines of block [43], slow conduction velocities [44] and short refractory periods [45]. Conduction velocity is slowed in ischemia [18, 46] but the refractory period lengthens due to the phenomenon of "post repolarization refractoriness" [2, 16, 24] in which the end of the refractory period occurs after repolarization has finished. The initiating event is a premature ventricular beat which originates from either the subendocardium [47] or the border zone probably by reflection rather than reentry [48]. Once it is set up, reentry may remain entirely intramural [49].

The initiation of the arrhythmia is an important problem, and reentry is one mechanism to explain it. In addition there is the possibility of arrhythmias being initiated by the flow of current between different parts of the myocardium at different voltages [48]. This can arise where adjacent areas of myocardium have different action potential durations and consequently when one has repolarized the other is still depolarized. There are other triggers. Acute ischemia may increase automaticity and early afterdepolarizations as well as delayed afterdepolarizations [2].

Finally, reentry and its predominance as the mechanism of arrhythmia in myocardial ischemia, implies that any integrative model should have three spatial dimensions.

APPLICATION TO MAN

The final result of this approach, as depicted in Fig. 2, is to integrate the models with the clinical data concerning ischemia in man. The experimental data is limited to relatively short periods of ischemia in conscious man. There are obvious differences in the size of the heart and the coronary anatomy which will have to be extrapolated from the range of experimental data in other models. There are other data indicating the complexity of extrapolating directly from cell to man. For example there is a diurnal variation in the incidence of sudden death, which is presumably arrhythmic. Cardiac related mortality is highest in the mornings. This is probably related to an increased sympathetic tone at the time. The autonomic nervous system probably plays a significant role in sudden arrhythmic death. It appears that both a raised catecholamine level as well as myocardial mechanical load bear on arrhythmia [50], and the question as to whether they interact has been briefly addressed. A preliminary study [51] showed that dobutamine, a B agonist, enhances mechanically induced arrhythmia in intact heart *in situ*. Figure 3 is an example where the load change under control conditions produced no arrhythmia, but produced it when the agonist was infused.

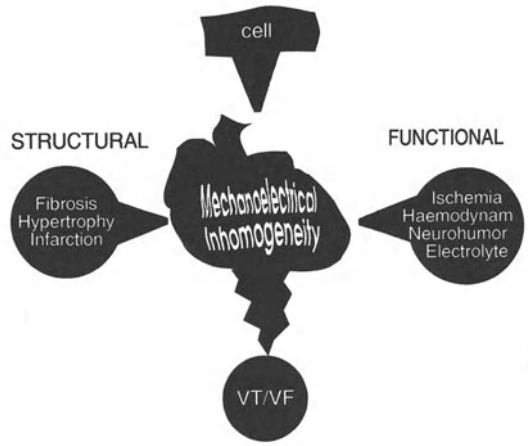

Figure 2. Diagram depicting integrative models incorporating the cell, structural (spatial), and functional factors. VT = ventricular tachycardia; VF = ventricular fibrillation.

Fairly detailed knowledge at the cellular level is required to make integrative experimental models of ischemia. The knowledge is limited to time dependent changes. However, spatial inhomogeneities are being described at subcellular levels. Structural and spatial alterations involving multicellular preparations are important, as is physical size. These include areas of fibrosis and scarring. Although the functional influences such as electrolyte disturbances apply uniformly to the heart, there are interdigitating spatial considerations that need integration. For example catecholamines have regionally different effects [52]. Also, an apparent overall uniform and functional hemodynamic change will produce regionally different stresses and strains. This applies to normal heart, and even more so in ischemia induced disease. This means that mechanoelectric feedback is also heterogeneous. It is this integrated response to ischemia that produces the unstable matrix that is conducive to lethal arrhythmia like ventricular tachycardia or fibrillation. Although

there are difficulties there are also important potential gains from an integrative model in the explanation of clinical phenomena which, whilst well documented, are poorly understood.

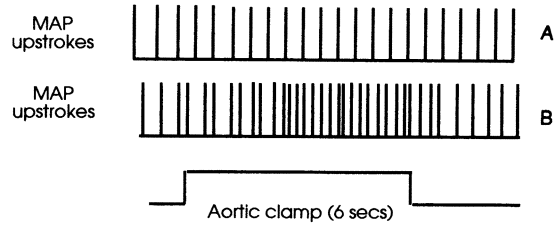

Figure 3. Monophasic action potentials (MAP) upstrokes plotted with time. **A:** Control. **B:** Ascending aortic occlusion produced no ventricular premature beats. During intravenous infusion of dobutrex 10 ug/kg, aortic occlusion produced runs of ventricular premature beats. Monophasic action potentials were recorded by suction electrode from the epicardium of anesthetized pig.

Despite the attempts at integration, we still have far to go. There are some shortcomings in scientific experiment to adequately account for the observed clinical phenomena. There are important questions. For example we need to explain: Why arrhythmias are more common in those with poor left ventricular function. In infarcts of the same size, why do some patients develop a serious arrhythmia and others do not. Why some patients die suddenly and others do not. Why in some patients reentry remains as stable ventricular tachycardia and in others degenerates into ventricular fibrillation. Precisely why is there such a strong association between heart rate variability and infarct related death.

CONCLUSION

Cellular events cannot be studied at the multicellular level and reentry arrhythmias cannot be studied in single cell preparations. In view of the number of simultaneously occurring events in each cell and the heterogeneous three dimensional nature of these events in multiple cells, there is a real need for integration of the two approaches. In the case of ischemia there are regional changes in metabolism, mechanical function and electrophysiology as well as changes in the peripheral circulation and autonomic nervous system. These changes affect the initiation and subsequent form of arrhythmias and make the need for an integrative model of the whole cardiovascular system particularly important in ischemia.

DISCUSSION

Dr. R. Reneman: I am surprised that the decrease in the ejection fraction is such a gradable parameter and a risk indicator. Are you aware of any studies that have related the decrease in ejection fraction to a prolongation of the conduction velocity in the heart under these circumstances of ischemia and partially infarcted patients? In our studies we introduced asynchrony in electrical activation on purpose; you can see that the heart can handle a conduction velocity delay of about 30 ms. As it becomes longer, at 40 ms delay, there is drop in ejection of about 15–20%. Are you aware of any correlations made between the decrease in ejection fraction and the prolongation in

the conduction velocity?

Dr. M. Lab: I know that there have been studies on refractory periods which change in sick hearts when they are dilated. The conduction velocity problem in normal myocardium is a difficult one. There have been some studies that show it goes up with stretch, and some show it goes down. The answer is not clear. I do not know what the answer is in abnormal hearts.

Dr. R. Reneman: Allessie and Wit do not know either. In their early work, Allessie and Wit [Wit *et al., Am J Cardiol.* 1982;49:166–185] studied electrophysiological changes in infarcted hearts, but did not relate their findings to hemodynamic changes.

Dr. M. Lab: In the more recent work with Reitèr [Reitèr *et al., Circulation.* 1994;89:423–431] they destroyed the inside of the myocardium and left a shell. They then dilated it and found that dilatation did effect electrophysiological properties.

Dr. R. Reneman: So it is impossible to relate it to ejection fraction in their model.

Dr. M. Lab: Absolutely.

Dr. A. Landesberg: You have shown the effect of verapamil and gadolinium on the ventricle cell membrane potential. What was the amount of calcium changes? After all, gadolinium is not a pure blocker of the stretch channels, it also blocks the other calcium currents, so maybe the cells that were treated with gadolinium were calcium depleted, and therefore the amount of calcium that was released after the stretch was insignificant and therefore the arrhythmia did not occur. My second question is about calcium release from the troponin versus the effect on the stretch activated channels. An enormous amount of calcium is bound to troponin, and this is a potential source for calcium release when a stretch is made. From the other side, as for the stretch activated channel, the quantify of stretch channel Ca entering via the sarcolemma is not so big. So quantitatively, I wonder how this can produce the changes you describe.

Dr. M. Lab: Gadolinium is a dirty drug. There is the possibility that it is an L–type calcium channel blocker, although some recent work suggests that it is not. Also, some of the L–type calcium channels are stretch sensitive. The second part of your comment about the quantitative side of things, I do not think is true. Fred Sacks [In: *Cell Mechanics and Cellular Engineering* (Mow VC, Guilak F. Tran–Son–Tay R, Hochmuth RM, eds) Springer Verlag, pp 308–328, 1994] has modeled the current changes and the stretch activated channel densities and he can actually change the action potential duration the appropriate amount and direction. He did these studies very carefully. I've tried to model it myself. You can modify, appropriately, the action potential by activating stretch activated channels.

Dr. M. Morad: My suggestion to you and all the modelers is that there is another interesting aspect that you have to plug into your models. That is the interstitial space; what we used to call the extracellular space. In this space ionic changes occur dramatically. If you put in a potassium or calcium microelectrode to look specifically in the extracellular space, enormous accumulations and depletions occur, specifically when you drive the preparation into ischemia. These changes have a dramatic effect on the action potential duration contraction, calcium transients, etc. My question is in some ways related to the issue of when you stretch or when you shorten. Surely, those spaces change. The amount of potassium dumped into that space, even on one single action potential, would change with respect to whether it is shortening or contracting. Also, if you are going after chloride current, I have a problem with the chloride current in that it seems that the effect that you got was at the resting potential, or at the end of the action potential. A change in the chloride conduction would have the least effect as compared to the plateau where the membrane impedance is the largest, so the smallest change in current, or opening of the channel, is going to have a dramatic effect on there vs the resting potential. How do you handle that?

Dr. M. Lab: Your comment on interstitial space is fundamentally true. In fact, when I first described this phenomenon, one of the mechanisms I invoked was diffusion restriction in the extracellular space, and I quoted your work [Kline and Morad, *Biophys J.* 1976;16:367–372]. Chloride is not the only ion involved. These channels are there, and 5–6 there are now described. Some of them are specific for sodium, some for potassium, some for calcium, and several channels for chloride. I think that only one study has shown a stretch chloride in the ventricular myocardium. In one of my earlier preparations, I stretched during the plateau, half-way down the plateau, stretched at end-plateau. The potential moves as if there is an equilibrium potential at round about -30 mV and you can model that with the chloride current. But coming back to your question about diastole, I agree, it is a little more difficult here, and you have to think more carefully during the resting membrane potential.

Dr. D. Brutsaert: Some time ago we were interested in volume induced arrhythmias and it confirmed that in *in vivo* condition, the volume induced arrhythmias are quite reproducible. But we have never been able to reproduce that in an isolated muscle, to our big surprise. If you have good isolated muscle, whatever the species, whatever the type of stretch you impose, during the twitch, during diastole, slow stretch, quick stretch, you will never be able to induce arrhythmias, at least in good muscles. In bad muscles, you sometimes do. So it seems that this phenomenon is inherent to the *in vivo* situation. Have you considered the possibility that it simply might be the result of the Purkinje fiber system being induced by balloon, or rubbing of the endocardium, or anything else?

Dr. M. Lab: It could be that the earlier studies were done on slightly sick papillary muscles. In the intact heart, it may well be different. We have excluded rubbing of the balloon because we can produce arrhythmia by injecting saline into the ventricle. It is more complicated in the intact heart. The Purkinje system is a little bit more stretch sensitive than the rest of the myocardium. Also, you have a lot of nerve endings. The extent to which the stretch is locally liberating catecholamines and changes cyclic AMP changes which interact with the stretch, could be important. It does seem to be a phenomenon more easily invoked in the intact preparation and maybe this could give us a handle on the mechanism.

Dr. H.E.D.J. ter Keurs: I agree with that comment. It is possible to generate extra systoles in cardiac muscle preparations, provided that you go to extremes of length changes. For example, keeping sarcomere length constant in the central area of a muscle, which requires substantial stretch, particularly in damaged regions, leads very systematically to arrhythmias and extra systoles. When you introduce a stretch activated channel you see a patch electrode with apparent suction in the device because the membrane is stretched into that electrode in an incredible way, like bubble-gum out of a kids mouth. One needs a pressure gradient of about 20 mmHg across the membrane in order to observe stretch activation of these channels. The degree of stretch that we are talking about in the heart, and even in muscle preparations, is only 20% and much smaller than in a patch.

Dr. M. Lab: That bothers me too, which is why I keep going to the intact preparation to see to what extent I can mimic the predicted effects of stretch activated channels. The possibility that stretch activated channels are artifacts was raised in a review by Morris [Morris E, *J Membr Biol.* 1990;113:93–107]. But Morris keeps on working on stretch activated channels so perhaps she does not really believe this. Also in some photographs that Fred Sacks has shown, you suck up all sorts of things in the patch. However, these mechanosensitive channels or mechanotransducer elements in the membrane have been found in almost every preparation in which it has been sought, from the bacterium all the way through to the nervous system. It seems to be a universally existing phenomenon. But perhaps we are studying a universal artifact. Some of the intact work we are doing seems to support the possibility that they exist. Finally, and this may be important, you can get whole cell current changing when you stretch cells.

Dr. S. Axelrod: How do you extrapolate this preparation to the clinical situation? In a preparation you have an active stretching, you have a step function. In the patient you have a steady state and

you do not necessarily have a dilatation. How do you relate your preparation to the clinical situation?

Dr. M. Lab: That is an important question. Most of these are abrupt changes. There are two ways of relating that to the patient. The first is that slow changes can do it. With slow changes you can actually measure slow increases in intracellular calcium, possibly through sodium getting in through the stretch activated channels and exchanging for calcium. The intracellular calcium goes up and that predisposes to arrhythmia. The second way, perhaps more important, is inhomogeneity. In a diseased myocardium one part of the myocardium can stretch while another part is not stretched. Moreover, where you have a premature ventricular beat, the wave form of propagation is entirely different. In one beat a bit of healthy myocardium is stretched by another bit of myocardium that is contracting. Then you have the sudden pertubation which relates to the clinical situation.

Dr. Y. Rudy: The afterdepolarizations that you have shown and termed early afterdepolarizations (EAD) occur close to full repolarization. Their mechanism is probably very different from that of plateau EADs that involve reactivation of the L-type calcium current. A second comment is in response to Dr. Morad's request that the interstitial space and its effects be appreciated and considered. The single cell model that I have presented here incorporates an interstitial cleft. In particular, the effects of extracellular potassium concentration changes on potassium channel conductances are represented in the model. A related issue is that, in addition to ion accumulation, there is an important effect of stretch that must play a major role in arrhythmogenesis in the whole heart. I refer to the change in cross-section of interstitial pathways for current flow during stretch. It is known that during ischemia, for example, interstitial resistance increases faster than intracellular resistance. The change of interstitial resistance can play a major role in the development of propagation-type arrhythmias such as conduction block, slow conduction, and reentry.

Dr. M. Lab: I agree with early afterdepolarization phenomenon, but, I think it is not strictly an early afterdepolarization; it is a different mechanism. We should call it "mechanically induced potential." By definition, you have to have it after repolarization, but you can get these in quiescent muscle. For example, the myocardium is quiet and you stretch it you produce depolarization. So we have to redefine it as being different to the conventional early afterdepolarization.

REFERENCES

1. Zipes DP, Jalife J (editors). *Cardiac Electrophysiology*. Philadelphia: W.B. Saunders, 1990.
2. Janse MJ, Wit AL. Electrophysiological mechanisms of ventricular arrhythmias resulting from myocardial ischemia and infarction. *Physiolog Rev*. 1989;69:1049-1169.
3. Report of the Working Group on Arteriosclerosis of the National Heart Lung and Blood Institute (Volume 2). Patient Oriented Research-Fundamental and Applied, Sudden cardiac death. DHEW, NIH Publication No.82-2035, in Washington D.C., U.S.Government Printing Office, 1981, pp 114-122.
4. Davies MJ, Thomas A. Thrombosis and acute coronary artery lesions in sudden cardiac ischemic death. *N Engl J Med*. 1984;310:1137.
5. Pantridge JF, Webb SW, Adgey AAJ, Geddes JS. The first hour after the onset of acute myocardial infarction. In: Yu PN, Goodwin JF, eds, *Progress in Cardiology*. Philadelphia: Lea and Febiger, 1974: 173.
6. Armstrong A, Duncan B, Oliver MF, Julian DG, Donald KW, Fulton M, Lutz W, Morrison SL. Natural history of acute coronary heart attacks. *Brit Heart J*. 1972;34:67-80.
7. Bayes de Luna A, Coumel P, Leclercq JF. Ambulatory sudden cardiac death: mechanisms of production of fatal arrhythmia on the basis of data from 157 cases. *Am Heart J*. 1989;117:151-159.
8. Campbell RWF, Murray A, Julian DG. Ventricular arrhythmias in the first 12 hours of acute myocardial infarction. *Brit Heart J*. 1981;46:351-357.
9. Horner SM. Efficacy of intravenous magnesium in acute myocardial infarction in reducing arrhythmias and mortality. Meta-analysis of magnesium in acute myocardial infarction. *Circ*. 1992;86:774-

779.

10. Avkiran M, Curtis MJ. Independent dual perfusion of left and right coronary arteries in isolated rat hearts. *Am J Physiol*. 1991;261:H2082–H2090.
11. Kleber AG. Resting membrane potential, extracellular potassium activity, and intracellular sodium activity during acute global ischemia in isolated perfused guinea pig hearts. *Circ Res*. 1983;52:442–450.
12. Coronel R, Fiolet JW, Wilms Schopman FJ, Schaapherder AF, Johnson TA, Gettes LS, Janse MJ. Distribution of extracellular potassium and its relation to electrophysiologic changes during acute myocardial ischemia in the isolated perfused porcine heart. *Circ*. 1988;77:1125–1138.
13. Downar E, Janse MJ, Durrer D. The effect of "ischemic" blood on transmembrane potentials of normal porcine ventricular myocardium. *Circ*. 1977;55:455–462.
14. Clusin WT, Buchbinder M, Harrison DC. Reduction of ischemic depolarization by the calcium channel blocker diltiazem. Correlation with improvement of ventricular conduction and early arrhythmias in the dog. *Lancet*. 1983;1:272–274.
15. Sobel BE, Corr PB, Robison AK, Goldstein RA, Witkowski FX, Klein MS. Accumulation of lysophosphoglycerides with arrhythmogenic properties in ischemic myocardium. *J Clin Invest*. 1978; 62:546–553.
16. Downar E, Janse MJ, Durrer D. The effect of acute coronary artery occlusion on subepicardial transmembrane potentials in the intact porcine heart. *Circ*. 1977;56:217–224.
17. Elharrar V, Foster PR, Jirak TL, Gaum WE, Zipes DP. Alterations in canine myocardial excitability during ischemia. *Circ Res*. 1977;40:98–105.
18. Kleber AG, Janse MJ, Wilms Schopmann FJ, Wilde AA, Coronel R. Changes in conduction velocity during acute ischemia in ventricular myocardium of the isolated porcine heart. *Circ*. 1986;73:189–198.
19. Kleber AG, Riegger CB, Janse MJ. Electrical uncoupling and increase of extracellular resistance after induction of ischemia in isolated, arterially perfused rabbit papillary muscle. *Circ Res*. 1987;61:271–279.
20. Kardesch M, Hogancamp CE, Bing RJ. The effect of complete ischemia on the intracellular electrical activity of the whole mammalian heart. *Circ Res*. 1958;6:715–720.
21. Wiegand V, Guggi M, Meesman W, Kessler M, Greitschus F. Extracellular potassium activity changes in the canine myocardium after acute coronary occlusion and the influence of b–blockade. *Cardiovasc Res*. 1979;13:297–302.
22. Dilly SG, Lab MJ. Changes in monophasic action potential duration during the first hour of regional myocardial ischaemia in the anaesthetised pig. *Cardiovasc Res*. 1987;21:908–915.
23. Lazzara R, el Sherif N, Hope RR, Scherlag BJ. Ventricular arrhythmias and electrophysiological consequences of myocardial ischemia and infarction. *Circ Res*. 1978;42:740–749.
24. Joyner RW, Ramza BM, Osaka T, Tan RC. Cellular mechanisms of delayed recovery of excitability in ventricular tissue. *Am J Physiol*. 1991;260:H225–H233.
25. Noma T. ATP –regulated potassium channels in cardiac muscle. *Nature*. 1983;305:147–148.
26. Lab MJ. Contraction–excitation feedback in myocardium: Physiological basis and clinical relevance. *Circ Res*. 1982;50:757–766.
27. Horner SM, Lab MJ, Murphy CF, Dick DJ, Zhou B, Harrison FG. Mechanically induced changes in action potential duration and left ventricular segment length in acute regional ischaemia and int *in situ* porcine heart. *Cardiovasc Res*. 1994;28:528–534.
28. Lee JA, Allen DG, Burgess MJ, Green LS, Millar K, Wyatt R, Abildskov JA. Mechanisms of acute ischemic contractile failure of the heart. Role of intracellular calcium The sequence of normal ventricular recovery. *J Clin Invest*. 1991;88:361–367.
29. el Sherif N, Scherlag BJ, Lazarra R, Samet P. Pathophysiology of tachycardia– and bradycardia–dependent block in the canine proximal His–Purkinje system after acute myocardial ischemia. *Am J Cardiol*. 1974;33:529–540.
30. Taggart P, Sutton PM, Spear DW, Drake HF, Swanton RH, Emanuel R. Simultaneous endocardial and epicardial monophasic action potential recordings during brief periods of coronary artery ligation in the dog: influence of adrenaline, beta blockade and alpha blockade. *Cardiovasc Res*. 1988;22:900–909.
31. Wilensky RL, Tranum–Jensen J, Coronel R, Wilde AAM, Fiolet JWT, Janse MJ. The subendocardial border zone during acute ischemia of the rabbit heart: an electrophysiologic, metabolic, and morphologic correlative study. *Circ*. 1986;74:1137–1146.
32. Litovsky SH, Antzelevitch C. Transient outward current prominent in canine ventricular epicardium

but not endocardium. *Circ Res*. 1988;62:116–126.

33. Cerati D, Schwartz PJ. Single cardiac vagal fiber activity, acute myocardial ischemia, and risk for sudden death. *Circ Res*. 1991;69:1389–1401.
34. Sakai K, Watanabe K, Millard RW. Defining the mechanical border zone: a study in the pig heart. *Am J Physiol*. 1985;249:H88–H94.
35. Dilly SG, Lab MJ. Is electrical alternans ubiquitous in myocardial ischaemia? Studies in anaesthetised pig. *J Physiol*. 1985;369:129P (abstract).
36. Lee HC, Mohabir R, Smith N, Franz MR, Clusin WT. Effect of ischemia on calcium-dependent fluorescence transients in rabbit hearts containing indo 1. Correlation with monophasic action potentials and contraction. *Circ*. 1988;78:1047–1059.
37. ISIS-2 (Second International Study of Infarct Survival) Collaborative Group . Randomised trial of intravenous streptokinase, oral aspirin, both, or neither among 17,187 cases of suspected acute myocardial infarction: ISIS-2. *Lancet*. 1988;2:349–360.
38. Kaplinsky E, Ogawa S, Michelson EL, Dreifus LS. Instantaneous and delayed ventricular arrhythmias after reperfusion of acutely ischemic myocardium: evidence for multiple mechanisms. *Circ*. 1981;63:333–340.
39. Pogwizd SM, Corr PB. Electrophysiologic mechanisms underlying arrhythmias due to reperfusion of ischemic myocardium. *Circ*. 1987;76:404–426.
40. Tan HL, Mazon P, Verberne HJ, Sleeswijk ME, Coronel R, Opthof T, Janse MJ. Ischaemic preconditioning delays ischaemia induced cellular electrical uncoupling in rabbit myocardium by activation of ATP sensitive potassium channels. *Cardiovasc Res*. 1993;27:644–651.
41. Janse MJ, van Capelle FJ, Morsink H, Kleber AG, Wilms Schopman F, Cardinal R, Naumann d'Alnoncourt D, Durrer D. Flow of "injury" current and patterns of excitation during early ventricular arrhythmias in acute regional myocardial ischemia in isolated porcine and canine hearts. Evidence for two different arrhythmogenic mechanisms. *Circ Res*. 1980;47:151–165.
42. Coronel R, Wilms-Schopman FJ, Opthof T, van Capelle FJ, Janse MJ. Injury current and gradients of diastolic stimulation threshold, TQ potential, and extracellular potassium concentration during acute regional ischemia in the isolated perfused pig heart. *Circ Res*. 1991;68:1241–1249.
43. Mehra R, Zeiler RH, Gough WB, El-Sherif N. Reentrant ventricular arrhythmias in the late myocardial infarction period. 9. Electrophysiological-anatomic correlation of reentrant circuits. *Circulation*. 1983;67:11–24.
44. de Bakker JMT, Coronel R, Tasseron S, Wilde AAM, Opthof T, Janse MJ, Van Capelle FJL, Becker AE, Jambrose G. Ventricular tachycardia in the infarcted langendorff perfused human heart. Role of the arrangment of surviving cardiac fibres. *J Am Coll Cardiol*. 1990;15:1594–1607.
45. Frame LH, Rhee EK. Spontaneous termination of reentry after one cycle or short nonsustained runs. *Circ Res*. 1991;68:493–502.
46. Elharrar V, Gaum WE, Zipes DP. Effect of drugs on conduction delay and incidence of ventricualr arrhythmias induced by acute coronary occlusion in dogs. *Am J Cardiol*. 1977;39:544–549.
47. Pogwizd SM, Corr PB. Reentrant and nonreentrant mechanisms contribute to arrhythmogenesis during early myocardial ischemia: results using three-dimensional mapping. *Circ Res*. 1987;61:352–371.
48. Janse MJ, Van Capelle FJL. Electrotonic interactions across an inexcitable region as a cause of ectopic activity in acute regional myocardial ischemia. *Circ Res*. 1982;50:527–537.
49. Pogwizd SM, Corr PB. Mechanisms underlying the development of ventricular fibrillation during early myocardial ischemia. *Circ Res*. 1990;66:672–695.
50. Dean JW, Lab MJ. Arrhythmia in heart failure: role of mechanically induced changes in electrophysiology. *Lancet*. 1989;1:1309–1312.
51. Dick DJ, Harrison FG, Horner SM, Murphy CF, Lab MJ. Effect of a b1-agonist on mechanically induced premature beats in the anaesthetised in-situ pig heart. *J Physiol (Lond)*. 1992;459:411P(Abstract).
52. Taggart P, Sutton P, Lab M, Dean J, Harrison F. Interplay between adrenaline and interbeat interval on ventricular repolarisation in intact heart *in vivo*. *Cardiovasc Res*. 1990;24:884–895.

CHAPTER 7

RICH DYNAMICS IN A SIMPLIFIED EXCITABLE SYSTEM

Shimon Marom,[1] Amir Toib[1] and Erez Braun[2]

ABSTRACT

The study aims at exploring effects of microscopic channel fluctuations on macroscopic dynamics of excitable systems. Molecular biology techniques are used in order to construct a minimal excitable system that is built of cloned channels embedded in a small (~1 μm^2) isolated patch of membrane. This simple synthetic "point" system exhibits dynamics in time scales that are several orders of magnitude longer then a single spike.

INTRODUCTION

Excitability stands in the basis of many physiological control systems. In most cases, the action potential (the excitation event itself) operates on a relatively fast time scale, whereas the system is modulated at time scales several orders of magnitude slower. The search for mechanisms to bridge this time gap, fuels an immense number of detailed studies which usually lead to additional intra- and inter-cellular complexities. Recent experiments [1-3] and theoretical considerations [4-5] suggest that intrinsic gating mechanisms of voltage-sensitive ion channels (the molecules of excitability) might contribute significantly to slow modulations in simple excitable systems. The study presented here aims at experimentally uncovering basic principles of modulations that are inherent to the process of excitation itself. For this purpose, a biological minimal excitable system is constructed using molecular biology techniques. The system is built of a binary mixture of cloned sodium and potassium voltage-gated ion channels embedded in a small (~1 μm^2 diameter) patch of an otherwise naive membrane. The dynamics of this "point" excitable system is studied under well controlled physico-chemical conditions, free of intracellular bio-chemical complications. This simplified excitable unit shows traces of what is usually ascribed to more complex systems, such as activity dependent excitability potentiation,

[1]Faculty of Medicine Rappaport Institute of Medical Science, and [2]Faculty of Physics, Technion-IIT, Haifa 31096, Israel.

Molecular and Subcellular Cardiology: Effects of Structure and Function
Edited by S. Sideman and R. Beyar, Plenum Press, New York, 1995

temporal integration and bistability. The challenge is to understand these sophisticated input–output functions. The hope is that the principles underlaying dynamics of the simplified unit can be carried up the scale to help us in the study of more complex ensembles.

METHODS

A mixture of *in vitro* made mRNA coding for mammalian sodium and potassium channels was injected to a frog oocyte which serves as a protein production line, so that the desired channels are expressed at the outer membrane of the oocyte. This membrane is otherwise non–excitable and for all practical purposes does not exhibit any voltage–dependent conductances in comparison to the ones carried by the expressed channels. mRNA coding for potassium channels is prepared from sequences of the Shaker related Kv1.3 gene [6]. mRNA coding for sodium channel gene type II [7] was used. Standard protocols for the preparation of DNA, RNA, and RNA injection to Xenopus oocytes are described elsewhere [8]. Recordings were made in the detached patch configuration. The pipet solution contains 96 mM NaCl, 2mM KCl, 1 mM $CaCl_2$, 1 mM $MgCl_2$ and 10 mM Hepes. The bath solution contained 100 mM KCl, 1 mM EGTA and 10 mM Hepes. Both solutions were at pH of 7.5. Generally, the resting potential ranges from −70 to −50 mV. An Axopatch 200A amplifier (Axon Instruments) was used.

RESULTS

The hallmarks of an excitable system containing a mixture of sodium and potassium channels in a detached patch are demonstrated in Fig. 1. The different traces of Fig. 1a are current responses to pulses of voltage. Figure 1b shows action potentials and aborted action potentials (i.e. below threshold reactions) recorded under current clamp conditions in which the current is held at zero except for a short stimulation period. The control parameter which determines the dynamics is the ratio of sodium to potassium peak conductances, measured in voltage clamp experiments as recorded in Fig. 1a. This parameter is coarsely controlled at the preparation phase by injection of different ratios of mRNA mixtures.

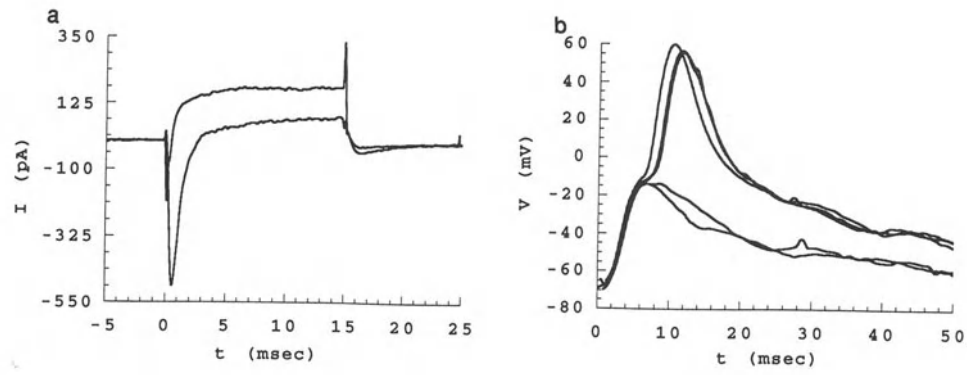

Figure 1. Current and voltage recordings from a detached patch of a membrane containing an embedded mixture of sodium and potassium ion channel proteins. **a:** Two typical voltage clamp traces. **b:** Action potentials and aborted action potentials recorded under current clamp conditions in which the current is held at zero, except for a short stimulation period.

To explore the *long term dynamics* of the system, we have studied its response to repetitive, constant amplitude, current stimulations. As shown in Fig. 2 these patches of membrane, which contain only a mixture of sodium and potassium channels, demonstrate dynamics at time scales much beyond the msec duration of a single spike. Figure 2a demonstrates a fairly trivial transient response of spike broadening and after-hyper-polarization modulation at a time scale of several seconds. This response reflects activity-dependent potassium conductance reduction (i.e. inactivation). About 30 sec of quiescent period, where no stimulation is applied, are required for full recovery of the channels and the reappearance of original profile spikes. Figure 2b demonstrates a less trivial long-term response, where the patch alternates between regions of low amplitude, passive responses to the current stimulus, and high amplitude, active responses in the form of action potentials. These clusters of responses have a wide range of durations, as shown in the binned data of Fig. 3. Apparently, there is no single characteristic time scale. As this simplified excitable system is devoid of any cellular complications the dynamical response must be intrinsic to the channels. The simplest interpretation of this behavior is that the threshold of the membrane for the generation of an action potential is not fixed by the

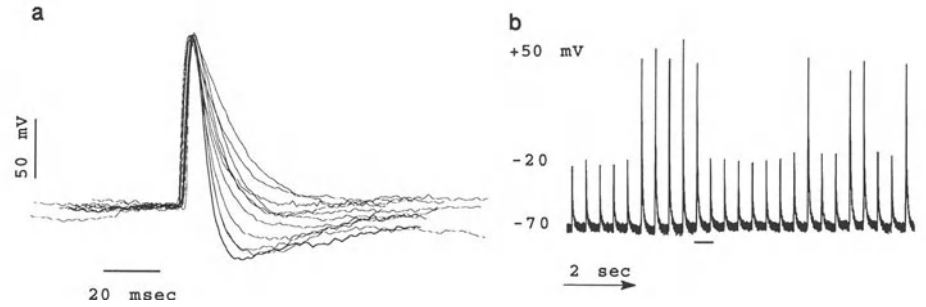

Figure 2. a: Modulation of after hyperpolarization and widening of action potential profiles in response to a series of short pulses every 400 msec. **b:** Clustering of active responses and aborted action potentials evoked by a long series of identical near threshold current stimulations.

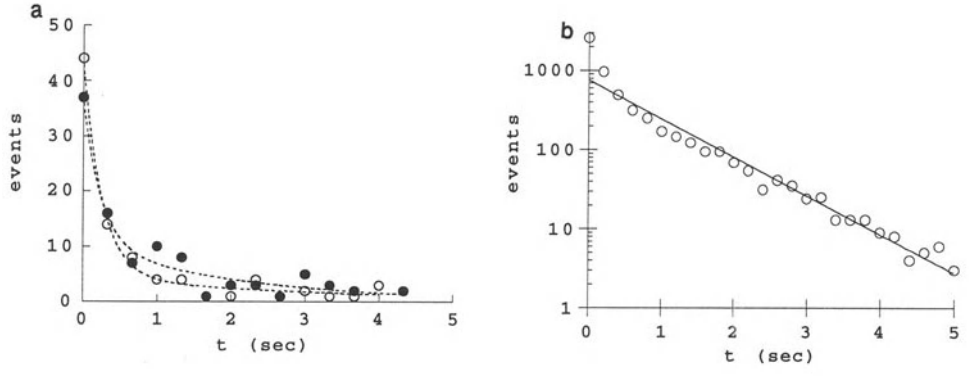

Figure 3. a: Binned clustered durations of action potentials (black circles) and sub-threshold responses (open circles) measured from data as in Fig. 2b, with interpulse intervals ranging from 100 to 400 msec. The broken lines are best fits to the data by sums of two exponents with time constants of approx. 250 msec and 2 sec. **b:** A summary of a Monte-Carlo simulation of 50 channels based on the three-state model above, where binned durations of responses, corresponding to the experimental results of Fig. 3a, are shown. The best fit of the results is by an exponent with a time constant of 1.3 sec, fairly similar to the data of Fig. 3a.

initial conditions of the sample (i.e. by the number of different channels), but itself becomes a slowly varying entity which fluctuates due to the stochastic activity of the ion channels.

To understand the source of the long term dynamics it is imperative to look into the microscopic operation of the ion channels. The reactions of the sodium channel are all within the msec time scales [9–10]. Therefore, we assume that slow modulation of activity in the excitable system arises from slow transitions of the potassium channel. The actual states of the potassium channel alone, and the transition rates between them, have been studied in detail under the same working conditions [3,8]. As shown in [3], the potassium channel can be simplified to a three–state system (Fig. 4) where v is the transmembrane voltage (in millivolts).

$$\text{Closed} \underset{\beta(v)}{\overset{\alpha(v)}{\rightleftharpoons}} \text{Open} \underset{\delta}{\overset{\gamma}{\rightleftharpoons}} \text{Inactivated}$$

Figure 4. Schematic of a three–state system of the potassium channel. The transition rates, in $msec^{-1}$ are: $\alpha(v) = -0.021\ (v + 8.3) / (\exp(-(v + 8.3) / 9.8) - 1)$; $\beta(v) = 0.0008 \exp(-(v + 23.6) / 20.7)$; $\gamma = 0.0074$; $\delta = 0.0002$.

The channel is conducting only when in the open state. The closed and inactivated states, both non–conducting, are different physical states of the channel and a direct transition between them is not possible. The transitions between the open and closed states are voltage dependent, and are fast (down to msec). The transitions between the inactive and open states (γ, δ) are voltage independent, and are relatively slow (up to sec). The coupling, of slow voltage–independent to fast voltage–dependent processes, is the source of the long–term dynamics. Recovery from inactivation is the slowest rate in our system so that any channel that made a transition into that state is trapped for a long time before being able to return to the pool of active channels available for conductance [3]. In the experiment, the number of available potassium channels becomes a dynamical parameter which affects strongly the excitable modes of the membrane. The activity dependent decrement of potassium channel availability leads to an increased excitability because the potassium current serves as a restoring force which acts against the sodium current exciting force. The passive restoring due to the leakage current is not significant during excitation – only a dynamical restoring can relax the membrane from an action potential. Therefore, the voltage threshold for action potential generation can be translated into a threshold in the number of available potassium channels. When this number is below the threshold, the patch responds to the stimulus by firing an action potential, and the system is highly excitable due to the weak restoring force.

The process described above is entirely based upon the stochastic nature of the channels. A typical patch, exhibiting fluctuations in its mode of firing action potentials as in Fig. 2, contains around 50 potassium and 500 sodium channels. This number of channels, when normalized to the capacitance of the experimental setup (1–2 pF, mostly contributed by the glass pipet) is a realistic representation of excitable systems [10]. To test if a simple three–state model is enough to determine the observed bursting of activity in Fig. 2, we ran a Monte–Carlo simulation for 50 channels, in which the probability of transition from one state to the other is given by: $f = \exp[-k \Delta t]$, where k is the actual transition rate and Δt is a small time step. Experimental values for the resting potential and

for the membrane voltage during sub-threshold responses and at the peak of an action potential, were used. We have arbitrarily chosen a critical number of active channels, Kc = 4, as the threshold below which the system starts to fire action potentials. The entire range of fluctuations which determines the value of Kc is very narrow, making the above choice (= 4) not unreasonable. The binned durations of the active-inactive states, chosen in such a way, are shown in Fig. 3b. The distribution is exponential with a mean time of 1.3 sec, very similar to the experimental data.

So far we have looked at the excitable system near the threshold for firing an action potential. What happens if we start with a large number of potassium channels so that the initial restoring force is large compared with the exciting force? If we repeatedly stimulate the membrane with an interpulse intervals smaller than the time scale of recovery from inactivation, a successively large amount of potassium channels will be trapped in the inactivated state. A continuous reduction of the restoring force is expected ("cumulative inactivation" [3, 4, 8, 11]). After some stimulation period the threshold for firing an action potential will start to be sensitive to the past history of stimulations. In fact, such temporal integration behavior can be observed in neurons [1]. Recently, a prediction was made [5] that in the limit where the small availability of potassium channels eliminates the threshold for firing action potential the system becomes an oscillator. Such a transition is observed in our experiment shown in Fig. 5, where an initially quiescent patch is stimulated to trap most of the potassium channels in the inactive state and becomes a spontaneous oscillator after the stimulations cease. The spontaneous firing of the patch is stable over the experimental life-time (many minutes) and seems to exhibit random bursts which originate from the fluctuations in the number of available channels. Note that there are large fluctuations also in the resting potential which presumably come due to weak, although still significant, leakage conductance. The strength of the sodium and leakage current components together with the capacitance of the membrane determine the minimal stimulation period needed to make this transition.

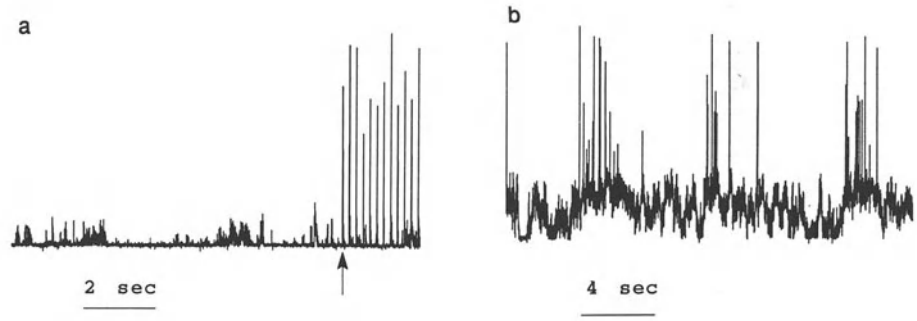

Figure 5. a: A silent patch is stimulated to fire action potentials, starting at the point marked by an arrow. The stimulation is ceased after ~0.5 min and, as shown in **b**,the patch becomes a free-running oscillator.

CONCLUSION

A conceptually simple construction - a point biological excitable system - enables us to study the temporal dynamics devoid of intra- and inter-cellular uncontrolled parameters. We have shown that, under realistic conditions, the microscopic fluctuations of the channels activity are imprinted on the macroscopic behavior of the system. These results raise the possibility that extended excitable systems can be treated as a continuous

mesh of excitable elements each of which has the ability to generate complex dynamics due to its internal structure.

DISCUSSION

Dr. H. Fozzard: I was interested in the calcium binding and its action. Where the histidine residue is responsible, then that should make the process quite pH sensitive. Have you looked at that.

Dr. S. Marom: Inactivation is sensitive to pH. Histidine is protonated at low pH and the rate of inactivation decreases as pH is reduced. This was shown by others as well, by *Busch et al.* two years ago [*Biochem & Biophys Res Comm.* 1991;179(3):1384–1390].

Dr. H. Fozzard: I trust you have experiments where you remove all of the calcium. Does the process occur?

Dr. S. Marom: The problem then is that we replace calcium by magnesium and we get a slight left over of activation that we do not know how to explain yet. It definitely removes the fast phases of inactivation that are seen with calcium. It fits 30 μM or so for calcium. Note that the calcium Kd is not in the physiological range. The potassium Kd is within a physiological range because we are talking abut 2–5 mM to prevent 50% of the channels to go into inactivation.

REFERENCES

1. Storm JF. Temporal integration by a slowly inactivating K current in hippocampal neurons. *Nature.* 1988;336:379–381.
2. Hsu H, Huang E, Yang X, Karschin A, Labarca C, Figl A, Ho B, Davidson N, Lester HA. Slow and incomplete inactivation of voltage–gated channels dominate encoding in synthetic neurons. *Biophys J.* 1993;65:1196–1206.
3. Marom S, Levitan IB. State–dependent inactivation of the Kv3 potassium channel. *Biophys J.* 1994;67:579–589.
4. Marom S, Abbott LF. Modeling state–dependent inactivation of membrane currents. *Biophys J.* 1994;67:515–520.
5. Marom S. A note on bi–stability in a simple synapseless "point neuron" model. *Network: Computation in Neural System.* 1994;5:327–331.
6. Stühmer W, Ruppersberg JP, Schroter KH, Sakmann B, Stocker M, Giese KP, Perschke A, Baumann A, Pongs O. Molecular basis and functional diversity of voltage–gated potassium channels in mammalian brain. *EMBO.* 1989; 8:3235–3244.
7. Noda M, Ikeda T, Kayano T, Suzuki H, Takeshima H, Kurasaki M, Takahashi H, Numa S. Exsitence of distinct Na channel messenger RNAs in rat brain. *Nature.* 1989;320:188–192.
8. Marom S, Goldstein SAN, Kupper J, Levitan IB. Mechanism and modulation of inactivation of Kv3 potassium channel. *Receptors and Channels.* 1993;1:81–88.
9. Patlak J B. Molecular kinetics of voltage–dependent Na channels. Physiol. Rev. 1991;71:1047–1080.
10. Hille B. Ionic channels of excitable membranes. 2nd ed., Sunderland, USA: Sinauer Ass; 1992.
11. Aldrich RW. Inactivation of voltage gated delayed potassium current in moluscan neurons. *Biophys J.* 1981;36:519–532.

CHAPTER 8

MODEL STUDIES OF CELLULAR EXCITATION

Yoram Rudy[1]

ABSTRACT

A mathematical model of the cardiac ventricular cell is used to describe ionic currents and dynamic concentration changes during a normal action potential. The model is also used to study arrhythmogenic activity of the single cell including early afterdepolarizations, delayed afterdepolarizations and rhythmic (spontaneous and triggered) activity under various degrees of calcium overload.

INTRODUCTION

Recently, we developed a mathematical model of the cardiac ventricular action potential, the L–R model [1–3], based on data from single cell and single channel preparations. The first phase in the model development [1] focused on the depolarization and repolarization phases of the action potential and concentrated on the kinetics of the following membrane ionic channels: I_{Na}, the fast sodium current; I_K, the time–dependent potassium current; I_{K1}, the time–independent potassium current; and I_{Kp}, a plateau potassium current. The dependence of the potassium currents on extracellular potassium concentration was introduced in the phase–1 model. However, this model did not account for dynamic changes in ionic concentrations and ionic fluxes during the action potential. In particular, the phase–1 model did not include pumps and exchangers that contribute to changes in ionic concentrations. It retained the Beeler and Reuter [4] formulation of the L–type calcium current and did not incorporate intracellular processes that regulate dynamically the intracellular concentration of calcium and determine the calcium transient during the action potential. The second phase in the model development [2, 3] focused on the formulation of processes that determine dynamic changes in ionic concentrations and ionic fluxes. The phase–2 model can simulate processes that regulate the dynamics of the intra–

[1]The Cardiac Bioelectricity Research and Training Center, Department of Biomedical Engineering, Case Western Reserve University, Cleveland, Ohio 44106–7207, USA.

Molecular and Subcellular Cardiology: Effects of Structure and Function
Edited by S. Sideman and R. Beyar, Plenum Press, New York, 1995

cellular calcium transient during the action potential. In addition, the model accounts for the effects of intracellular calcium changes on ionic currents (e.g. calcium–dependent inactivation of the calcium current through the sarcolemma, sodium–calcium exchange current, non–specific calcium–activated current). These properties of the model make it possible to study, using simulations, physiological phenomena that are related to the excitation–contraction coupling process in cardiac myocytes. It is also possible to simulate the behavior of the cell under conditions of calcium overload and to suggest mechanisms of related arrhythmogenic activity of the single cell such as early and delayed after–depolarizations and triggered activity.

In this chapter we use the L–R phase–2 model to describe ionic currents and concentration changes during a normal action potential and to examine the role played by these individual processes in generating the action potentials (details can be found in [2]). We also investigate cellular behavior under conditions of calcium overload and study arrhythmogenic activity of the single cell including early afterdepolarizations (EADs), delayed afterdepolarizations (DADs) and rhythmic activity. EADs and DADs are single–cell phenomena that can induce abnormal rhythmic activity and cardiac arrhythmias [5, 6]. An afterdepolarization is defined as a depolarizing after potential that occurs before (early) or after (delayed) the completion of action potential repolarization. Rhythmic activity can be spontaneous or can be triggered by pacing a quiescent cell for a certain time period. All of these arrhythmogenic phenomena involve dynamic changes in intracellular calcium such as spontaneous calcium release from the SR and activation of membrane currents through calcium–modulated processes. These processes are incorporated in our model and their complex effects (these processes interact and influence each other, in addition to their direct effect on the cell membrane) on the action potential can be simulated. Details of the afterdepolarizations and rhythmic–activity simulations can be found in [3]. Additional related studies are described in [7–9].

METHODS

Methods for computing the action potential and the formulation of underlying processes are described in [2]. A diagram of the cell model is provided in Fig. 1 (symbols are defined in the figure legend). Several important properties of the model are summarized here. (1) Based on recent data [10], activation of I_{Ca} in the model is very fast (it can be activated in 2 msec, an order of magnitude faster than in the Beeler & Reuter model). Inactivation of I_{Ca} depends on both the membrane voltage and the intracellular concentration of calcium, $[Ca]_i$. (2) Two sarcolemmal currents are activated by an increase of $[Ca]_i$. These are I_{NaCa} (sodium–calcium exchange current) and $I_{ns(Ca)}$ (non–specific, calcium activated current). The total $[Ca]_i$ – activated transient inward current, I_{TI}, is defined as the sum of these two currents: $I_{TI} = I_{NaCa} + I_{ns(Ca)}$. (3) The sarcoplasmic reticulum (SR) is divided into two compartments: network SR (NSR) and junctional SR (JSR). Calcium uptake occurs at the NSR and calcium release at the JSR. Ca^{2+} is transferred from NSR to JSR via a monoexponential translocation process with a time constant of 180 msec. (4) Calcium release from JSR can be triggered in two ways: externally by a sufficiently fast increase in total myoplasmic calcium (calcium–induced–calcium–release) or internally by calcium overloading of the JSR above a threshold level (spontaneous release). Calcium–induced–calcium–release occurs if the total myoplasmic $[Ca]_i$ (free + buffered) increases by more than 0.18 mmol/L in the first 2 msec of the action potential. (5) The model includes buffering of calcium ions both in the myoplasm (by calmodulin and troponin) and in the JSR (calsequestrin). Spontaneous calcium release from JSR occurs if more than a

threshold percentage of total calsequestrin binds with calcium ions (70% for the rat, higher for other species).

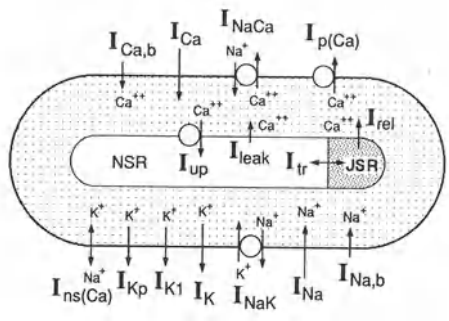

Figure 1. Schematic diagram of the L–R single ventricular cell model. I_{Na}: fast sodium current; I_{Ca}: L–type calcium current; I_K: delayed rectifier potassium current; I_{K1}: inward rectifier potassium current; I_{Kp}: plateau potassium current; I_{NaK}: sodium–potassium pump current; I_{NaCa}: sodium–calcium exchange current; $I_{p(Ca)}$: calcium pump in the sarcolemma; $I_{Na,b}$: sodium background current; $I_{Ca,b}$: calcium background current; $I_{ns(Ca)}$: non–specific calcium–activated current; I_{up}: calcium uptake from myoplasm to network sarcoplasmic reticulum (NSR); I_{rel}: calcium release from junctional sarcoplasmic reticulum (JSR); I_{leak}: calcium leakage from NSR to myoplasm; I_{tr}: calcium translocation from NSR to JSR. Dotted areas indicate presence of calcium buffers. For details, see [2]. (From [2], by permission of the American Heart Association, Inc.).

RESULTS

Ionic Currents and Concentration Changes during the Action Potential

Figures 2, 3 and 4 depict the simulated time course of selected processes during an action potential. Figure 2 shows major ionic currents that determine the shape of the action potential. For the purpose of presentation, all time–independent currents are lumped together and represented as I_v (panel E); $I_v = I_{NaK} + I_{K1} + I_{Kp} + I_{Na,b} + I_{Ca,b} + I_{p(Ca)}$. Once the cell is excited by a suprathreshold stimulus, I_{Na} depolarizes the membrane with a maximum rate $(dV/dt)_{max}$ of 388 V/sec to the overshoot potential of 46.5 mV (see Fig. 2) and inactivates immediately. Subsequently, I_{Ca} is activated to support the action potential plateau against the repolarizing currents I_v (determined mostly by I_{Kp} at this range) and I_K. I_{Ca} reaches its peak value of −6.27 μA/μF in 3.23 msec after the onset of stimulation, while I_{Na} reaches its (much larger) peak value of −380 μA/μF in 1 msec, a time when I_{Ca} is still very small (−0.97 μA/μF). Therefore, the early peak of I_{Ca} contributes very little to the rising phase of the action potential. However, the early peak of I_{Ca} determines the cumulative calcium entry 2 msec after $(dV/dt)_{max}$, and, in turn, the release of Ca^{2+} from the JSR and the resulting $[Ca]_i$ transient (see below). Finally, the large increase of the delayed I_K together with I_v that operates at its negative slope range (peak I_v at about 180 msec, contributed by I_{K1}) repolarizes the membrane to the resting potential. In the last panel of Fig. 2, I_{NaCa} has almost zero contribution during most of the action potential plateau, but is activated during the late plateau and repolarization phases to extrude calcium ions out of the cell [11]. Note that at the late repolarization phase I_{Ca} is inactivated, while I_{NaCa} is activated and slows down the rate of membrane repolarization [12]. The action potential duration is about 180 msec, in the measurement range of 207±31 msec [13] and close to the value of 184.6 msec estimated from the experimental results of Doerr *et al.* [12].

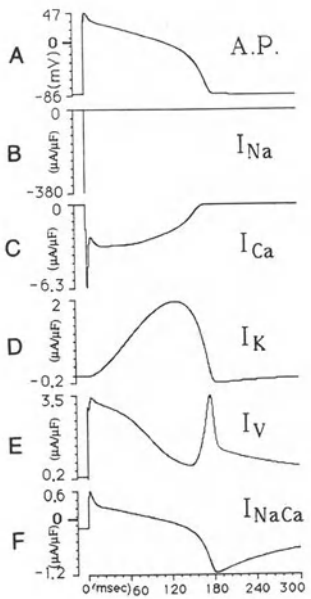

Figure 2. Major ionic currents that determine the shape of the action potential. (From [2], by permission of the American Heart Association, Inc.). Symbols are defined in Fig. 1.

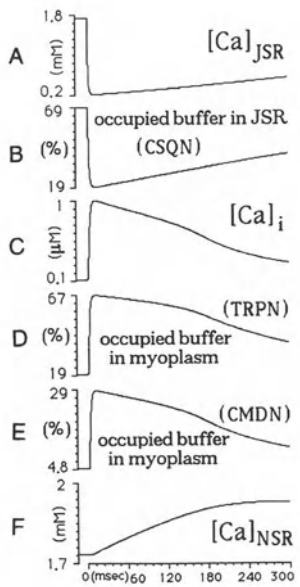

Figure 3. Calcium concentration changes in the myoplasm and in the SR during an action potential. **A:** free calcium in JSR; **B:** calcium buffered by CSQN (calsequestrin) in JSR **C:** free calcium in myoplasm ("the calcium transient"); **D, E:** calcium buffered by TRPN (troponin) and CMDN (calmodulin), respectively, in myoplasm; **F:** calcium in NSR. (From [2], by permission of the American Heart Association, Inc.).

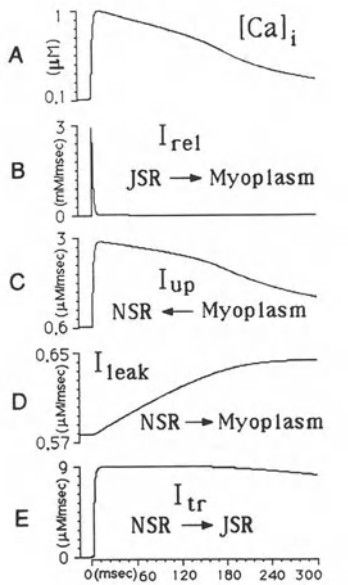

Figure 4. Calcium fluxes during an action potential. **A:** free calcium in myoplasm ("the calcium transient"); **B:** calcium release by JSR; **C:** calcium uptake by NSR; **D:** calcium leakage from NSR; **E:** calcium translocation from NSR to JSR. (From [2], by permission of the American Heart Association, Inc.).

Figures 3 and 4 describe the processes that regulate calcium concentration in the cell. In Fig. 3, cumulative calcium entry of 0.375 μM 2 msec after $(dV/dt)_{max}$ results in an increase of $[Ca]_i$ from 0.12 μM to only 0.1235 μM due to the buffering of calcium in the myoplasm. The calcium entry triggers the release of calcium ions from the JSR into the myoplasm (upper two panels) following the kinetics of the CICR process. The total amount of calcium ions released is 6.37 mM (based on the small volume of the JSR), which is equivalent to 45 μM in the large volume of the myoplasm. The value of 6.37 mM released by the JSR is made up of 1.53 mM of free Ca^{2+} and 4.84 mM of Ca^{2+} buffered by CSQN (calsequestrin), demonstrating the importance of buffering in the JSR to increase its calcium storage capacity. Due to the large capacity buffers in the myoplasm, 97.8% of the released calcium ions are buffered (71.7% by TRPN (troponin) and 26.1% by CMDN (calmodulin)), resulting in a peak $[Ca]_i$ transient of 1 μM (panel C). These simulated results demonstrate the importance of the myoplasm buffers in maintaining the low level of $[Ca]_i$. Throughout the action potential, calcium ions enter the NSR by the uptake process, increasing calcium concentration in the NSR from 1.73 mM to 1.92 mM (last panel). Figure 4 depicts the movement of calcium ions inside the cell. As indicated in panel B, the calcium ions are released from the JSR into the myoplasm as a spike with a peak rate of 3 mM/msec, then reenter the NSR (panel C) with a maximum uptake rate of 2.6 μM/msec, resulting in a net loading of calcium ions into the NSR as shown in Fig. 3, panel F. Finally, the calcium ions that loaded the NSR are translocated into the JSR with a rate of 0.86 μM/msec (last panel), and, therefore, the calcium content of the JSR increases, as shown in Fig. 3, panels A and B.

Delayed Afterdepolarizations Under Normal Conditions (no calcium overload)

Two delayed afterdepolarizations (DAD) are observed in Fig. 5, where the cell is paced by a train of stimuli at BCL=400 msec for 11 beats, and the pacing is terminated. These two DADs are associated with spontaneous calcium release (panel B) from the overloaded JSR (panel F). As shown in panel E, NSR is loaded with calcium ions to 2.42 mM at the last paced beat (full arrow). Then, translocation of calcium from the NSR loads the JSR (panel F). When JSR is loaded up to the 70% threshold of buffered CSQN, spontaneous calcium release occurs, bringing about an increase of $[Ca]_i$ (panel B). This increase in $[Ca]_i$ activates both the sodium–calcium exchanger (I_{NaCa}, panel C) and the non-specific, calcium activated current ($I_{ns(Ca)}$, panel D). These two depolarizing currents result in the DADs shown in panel A (arrows). Note that $[Ca]_{NSR}$ decreases monotonically towards its resting level (panel E) as a result of calcium extrusion by I_{NaCa}. After two episodes of spontaneous calcium release, $[Ca]_{NSR}$ is reduced to almost its resting value of 1.73 mM. As a result, JSR can not be overloaded to the threshold level and additional episodes of spontaneous release can not occur. Under the simulated normal conditions, the peak $[Ca]_i$ transient caused by one spontaneous calcium release is only 0.54 μM, and, $I_{ns(Ca)}$ is only partially activated (about one twelfth of its fully-activated value). Therefore, its amplitude is only −0.49 μA/μF, less than one half the I_{NaCa} amplitude of −1.13 μA/μF. This means that I_{NaCa} is more important than $I_{ns(Ca)}$ in generating the DAD under normal conditions. Note that during the pacing period peak $[Ca]_i$ transient (panel B) increases monotonically from 0.68 μM (second beat) to 0.8 μM (last driven beat). This reflects the loading of NSR (panel E) that, through the translocation process, provides more calcium ions for release from the JSR.

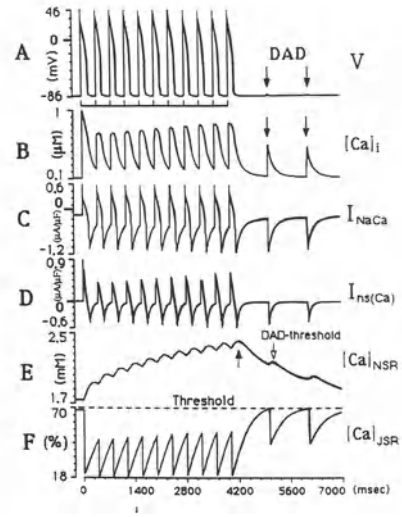

Figure 5. Delayed afterdepolarizations (DADs) following pacing under normal conditions. Pacing at BCL=400 msec. Spontaneous SR calcium release occurs twice (arrows in panel **B**) to generate two DADs (arrows in panel **A**). The amplitude of I_{NaCa} during the DADs is more than twice the $I_{ns(Ca)}$ amplitude. DAD-threshold (empty arrow in panel **E**) is defined as the value of $[Ca]_{NSR}$ that generates a single DAD. **A:** membrane potential; **B:** calcium in myoplasm; **C:** sodium-calcium exchange current; **D:** non-specific, calcium activated current; **E:** calcium in NSR; **F:** calcium content of JSR (threshold for spontaneous release is at 70% as indicated). (from [3], by permission of the American Heart Association, Inc.).

Early and Delayed Afterdepolarizations (minimum calcium overload)

We create conditions of minimum calcium overload by setting $[Ca]_i$ = 0.3 μM at the resting state (normal value is 0.12 μM). As a result of the overload, the first action potential shown in Fig. 6A is generated by spontaneous calcium release, and is followed by an EAD (early afterdepolarization) and a DAD before a stimulus (indicated by a vertical bar at the bottom of panel A) is applied. Peak $I_{ns(Ca)}$ associated with the initiation of the spontaneous action potential is only 0.6 μA larger than peak I_{NaCa} (panel E). Therefore, under minimum overload conditions, both currents are equally important for the generation of a spontaneous action potential, although $I_{ns(Ca)}$ is somewhat larger. The EAD at the plateau phase of the spontaneous action potential (takeoff at −21.6 mV with amplitude of 19.4 mV) is generated by the double-peak behavior of the L-type calcium current, I_{Ca} ("*" in panel C) in contrast to the single-peak (normal) behavior of I_{Ca} ("#" in panel C) for the action potential elicited by the stimulus. This comparison clearly demonstrates that secondary activation of I_{Ca} during the action potential generates the plateau EAD.

By applying a stimulus at the decaying phase of the first DAD (Fig. 6A), an action potential is elicited. Following this action potential, a DAD of a relatively large amplitude is generated, followed by additional four DADs of monotonically decreasing amplitudes (Fig. 6A). This decrease in amplitude of the subsequent DADs was also observed experimentally by Stern *et al.* [14]. Note that, in contrast to the plateau EAD, the DADs do not involve I_{Ca} at all (panel C) but result from the depolarizing currents $I_{ns(Ca)}$ and I_{NaCa} (panel D and panel E, respectively).

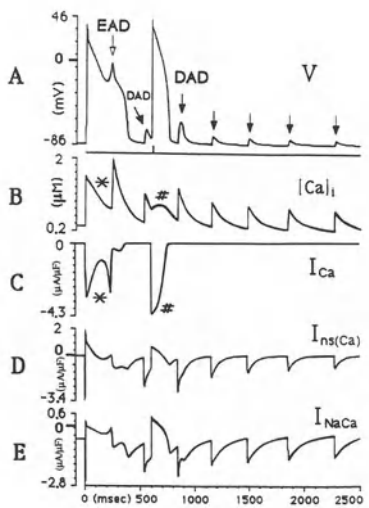

Figure 6. Cellular responses under minimum calcium–overload. EAD – early afterdepolarization; DAD – delayed afterdepolarization (from [3], by permission of the American Heart Association, Inc.).

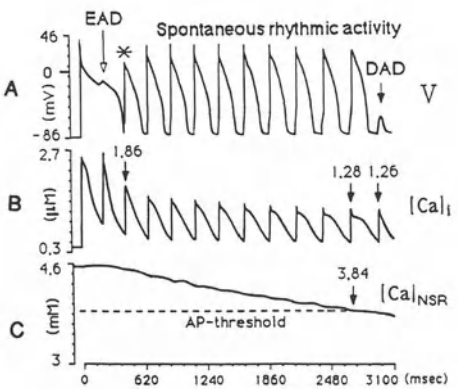

Figure 7. Spontaneous rhythmic activity under high calcium–overload. Rhythmic activity (panel **A**) is generated by a series of spontaneous calcium–release events (panel **B**) before the degree of overload is decreased below the threshold for generating an action potential (panel **C**; AP–threshold). (From [3], by permission of the American Heart Association, Inc.).

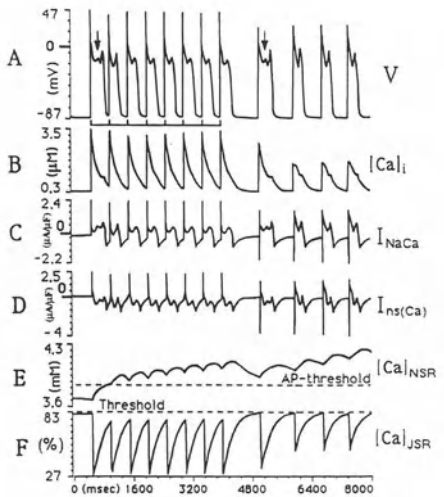

Figure 8. Triggered activity under maintained calcium overload. Note that threshold for spontaneous calcium release is set at 82.5% (panel **F**). See text for details. (From [3], by permission of the American Heart Association, Inc.).

Spontaneous Rhythmic Activity (high calcium overload)

In the case of high level calcium overload conditions (resting $[Ca]_i$ is set at 0.4 μM in the model), we observe spontaneous rhythmic activity resulting from spontaneous calcium release from the JSR (Fig. 7). Except for the first action potential that is elicited from the resting state, all other action potentials display a very short duration (short APD) and the basic cycle length of the rhythmic activity increases monotonically until failure occurs and a DAD is observed. The short APD implies small total calcium entry into the cell during the action potential. As a result of the increased imbalance between calcium extrusion by I_{NaCa} and the reduced calcium entry, $[Ca]_{NSR}$ decreases monotonically (except for the long-duration first action potential) until the rhythmic activity ceases and a DAD is observed.

Triggered Activity with Maintained Calcium Overload Conditions

In Fig. 5, spontaneous SR calcium release occurred as a result of pacing under normal conditions (no calcium overload). In that particular simulation, JSR threshold for spontaneous release was set at a low level of 70%; low threshold for release is known to exist in the rat. If we set a higher threshold of 82.5%, spontaneous release does not occur under normal conditions (this behavior is typical of dog and guinea pig myocytes). With the higher threshold, the cell maintains calcium overload conditions but remains quiescent. We pace the cell under these conditions to investigate the possibility of triggered activity. As shown in Fig. 8, the cell is paced with a train of eight stimuli (vertical bars at bottom of panel A) at a BCL=500 msec. Following the last paced beat, a triggered action potential is generated. It is generated by spontaneous calcium release from the SR (panels B and F), the same mechanism as we described previously for DADs. The subsequent triggered action potentials are elicited earlier and earlier (shorter coupling intervals) due to the increase of $[Ca]_{NSR}$ (panel E). The rhythm becomes faster and faster until a dynamic steady state is reached. Note that the level of $[Ca]_{NSR}$ after the pacing period (panel E) is always above the AP-threshold. Therefore, sustained triggered activity is maintained by spontaneous calcium release.

CONCLUSIONS

The L-R model of the mammalian ventricular action potential was used to examine electrophysiological processes during the normal action potential and cellular behavior during abnormal arrhythmogenic activity. The model is based mostly on the guinea pig ventricular cell but provides the framework for modeling other types of ventricular cells with appropriate modifications made to account for species differences. The formulation integrates many individual processes (e.g. ionic currents, SR calcium release, calcium buffering, etc.) into a model of the cell that can be used to study possible interactions between these components and to simulate the resulting qualitative cellular behavior.

The time course of selected ionic currents and concentration changes during an action potential were described and depicted in Figs. 2 to 4. It is clear from the simulations that in spite of its fast activation relative to the B-R model, I_{Ca} does not contribute significantly to the rising phase of the action potential. However, the early peak of I_{Ca} is important since it determines the magnitude of early calcium-entry into the cell and, in turn, the release of calcium from the SR and the $[Ca]_i$-transient. It is interesting to note that $[Ca]_i$ inactivates I_{Ca} through the $[Ca]_i$-dependent inactivation process. This suggests

a negative feedback control mechanism by which the early I_{Ca}-peak influences the inactivation of I_{Ca}. The $[Ca]_i$-transient also influences other currents such as I_{NaCa} and, under certain conditions, $I_{ns(Ca)}$. The simulations demonstrate the importance of buffering processes in the myoplasm in controlling cellular calcium and, therefore, in regulating these currents. A related observation is that I_{NaCa} does not contribute significantly during most of the plateau, but influences the rate of membrane repolarization during the repolarization phase and, consequently, the action potential duration. This simulated behavior is in agreement with the experimental observation of Doerr *et al.* [12].

Various patterns of arrhythmogenic activity, simulated using the L-R model, are depicted in Figs. 6 to 8. These include DADs, rhythmic activity (both spontaneous and triggered) and EADs. The simulations support the hypothesis that the underlying mechanism of DADs and of rhythmic activity in mammalian ventricular cells is spontaneous calcium release from the overloaded JSR. When spontaneous calcium release occurs, the $[Ca]_i$ transient reaches its peak value quickly and activates a transient inward current, I_{TI}. This, in turn, generates a DAD or an action potential. Two different calcium-activated membrane processes can potentially contribute to I_{TI}. These are I_{NaCa}- the sodium-calcium exchanger and $I_{ns(Ca)}$- a non-specific, calcium-activated channel. The relative contribution of these processes to I_{TI} (and therefore their relative importance to arrhythmogenesis) is still a matter of controversy. Experimentally it is difficult to separate these two components. An important result of the simulations is that the relative importance of I_{NaCa} and $I_{ns(Ca)}$ depends on the degree of calcium overload. For DADs that develop following pacing under normal conditions (Fig. 5), I_{NaCa} is the major component of I_{TI}. Under conditions of minimum calcium overload (Fig. 6) and high calcium overload (Fig. 7), both I_{NaCa} and $I_{ns(Ca)}$ are equally important in their contribution to I_{TI}. During the triggered activity simulated in Fig. 8, $I_{ns(Ca)}$ is the major component of I_{TI} and is more important than I_{NaCa} to the generation of sustained triggered activity.

The simulations suggest that DADs and EADs do not share a common mechanism. EADs at plateau potentials are generated by recovery from inactivation and reactivation of I_{Ca} during the action potential (Fig. 6). Unlike DADs, EADs do not involve spontaneous calcium release from the SR and activation of I_{NaCa} and/or $I_{ns(Ca)}$. This conclusion is consistent with experimental observations that also suggest that I_{Ca}, and not SR release, underlies the generation of plateau EADs [15, 16].

Acknowledgment

This study was supported by the National Institutes of Health, Grant #HL-49054 (National Heart, Lung and Blood Institute), USA.

DISCUSSION

Dr. H. Fozzard: I am puzzled over the EAD mechanisms in terms of the voltage dependence of recovery of the current, so that it can be reactivated, versus the decline in intracellular calcium, as the SR takes up calcium and recovery as a result of removal of calcium. Can you talk about the balance of those two phenomena?

Dr. Y. Rudy: Both voltage-dependent and calcium-dependent inactivation processes are important in the model. The removal of calcium brings about recovery of the fCa inactivation gate. As shown in conjunction with the Bay K8644 simulations, fCa recovers faster than the voltage-dependent

inactivation. When the action potential is prolonged, the calcium-dependent inactivation gate starts to recover first. This is followed by slower recovery of the voltage-dependent inactivation gate and reactivation of the activation d-gate, leading to EAD formation (detailed plots of these kinetics can be found in Figure 4, reference 9 of this chapter). Since the voltage-dependent recovery is the slowest process, it is also the time-limiting process and, therefore, is reflected in most experiments that study the characteristics of EAD formation. Fast recovery of the calcium-dependent inactivation is necessary, however, for the generation of EADs.

I should mention an important limitation of the model. It does not incorporate inhomogeneities of calcium concentration in the cell. That is, we do not represent the local calcium concentration in restricted spaces, at the mouth of the L-type calcium channel, or the geometrical relationship of the SR release sites to the L-type calcium channel or to the sodium-calcium exchanger. At present, there is not enough known experimentally with sufficient resolution, and I hope to hear more about it from Gil Wier's presentation of recent work in his laboratory. Confocal microscopy may describe how calcium is divided in the cell in terms of restricted spaces, proximity to SR release sites, L-type modulation sites and so on. These properties are difficult to simulate because one has to formulate restricted diffusion and to incorporate very intimate knowledge of the submicro organization of the cell. We have started to think how this can be accomplished but it will require a major effort and additional experimental data that are not available at the present time.

Dr. H. Fozzard: Whose experimental work did you use to formulate the voltage and calcium-dependent inactivation processes in your model?

Dr. Y. Rudy: The way the model was constructed was to first formulate and test every component individually based on published experimental data. Only then were the various components allowed to interact in a model of the entire cell where, again, the behavior was tested in comparison to experiments. This is also true for the L-type calcium current and its voltage-and calcium-dependent inactivation kinetics. A detailed discussion, including references to the extensive experimental literature that we have used to formulate the kinetics of ICa, is provided in our original publication of the model [2].

Dr. E. Marban: I was always very skeptical about the idea that calcium currents would recover from inactivation during the decline of the calcium transient because what was known about the calcium current and calcium transients under conditions of normal calcium loading was that the calcium current apparently entered some inactivated state despite the fact that calcium returned to baseline. Karen Sippito, Gert Calloran and Edward Carmeliet have a paper in press in *Circ Res* which shows that in calcium overload you actually do get this recovery phenomenon.

Dr. Y. Rudy: I have heard about these recent results. It is very consistent with the fact that calcium changes do contribute to the control of the calcium current. But the exact kinetics depend on local calcium concentrations.

Dr. H. ter Keurs: Most of the DADs that you have described that can be generated in single cells require rather unscrupulous interventions, raising the calcium levels. I would like to comment on one of the types of DADs that we have observed in muscle following focal damage. I think that it may be relevant to the situation in real hearts in real life, although very late in life. Focal damage causes local release of calcium during the relaxation phase of the normal contraction, which then causes a process of propagated calcium release throughout a preparation which otherwise is not calcium overloaded. There are various means of interrupting such a propagated process, showing that it is not a matter of calcium overload of the general preparation. I agree with Dr. Fozzard that you have made plenty of assumptions already. Could you speculate what happens if you put two cells in series and cause local calcium release in one cell, what is going to happen in the other cell?

Dr. Y. Rudy: We have incorporated the cell model into a propagating mode in a series of cells that are connected by models of gap junctions. We have looked at propagation during ischemic condi-

tions for example, but not at propagated EADs or DADs. I can only speculate that loading the afterdepolarizing cell with another coupled cell (or cells) will interfere with EAD or DAD formation. This is because the coupled cell will create a sink that will take current away from the afterdepolarizing cell. It will probably take a certain degree of cellular uncoupling for EADs or DADs to develop and to propagate. But, reduced coupling exists during pathology and damage (e.g. ischemia and infarction), favoring the formation and propagation of EADs and DADs under these conditions. Your suggestion that focal, rather than global, calcium overload is sufficient for afterdepolarizations to occur and propagate is consistent with the model behavior since EAD and DAD formation is a single-cell phenomenon that requires only local conditions to exist. Of course, EADs and DADs can be arrhythmogenic in many other ways, without propagating and capturing the tissue. For example, they can prolong action potential and refractoriness regionally, creating conditions that favor the initiation of reentry.

REFERENCES

1. Luo CH, Rudy Y: A model of the ventricular cardiac action potential, depolarization, repolarization, and their interaction. *Circ Res.* 1991; 68: 1501–1526.
2. Luo CH and Rudy Y: A dynamic model of the cardiac ventricular action potential I: Simulations of ionic currents and concentration changes. *Circ Res.* 1994; 74: 1701–1096.
3. Luo CH and Rudy Y: A dynamic model of the cardiac ventricular action potential II: Afterdepolarizations, triggered activity, and potenitation. *Circ Res.* 1994; 74: 1097–1113.
4. Beeler GW, Reuter H: Reconstruction of the action potential of ventricular myocardial fibres. *J Physiol (Lond).* 1977; 268: 177–210.
5. Cranefield PF, Aronson RS: *Cardiac Arrhythmias: The Role of Triggered Activity and Other Mechanisms.* Futura Publishing Company, Inc., New York, USA, 1988.
6. Rosen MR: The concept of afterdepolarization. In: *Cardiac Electrophysiology: A Textbook* (Rosen MR, Janse MJ, and Wit AL, editors). Futura Publishing Co., New York. 1990; Chapter 3: 267–282.
7. Zeng J, Rudy Y.: Simulation studies of the mechanism of arrhythmogenic early afterdepolarizations in cardiac myocytes. 38th Annual Meeting of The Biophysical Society. *Biophys J.* 1994;66:A322.
8. Zeng J, Rudy Y: Simulation studies of the rate dependence mechanism of early and delayed afterdepolarizations. *FASEB J.* 1994;6:A77.
9. Zeng J, Rudy Y. Early afterdepolarizations in cardiac myocytes: Mechanism and rate dependence. *Biophys J.* 1995; in press.
10. Isenberg G, Klockner U: Calcium current of isolated bovine ventricular myocytes are fast and of large amplitude. *Pflugers Archiv.* 1982; 395: 30–41.
11. Campbell DL, Giles WR, Robinson K, Shibata EF: Studies of the sodium–calcium exchanger in bull–frog atrial myocytes. *J Physiol (Lond).* 1988; 403: 317–340.
12. Doerr T, Denger R, Doerr A, Trautwein W: Ionic currents contributing to the action potential in single ventricular myocytes of the guinea pig studied with action potential clamp. *Pflugers Archiv.* 1990; 416: 230–237.
13. Priori SG, Corr PB: Mechanisms underlying early and delayed afterdepolarizations induced by catecholamines. *Am J Physiol.* 1990; 258: H1796–H1805.
14. Stern MD, Capogrossi MC, Lakatta EG: Spontaneous calcium release from the sarcoplasmic reticulum in myocardial cells: mechanisms and consequences. *Cell Calcium.* 1988; 9: 247–256.
15. Marban E, Robinson SW, Wier WG: Mechanisms of arrhythmogenic delayed and early afterdepolarizations in ferret ventricular muscle. *J Clin Invest.* 1986; 78: 1185–1192.
16. January CT, Riddle JM: Early afterdepolarizations: mechanism of induction and block, a role for L-type Ca^{2+} current. *Circ Res.*1989; 48: 720–727.

Intracellular Calcium and Muscle Function:

SR and Filaments

CHAPTER 9

CONFOCAL MICROSCOPY REVEALS LOCAL SR CALCIUM RELEASE IN VOLTAGE-CLAMPED CARDIAC CELLS

Withrow Gil Wier[1]

ABSTRACT

Confocal microscopy during voltage-clamp depolarization of mammalian heart cells revealed distinct local $[Ca^{2+}]_i$-transients that resulted from Ca^{2+} released through sarcoplasmic reticulum (SR) release channel(s). When voltage was varied, the latency to occurrence and the relative probability of local $[Ca^{2+}]_i$-transients varied as predicted if SR Ca^{2+}-release is linked tightly to Ca^{2+} flux through co-associated L-type Ca^{2+}-channels.

INTRODUCTION

Conventionally, excitation-contraction (EC) coupling in the heart has been studied by observing 'whole-cell' $[Ca^{2+}]_i$-transients and whole-cell Ca^{2+}-currents [1, 2]. Such studies have failed to resolve the central paradox of EC coupling in the heart: how can the relatively small amount of Ca^{2+} that enters the cell via L-type Ca^{2+}-channels both activate and control the release of a much larger amount of Ca^{2+} from the SR. Recently, Stern [3] has recognized that the solution to this paradox may lie in the concept of a microscopic 'coupling' between individual L-type Ca^{2+}-channels and SR release channels (or ryanodine receptors, RyR), perhaps arranged in 'clusters'. Briefly, if such 'clusters' are *functionally* independent and are 'recruited' by Ca^{2+} that enter via co-associated L-type Ca^{2+}-channels then control of SR release by Ca^{2+}-current is gained, since the flux from one cluster would not activate or influence flux from another. This view of EC coupling has been termed 'local control'[3]. We have already suggested [4] that, in addition to the open probability of L-type Ca^{2+}-channels (P_o), the amplitude of the single L-type Ca^{2+}-channel current (i) was an important determinant of the peak rate of release of Ca^{2+} from the SR, since Ca^{2+}-

[1]Department of Physiology, University of Maryland at Baltimore, 655 West Baltimore St., Baltimore, MD 21201, USA.

Molecular and Subcellular Cardiology: Effects of Structure and Function
Edited by S. Sideman and R. Beyar, Plenum Press, New York, 1995

currents comprised of relatively few large single-channel currents (i.e. those in which P_o is low, but i is large) are much more efficacious in activating SR Ca^{2+}-release than Ca^{2+}-currents comprised of a relatively large number of small single-channel currents (i.e. those in which P_o is high, but *i* is small). From similar (indirect) studies, others [5] have recently concluded that the rate of SR Ca^{2+}-release is determined by the time and voltage-dependent opening of L-type Ca^{2+}-channels after depolarization. In the present manuscript I present more direct evidence for this view of EC coupling, through the use of confocal microscopy to observe directly local $[Ca^{2+}]_i$-transients that are the result of SR Ca^{2+}-release.

METHODS

Two-month old Wistar rats were anaesthetized with sodium pentobarbitone (17 mg /kg injected intra-peritoneally) and hearts were removed from the animal via midline thoracotomy. Single ventricular cells were obtained by an enzymatic dispersion technique described in detail previously [6]. The external solution used during giga-seal formation, break-in, and voltage-clamp recordings was comprised of the following (in mM): NaCl, 140; dextrose, 10; HEPES, 10; CsCl, 10; $MgCl_2$, 1; $CaCl_2$, 1; pH adjusted to 7.3-7.4 with NaOH. When necessary, ryanodine (50.0 μM) was added to this solution. The electrode filling solution composed of (mM): NaCl, 12.0; Cs-glutamate, 130; HEPES, 10; TEA-Cl, 20; $MgCl_2$, 0.33; Mg-ATP,4; Fluo-3, (pentapotassium salt), 0.1; pH adjusted to 7.1-7.2 with CsOH. The holding potential was usually -40 mV and all experiments were performed at room temperature (21-23°C). When filled, micro-pipette electrodes had resistances of 1.5-2.5 Mohms. Voltage clamp was performed with an Axopatch 1B clamp amplifier (Axon Instruments Inc., Foster City, CA). Current was filtered at 5 kHz and digitized at 1 kHz with 12-bit resolution.

As described in detail elsewhere [7] and briefly reiterated here, cells were studied in a recording chamber mounted on the stage of a Nikon Diaphot TMD inverted microscope (Nikon Inc. Melville, NY) to which a Bio-Rad MRC-600 confocal imaging system was attached (Bio-Rad, Microscience Division, Herts, U.K.). Fluo-3 fluorescence was excited with light at 488 nm (25 mW argon-ion laser, attenuated intensity to 10%) and measured at wavelengths greater than 515 nm. The objective lens was a plan-apo, oil-immersion lens of magnification 60 and n.a. of 1.4 (Nikon Inc.). The imaging system was operated in the 'line scan' mode with the control micrometer of confocal aperture set to two (small) divisions. Analog recording of fluorescence intensity during one scan was digitized into 768 pixels, giving pixel dimensions of 0.271 μm and 2.60 μs. If, under these conditions, the optical section ('z' axis) is approximately 1.0 μm, and the point being scanned is limited by diffraction at 1. 0 mm, then the volume from which fluorescence is detected and represented by a single pixel in the line will be approximately 1.0 μm^3. Although each pixel nominally represents fluorescence over 0.271 μm of scan line, it actually also contains fluorescence arising from points as far away as 1.0 μm.

For the quantification of 'local $[Ca^{2+}]_i$-transients' within the cell, the intensity levels of four selected adjacent pixels along a scanned line were averaged. The specimen was scanned 512 times at 2.0 ms per scan; this provided a record of $[Ca^{2+}]_i$ detected in a region of approximately 2.0 μm^3 (4 pixels, convolved with 1.0 μm spot) with a temporal resolution of 2.0 ms/point, over 1.024 s. $[Ca^{2+}]_i$-transients were also computed from the entire volume scanned. These $[Ca^{2+}]_i$-transients are referred to as the 'line $[Ca^{2+}]_i$-transients'. In this case, the intensity levels of all the pixels along the scanned line were averaged. $[Ca^{2+}]_i$ was calculated from the fluo-3 fluorescence through the use of a 'pseudo-ratio' using an

equation and calibration parameters given previously [8]. Computations and image analysis were performed on an IBM Risc System/6000 workstation (IBM Corp., Armonk NY) using the software, IDL (Research System, Inc., Boulder, CO).

RESULTS

Calcium Sparks

Confocal microscopy has recently been used to observe, in unstimulated heart cells, *spontaneous, non-propagating* local changes in $[Ca^{2+}]_i$, termed 'Ca^{2+}sparks' [8]. Ca^{2+}-sparks result from release of Ca^{2+} through SR Ca^{2+}-release channels and they can trigger propagating Ca^{2+}-waves, probably when the SR is highly loaded with Ca^{2+}. Ca^{2+}-sparks are of substantial interest because they represent release of Ca^{2+} from the SR, but under conditions in which this release does not feedback to cause further release and the propagation of a Ca^{2+} wave. Also, it has been hypothesized that such calcium sparks can also be evoked by electrical activity and thus form the basis for EC coupling [7-9]. Examples of Ca^{2+}-sparks recorded with our confocal imaging system (MRC-600, Bio-Rad Microscience Division, Herts, UK) are presented in Fig. 1 [10].

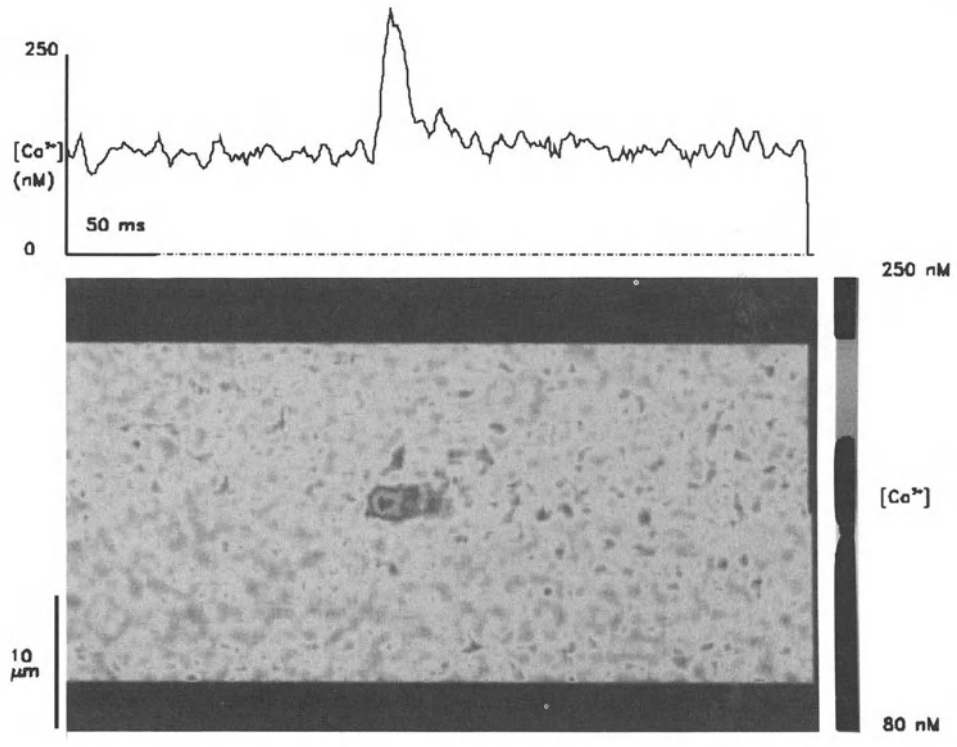

Figure 1. A Ca^{2+}-spark obtained in a rat ventricular myocyte perfused internally with fluo-3 (100 mM). The holding potential was -40 mV. The confocal line-scan image is shown at the bottom. Upper recording represents the time course of the spatial average $[Ca^{2+}]_i$ over the entire length of cell scanned, recorded at the sites indicated by the short white lines marked correspondingly in the line-scan image. (The line extends through the center of the calcium spark). Data reproduced from [10] with permission.

Confocal $[Ca^{2+}]_i$-Transients

Confocal microscopy of $[Ca^{2+}]_i$ in heart cells has the potential to reveal spatial heterogeneity of $[Ca^{2+}]_i$ during EC coupling, should it actually exist, just as it revealed the spontaneous calcium sparks. Figure 2 illustrates $[Ca^{2+}]_i$-transients recorded with confocal microscopy during EC coupling. The striking finding is that there are local calcium transients that are distinctly different from the whole-cell, or spatial average calcium transient [7]. In addition, the local calcium transients occurring during EC coupling have elements in them that appear identical to the spontaneous calcium sparks in Fig. 1. In addition, our previously published results [7] illustrate that $[Ca^{2+}]_i$-transients studied in this way exhibit the graded, (i.e. 'controlled') release of Ca^{2+} in response to Ca^{2+}-current and other phenomena established previously using whole cell recording techniques in mammalian cardiac cells.

Confocal $[Ca^{2+}]_i$-Transients in the Presence of L-Type Ca^{2+}-Channel Block

Because local calcium transients seem to occur at quite high frequency during strong depolarizations (i.e. > -30 mV), we reduced the probability of local calcium transients by applying a blocker of L-type Ca^{2+}-channels, such as cadmium ions or verapamil. In the presence of verapamil (10 μM), local $[Ca^{2+}]_i$-transients were evoked at most clamp-pulse

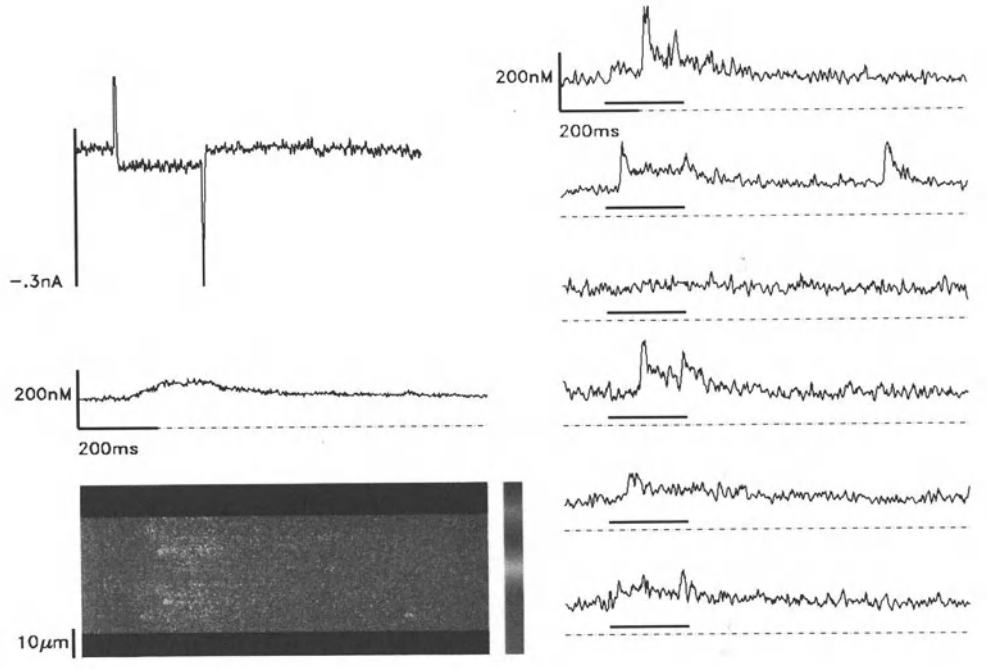

Figure 2. Confocal $[Ca^{2+}]$i-transients and Ca^{2+}-currents in a voltage-clamped rat ventricular myocyte perfused internally with fluo-3 (100 mM). This figure illustrates that local $[Ca^{2+}]$i -transients in subcellular regions during EC coupling are distinct from each other and from the spatial average $[Ca^{2+}]$i -transient. The cell was depolarized for 200 ms from a holding potential of -40 mV to -30 mV. Traces on right are individual 'line $[Ca^{2+}]$i-transients', obtained at different places from the line-scan image (left bottom) as described in Ref. [7]. The Ca^{2+}-current, the plot of average $[Ca^{2+}]$i (whole-cell $[Ca^{2+}]$i-transient) have been aligned temporally on the left with the line-scan image. Whole-cell and local $[Ca^{2+}]_i$-transients: - 30 mV.

voltages. A preliminary report of this work has appeared [11]. At this concentration of verapamil, the whole-cell Ca^{2+}-currents were too small to be measured reliably against the background of other ionic currents, although single L-type Ca^{2+}-channel activity would have been expected to be present at a very low level. The local $[Ca^{2+}]_i$-transients were similar to those we observed previously [7] as a result of small clamp-pulse depolarizations in the absence of verapamil, and to those observed by others during action potentials in the presence of the Ca^{2+}-channel blocker, Cd^{2+} [8, 9]. The voltage-clamp pulse protocol, which consisted of repetitive pre-pulses to a positive potential followed by the test pulse was designed to ensure both uniform loading of the SR via 'reverse mode' Na/Ca exchange at positive potentials (16) and a constant level of 'use-dependent' block of the Ca^{2+}-current by verapamil. The local $[Ca^{2+}]_i$-transients under these conditions are the result of Ca^{2+} released from the SR, since local $[Ca^{2+}]_i$-transients were never observed in the presence of ryanodine (data not shown).

If local $[Ca^{2+}]_i$-transients are evoked by the opening of L-type Ca^{2+}-channels, then the waiting time histogram of evoked local $[Ca^{2+}]_i$-transients under the low-probability conditions used in these experiments should be explicable in terms of L-type Ca^{2+}-channel gating. It has recently been suggested that 'release units' or 'clusters' of RyRs are activated by the *first* opening of an L-type Ca^{2+}-channel (10). This prediction was tested by measuring the latencies of evoked local $[Ca^{2+}]_i$-transients at different clamp-pulse potentials. Most local $[Ca^{2+}]_i$-transients were evoked within the first 40 ms (the first two bins). At pulse voltages between -20 mV and +10 mV, the numbers of evoked local $[Ca^{2+}]_i$-transients declined sharply with time and the latency histograms could be fit by exponentially declining functions. At more negative and more positive clamp-pulse potentials, exponential fitting of the data was uncertain, but the histograms clearly fell more slowly than at the intermediate potentials.

As described above, it is clear that the probability of evoking local $[Ca^{2+}]_i$-transients is both a function of time and voltage. To test the effect of voltage on the size of local $[Ca^{2+}]_i$-transients, the peak amplitudes of the local $[Ca^{2+}]_i$-transients were measured as a function of clamp-pulse potential. No effect of clamp-pulse potential on amplitude could be detected.

A controversial issue, important to the mode of control' of EC coupling, has been whether Ca^{2+} entering cells via 'reverse mode' Na/Ca exchange can also trigger SR Ca^{2+} release [12]. To investigate this issue, we voltage-clamped cells for 200 ms to membrane potentials as high as +100 mV, at which potential entry of Ca^{2+} via 'reverse mode' Na/Ca exchange occurs but not entry of Ca^{2+} via L-type Ca^{2+}channels. Local $[Ca^{2+}]_i$-transients were never observed during clamp-pulses to these potentials, although the spatially averaged $[Ca^{2+}]_i$ increased slowly to relatively high levels. Clearly, Ca^{2+} entry via L-type Ca^{2+}-channels (Vp of -20 mV) was much more effective in triggering local $[Ca^{2+}]_i$-transients than the simple elevation of the average $[Ca^{2+}]_i$ in the cell (V_p of +80 mV).

CONCLUSIONS

The data support the concept that $[Ca^{2+}]_i$-transients under normal conditions (i.e., without verapamil) can be explained by the simple 'recruitment' of more local $[Ca^{2+}]_i$-transients, with the same characteristics as those observed here. First, the bell-shaped voltage-dependence of the number of local $[Ca^{2+}]_i$-transients is similar to that of the spatial average $[Ca^{2+}]_i$-transient, as measured previously [4]. Second, the time courses of the latency histograms are similar to those of the whole-cell SR release flux (FSR,rel) that we have measured previously (in rat cells). This is the expected result if normal 'whole-

cell' $[Ca^{2+}]_i$–transients are the spatial and temporal summation of local $[Ca^{2+}]_i$–transients of the type described here.

Acknowledgement

This work was supported by Public Health Service awards HL29473 (W.G.W.), HL02466 and HL50435 (C. Willaim Balke.), American Heart Association–Maryland Affiliate, Grant–in–Aid (C.W.B.), and the Division of Cardiology, Dept. of Medicine, University of Maryland at Baltimore.

DISCUSSION

Dr. H. Strauss: Were oscillations in calcium release associated with these sparks and if so, were they elevated by low amplitude test potential?

Dr. W.G. Wier: If you have a leaky electrode, or if the cell is not healthy and the SR is over–loaded, then you get calcium waves and oscillations, even under these conditions. We regard those as being the *sine qua non* of an overloaded cell. We did not include such cells in this kind of study.

Dr. M. Morad: Congratulations. It is a beautiful story. For those of us working in the field, I know how tough it is. One of the things that you pointed out and I was very excited to get an answer to, was your variable gain idea. It is an appealing idea and this sort of spark idea should tell us something about it. I understood that it was the recruitment of different subunits, which I agree on. But how does one unit, at say –30 mV, recruit 10 subunits at the same calcium current? At 40 mV you recruit only two units with the same calcium. I did not get it.

Dr. W.G. Wier: What you are referring to is that at the whole cell level we can observe similar calcium currents at very different membrane potentials, one negative and one positive, with one being more effective in eliciting release during the pulse than the other. At the single channel level, we know that this current must be composed of a relatively few large single channel currents because it is in a negative potential where open probability is low but the driving force is high. The other current, at the positive potential, is comprised of a much larger number of relatively small currents because it is at a potential where probability is high but the driving in force is low. The idea that we now favor is that these small currents are simply below a threshold or level at which they can produce these local calcium events so that very few calcium events, or sparks, are recruited at this membrane potential. That is in fact what we measure. The number of events fell off steeply as a function of membrane potential and at the positive potentials we did not get very many events. Currents at negative potentials are much more effective because the single channel current is large. Perhaps this creates microdomain of high calcium in the region of the L–type calcium channel and the ryanodine receptors and that is very effective in triggering a calcium spark.

Dr. W. Barry: The sodium–calcium exchange trigger has been reported to increase by higher temperatures and also, of course, by increasing intracellular sodium. What was this sodium concentration was in your pipette in these experiments, and also, what was the temperature?

Dr. W.G. Wier: That is a good point because the sodium–calcium exchanger is very temperature sensitive. We worked at room temperature, which was about 21°C in this case, and the sodium in the pipette was, what we thought was normal for a guinea pig cell, at a concentration of 12 mM.

Dr. H. Strauss: The findings are very convincing and very attractive because they simplify a very complex problem. How confident are you about the quantification of unitary amplitudes, because that is obviously very critical to the interpretation?

Dr. G. Wier: That is a difficult issue because even if they are totally stereotypical events, there will still be a distribution of amplitudes. The reason for that is that sparks could occur outside the focal plane and if then calcium diffuses into the focal plane, where it is observed, this will appear as a smaller, slower spark, presumably. The characterization of these is not easy from that standpoint. Basically, what we did was to take the approach of reducing the probability to such low levels that they were distinct individual events. We got a mean value at each membrane potential and there was a fairly broad distribution at each membrane potential, probably reflecting the fact that some of them were originating from sites outside the focal plane. Nevertheless, at each membrane potential, the mean peak value was the same. We could not martial any evidence whatsoever that there was effect of amplitude on them.

Dr. H. Strauss: In follow-up of that comment, are they distributed in such a manner that is consistent purely to just out of focus fluorescence, a sort of normally distributed amplitudes?

Dr. G. Wier: Yes.

Dr. H. Strauss: The second question concerns the resting sparks, the ones you get at a negative potential. Do you believe they are triggered by calcium entry at very rare openings of L-type channels, or do you think they are not?

Dr. G. Wier: We have not looked at the resting sparks specifically. There is no doubt that under some conditions, sparks can be triggered by an elevation of background calcium, so that they may not require an L-type calcium channel opening to occur, and, when the SR is highly loaded with calcium, then these things tend to occur spontaneously more often. But, under normal conditions, when you see an occasional spark, I do not know whether there was an L-type calcium channel opening that accompanied that or not. One would expect that at the holding potentials we used at -40 mV there would be only rare L-type channel openings.

Dr. Y. Rudy: In your experiments, you loaded the SR through the sodium-calcium exchange in a reverse direction. Was the SR normally loaded or overloaded in the experiments that you showed?

Dr. G. Wier: No, it was not overloaded. Our measure of calcium overload is whether or not waves or oscillatory calcium release was triggered, something which is not part of normal cardiac function. We had to titrate the number of conditioning pulses to avoid overloading.

Dr. H.E.D.J. ter Keurs: Concerning the resolution of your observations, can you indicate how many ryanodine channels may be involved in a single spark and whether that can indicate whether ryanodine channel calcium releases may be coupled between their channels. Related to that is, of course, the threshold of the channel. If one wants to know about the threshold, I would like to know how much of the spark is actually an integrated calcium current through the DHP receptor.

Dr. G. Wier: I do not think that any of the sparks are the direct result of calcium entry through the DHP receptor. I think that micro-domain of high calcium established by the flux through the L-type channel is so brief that we never have a chance to observe it. It dissipates and we never have a chance of seeing it. But it does trigger the ryanodine receptors. Whether it is one or a group, neither we nor anyone else knows. It is most likely that it is a small cluster of receptors. That is the beauty of this hypothesis, that the problem of uncontrolled positive feedback is avoided in a way, because you allow it to occur within a cluster so that once a ryanodine receptor starts releasing calcium, then the whole cluster fires and if it is far enough away from another cluster, then you do not have any further release.

REFERENCES

1. Bers DM. *Excitation–contraction coupling and cardiac contractile force.* Kluwer, Dordrecht, 1991.
2. Beuckelmann DJ, Wier WG. Mechanism of release of calcium from sarcoplasmic reticulum of guinea–pig cardiac cells. *J Physiol.* 1988;405:233–255.
3. Stern MD. Theory of excitation–contraction coupling in cardiac muscle. *Biophys J.* 1992;63:497–517.
4. Wier WG, Egan TM, López–López JR, Balke CW. Local control of excitation–contraction coupling in rat heart cells. *J Physiol.* 1994;474:463–471
5. Isenberg G, Han S. Open probability of L–type Ca^{2+} channels grades SR Ca^{2+} release by recruiting of clusters of active release channels. *J Physiol.* 1994;480:423–438.
6. Balke CW, Wier WG. Modulation of L–type calcium channels by sodium ions. *Proc Natl Acad Sci USA.* 1992;89:4417–4421.
7. López–López JR, Shacklock PS, Balke CW, Wier WG. Local, stochastic release of Ca^{2+} in voltage–clamped rat heart cells: visualization with confocal microscopy. *J Physiol.* 1994;480.1:21–29.
8. Cheng H, Lederer WJ, Cannell MB. Calcium sparks: Elementary events underlying excitation–contraction coupling in heart muscle. *Science.* 1993;262:740–744.
9. Cannell MB, Cheng H, Lederer WJ. Spatial non–uniformities in $[Ca^{2+}]i$ during excitation–contraction coupling in cardiac myocytes. *Biophys J.* 1994;67:1942–1956.
10. Wier WG, López–López JR, Shacklock PS, Balke CW. Calcium signalling in cardiac muscle cells. In: Bock G, Ackrill K (eds), *Calcium waves, gradients and oscillations.* Wiley: Chichester (Ciba Foundation Symposium 188). 1995:146–164.
11. López–López JR, Shacklock, PS, Balke CW, Wier WG. Evoked calcium sparks in voltage–clamped heart cells (abstract). *Biophysical J.* 1995; in press.
12. Leblanc N, Hume JR. Sodium current–induced release of calcium from cardiac sarcoplasmic reticulum. *Science.* 1990;248:372–376.

CHAPTER 10

SIGNALING OF Ca^{2+} RELEASE AND CONTRACTION IN CARDIAC MYOCYTES

Martin Morad[1]

ABSTRACT

Cross signaling between Ca^{2+} channel and ryanodine receptor was explored in whole cell clamped rat ventricular myocyte under conditions where global myoplasmic Ca^{2+} concentrations were strongly buffered by dialyzing the myocytes with high concentrations of Fura 2 and EGTA. Ca^{2+} channel and ryanodine receptor were respectively activated by a depolarizing pulse to −10 mV and rapid (<50 ms) application of 5 mM caffeine. Temporal analysis of kinetics of inactivation of Ca^{2+} channel with respect to the time of application of caffeine pulse provided experimental evidence that signalling between the ryanodine and Ca^{2+} channel is mediated exclusively through the Ca^{2+} microdomains surrounding the DHP/ryanodine receptor complex independent of global myoplasmic Ca^{2+} concentrations.

INTRODUCTION

The ultra-structural location of a host of processes, known as excitation-contraction coupling, is the T-SR juncture in the mammalian ventricular myocyte. In this structural complex, the L-type Ca^{2+} channels of the sarcolemma (DHP-receptors) come within about 10 nm of the ryanodine receptors (Ca^{2+}-release channels) of sarcoplasmic reticulum. Quantitative analyses of the number of DHP- and ryanodine-binding sites suggest a ratio of 5 to 9 ryanodine receptors to one DHP receptor in rat ventricle depending on the age of the animal [1]. In skeletal muscle, where the ratio of ryanodine receptor to Ca^{2+} channels is 2:1, every other DHP receptor is closely apposed to the ryanodine receptor within the "feet" structures of TSR-junctions [2, 3]. In cardiac muscle, on the other hand, no distinct ultra-structural pattern between the two sets of receptors has been thus far identified. These

[1]Georgetown University School of Medicine, 3900 Reservoir Road, NW, Washington, DC 20007, USA.

Molecular and Subcellular Cardiology: Effects of Structure and Function
Edited by S. Sideman and R. Beyar, Plenum Press, New York, 1995

structural differences in the microanatomy of excitation–contraction coupling in skeletal and cardiac muscle are expressed functionally in the different modes of gating of the ryanodine receptors in the two types of muscles.

Evidence in intact tissue supporting the differential gating of cardiac and skeletal muscle includes the findings that: a) the voltage–dependence of tension was bell shaped (similar to voltage–dependence of I_{Ca}) in cardiac [4, 5] but sigmoid in skeletal muscle (similar to voltage–dependence of intra–membranous charge movement) [6, 7]; b) $[Ca]_o$ determines the strength of contraction in cardiac [8] but not in skeletal muscle, further skeletal muscle unlike cardiac muscle continues to contract in the absence of $[Ca]_o$ [9]; c) the voltage–dependence of the intrinsic birefringence signal, related to the release of Ca^{2+} from the SR, was bell shaped in cardiac [10] and sigmoid in skeletal muscle [11]. Thus, these early studies suggested that signaling of Ca^{2+} release was regulated by the influx of Ca^{2+} in cardiac and intra–membranous charge movement in skeletal muscle.

Ca^{2+} CURRENT AND SIGNALING OF Ca^{2+} RELEASE

The development of whole cell clamp technique combined with optical measurement of Ca^{2+} activity in single myocytes have made it possible to probe the mechanisms regulating Ca^{2+} release from the SR and determine the nature of signaling between DHP and ryanodine receptors. Uncertainties regarding the role of transmembrane Ca^{2+} influx in regulating Ca^{2+} release from the SR were to a great extent removed when it was shown that complete suppression of I_{Ca} by rapid (<50ms) removal of Ca^{2+} from extracellular solutions bathing the cell totally suppressed Ca^{2+} release and contraction in single cardiac myocytes [12]. Further, the influx of Ca^{2+} through the Ca^{2+} channel was critical for the release process as the influx of Na^+ or Ba^{2+} through the Ca^{2+} channel failed to release Ca^{2+} from the SR [12]. Consistent with earlier studies in intact ventricular strips [4, 5], the voltage–dependence of Ca_i–transients and contraction were found to be essentially similar to the voltage–dependence of I_{Ca} [13–15]. Arguments regarding whether the I_{Ca}–induced Ca^{2+} release was regulated in addition by membrane voltage [16] were weakened significantly by the findings that Ca^{2+} release could be terminated as effectively by deactivation of Ca^{2+} current through repolarization as by depolarizations to potentials near E_{Ca} [13]. Further, myoplasmic photo release of Ca^{2+}, triggered equivalent Ca^{2+} releases from the SR independent of conditioning holding potentials [17]. Thus it appears that the Ca^{2+}–induced Ca^{2+} release mechanism not only induces Ca^{2+} release in skinned myocytes [18] but also effectively gates the release of Ca^{2+} in intact cardiac myocytes [13]. Since rapid photo release of Ca^{2+} triggers the release of Ca^{2+} in intact myocytes at resting potentials without activation of Ca^{2+} channel [19], Ca^{2+} rather than Ca^{2+} channel was the signaling molecule for Ca^{2+} release. Although the data obtained using isolated cardiac ryanodine receptor incorporated in isolated vesicles or lipid bilayers are consistent with Ca^{2+} as the transmitter molecule in cardiac muscle [20, 21], similar results were obtained using skeletal ryanodine receptor [22, 23]. This finding in isolated skeletal ryanodine receptor raises the intriguing possibility that the Ca^{2+}–sensitive site may be "masked" in intact skeletal muscle where movement of intra–membranous charge rather than influx of Ca^{2+} gates the Ca^{2+}–release process. The presence of an additional 125 AA intracellular peptide between domains II and III of skeletal DHP receptor (not present in cardiac Ca^{2+} channel) [24] may represent the "masking" molecule which could provide the direct electrical signaling between the DHP and skeletal ryanodine receptors.

EFFECTIVENESS OF Ca^{2+} CHANNEL VS. Na^+–Ca^{2+} EXCHANGER IN REGULATION OF Ca^{2+} RELEASE

Since Ca^{2+} rather than Ca^{2+} channel appears to be the signaling molecule, multiple efforts have been made to delineate the role of the exchanger in the Ca^{2+} release process. In rat ventricular myocytes the role of the exchanger in gating Ca^{2+} release was found to be significantly smaller than Ca^{2+} channel [24, 25, 26]. Influx of Ca^{2+} via the exchanger was found to be, in fact, 20 to 100 times less effective than I_{Ca} in gating Ca^{2+} release from the ryanodine receptors, suggesting that Ca^{2+} channel had better access to the ryanodine receptors than the exchanger. The differential accessibility of these two sarcolemmal Ca^{2+} transporters may vary significantly between species or with growth and development. Such species variations may, in fact, be the reason for the reported much higher contribution of the exchanger to the release of Ca^{2+} in guinea-pig ventricular myocytes [28]. In addition to possible species differences, critical in evaluation of the role of exchanger versus Ca^{2+} channel in release of SR Ca^{2+}, are the activities of intracellular Ca^{2+} and Na^+ which in part are determined by the metabolic state of the myocyte or the dialyzing concentrations of the cations in the intracellular solutions of the patch pipette. Most studies showing evidence in favor of significant Ca^{2+}–influx via the exchanger to trigger Ca^{2+} release appear to use high $[Na^+]_i$ conditions which would tend to overload the intracellular Ca^{2+} stores. Recently two independent studies have attempted to evaluate the role of the exchanger in guinea pig myocytes dialyzed with low (5 mM) $[Na]_i$, and have obtained diametrically opposite results. Lipp and Niggli conclude that the exchanger can produce sufficient influx of Ca^{2+} to trigger Ca^{2+} release [29]. Evans and Cannell, under the exact same experimental conditions, find that I_{Na} and the exchanger could not trigger Ca^{2+} release and suggest that variability in complete block of Ca^{2+} channel and problems related to poor voltage control during activation I_{Na} are possible reasons for the discrepancy between the two sets of data [30, *see also* 25].

ACCESSIBILITY OF Ca^{2+} CHANNELS TO RYANODINE RECEPTORS

To probe the degree of accessibility of Ca^{2+} channel to the ryanodine receptor vs. the Na^+–Ca^{2+} exchanger, we monitored the kinetics of inactivation of Ca^{2+} channel in response to Ca^{2+} release caused by short pulses of caffeine. In the rat heart, ventricular myocytes were dialyzed with high concentrations of Ca^{2+} buffer (for instance 2 mM Fura 2 and 14 EGTA). Even under such conditions, Ca^{2+} channel continued to signal the release of Ca^{2+} from the SR, SR continued to reuptake the released Ca^{2+}, and the released Ca^{2+} continued to regulate the inactivation kinetics of L-type Ca^{2+} channels in myocytes dialyzed with small concentrations of Ca^{2+} buffers. The high degree of accessibility of the two receptors to Ca^{2+} transported by each other is illustrated in Fig. 1. In this experiment, Ca^{2+}–release channels were activated by rapid (<50 ms) application of 5 mM caffeine. When the caffeine-pulse was applied for periods longer than 500 ms prior to the activation of I_{Ca}, Ca^{2+} channels inactivated significantly slower than in myocytes not exposed to caffeine. On the other hand, when caffeine-induced Ca^{2+} release was timed to occur simultaneous with or 30–50 ms prior to the activation of I_{Ca}, the kinetics of inactivation of Ca^{2+} channel were significantly enhanced. These findings suggest that even when cytoplasmic Ca^{2+} was highly buffered with 14 mM EGTA and 2 mM Fura 2, Ca^{2+} release from the SR, though insufficient to raise the global myoplasmic Ca^{2+} concentrations, was nevertheless sufficient to increase the Ca^{2+} concentrations in the microdomains surrounding the cytoplasmic side of the Ca^{2+} channel to inactivate it. Thapsygargin (Ca-ATPase inhibitor) or

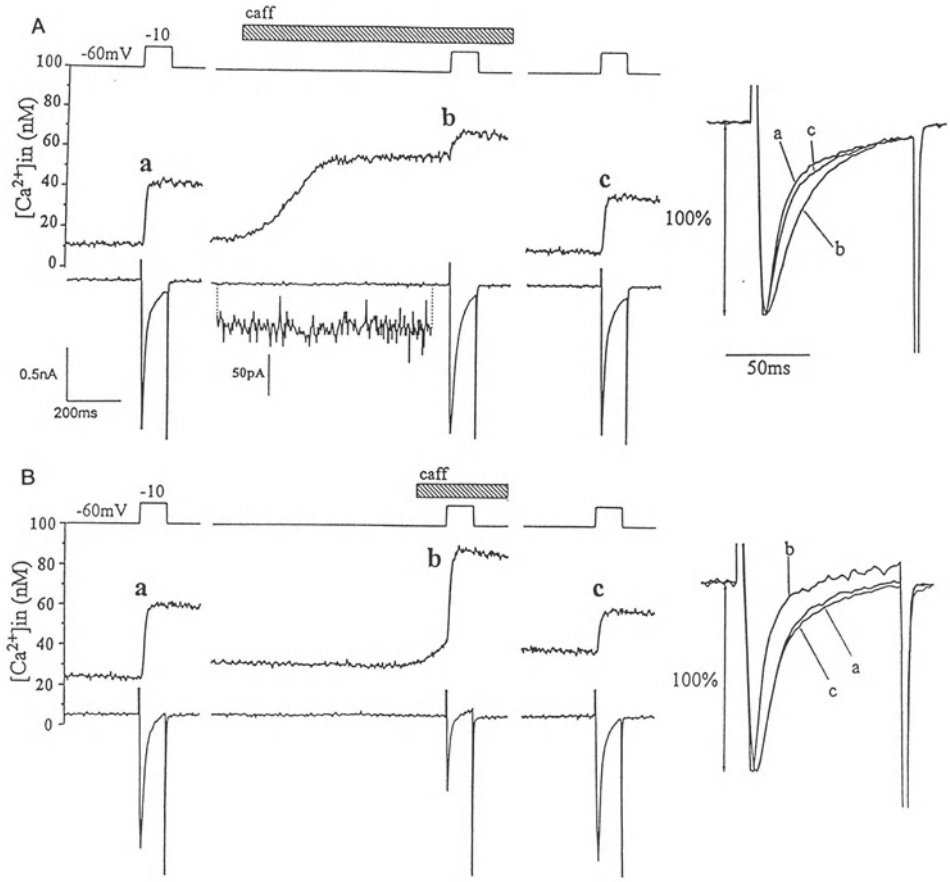

Figure 1. Effect of rapid application of caffeine (5 mM) on I_{Ca} and $[Ca^{2+}]_i$ in rat ventricular myocyte dialyzed with 2 mM Fura-2. The effects of the caffeine exposure depended on its timing relative to the voltage clamp depolarizations. The upper part of panel **A** shows the protocol where voltage clamp depolarizations were applied. Caffeine (5 mM) was applied yielding slow Ca^{2+} release 850 ms (**A**) and 50 ms (**B**) prior to the activation of I_{Ca}. Each panel shows only three of a sequence of about eight voltage clamp depolarizations. Thus, exposure to caffeine was preceded by 2 or more depolarizations to make sure the stability of the amplitude of I_{Ca} and Ca^{2+} transients, and followed by 4 or more to allow washout and complete re-equilibration. Ca^{2+} transients (middle trace) and I_{Ca} (lower trace) were measured before (**a**), during (**b**), and after (**c**) the exposure to caffeine. The normalized membrane currents are superimposed on the right side of each panel to yield the same maximal downward deflection with expanded time base. The current traces are shown without the leak current subtraction (from Adachi-Akahane S, Cleemann L, and Morad M, unpublished).

ryanodine, which deplete the Ca^{2+} stores of the SR, blocked the dual effects of caffeine on the kinetics of Ca^{2+} channel, suggesting that Ca^{2+} release from the SR was responsible for the dual caffeine effects.

Figure 2 illustrates schematically the sequence of events starting with influx of Ca^{2+} through the Ca^{2+} channel, to binding of Ca^{2+} to the ryanodine receptor, to the release of Ca^{2+} from the SR, and the kinetics of Ca^{2+} channel in turn by the released Ca^{2+}. Thus, in the Ca^{2+} microdomains surrounding the DHP/ryanodine receptor complex, cross talk between the two sets of proteins takes place via the "messenger" Ca^{2+}. Since slight buffering (200–500 μM Fura 2) of myocytes significantly suppressed or abolished I_{Na-Ca} activated

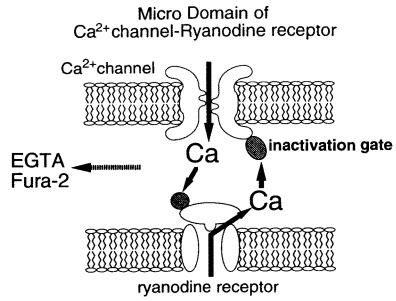

Figure 2. Schematics of the Ca^{2+} channel–Rayanodine receptor.

by caffeine–induced, or Ca^{2+} channel–gated Ca^{2+} release, the data suggest that Ca^{2+} released from the ryanodine receptor may not reach the micro environment of the exchanger protein in sufficient concentrations as to activate it. In sharp contrast, even much higher concentrations of Ca–buffers (2 mM Fura 2 and 14 mM EGTA) failed to inhibit cross signaling between the DHP and ryanodine receptors suggesting that Ca^{2+} concentrations in microdomains of DHP/ryanodine receptor complex are much higher than those postulated ($\approx$ 0.5 mM) or that the space between the two receptors is somewhat restricted. I_{Na-Ca} exchanger protein on the other hand appears to monitor primarily the global cytosolic Ca^{2+} concentrations without significant privileged access to the microdomains of Ca^{2+} around the DHP or ryanodine receptors. As the density of exchanger proteins or its geometrical proximity vis a vis Ca^{2+} channel and ryanodine receptor changes, the contribution of the exchanger protein to the release of Ca^{2+} from SR or its modulation by the released Ca^{2+} may change significantly.

CONCLUSION

Ca^{2+} influx through Ca^{2+} channel in rat ventricular myocyte has exclusive access to the ryanodine receptor so that Ca^{2+} influx via other Ca^{2+} transporting mechanisms, such as Na^{+}–Ca^{2+} exchanger, are essentially ineffective in activating the ryanodine receptor under physiological conditions. The strong modulation of kinetics of inactivation of Ca^{2+} channel by the Ca^{2+} released from the ryanodine receptor even in highly Ca^{2+}–buffered myocytes strongly imply that ryanodine receptor closely regulates the activity of the cardiac Ca^{2+} channel in a negative feedback manner.

DISCUSSION

Dr. S. Sideman: Could you relate to your most recent studies which deal with regulation of the Na^{+}–Ca^{2+} exchanger by isoproterenol?

Dr. M. Morad: Adrenergic β–agonists are known to enhance the force of cardiac contraction and accelerate the rate of its relaxation. The increase in the force of contraction results primarily from enhanced Ca^{2+} current and Ca^{2+} release secondary to cyclic AMP–dependent phosphorylation of the Ca^{2+} channel. On the other hand, the phosphorylation of phospholamban and the subsequent simulation of Ca^{2+} pump, in addition to decreased myofilament Ca^{2+} sensitivity, are thought to

mediate the relaxant properties of β-agonists. Quite similar to the mammalian myocardium, the frog heart also exhibits all the functional characteristics associated with the β-agonist response. In light of recent reports suggesting low content of Ca-ATPase, absence of mRNA message for Ca-ATPase, and functionally insignificant Ca^{2+}-release stores in the frog heart, the similarity in the β-agonist relaxant effects in mammalian and amphibian hearts is surprising and unexpected if the relaxant response of β-agonist were mediated solely by the cyclic-AMP induced phosphorylation of the phospholamban. We have now found a novel regulatory property of isoproterenol on the frog heart which results in suppression of Ca^{2+} influx by the Na^{+}-Ca^{2+} exchanger mediated via the β-receptor/adenylate-cyclase/cAMP-dependent cascade. This regulatory effect is independent of $[Ca^{2+}]_i$ and membrane potential and provides the molecular mechanism for the well documented contracture-relaxant effect of the hormone on heart muscle. Recent discovery of the presence of a putative nucleotide binding domain in the frog cardiac exchanger may represent the molecular site that mediates this β-agonist tension-suppressant effect. Adrenergically-induced temporal shift in preferred Ca^{2+} influx pathways in the heart, i.e., simultaneous enhancement of I_{Ca} and suppression of I_{Na-Ca}, may have evolved to accommodate cellular ultra-structural modification of the SR imposed by the evolutionary and developmental needs. The implication of these findings for pre- and neonatal mammalian myocardium which have ultrastructural and functional characteristics similar to those of amphibian hearts remain to be evaluated.

Dr. W.H. Barry: Do you see any difference in relaxation phase in the frog, loaded with Fura, since presumably it is dependent on sodium-calcium exchange? One might anticipate markedly slowed relaxation after exposure to isoproterenol.

Dr. M. Morad: I can not answer you since we did not measure cell shortening. But based on measurements of I_{Na-Ca} we see that calcium influx decreases. The kinetics of the exchanger, on the other hand, do not change at all with isoproterenol. This is a surprise! This might suggest that relaxation remains unaltered, but there is, of course, the isoproterenol-induced decrease in myofilament sensitivity and the activity of sarcolemmal Ca^{2+}-ATPase which together with decreased influx of Ca^{2+} will tend to accelerate cardiac relaxation.

Dr. E. Marban: You see a relaxant effect in the frog and you believe that this relaxant effect in the frog may be due to this effect of isoproterenol on the sodium-calcium exchange. Do you think this phosphorylation or a direct cyclic effect?

Dr. M. Morad: I have not done the experiment where I put the catalytic subunit of PKA into the myocyte and examine the effect on I_{Na-Ca}. My evidence for phosphorylation is simply that the various steps in cAMP-cascade seem to be involved, that is, forskolin does it, cyclic AMP itself does it, theophylline does it. Of course, all these steps may simply lead to increased $[cAMP]_i$ enhancing nucleotide binding without inducing phosphorylation. The process though has to be fairly specific to cAMP, since the experiments were all carried out in the presence of 5 mM Mg ATP.

Dr. J. Bassingthwaighte: Why did the reversal potential change with the isoproterenol?

Dr. M. Morad: If you change the intracellular calcium in poorly Ca^{2+}-buffered cells, the reversal potential of the exchanger is going to shift. If you raise the calcium, it is going to shift to the right, and if you decrease intracellular calcium, it will shift to the left. That is according to theory.

Dr. J. Bassingthwaighte: But it was 20 mV, which indicates a 2/3 of a decade change in calcium concentration.

Dr. M. Morad: From the theoretical point of view it comes right on the button. Do not forget that we are not buffering $[Ca]_i$ significantly. If we buffer the Ca^{2+} we see no shift in the reversal potential of the exchanger in response to isoproterenol effect.

Dr. H.E.D.J. ter Keurs: If I understand you correctly, isoproterenol in the frog is not a relaxing factor. It is an inhibitor of activation. Did you study the effect of varying the external sodium concentrations in the relaxation phase of contraction?

Dr. M. Morad: Yes, we have done those types of studies going all the way back to 1980. If you were to remove extracellular sodium, you block the isoproterenol effect, i.e., there is no relaxant effect. Second, the time constant of the relaxation which is around 100 ms in the frog heart increases to 5 sec in the absence of sodium. Sodium plays an incredible role in the removal of calcium. But the isoproterenol effect is not what I would have predicted it to be. The relaxant effect may have a number of components including the suppression of influx during long depolarization periods.

REFERENCES

1. Wibo M, Bravo G, Godfraind T. Postnatal maturation of excitation–contraction coupling in rat ventricle in relation to the subcellular localization and surface density of 1, 4–dihydropyridine and ryanodine receptors. *Circ Res.* 1991;68:662–73.
2. Block BA, Imagawa T, Campbell KP, Franzini–Armstrong C. Structural evidence for direct interaction between the molecular components of the transverse tubule/sarcoplasmic reticulum junction in skeletal muscle. *J Cell Biol.* 1988;107:2587–600.
3. Lamb GD. DHP receptors and excitation–contraction coupling. *J Musc Res and Cell Motility.* 1992;13:394–405.
4. Morad M, Goldman Y. Excitation–contraction coupling in heart muscle: Membrane control of development of tension. *Prog Biophys Molec Biol.* 1973;27:257–313.
5. Morad M, Cleemann L. Role of Ca^{2+} channel in development of tension in heart muscle. *J Mol Cell Cardiol.* 1987;19:527–553.
6. Hodgkin AL, Horowicz P. Potassium contractures in single muscle fibers. *J Physiol London.* 1960;153:386–403.
7. Schneider MF, Chandler WK. Voltage–dependent charge movement in skeletal muscle: a possible step in excitation–contraction coupling. *Nature.* 1973;242:244–6.
8. Ringer S. A further contribution regarding the influence of different constituents of blood on contraction of the heart. *J Physiol.* 1983;4:29–42.
9. Armstrong CM, Bezanilla FM, Horowicz P. Twitches in the presence of ethylene glycol bis (beta–aminoethyl ether) –N, N'–tetraacetic acid. *Biochimica et Biophysica Acta.* 1972;267:605–608.
10. Maylie J, Morad M. A transient outward current related to calcium release and development of tension in elephant seal atrial fibres. *J Physiol.* 1984;357:267–292.
11. Baylor SM, Chandler WK. Optical indications of excitation–contraction coupling in striated muscle. In *Biophysical Aspects of Cardiac Muscle,* M. Morad, ed., Academic Press, New York, pp. 207–228, 1978.
12. Näbauer M, Callewaert G, Cleemann L, Morad M. Regulation of calcium release is gated by calcium current, not gating charge, in cardiac myocytes. *Science.* 1989;244:800–803.
13. Cleemann L, Morad M. Analysis of role of Ca^{2+} in cadiac excitation–contraction coupling: Evidence from simultaneous measurements of intracellular Ca^{2+} contraction and Ca^{2+} current. *J Physiol.* 1991;432:283–312.
14. Beuckelmann DJ, Wier WG. Mechanism of release of calcium from sarcoplasmic reticulum of guinea pig cardiac cells. *J Physiol.* 1988;405:233–255.
15. Callewaert G, Cleemann L, Morad M. Epinephrine enhances Ca^{2+} current–regulated Ca^{2+} release and Ca^{2+} reuptake in rat ventricular myocytes. *Proc Natl Acad Sci USA.* 1988;85:2009–2013.
16. Cannel MB, Berlin JR, Lederer WJ. Effect of membrane potential changes on the calcium transient in single rat cardiac muscle cells. *Science.* 1987;238:1419–1423.
17. Niggli E, Lederer WJ. Voltage–independent calcium release in heart muscle. *Science.* 1990;250:565–568.
18. Fabiato A, Fabiato F. Contractions induced by a calcium–triggered release of calcium from the sarcoplasmic reticulum of single skinned cardiac cells. *J Physiol.* 1975;249:469–495.
19. Näbauer M, Morad M. Ca^{2+}–induced Ca^{2+}–release as examined by photolysis of caged Ca^{2+} in single ventricular myocytes. *Am J Physiol.* 1990;258:C189–C193.

20. Rousseau E, Meissner G. Single cardiac sarcoplasmic reticulum Ca^{2+}-release channel: Activation by caffeine. *Am J Physiol.* 1989;256:H328–H333.
21. Meissner G, Henderson JS. Rapid calcium release from cardiac sarcoplasmic reticulum vesicles is dependent on Ca^{2+} and is modulated by Mg^{2+}, adenine nucleotide, and calmodulin. *J Biol Chem.* 1987;262:3065–3073.
22. Smith JS, Coronado R, Meissner G. Single channel measurements of the calcium release channel from skeletal muscle sarcoplasmic reticulum. *J Gen Physiol,* 1986;88:573–588.
23. Endo M, Tanaka M, Ogawa Y. Calcium induced release of calcium from the sarcoplasmic reticulum of skinned skeletal muscle fibres. *Nature.* 1970;228:34–36.
24. Tanabe T, Beam KG, Adams BA, Niidome T, Numa S. Regions of the skeletal muscle dihydropyridine receptor critical for excitation–contraction coupling. *Nature.* 1990;356:567–569.
25. Sham JSK, Cleemann L, Morad M. Gating of cardiac release channels by Na^+ current and Na^+–Ca^{2+} exchange. *Science.* 1992;255:850–853.
26. Sham JSK, Cleemann L, Morad M. Functional coupling of Ca^{2+} channels and ryanodine receptors in cardiac myocytes. *PNAS.* In press 1995.
27. Beuckelmann DJ, Wier WG. Sodium–calcium exchange in guinea–pig cardiac cells: Exchange current and changes in intracellular Ca^{2+}. *J Physiol.* 1989;414:499–520.
28. Leblanc N, Hume JR. Sodium current–induced release of calcium from cardiac sarcoplasmic reticulum. *Science.* 1990;248:372–376.
29. Lipp P, Niggle E. Na^+ current–induced Ca^{2+} signals in isolated guinea–pig ventricular myocytes. *J Physiol.* 1994;474:439–446.
30. Evans AM, Cannell MB. Calcium influx through L–type Ca^{2+} channels provides the major trigger for Ca^{2+}–induced Ca^{2+} release in guinea–pig myocytes (abstract). *J Physiol.* 1994, p. 31.

CHAPTER 11

A MODEL OF Ca^{2+} RELEASE FROM THE SARCOPLASMIC RETICULUM

Arkady Glukhovsky,[1] Giora Amitzur,[2] Dan Adam,[1] and Samuel Sideman[1]

ABSTRACT

Various functions in the myocyte depend on Ca^{2+} transport, yet the control of these processes is still obscure. In order to better understand the intracellular Ca^{2+} processes, a model of Ca^{2+} release from the cardiac sarcoplasmic reticulum (SR) is suggested, in which the release of Ca^{2+} from the SR is mainly regulated by the kinetics of Ca^{2+} channels within the SR membrane. These kinetics are controlled by changes in the concentration of free Ca^{2+} near the openings of Ca^{2+} channels, and are affected by Ca^{2+} competitors, e.g., ryanodine. The control mechanism is based on a combination of positive and negative control loops, associated with two respective types of Ca^{2+} binding sites located on the SR membrane: 1) activating sites with low affinity to Ca^{2+} and high binding rate, and 2) inactivating sites with high affinity but low binding rate. The model also assumes that the activation of the Ca^{2+} channels depends on the preceding stimulation pattern (short term memory), an additional activation mechanism which is Ca^{2+} independent. This report describes the cytoplasmatic Ca^{2+} concentration in response to Ca^{2+} release from the SR, including the dependence on the beat intervals, either in the steady state or during response to premature and delayed beats. The analysis of ryanodine intervention supports a control mechanism based on two feedback loops, and available interval-dependent data favors inclusion of the short-term memory mechanism in the proposed model.

INTRODUCTION

The sarcoplasmic reticulum (SR) is the main intracellular store of Ca^{2+} which plays an important role in the regulation of muscle contraction and relaxation. The strength of

[1]The Julius Silver Institute of Biomedical Engineering, Technion-IIT, Haifa, 32000, Israel; [2]Neufeld Cardiac Reserach Institute, Sackler Faculty of Medicine, Chaim Sheba Medical Center, Tel Hashomer, Israel.

Molecular and Subcellular Cardiology: Effects of Structure and Function
Edited by S. Sideman and R. Beyar, Plenum Press, New York, 1995

contraction is determined by the amount of Ca^{2+} released from the SR [1], and the relaxation phase is strongly affected by the sequestration of Ca^{2+} back into the SR. The intracellular process of contraction of the cardiac muscle is initiated by a rapid increase of free [Ca^{2+}] in the cytoplasm, especially in the area of junctional SR (JSR) which is located near invaginations of the external sarcolemma (T-tubules). This localized rapid elevation of [Ca^{2+}] usually occurs when extracellular Ca^{2+} enters the cell near the T-tubule area in response to external membrane changes induced by the action potential . The elevation of Ca^{2+} concentration triggers the famous "calcium induced calcium release" (CICR) [1].

Although the detailed mechanism of physiological Ca^{2+} release is still undetermined, some results of the functional and structural investigations are instructive:

1) Skinned cell experiments show that the amount of Ca^{2+} released from the SR depends on the rate of application and the amount of the trigger Ca^{2+}: faster application produces larger response [1]. This sensitivity to the trigger Ca^{2+} typically characterizes a positive feedback mechanism. However, the amount of the released Ca^{2+} is reduced at high levels of the applied Ca^{2+} trigger [1]. This response typically suggests a negative feedback mechanism.

2) Only part of the stored Ca^{2+} in the SR is released during a normal contraction [2]. This phenomenon is related to the negative (inactivating) feedback loop.

3) Addition of ryanodine, which is widely used as a selective and specific ligand for the SR Ca^{2+} channel, affects the kinetics of Ca^{2+} release. At low concentrations (< 1 mM) ryanodine causes depletion of Ca^{2+} from the SR, while at high concentrations (> 100 mM) it inhibits Ca^{2+} release from the SR [3]. The data suggests the existence of two types of ryanodine receptors [4].

4) Most species demonstrate positive force-frequency dependence, i.e. increase of the steady state stimulating frequency produces higher Ca^{2+} transients in the cytoplasm. This increase of response is usually related to higher content of Ca^{2+} in the SR, due to more frequent entry of Ca^{2+} through the sarcolemma (higher duty cycle). It was also shown that the interval dependence exists in the steady state [2, 5], as well as in the extra- and post-extra-systolic stimulation [6]; the extra-systolic response is usually smaller than the steady state response, while the post-extra-systolic beat is significantly higher.

The available experimental data does not provide a complete explanation as to how the Ca^{2+} controls the release mechanism. A model which describes the regulation of Ca^{2+} release is proposed here to study the release of Ca^{2+} from the SR, including the interval dependence, and the way that ryanodine may affect, and thus explain, the kinetics of Ca^{2+} release.

THE MODEL

The model of Ca^{2+} release from the SR is essentially based on the classical model of Hodgkin and Huxley (HH) of the ion channels kinetics [7]. The channel is open if, and only if, a unique combination of "particles" is bound to specific sites, thus regulating the state of the ion channel.

It is assumed here that the state of each channel (or group of channels), is controlled by two activating sites having a low affinity to Ca^{2+} but a high binding rate, and one inactivating site with a high affinity to Ca^{2+} but a low binding rate. In addition, it is assumed that the state of the channel is controlled by a calcium-independent activation process, which is assumed to depend on the preceding stimulation process. The formalism of the HH model is thus slightly modified, and is similar to that proposed by Marom and Abbot [8] for the time-dependent inactivation of the sodium channels.

It is assumed that Ca^{2+} entering the sarcolemma and the Ca^{2+} released from the SR are mixed in the region proximal to the openings of the release channels. It is also assumed that an ion released from one site may diffuse and bind to any other control site in any channel within the SR release area. There are no obstacles that can prevent the Ca^{2+} ion from diffusing and binding with a control site of any Ca^{2+} channel (or group of channels) in the JSR area.

States of the Ca^{2+} Release Channels

The physical states of the Ca^{2+} release channels are depicted in Fig. 1. A channel is open—State O—if, and only if, both activating sites are occupied by Ca^{2+} ions and the inactivating site is not simultaneously occupied. Additional condition enabling the open state is imposed by the status of calcium-independent activation process. Thus, the probability of single channel to be in an open state is:

$$p = a^2 \cdot (1 - i) \cdot (1 - h) \tag{1}$$

where a is the probability of an activating site to be occupied by Ca^{2+} ions, i is the probability of the inactivating site being occupied, and $(1 - h)$ is the probability of the channel to be in the calcium-independent activated state.

The channel is transferred from State O to the inactivated state I^* when the inactivating site is also occupied, in addition to both activating sites being occupied by Ca^{2+}. From this state, the channel can either return to the open state O or to one of the closed states, C_0 or C_1^*. The channel can transform to (or from) the calcium-independent inactivated state (I_h^*) from any of the other states.

The probabilities of the channel to be in any of these states are characterized by the equation describing the binding and unbinding of Ca^{2+} to the control sites:

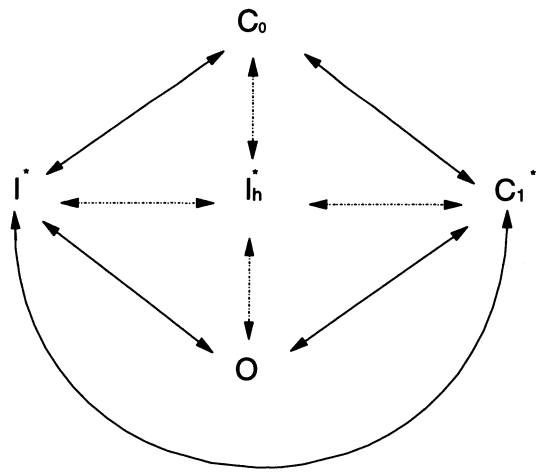

Figure 1. Possible states of the Ca^{2+} release channel. During the diastolic period the channel is in the closed state (C_0), and neither the activating site or the inactivating site are occupied by the Ca^{2+} ions. Whenever rapid increase in $[Ca^{2+}]$ occurs near the openings of the channels, the probability of Ca^{2+} binding to one of the activating sites increases. When this happens, the channel is transformed to the closed state. The channel is in the closed, or inactivated state, once any one of the two activating sites is occupied: the asterisk denotes this particular state. I^* – inactivated state; I_h^* – Ca^{2+} independent inactivated state.

$$\frac{ds}{dt} = \alpha_s \cdot s - \beta_s \cdot (1 - s) \tag{2}$$

where s denotes the probability of binding the Ca^{2+} ion either to the activating (a) site or to the inactivating (i) site. The probability constants α_s and β_s are determined by the kinetic constants of the sites (k_{on} and k_{off}), and the concentration of calcium in the proximity of the control sites, $[Ca^{2+}]_{prox}$:

$$\alpha_s = k_{on}^s \cdot [Ca^{++}]_{prox} \; ; \qquad \beta_s = k_{off}^s \; ; \qquad s \in (a,i) \tag{3}$$

The activating and inactivating kinetic constants have been estimated, and the corresponding dissociation constants have been calculated, for different cell geometries and various diffusion rates of Ca^{2+} ions in the cytoplasm. The values of the corresponding dissociation constants were found to be $k_d^a = k_{off}^a / k_{on}^a = 2 \div 3\,\mu M$ for an activating site, and $k_d^i = k_{off}^i / k_{on}^i = 10 \div 200\,nM$ for an inactivating site.

The Ca^{2+} flux through the SR membrane (J_{sr}) is a passive process determined by the gradient of Ca^{2+} concentrations between the inner side of the SR membrane ($[Ca^{2+}]_{sr}$) and the cytoplasm near the openings of the Ca^{2+} channels, ($[Ca^{2+}]_{prox}$). Thus,

$$J_{sr} = G \cdot \{[Ca^{++}]_{sr} - [Ca^{++}]_{prox}\} \tag{4}$$

where G, the permeability of the SR membrane, is determined by the number of open channels. This number is equal to the total number of channels multiplied by the probability p of a single channel to be in the open state. Thus, the permeability of the SR membrane is given by the maximal membrane permeability (G_0) multiplied by the probability of single channel to be in the open state (p):

$$G = G_0 \cdot p = G_0 \cdot a^2 \cdot (1 - i) \cdot (1 - h) \tag{5}$$

The Ca^{2+} Release Mechanism

The schematic description of the release mechanism is presented in Fig. 2. Experimental results obtained for most species show that the amount of the Ca^{2+} in the SR

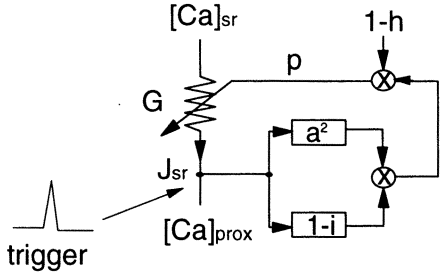

Figure 2. Model of Ca^{2+} release from the SR, based on specific sites controlling the state of the channel: the activating site, associated with the positive feedback, and the inactivating site, associated with negative feedback loop. The calcium–independent activation (1–h) is also shown here. The trigger is applied in the area near the openings of the release channels, causing elevation in the $[Ca^{2+}]_{prox}$, and subsequently affecting both activating and inactivating branches of the control mechanism.

increases with the stimulation frequency [5]. However, as the intervals between beats decrease, the degree of the restitution of the Ca^{2+} channels from the calcium–dependent inactivation also decreases. Thus, the amount of the released Ca^{2+} from the SR will not increase significantly with frequency unless a frequency dependent mechanism is incorporated in the model. This is introduced in Fig. 2 as a calcium–independent activation mechanism with a short–term memory which modifies the number of available channels according to the interval between the preceding beats.

SIMULATION OF Ca^{2+} TRANSPORT

Ca^{2+} Cycling in the Intact or Skinned Cell

The Ca^{2+} cycling path is schematically presented in Fig. 3A for the intact or skinned cardiac cell and in Fig. 3B for the isolated SR vesicles. The model represents either a single cluster of Ca^{2+} channels or the entire ensemble of the channels associated with the half–sarcomere being modeled.

The parameters in Fig. 3A are based on known experimental measurements from a myocyte of a small mammal. These include the geometrical size (sarcomere radius 0.5 μm, sarcomere length 2.0 μm [9]), rate of Ca^{2+} diffusion in the myoplasm ($7{\cdot}10^{-10}m^2s^{-1}$ [10]), $[Ca^{2+}]$ in the different compartments of the sarcomere (2 mM in the SR [11], 0.1 μM in the cytoplasm during diastole [12]), as well as concentrations of the major Ca^{2+} buffers in the cytoplasm (50 μM calmodulin [13], 50 μM troponin [14]) and in the SR (5 mM calsequestrin [15]).

Upon excitation, a small amount of Ca^{2+}, "trigger Ca^{2+}," enters the cytoplasm near the openings of the SR Ca^{2+} channels. Elevation of $[Ca^{2+}]$ near these openings activates the Ca^{2+} release mechanism. The flux (J_{sr}) of Ca^{2+} from the SR increases $[Ca^{2+}]_{prox}$ even more. Finally, the inactivation process slows and terminates the release process. The Ca^{2+}

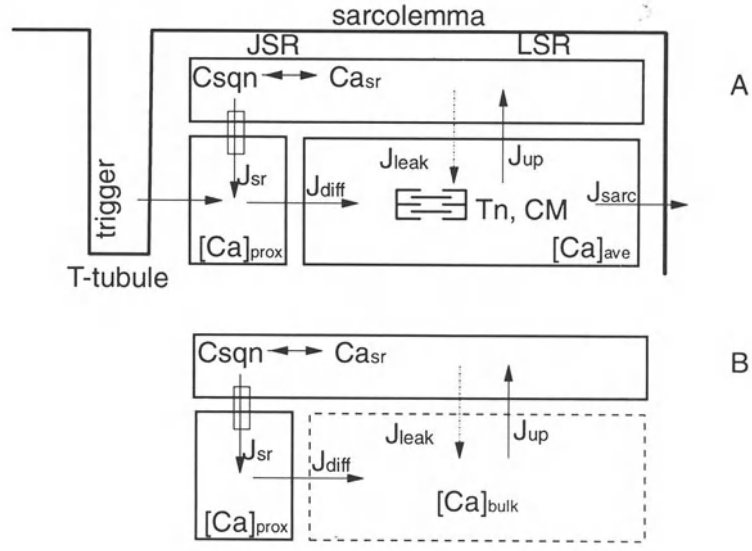

Figure 3. A: Schematic presentation of the Ca^{2+} cycling path in the myocyte. **B:** Schematic presentation of Ca^{2+} cycling path when a SR vesicle is in solution with a constant Ca^{2+} concentration ($(Ca^{2+})_{bulk}$).

in the proximity of the release area diffuses to other parts of the cytoplasm. The free calcium ($[Ca^{2+}]_{ave}$) in the cytoplasm reacts with troponin (Tn) and calmodulin (CM). The Ca^{2+} is then pumped from the myoplasm (J_{up}) into the longitudinal fraction of the SR (LSR), completing a single excitation cycle.

Small amount of Ca^{2+} is also pumped through the sarcolemma into the extracellular space. This flux (J_{sarc}) is generated by the ATP-active sarcolemmal Ca^{2+} pump and the sarcolemmal Na/Ca exchanger, which under normal physiological conditions pumps Ca^{2+} out of the cell. Under normal physiological steady state conditions the amount of Ca^{2+} entering the cell through the sarcolemma (trigger Ca^{2+}) is equal to the amount of the Ca^{2+} pumped back (J_{sarc}) during the beat interval.

During the rest period, the free calcium in the SR, $[Ca_{sr}^{2+}]$ is assumed to be in equilibrium with the Ca^{2+} buffer calsequestrin (Csqn). Only small Ca^{2+} fluxes occur from and into the SR. The leakage of Ca^{2+} through the non-specific Ca^{2+} channels (J_{leak}) is limited mainly to the LSR area; the leakage of Ca^{2+} through the specific Ca^{2+} channels occurs mainly in the JSR area (J_{sr}). Both fluxes are compensated during the rest period by the flux generated by the ATP-active Ca^{2+} pump (J_{up}).

Ca^{2+} Transport in Isolated SR Vesicles

The model of Ca^{2+} transport in the isolated SR vesicle depicted in Fig. 3B indicates that neither Ca^{2+} trigger nor sarcolemmal pumps need be considered in this situation. The concentration of calcium in the bulk solution ($[Ca^{2+}]_{bulk}$) is assumed to be constant, independent of Ca^{2+} release from the SR.

Interaction with Ryanodine

Ryanodine competes with Ca^{2+} in binding to the regulating sites. Experimental evidence supports the hypothesis that it does not interact with other cellular processes [3, 4]. It is assumed that site affinities are either high or low for both Ca^{2+} and ryanodine. The measured dissociation constants of ryanodine vary from 3 nM [16] to 17 nM [17] for the high affinity site, and between 1 μM and 3 μM [18] for the low affinity site.

Comparison of the affinity of ryanodine data to the calculated affinity of Ca^{2+} indicates that ryanodine has a higher affinity than Ca^{2+} for both types of binding sites; it is significantly higher for the high affinity (inactivating) site, and only slightly higher for the low affinity (activating) site.

Binding of ryanodine to the specific sites is based here on the steady state solution, assuming that the concentration of ryanodine does not change near these sites during the release of Ca^{2+}. Although ryanodine and Ca^{2+} compete on binding to these sites, the changes in $[Ca^{2+}]_{prox}$ between its diastolic and systolic values do not significantly affect the number of sites occupied by ryanodine (see Results).

It is assumed that binding ryanodine to the regulating sites does not change the state of the channel. However, bound ryanodine at a specific site prevents binding of Ca^{2+} to this site. Thus, binding of ryanodine to an inactivating site inhibits inactivation of the release mechanism, and consequently increases the probability of the channel to remain in the open state. Similarly, binding of ryanodine to the activating site inhibits opening of the channel.

RESULTS

The model is used to simulate various experimental studies which involve the Ca^{2+} release mechanism and its dependence on several factors: 1) dependence of the released

amount of Ca^{2+} on the stimulation frequency in steady state, and dependence on the time interval in the extra- and post-extra-systolic stimulation, and 2) interaction with ryanodine.

Dependence on the Stimulation Pattern

The model of Ca^{2+} cycling in the myocyte depicted in Fig. 3A was used to calculate the amount of the Ca^{2+} inside the SR and the amount of the Ca^{2+} being released from the SR for various stimulation patterns. In general, the mechanism of Ca^{2+} -independent activation provided responses, which were similar to the experimentally observed responses during steady state [2,5], extra-systolic and post-extra-systolic stimulation pattern [6]. The Ca^{2+} -independent mechanism (Fig. 2) defined the frequency pattern in steady state whereby the response increased with the increase of the stimulating frequency. The response obtained for an extra-systolic beat decreased with the decrease of the extra-systolic interval. However, the corresponding post-extra-systolic beat showed an opposite behavior. The model predicts also that the decrease in the extra-systolic stimulation occurs mainly due to the incomplete restitution of the inactivating control sites. The nature of the increase of the post-extra-systolic beat in the model is primarily due to the additional apparatus of the calcium independent inactivation response.

Effect of Ryanodine

The simulations were performed assuming various concentrations of ryanodine in the cytoplasm. Trigger Ca^{2+} was injected, with a flux of 0.6 μmol/liter/ms, during 10 ms, near the openings of the Ca^{2+} channels. Figure 4 depicts the calculated transient of free $[Ca^{2+}]$ in the SR, after the application of trigger Ca^{2+}, for different concentrations of ryanodine.

As seen in Fig. 4, the inactivation site is not significantly inhibited at the lowest range of ryanodine concentrations (1nM, 10nM), and the release of Ca^{2+} is terminated in a relatively short period, returning $[Ca^{2+}]$ in the SR returns almost to its initial value.

The inactivating mechanism is inhibited significantly at higher concentrations of ryanodine (0.1 μM, 1 μM) and the release of Ca^{2+} continues until the SR is almost depleted. At higher levels of ryanodine (10 μM), the ryanodine binds also to the low affinity activating site, and thus inhibits the activation of Ca^{2+} release. Ca^{2+} release can no longer be observed at this level. The leak of Ca^{2+} is also reduced, and the Ca^{2+} contents of the SR increases gradually to a level higher than it was before the triggering occurred.

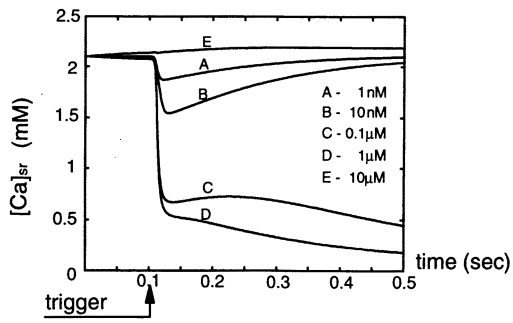

Figure 4. Changes of Ca^{2+} concentration in the SR in response to trigger Ca^{2+} injected at 100ms, for five different concentrations of ryanodine.

Simulations of the Ca^{2+} release process in *isolated SR vesicles* (Fig. 3B), and the effects of ryanodine under these conditions, provide a tool for investigating of the release mechanism under "open loop" conditions, when the release process is not affected by the feedback loops. The time of half Ca^{2+} depletion from the vesicles was calculated, when vesicles loaded with Ca^{2+} were transferred to solutions containing various Ca^{2+} concentrations. Simulated effect of various concentrations of ryanodine in the solution is consistent with the available experimental data [8].

The model predicts that the maximal rate of Ca^{2+} release, in the absence of ryanodine, is within the range of the systolic Ca^{2+} concentrations (5 μM ÷ 50 μM); the release rate is slower for both lower and higher Ca^{2+} concentrations. Addition of 10 nM to 0.1 μM of ryanodine to the solution promotes higher release rates, when $[Ca^{2+}]$ in the solution is systolic and higher. This occurs due to the inactivating mechanism being partially inhibited by the ryanodine. Addition of 1 μM ryanodine produces a maximal release rate that does not differ significantly from the maximal rate with no ryanodine. However, high release rate values hold over much wider range of Ca^{2+} concentrations. This happens since ryanodine partially inhibits the activating mechanism of the channels. Higher doses of ryanodine (> 10 μM) prevent the release of Ca^{2+} from the vesicles almost totally; this is in agreement with available experimental data [3]. The slow dilution rate occurs due to a significant inhibition of the release mechanism.

DISCUSSION

Interval-Dependent Activation

The simulations of the dependence of the $[Ca^{2+}]$ fluctuations during the excitation–contraction on the interval between beats, both in the steady state and in the extra– and post–extrasystolic stimulation patterns, agrees well with the available experimental data [2, 5, 6]. This is mainly due the assumed mechanism of calcium–independent activation, which depends on the interval between preceding beats. Similar behavior was observed in other types of ion channels, as, for example, the membrane potassium channels [19]. This observed behavior is related [8, 19] to the inactivation of these channels. It supports, however, the suggested additional mechanism which controls the state of the channel as function of the stimulation interval. This observation supports the proposed hypothesis that such a mechanism may be present in other kind of channels, e.g., the SR Ca^{2+} release channels.

Several types of mechanisms can be proposed to explain this kind of activation. One of these mechanism may be based on changes in concentration of other than Ca^{2+} ions in the area proximal to the release region. However, such a specific mechanism was not assumed in this study.

Influence of Ryanodine

The simulation results of ryanodine competing with Ca^{2+} on the same control sites agree well with the experimental data [1, 3, 4, 18]. These results show that binding of ryanodine to these sites prevents the binding of Ca^{2+} to those sites, while ryanodine has no effect on the state of the release channel.

An alternative explanation of the effect of ryanodine is that ryanodine changes the state of the release channel. This implies that ryanodine in low concentrations binds mostly to the site that opens the Ca^{2+} channel, while in high concentrations ryanodine will bind to the site that closes the channel. It requires that the channel's activating site has a high affinity for ryanodine, and that the inactivating site will be a low affinity site. This is

contradictory to the interaction of Ca^{2+} with these sites, suggesting that ryanodine does not control the state of the channel.

The Release Mechanism

It is assumed here that the regulating sites are located on the outer side of the SR membrane. Other alternative mechanisms may be associated with Ca^{2+} processes within the SR. Experimental data based on rapid cooling contracture (RCC) experiments [2] indicate that the processes in the SR are not rate limiting in the regulation of Ca^{2+} availability. It can be argued that the RCC experimental setup significantly affects the rate of these processes, increasing the Ca^{2+} gradient in the LSR by locking Ca^{2+} release channels in the open state. However, additional control of the Ca^{2+} release near the SR membrane is still required even when assuming the existence of a more significant delay due to Ca^{2+} translocation within the SR,. No reasonable explanation otherwise can be given to phenomenon such as CICR, which demonstrates dependence of the released Ca^{2+} on $[Ca^{2+}]$ at the outer side of the SR membrane, and the influence of ryanodine, which affects the release mechanism at the outer side of the SR membrane (since it does not penetrate the SR).

Another basic assumption of the model is that the trigger Ca^{2+} entering the sarcolemma and the Ca^{2+} released from the SR are mixed in the proximity of the release area. It is assumed that there is no physical barrier preventing the movement of calcium ions. Thus, any Ca^{2+} ion can bind to any regulating site within the entire release area. Obviously, if some kind of barrier does exist, then the simplified description of the release process by a single mechanism may be insufficient. The alternative description will require divide of the entire release area into small parts with local release mechanisms. This concept was proposed in the "cluster bomb" model [20] where it was assumed that Ca^{2+} ion released from one group of channels (cluster) can not affect other clusters. This "cluster bomb" model is supported by recent experimental data [21]. However, this local release mechanism still can be based on the existence of activating and inactivating sites controlling the state of the release channel (or group of channels).

CONCLUSION

The model presented here successfully describes and explains the phenomena related to the release of Ca^{2+} from the SR, the recovery mechanism of Ca^{2+} availability, interval dependence, and the effects of ryanodine intervention. The results support the basic hypothesis of the model that the SR Ca^{2+} release channels are controlled by regulating sites located outside the SR. Understanding the regulation of the release process provides a better insight into cardiac pathophysiology and the excitation–contraction coupling that controls the cardiac muscle function.

Acknowledgment

This study was sponsored by the Women's Division of The American Technion Society and supported in part by a grant from Mr. J Schneider, Las Vegas, USA, and the Al & Phyllis Newman and the Joseph & Edythe Jackier Endowment Funds, Detroit, USA. This research was also supported by the Fund for the Promotion for Research at the Technion. We greatly appreciate this generous support, without which these interesting and important results could not have been obtained.

DISCUSSION

Dr. M. Lab: Is it possible to use your model for calculating calcium recirculation fractions? Is it possible to calculate the amount of Ca^{2+} that goes back into the SR after a post–extra systolic potentiation compared to the extra systole itself?

Dr. D. Adam: The model can be used to calculate the fraction of calcium released from the SR vs. the amount present in the SR during diastole, and the fraction of calcium pumped back into the SR during the intervals between beats, for different intervals (either regular, extra systole, or post–extra systolic beats). We did not perform exact quantitative analysis of these fractions. Qualitative observations of the model allow us to predict that almost 90% of the calcium released from the SR is pumped back during the extra–systolic and similarly during post–extra–systolic stimulation. It seems that the recirculation fraction is not the crucial factor distinguishing between the extra– and post–extra–systolic beat.

Dr. G. Wier: Mike Stern [20] has published a theoretical model of the SR release process. He noted that it is often difficult to achieve high gain and stability at the same time in these models. Did you have similar difficulty with this model? Or is there some characteristics built into your model that circumvented that problem?

Dr. D. Adam: Stern [20] argues that the common–pool models can not combine two basic features of the calcium release process: high gain (released calcium versus the trigger calcium) and stability (spontaneous release occurs only for extreme pathophysiological concentrations of calcium). This analysis of stability is applicable to any mechanism which includes positive feedback. The presented model, however, can not be treated straightforward as a common–pool model: the time of diffusion of the calcium ions in the cytoplasm is similar to the characteristic time of the response of the positive feedback of the release mechanism. Thus two pools of calcium are actually present in the model: the proximal pool (in the proximity to the release area), and the rest of the cell. Another stabilizing factor is the hypothesized mechanism of multiple, rather than single, activation site associated with the positive feedback loop. This assumption implies non–linear behavior of the model, enforcing small gain at low calcium concentrations, and larger gain at higher concentrations. Additionally, negative feedback path is included in the model, which also prevents instability.

Dr. M. Morad: You may consider one interesting thing from an experimental point of view. None of the intact myocyte studies in the past 10–15 years, done under various complicated methodologies, have been able to show calcium induced inactivation, exception of the Fabiato's data. This is a problem. I do not know what the answer is, but certainly the Stern model [20] does explain it from a stochastic point of view, which basically gets around this issue. Can your model address these different experimental findings in any way?

Dr. D. Adam: It is correct that no major experimental evidence has been provided recently to support Fabiato's data, which was measured in the intact myocyte. However, Meissner *et al.* [3, 4] reported on experimental data regarding the release of calcium from the isolated SR vesicles, both in the presence and in the absence of ryanodine. The analysis of this data shows that the rate of release of calcium from these vesicles declines for high concentrations of calcium in the solution. The reasonable conclusion from this series of experiments is that there exists some mechanism that inactivates the release process for high concentrations of calcium. In our model the inactivating site provides this calcium inactivation mechanism. The stochastic approach does not necessarily contradict the proposed calcium inactivation mechanism.

Dr. J. Bassingthwaighte: Did you run your model against the Fabiato data, and have you made any comparisons with the modeling that Wong and Fabiato and I [22] did on those data?

Dr. D. Adam: The simulation results of our model were also compared to the Fabiato's data [1]. His data shows the dependence of the tension developed by the skinned Purkinje cells on the amount and the rate of injection of the trigger calcium. Fabiato also showed that tension is proportional to the free calcium transient in cytoplasm, a transient which occurs mainly due to calcium released from the SR. According to his data, the release of calcium from the SR is proportional to the rate of injection of the trigger calcium. Our model succeeds well in simulating these results due to a much faster response of the positive feedback than the response of the negative feedback. Another feature revealed by the experimental data is that the maximal tension is developed in intermediate amounts of the trigger calcium. The tension declines both for low and for high amounts of the trigger calcium. Our model succeeds well in describing this behavior for low and intermediate values. However, for high amounts of trigger calcium, the simulated behavior differs from the experimental one, as the amount of trigger calcium itself is sufficient to affect the developed tension. There are several possible explanations for the observed experimental behavior. One of the explanations (as assumed in the model of Wong *et al.* [22]), is that the trigger calcium first enters the SR, and only then is the release mechanism operated. The problem with this assumption is that relatively small addition of free calcium in the SR triggers the release process, suggesting high sensitivity of the system, and consequent problems of instability. The other possible explanation is that the injection of trigger calcium into the skinned Purkinje cells, as in the experiments by Fabiato, does not occur in the same place that the physiological injection occurs.

Dr. H. Fozzard: As I understand it, there is a coupling in your model there is a coupling between the radius of the proximal space, the Ca^{2+} diffusion coefficient from this space to the cytoplasm, and the ryanodine receptor threshold for the calcium release. Is there any constraint? Are those completely arbitrary related variables or is there any constraint on, for example, the radius of the subsarcolemmal space?

Dr. D. Adam: There are no constraints. The assumed diffusion coefficient does not influence, nor is it related, to the size of the proximal space of the model. The diffusion coefficient affects, of course, the transfer rate of calcium from the proximal space to the rest of the cell. In our study we checked the concentration of calcium as a function of distance from the opening of the release channel. It appears that this concentration is relatively constant near the openings, and it gradually declines at larger distances. The size of the proximal space was chosen so that the concentration of calcium in it can be treated as uniform throughout the entire proximal volume.

REFERENCES

1. Fabiato A. Time and calcium dependence of activation and inactivation of calcium-induced release of calcium from the sarcoplasmic reticulum of skinned canine cardiac purkinje cell. *J Gen Physiol.* 1985;85:247-289.
2. Bers DM. SR Ca loading in cardiac muscle preparations based on rapid-cooling contractures. *Am J Physiol.* 1989;256:C109-C120.
3. Meissner G. Ryanodine activation and inhibition of the Ca^{2+} release channel of sarcoplasmic reticulum. *J Biol Chem.* 1986;261:6300-6306.
4. Meissner G, Henderson JS. Rapid calcium release from cardiac sarcoplasmic reticulum vesicles is dependent on Ca^{2+} and is modulated by Mg^{2+}, adenine nucleotide, and calmodulin. *J Biol Chem.* 1987;262:3065-3073.
5. Edman KAP, Johannsson M. The contractile state of rabbit papillary muscle in relation to stimulation frequency. *J Physiol.* 1976;254:565-581.
6. Wier WG, Yue DT. Intracellular calcium transients during the short-term force-interval relationship in ferret ventricular myocardium. *J Physiol.* 1986;376:507-530.
7. Hodgkin AL, Huxley AF. A quantitative description of membrane current and its application to conduction and excitation in nerve. *J Physiol.* 1952;117:500-544.
8. Marom S, Abbott LF. Modeling state-dependent inactivation of membrane currents. *Biophys J.* 1994, 67:515-520.

9. Sommer JR, Johnson EA. Ultrastructure of cardiac muscle. In: Geiger SR, Berne RM, eds., *Handbook of Physiology, The Cardiovascular System, Vol. 1.* Bethesda MD: American Physiological Society, 1979; 113–186.
10. Wang JH. Tracer diffusion in liquids. IV. Self-diffusion of calcium ion an dchloride ion in aequeous calcium chloride solutions. *J Am Chem Soc.* 1953;75:1769–1770.
11. Bers DM, Bridge JBH, Spitzer KW. Intracellular Ca transients during rapid cooling contractures in guinea-pig ventricular myocytes. *J Physiol.* 1989;417:537–553.
12. Blinks JR. Intracellular [Ca] measurements. In: Fozzard HA, Haber E, Jennings RB, Katz AM, Morgan HE, eds, *The Heart and Cardiovascular System, Vol 2.* New York: Raven Press, 1991; 1171–1201.
13. Cheung WY. Calmodulin plays a pivotal role in cellular regulation. *Science.* 1980;207:19–27.
14. Solarao RJ, Wise RM, Shiner JS, Briggs NF. Calcium requirements for cardiac myofibrillar activation. *Circ Res.* 1974;34:525–530.
15. Bers DM. *Excitation–Contraction Coupling and Cardiac Contractile Force.* Dordrect/Boston/ London: Kluwer Academic Publishers, 1991; 98.
16. Inui M, Wang S, Saito A, Fleisher S. Characterization of junctional and longitudinal sarcoplasmic reticulum from the heart muscle. *J Biol Chem.* 1988;263:10843–10850.
17. Anderson K, Lai FA, Liu QY, Rousseau E, Erickson P, Meissner G. Structural and functional characterization of the purified cardiac ryanodine receptor–Ca^{2+} release channel complex. *J Biol Chem.* 1987;264:1329–1335.
18. Lai FA, Mistra M, Xu L, Smith AA, Meissner G. The ryanodine receptor–Ca^{2+} release channel complex of skeletal muscle sarcoplasmic reticulum. *J Biol Chem.* 1989;264:16776–16785.
19. Marom S, Levitan IB. State-dependent inactivation of the Kv3 potassium channel. *Biophys J.* 1994;67:579–589.
20. Stern DM. Theory of excitation–contraction coupling in cardiac muscle. *Biophys J.* 1992;63:497–517.
21. Lopez-Lopez JR, Shaclock PS, Balke CW, and Wier WG. Local, stochastic release of Ca^{++} in voltage–clamped rat heart cells: visualization with confocal microscopy. *J Physiol.* 1994;480.1:21–29.
22. Wong AYK, Fabiato A, Bassingthwaighte JB. Model of Ca release mechanism from the sarcoplasmic reticulum: Ca–mediated activation, inactivation and reactivation. In: *Activation, Metabolism and Perfusion of the Heart*, Sideman S, Beyar R, eds. Martinus Nijhoff Publ.:Dordrecht/Boston, 1987: 281–295.

CHAPTER 12

TROPONIN C - TROPONIN I INTERACTIONS AND MOLECULAR SIGNALLING IN CARDIAC MYOFILAMENTS

R. John Solaro[1]

ABSTRACT

This chapter describes a current perception of the molecular interactions regulating myofilament activity in heart cells. The focus is on the interaction between troponin-C (TnC), the Ca^{2+}-receptor and troponin I (TnI), an inhibitory protein. It is this interaction that appears to form a molecular switch that turns on the thin filament. It will be seen that control of the actin-myosin reaction is not only through Ca^{2+}-binding to TnC, but also through steric, cooperative and allosteric processes involving all of the main myofilament proteins-actin, myosin, tropomyosin (Tm), troponin T (TnT), TnC, and TnI. The process is modulated by covalent and non-covalent mechanisms. The process is altered in diverse myopathies and pathologies of the heart and is a target for pharmacological manipulation by a new class of inotropic agents, the "Ca^{2+}-sensitizers".

INTRODUCTION

There are compelling reasons for understanding the molecular processes by which regulatory proteins signal cardiac myofilaments to turn on and to turn off. Length dependence of myofilament response to Ca^{2+} forms the basis of Starling's Law [1-3]. There is also substantial evidence that adrenergic stimulation of the heart is associated with phosphorylation of the myofilaments by protein kinase A, protein kinase C and also Ca^{2+}-calmodulin dependent protein kinase to name the most well studied [4, 5]. Importantly, co-valent modulation of the myofilament proteins via these kinases affects their activity and their control by Ca^{2+} [4, 5]. Alterations in the response of the myofilaments to Ca^{2+} also occur during conditions associated with depressed cardiac function. One example is during

[1]Department of Physiology & Biophysics, College of medicine (M/C 901), University of Illinois-Chicago, 901 South Wolcott, Chicago, IL 60612-7342, USA.

Molecular and Subcellular Cardiology: Effects of Structure and Function
Edited by S. Sideman and R. Beyar, Plenum Press, New York, 1995

acidosis and hypoxia, where it has been shown that force generating capabilities of heart muscle are considerably depressed under conditions in which the amplitude of Ca^{2+}-transient during the twitch is, in fact, increased [1, 6]. There are also potential long term changes in structure/function relations of the myofilaments associated with breakdown of myofilament proteins [7] or altered gene expression [8–10] that may affect the myofilament response to Ca^{2+}. Familial hypertrophic myopathy is now characterized as a "sarcomeric disease" on the basis of evidence that missense mutations in the myosin heavy chain [9] and in tropomyosin (Tm) and troponin T (TnT) [10] are causal. Finally, recent evidence indicates that pharmacological manipulation of the response of the myofilaments to Ca^{2+} by agents increasing Ca^{2+} affinity of TnC [11] may alter the energy requirements for the pumping function of the heart [12].

SWITCHING THE THIN FILAMENT "ON" THROUGH Ca-TnC

It is apparent that Ca^{2+} binding to TnC promotes the reaction between actin and myosin by affecting a slow step involving isomerization of a weak binding state, actin–myosin–ADP [13–15]. However, a current unresolved issue is just what is regulated when Ca^{2+} binds to TnC. One possibility is that Ca^{2+} acts as a switch and promotes the transition from the weak to the strong state in an "all or none" fashion [16]. In this case Tm acts to enhance the affinity of crossbridges for actin, and relative activation of the myofilaments by Ca^{2+}, say at the 50% level would involve 50% of the crossbridges "recruited" to the strong state. A different view is that Ca^{2+} increases the rate of transition from the weak to the strong state in a "graded" fashion [17]. In this case, 50% relative activation of the myofilaments could involve all of the crossbridges in an activated state, but with the forward rate of transition between weak and strong states at some sub-maximal level [17]. A choice between these possibilities is difficult in that the conclusions from particular experiments are dependent on the methods used and may be model dependent [7].

Whether "all or none" or "graded" in terms of activation of the thin filament, there is an emerging picture of how the reaction of Ca^{2+} with TnC is transduced to affect the reactivity of actin [1, 2]. Figure 1 illustrates the molecular processes that are believed to occur in triggering the actin–myosin crossbridge reaction and shows the thin filament in "on" and "off" states. The "off" state is associated with low cytosolic Ca^{2+}; there are weak interactions between TnC and TnI and possibly between TnC and TnT; TnI binds to actin strongly [1, 2]. The "off" state may also be characterized by a poorly understood interaction of TnI with TnT, and a potential interaction of TnT with actin [18]. These interactions, which are transmitted to Tm through TnT, hold Tm in a conformational state or location that alters actin activity such that the actin–crossbridge reaction is impeded. The strong interaction of TnI with actin in relaxing conditions also is likely to inhibit the reaction of crossbridges and has been speculated to produce the "blocked" state [19]. As depicted in Fig. 1, these inhibitory reactions are reversed when Ca^{2+} binds to TnC and result in an activation of myofilament activity.

A key reaction central to the release from inhibition is the tight binding of TnC with TnI upon Ca^{2+}–binding to the regulatory site of TnC. The topology of the interactions are presently being sorted out and a current working model is depicted in Fig. 2. The regulatory Ca^{2+}–binding domain (II) is at the NH_2–terminal (N) domain. Site I is a mutated site that, unlike the case with sTnC, does not bind Ca^{2+} in the physiological range of concentrations. Site III and IV, which are joined to the N domain of cTnC by an alpha-helical stalk, are the high affinity Ca^{2+}/Mg^{2+} sites. The domains of cTnI are depicted as a

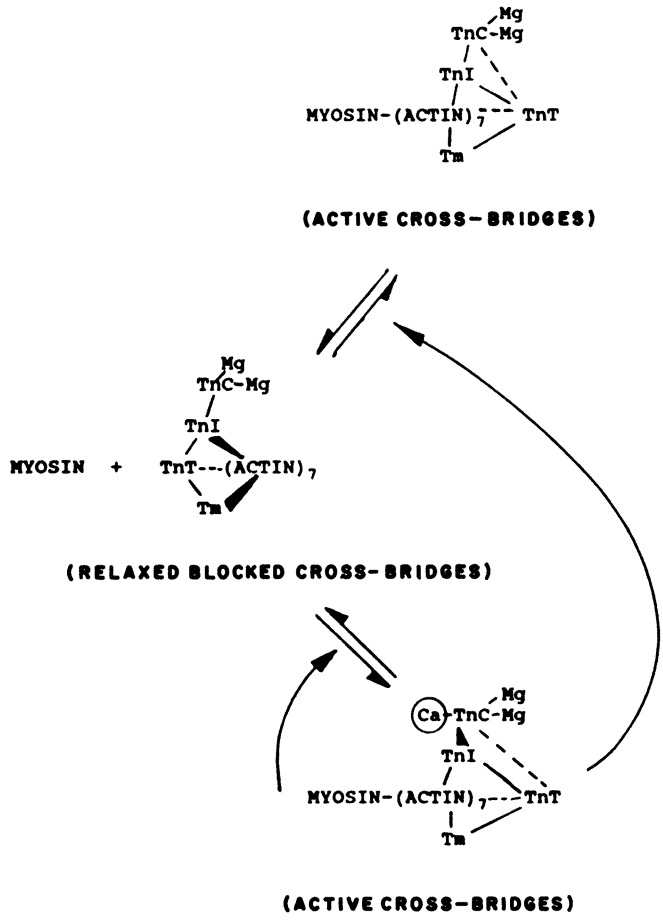

Figure 1. Scheme depicting modes of activation of thin cardiac myofilaments by calcium–TnC and by strong crossbridges. The figure demonstrates that thin filaments are turned on by calcium through TnC and by the binding of the crossbridge.

COOH-terminal (C) domain, an inhibitory domain (I) and an N domain. The N domain demonstrates a unique extension of some 32 amino acids not present in skeletal TnI [1]. As shown in Fig. 2, this stretch of amino acids contains Ser 23/24 that are substrates for protein kinase A [4, 5]. Also shown in Fig. 2 are primary structures of some other important domains of cTnI– the I domain which shuttles between binding to TnC and actin; the putative cTnT binding and pH sensitive domains. The sequences shown below the cardiac sequence are homologous regions of the slow skeletal TnI (ssTnI), which is the embryonic isoform [6]. Functional differences between myofilaments containing ssTnI and cTnI suggest that isoform switching that occurs with development is associated with a reduced ability of acidic pH to deactivate the pCa–force relation. Using NMR spectroscopy and selective isotope labeling [20], we have shown that the arrangement of cTnI with cTnC is anti-parallel. Our studies indicate a strong interaction between the cTnI N domain and the C domain of cTnC [20]. Our hypothesis is that the C domain of cTnI (amino acids 81–211) also makes strong Ca^{2+}–dependent interactions with the helix D in the N domain of cTnC. In the case of sTnC–sTnI, a similar arrangement is obtained [21], yet the characterization

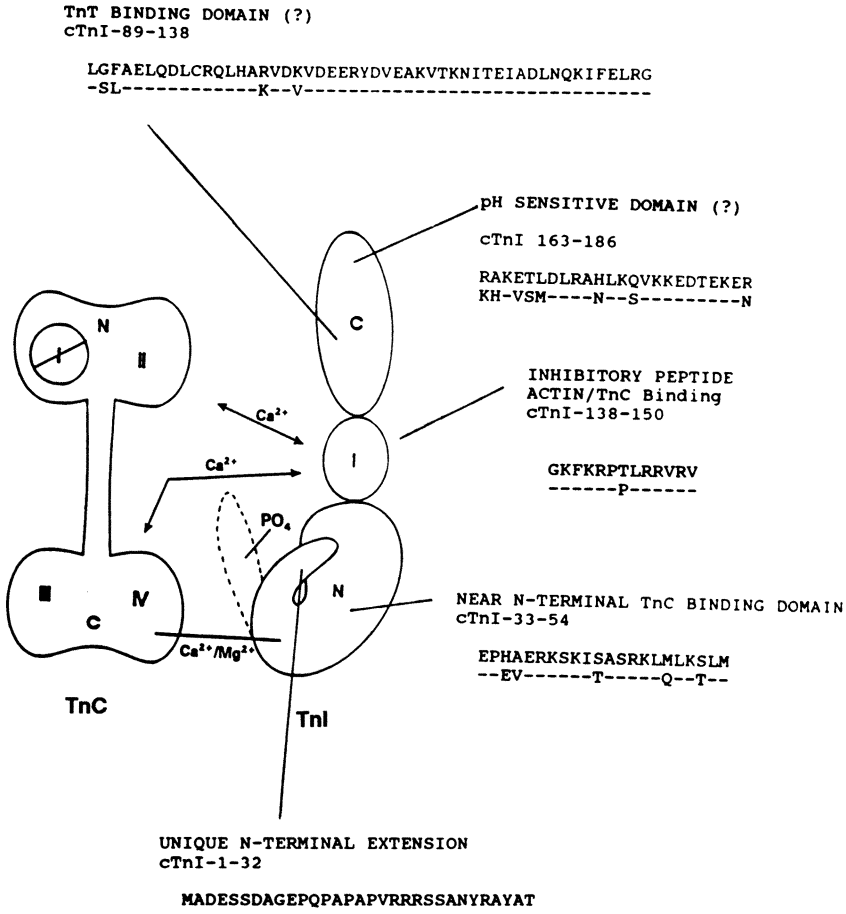

Figure 2. Schematic representation of the cTnC and cTnI interactions. Primary structures of various domains is shown in the upper lines for the cardiac variant with the homologous structure of slow skeletal variant (ssTnI) below.

of the N domain of TnI as purely structural [21] cannot be the case in cTnI. Although we [22] have also shown that removal of the N domain of cTnI has no effect of Ca^{2+} activation of myofibrillar ATPase activity, or its inhibition by acidic pH, phosphorylation of amino acids (Ser 23/24) in the unique N domain affects the Ca^{2+}-sensitivity of myofilament activation [4, 5]. There are prolines in this domain suggesting that phosphorylation results in a movement of the extension as shown in Fig. 2.

SWITCHING THE THIN FILAMENT "ON" THROUGH STRONG CROSSBRIDGES

There is much evidence that, in striated muscle, myosin is not only a molecular motor but is involved in activation of the thin filament [19, 23]. Important conclusions from these studies are as follows: 1) Although Ca^{2+} is a required co-factor, strong crossbridges are required to fully turn on the thin filament. 2) Myosin heads bind cooperatively;

crossbridge binding may compete for the same thin filament sites with Tm and perhaps TnT–TnI, as well. 3) The size of the cooperative unit may involve more than 7 actins and be altered by Tn. Thus, strong crossbridges are themselves able to reverse the inhibited state and it is apparent that the state of activity of TnI may modulate this mode of activation. TnI could do this sterically by modulating a blocked state in which TnI impedes the actin–crossbridge reaction or allosterically by modulating actin activity. A potential mechanism is phosphorylation of cTnI by protein kinase C, which inhibits myosin head binding and maximum actomyosin ATPase rate even at saturating levels of free Ca^{2+} [24]. Sites on cTnI involved in this effect appear to be Ser 43/45 in the near N–terminal TnC binding domain (Fig. 2; Noland, Guo, Solaro and Kuo, unpublished observations).

CONCLUSION

A useful working model of the molecular switch that turns on the thin filament is as follows: In diastole, cTnI is fixed to cTnC by Ca^{2+}/Mg^{2+} binding to sites III and IV of the N domain, which binds tightly to the N domain of cTnI. Release of Ca^{2+} into the myofilament space results in Ca^{2+}–binding to a single regulatory site on TnC (Site II). cTnI moves away from actin and binds tightly to cTnC through the C domain of cTnI. Phosphorylation of the N domain reduces the affinity of TnI for TnC as well as it reaction with actin–Tm–Tn. Moreover, the molecular switch may involve two types of processes, a release from a blocked state and an increase in the rate constants for transition from the weak to the strong binding state. Tropomyosin or TnI (and potentially TnT) may modulate activation of functional units by strong crossbridges. Thus, a particular contractile state may be perceived as a balance between the steric/allosteric activation of the myofilaments by Ca^{2+} working through TnC–TnI–TnT–Tm and the cooperative activation of the myofilaments by crossbridges.

Acknowledgments

The author is supported by research grants NIH RO1–HL22231 and R01 HL49934.

DISCUSSION

Dr. M. Lab: How fast can you get these phosphorylation changes? Can you have a microenvironment where you can have a beat–to–beat change in phosphorylation?

Dr. J. Solaro: It is not unlikely that one could get beat–to–beat changes in pH. The phosphorylation seems slower than that, but it may be related to the time resolution of the measurements.

Dr. A. Landesberg: Hoffman and Fuchs [*Am J Physiol.* 1987;253:C90–C96; *Am J Physiol.* 1987;253:C541–C546] have shown that crossbridge binding affects the affinity of calcium to troponin in the cardiac muscle. This phenomena was not described in the skeletal muscle. Do you have any explanations for this difference between cardiac troponin and skeletal muscle troponin in the molecular structure?

Dr. J. Solaro: When you lock all the crossbridges on the thin filament in a rigor state, then you can see a change in affinity, which suggests that there is, and by a detailed balance you would

expect that to occur. When we made very careful measurements of that, we saw small effects that are insignificant when one looks at direct measurements using calcium 45. So we have not actually seen much of an effect of active crossbridges on calcium binding. If there is an effect I think it is probably relatively small.

Dr. D. Burkhoff: Could you comment, on the other hand, about how length might affect calcium binding?

Dr. J. Solaro: We think that the major effect of length on activation is probably through interfilament spacing and not on calcium binding to troponin-C. Our reason for this is that with the cardiac TmC variant that exists in slow skeletal muscle, one still gets a length dependence of activation, independent of changes in calcium binding. In our own measurements of calcium binding with length, we have seen some relatively small changes. But I think its an epiphenomenon, and it is not the main basis for the length dependent activation. Skeletal muscle does not seem to require it.

Dr. H. ter Keurs: Every thin filament in cardiac muscle is accompanied by, and probably according to recent reports bound to, titan filaments. I did not see any titan there. Could you speculate how titan might interact with the protein regulatory proteins that you have described?

Dr. J. Solaro: We have never made any measurements of exactly how titan interacts with any of these components across the filaments. It would be pure guess work. But indeed, there is a calcium binding domain. There are calmodulin-like domains that can bind calcium with relatively low affinity. One could possibly imagine that there may be some interaction, but I do not know of any evidence for it myself. There is also a whole range of phosphorylation sites.

REFERENCES

1. Solaro RJ, Pan BS. Control and modulation of contractile activity of cardiac myofilaments, in Sperelakis N (ed): *Physiology and Pathophysiology of the Heart.* Boston: Kluwer Academic Publishers; 1988:291–293
2. Moss RL. Ca^{2+} regulation of mechanical properties of striated muscle: mechanistic studies using extraction and replacement of regulatory proteins. *Circ Res.* 1992;70:865–884.
3. Allen DG, Kentish JC. The cellular basis of the length-tension relation in cardiac muscle. *J Mol Cell Cardiol.* 1985;17:821–840.
4. Solaro RJ. Protein phosphorylation and the cardiac myofilaments. In: Solaro RJ, ed. *Protein Phosphorylation in Heart.* Boca Raton: CRC Press, Inc.; 1986:129–156.
5. Solaro RJ. Modulation of activation of cardiac myofilaments by beta-adrenergic agonists. In: Lee JA, Allen DG, eds. *Modulation of Cardiac Calcium Sensitivity*, Oxford: Oxford University Press; 1993:161–177.
6. Solaro RJ, Lee J, Kentish J, Allen DA. Differences in the response of adult and neonatal heart muscle to acidosis. *Circ Res.* 1988;63:779–787.
7. Westfall MV, Solaro RJ. Alterations in myofibrillar function and protein profiles following global ischemia in rat hearts. *Circ Res.* 1992;70:302–313.
8. Anderson PAW, Malouf NN, Oakeley A, Pagani ED, Allen PD. Troponin T isoform expression in humans: A comparison among normal and failing adult heart, fetal heart, and adult and fetal skeletal muscle. *Circ Res.* 1991;60:1226–1233.
9. Tanigawa G, Jarcho JA, Kass S, Solomon SD, Vosberg JG, Seidman JG, Seidman CE. A molecular basis for familial hypertrophic cardiomyopathy: an α/β cardiac myosin heavy chain hybrid gene. *Cell.* 1990; 622:991–998.
10. Thierfelder L, Watkins H, MacRae C. Alpha-tropomyosin and cardiac troponin T mutations cause familial hypertrophic cardiomyopathy: a disease of the sarcomere. *Cell.* 1994;77:701–712.
11. Fujino K, Sperelakis N, Solaro RJ. Sensitization of dog and guinea pig cardiac myofilaments to Ca^{2+}-activation and inotropic effect of pimobendan: Comparison with milrinone. *Circ Res.* 1988;63:911–922.

12. Mori M, Takeuchi M, Takaoka H, Hata K, Yamakawa H. New Ca^{2+} sensitizer, MCI-154, reduces myocardial oxygen consumption for non-mechanical work in diseased human hearts. *Circulation.* 1994;92(4) Part 2, I-217.
13. Millar N, Homsher E. The effect of phosphate and Ca on force generation in glycerinated rabbit skeletal muscle fibers. *J Biol Chem.* 1990;265:20234-20240.
14. Kawai M, Saeki Y, Zhao Y. Crossbridge scheme and the kinetic constants of elementary steps deduced from chemically skinned papillary and trabecular muscles of the ferret. *Circ Res.* 1993;73:35-50.
15. Walker JW, Lu Z, Moss RL. Effects of Ca^{2+} on the kinetics of phosphate release in skeletal muscle. *J Biol Chem.* 1992;267:2459-2466.
16. Kress M, Huxley HE, Faruqi AR, Hendrix J. Structural changes during activation of frog muscle studied by time resolved X-ray diffraction. *J Mol Biol.* 1986;188:325-342.
17. Brenner B. Changes in calcium sensitivity at the crossbridge level. In: Lee JA, Allen DG, eds. *Modulation of Cardiac Calcium Sensitivity*, Oxford: Oxford University Press; 1993:197-214.
18. Heeley DH, Smillie LB. Interaction of rabbit skeletal muscle troponin T and F-actin at physilogical ionic strength. *Biochemistry.* 1988;27:8227-8231.
19. Lehrer S. The regulatory switch of the muscle thin filament: Ca^{2+} or myosin heads? *J Mus Res Cell Motility.* 1994;15:232-236.
20. Krudy G, Kleerkoper Q, Guo X, Howarth JW, Solaro RJ, Rosevear PR. NMR studies delineating spatial relationships within the cardiac troponin I-troponin C complex. *J Biol Chem.* 1994;269:23731-23735.
21. Farah CS, Miyamoto CA, Ramos CHI. Structural and regulatory functions of the NH_2 and COOH-terminal regions of skeletal muscle troponin I. *J Biol Chem.* 1994;269:5230-5240.
22. Guo X, Wattanapermpool J, Palmiter KA, Murphy AM, Solaro RJ. Mutagenesis of Cardiac Troponin I. Role of the Unique NH_2-Terminal Peptide in Myofilament Activation. *J Biol Chem.* 1994;269:15210-15216.
23. Bremel R, Murray J, Weber A. Manifestations of cooperative behavior in the regulated actin filament during actin-activated ATP hydrolysis in the presence of calcium. *Cold Spring Harbor Symp Quant Biol.* 1973;37:267-275.
24. Noland TA Jr, Kuo JF. Protein kinase C phosphorylation of cardiac troponin I or troponin T inhibits Ca^{2+}-stimulated actomyosin MgATPase activity. *J Biol Chem.* 1991;266:4974-4978.

CHAPTER 13

THE GATA-4 TRANSCRIPTION FACTOR TRANSACTIVATES THE CARDIAC-SPECIFIC TROPONIN C PROMOTER-ENHANCER IN NON-MUSCLE CELLS

Hon S. Ip,[1] David B. Wilson,[3,4] Markku Heikinheimo,[3,4] Jeffrey M. Leiden,[1,2] and Michael S. Parmacek[1]

ABSTRACT

The unique contractile phenotype of cardiac myocytes is determined by the expression of a set of cardiac-specific genes. By analogy to other mammalian developmental systems, it is likely that the coordinate expression of cardiac genes is controlled by lineage-specific transcription factors that interact with promoter and enhancer elements in the transcriptional regulatory regions of these genes. Here, we demonstrate that the slow/cardiac-specific troponin C (cTnC) enhancer contains a specific binding site for the lineage-restricted, zinc finger transcription factor, GATA-4 and that GATA-4 mRNA and protein is expressed in cardiac myocytes. In addition, GATA-4 binding sites were identified in several previously characterized cardiac-specific transcriptional regulatory elements. The cTnC GATA-4 binding site is required for transcriptional enhancer activity in primary cardiac myocytes. Moreover, the cTnC enhancer can be transactivated by overexpression of GATA-4 in non-cardiac muscle cells such as NIH 3T3 cells. Taken together, these results are consistent with a model in which GATA-4 functions to direct tissue-specific gene expression during mammalian cardiac development.

INTRODUCTION

Vertebrate striated muscle is composed of two functionally distinct mesodermally-derived cell lineages: cardiac and skeletal (fast and slow) muscle. The diverse functional

Departments of Medicine[1] and Pathology[2] University of Chicago, Chicago, IL, and Departments of Pediatrics[3] and Molecular Biology and Pharmacology[4], Washington University School of Medicine, St. Louis, MO, USA.

Molecular and Subcellular Cardiology: Effects of Structure and Function
Edited by S. Sideman and R. Beyar, Plenum Press, New York, 1995

capacities of these lineages are determined by the expression of distinct sets of tissue-specific genes including those encoding myofibrillar isoforms, cell-surface receptors, and lineage-specific enzymes. The tissue-specific pattern of expression of many muscle genes is controlled at the level of transcription. Therefore, an understanding of muscle cell development must at some level be based upon elucidating the molecular mechanisms that control lineage-specific gene expression during myogenesis.

Recent studies have suggested that GATA-4, a newly identified GATA transcription factor, may play a role in cardiac development [1, 2]. In the mouse, the GATA-4 gene is first expressed in the coelomic epithelial cells of the primitive streak embryo at p.c. day 7 [3]. GATA-4 mRNA is clearly detectable within the primordial heart tube at p.c. day 8, and it continues to be expressed in the heart throughout the life of the animal. Later in embryonic development, GATA-4 is expressed in the intestinal epithelial cells and in the germ cells within the seminiferous tubule. Although this tissue-restricted pattern of expression suggested that GATA-4 might play a role in regulating lineage-restricted gene expression in the heart, GATA-4 has not been shown to date to bind to or regulate the expression of cardiac-specific genes.

The murine slow/cardiac troponin C (cTnC) gene has been used as a model system to examine the molecular mechanisms that regulate cardiac-specific transcription during mammalian development [4, 5]. cTnC gene expression is restricted to adult slow skeletal and cardiac muscle and is controlled at the level of transcription [4]. We have previously identified a cardiac-specific transcriptional enhancer located within the immediate 5' flanking region of the cTnC gene (bp −79 to −124). This enhancer functions in concert with the cTnC promoter to program high-level transcription in both cultured cardiac myocytes and in cardiac muscle *in vivo* [5]. The cTnC enhancer contains two functionally important nuclear protein binding sites designated CEF-1 and CEF-2. Both sites have been shown to bind cardiac-restricted nuclear protein complexes [5]. In this report, we present data which demonstrate that GATA-4 plays an important role in regulating cTnC gene expression in the heart and suggest that GATA-4, like GATA-1 and GATA-3, may be an important regulator of lineage-specific gene expression during mammalian development.

MATERIALS AND METHODS

Cells and media. NIH 3T3 and COS-7 cells were grown in Dulbecco's modified Eagle's medium (DMEM)-10% fetal bovine serum-1% penicillin and streptomycin (GIBCO, Gaithersburg, MD). Primary cultures of neonatal rat cardiac myocytes and fibroblasts were isolated and grown as described previously [5].

Plasmids. The promoterless control plasmid, pCAT-Basic (Promega, Madison, WI), and the p-124CAT plasmid, containing the 156-bp (bp −124 to +32) cTnC cardiac-specific promoter and enhancer subcloned 5' of the chloramphenicol-acetyl transferase (CAT) reporter gene have been described previously [5]. The p-124CATmCEF-1 plasmid containing five nucleotide substitutions within the CEF-1 GATA-4 binding site within the context of the 156-bp cTnC promoter-enhancer was constructed using PCR-mediated site-directed mutagenesis and subcloned into HindIII/XbaI digested pCAT-Basic plasmid as described previously [5]. The sequence of the mutated 156-bp fragment was confirmed by dideoxy-sequence analysis. The pMSVβgal reference plasmid contains the β-galactosidase gene under the control of the MSV LTR. The control expression plasmid pMT2 and the eukaryotic expression plasmid pMT2-GATA-4 were described previously [1]. The plasmid GATA-4/pGEM7Z contains the full-length murine GATA-4 cDNA [1] cloned into the EcoRI site of pGEM7Z (Promega).

Transfections and CAT assays. Cultures of rat neonatal cardiac myocytes were transfected as described previously [5].

EMSAs. Nuclear extracts were prepared from cultures of primary neonatal rat cardiac myocytes and fibroblasts as described previously [5]. In addition, nuclear extracts were prepared 48 hours following transient transfection of COS-7 cells with either the pMT-2 or pMT2-GATA-4 expression vectors according to the procedure of Andrews and Faller [6]. The following complementary oligonucleotides were synthesized with BamHI and BglII overhanging ends on an Applied Biosystems model 380B DNA synthesizer:

CEF-1	5' CCAGCCTGAGATTACAGGGA 3'
mCEF-1	5' CCAGCCTGGGGCCCCAGGGA 3'
CEF-2	5' GGTGGAGGATATTCCAGG 3'
mCEF-2	5' GGTGGAGGGCCCTCCAGG 3'
αglobin	5' TCCGGCAACTGATAAGGATTCCCT 3'

Electrophoretic mobility shift assays were carried out as described previously [5].

RESULTS

Identification of a GATA-4 Binding Site in the cTnC Enhancer

Previous studies have identified four functionally important nuclear protein binding sites in the murine cTnC promoter-enhancer (Fig. 1A) [5]. The first of these sites, termed CEF-1, contains the nucleotide sequence AGATTA which conforms to one of the high affinity GATA binding sites identified by random site selection analyses, but differs from the consensus GATA-binding sequence (WGATAR) by a single nucleotide substitution (Fig. 1A) [7-9]. In addition, the second nuclear protein binding site in the cTnC enhancer,

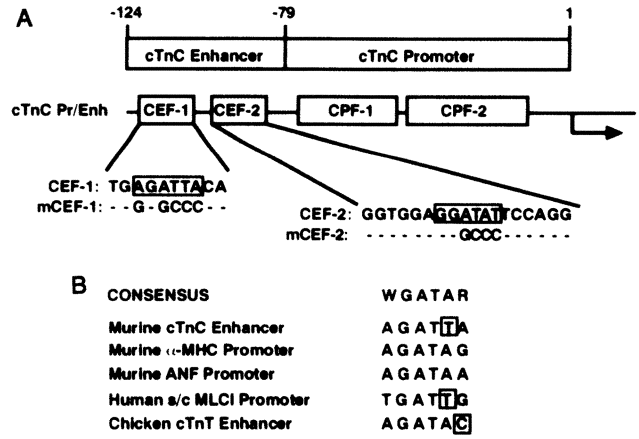

Figure 1. Identification of potential GATA binding sites in the cTnC enhancer and other cardiac genes. **A:** Schematic representation of the cTnC cardiac-specific promoter-enhancer (bp -124 to +1) (54). The four functionally important nuclear protein binding sites designated CEF-1, CEF-2, CPF-1 and CPF-2 are boxed (5). The nucleotide sequence of the putative CEF-1 and CEF-2 GATA binding sites (boxed) are shown beneath the respective binding sites. The nucleotide substitutions in the GATA site of CEF-1 (mCEF-1) and CEF-2 (mCEF-2) are shown. **B:** Comparison of the nucleotide sequences of the consensus GATA binding site (CONSENSUS) with potential GATA binding sites in other cardiac muscle genes: murine cTnC enhancer, murine α-myosin heavy chain (MHC) promoter, murine atrial natriuretic factor (ANF) promoter, human slow/cardiac myosin light chain 1 (MLC1) promoter, and chicken cardiac troponin T (cTnT) promoter-enhancer.

CEF–2, contains the nucleotide sequence GGATAT which contains the GATA core motif, but differs from the consensus GATA–binding sequence in its flanking residues (Fig. 1A). Of note, related motifs are present in the transcriptional regulatory elements of multiple cardiac genes (Fig. 1B).

Binding GATA–4 from Cardiac Nuclear Extracts to CEF–1

To determine if cardiac nuclear extracts contained GATA–4 that could bind to the CEF–1 element of the cTnC enhancer, cardiac nuclear extracts were used in EMSAs in conjunction with a radiolabeled CEF–1 probe and a GATA–4–specific antiserum (Fig. 2). Cardiac nuclear extracts contained a major CEF–1 binding activity (lane 2, arrow) which was identical to GATA–4 by several criteria. First, it was competed by unlabelled CEF–1 oligonucleotide (lanes 3 and 4) and by the GATA binding site from the α1–globin promoter [10] (lanes 5 and 6). In contrast, it was not competed by the mCEF–1 oligonucleotide containing five nucleotide substitutions in the GATA site (lanes 7 and 8). Second, this complex was supershifted by a GATA–4–specific antiserum (lane 10, dashed arrow), but not by a preimmune serum (lane 9). Finally, this cardiac nuclear complex co–migrated with recombinant GATA–4 protein prepared by transfection of COS–7 cells with a GATA–4 eukaryotic expression vector (compare lanes 2 and 12). Thus, we concluded that cardiac nuclear extracts contain GATA–4 that can bind to CEF–1. Two additional CEF–1 binding activities were observed in the cardiac nuclear extracts. The rapid mobility

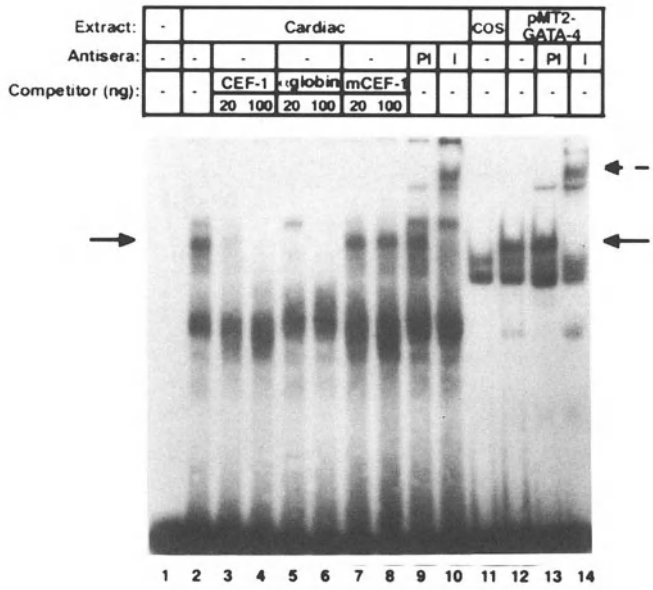

Figure 2. Binding of GATA–4 from nuclear extracts to the CEF–1 site of the cTnC enhancer. Radiolabeled CEF–1 oligonucleotides were used in EMSAs with nuclear extracts prepared from neonatal rat hearts (Cardiac), COS–7 cells transfected with the control plasmid pMT–2 (COS) and COS–7 cells transfected with the GATA–4 eukaryotic expression plasmid pMT–2–GATA–4 (pMT2–GATA–4). Where indicated, binding reactions were pre–incubated with either control preimmune rabbit antiserum (PI), a GATA–4–specific rabbit antiserum (I), or 20–100 ng of unlabelled competitor oligonucleotides. The bands corresponding to the GATA–4 nuclear protein complex and the antibody supershifted GATA–4 protein complex are indicated with black and dashed arrows, respectively.

complex does not appear to represent a specific binding activity as it was not competed by excess unlabelled CEF-1 oligonucleotide. The slower mobility complex does not appear to represent a GATA binding activityas it is not competed by excess unlabelled oligonucleotide corresponding to the GATA binding site from the α1-globin promoter.

Functional Significance of the GATA Site for cTnC Enhancer Activity

To determine the role of the CEF-1 GATA binding site in the transcriptional activity of the cTnC promoter-enhancer in cardiac myocytes, CAT reporter constructs containing the wild-type cTnC promoter-enhancer (p-124CAT) or the cTnC promoter-enhancer containing a mutated GATA-4 binding site (p-124CATmCEF-1) were transfected into primary cardiac myocytes. The wild-type cTnC promoter-enhancer increased CAT expression by 50-fold as compared to a control CAT reporter construct lacking a functional promoter or enhancer (pCAT-Basic) (Fig. 3). Mutation of the GATA-4 binding site in CEF-1 resulted in a 90% reduction in the transcriptional activity of the cTnC promoter-enhancer (Fig. 3). Thus, the GATA-4 binding site is required for the transcriptional activity of the cTnC gene in cardiac myocytes.

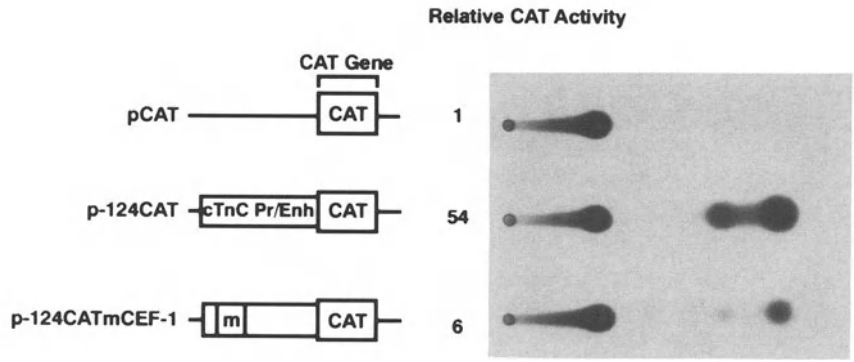

Figure 3. The GATA-4 binding site is required for the activity of the cTnC promoter-enhancer in neonatal cardiac myocytes. Fifteen μg of the cTnC-CAT reporter plasmids (schematically represented at the left) and 5 μg of the pMSVβgal reference plasmid were transfected into cultures of primary neonatal rat cardiac myocytes, and CAT and β-galactosidase activities were determined. CAT activities, corrected for differences in transfection efficiencies, were normalized to the CAT activity observed following transfection of the promoterless control plasmid, pCAT-Basic, which produced 0.5% acetylation. A representative CAT assay is shown at the right.

GATA-4 Activates Transcription of the cTnC Enhancer in Non-Muscle Cells

The cTnC transcriptional enhancer is not active in non-cardiac muscle cell lineages [5]. Similarly, GATA-4 is not expressed in non-cardiac muscle cells such as NIH 3T3 cells. Therefore, it was of interest to determine whether forced expression of GATA-4 can activate transcription from the cTnC promoter-enhancer in 3T3 cells. 3T3 cells were co-transfected with a CAT reporter construct containing the intact cTnC promoter-enhancer and a GATA-4 eukaryotic expression vector (pMT2-GATA-4) (Fig. 4). Consistent with previous reports [5], the p-124CAT reporter construct was inactive in 3T3 cells (lane 1). However, co-transfection of the pMT2-GATA-4 expression plasmid with the p-124CAT reporter construct resulted in a 45-fold increase in transcription from the cTnC promoter-

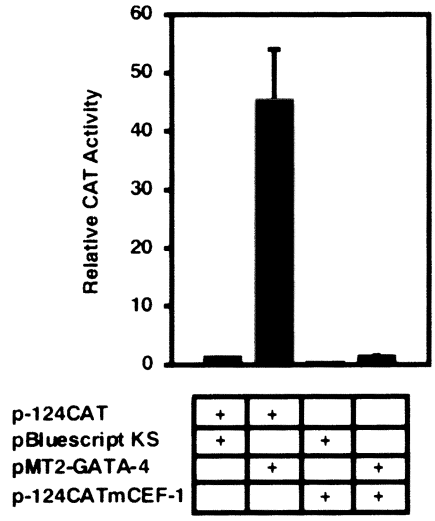

Figure 4. GATA-4-modulated transactivation of the cTnC promoter-enhancer in NIH 3T3 cells. NIH 3T3 cells were transfected with 24 μg of the p-124CAT reporter plasmid containing the wild-type cTnC promoter-enhancer (p-124CAT +) or the p-124CATmCEF-1 reporter plasmid containing a five nucleotide substitution in the CEF-1, GATA-4 binding site (p-124CATmCEF-1 +), and either 6 μg of the control plasmid pBluescript KS (pBluescript +) or 6 μg of the GATA-4 expression plasmid pMT2-GATA-4 (p-124CATmCEF-1 +). All transfections also contained 5 μg of the pMSVβgal reference plasmid. Forty-eight hours after transfection, CAT and β-galactosidase activities were determined. CAT activities, corrected for differences in transfection efficiencies, were normalized to the CAT activity obtained following transfection of the p-124CAT plasmid with the pBluescript KS control plasmid, which produced 0.1% acetylation. The data are presented as relative CAT activities ± S.E.M.

enhancer (lane 2). To determine whether this increase in transcription was dependent upon an intact CEF-1 GATA-4 binding site, we tested the effects of GATA-4 expression on the transcriptional activity of the p-124CATmCEF-1 reporter plasmid containing a 5 nucleotide substitution in the CEF-1 GATA-4 site of the cTnC enhancer (lanes 3 and 4). GATA-4 did not significantly activate transcription of the cTnC enhancer containing a mutant GATA-4 binding site. Thus, GATA-4 can transactivate the intact cTnC promoter-enhancer in non-muscle cells and this transactivation requires the CEF-1 GATA-4 binding site.

DISCUSSION

A large number of studies have provided evidence for the importance of the skeletal muscle-restricted bHLH and MEF-2 transcription factors in the regulation of skeletal muscle development. Several lines of evidence now suggest that GATA-4 may play an important role in cardiac muscle development. GATA-4 is expressed early during cardiac myogenesis in the mouse, and its expression is restricted to the developing heart and pre-cardiac mesoderm during early murine development [1, 3]. GATA-4 binding sites are present in the transcriptional regulatory regions of multiple cardiac genes (Fig. 1B). Most importantly, GATA-4 can directly activate the expression of at least one cardiac-specific gene in non-muscle cells. Despite these results, the findings that GATA-4 is expressed in

non-cardiac muscle in later development, and that other GATA family members which have been reported to bind to similar sequence motifs are widely expressed in the mouse, raise important questions about the mechanisms by which GATA-4 might regulate lineage-specific gene expression during cardiac myogenesis.

Previous studies of the role of the GATA proteins in regulating lineage-specific gene expression in T cells and erythroid precursors have strongly suggested that GATA proteins interact cooperatively with other transcription factors to regulate lineage-specific gene expression in these systems (reviewed in [9, 11]). For example, GATA-1 functions in conjunction with NF-E2 in regulating the transcription of the globin locus control region (LCR). In addition, the α- and β-globin promoters contain binding sites for both GATA and CACCC box-binding factors. In this light, it is of interest that the cTnC promoter-enhancer contains at least three additional nuclear protein binding sites, each of which has been shown to be important for the activity of this enhancer in cardiac myocytes [5]. Of note, the CEF-2 nuclear protein binding site, which contains the nucleotide sequence GGATAT, failed to bind GATA-4. However, EMSAs revealed that the CEF-1 and CEF-2 probes (each of which contain the nucleotide sequence GANATTNCAGG) do bind a common lineage-restricted nuclear protein complex. Moreover, a four nucleotide substitution in CEF-2 which abolished the binding of this complex (see Fig. 1A, mCEF-2) dramatically reduced the activity of the cTnC in cardiac myocytes (data not shown). Taken together, these data suggest that a potentially novel lineage-restricted transcription factor (or factors) binds to both the CEF-1 and CEF-2 elements and may, in conjunction with GATA-4, CACCC box binding factors and M-CAT/TEF-1, play an important role in regulating transcription of the cTnC gene in cardiac myocytes. The identity of this novel factor, which is clearly distinct from GATA-4, is currently under investigation.

CONCLUSION

In addition to playing a potentially important role in controlling lineage-specific gene expression during cardiac development, GATA-4 serves as an early marker of differentiating cardiac mesoderm [1-3]. Thus, it will be of interest to elucidate the transcriptional mechanisms controlling GATA-4 expression in pre-cardiac mesoderm. We have shown previously that GATA-4 can be induced in F9 cells by treatment with retinoic acid [1]. It is possible that GATA-4 can function as a retinoic acid-responsive transcription factor during cardiac development. Recent studies have described an evolutionarily conserved homeobox gene, Csx-1/Nkx 2.5 [12, 13] which, like GATA-4, is expressed early during cardiac development. Future studies should elucidate the relationship between GATA-4, Csx-1 and other cardiac-restricted transcription factors expression in developing cardiac myocytes.

Acknowledgments

Some of the material in this manuscript was originally published in *Molecular and Cellular Biology* 1994;14:7517-7526 and is reprinted with permission from the publisher. This work was supported in part by Public Health Service grant 1R01HL51145-01 and an American Heart Association Grant-In-Aid to M.S.P.

DISCUSSION

Dr. G. Kessler-Icekson: How about the time course of expression of these transcription factors and do they respond to embryonic morphogenic factors like retinoic acid?

Dr. M. Parmacek: We have done very careful studies. In the very best study, Dave Wilson in Development looked at the time course very carefully. GATA-4 is first at Day 7 to 7.25 of mouse development. It preceeds other cardiac specific contractile proteins by about a half day; those are expressed at about Day 7.5 to 7.75. That is fairly uniform amongst many of the contractile proteins, although interestingly, the ANF gene does not come out until much later in development, at about Day 16. Nemer in Montreal has suggested [14] that GATA-4 regulates ANF gene expression. There is an interesting time discrepancy suggesting that other factors are important for ANF.

Does retinoic acid play a role? The first paper which described GATA-4 suggested that retinoic acid induced GATA-4 expression in F9 cells, which are undifferentiated mesodermal cells. Again, we are performing experiments with other groups, trying to determine if retinoic acid serves as an inducer of GATA-4 gene expression in cardiac development. It is unclear yet. There are retinoic acid receptor knockout mites produced in San Diego now. No one has looked to see if they express GATA-4. So that will be an interesting study to do.

REFERENCES

1. Arceci RJ, King AA, Simon MC, Orkin SH, Wilson DB. Mouse GATA-4: a retinoic acid-inducible GATA-binding transcription factor expressed in endodermally derived tissues and heart. *Mol Cell Biol.* 1993;13:2235-2246.
2. Kelley C, Blumberg H, Zon LI, Evans T. GATA-4 is a novel transcription factor expressed in endocardium of the developing heart. *Development* 1993;118:817-827.
3. Heikinheimo M, Scandrett JM, Wilson DB. Localization of transcription factor GATA-4 to regions of the mouse embryo involved in cardiac development. *Devel Biol.* 1994;164:361-373.
4. Parmacek MS, Leiden JM. Structure and expression of the murine slow/cardiac troponin C gene. *J Biol Chem.* 1989;264:13217-13225.
5. Parmacek MS, Vora AJ, Shen T, Barr E, Jung F, Leiden JM. Identification and characterization of a cardiac-specific transcriptional regulatory element in the slow/cardiac troponin C gene. *Mol Cell Biol.* 1992;12:1967-1976.
6. Andrews NC, Faller DV. A rapid micropreparation technique for extraction of DNA-binding proteins from limiting numbers of mammalian cells. *Nucleic Acids Res.* 1991;19:2499.
7. Ko LJ, Engel JD. DNA-binding specificities of the GATA transcription factor family. *Mol Cell Biol.* 1993;13:4011-4022.
8. Merika M, Orkin SH. DNA-binding specificity of GATA family transcription factors. *Mol Cell Biol.* 1993;13:3999-4010.
9. Orkin SH. GATA-binding transcription factors in hematopoietic cells. *Blood* 1992;80:575-581.
10. Martin D, Orkin SH. Transcriptional activation and DNA binding by the erythroid factor GF-1/NF-E1/Eryf 1. *Genes Dev.* 1990;4:1886-1898.
11. Orkin SH. Globin gene regulation and switching: circa 1990. *Cell* 1990;63:665-72.
12. Komuro I, Izumo S. Csx: a murine homeobox-containing gene specifically expressed in the developing heart. *Proc Natl Acad Sci USA.* 1993;90:8145-8149.
13. Lints TJ, Parsons LM, Hartley L, Lyons I, Harvey, RP. Nkx-2.5: a novel murine homeobox gene expressed in early heart progenitor cells and their myogenic descendants. *Development* 1993;119:419-431.
14. Grépin C, Dagnino L, Robitaille L, Haberstroh L, Antakly T, Nemer M. A hormone-encoding gene identified a pathway for cardiac but not skeletal muscle gene transcription. *Mol Cell Biol.* 1994;14: 3115-3129.

CHAPTER 14

SARCOMERE FUNCTION AND CROSSBRIDGE CYCLING

Henk E.D.J. ter Keurs[1]

ABSTRACT

The power of the heart is dictated by the force development and velocity of shortening (V) of the cardiac sarcomere. Both depend on the amount of Ca^{++} released by the sarcoplasmic reticulum during the action potential. We have investigated the inter-relationship between force (F) sarcomere length (SL) and V and the intracellular Ca^{++} concentration ($[Ca^{++}]_i$) in trabeculae isolated from the right ventricle of rat heart. Activation of the contractile filaments during a normal heartbeat requires approximately 30 μM Ca^{++} ions, which rapidly bind to cytosolic ligands. Consequently the $[Ca^{++}]_i$ transient detected by intracellular probes is less than 2 μM. Length dependent binding of Ca^{++} to Troponin-C is responsible for the shape of the F-SL relationship. Ca^{++} ions are bound to Troponin-C long enough to allow the F-SL relationship, and consequently the end-systolic pressure volume relationship in the intact ventricle, to be largely—but not completely—independent of the loading conditions. V increases hyperbolically with decreasing load during contraction against a load. Stiffness studies reveal that the number of attached crossbridges increases in linear proportion to an increase of the external load. At low external loads the V was large enough to induce a substantial viscoelastic load within the sarcomere itself. The F-V relationship of a single crossbridge appeared to be linear after correction for the observed viscoelastic properties of the muscle and for load dependence of the number of crossbridges. Maximal V of sarcomere shortening without an external load (V_0), depends on the level of activation by Ca^{++} ions because of the internal viscous load. Our studies of the rate of ATP hydrolysis by the actin-activated S_1 fragment of myosin suggest that V_0 is limited by the detachment rate of the crossbridge from actin. These studies also suggest that the difference between the fast (V_1) and slow (V_2) myosin iso-enzyme can be explained by a difference in the amino acid domain on S_1 involved in binding of the crossbridge to the actin filament.

[1]Departments of Medicine and Medical Physiology, the Faculty of Medicine, University of Calgary, Canada.

Molecular and Subcellular Cardiology: Effects of Structure and Function
Edited by S. Sideman and R. Beyar, Plenum Press, New York, 1995

INTRODUCTION

The strength of the heart beat can be modulated by interventions which affect the amount of Ca^{++} released into the cytosol of the myocytes, the sensitivity of the contractile system to Ca^{++} ions, and the sarcomere length at which the cardiac fibers contract. The rate of relaxation is modulated by interventions which determine the rate of Ca^{++} extrusion from the cytosol. Regulatory mechanisms involved in the control of the circulation affect the intact heart both through regulation of the interval between the heartbeats and via the effects of catecholamines on the cardiac myocytes, whereas variation of the fiber length is brought about by control of the filling pressure of the ventricles via control of the capacitance of venous system. To appreciate this component of the cardiovascular control we will discuss the fundamental aspects of cardiac excitation–contraction coupling and length dependence of the force of the heart beat in the following paragraphs.

CARDIAC EXCITATION–CONTRACTION COUPLING

It is well accepted that, during the action potential, Ca^{++} ions enter the cell through the dihydropyridine–sensitive channels. Most of this Ca^{++} is immediately bound to the Ca^{++} pump in the SR. Therefore, the amount of Ca^{++} that enters the cell during a given interval will depend upon the action–potential duration and heart rate. The Ca^{++} ions which enter through the T–tubuli start the process of excitation–contraction coupling by triggering release of Ca^{++} from the SR. The amount of Ca^{++} that is released is proportional to the Ca^{++} content of the SR and dictates the force of the cardiac contraction. The released Ca^{++} activates the contractile machinery and is subsequently eliminated from the cytosol via two pathways: i) Ca^{++} that was released by the SR together with Ca^{++} that entered the cell through the Ca^{++} channels during the action potential is re–sequestered by the SR [1]; ii) the remaining Ca^{++} is most probably extruded immediately after activation of contraction [2] through the cell membrane by the low–affinity, high–capacity, Na^{+}/Ca^{++} exchanger.

During the diastolic interval, the low–capacity high–affinity Ca^{++} pump in the cell membrane lowers the cytosolic Ca^{++} level further [3]. In the steady state, Ca^{++} efflux during the diastolic interval must balance the influx during the action potential. It follows that the amount of Ca^{++} that is accumulated in the SR also depends on the action–potential duration and the heart rate. It also follows from the above that a fraction of the Ca^{++} ions that is involved in the activation of contraction is re–circulated into the SR and becomes available for activation of the next beat, so force of the heart beat will depend on the force of the previous beat. Also, it takes some time before the Ca^{++} release process recovers completely from the last release and sequestered Ca^{++} can again be released from the SR. The force of the heartbeat will, therefore, depend strongly on heart rate and on the interval preceding an individual beat, as well as on the duration of the action potential [4.5]. The force of contraction of the quietly beating heart is probably only approximately one–third of the maximal force that can be generated by the contractile filaments, implying that the normal heart has a wide margin before its contractile reserves are exhausted.

CYTOSOLIC Ca^{++} AND STRENGTH OF THE HEART BEAT

Figure 1 shows twitch force and the estimated cytosolic $[Ca^{++}]$ as a function of time at an external $[Ca^{++}]_o$ of 1 mM in a preparation loaded by micro–injection of Fura–2 salt [4, 6]. The results are representative of contractions at short and long end–systolic

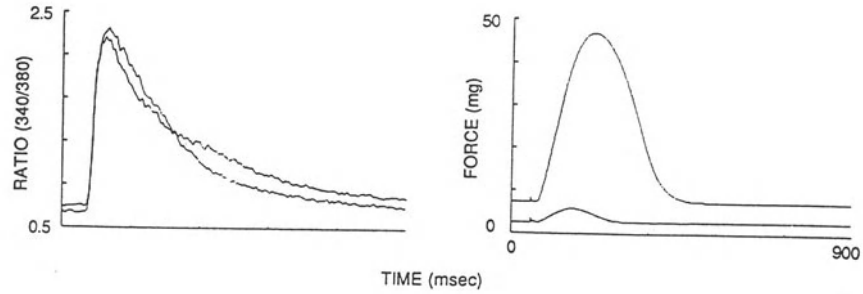

Figure 1. Left: transient changes of $[Ca^{++}]_i$ (as measured by the fluorescence ratio 340/380 of the compound FURA-2) during a twitch at two sarcomere lengths. **Right:** the corresponding forces at the two sarcomere lengths; the larger force corresponds to that recorded at an end-systolic sarcomere length of 2.15 μm while the smaller force corresponds to that at a sarcomere length of 1.6 μm. The Ca^{++} transient at the longer sarcomere length relaxes more rapidly in the early phase of relaxation than at the shorter sarcomere length. However, later in the relaxation process the Ca^{++} transient at the longer sarcomere length relaxes more slowly than at the shorter sarcomere length. As a result, the Ca^{++} transients at the two sarcomere lengths cross-over during the relaxation period (modified from Backx and ter Keurs [6], with permission).

sarcomere lengths, i.e. at the extremes of the function curve of cardiac muscle. Figure 1 shows typical behavior of mammalian cardiac muscle: the peak and time course of the Ca^{++} transients are remarkably independent of length, albeit the relaxation phases differ between the short and long muscle. The interpretation of the $[Ca^{++}]_i$ transients and their relation to force development requires caution, since it is known that full activation of the contractile system requires saturation of all the Troponin-C Ca^{++} sites (for which approximately 70 μM of $Ca^{++}$is needed) with simultaneous binding of another 50 μM of Ca^{++} to calmodulin [7]. Hence, even activation of the muscle at only 25% of maximum such as in this example, is accompanied by Ca^{++} turnover of ~30 μM. Only a small fraction of this Ca^{++} is "visible" in the cytosol.

It is unlikely that muscle stretch only affects the rate and/or amount of Ca^{++} release. Rather, the stretch-induced changes in the kinetics of the transient are consistent with the hypothesis that the force-length relation (as shown in Fig. 3) is determined principally by the length-dependent sensitivity of the contractile system (Fig. 2). It has been suggested that the length-dependent Ca^{++} sensitivity of the contractile system is actually due to troponin's stretch-dependent Ca^{++} affinity [8, 9]. Thus, much more Ca^{++} is bound by troponin-C in the stretched myocardium [9]. The peak amplitude of the $[Ca^{++}]_i$ transient is probably unchanged following stretch, both because more Ca^{++} is released by the SR and because more Ca^{++} is bound to the contractile filaments. This concept of the effect of length changes sounds attractive, but it should be remembered that an increase of the amount of Ca^{++} release by the SR has not yet been shown experimentally.

The relaxation phase of the Ca^{++} transient depends also on the rate of binding of Ca^{++} ions to the sarcolemmal Na^+/Ca^{++} exchanger and to the SR Ca^{++} pump as well as on their respective transport rates. Hence, studies at fixed muscle length allow evaluation of the influence of interventions on the rate of transport by those two mechanisms. Such evaluations have indicated that the rate of decline of the Ca^{++} transient depends about equally on the activity of the Na^+/Ca^{++} exchanger and the SR Ca^{++} pump [2]; the latter is modulated by phosphorylation of phospholamban due to second-messenger activation and probably due to Ca^{++}-activated calmodulin action [10].

THE FRANK-STARLING LAW OF THE HEART

Upon arrival of Ca^{++} ions in the vicinity of actin, Ca^{++} binds to Troponin-C and contraction begins. Figure 2 shows that the response of the contractile apparatus to Ca^{++} ions consists of a classical, sigmoidal, dose-response curve. These dose-response curves shift leftward (toward lower $[Ca^{++}]_i$) with stretch of the sarcomeres [8, 9]. This results in length dependence of force development, even when the Ca^{++} release by the SR is constant.

The force at the peak of a contraction is rather insensitive to the way in which the muscle contracted prior to the peak of force, and depends only upon the sarcomere length that exists at that moment. This means that the instantaneous force development of two contractions at the same "end-systolic" length is identical, even though one of the contractions is isometric while the other contraction, which started at a greater sarcomere length, has shortened to the given length while contracting against a load. Consequently, the same force-sarcomere length relationships are obtained from both isometric contractions and contractions in which substantial shortening occurs. This unique character of the force-length relationship has been found in many mammalian species [11]. The same unique relationship has been observed in the intact heart in the form of the end-systolic pressure-volume relationship (ESPVR) [12, 13]. The existence of a fixed ESPVR is extremely important conceptually because it predicts that the stroke volume of a ventricle, which ejects blood against a fixed aortic pressure, will increase in linear proportion to the increase in end-diastolic volume. The resultant stroke volume to end-diastolic volume relationship has an intercept with the abscissa at a volume at which the ventricle can just attain aortic pressure during isovolumic contraction. This behavior of the heart has been known as the Frank-Starling Law of the Heart since the beginning of this century [14, 15].

Let us return to the force-sarcomere length relationship. Figure 3 shows that the unstimulated passive muscle displays elastic behavior, i.e. an elastic force is generated with stretch. It is clear from Fig. 3 that this passive force rises steeply when the sarcomeres in mammalian myocardium are stretched to a length of approximately 2.3 μm.

At this length the overlap between the contractile filaments is close to optimal. The consequence of the steep rise of the passive force-length relation is that the sarcomeres in

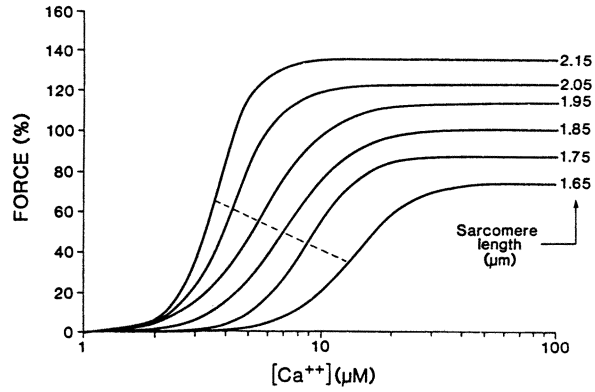

Figure 2. Relationship between active force and $[Ca^{++}]$ in skinned muscles at various sarcomere lengths. The solid lines are best-fits to the modified Hill equation: Force = Maximum Force · $[Ca^{++}]^n/(K^n + [Ca^{++}]^n)$. The dashed line joins the points corresponding to half-maximal activation for each curve. It can be seen that increasing the sarcomere length raises both maximum force production and the Ca^{++} sensitivity of the myofibrils (from Kentish *et al.* [8], with permission of the American Heart Association).

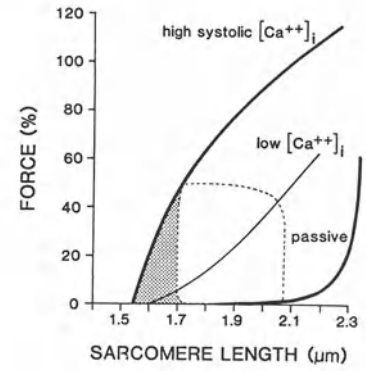

Figure 3. The force–sarcomere length relationship observed at a low (light line) and at a high (heavy line) $[Ca^{++}]_i$ in intact cardiac trabeculae. The relationships coincide with the relationships predicted by the curves in Fig. 6. The dotted line indicates the force sarcomere length loop (FSLL) during cardiac systole. The dotted area together with the FSLL form the basis for the pressure–volume area in the heart. The heavy solid line is the passive force–sarcomere length relation, indicating that stretch of the cardiac sarcomere is limited to a length of ~2.3 to 2.4 μm.

the heart cannot be stretched beyond the length that effects an optimal overlap of the contractile filaments. Hence, the systolic force–sarcomere length relationship increases up to a length of ~2.3–2.4 μm and simply stops when further stretch becomes impossible. Similarly, the ESPVR shows a monotonic rise of systolic pressure with end–systolic volume without a declining phase. The predicted stroke volume—end–diastolic volume relationship also stops at high end–diastolic volumes because of the limit to further stretch. This behavior is different from that of a heart which operates at high end–diastolic pressures, in which stroke volume may decrease as filling pressure increases. Contrary to the widely held belief, it is now clear that the descending limb of the Frank–Starling curve is not due to any intrinsic property of the mammalian cardiac sarcomere. This so–called descending limb at high end–diastolic pressures probably results from a complex of factors, including subendocardial ischemia, mitral regurgitation, and increased pulmonary pressures (which reduce right ventricular output).

VELOCITY OF SARCOMERE SHORTENING

It is well known that the velocity of shortening is a hyperbolic function of the load imposed on the muscle (Fig. 4A). In the absence of an external load the muscle reaches its maximal velocity of shortening (V_0). Both F_0 and V_0 are sigmoidal functions of $[Ca^{++}]_0$ [16–19]. SL has a prominent effect on V_0, which could be modulated by $[Ca^{++}]_0$. At lengths below slack length, V_0 decreased in proportion to SL at all levels of contractile activation. At close to maximal levels of activation (i.e. $[Ca^{++}]_0$=1.5 mM), V_0 is independent of SL above slack length [16, 18]. The decline of V_0 below slack SL is probably the result of restoring forces, which would act as internal elastic load on the cardiac sarcomere. At sub–maximal levels of contractile activation, V_0 declines in proportion to SL over the full range of SLs [18, 19].

V_0 of intact myocardium depends on the level of contractile activation. This raises the question of how the overall amount of calcium binding to troponin–C [20] can regulate

the actomyosin interaction of individual sites, i.e. affect crossbridge cycling rate, and thus regulate V_0. One possible explanation is the presence of an additional calcium regulatory site on myosin, as has been proposed [21]. Another possibility is the existence of an internal load [22–25]. I the following section evidence will be provided that it is likely that this internal load may be a viscous load generated by titin molecules, which form a filamentous support for the thick filament.

Passive Viscoelastic Properties of Cardiac Trabeculae

The force response to a linear stretch of the sarcomeres in unstimulated trabeculae is characteristic of an arrangement of an elastic (stiffness = k_{series}) and a viscous element (viscosity = η) in series. The steady force during the length change evidently reflects the viscosity of the viscous component ($F_\upsilon = \eta \cdot \upsilon$), while the time constant τ of increase of force to F_υ reflects the time course of the length change of the elastic element in series with the viscous element. It can be shown that $\tau = \eta / k_{series}$.

The diastolic viscosity of cardiac muscle is non–Newtonian [26] and generates a few percent of F_0 at V in the range of V_0. The magnitude of the viscosity is comparable to that in skeletal muscle [27, 28]. It is unlikely that the viscous behavior is explained by properties of the sarcolemma or of the mitochondria, because the density of sarcolemma and mitochondria is approximately tenfold greater in cardiac muscle than in fast twitch skeletal muscle fibers. Neither is it likely that the passive viscosity measured in the present study is due to 'weakly attached' crossbridges [29], which have been postulated on the basis of the force response to length changes at velocities far exceeding those discussed here. Furthermore, it is unlikely that the viscous properties of the trabeculae are caused by residual attached Ca^{++} dependent crossbridges, since reduction of $[Ca^{++}]_0$ to very low levels (pCa = 9) does not reduce the viscosity [30]. Furthermore the magnitude of k_{series} is at least 175 times lower than that of the crossbridges.

Exclusion of the contribution by other structures leaves the titin as the remaining possible structural basis for the passive viscoelasticity of the passive muscle. Further evaluation of the mechanical properties of titin is needed, but several of the characteristics

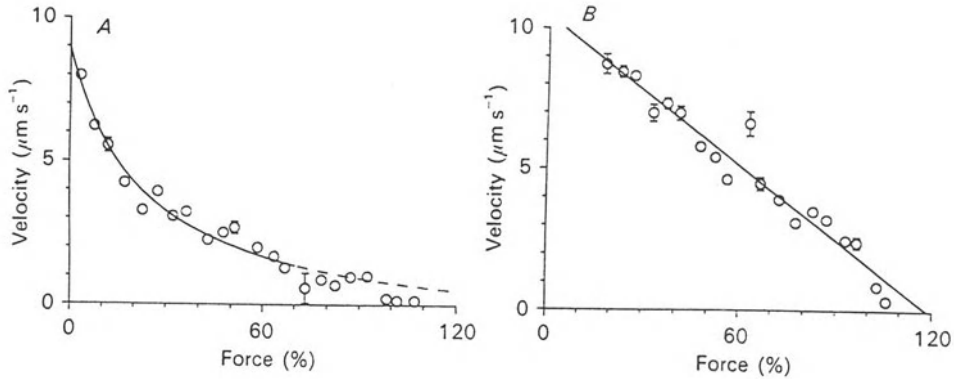

Figure 4. Force–velocity relationship of cardiac muscle and the same relationship calculated for a single crossbridge. Panel **A** shows the average velocity as a function of the external load in seven trabeculae. Panel **B** shows the relationships after the load supported by the muscle had been divided by the stiffness of the muscle during sinusoidal length fluctuations at 500 Hz. It is clear that hyperbolic F–V relationship in the intact muscle. converts to a linear relationship at the level of the single crossbridge (from de Tombe and ter Keurs [30] *J Physiol* with permission).

of the behavior of the viscoelastic element support its candidacy. Although k_{series} is much lower than that of the crossbridges it is still substantial, e.g. it is approximately five times larger than the stiffness of the parallel elastic element of the sarcomere at lengths between 1.9 and 2.1 μm. This suggests the presence of a moderately stiff—probably protein—element in series with the viscous component. Titin would be a plausible candidate for this arrangement; the molecule is arranged in the form of a series of large macromolecular domains which can be extended enormously by unfolding [31], and which are coupled to each other by shorter protein domains. The shorter protein domains may provide the basis for k_{series}, while unfolding of the large domains could underlie the viscous behavior. The unfolded domains could provide a basis for: i) the parallel elastic behavior that is observed in isolated myocytes [32] and; ii) the compliant part of the parallel elastic structures that respond with a small increase of force with stretch of cardiac muscle above slack length.

Force–Velocity Relation of the Cardiac Crossbridge

Dynamic stiffness of cardiac muscle decreases with decreasing load during shortening, as has been observed in skeletal muscle [28, 33–35]. A finite stiffness is observed at zero external force (about 12%) which is smaller than that in skeletal muscle, probably due to the 50% lower level of activation of cardiac muscle. This suggests that the stiffness at zero load is a function of the level of contractile activation. The average force–velocity relation calculated from the load and the corresponding stiffness at the level of a single crossbridge was close to linear (see Fig. 4B). A similar result has recently been reported for frog skeletal muscle [35]. A close to linear average force–velocity relation at the level of a single crossbridge is in fact predicted by the 1957 Huxley model [36].

Effect of Activation on Unloaded Velocity of Shortening

The effect of activation on unloaded velocity of shortening can be explained quantitatively on the basis of the above mentioned observations that, during shortening, the velocity of shortening is linearly proportional to the average load per attached crossbridge (slope coefficient: k_2); second, the number of crossbridges at zero external load is assumed to be proportional (k_1) to the level of activation; third, the viscous force (η) generated by the shortening sarcomere is proportional to the velocity of shortening (V_0). Then it can be shown [30] that:

$$V_0 = (V_{intr} \cdot F_0) / (K + F_0) \quad (1)$$

in which $K = k_2 \cdot \eta / k_1$ and V_{intr} is the intrinsic maximal velocity.

Figure 5 shows that this relationship fits excellently to data from cardiac muscle of euthyroid rat (and cat and hypothyroid rat) myocardium. The expected value for K, estimated from the values for k_1,k_2 and for viscosity of euthyroid rat myocardium varied from 23 to 38 and matched the value calculated from the V_0–F_0 relation (26.8) well. Thus, a passive viscosity together with a reduction of the number of crossbridges at V_0 seemed sufficient to account for the limiting effect of contractile activation on V_0.

DISCUSSION AND CONCLUSIONS

It should be stressed that this last conclusion is based on several assumptions. First, we assumed that the finite stiffness at zero external load is a function of the level of

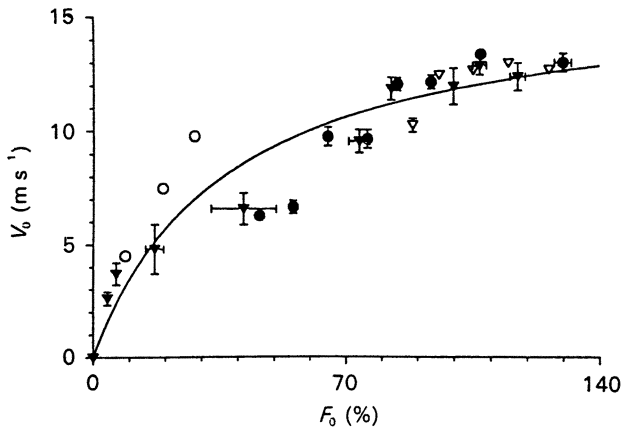

Figure 5. The relationship between the maximal velocity of sarcomere shortening V_0 and the maximal isometric force F_0 under the same conditions. The data were obtained at varied sarcomere length (Ca^{++} = 1.5 mM open triangles; 0.5 mM filled circles and; 0.2 mM open circles), or at varied $[Ca^{++}]o$ (filled triangles). The relationship between V_0 and F_0 could be explained fully by assuming that the number of crossbridges involved in shortening at zero external load is function of the $[Ca^{++}]o$ and that the internal load is determined by the viscous properties of the muscle, as is described in the text. The solid line is the fit to Eq. (1) (from de Tombe and ter Keurs [30] *J Physiol*, with permission).

activation. Even though this assumption appears to be reasonable, further experiments are necessary to confirm this assumption (i.e. measurement of dynamic stiffness during shortening at different levels of activation). Second, we have measured passive viscosity during a stretch in unstimulated muscles. We then assumed that this property also applied in the active muscle during shortening. The reports [27, 37] that in the analysis of instantaneous elasticity (F_1) of active muscle a viscous response remained undetected, seem to be at odds with the above assumption. The absence of a viscous response seems puzzling at first glance, but is readily explained if one realizes that during a rapid release (e.g. 18 nm in 200 μs) to zero force the viscous force amounts to only 15% of F_0. The contribution of viscosity to the F_1 curve is proportionally less if smaller quick releases are applied.

Analysis of the temperature dependence of V_0 revealed a high Q_{10}(4.5); this Q_{10} is similar to that of actin-activated myosin ATPase. Further study of the Q_{10} of the ATPase rate of myosin-S_1 with actin in solution, and of the Q_{10} for ATPase of myosin-S_1 cross-linked to actin, strongly supports the hypothesis that detachment of myosin is the step in the crossbridge cycle that limits shortening velocity ($Q_{10} \geq 4$). We have also demonstrated that ATP hydrolysis by the fast isoenzyme of myosin (V_1) in solution with actin is twice as fast as the ATPase rate of slow myosin (V_3); the difference is identical to the difference in V_i of these muscles. Cross-linking fast or slow S_1 to actin accelerated the ATPase rate up to hundredfold and eliminated the difference between the ATPase rate of slow and fast myosin S_1-actin, showing that the difference in kinetic properties of fast and slow myosin resides in a short amino acid domain on S_1 involved in attachment and detachment to and from actin [38].

DISCUSSION

Dr. J. Solaro: The dynamics of the calcium transients as you increase length seem very similar, yet the relaxation times were dissimilar. Are you suggesting that this is due to an enhanced affinity

of troponin–C for calcium? One may expect the calcium transients to be more different if it could account for the big changes that you saw.

Dr. H.E.D.J. ter Keurs: A critical evaluation of calcium transients is in place here. If the muscle generates full force, 100% of the maximal force in skinned fibers, a reasonable estimate indicates that all troponin–C is bound to calcium, which would require about 70 μM of calcium. While in the myofilament domain, 70 μM of calcium is bound, we find a maximal cytosolic calcium concentration of 1 μM. At this moment, we need extremely careful parameter control in order to dare make statements about the implications of the kinetics of the small Ca^{++} transients.

Dr. J. Solaro: I agree with you. It is very difficult to know how much calcium is bound from the calcium transient. But I would like to suggest that there is a possibility that you have more crossbridges that are activating the thin filament and that this process may just be slower to decay. It could be that the calcium binding does not have to change very much too, due to this crossbridge dependent activation of the thin filaments. I do not think we truly understand how that aspect of activation plays a role in these kinds of manipulations of crossbridge interaction.

Dr. H.E.D.J. ter Keurs: I agree. Essentially what you are asking for is a mechanism for length dependent activation of this system. There are several mechanisms that have been proposed and pursued over time. Troponin–C properties have been one of them. Following your presentation I tried to tempt you into a statement about a possible interaction between titin filaments and thin filaments and their role in regulation of length dependence. Secondly, feedback of crossbridges and the number of available crossbridges for each thin filament will vary with length, and activation of crossbridges by themselves may influence calcium sensitivity and binding to Troponin–C. Assuming only that the number of crossbridges would be enough to explain variation in force would not work as a model. One needs feedback from binding of crossbridges of which the number in the cardiac muscle will vary approximately two–fold over the full range of sarcomere lengths. Feedback from crossbridges and their force generating states to calcium binding is a necessary ingredient to the behavior of the system. This concept is supported by the observation that the rate of decline of force development is extremely sensitive to the actual force from which that decline starts.

Dr. M. Lab: How difficult is it to differentiate between a length dependence of troponin–C sensitivity to calcium, and a force dependence.

Dr. H.E.D.J. ter Keurs: It is fairly complicated because every force change has to be accompanied or preceded by a length change. But lets look at the effect of instantaneous, or near instantaneous, releases. In that case, force development drops to virtually zero following a length change of only 8 nm. One finds a very substantial release of calcium from the thin filaments. An important observation is that force recovery following that mechanical release (and the release of calcium from the filaments) accompanies the rebinding of calcium to the filaments very tightly. Given the small magnitude of the length change and the close correspondence of force and calcium binding to the filaments, one would be inclined to give most of the weight to force as the controlling feedback parameter.

Dr. M. Lab: I agree with you. Together with David Allen [Lab et al. *Circ Res.* 1984;55:825–829], I showed the same kind of thing. With a release, the corresponding change in calcium is more pronounced. My interpretation is more force related than length related.

Dr. M. Morad: You were concerned in the past about sarcomere length variations in such a multicellular preparation. If there was a problem with quick releases, the different sarcomeres would not be released to the same extent. Could dispersion of the calcium signal at these long lengths be, in part, related to that? How confident are you of this?

Dr. H.E.D.J. ter Keurs: You are relating to the time that we woke you up at 5 am after you went

to bed at 4 am in New Orleans at the Biophysical Society Meeting, and we wanted you to attend our three presentations which were dealing with skeletal muscle and a descending limb in which one has the fundamental problem that there may be nonuniformity which may be unstable and therefore may be enhanced during any intervention that an experimentalist imposes upon the muscle. Two things about the cardiac muscle. First, it operates on the ascending limb; therefore nonuniformity, which is based on instability, is less prone to occur. Second, in our experiments we have always very obsessively and compulsively looked at the diffraction patterns to make sure that the uniformity that was present in the native state of the muscle was maintained during the interventions. I believe that uniformity within the central segment of cardiac muscle preparations is quite well preserved. In contrast, nonuniformity in damaged and elastic elements that link the central sarcomeres in the muscle to the recording and motor set-up could interfere with the interpretation. But not if one works purely at the level of the central sarcomeres. I have limited the discussion to that situation.

REFERENCES

1. Bers DM. *Excitation-Contraction Coupling and Cardiac Contractile Force*. Kluwer Academic, Boston/London, 1991.
2. Bridge JHB, Spitzer KW, Ershler PR. Relaxation of isolated ventricular cardiomyocytes by a voltage-dependent process. *Science*. 1988;241:823-825.
3. Carafoli E. Intracellular calcium homeostasis. *Ann Rev Biochem*. 1987;56:395-433.
4. Schouten VJA, Deen JK, Tombe PP, Verveen AA. Force-interval relationship in heart muscle of mammals. A calcium compartment model. *Biophys J*. 1987;51:13-26.
5. Wohlfart B. Relationship between peak force, action potential duration, and stimulus interval in rabbit myocardium. *Acta Physiol Scand*. 1979;106:395-409.
6. Backx PH, ter Keurs HEDJ. Fluorescent properties of rat cardiac trabeculae microinjected with fura-2 salt. *Am J Physiol (Heart Circ Physiol)*. 1993;264: H1098-H1110.
7. Wier WG, Yue DT. Intracellular calcium transients underlying the short-term force-interval relationship in ferret ventricular myocardium. *J Physiol*. 1986;376:507-530.
8. Kentish JC, ter Keurs HEDJ, Ricciardi L, Bucx JJJ, Noble MIM. Comparison between the sarcomere length-force relations of intact and skinned trabeculae from rat right ventricle. *Circ Res*. 1986;58:755-768.
9. Hofmann PA, Fuchs F. Bound calcium and force development in skinned cardiac muscle bundles: Effect of sarcomere length. *J Mol Cell Cardiol*. 1988;20:667-677.
10. Morris GL. The regulatory interaction between phospholamban and SR (Ca++-Mg++) ATPase. Ph.D. Thesis, The University of Calgary, 1993.
11. ter Keurs HEDJ, Kentish JC, Bucx JJJ. On the force-length relation in myocardium. In: ter Keurs HEDJ, Tyberg JV, eds. *Mechanics of the Circulation*. Dordrecht, The Netherlands: Martinus Nijhoff, 1987; 91-105.
12. Sagawa K, Suga H, Shoukas AA, Bakalar KM. End-systolic pressure-volume ratio: a new index of ventricular contractility. *Am J Cardiol*. 1977;40:748-753.
13. Sagawa K, Maughan L, Suga H, Sunagawa K. *Cardiac Contraction and the Pressure-Volume Relationship*. New York/Oxford: Oxford University Press; 1988: 139-143
14. Patterson SW, Piper H, Starling EH. The regulation of the heart beat. *J Physiol (London)*. 1914;48:465-513.
15. Starling EH. *Human Physiology*. Philadelphia/New York: Lea and Febiger; 1912: 880-884, 909-9
16. Daniels M, Noble MIM, ter Keurs HEDJ, Wohlfart B. Velocity of sarcomere shortening in rat cardiac muscle: Relationship to force, sarcomere length, calcium and time. *J Physiol*. 1984;355:367-381.
17. de Tombe PP, ter Keurs HEDJ. Lack of effect of isoproterenol on unloaded velocity of sarcomere shortening in rat cardiac trabeculae. *Circ Res*. 1991;68:382-391.
18. de Tombe PP, ter Keurs HEDJ. Sarcomere dynamics in cat cardiac trabeculae. *Circ Res*. 1991;68:588-596.
19. Martyn DA, Rondinone JF, Huntsman LL. Myocardial segment velocity at a low load: Time, length, and calcium dependence. *Am J Physiol*. 1983;244:H708-H714.

20. Woledge RC, Curtin NA, Homsher E. *Energetic Aspects of Muscle Contraction*. London: Academic Press, 1985.
21. Lehman W. Thick-filament-linked calcium regulation in vertebrate striated muscle. *Nature*. 1978;274:80-81.
22. Gulati J, Babu A. Contraction kinetics of intact and skinned frog muscle fibers and degree of activation. *J Gen Physiol*. 1985;86:479-500.
23. Chiu YL, Ballou EW, Ford LE. Force, velocity and power changes during normal and potentiated contractions of cat papillary muscles. *Circ Res*. 1987;60:446-458.
24. Tsuchiya T. Passive interaction between sliding filaments in the osmotically compressed skinned muscle fibers of the frog. *Biophys J*. 1988;53;415-423.
25. Chiu YL, Ballou EW, Ford LE. Velocity transients and viscoelastic resistance to active shortening in cat papillary muscle. *Biophys J*. 1982;40:121-128.
26. Noble MIM. The diastolic viscous properties of cat papillary muscle. *Circ Res*. 1977;40:288-292.
27. Ford LE, Huxley AF, Simmons RM. Tension responses to sudden length changes in stimulated frog muscle fibers near slack length. *J Physiol*. 1977;269:441-515.
28. Ford LE, Huxley AF, Simmons RM. Tension transients during steady shortening of frog muscle fibers. *J Physiol*. 1985;361:131-150.
29. Brenner BM, Schoenberg M, Chalovich JM, Greene LE, Eisenberg E. Evidence for cross-bridge attachment in relaxed muscle at low ionic strength. *Proc Nat Acad Sci*. 1982;79:7288-7291.
30. de Tombe PP, ter Keurs HEDJ. An internal viscous element limits unloaded velocity of sarcomere shortening in rat myocardium. *J Physiol*. 1992;454:619-642.
31. Wang K, Wright J. Architecture of the sarcomere matrix of skeletal muscle: Immunoelectron microscopic evidence that suggests a set of parallel inextensible nebulin filaments anchored at the Z line. *J Cell Biol*. 1988;107:2199-2212.
32. Brady AJ. Mechanical properties of isolated cardiac myocytes. *Physiological Rev*. 1991;71:413-428.
33. Julian FJ, Morgan DL. Variation of muscle stiffness with tension during tension transients and constant shortening in the frog. *J Physiol*. 1981;319:193-203.
34. Ford LE, Huxley AF, Simmons RM. The relation between stiffness and filament overlap in stimulated frog muscle fibers. *J Physiol*. 1981;311:219-249.
35. Haugen P. The stiffness under isotonic releases during a twitch of a frog muscle fibre. In: Sugi H, Pollack GH, eds. *Molecular Mechanism of Muscle Contraction*. New York: Plenum Press, 1988; 461-469.
36. Huxley AF. Muscle structure and theories of contraction. *Prog in Biophys Chem*. 1957;7:255-318.
37. Backx PH, ter Keurs HEDJ. Restoring forces in rat cardiac trabeculae. *Circulation*. 1988;78II:68.
38. Nguyen TTT, ter Keurs HEDJ, unpublished data, 1994.

CHAPTER 15

CROSSBRIDGE DYNAMICS IN MUSCLE CONTRACTION

Amir Landesberg, Rafael Beyar, and Samuel Sideman[1]

ABSTRACT

The study deals with the description of muscle contraction based on biochemical studies and describes four major approaches for coupling calcium kinetics with crossbridge (Xb) cycling. The analysis illuminates two controversial points: 1) the relationship between Xb attachment/detachment and Xb cycling, i.e., the transition between weak to strong conformations, and 2) the effect of calcium on Xb function: does it regulate Xb kinetics or Xb recruitment.

INTRODUCTION

The force is generated by the sarcomere but is regulated by the transient free calcium concentration. The sarcomere consists of an actin and myosin filaments (Fig. 1). The myosin heads, denoted as the crossbridges (Xbs), project from the myosin filaments and bind to the actin molecules. According to Huxley [1], the Xb can be either in the attached or the detached state and the force is generated by the Xbs in the attached state. Moreover, the classical Huxley's model [1] links the biochemical process of ATP hydrolysis to the physical process of Xb attachment/detachment, with one molecule of ATP hydrolysed for each stroke work of the Xbs.

Recent biochemical studies [2, 3] suggest that the Xbs cycle between two conformations: a strong, force generating, conformation and a weak, non force generating, conformation. The Xbs in the weak and the strong conformation can be either in the attached or the detached state [2, 4], and force is generated by the Xbs in the strong conformation. The two conformations differ in their biochemical structure, and Xb cycling

[1]Heart System Research Center, The Julius Silver Institute, Department of Biomedical Engineering, Technion-IIT, Haifa, 32000, Israel.

Molecular and Subcellular Cardiology: Effects of Structure and Function
Edited by S. Sideman and R. Beyar, Plenum Press, New York, 1995

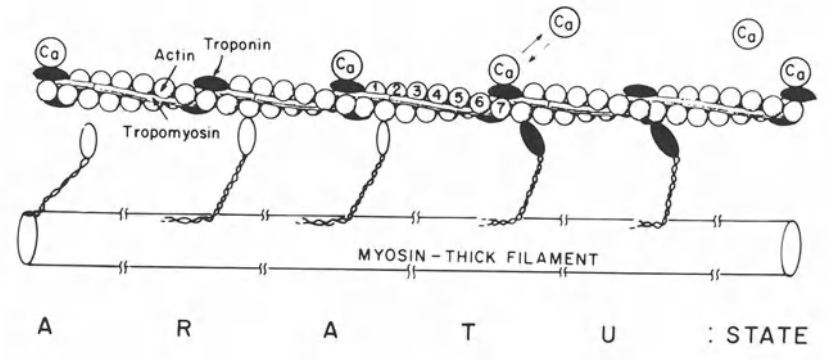

Figure 1. The Physiological Model. The structure of the sarcomere in the single overlap region.

between the two conformations is related to nucleotide binding and release: ATP hydrolysis and phosphate release turns the Xb to the strong conformation, while the release of ADP from the head of the myosin and ATP binding turn the Xb back to the weak conformation. Obviously, the physical attachment/detachment phenomenon is not identical with the biochemically defined strong conformations, and different models were proposed to relate these phenomena to the mechanical performance of the Xb in the contraction process. The basic models will be reviewed here, and the difference between the attached/detached states and the strong/weak conformations will be discussed. Particular attention is given to the ability of models to describe the mechanical characteristic of the Xbs and the energy consumption.

Another basic question relates to the effect of calcium binding to troponin on the regulation of Xb function. Wong [5] has suggested that calcium affects the rate of Xb attachment. Brenner [6] has suggested that calcium regulates the rate of Xb transition from the weak to the strong conformation. while Zahalak and Shi-ping [7] have proposed that calcium regulates Xbs recruitment, i.e., the number of available Xbs for force generation. Of particular interest here is the question whether the experimental data that has led to the hypothesis that calcium affects rate kinetics [6] can support the assumption that calcium regulates Xb recruitment.

The objectives of this study are thus to highlight the following points: 1) The kinetics of Xb attachment/detachment vs. Xb cycling between the strong and weak conformations, and 2) the effect of calcium on the regulation of Xb function: Xb kinetics versus Xb recruitment. A realistic description of the intracellular control mechanism should provide a better understanding of muscle function and LV performances.

BASIC MODELS OF CROSSBRIDGE KINETICS

In pursuing our objective, we relate to four different models (Fig. 2) that highlight these controversial points. The basic ***Huxley's model*** [1] is a two-state model (Fig. 2A) which focuses on the ensemble of the head of the myosin. Each Xb is assumed to act independently, and only with one actin site. Each Xb can be either in the attached state or in the detached state.

Huxley's model [1] assumes that the rate of Xb attachment (f_h) and the rate of Xb detachment (g_h) are function of the displacement (x) of the Xb from the equilibrium state (x=0), i.e.:

$$\begin{cases} x < 0 & f_h = 0 & g_h = g_{h2} \\ 0 \le x \le H & f_h = f_{h1}x/H & g_h = g_{h1}\, x/H \\ x > H & f_h = 0 & g_h = g_{h1}\, x/H + g_{h3}\, x/H \end{cases} \quad (1)$$

where H is the maximal displacement at which the Xb can attach to the actin sites. The distribution of the Xbs, n(x, t), as a function of the time (t) and the displacement (x) is given by:

$$\frac{\partial n(x,t)}{\partial t} - V_{SL}(t)\frac{\partial n(x,t)}{\partial x} = [1 - n(x,t)]f_h(x) - n(x,t)g_h(x) \quad (2)$$

where V_{SL} is the sarcomere shortening velocity.

As seen, Huxley's model (Eqs. (1) and (2)) was developed for full activation, as is the case in skeletal muscle at tetanus.

Two different approaches were developed to account for the transient effects of free calcium changes on Xb function. Wong [5] (Fig. 2A) assumed that calcium affects the rate of Xb attachment. The Xb distribution function is given by Eq. (1) but the rate of attachment depends on an activation function, $\gamma_{Wong}(t)$ which expresses the time course of calcium binding to troponin:

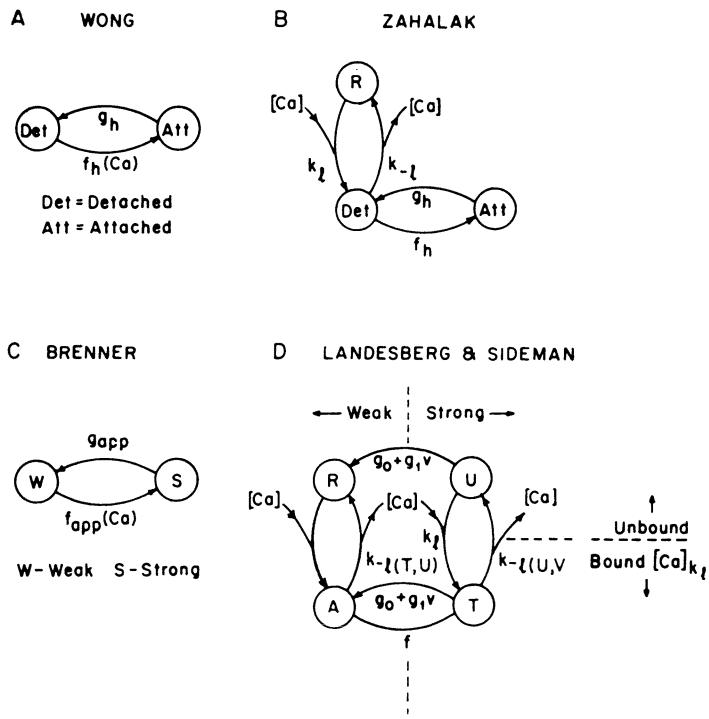

Figure 2. Models describing coupling calcium binding to troponin with Xb turnover. **A:** Wong's modification of Huxley's model [5]; **B:** Zahalak's model [7]; **C:** Brenner's model [6]; **D:** Landesberg and Sideman's model [8, 9]. A and B are based on Huxley's model. C and D are based on the biochemical studies. In A and C calcium affects Xb kinetics and in B and D calcium determines Xb recruitment.

$$\begin{cases} x < 0 & f_h = 0 & g_h = g_{h2} \\ 0 \le x \le H & f_h = \gamma_{Wong}(t) \cdot f_{h1} x/H & g_h = g_{h1} x/H \\ x > H & f_h = 0 & g_h = g_{h1} x/H + g_{h3} x/H \end{cases} \quad (3)$$

Zahalak [7], on the other hand, assumed that calcium regulates Xb recruitment; Xb can bind to the actin site, provided that the site has been activated by calcium, and that the binding site is exposed (Fig. 2B). State R represents the Rest state, i.e., there is no bound calcium and the Xb is detached. Calcium binding to troponin leads to state "Det" – where the actin site is activated but the Xb is in the detached state. Thereafter, Xb binding to actin, the attached state, ("Att") generates force. The rates of attachment and detachment are as in the original Huxley's model (Eq. (1)). However, Huxley's equation for Xb distribution (Eq. (2)) is modified:

$$\frac{\partial n(x,t)}{\partial t} - V_{SL}(t)\frac{\partial n(x,t)}{\partial x} = \left[\gamma_{Zah} - n(x,t)\right] f_h(x) - n(x,t) g_h(x) \quad (4)$$

where $\gamma_{Zah}(t)$ defines the number of actin sites available for Xb attachment, which is determined by the amount of bound calcium to troponin. In contrast to Wong's model, the rate of attachment is constant but calcium determines the number of cycling Xbs.

Brenner [6] has suggested another two–state model for Xbs cycling (Fig. 2C). This model is based on biochemical studied: the Xbs cycle between a weak non–force generating state and a strong force generating state. Each of these states includes several biochemical steps. Xb cycling between these two states is described by two rate limiting kinetics: f_{app}, the apparent turnover rate from the weak to the strong state, and g_{app}, the apparent turnover rate from the strong to the weak state. Brenner [6] has measured the rate of isometric force redevelopment at various free calcium concentrations, starting from different initial force levels, following isotonic shortening and restretch to the initial sarcomere length. The rate of force redevelopment, τ_{RED}, for his two–state model is given by (Appendix A):

$$\tau_{RED} = f_{app} + g_{app} \quad (5)$$

Brenner [6] has also shown that an increase in the free calcium concentration increases the rate of force redevelopment. Based on this two–state model for Xb cycling, Brenner has concluded that calcium affects the kinetics of Xb cycling, i.e., the turnover rate from the weak to the strong state, f_{app}, depends on the free calcium concentration.

Our model (Fig. 2D) is also based on biochemical studies where the Xbs cycle between the weak and strong conformation [8, 9]. However, the main difference from Brenner's model relates to the effect of calcium. Brenner has suggested that calcium regulates the rate of Xb transition from the weak to the strong conformation, while our model suggests that calcium regulates Xbs recruitment.

Two criteria determine the "state" of the regulatory troponin units in our model: 1) The existence of bound calcium to troponin, and 2) the conformation of the Xb is either 'strong' or 'weak'. The physical configuration of the four states are defined in Fig. 1; Fig. 2D shows the relationship between the states: State R represents the 'Rest' state: no calcium is bound to troponin, and the Xbs are in the weak conformation. Calcium binding to troponin leads to Activation state A, which represents the mechanical activation level, i.e.,

the number of Xbs in the non force generating conformation that can turn to the force generating conformation, and thus represents the ability of the muscle to generate force. Xbs turnover to the strong conformation leads to the Tension state T which represents the tension generating state. Calcium dissociation from troponin, at state T, leads to the Unbound calcium state, U, wherein the Xbs are still at the force generating conformation but without bound calcium.

MODEL RESULTS

Rates of Attachment and Detachment

To estimate the rates of attachment and detachment, and to evaluate the ability of Huxley's [9] model to describe Xb mechanics, we can calculate the dependence of the stiffness on the frequency of sinusoidal length perturbation (Appendix B). The stiffness is defined by the change in the magnitude of the force oscillation, relative to change in the sarcomere length.

Figure 3 compares the stiffness calculated based on Huxley's model and the stiffness based on the force and length oscillations measured by Gao and ter Keurs [10]. The commonly used values for the rate of attachment and detachment, as presented in Appendix B, yields the upper curve which exhibits the lowest cutoff frequency. The increase in the frequency of the sinusoidal length perturbation increases the magnitude of the force oscillation. At high frequency of oscillations, the length perturbation is faster than the rate of Xb detachment, and the Xbs do not succeed to detach. The Xbs remain "fixed" to actin and the arms of the Xbs stretch and release, resulting in a high stiffness.

It is evident that the cutoff frequency of the stiffness calculated based on Huxley's model with the commonly used rate parameters is by far lower then the experimental one. For the commonly used Huxley's parameters, when g_{h1} is about 10 per second, the cutoff frequency is 10Hz. Using a set of rate parameters which are 100-fold faster (g_{h1} = 1000 sec^{-1}) yields a cutoff frequency at 1000 Hz (lower curve in Fig. 3).

Note that the new cutoff frequency is determined by the rate of Xb detachment, g_{h1}. As discussed below, the experimental data suggest that g_{h1} should be at least 100 sec^{-1}, in contrast to Huxley's low rate value of detachment. Note that the commonly used rate of detachment is low in order to describe the relatively slow time course of the twitch.

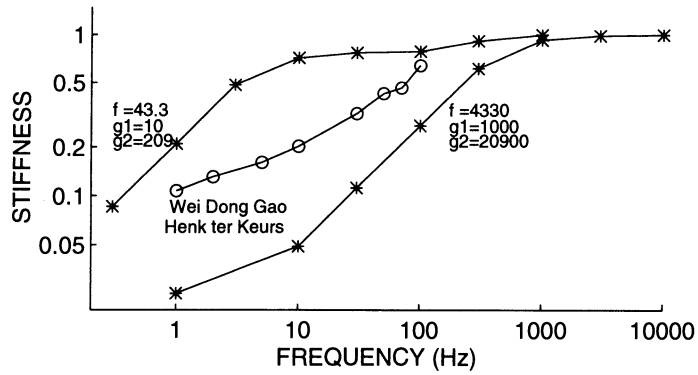

Figure 3. Stiffness as a function of the frequency of length perturbation. Comparison of experimental data of Gao and ter Keurs [10], and two simulations based on Huxley's model, each with different rate constants.

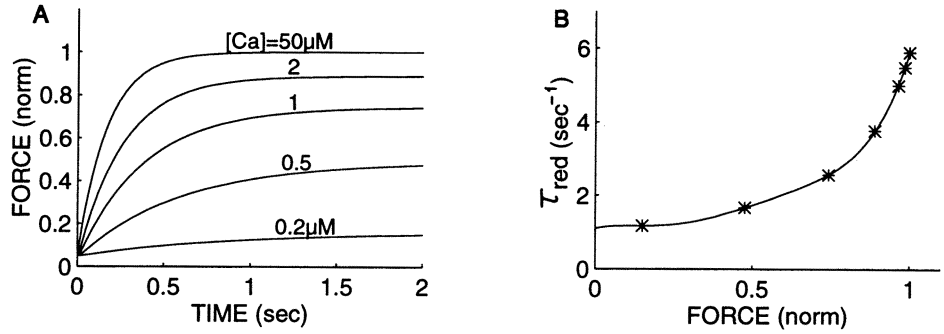

Figure 4. Simulation of rate of force development in skeletal muscle. **A.** Force development from an initial force level (0.05 F_{max}) at various free calcium concentrations. **B.** Effect of free calcium concentration on rate of force development. Abscissa represents steady state force at the various free calcium concentrations.

Effect of Calcium: Xb Kinetics versus Xb Recruitment

Brenner [6] measured the rate of isometric force redevelopment and suggested that calcium affects Xb kinetics. Following Brenner's experiments, we address the question of whether Brenner's experimental data can be interpreted by another mechanism as well. Thus, the rates of isometric force redevelopment in our four-state model [8, 9] were calculated from different initial force levels and different free calcium concentrations. Assuming that the rate of calcium association and dissociation from the troponin is faster than the rates of Xb cycling [11, 12], the rate of isometric force redevelopment in the four-state model is given by (Appendix A):

$$\tau_{RED} = \frac{g_0}{1 - c \cdot F} \qquad c = \frac{f}{f + g_0} \cdot \frac{1}{F_{max}} = \text{const} \tag{6}$$

where F is the isometric force and F_{max} is the isometric force generated at maximal calcium concentration. Simulation of the rates of force redevelopment from the same initial force, at various free calcium concentration is demonstrated in Fig. 4A. Increasing the free calcium concentration elevates the steady state force level and the rate of force development (Fig. 4B). The analytical (Eq. (6)) and numerical results are in agreement with Brenner's experimental data, where the rate of force redevelopment is affected by the free calcium concentration, and hence the rate of force redevelopment increases with the increase in the isometric force, consistent with Brenner's analysis. Note that the calculations were performed [8] for a skeletal muscle with four calcium binding sites on each troponin, since Brenner's experimental study was performed on rabbit psoas fiber [6].

DISCUSSION

Attachment/Detachment Rates

Huxley has suggested that the kinetics of Xb attachment/detachment can explain both the physical mechanisms of force generation as well as the biochemical process of nucleotide binding and release and the related biochemical energy consumption. The rate

constants of attachment and detachment were estimated indirectly from the time course of the twitch, the force–velocity relationship, and some energetic consideration, and not from direct measurements of the rate of attachment and detachment.

Brenner [4] has measured the stiffness–speed relationship derived from the T plots, of force vs imposed length change. Brenner [4] has concluded that the rate constants of reversible Xb attachment and detachment are greater then 50–1000 sec^{-1}, which are an order of magnitude greater than the rate constants that are commonly used for the description of muscle mechanics based on Huxley's model.

The experimentally measured dependence of the stiffness on the frequency of length perturbation was compared, in Fig. 3, with simulations based on Huxley's model. An increase in the frequency of length perturbation increases the stiffness, reaching a cutoff frequency beyond which the stiffness is almost constant. As shown in Fig. 3, the cutoff frequency is determined by the rate of detachment, g_{h1}. The commonly used values for the rates of attachment and detachment gives a cutoff frequency which is by far lower then the cutoff frequency observed experimentally. When the experimental data [10] is related to Huxley's model in Fig. 3, it suggests that the rate of detachment should be of the order of 100 Hz, rather than the low rate of detachment (1–10 sec^{-1}) which is commonly used to describe the relative slow time course of the twitch.

As reported by Brenner [4], the actual rate constant for active Xb turnover between the weak and strong states, denoted as the apparent f (f_{app}) and the apparent g (g_{app}), are of the order of 1–10 s^{-1}. Thus, the relative low constants which were used in Huxley's model to represent the rates of attachment and detachment, do, in fact, represent the rates of Xb turnover between the weak and strong conformations, and not the attachment/ detachment rates.

These qualitative findings suggest the existence of two types of interdependent processes: 1) A physical process involved in the force generation by the Xbs, which may relate to Xb attachment and detachment phenomena, and 2) the biochemical process of Xb cycling between the force generating (strong) and non–force generating (weak) conformation. These two interdependent processes differ in their rate kinetics; the rate of attachment/ detachment is by far faster than the rate of Xb cycling between the weak and strong conformations. It is noteworthy that no fixed coupling is known to exist between Xb attachment/detachment and Xb cycling between the weak to strong conformation [4, 6], particularly since one ATP can be used for several stroke work of attachment/detachment [13].

Effect of Calcium on Xb Kinetics and Xb Recruitment

The above information raises some doubts as to the applicability of Huxely's attachment/detachment theory to stiffness and energy consumption. Moreover, Chalovich and Eisenberg [14, 15], who have measured the rate of ATP hydrolysis and the fraction of myosin subfragment–1 bound to actin in the presence and absence of calcium, have concluded that calcium has an insignificant effect on the rate of attachment/detachment. However, they have suggested [13, 14] that calcium affects the actomyosin ATP_{ase} activity.

These doubts have led to the development of models that describe Xb cycling between the weak and strong conformations, which biochemically relate to nucleotide binding and release [2, 3]. As already noted, Brenner, using a simple two–state model (Fig. 2C) [6], concluded that the main regulatory mechanism of calcium was through the control of Xb kinetics, although he found some regulation of the number of turning–over Xbs, especially at low levels of free calcium. The question is whether calcium binding to

troponin regulates mechanical activity by modulating Xbs kinetics [6] or by recruitment of Xbs and controlling the number of Xbs that can generate force [7–9].

The four–state model describes the biochemical–mechanical coupling between calcium binding to troponin and Xb cycling. Brenner's two–state model and our four–state models yield similar expressions for the isometric force at full activation. Furthermore, our four–state model describes analytically (Eq. (6)) and numerically (Fig. 4) the dependence of the rate of force redevelopment on the free calcium concentration, or on the isometric steady state force. The results are in agreement with Brenner's experimental results [2], although, in contrast to Brenner's conclusion, the rates of Xb cycling in the four–state model are constant (f=const) and calcium regulates Xb recruitment. Moreover, the increase of the number of cycling Xbs with the increase of the activation level demonstrated by Brenner is closely predicted by our model [8].

Chalovich and Eisenberg [15] experimental data also suggests that calcium affects Xb recruitment. They measured the rate of ATP hydrolysis by the activated subfragment–1 ATPase in the presence and absence of calcium. They have shown that the primary effect of the regulatory troponin–tropomyosin complexes is in the regulation of the activity of the actomyosin ATPase. Their experimental data fits the Michaelis–Menten description of enzymatic reaction:

$$\mathrm{ATP} + [\mathrm{E}] \underset{k_{-1}}{\overset{k_1}{\rightleftarrows}} \mathrm{E\text{–}ATP} \xrightarrow{k_2} [\mathrm{E}] + \mathrm{ADP} + \mathrm{P}$$

and the rate of ATP hydrolysis (V) by the actomyosin ATPase, denoted by E, is given by:

$$\frac{1}{V} = \frac{1}{V_{max}} + \frac{K_{ATPase}}{V_{max} \cdot [E]} \tag{7}$$

where, based on the enzymatic reaction:

$$K_{ATPase} = \frac{k_{-1} + k_2}{k_1} \qquad \text{and} \qquad V_{max} = k_2 \cdot [E] \tag{8}$$

The data [15] shows that calcium increases the maximal rate of ATP hydrolysis (V_{max}) by the actomyosin ATPase from 0.9 to 11.2 sec^{-1}, but has a relatively small effect on K_{ATPase}, increasing it from $1.6 \cdot 10^4$ to $2.6 \cdot 10^4$. The relative small change in the K_{ATPase} suggests that calcium has a small effect on the rate kinetics. These data confirm that the regulatory troponin complexes block a kinetic step in the actomyosin ATPase cycle in the absence of calcium, and that calcium releases this block and thus increases the number of activated actomyosin ATPase. As stated, calcium has a larger effect on V_{max} than on K_{ATPase}. As seen in Eq. (8), the maximal rate of the enzymatic reaction, V_{max}, is proportional to the amount of available enzyme, and the significant effect of calcium on the V_{max} relative to the small change in K_{ATPase} support the hypothesis that the major effect of calcium in on the regulation of Xb recruitment.

Our four–state model also suggests an explanation for the findings of Grabarek *et al.* [16] that the relationship between ATPase activity and pCa exhibits a Hill coefficient and a transition midpoint ($pCa_{1/2}$) greater than those obtained in the bound calcium–pCa curve. This is explained by assuming that more troponin complexes are in state U than in state T at low values of pCa, i.e., the majority of the Xbs are in the strong conformation without bound calcium. Thus, the increase in the normalized force with the rise in free

calcium at low free calcium concentrations is higher than the rise in the bound calcium. Consequently, the Hill coefficient for the force and ATPase activity is higher than Hill's coefficient for the bound calcium.

Other advantages of the four-state model over Brenner's two-state model, are not necessarily related to the regulation of calcium in Xb cycling. Unlike Brenner's two-state model, our four-state model can also describe the effect of shortening velocity on force generation and the related force-velocity relationship [9], the control of relaxation [17] and the effect of loading conditions on the free calcium transient [9, 17].

CONCLUSION

The study views four basic models of coupling calcium kinetics with Xb function in the light of two controversial points: 1) the relationship between Xb attachment/ detachment and Xb cycling, i.e., weak to strong transitions. 2) the effect of calcium on Xb function: does it regulate Xb kinetics or Xb recruitment. The analysis emphasizes the importance of the description of Xb cycling between the weak and strong conformations to the understanding of the contraction dynamics. The analysis suggests that calcium enhances Xb recruitment rather than Xb kinetics.

APPENDIX A. THE RATE OF FORCE REDEVELOPMENT

Brenner's Model

The number of Xbs in the strong conformation (S), in the two-state model proposed by Brenner (Fig. 2C), is given by:

$$\frac{dS}{dt} = f_{app} \cdot (1 - S) - g_{app} \cdot S \qquad \text{(A-1)}$$

Since the isometric force (F) is equal to $F = \bar{F} \cdot S$, where $\bar{F}$ is the average isometric force generated by each Xb, the instantaneous isometric force is given by:

$$F(t) = \frac{f_{app}}{f_{app}+g_{app}} \bar{F} + \left(F_0 - \frac{f_{app}}{f_{app}+g_{app}} \bar{F}\right) \cdot e^{-(f_{app}+g_{app}) \cdot t} \qquad \text{(A-2)}$$

where F_0 is the initial isometric force level. Therefore, the rate of force redevelopment τ_{RED} in the two-state model is:

$$\tau_{RED} = f_{app} + g_{app} \qquad \text{(A-3)}$$

Landesberg and Sideman's Model

The number of Xbs in isometric contraction in the four-state model (Fig. 2D), in the strong conformation, S = T + U, is given by:

$$\frac{dS}{dt} = f \cdot A - g_0 \cdot S \qquad \text{(A-4)}$$

Assuming that the rate of calcium association and dissociation from the troponin is faster then the rate of Xb cycling ($f, g_0 \ll k_{-\ell}$, $k_\ell \cdot [Ca]$), then:

$$\frac{A}{R} \simeq \frac{T}{U} \simeq \frac{k_\ell [Ca]}{k_{-\ell}} = K \cdot [Ca] \tag{A-5}$$

Using Eq. (A-5), the state variable can be approximate by:

$$\begin{aligned} R + A + T + U &= (1 + K[Ca]) \cdot (R + U) = TRo \\ S = T + U &= (1 + K[Ca]) \cdot U \end{aligned} \tag{A-6}$$

where TRo is the total amount of troponin regulating units, and state A, the activation level, is given by (from Eq. (A-5) and (A-6)):

$$A = K[Ca] \cdot R = K[Ca] \frac{Tro - S}{1 + K[Ca]} \tag{A-7}$$

The number of Xbs in the strong conformation (Eq. (A-4) and (A-7)) is:

$$\frac{dS}{dt} = f \frac{TRo \cdot K[Ca]}{1 + K[Ca]} - \left(g_0 + \frac{K[Ca]}{1 + K[Ca]} f \right) \cdot S \tag{A-8}$$

Thus, the rate of force redevelopment is:

$$\tau_{RED} = g_0 + \frac{K[Ca]}{1 + K[Ca]} f \tag{A-9}$$

However, since Brenner did not measure the free calcium concentration and he expressed the rate of force redevelopment as a function of the steady state isometric force, we too express the rate of force redevelopment by the steady state isometric force (F_{ss}). At steady state

$$\frac{dS_{ss}}{dt} = f \cdot A_{ss} - g_0 \cdot S_{ss} = 0 \tag{A-10}$$

and the state variable can be approximate by:

$$f K[Ca] \cdot R_{ss} \simeq g_0 (1 + K[Ca]) \cdot U_{ss} \tag{A-11}$$

Using Eq. (A-6), the steady state isometric force is thus:

$$F_{ss} = \bar{F} \frac{TRo\, f K[Ca]}{g_0 + K[Ca](f + g_0)} \tag{A-12}$$

At maximal calcium concentration, $K[Ca]\,(f + g_0) \gg g_0$, and the maximal force generated at maximal calcium activation (F_{max}) is:

$$F_{max} = \bar{F}\, TRo \frac{f}{f + g_0} \tag{A-13}$$

From Eq. (A-9), (A-11) and (A-12), the rate of force redevelopment is given by:

$$\tau_{RED} = \frac{g_0}{1 - cF_{ss}} \quad ; \quad c = \frac{f}{f + g_0} \frac{1}{F_{max}} \tag{A-14}$$

in agreement with Brenner's experimental study [6].

APPENDIX B. THE STIFFNESS-FREQUENCY RELATION BASED ON HUXLEY'S MODEL

The rates of attachment and detachment in Huxley's model are estimated by calculating the dependence of the stiffness on the frequency of sinusoidal length perturbation. Figure B1 presents the force response to sinusoidal length perturbation at 1 Hz and 100 Hz. The sinusoidal length perturbation is in an amplitude of half the maximal Xb stroke length (H). Xb distribution at various instants during the oscillations, denoted by the numbers 0 to 3, are also presented in Fig. B1 (bottom).

The force and the Xb distribution are calculated based on Huxley's model (Eq. (1)), with the parameters used by Zahalak for the rate of attachment and detachment. The x axis is the Xb displacement, normalized by H. The distance of the Xb from the equilibrium position is denoted by 0. The y axis is the fraction of Xbs bound to the actin site. For the isometric regime, we have a constant distribution between x=0 and x=H. For a relative slow length perturbation, when the rates of attachment and detachment are faster than the rate of Xb displacement, the majority of the Xbs are distributed between x=0 and x=H

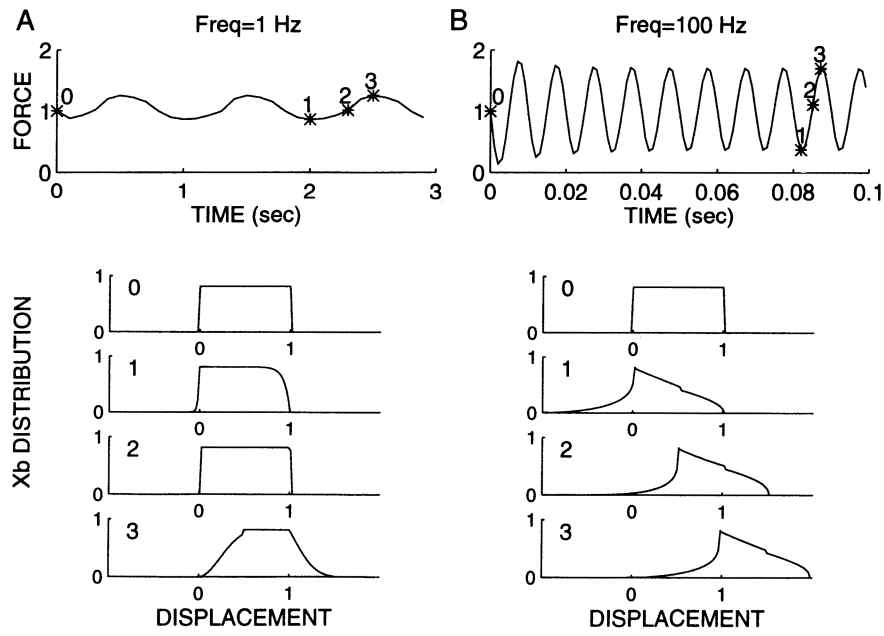

Figure B1. The effect of sinusoidal length perturbation on (upper) the generated force and on (lower) the distribution of the Xbs at various instant during the oscillation, based on Huxley's model with fR = 43.3; g_{ha} = 10; g_{h2} = 209; g_{h3} = 50. The frequency of length perturbation is **(A)** 1 Hz; **(B)** 100 Hz.

(Fig. B1–A). Thus, the magnitude of the force oscillations for slow length perturbations is small. As shown in Fig. B1–B, an increase in the frequency of length perturbation scatters the Xbs over a wider range. Note the increase in the amount of Xbs distributed in the region that generates negative force, and the rather peculiar bond distribution functions.

DISCUSSION

Dr. H.E.D.J. ter Keurs: Moss' group [Wolff and Moss. *Circ Res.* 1995;76:154–160] studied the rate of force redevelopment in skinned fibers under sarcomere length control. They argue that the rate of force redevelopment is strongly calcium dependent. The group of Huntsman [Huntsman HM. *Circ Res.* 1993;73:603–611] finds no calcium dependence. Which model would you apply to their results?

Dr. A. Landesberg: We have shown here that the dependence of the rate of force redevelopment on calcium concentration, as shown by Brenner [2], does not necessarily mean that calcium affects Xb kinetics. If you are using a two-state model, then the experimental data can be explained only by assuming that calcium affects the rate of Xb transition from the weak to the strong conformation. However, in our four-state model, calcium affects the rate of Xb recruitment rather than Xb kinetics. The question is, what is the right model? The two-state model of Brenner or our four-state model? Based on the experimental study of Chalovich and Eisenberg [14], it seems that calcium determines V_{max} of the enzymatic reaction mainly by affecting the number of available enzymes, while the rate of the enzymatic reaction remains almost the same. Thus, calcium regulates Xb recruitment. Moreover, the four-state model assumes a loose coupling between calcium dissociation from the troponin and Xb weakening [8, 9] and can explain other phenomena, such as the effect of loading condition on the free calcium transient [9], the rate of force development after a quick releases at various instant during the twitch [11] and the load dependent of relaxation [17].

Dr. J. Solaro: I was glad to see that you address this attachment regulation too. There is now increasing evidence for a blocked state of the thin filament, from *in vivo* studies which suggests that recruitment is probably a viable mechanism which can be modeled. Also, Kawai *et al.* [*Circ Res.* 1993;73:35–50, 1993] have shown a lack of calcium dependence when they use a sinusoidal analysis. Have you ever perturbed your model with sinusoidal length changes, the way they do?

Dr. A. Landesberg: No, we have not analyzed the dependence of the stiffness on the frequency of sinusoidal length perturbations, as was performed by Kawai *et al.* However, they have used tools from the field of the linear time invariant system to analyze the mechanical performances of the cardiac muscle, which is a nonlinear and time variant system. Moreover, they assume a schematic model in which the steps of nucleotide binding and release occur in sequence with the process of Xb attachment/detachment. Our model relates to large scale perturbations, as well as coupling Xb cycling with calcium kinetics, and understanding the force–length and force–velocity relationships. The description of the average force generated by a single Xb is based on the experimental studies of de Tombe and ter Keurs [*J Physiol.* 1992;454:619–642]. Our model establishes the existence of mechanical feedback, where the rate of Xb weakening is affected by the sarcomere sliding velocity, which has an important significance in the understanding of the biochemical–mechanical coupling, and the control of ATP hydrolysis.

Dr. D. Burkhoff: If I understand it correctly, you have an up–down, right–left symmetry in the rate constants so that in the unbinding of actinomycin or the transformation from strong to weak, it does not matter whether calcium is bound or not. I wonder whether that is reasonable.

Dr. A. Landesberg: Yes. The rate of Xb weakening does not depend on the existence of bound calcium. There is a loose coupling between the Xb cycling and calcium kinetics.

Dr. D. Burkhoff: What is the experimental evidence. If calcium is unbound, then I would think that the rate of uncoupling is quicker.

Dr. A. Landesberg: The independence of the rate of Xb transition from the strong to the weak conformation on the existence of bound calcium to adjacent troponin is based on the experimental studies of Brenner [6] and others [Potma *et al. J Physiol.* 1994;474:303–317] where a linear dependence between the rate of ATPase hydrolysis and the isometric force was found. The only possibility to obtain such linear relation between the rate of ATP hydrolysis and the isometric force, for various free calcium concentration, is when the rate of Xbs weakening does not depend on the existence of bound calcium to troponin. We have also proven this point analytically [8].

Dr. D. Burkhoff: That is a derived answer from analyzing complicated experiments. Is the rate of uncoupling of the actin–myosin bond dependent on whether calcium is there?

Dr. J. Solaro: Sure it is.

Dr. A. Landesberg: I am afraid that you have missed the point. It is not a derived answer from complicated experiments, since the experiments are quite simple: you measure the isometric force and the rate of ATP hydrolysis at different calcium concentrations. I suspect that you are making a wrong assumption, that calcium determines the rate of Xbs detachment or weakening. If you propose that calcium affects the rate of Xb detachment, than Chalovich and Eisenberg [3] have shown that calcium binding to troponin has insignificant effect on the rate of Xb attachment/ detachment. However, you should understand the difference between attachment/detachment and Xb cycling between the weak and strong conformation. The weakening rate relates to the transition from the strong to the weak conformation. This rate constant relates also to the energy turnover from chemical energy to mechanical energy. If you assume that Xb with adjacent bound calcium turns back to the weak conformation at a lower rate than the Xb without an adjacent bound calcium, for the same shortening velocity, then the Xb with the bound calcium perform more mechanical work per hydrolysis of ATP. Do you have any evidence for this? Does it seem logical?. Moreover, all the best models have so far proposed that the calcium affects the rate of Xb attachment [5] or the rate transition from the weak to the strong conformation [6], or Xb recruitment [7], but nobody has suggested that calcium affects the rate of Xb detachment or Xb weakening. Furthermore, the Lema that the rate of Xb weakening is independent of the existence of bound calcium is very simple to prove mathematically, and we have shown it previously [8].

Dr. D. Burkhoff: I also wonder whether this left–right symmetry is not somewhat bizarre, that the calcium binding should not be a function of whether actin and myosin are bound, that there is a cooperativity between crossbridge coupling and calcium binding.

Dr. A. Landesberg: We have discussed this point in detail elsewhere [8]. The symmetry is based on the idea that the activation function spreads along the thin filament. The idea was proposed originally by Guth and Potter [*J Biol Chem.* 1987;262:15883–15890] and is also supported by other experimental studies. For example, Brandt *et al.* [*J Mol Biol.* 1987;195:885–896]. You can find a detailed explanation in our previous study [8].

Dr. D. Burkhoff: In your conclusion that length was not affecting the rate constants, you used the data of Hibberd and Jewell [*J Physiol.* 1982;329:527–540], in which the Hill coefficient was not changing with length. But the more recent data from, for instance, Kentish, ter Keurs, and Marban, and we have measured it too, show that when you change the length or volume of the ventricle in

the intact ventricle, the Hill coefficient does change. So, if the Hill coefficient changes, would that modify your plots of the rate constants.

Dr. A. Landesberg: No, since our model suggests that the Hill coefficient for the force–free calcium relation depends on the sarcomere length. Hibberd and Jewell have found that the sensitivity of the sarcomere increases with the increase in the sarcomere length, and the Hill coefficient increases from 2.5 at short sarcomere length to 2.94 at longer length. However, the T–test showed no statistical difference. Maybe the sarcomere length measurements were not precise enough. We have also analyzed the data of Kentish and ter Keurs [8].

The cooperativity mechanism that we have suggested can explain the increase in Hill coefficient with the increase in the sarcomere length. You should realize that Hill's equation is only a phenomenological description. In your model you took the Hill coefficient as a characteristic feature of the muscle, without trying to understand the basic phenomena. In our model there is no Hill's coefficient, but we can simulate the effect of the length on the force–free calcium relation. The same is true for Hill's force–velocity relationship. We search for a better physiological understanding, to understand the cellular control mechanism, and there is a reason for this. The Hill force–velocity relationship is precise only for a certain point during the twitch – the instant of peak isometric force, since the shortening velocity is affected by the activation level, which is never at steady state during the twitch. Also, the Hill coefficient for the force–free calcium describes only the relation at steady state. Our model can describe the transient response. In a nonlinear time varying system as the cardiac muscle it is not recommended to assume that the steady state measurements can characterized the transient response.

Dr. D. Burkhoff: Does the calculation of that apparent rate constant, and I do not know exactly how you did that, depend on the fact that the number of available crossbridges will change with length? Is that built into the calculation?

Dr. A. Landesberg: Yes.

Dr. D. Burkhoff: So, therefore, if you make the assumption that the number of crossbridges are changing with length, then you are already having a predetermined assumption of how the length is affecting the function.

Dr. A. Landesberg: You seem to miss the point. We assume that the distribution of the heads of myosin is uniform along the heavy myosin filament, as is described in the literature. Thus, changing the sarcomere length will change the single overlap length. However, the amount of Xbs in the strong conformation depends on amount of Xbs available for force generation, and as we have shown, Xb recruitment is determined by the free calcium concentration and the cooperativity mechanism. It is well established that there is a length dependent calcium sensitivity. The question is, how does the muscle sense the changes in length. We propose that the sensor is the number of force generating Xbs!

Dr. D. Burkhoff: You are making a conclusion that length does not affect the apparent rate constant. I believe that length is modifying one of the assumptions in your calculation.

Dr. A. Landesberg: The number of available Xbs in the strong conformation is not determined exclusively by the length. It is well known that the force approaches zero at sarcomere length of 70% of the maximal sarcomere length. The main mechanism is Xbs recruitment from the rest state. and Xb recruitment depends on calcium concentration and on the affinity of troponin for calcium, and hence on the cooperativity mechanism.

Dr. D. Burkhoff: But what if you assume that the available number of crossbridges is constant with length. Would you come up with a different answer?

Dr. A. Landesberg: How can you assume that? The total amount of Xbs is constant, but part of them are in the single overlap and part are in the double overlap region.

Dr. D. Burkhoff: When you do theoretical modeling, you cannot restrict yourself. It is circular reasoning. You have to allow all possibilities since you are not making the measurements, you do not know what the right answer is. So your result is a function of what your starting assumptions are.

Dr. A. Landesberg: The starting assumption is the well established experimental data. In our terms, your approach does not distinguish between the "total amount of Xbs" (R+A+T+U), and the "available crossbridge (A). Also, you do not distinguish between the single overlap and the effect of the double overlap on force development. Again, we do assume that the distribution of the Xb is uniform. The effect of the double overlap in the sarcomere length of 1.8–2.3 μm is based on the experimental studies of Stephenson *et al.* [*J Physiol.* 1989;410:351–366] and Kentish and Stienen [*J Physiol.* 1994; 475:175–184]. You propose to assume that the number of XBs in the single overlap is constant at the various sarcomere lengths, which is incorrect, based on experimental data.

Dr. J. Solaro: Your model [8] includes a cooperativity mechanism, whereby the number of cycling Xbs determines the affinity of troponin for calcium. If you stretch a slow skeletal muscle which has cardiac troponin–C beyond optimal overlap when the force is falling, it becomes more sensitive to calcium. So there is not a unique relationship. The other thing is that in the slow skeletal muscle, there is no change in calcium binding which occurs throughout the whole force–length relation, although calcium sensitivity changes dramatically. It may be interesting to do more experiments on slow skeletal muscle and we are trying to substitute slow skeletal troponin–I into cardiac myofilaments, because the two muscles have the same troponin–C. The other thing, are you saying that you could peel out the Hofmann and Fuchs data, the binding constant for calcium binding to troponin–C that was highly cooperative? Because they did not do that; they were afraid to do that.

Dr. A. Landesberg: It is generally accepted that the steep force–length relationship in the cardiac muscle is largely attributed to the "length dependence of myofilament calcium sensitivity", as was shown by Hibberd and Jewell [*J Physiol.* 1982;329:527–540], and by Allen and Kentish [*J Mol & Cellular Biol.* 1985;17:821–840]. The studies of Hofmann and Fuchs [*Am J Physiol.* 1987;253: C90–C96; *Am J Physiol.* 1987;253:C541–C546] suggest that the mechanism behind this phenomena is the length dependence of troponin for calcium. Our analysis of the Force–Length–Free calcium concentration relation [8] and the experimental study of Hofmann and Fuchs [*Am J Physiol.* 1987;253:C541–C546] propose that the troponin sense the changes in the muscle length by sensing the number of Xbs in the strong force generating conformation. The increase in the sarcomere length increases the amount of Xbs in the strong conformation and this increases the affinity of troponin for calcium. Hofmann and Fuchs [*ibid*] have demonstrated that suppression of Xb cycling by vanadate reduces the amount of calcium bound to troponin. The study of Allen and Kentish [*J Physiology* 1982;327:79–94] have also demonstrated that the affinity of troponin for calcium depends on the number of cycling crossbridges and not on the length. They have shown that the amount of calcium dissociates from the troponin due to quick release is correlated with the changes in the tension and not with the changes in the length. I agree that the question remains how to explain the increase in calcium sensitivity with the increase in the sarcomere length beyond the ascending limbs, where the number of crossbridges decrease with the increase in the sarcomere length. However, this is beyond the scope of the present model for the cardiac muscle, but there are several explanation for the phenomena, and the role of troponin–C in the length dependence calcium sensitivity in the skeletal muscle is not clear. As was shown by Fuchs and Wang [*Am J Physiol.* 1991;261:C787–C792] the affinity of troponin for calcium in the skeletal muscle is constant and does not depend on the force, shortening velocity or length. Moreover it is not clear whether the length dependence of calcium sensitivity depends on the specific isoform of the troponin–C or to the entire myofilament assembly, since the replacement of skeletal troponin–C with cardiac

troponin-C does not alter the length dependence of force development in the skeletal muscle [*Biophys J.* 1990;57:146a].

As to the question concerning the calculation of calcium affinity, I agree that the data of Hofmann and Fuchs includes only 4–5 points. However, I do not take their study as the only justification for the cooperativity mechanisms. Using our four-state model, which is based on biochemical studies, we analyzed the force-length relationship presented by Kentish *et al.* [*J Physiol.* 1983;345:24P] at various free calcium concentrations, and Hibberd and Jewell's [*J. Physiol.* 1982; 329:527–540] force-free calcium relationship at two different sarcomere lengths. These studies describe the force-length-free calcium relationship at steady state isometric contraction in skinned cardiac muscle. We have also calculated the apparent calcium binding coefficient. The analysis suggests that the affinity of troponin for calcium depends on the isometric force and not on the sarcomere length. The length dependence is attributed to the effect of the length on the amount of available crossbridges for force generation in the single overlap region.

Dr. J. Solaro: What you are saying is that if the measurements were made much better, they would fit the Kentish data.

Dr. A. Landesberg: Yes, I suspect so.

Dr. H.E.D.J. ter Keurs: I have a question about the kinetics of the system. You have shown [9] a time to peak tangent that varies four-fold with sarcomere length. How did you get the experimental data from muscle isometric contractions for sarcomere isometric contractions? Another question: I interpret the calculated force-velocity relationship in your model [9] as the force-velocity relation of the crossbridge system and I wonder how you can get a hyperbola vs the linear relation that we get for the single crossbridge. In other words, where has all the stiffness gone?

Dr. A. Landesberg: The time to peak tension was described by Allen and Kurihara [*J Physiol.* 1982;327:79–94], but they have measured the muscle length rather than the sarcomere length. Also, in your study with Backx [*Am J Physiol.* 1993;264:H1098–H1110], a significant difference between the time to peak force is noticed when you compared the normalized force at the sarcomere length of 2.3 μm against the normalized force at sarcomere length of 1.6 μm.

Dr. H.E.D.J. ter Keurs: Backx *et al.*'s study includes internal shortening too. If you make a truly isometric contraction, time to peak force tangent varies by 30%.

Dr. A. Landesberg: What are the major determinants of the time to peak force? There are three components: the time course of the free calcium transient, the uprise of the free calcium, and the time to peak free calcium. In our simulation [9], the free calcium transient is described based on Lee and Allen's [*Circ Res.* 1991;69:927–936] model for the current from the SR and membrane. This is only a rough approximation of these currents, but the aim of our study is to describe performances of the sarcomere. The second factor is the cooperativity mechanism and the third factor is the rate of crossbridge cycling. However, the increase in the time to peak force with the increase in the sarcomere length is attributed mainly to the cooperativity mechanism. The other factors only modulate the magnitude of this phenomena.

As to the force-velocity relationship, the effect of shortening on force generation in our model is attributed to four phenomena. 1) The effect of the force-length relation on the sarcomere force. This effect has a negligible contribution to the force-velocity relation. 2) Reduction in the average force generated by the Xbs, based on your study [*J Physiol.* 1992;454:619–642]; we assume that the average force generated by the Xbs decreases linearly with the increase in the shortening velocity. 3) The mechanical feedback, whereby the rate of Xbs turnover from the strong to the weak conformation depends linearly on the sarcomere shortening velocity. An increase in the shortening velocity decreases the number of crossbridges in the strong conformation. This effect was studied in detail in our previous study [9]. This feedback is responsible for the hyperbolic slope of

the force velocity relationship. 4) The cooperativity mechanism. The combined effect of the cooperative and mechanical feedback mechanisms produces the phenomena of shortening deactivation. The shortening velocity reduces the number of Xbs in the strong conformation, through the mechanical feedback. Reduction in the number of cycling Xbs, reduces the affinity of troponin for calcium. Since calcium regulate the rate of ATPase activity, then the calcium dissociation from the troponin reduces the activation level, the ability of the muscle to generate force.

REFERENCES

1. Huxley AF. Muscle contraction. *J Physiol.* 1974;243:1–43.
2. Eisenberg E, Hill TL. Muscle contraction and free energy transduction in biological system. *Science.* 1985;227:999–1006.
3. Fozzard HA, Haber E, Jennings RB, Katz AM, Morgan HE. *The Heart and Cardiovascular System, Scientific Foundations.* Second edition. NY: Raven Press. 1991:1281–1295.
4. Brenner B. Rapid dissociation and reassociation of actomyosin crossbridge during force generation: a newly observed facet of crossbridges action in muscle. *Proc Natl Acad Sci.* 1991;88:10490–10494.
5. Wong ALK. Mechanics of cardiac muscle, based on huxley's model: mathematical simulation of isometric contraction. *J Biomechanics.* 1971;4:529–540.
6. Brenner B. Effect of Ca^{2+} on crossbridge turnover kinetics in skinned single rabbit psoas fibers: implication for regulation of muscle contraction. *Proc Nat Acad Sci.* 1988;85:3265–3269.
7. Zahalak IG, Shi–ping MA. Muscle activation and contraction: constitutive relations based directly on crossbridge kinetics. *J Biomechan Eng.* 1990;112:52–62.
8. Landesberg A, Sideman S. Coupling calcium binding to Troponin–C and cross–bridge cycling kinetics in skinned cardiac cells. *Am J Physiology* 1994;266(*Heart Circ Physiol* 35): H1260–H1271.
9. Landesberg A, Sideman S. Mechanical regulation in the cardiac muscle by coupling calcium binding to troponin–C and crossbridge cycling. A dynamic model. *Am J Physiol* 1994;267(*Heart Circ Physiol* 36):H779–H795.
10. Gao WD, ter Keurs HEDJ, Typberg JV, Zeverson D, MacIntosh RB, Suga H. Energy erivation and cardiac mechanics. *Ph.D. Thesis*, University of Calgary, Dept. of Medical Science, December, 1991.
11. Peterson JN, Hunter WC, Berman MR. Estimated time course of calcium bound to troponin–c during relaxation in isolated cardiac muscle. *Am J Physiol.* 1991;260:H1013–H1024.
12. Robertson SP, Johnson P, Potter JD. The time course of calcium exchange with calmodulin, troponin, paralbumin and myosin in response to transient increase in calcium. *Biophys J.* 1981;34:559–569.
13. Lombardi V, Puazzesi G, Linari M. Rapid regeneration of actin–myosin power stroke in contracting muscle. *Nature.* 1992;355:638–641.
14. Chalovich J, Chock MPB, Eisenberg E. Mechanism of action of troponin–tropomyosin. *J Biol Chem.* 1981;256:557–578.
15. Chalovich JM, Eisenberg E. The effect of troponin – tropomyosin on the binding of heavy meromyosin to actin in the presence of ATP. *J Biol Chem.* 1986;261:5088–5093.
16. Grabarek Z, Grabarek J, Leavis PJ, Gergely J. Cooperative binding to Ca – specific sites of troponin C in regulated actin and actomyosin. *J Biol Chem.* 1983;258:14098–14102.
17. Landesberg A, Sideman S. Calcium kinetic and mechanical regulation of the cardiac muscle. In: Sideman S, Beyar R (eds) *Interactive Phenomena in the Cardiac System*, Proc of the 8th Henry Goldberg Workshop, Bethesda, MD, 1992. NY:Plenum Publishing Corp, 1993:59–77.

CHAPTER 16

MECHANISMS OF THE FRANK–STARLING PHENOMENA STUDIED IN INTACT HEARTS

Daniel Burkhoff,[1] Richard A. Stennett,[2] and Kazuhide Ogino[1]

ABSTRACT

The impact of ventricular volume on the relationship between intracellular calcium and ventricular pressure under steady–state conditions was determined in intact ferret hearts. The results reveal major quantitative differences and minor qualitative differences between these relations and those previously measured in isolated intact and skinned cardiac muscle. The importance of these differences is discussed within the context of developing a comprehensive mechanistic theory to describe load–dependence of the intact ventricle.

INTRODUCTION

The course of research in cardiovascular physiology has been influenced greatly by the time–varying elastance [E(t)] theory of ventricular contraction which was introduced in the early 1970's [1]. In principle, the E(t) function describes the time variations in instantaneous ventricular volume–elastance during a beat and was proposed as a load–independent characterization of dynamic ventricular pump properties. However, several shortcomings of this theory have been identified which have brought into question the fundamental assumptions of the theory. Most importantly, it has been shown that, in general, the end–systolic pressure–volume relationship (ESPVR) is nonlinear, is load dependent and that the entire time course of contraction is highly load dependent [2–4]. Furthermore, there has been increasing recognition of the fact that the E(t) theory provides a phenomenologic description of ventricular properties. While this theory has proved to be useful in understanding the role of the heart in overall cardiovascular performance [5], there is increasing interest in being able to describe ventricular contractile properties in terms of the fundamental processes responsible for contraction.

---

[1]Departments of Medicine[1] and Anesthesiology[2], Columbia University, 630 W. 168th Street, New York, NY, USA.

Molecular and Subcellular Cardiology: Effects of Structure and Function
Edited by S. Sideman and R. Beyar, Plenum Press, New York, 1995

Towards this end, investigators have already attempted to explain several aspects of observed ventricular behavior, including load-dependence of ESPVR, based on simple models of excitation-contraction coupling and upon the notion that loading conditions can impact on the kinetic interactions between calcium, actin and myosin [6]; a phenomenon broadly referred to as *length-dependence of activation* [7, 8].

However, in attempting to explain whole heart behavior in terms of fundamental concepts derived from studies of isolated (intact or skinned) muscles, one is always faced with two interrelated questions. First, to what degree can fundamental concepts be used to directly explain whole heart function without the need for complex mathematical models to account for the geometry, architecture, activation sequence and heterogeneity of cellular properties that exist in the heart? Second, since the physiologic conditions under which isolated (intact or skinned) muscle studies are performed differ significantly from those in which muscles exist in a perfused heart, do the results obtained from the muscle studies apply both qualitatively and quantitatively to muscle in the intact wall of the ventricle? As we move from phenomenologic to mechanistic descriptions of LV performance, these questions present themselves once more.

The purpose of this study was to examine the impact of ventricular volume on the relationship between intracellular calcium and ventricular pressure under steady-state conditions at the whole heart level. This was possible because of the recent development of techniques to measure intracellular calcium transients from a small region of the intact heart using macro-injected aequorin [9] and by techniques to tetanize the whole heart after exposure to ryanodine [10, 11]. The analogous muscle level relationship (the steady-state intracellular calcium-force relationship) provides one way of characterizing a fundamental aspect of cardiac muscle physiology and has already been studied extensively in isolated skinned and intact cardiac muscle. This relationship is so fundamental that it could provide a major portion of the foundation on which a mechanistic description of ventricular properties can be built. The results demonstrate important quantitative differences and minor qualitative differences between phenomena measured at the ventricular level and previous results obtained in isolated muscle. The importance of these differences is discussed within the context of developing a comprehensive mechanistic theory to describe load-dependence of the intact ventricle.

METHODS

Studies were performed in isolated ferret hearts using standard perfusion techniques. Briefly, hearts were excised from anesthetized ferrets and perfused on a modified Langendorff perfusion apparatus with Tyrode solution. A balloon was placed in the LV chamber through the mitral valve and balloon volume was adjusted as dictated by the protocol (see below). After stabilization of the isolated heart in modified Tyrode solution containing 2 mM [Ca^{2+}], ryanodine 3 mM was added to the perfusate and maintained for 20 to 30 min until the developed pressure, which decreased significantly with ryanodine infusion, remained unchanged for several minutes [11]. To elicit tetanizations on demand, rectangular pulses of 50 msec duration, 1.5 times voltage threshold at 10 Hz were used. Tetanic stimulation was maintained for 5 sec in most cases and maximum developed pressure (steady state) was achieved usually within 1 to 2 sec. Rest periods of at least 2 min, during which the heart contracted spontaneously, were imposed between successive tetanic contractions.

Near the end of the ryanodine infusion (when the heart became quiescent), between 3 and 5 μl of an aequorin solution (aequorin 1 mg/ml, NaCl 154 mM, KCl 5.4 mM, $MgCl_2$ 1 mM, HEPES 12 mM, glucose 11 mM and EDTA 0.1 mM) is injected just under the epi-

mysium of the infero-apical region of the heart. It has been shown that the aequorin diffuses into epicardial cells with minimal damage to the cells near the injection site (as evidenced by light microscopy) [9]. The heart and perfusion apparatus are placed inside a light tight box with a glass organ bath; the aequorin injection site is placed in contact with the base of the bath so that the aequorin luminescence is emitted through the bottom of the bath. Emitted light is focused on a photo-multiplier tube (9235QA, Thorn EMI, Fairfield NJ).

The method of calibrating the light signal into an absolute concentration of calcium is the same as used in papillary muscles [9]. At the end of the experiment, the heart was perfused with an 50mM calcium-5% Triton X-100 solution which lysed the cells and exposed the remaining aequorin to high amounts of calcium [12]. In order to calibrate a particular calcium transient, a quantity referred to as L_{max} must be determined which is the integral of the aequorin signal from the time of the chosen transient to the end of the experiment including the light collected during the lysis procedure. After determining the appropriate L_{max}, the particular light transient [L(t)] is converted to $[Ca^{2+}]_i(t)$ using a previously determined calibration curve [9].

Protocol and Data Analysis

The steady-state relationship between intracellular calcium and developed pressure was determined at different volumes by varying perfusate calcium concentration $\{[Ca^{2+}]_o\}$. After ryanodine infusion and aequorin macroinjection, $[Ca^{2+}]_o$ was varied between 0.3 and 20 mM. At each $[Ca^{2+}]_o$, developed pressures during tetanization at 2 or 3 volumes corresponding to approximate EDPs of 0, 10 and 30 mmHg were measured. After having constructed the curves relating intracellular calcium to pressure, the following standard cooperative binding curve was fit to the data:

$$LVP_{max} = [Ca^{2+}]_i^N / \{K_m^N + [Ca^{2+}]_i^N\} \quad (1)$$

where LVP_{max} is the plateau of the LVP curve at high $[Ca^{2+}]_i$ levels, N is the Hill coefficient and K_m is the calcium concentration that will provide half maximal activation.

RESULTS

Representative tracings of ventricular pressure and intracellular calcium estimated from aequorin luminescence during tetanic contractions at different perfusate calcium concentrations at a fixed LV volume are shown in Fig. 1. These tracings are similar to those previously published in isolated intact cardiac muscle exposed to ryanodine [10]. As seen in Fig. 1, neither calcium nor pressure attain a true steady state and, as in previous studies of isolated muscle, the values of both measured 1.5s after the onset of tetanus are designated as the respective "steady-state" values. From these data, we plot the relationship between intracellular calcium and pressure during the tetanus. Figure 2 shows such relations when data from 6 hearts were pooled and averaged (standard deviation bars left off for clarity); results are presented at the three different volumes. Also shown in the figure are the best fit Hill curves according to Eq. 1. K_m, indicated by the vertical lines, decreases as LV volume is increased; at the highest volume the K_m is approximately 0.4 μM and this increased to 0.54 μM at the lowest volume. Also, LVP_{max} was attained at a calcium concentration of ~0.75 μM at the high volume, and this increased to ~1.25 μM at the low volume. It is also evident that the rising portion of the curve is much steeper at the higher

than at the lower volume. This indicates that there is a change in the degree of apparent cooperativity (as indexed by the Hill coefficient, N) between calcium binding and force generation between the two loading conditions. When raw data from 6 hearts are pooled and N and K_m are determined for the three volumes studied, the results summarized in Table 1 are obtained.

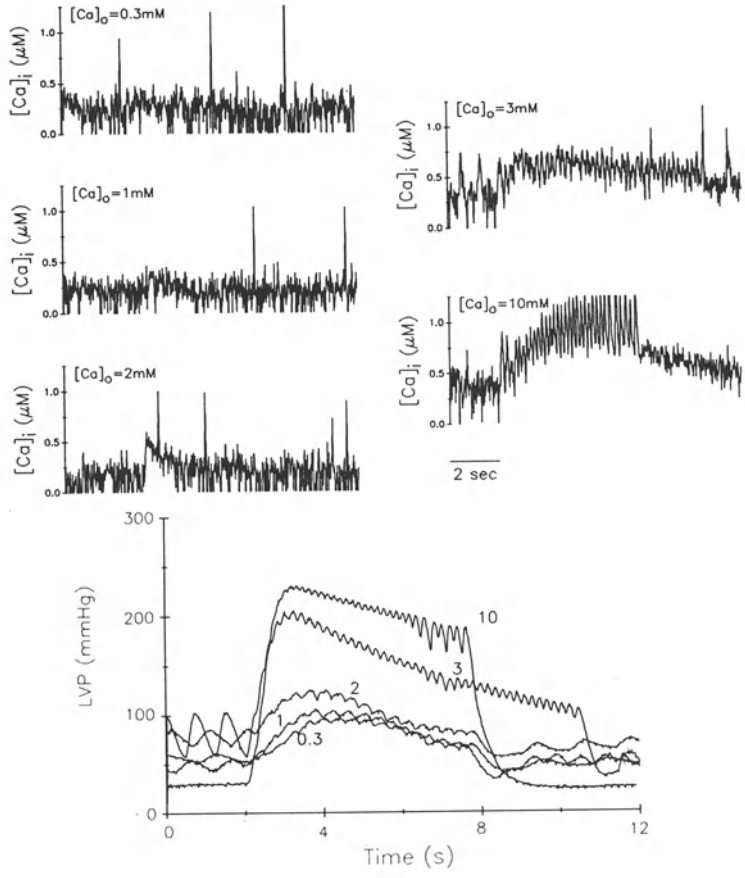

Figure 1. Tracings of LV pressure versus time during a tetanus at high LV volume with different perfusate calcium concentrations ($[Ca]_o$, as indicated in mM) are shown in the bottom panel. Upper panels show estimated intracellular calcium transient for different $[Ca]_o$ values. Note the discrete calcium transients during tetanus seen with high $[Ca]_o$; in such a case, $[Ca^{2+}]_i$ was set as the average value during the plateau.

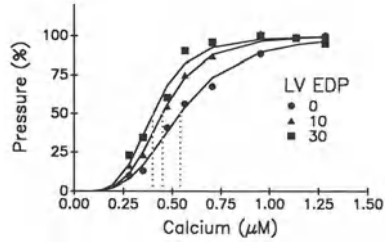

Figure 2. Average relations (n=6) between intracellular calcium and LV pressure (expressed as a % of the plateau value) during tetanic contractions at three different volumes chosen to provide end-diastolic pressure (LV EDP) of 0, 10 and 30 mmHg. Vertical lines indicate calcium concentration for half maximal activation.

Table 1. Values for Hill Coefficient (N) and Calcium Concentration for Half Maximal Activation (K_m) Obtained from Average Data Shown in Fig. 2

	Volume		
	High	Medium	Low
LVEDP (mmHg)	30	10	0
N	4.44	4.42	3.77
K_m (μM)	0.44	0.45	0.54

DISCUSSION

The relationship between intracellular calcium and muscle force determined under steady–state conditions provides a fundamental characterization of lumped myofilament properties. It is well known from previous studies that muscle length modulates this relationship, though the mechanism remains to be fully elucidated. The data presented in this study demonstrate that, with a few exceptions, the intact ventricle behaves qualitatively in a similar manner with regard to this phenomenon as does isolated muscle. However, important quantitative differences exist.

First, the degree of cooperativity of crossbridge interactions (indexed by the Hill coefficient of the calcium–pressure relation) is similar to that measured in intact and skinned muscle. Hill coefficients have been reported between ~4 and 6 in both skinned and intact muscle when measured at L_{max}. However, previous studies of muscle have that the Hill coefficient increases steadily as muscle length is increased. The data of the present study reveal that there is a volume–dependence of this parameter, but it is nonlinear, tending to reach a maximum as volume rises above the level which provides an end–diastolic pressure of 10 mmHg.

The calcium concentration for 50% maximal activation (K_m) at a high ventricular volume is much lower than that obtained in skinned muscle at L_{max} [13], though comparable to that measured in intact muscle [10]. In addition, the range over which K_m varies in the intact heart, presented for the first time in this report, is much narrower than the range over which K_m varies with sarcomere length in skinned preparations.

Finally, the data reveal that the plateau of the pressure–$[Ca^{2+}]_i$ relationship is reached at levels which are comparable to peak calcium measured during a twitch contraction despite the fact that the pressures are much lower during a twitch. This indicates, consistent with many previous reports, that the crossbridges are far from an equilibrium state with regard to calcium binding and crossbridge attachment during a twitch.

CONCLUSIONS

It has recently been proposed that dynamics of whole heart contraction could be explained on the basis of fundamental concepts derived from studies of isolated muscles [6]. Since it is the kinetics of calcium and myofilament interactions that determine the time course of force generation in cardiac muscle, this is likely to be a good starting point on which to build such a theory. As a prelude to explaining dynamic aspects of ventricular contraction, it is required that a thorough characterization of equilibrium behavior

conditions be available. The data presented in this report provide important quantitative and qualitative information about how two important parameters that describe equilibrium behavior vary with ventricular volume. Because of the overall striking similarity of ventricular to muscle behavior, we propose that fundamental concepts can be used to directly explain whole heart function without the need for *complex* mathematical models to account for the geometry, architecture, activation sequence and heterogeneity of cellular properties. However, we hypothesize that the important quantitative differences from muscle behavior observed relate to the fact that the conditions under which isolated muscle studies are performed differ significantly from those in which muscles exist in a perfused heart. This highlights the importance of performing such experiments in the intact ventricle.

Acknowledgements

This work was supported by grants from NIH (1-R29-HL51885-01) and the Whitaker Foundation. D. Burkhoff was supported by an Investigatorship Award from the American Heart Association, New York City Affiliate, Inc.

DISCUSSION

Dr. W.H. Barry: What kind of calcium levels do you see in your injected preparations during a normal twitch? I would expect them to be close to the peak that you have measured during your tetanic stimulation.

Dr. D. Burkhoff: The peak calcium that we have been measuring with 1.5 mM extracellular calcium ranges between 0.8 and maybe 1.1 μM as the peak.

Dr. W.H. Barry: The levels you achieved during tetany in the presence of ryanodine were not much greater than that.

Dr. D. Burkhoff: That is correct, and this is consistent with what has been observed recently in intact papillary muscles.

Dr. W.H. Barry: Dr. Marban, did you find an increase of about 0.5 μM or so above the normal peak twitch?

Dr. E. Marban: In our previous studies, we observed myofilament saturation by 1 μM at steady state.

Dr. H.E.D.J. ter Keurs: If aequorin studies report a diastolic calcium level of about 300 nM, I would ask myself the question, where is it located. Is it adhering to glycoproteins of the glycocalyx? Is it all intracellular, or is it all extracellular? Is it in myocytes or is it in fibroblasts or in endothelium? Is it in the mitochondria? And last but not least, how do you get away with relaxation time after the tetanus for aequorin of 30 sec?

Dr. D. Burkhoff: I think that the high diastolic calcium and the long relaxation time suggest that the aequorin is not all intramyocellular but may be, as you suggest, in fibroblasts as well.

Dr. H.E.D.J. ter Keurs: What happens if you do not put one of those egg shells on top of the heart, but simply a microscope and you look at what glows. Your eyes are usually better than egg shells.

Dr. E. Marban: Aequorin luminescence, as Gil Wier once proved to me, is very difficult to see.

Dr. G. Wier: No, I do not think you can see with your eyes inside a muscle cell. Its been tried!

REFERENCES

1. Suga H, Sagawa K. Instantaneous pressure–volume relationships and their ratio in the excised, supported canine left ventricle. *Circ Res.* 1974;35:117–126.
2. Burkhoff D, Sugiura S, Yue DT, Sagawa K. Contractility–dependent curvilinearity of end–systolic pressure–volume relations. *Am J Physiol (Heart Circ Physiol.)* 1987;252:H1218–H1227.
3. Burkhoff D, de Tombe PP, Hunter WC, Kass DA. Contractile strength and mechanical efficiency of left ventricle are enhanced by physiological overload. *Am J Physiol (Heart Circ Physiol.)* 1991;60:H569–H578.
4. Burkhoff D, de Tombe PP, Hunter WC. Impact of ejection on the magnitude and time course of ventricular pressure generating capacity. *Am J Physiol (Heart Circ Physiol.)* 1993;265:H899–H909.
5. Sagawa K, Maughan WL, Suga H, Sunagawa K. *Cardiac Contraction and the Pressure–Volume Relationship*, Oxford, Oxford University Press, 1988, pp 1–480.
6. Burkhoff D. Explaining load dependence of ventricular contractile properties with a model of excitation–contraction coupling. *J Mol Cell Cardiol.* 1994;26:959–978.
7. Jewell BR. Review: A reexamination of the influence of muscle length on myocardial performance. *Circ Res.* 1977;40:221–230.
8. Allen DG, Kentish JC. The cellular basis of the length–tension relation in cardiac muscle. *J Mol Cell Cardiol.* 1985;17:821–840.
9. Kihara Y, Grossman W, Morgan JP. Direct measurement of changes in intracellular calcium transients during hypoxia, ischemia, and reperfusion of the intact mammalian heart. *Circ Res.* 1989;65:1029–1044.
10. Yue DT, Marban E, Wier WG. Relationship between force and intracellular [Ca2+] in tetanized mammalian heart muscle. *J Gen Physiol.* 1986;87:223–242.
11. Marban E, Kusuoka H, Yue DT, Weisfeldt ML, Wier WG. Maximal Ca2+–activated force elicited by tetanization of ferret papillary muscle and whole heart: mechanics and characteristics of steady contractile activation in intact myocardium. *Circ Res.* 1986;59:262–269.
12. Bentivegna LA, Ablin LW, Kihara Y, Morgan JP. Altered calcium handling in left ventricular pressure–overload hypertrophy as detected with aequorin in the isolated, perfused ferret hearts. *Circ Res.* 1991;69:1538–1545.
13. Kentish JC, ter Keurs HEDJ, Ricciardi L, Bucx JJJ, Noble MIM. Comparison between sarcomere length–force relations of intact and skinned trabeculae from rat right ventricle: Influence of calcium concentrations on these relations. *Circ Res.* 1986;58:755–768.

MOLECULAR MANIFESTATIONS OF CELL ADAPTATION

CHAPTER 17

METABOLIC OSCILLATIONS IN HEART CELLS

Brian O'Rourke, Brian M. Ramza, Dmitry N. Romashko, and Eduardo Marban[1]

ABSTRACT

Oscillatory rhythms underlie biological processes as diverse and fundamental as neuronal firing, secretion, and muscle contraction. We have detected periodic changes in membrane ionic current driven by intrinsic oscillations of energy metabolism in guinea pig heart cells. Withdrawal of exogenous substrates initiated oscillatory activation of ATP-sensitive potassium current and cyclical suppression of depolarization-evoked intracellular calcium transients. The oscillations in membrane current were not driven by pacemaker currents or by alterations in intracellular calcium and thus represent a novel cytoplasmic cardiac oscillator. The linkage to energy metabolism was demonstrated by monitoring oscillations in the oxidation state of pyridine nucleotides. Interventions which altered the rate of glucose metabolism modulated the oscillations, suggesting that the rhythms originated at the level of glycolysis. The metabolic oscillations produced cyclical changes in electrical excitability, underscoring the potential importance of this intrinsic oscillator in the genesis of cardiac arrhythmias.

INTRODUCTION

Biological oscillators with periods as brief as milliseconds or as long as years have been identified in numerous physiological systems [1]. While the intrinsic timer underlying physiological rhythms is often difficult to pinpoint, cellular oscillators can be segregated into two major categories [2]: 1) oscillators of the surface membrane (involving ionic currents, pumps or transporters) and 2) oscillators of intracellular origin (involving enzymatic pathways, Ca^{2+} release or sequestration). Extracellular and intracellular inputs modulate the activity of both types of oscillators and interactions between the two may be necessary for a maintained response, as in the case of IP_3-mediated oscillations of cytosolic Ca^{2+} in

[1]The Johns Hopkins University, Department of Medicine, Division of Cardiology, 844 Ross Building, 720 N. Rutland Avenue, Baltimore, MD 21205, U.S.A.

Molecular and Subcellular Cardiology: Effects of Structure and Function
Edited by S. Sideman and R. Beyar, Plenum Press, New York, 1995

response to surface receptor stimulation [3]. Descriptions of several oscillatory biochemical pathways have lent support to the notion that single rate-controlling enzymes possess regulatory properties capable of supporting stable nonequilibrium oscillatory states under defined conditions [4]. One such system is the glycolytic oscillator, which is primarily controlled by phosphofructokinase [5, 6]. Although identified in intact yeast cells, most of the information about this oscillator has been obtained from cell-free extracts. Despite a dearth of information on the behavior or significance of the system in intact mammalian cells, the ubiquitous distribution of glycolytic enzymes has motivated proposals that the oscillator could mediate various oscillatory physiological behaviors, including slow waves of contraction in smooth muscle [7], bursting electrical activity in *Aplysia* neurons [8], and insulin release from the β islet cells of the pancreas [9].

Here we describe a previously unrecognized metabolic oscillator revealed by substrate deprivation that drives oscillations in background potassium conductance and Ca^{2+} transient amplitude in ventricular myocytes. Examination of the mechanism of this phenomenon indicates that the glycolytic oscillator is likely to be the primary rhythm generator underlying the observed changes in membrane currents and excitation-contraction coupling. The apparent linkage between energy metabolism and ion channel function has major implications for understanding the abnormal electrophysiology of the heart during ischemia or other forms of metabolic compromise. These inherent metabolic fluctuations, perhaps latent in every cell, introduce a source of time-dependent microheterogeneity of cellular excitability in the myocardium and thus may constitute a novel mechanism for the generation of lethal arrhythmias.

THE OSCILLATORY PHENOMENA

Description of the Oscillatory Phenomenon

Membrane current and fluorescence were measured [10] in guinea-pig ventricular myocytes equilibrated with intracellular and extracellular solutions containing physiological concentrations of ions. When external glucose was supplied, the myocytes responded to depolarizations with relatively unremarkable Na^+, Ca^{2+}, and K^+ currents for 30 mins or more. By simply omitting fuel substrates from the bathing medium, we found that large periodic increases in a background membrane conductance were initiated. In each cycle of oscillation, the current developed over 15 secs, peaked briefly, and resolved within the next 60 secs (Fig. 1). In the absence of external substrate, spontaneous oscillations in membrane conductance were observed in approximately 50% of myocytes studied. In myocytes which did not spontaneously oscillate at the onset of the experiment, latent oscillatory membrane currents could often be revealed after prolonged observation or after perturbations of intracellular metabolites. Simultaneous measurement of depolarization-evoked intracellular Ca^{2+} transients revealed that the amplitude was suppressed in phase with the development of the oscillatory current, but was fully restored when the background current returned to baseline. The peak-to-peak period of spontaneous oscillations obtained by analysis of multiple cycles of oscillations (Fig. 1) averaged 1.66 ± 0.21 mins (mean ± SD; N = 8), with remarkably little cell-to-cell variation in myocytes displaying regular periodicity. Some cells oscillated aperiodically, as shown in Fig. 2. Spontaneous oscillations in current and in the Ca^{2+} transient were stable over long periods of time, with the longest observations of self-sustained oscillations being more than 2 hrs.

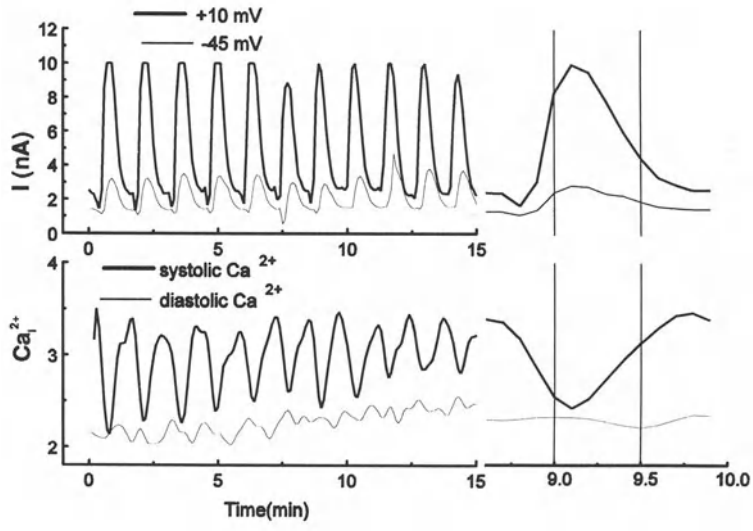

Figure 1. Spontaneous oscillations in membrane currents **(upper)** and intracellular calcium transient **(lower)**, as a result of glucose omission from the medium. Figures excerpted with permission from O'Rourke B, Ramza BM, MArban E. *Science*. 1994;265:962–966. Copyright 1994 American Association for the Advancement of Science [10].

Nature of the Oscillatory Current

Analysis of the current–voltage relationship for background currents during membrane voltage ramps revealed that the reversal potential of the background current at the peak of an oscillation was the same as that during the nadir. Under normal conditions, this reversal potential is largely determined by ionic conductance through inwardly–rectifying potassium channels. The reversal potential of the background currents always remained near the estimated reversal potential for potassium (E_K; −86 mV for the experimental solutions) and could not be accounted for by alterations in the membrane conductance of other cations or that of chloride. Since the oscillating potassium current showed weak inward rectification at positive potentials and was observed only during metabolic stress, ATP–sensitive potassium channels ($I_{K,ATP}$) were suspected as mediators of the response. Consistent with a mechanism involving $I_{K,ATP}$, the oscillations were shown to be sensitive to glibenclamide [10]. Changes in membrane potential or in intracellular [Ca^{2+}] were not required to support the oscillations in $I_{K,ATP}$. In a myocyte undergoing spontaneous oscillations in membrane current and Ca^{2+} transient amplitude during depolarizing steps, the voltage protocol was temporarily switched to one in which the membrane potential was held constant at −80 mV. Elimination of voltage–activated currents abolishes the intracellular Ca^{2+} transient without affecting the oscillations in holding current. Thus, the oscillatory phenomenon is distinguishable from conventional oscillatory mechanisms relying on feedback control by intracellular Ca^{2+}, including the widely–studied oscillations due to spontaneous Ca^{2+} release from the sarcoplasmic reticulum [2, 11], IP_3–induced Ca^{2+} release [3], and Ca^{2+}/cyclic AMP feedback loops [12]. The observation of oscillations of $I_{K,ATP}$ in substrate–depleted cells suggested that intrinsic oscillations of energy metabolism might be driving the oscillations in ionic current, prompting further investigation into the site of generation of the physiological rhythms.

Linkage with Metabolic Flux

Stable oscillations in the flux of substrates through glycolysis have been extensively documented in the literature [4, 13, 14]. In intact yeast, glycolytic oscillations can be recorded by monitoring the levels of reduced nicotinamide adenine dinucleotides (primarily NADH) with fluorescence spectroscopy [15]. Using NADH fluorescence as an index of cellular energy metabolism, we found that the oscillations in $I_{K,ATP}$ were directly correlated with transient decreases in NADH (Fig. 2A). Analysis of the first derivative of the time course of oscillations in current and NADH indicated that the decrease in NADH consistently preceded the increase in membrane currents (Fig. 2B), suggesting that a change in the rate of energy metabolism initiated the change in membrane conductance. Further support for this idea was obtained by altering the rates of glycolysis or oxidative phosphorylation using exogenous substrates or metabolic inhibitors. Provision of glucose to cardiomyocytes displaying the oscillatory response often resulted in modulation of the frequency or complete cessation of oscillation – in some cells, a strong amplitude damping effect was observed upon exposure to glucose, with little effect on the frequency (Fig. 3). These results suggest that the oscillatory response is closely associated with alterations in glycolytic flux. We have also observed damped oscillations in $I_{K,ATP}$ during transient increases in glycolytic flux following severe metabolic inhibition [10], emphasizing the potential importance of the oscillator during the reperfusion of ischemic cardiac tissue, when the risk of arrhythmias is high [16].

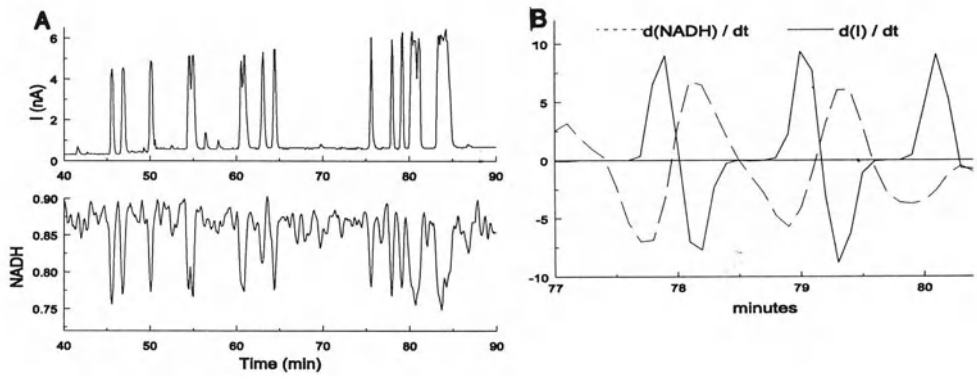

Figure 2. The relationship between the oscillations in membrane current and cellular energy metabolism, recorded by monitoring NADH fluorescence. **A:** time courses; **B:** time derivatives. Note that changes in energy metabolism precede the changes in membrane currents (adapted from [10] with permission).

Taken together, the evidence indicates that, over a crucial range of glycolytic rates, an oscillatory pattern can be sustained – a decrease in flux below or an increase above the window pushes the system out of the oscillatory domain. This interpretation agrees with the predictions of models of the glycolytic oscillator, in which a stable oscillatory domain is surrounded by states responding with monotonic changes in activity [17]. Experimental results have confirmed the critical dependence on substrate influx rate in supporting the glycolytic oscillations in yeast [18]. Although within the critical substrate input range the system is relatively resistant to deviation from the mean autonomous oscillatory frequency, certain rates of periodic substrate influx can result in entrainment of the oscillator to the input frequency [18], while others may induce chaotic behavior [19]. In cardiac cells, which

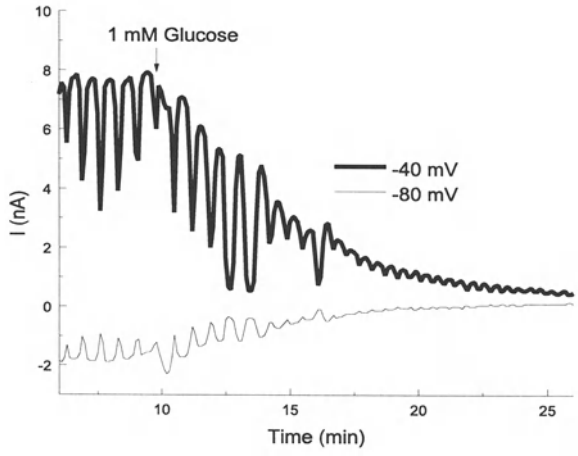

Figure 3. Effect of adding glucose on oscillations in membrane currents. Note in this example that the amplitude damped when glucose was provided, with little effect on the frequency (adapted from [10] with permission).

normally rely on oxidative metabolism, another type of entrainment must be considered. The cyclical changes in adenine nucleotides, NADH, and pyruvate generated in bursts by glycolysis may serve to entrain mitochondrial function to the cytoplasmic oscillator, thus amplifying the effect. Feedback on the glycolytic oscillator by oxidative metabolism has been reported in yeast [20] and may also play an important modulatory role in the present response. We have recently found that computer simulation of the glycolytic oscillator coupled to ADP-dependent control over the mitochondrial oxidation rate adequately describes the phase relationships of K,ATP channel activation and NADH oscillation if we assume that the NADH signal is largely mitochondrial in origin [15].

Allosteric Modulation of Oscillations

Oscillations in the levels of glycolytic intermediates have been measured in cell-free extracts of skeletal muscle [21], heart [14], yeast [22], and blowfly thorax [13]. Similar oscillations in NADH fluorescence of intact yeast [23] and ascites tumor cells [24] have been detected. Examination of the phase shift between oscillations in the various glycolytic metabolites has revealed key rate-limiting control points. In some systems, a single "master" enzyme possessing the regulatory properties necessary for maintaining a stable nonequilibrium oscillatory state can entirely account for the oscillations [5]. Prerequisites for such a control enzyme include a non-linear response to effectors (provided by allosteric binding sites) and multiple pathways for positive and negative feedback on the enzyme [6, 12]. Phosphofructokinase (PFK), the major control point for glycolysis catalyzing the conversion of fructose 6-phosphate to fructose 1,6 diphosphate, fulfills these criteria for maintaining stable oscillations in glycolysis. PFK activity is regulated by the positive allosteric effectors AMP, ADP, and P_i and the negative effectors ATP and citrate. A decline in the ATP/ADP ratio or a rise in AMP has been proposed to initiate the cyclical activation of PFK in yeast extracts [25], while in muscle extracts, the autocatalytic activation of PFK by fructose 1,6 - diphosphate also plays a role in rapidly switching on enzyme activity [6]. Allosteric modulators of PFK have been shown to alter the frequency and amplitude of the oscillations, often in a phase-dependent manner [25-27], consistent with the idea that the

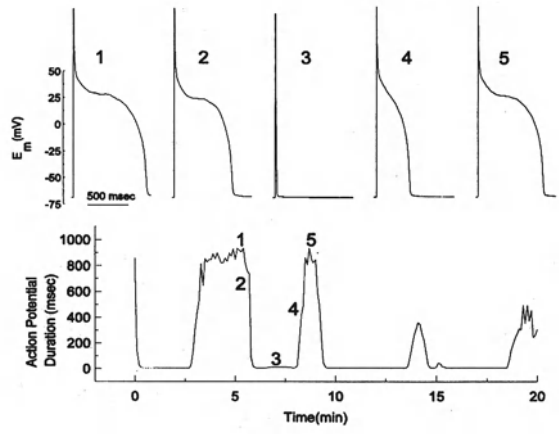

Figure 4. Action potential in a spontaneous oscillating cell. The period of inexcitability parallels the time course of current oscillations recorded in voltage clamp experiments (adapted from [10] with permission).

enzyme cycles between different activity states [28]. We tested whether the oscillations in membrane current that we observed respond to interventions known to alter the activity of the glycolytic oscillator. Early studies on the effect of nucleotides on NADH fluorescence oscillations in glycolytic extracts showed that the application of ADP to the system could reset the phase or alter the amplitude of the oscillations [27]. Furthermore, if changes in the ATP/ADP ratio trigger oscillations, we reasoned that a rapid increase in cytosolic ADP might initiate the response. This prediction was borne out by experiments in which cytosolic ADP was rapidly increased by flash photolysis of intracellular caged ADP [10]. In cells which were not oscillating in zero glucose, ADP release immediately induced a series of oscillations. The effect of the photolytically-released ADP on the oscillations was consistent with the hypothesis that adenine nucleotides acted directly on the glycolytic oscillator by regulating PFK activity.

Effects on Action Potentials

The large oscillations of membrane current measured under voltage clamp conditions implied that electrical excitability would be altered cyclically. The resting membrane potential, which is close to E_K, should be minimally influenced by the oscillatory increases in background potassium conductance. In contrast, the repolarizing influence of the background conductance should greatly reduce excitability and speed repolarization when an action potential can be generated. These predictions held true when we recorded action potentials in a spontaneously oscillating cell (Fig. 4). Periods of inexcitability paralleled the time course of the current oscillations recorded in voltage clamp mode and were preceded and followed by transition periods of shorter action potential duration. The cyclical changes in action potential shape and duration indicate that temporal action potential heterogeneity can be present in individual cells even under constant external conditions.

PATHOPHYSIOLOGICAL IMPLICATIONS

The discovery of oscillations in the ionic conductance of the cardiac sarcolemma under conditions of metabolic stress provides new clues towards understanding the mech-

anisms of arrhythmogenesis during myocardial ischemia and reperfusion. Although there is a wealth of information documenting the various forms of anomalous electrical behavior in metabolically-compromised myocardium, little is known about the root cause of the disturbances at the cellular level. This deficit of knowledge about the cellular basis of ventricular arrhythmias has restricted our ability to treat or to prevent the lethal arrhythmias underlying "sudden cardiac death" [29]. Oscillations in the electrical excitability of individual cells or small regions of the heart may explain the unpredictable initiation of reentrant circuits and chaotic progression toward fibrillation by affecting both the conduction velocity and the effective refractory period in segments of the conduction pathway in a time-varying manner. In addition to the importance of spatial heterogeneity of the action potential [16], temporal alterations in cellular excitability must be taken into account when dispersion of refractoriness is considered as a cause of arrhythmias. With regard to the role of $I_{K,ATP}$ in ischemia-related arrhythmias, activation of K,ATP channels with pinacidil increases the incidence of ventricular tachycardia and fibrillation during ischemia [30, 31], while glibenclamide block of $I_{K,ATP}$ attenuates ventricular arrhythmias during ischemia [31-34].

The pathophysiological implications of the oscillations will, in part, be determined by whether or not the oscillations are entrained in a multicellular preparation. In yeast cell suspensions, the entire population of cells must be oscillating in phase to detect NADH oscillations on a macroscopic level, and rapid synchronization of two populations of yeast oscillating 180° out of phase has been demonstrated upon mixing [35]. Similarly, bursting patterns occur independently in single pancreatic β cells but are synchronized in intact islets [36]. Damped oscillations in NADH fluorescence in an intact heart have been observed when glucose was added to the perfusate after a brief period of anoxia and reoxygenation [37], suggesting that cell-to-cell entrainment is possible. The synchronizing factor for these forms of cellular communication is unknown, but could be mediated by diffusible extracellular messengers or transmission through gap junctions. It is interesting to note that oscillation in the generation of metabolites coupled with diffusion away from the point of generation establishes waves of sharp concentration gradients which facilitate the propagation of a diffusible messenger [38].

CONCLUSION

The present study is the first to describe a direct linkage between the glycolytic oscillator and the primary function of a cell, in this case cardiac excitation-contraction coupling. Whether the oscillations are advantageous to the function of the cell during physiologic stress or simply reflect a complex control process gone awry [6, 38], the recognition of a metabolic oscillator dynamically linked to excitability may have a profound influence on the susceptibility to arrhythmias in the metabolically-challenged heart.

DISCUSSION

Dr. M. Lab: Have you tried to influence your oscillations by metabolic manipulation? For example, have you tried insulin? Insulin resistance is becoming prominent in cardiology.

Dr. B. O'Rourke: Yes; we have not seen very reproducible effects of insulin on the rate of oscillation. We think that when the glucose is taken away, the cell becomes dependent on glycogenolysis to supply substrates to the glycolytic pathway and slowing of the input rate pushes it into

the oscillatory range. We have done some experiments using metabolic inhibitors like 2-deoxyglucose and 2,4 dinitrophenol. In a cell that was showing oscillations when we added 2-deoxyglucose, the oscillations stopped. Then we induced severe metabolic inhibitions with dinitrophenol in zero glucose which activated I_{KATP} strongly. At this point we restored glucose metabolism by washing out the dinitrophenol in the presence of glucose and saw a return to baseline of the KATP current. We also observed damped oscillations on restoration of glucose metabolism. Again, we think we are going through this window of oscillation as we turn glucose metabolism back on, but we are continuing to study various points in the system using the model as a guide to test various steps in the system with specific inhibitors of those steps. But I do not have specific results on those yet.

Dr. G. Kessler-Icekson: What proportion of the cells display this phenomenon of oscillation? If you take, for instance, thyroid treated animal, will this proportion be changed.

Dr. B. O'Rourke: We have not found anything that will change the proportion directly at this point in time. We see it in approximately 50% of the cells, 50 out of 105 cell studies so far. The problem that we have now is trying to get this thing under complete control and figure out what the most important factor controlling it is. We are limited in that regard because, as I said, I think that the rate of glycogenolysis might be important, but we have not gotten any reproducible intervention that can make it active in 100% of the cells. We are trying to do that by infusing various glycolytic intermediates in the internal solution right now and blocking other inputs. We are limited by input control at this point so we are trying to work that out.

Dr. D. Burkhoff: Normally, of course, there are fatty acids present. When fatty acids are present pyruvate hydrogenase is inhibited and the flux through glycolysis is decreased. Have you tried experiments where you have given only fatty acids, or a combination of glucose with fatty acids. In other words, if you decrease the flux through glycolysis, does that decrease the importance of these feedback mechanisms that you are talking about, and then suppress the oscillations?

Dr. B. O'Rourke: We have not used fatty acids *per se*. We have tried to add pyruvate or acetate to get at the oxidative metabolism by the mitochondria in that way. We have seen situations where pyruvate had no effect so we think that the oscillator does reside at the level of glycolysis. I am not sure, in the absence of substrate, whether the cell is still metabolizing endogenous fatty acids as a primary substrate. I think there is competition between the acetyl coenzyme A (CoA) pool and the acetyl CoA pool for a limited supply of CoA.

Dr. D. Burkhoff: But still, when you give glucose, it is primarily using the glucose.

Dr. B. O'Rourke: Yes, we think that about 98% of the glucose is oxidized when there is external glucose.

Dr. D. Burkhoff: So there is not much from endogenous triglycerides.

Dr. B. O'Rourke: Something is inhibiting fatty acid metabolism in the absence of external substrate, even though the cell prefers to use fatty acids under normal conditions.

REFERENCES

1. Rapp PE. An atlas of cellular oscillators. *J Exp Biol.* 1979;81:281-306.
2. Tsien RW, Kass RS, Weingart R. Cellular and subcellular mechanisms of cardiac pacemaker oscillations. *J Exp Biol.* 1979;81:205-215.

3. Tsien RW, Tsien RY. Calcium channels, stores, and oscillations. *Annu Rev Cell Biol.* 1990;6:715–760.
4. Andrés V, Schultz V, Tornheim K. Oscillatory synthesis of glucose 1,6-bisphosphate and frequency modulation of glycolytic oscillations in skeletal muscle extracts. *J Biol Chem.* 1990;265:21441–21447.
5. Hess B, Plesser T. Temporal and spatial order in biochemical systems. *Ann NY Acad Sci.* 1979;316:203–213.
6. Tornheim K. Oscillations of the glycolytic pathway and the purine nucleotide cycle. *J Theor Biol.* 1979;79:491–541.
7. Connor JA. On exploring the basis for slow potential oscillations in the mammalian stomach and intestine. *J Exp Biol.* 1979;81:153–173.
8. Meech RW. Membrane potential oscillations in molluscan "burster" neurones. *J Exp Biol.* 1979;81:93–112.
9. Corkey BE, Tornheim K, Deeney JT, Glennon MC, Parker JC, Matschinsky FM, Ruderman NB, Prentki M. Linked oscillations of free Ca^{2+} and the ATP/ADP ratio in permeabilized RINm5F insulinoma cells supplemented with a glycolyzing cell-free muscle extract. *J Biol Chem.* 1988;263:4254–4258.
10. O'Rourke B, Ramza BM, Marban E. Oscillations of membrane current and excitability driven by metabolic oscillations in heart cells. *Science.* 1994;265:962–966.
11. Kort AA, Lakatta EG, Marban E, Stern MD, Wier WG. Fluctuations in intracellular calcium concentration and their effect on tonic tension in canine cardiac purkinje fibres. *J Physiol (Lond).* 1985;367:291–308.
12. Rapp PE, Berridge MJ. Oscillations in calcium-cyclic AMP control loops form the basis of pacemaker activity and other high frequency biological rhythms. *J Theor Biol.* 1977;66:497–525.
13. Collatz K-G, Horning M. Age dependent changes of a biochemical rhythm – the glycolytic oscillator of the blowfly phormia terraenovae. *Comp Biochem Physiol.* 1990;96:771–774.
14. Frenkel R. Control of reduced diphosphopyridine nucleotide oscillations in beef heart extracts. II. Oscillations of glycolytic intermediates and adenine nucleotides. *Arch Biochem Biophys.* 1968;125:157–165.
15. Eng J, Lynch RM, Balaban RS. Nicotinamide adenine dinucleotide fluorescence spectroscopy and imaging of isolated cardiac myocytes. *Biochem J.* 1989;55:621–630.
16. Wit AL, Janse MJ. *The ventricular arrhythmias of ischemia and infarction: electrophysiological mechanisms.* Mount Kisco, Futura, 1993.
17. Hess B. Non-equilibrium dynamics of biochemical processes. *Hoppe-Seyler's Z Physiol Chem.* 1983;364:1–20.
18. Boiteux A, Goldbeter A, Hess B. Control of oscillating glycolysis of yeast by stochastic, periodic, and steady source of substrate: a model and experimental study. *Proc Natl Acad Sci USA.* 1975;72:3829–3833.
19. Markus M, Kuschmitz D, Hess B. Chaotic dynamics in yeast glycolysis under periodic substrate input flux. *FEBS Lett.* 1984;172:235–238.
20. Aon MA, Cortassa S, Westerhoff HV, Berden JA, Van Spronsen E, Van Dam K. Dynamic regulation of yeast glycolytic oscillations by mitochondrial functions. *J Cell Sci.* 1991;99:325–334.
21. Tornheim K, Lowenstein JM. The purine nucleotide cycle. IV. Interactions with oscillations of the glycolytic pathway in muscle extracts. *J Biol Chem.* 1974;249:3241–3247.
22. Ghosh A, Chance B. Oscillations of glycolytic intermediates in yeast cells. *Biochem Biophys Res Comm.* 1964;16:174–187.
23. Hess B, Boiteux A. Mechanism of glycolytic oscillation in yeast. I. Aerobic and anaerobic growth conditions for obtaining glycolytic oscillation. *Hoppe-Seyler's Z Physiol Chem.* 1968;349:1567–1574.
24. Ibsen KH, Schiller KW. Oscillations of nucleotides and glycolytic intermediates in aerobic suspension of ehrlich ascites tumor cells. *Biochim Biophys Acta.* 1967;131:405–407.
25. Chance B, Schoener B, Elsaesser S. Metabolic control phenomena involved in damped sinusoidal oscillations of reduced diphosphopyridine nucleotide in a cell-free extract of *Saccharomyces carlsbergensis*. *J Biol Chem.* 1965;240:3170–3181.
26. Frenkel R. Reduced diphosphopyridine nucleotide oscillations in cell-free extracts from beef heart. *Arch Biochem Biophys.* 1966;115:112–121.
27. Chance B, Schoener B, Elsaesser S. Control of the waveform of oscillations of the reduced pyridine nucleotide level in a cell-free extract. *Biochemistry.* 1964;52:337–341.

28. Monod J, Wyman J, Changeux J-P. On the nature of allosteric transitions: a plausible model. *J Mol Biol.* 1965;12:88–118.
29. Stevenson WG, Stevenson LW, Middlekauff HR, Saxon LA. Sudden death prevention in patients with advanced ventricular dysfunction. *Circ.* 1993;88:2953–2961.
30. Chi L, Black SC, Kuo PI, Fagbemi SO, Lucchesi BR. Actions of pinacidil at a reduced potassium concentration: a direct cardiac effect possibly involving the ATP-dependent potassium channel. *J Cardiovasc Pharmacol.* 1993;21:179–190.
31. Wolleben CD, Sanguinetti MC, Siegl PKS. Influence of ATP-sensitive potassium channel modulators on ischemia-induced fibrillation in isolated rat hearts. *J Mol Cell Cardiol.* 1989;21:783–788.
32. Lynch JJ, Jr., Sanguinetti MC, Kimura S, Bassett AL. Therapeutic potential of modulating potassium currents in the diseased myocardium. *FASEB J.* 1992;6:2952–2960.
33. Kantor PF, Coatzee WA, Carmeliet EE, Dennis SC, Opie LH. Reduction of ischemic K^+ loss and arrhythmias in rat hearts. Effect of glyburide, a sulfonylurea. *Circ Res.* 1990;66:478–485.
34. Gwilt M, Norton B, Henderson CG. Pharmacological studies of K^+ loss from ischaemic myocardium *in vitro*: roles of ATP-dependent K^+ channels and lactate-coupled efflux. *Eur J Pharmacol.* 1993;236:107–112.
35. Pye EK. Biochemical mechanisms underlying the metabolic oscillations in yeast. *Can J Bot.* 1969;47:271–285.
36. Longo EA, Tornheim K, Deeney JT, Varnum BA, Tillotson D, Prentki M, Corkey BE. Oscillations in cytosolic free Ca^{2+}, oxygen consumption, and insulin secretion in glucose-stimulated rat pancreatic islets. *J Biol Chem.* 1991;266:9314–9319.
37. Chance B, Williamson JR, Jamieson D, Schoener B. Properties and kinetics of reduced pyridine nucleotide fluorescence of the isolated and *in vivo* rat heart. *Biochemische Zeitschrift.* 1965;341:357–377.
38. Goldbeter A, Caplan SR. Oscillatory enzymes. *Ann Rev Biophys Bioeng.* 1976;5:449–476.

CHAPTER 18

ALTERED GENE TRANSCRIPTION FOLLOWING BRIEF EPISODES OF CORONARY OCCLUSIONS

Ralph Knöll, René Zimmermann, and Wolfgang Schaper[1]

ABSTRACT

This study was designed to elucidate whether previously observed enhanced mRNAs were due to accelerated transcription, enhanced mRNA stability or both mechanisms. We employed the nuclear run-on technique on myocardial nuclei and found the transcriptional induction of several genes, especially nuclear protooncogenes, Ca^{2+} regulating and heat shock protein genes.

INTRODUCTION

Coronary occlusions cause mainly two phenomena: 1) Long lasting, hours to days, contractile dysfunction, and 2) effect of ischemic preconditioning [1]. In order to evaluate whether altered gene expression occurs or may be responsible for these phenomena we, and others [2–5], found a variety of different mRNAs upregulated during or after short coronary occlusions. This study was designed to elucidate whether these upregulated mRNAs were due to accelerated transcription, enhanced mRNA stability or both mechanisms. We investigated several members of the leucine zipper nuclear transcription factors like c-jun, c-fos, jun B, jun D and c-myc, all of them known to be potent regulators of gene transcription. We also included the calcium regulating genes coding for phospholamban, calsequestrin, calmodulin and Ca^{2+} ATPase as well as heat shock protein genes like hsp27, hsp70 and ubiquitin. Furthermore, the gene coding for the glycolytic enzyme glyceraldehyde-phosphate-dehydrogenase (GAPDH), the contractile protein β myosin heavy chain (βMHC), as well as the gene for plasminogen activator inhibitor-1 (PAI-1), were included in this study. Additionally, we included the genes coding for different growth

[1]Max-Planck-Institute, Department of Experimental Cardiology, Benekestrasse 2, D-61231 Bad Nauheim, F.R. Germany.

Molecular and Subcellular Cardiology: Effects of Structure and Function
Edited by S. Sideman and R. Beyar, Plenum Press, New York, 1995

factors like transforming growth factor β_1, ($TGF\beta_1$), acidic fibroblast growth factor (aFGF), interleukin 6 (IL6), insulin like growth factor 1 (IGF-I) and insulin like growth factor 2 (IGF-II).

METHODS, MATERIALS AND PROCEDURES

Animal Preparation

Animals used in this study were handled in accordance with the American Physiological Society guidelines for animal welfare and the experimental protocol was approved by the bioethics committee of the District of Darmstadt, Germany.

Seven castrated male mixed breed Landrace-type domestic pigs were sedated with azaperone 2 mg/kg i.m. and then anesthetized with intravenous pentobarbitone 30 mg/kg. After intubation, the pigs were mechanically ventilated with a respirator (Mark 7, Bird Products, Palm Springs, California) with room air supplemented with oxygen (2 liters/min). The thorax was opened, the heart was exposed and a stabilization period of 30 mins was allowed. The left anterior descending coronary artery (LAD) was then occluded for 10 mins followed by 30 mins of reperfusion and again occluded for a further 10 mins (timepoint 10-30-10). Pigs were sacrificed immediately after the second occlusion, or after 30 mins (timepoint $(10\text{-}30)_2$) or 90 mins (timepoint $(10\text{-}30)_2$+60) of reperfusion (Fig. 1). Experimental tissue was removed from the LAD area and control tissue was removed from the region of the left circumflex coronary artery (Cx) area.

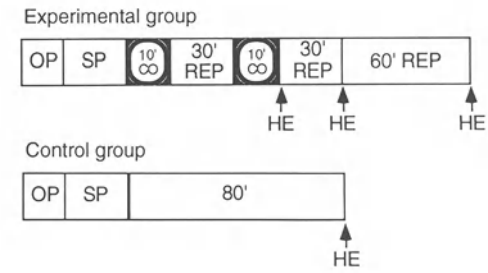

Figure 1. Protocol for the coronary occlusions. HE - heart excision; OP - operation; SP - stabilization period (~ 30 min); REP - reperfusion; CO - occlusion.

Nuclei Isolation

Nuclei were isolated with slight modifications of the nonenzymatic procedure described earlier [6]. Briefly, our methods were as follows: All steps were carried out at 4°C. Approximally 6 g of experimental and of control myocardial tissue were minced with scissors and homogenized for 30 seconds at 13500 RPM with a homogenizer (Ultraturrax T25, Janke und Kunkel) in 20 ml of MA buffer (10 mM Tris/HCl, pH 7.4; 10 mM $MgCl_2$; 0.25 M sucrose; 0.1 mM PMSF (phenylmethanesulphonyl fluoride); 2.8 mM DTT (dithio-threitol). The homogenate was centrifuged for 10 mins at 750 g and resuspended in 20 ml of MA buffer, homogenized with six strokes in a dounce homogenizer and filtered through a nylon membrane (sieve mesh 100 nm; Züricher Beuteltuchfabrik; Switzerland). The filtrate was then centrifuged for 10 mins at 750 g. The pellet was resuspended in 20 ml MB

buffer (0.5% Triton X-100 in MA buffer) and centrifuged again for 10 mins at 750 g. The pellet was then resuspended in 25 ml of MC buffer (2.2 M sucrose; 10 mM Tris/HCl pH 7.4; 10 mM $MgCl_2$; 0.1 mM PMSF; 2.8 mM DTT) and loaded onto a sucrose gradient consisting of 5 ml 2.7 M and 2 ml 2.4 M sucrose. Ultracentrifugation was carried out for 1 h at 25000 RPM in a Beckman type ultracentrifuge. The relatively pure myocyte nuclei population was localized at the interphase between the 2.4 M and the 2.7 M sucrose bands, whereas non-myocyte nuclei, depending on their size and density, were located at the bottom of the tube. Nuclei were recovered, resuspended in 40 ml of MA buffer and centrifuged for 20 mins at 750 g. Nuclei were then resuspended in 1 ml of MA buffer, counted in a Neubauer chamber and spun down in an Eppendorf centrifuge.

Nuclear Transcription

Reactions were performed as described by Cox *et al.* [7]. The centrifuged nuclei were resuspended in 100 µl of Keller storage buffer [8] (10 mM Tris/HCl pH 7.5; 5 mM $MgCl_2$; 0.5 M sorbitol; 2.5% Ficoll; 0.008% spermidine; 1 mM DTT; 200 U RNasin/ml; 50% glycerol) and 87.5 µl of reaction mixture (80 mM Tris/HCl, pH 8.3; 300 mM NH_4Cl; 15 mM $MgCl_2$; 625 µM ATP; 312 µM CTP; 312 µM GTP) were added. Nuclear transcription reactions were started by the addition of 12.5 µl of α^{32}P UTP solution (125 µCi; 3000 Ci/mM; Amersham) and incubated at 27°C for 20 mins. The reaction was stopped by quick centrifugation in an Eppendorf centrifuge and the nuclear pellet was resuspended in 500 µl of guanidinium buffer (4 M guanidiniumisothiocyanate; 25 mM sodium citrate; 0.5% sarcosyl; 0.1 M 2 mercaptoethanol).

Isolation of Nuclear RNA

Nuclear RNA was isolated by the method of Chomczynsky and Sacchi [9] Briefly, 50 µl of 2 M sodium acetate pH 4.0, 500 µl water-saturated phenol and 100 µl of chloroform isoamylalcohol were added to the above suspension of nuclei-guanidiniumisothiocyanate buffer, and thoroughly mixed after each addition. The suspension was cooled on ice for 20 mins and centrifuged for 20 mins at full speed in an Eppendorf centrifuge. The upper phase was removed and precipitated by the addition of 1 volume of isopropanol at -20°C for 1 h. The RNA was pelleted, washed with 70% ethanol, dissolved in 100 µl of guanidinium buffer and precipitated again by addition of 1 volume of isopropanol for 1 h at -20°C. After centrifugation the pellet was washed twice with 70% ethanol and finally dissolved in 50 µl of autoclaved water.

Hybridization Conditions

Double-stranded cDNA plasmids were linearized, denatured and 10 µg per slot were blotted onto Hybond N membrane filters by the use of a water aspirator and a Milli-Blot™ chamber. The membranes were fixed with a UV strata linker (Stratagene) and processed for hybridizations. Experimental as well as control RNAs were hybridized utilizing 10^6 cpm/ml. Prehybridizations were performed overnight and hybridizations were carried out for 2 days at 42°C in the same buffer consisting of 5 X SSC, 0.1% sodium dodecyl sulphate (SDS), 1 X Denhardt solution (50 X Denhardt solution = 5 g Ficoll, 5 g polyvinylpyrrolidone, 5 g bovine serum albumin and H_2O to 500 ml), 50% formamide, 50 mM sodium phosphate pH 7.7, and 50 µg/ml yeast tRNA. The filters were washed four times at 60°C for 20 mins, each time in 1 X SSC (20 X SSC = 3 M NaCl; 0.3 M Na-citrate) containing 0.1% SDS and then twice for 45 mins each time in 0.2 X SSC

containing 0.1% SDS. Thereafter the filters were incubated for 30 mins at 37°C in the presence of 10 μg/ml RNase A in 2 X SSC and then washed for further 60 mins in 2 X SSC. The filters were then exposed to Kodak XR Omat films with two intensifying screens at −70°C for 3–7 days. Quantification of autoradiograms was performed by laserdensitometry (Elscript 400, Hirschmann Unterhaching, FRG). All data were expressed as the ratio between experimental and corresponding control values.

Plasmids

Recombinant plasmids used in our study, were as follows: GAPDH (glyceraldehyde 3 phosphodehydrogenase, human, 720 bp, ATCC), fibronectin (rat, 997 bp, kindly provided by Dr. K. Boheler), PAI-1 (human, 2200 bp, kindly provided by Dr. S. Degen), c-myc (human, 2500 bp, Amersham), c-jun (mouse, 2600 bp, kindly provided by Dr. R. Bravo), jun-B (mouse, 1800 bp, kindly provided by Dr. R. Bravo), jun-D (1000 bp, kindly provided by Dr. R. Bravo), Ca^{2+}ATPase (rat, 1200 bp, kindly provided by Dr. K. Schwartz), hsp27 (human, 500 bp, Stressgene), hsp70 (human, 2300 bp, ATCC), βMHC (rat, 69 bp, kindly provided by Dr. K. Schwartz). The probes for calsequestrin, calmodulin and phospholamban (pig, 300–400 bp) were prepared by rt-PCR in our laboratory, c-fos (rat, 2100 bp, kindly provided by Dr. T. Curran; and mouse, 720 bp kindly provided by Dr. R. Bravo, in a former study used for northern blotting), 18S (mouse, 735 bp, kindly provided by Dr. I. Oberbäumer), aFGF (human, 2100 bp, kindly provided by Dr. T. Maciag), $TGF\beta_1$ (human, 1050 bp, kindly provided by Dr. R. Derynck), IL-6 (human, 505 bp, Dr. R. Zimmerman), IGF-I and IGF-II (human, ATCC, Rockville, USA). More details about the experimental conditions, hybridizations and hybridization efficiency, northern analysis and experiments with α-amanitin are given in [6].

RESULTS

Fibronectin, believed to be expressed in non-myocytes, like fibroblasts or smooth muscle cells, was included during all hybridizations and never gave any hybridization signal. We interpret this to indicate the purity of our myocyte nuclei preparation. The absence of any hybridization signal for pGEM indicates that no crosshybridization had occurred. GAPDH, previously believed to be constantly expressed, was 2.3-fold induced after 90 mins of the second cycle of reperfusion. We found early transcriptional inductions in the range of 1.5 to 2.4-fold for the nuclear transcription factors c-jun, jun-B, jun-D and c-myc, whereas c-fos was never detectable. The PAI-1 gene became 2.1 and 2.5-fold upregulated only after 30 and 90 mins of reperfusion. The genes coding for Ca^{2+}ATPase, phospholamban, calsequestrin and calmodulin were transcribed at highest levels, between 1.7 and 2.5-fold, after 90 mins of the second reperfusion period. The heat shock protein genes hsp27 and hsp70 were up to 3.6-fold transcribed after 90 mins of reperfusion, whereas ubiquitin was highly transcribed (2 to 3-fold) at all the timepoints examined. In contrast, transcription of the contractile protein βMHC remained constant. Among the growth factors examined we found IL6 4.3, IGF-I 2.7 and IGF-II 1.4-fold transcribed after 90 mins of reperfusion, whereas $TGF\beta_1$ was never found to be transcriptionally induced. During all the experiments aFGF remained undetectable. All results are summarized in Tables 1 to 3.

Table 1. Summary of Results at the Three Timepoints

	10–30–10	$(10–30)_2$	$(10–30)_2$ + 60
GAPDH	0.8	1.1	2.3* [2]
PGEM	n.d.	n.d.	n.d.
Fibronectin	n.d.	n.d.	n.d.
c–myc	1.2	1.9 [2]	1.9 [2]
c–jun	1.5	1.1	1.6* [2]
jun–B	1.4	1.7 [2]	2.2 [2]
jun–D	2.4	1.0	1.1
c–fos	n.d.	n.d.	n.d.
PAI–1	faint	2.1** [2]	2.5
Calmodulin	1.4	1.8* [2]	2.4 [2]
Ca^{2+}ATPase	2.5	1.8	2.4 [2]
Calsequestrin	1.2	1.5	1.7* [2]
Phospholamban	faint	0.8 [1]	2.5 [2]
Ubiquitin	2.7	1.9	2.8 [2]
hsp27	1.0	1.1	3.6 [2]
hsp70	0.4	0.9	2.2
aFGF	n.d.	n.d.	n.d.
$TGF\beta_1$	1.0	1.0	1.0
βMHC	1.0	1.0	1.0

Each value represents the result of the quotient of the experimental signal divided by the control signal. As a negative control we used a pGEM vector. Fibronectin was an indicator for non–myocyte nuclei contamination (see discussion). The table shows the early induction of several nuclear protooncogenes and the late induction of calcium binding protein genes, ubiquitin and heat shock protein genes. Timepoints $(10–30)_2$ and $(10–30)_2$+60 were performed twice and the values shown are averages. Statistical analysis between experimental (E) and control (C) values from the same heart was obtained by normalizing the data [(E–C)/C] and then comparing the expression t_{crit} – mean/SEM with the Student's t–distribution. Statistical significance was accepted at $p<0.05$. *$p<0.05$; **$p<0.01$; n.d. – not detectable; faint – weak signals, impossible to count; [1]phospholamban was included at $(10–30)_2$ only for one experiment; [2]two values from two experiments showed an increase of more than 1.5 at that timepoint.

DISCUSSION

We have previously shown [3–5] that brief coronary occlusions increase the mRNA tissue concentration of a large number of genes, i.e., transient ischemia and intermittent reperfusion is a strong stimulus for gene expression. This is true for the transcription factor genes (fos, jun, myc), the calcium binding protein, and for the heatshock protein genes. Some members of the growth factor family show increased expression (IGF–II), as well as procoagulant factors (PAI–1) and glycolytic enzymes (GAPDH). The change in the mRNA tissue concentration is, however, not necessarily caused by increased transcription; a change in the mRNA stability can also contribute. Ischemia itself is known to strongly influence translation, a process that consumes mRNA, so that translational inhibition may indirectly increase the mRNA concentration. These problems can only be addressed by run–on synthesis experiments using isolated nuclei where problems of translational changes and of stability do not exist. Our studies show that transcriptional regulation in ischemia–reperfusion can be surprisingly complex. In many cases an increase in the mRNA concentration is indeed caused by transcriptional upregulation (this is true for most of the

genes examined), in others a stability change must be assumed, because run-on studies did not show transcripts ($TGF\beta_1$, c-fos, hsp70 early in the experiment) at timepoints where mRNA was increased. In a few cases both possibilities must have occurred sequentially on the basis of comparison of transcript data with mRNA concentration (c-jun, jun-B).

For the members of the leucine zipper nuclear transcription factors, we show that these genes were most probably transcriptionally regulated. An exception is c-fos, whose transcription was never detectable. Since this gene, known to be rapidly induced after a stimulus (within 5 mins) [10] and since it is also known that the gene product can transrepress its own transcription, it may be possible that the chosen timepoints were too late to detect any transcription. On the other side, c-fos knock out mice are also available and these animals do not exhibit deficiencies in AP-1 binding [11]. It might be a possibility that adult cardiocytes *in vivo* do not produce c-fos.

It is interesting to note the transcriptional induction of PAI-1, which contains AP-1 binding sites in its 5' sequence (Table 2) and may be responsible for the well known procoagulent effects during the reperfusion periods.

Table 2. The Relevance of AP-1, CRE and Myc-Max Binding Sites for Eight of the Late Induced Genes

	Responsive Elements		
	CRE	AP-1	Myc-Max
Ubiquitin	X		
hsp70	X		
Ca^{2+}ATPase	X		X
Phospholamban		X	
Calsequestrin		X	
Calmodulin		X	
PAI-1		X	
GAPDH		X	X

Among the growth factors investigated we found a constitutive transcription for $TGF\beta_1$ at any timepoint examined. $TGF\beta_1$, which plays a crucial role during myocardial differentiation, is known to be posttranslationally activated [12] and is a regulator of different cardiac genes including Ca^{2+}ATPase [13]. $TGF\beta_1$ may therefore be a autocrine regulator of cardiac gene transcription during ischemia. aFGF, which is also known to be present in the heart [14], as well as a regulator of myocardial gene transcription [15], could never be detected. It might be that aFGF, a potent growth factor, is transcribed only at a very low level and remained undetectable by nuclear run on assays. The results for IL-6, IGF-I and IGF-II (Table 3) clearly show that these genes were transcribed in myocytes of the control as well as of the experimental areas. Only after 90 mins of reperfusion we found a induction for IL6, IGF-I and IGF-II. These data also support other findings of our group [16].

The calcium handling protein genes Ca^{2+}ATPase, phospholamban, calsequestrin and calmodulin were transcribed at highest levels after 90 mins of reperfusion. The same is true for the heat shock protein genes hsp27 and hsp70. Ubiquitin transcription was accelerated transcribed during all the timepoints examined. Since leucine zipper nuclear transcription factors can recognize and bind to AP-1 (activator protein-1; TGA(G/C)TCA) as well as

Table 3. Transcriptional Induction of the Genes Coding for IL-6, IGF-I and IGF-II.

	IL-6	IGF-I	IGF-II
10-30-10	faint	0.8	0.8
$(10\text{-}30)_2$+60	4.3	2.7	1.4

Each value represents the quotient of the experimental signal divided by the control signal. All results were obtained from one experiment for each timepoint. Faint = weak signals, impossible to count.

to CRE (cAMP responsive element; TGAGCT) sequences [17], and since eight of the late induced genes contain these sequences, leucine zippers may have influenced their gene expression (Table 1). It may also be possible that c-myc, provided it is translated, may bind to Max [18-20] and also influence the transcription of the GAPDH and Ca^{2+}ATPase genes through CACGTG sequences (Table 2).

DISCUSSION

Dr. R. Reneman: I believe it takes about 20-24 hrs before the hsps are functional.

Dr. R. Knöll: Yes, it does.

Dr. B. O'Rourke: Did you do any interventions to block protein kinase-C, especially with the immediate early gene activation? What is the role of PKC?

Dr. R. Knöll: We found during the preconditioning experiments that protein kinase-C is activated after short coronary occlusions. After we blocked protein kinase-C, the preconditioning effect was still there. This is probably an epi-phenomena, or something else. We have not tested whether protein kinase-C leads to the transcriptional induction. But, it is probably that protein kinase-C is needed to induce these nuclear proto-oncogenes and to induce a delayed gene response.

Dr. M. Lab: How did you make the pigs ischemic? Was it global ischemia or regional ischemia?

Dr. R. Knöll: It was regional ischemia. The LAD was occluded for 2 cycles of 10 min of occlusion and 30 min of reperfusion.

Dr. G. Kessler-Icekson: Why did you decide to look for IL6? As for the angiogenic factors, how early did you see an upregulation of the angiogenic factors?

Dr. R. Knöll: The angiogenic factors for which we have looked were TGF β, as well as several other growth factors. Some of them were not detectable by nuclear run-on analysis. The transcription of transforming growth factor β remained unchanged but it is also known that this protein is activated post-translational. I cannot exclude that this protein is in need during the cascade of events after short coronary occlusions.

Dr. G. Kessler-Icekson: Are you referring to the IGF and FGF?

Dr. R. Knöll: It is quite difficult to say anything about the IGFs. We showed the accelerated transcription. We know that there are receptors on myocytes for these two growth factors, but we cannot answer whether they have any specific effect during this cascade. What we have shown was the transcription in myocytes.

Dr. G. Kessler-Icekson: What would be the role of interleukin-6? In one of your protocols there is a four-fold increase in interleukin-6. Have you any explanation for this?

Dr. R. Knöll: I do not have any explanation.

Dr. W. Barry: The nuclear run on results are very nice. I wonder, how did you separate the myocardial cell nuclei from the nuclei of the other cell types of the tissue.

Dr. R. Knöll: The tissue is removed from the heart and homogenized during several steps by a ultrathorax, as well as by teflon homogenizers, and filtered several times through nylon membranes. An important step is the ultracentrifugation by the use of a discontinuous sucrose gradient consisting of 2.4 and 2.7 molar sucrose. Myocyte nuclei were found only between the 2.4 and 2.7 molar sucrose. One can remove these myocyte nuclei and use them immediately for the transcription reactions.

Dr. M. Parmacek: AP1 family members are often induced in a variety of circumstances in any cell type which is perturbed in any way. Is there any specificity in particular family members or particular targets that you have been able to identify that can distinguish the expression of fos and jun as anything other than a nonspecific response to any stimuli in this system.

Dr. R. Knöll: This is quite difficult to answer. What we can say is that we tested several other nuclear transcription factors including N-myc, L-myc, egr-1 or fos B. They all remained unchanged or were not detectable. We tested all these transcription factors, but only a few were detectable, induced by Northern blotting as well as by nuclear run-on analysis. Since we found the corresponding responsible elements in the promoters of the late upregulated genes, it is likely that this transcription factor might have induced the late upregulated genes.

Dr. M. Parmacek: I would like to caution you on that conclusion; fos and jun AP1 family members are, as you probably know, not only in those proteins, but in a whole host of proteins expressed in the heart, so it is hard to confer that conclusion from that set of data.

Dr. H.E.D.J. ter Keurs: Did you ever look at the polymerase activity in nonmyocyte nuclei?

Dr. M. Parmacek: No, not yet.

REFERENCES

1. Murry CE, Richard V, Reimer KA, Jennings RB. Ischemic preconditioning slows energy metabolism and delays ultrastructural damage during a sustained ischemic episode. *Circ Res.* 1990;66:913-931.
2. Das DK, Moraru II, Maulik N, Engelman RM. Gene expression during myocardial adaptation to ischemia and reperfusion. *Ann NY Acad Sci.* 1994;723:292-307.
3. Frass O, Sharma HS, Knöll R, Duncker DJ, McFalls EO, Verdouw PD, Schaper W. Enhanced gene expression of calcium-regulatory proteins in stunned porcine myocardium. *Cardiovasc Res.* 1993;27:2037-2043.
4. Brand T, Sharma H, Fleischmann K, Duncker DJ, McFalls EO, Verdouw PD, Schaper W. Protooncogene expression in porcine myocardium subjected to ischemia and reperfusion. *Circ Res.* 1992;71:1351-1360.
5. Andres J, Sharma H, Knöll R, Stahl J, Sassen LMA, Verdouw P, Schaper W. Expression of heat shock proteins in the normal and stunned porcine myocardium. *Cardiovasc Res.* 1993;27:1421-1429.
6. Knöll R, Arras M, Zimmermann R, Schaper J, Schaper W. Changes in gene expression following short coronary occlusions studied in porcine hearts with run-on assays. *Cardiovasc Res.* 1994;28:1062-1069.
7. Cox RD, Garner I, Buckingham ME. Transcriptional regulation of actin and myosin genes during differentiation of a mouse muscle cell line. *Differentiation.* 1990;43:183-191.

8. Konieczny SF, Emerson JR. Differentiation, not determination, regulates muscle gene activation: transfection of troponin I genes into multipotential and muscle lineages of 10T1/2 cells. *Mol Cell Biol.* 1985;5:2423–2432.
9. Chomezynski P, Sacchi N. Single step method of RNA isolation by acid guanidinium thiocyanate–phenol–chloroform extraction. *Anal Biochem.* 1987;162:156–159.
10. Greenberg ME, Ziff EB. Stimulation of 3T3 cells induces transcription of the c–fos proto–oncogene. *Nature.* 1984;311:433–438.
11. Hu E, Mueller E, Oliviero S, Papaioannou E, Johnson R, Spiegelman BM. Targeted disruption of the c–fos gene demonstrates c–fos–dependent and –independent pathways for gene expression stimulated by growth factors or oncogenes. *EMBO J.* 1994;13:3094–3103.
12. Sporn MB, Roberts AB, Wakefield LM, de Crombrugghe B. Some recent advances in the chemistry and biology of transforming growth factor–beta. *J Cell Biol.* 1987;105:1039–1045.
13. Parker TG, Chow K–L, Schwartz RJ, Schneider MD. Differential regulation of skeletal alpha–actin transcription in cardiac muscle by two fibroblast growth factors. *Proc Natl Acad Sci USA.* 1990;87:7066–7070.
14. Quinkler W, Maasberg M, Bernotat–Danielowski S, Lüthe N, Sharma HS, Schaper W. Isolation of heparin–binding growth factors from bovine, porcine and canine hearts. *Eur J Biochem.* 1989;181:67–73.
15. Parker T, Schneider M. Growth factors, proto–oncogenes and plasticity of the cardiac phenotype. *Ann Rev Physiol.* 1991;53:179–200.
16. Kluge A, Zimmermann R, Münkel B, Verdouw P, Schaper J, Schaper W. Insulin–like growth factor II is a stress–inducible gene in a porcine modle of brief coronary occlusions. *Cardiovasc Res.* 1995; in press.
17. Macgregor PF, Abate C, Curren T. Direct cloning of leucine zipper proteins: jun binds cooperatively to the CRE with CRE–BP1. *Oncogene.* 1990;5:451–458.
18. Cole MD. Myc meets its max. *Cell.* 1991;65:715–716.
19. Blackwell TK, Kretzner L, Blackwood EL, Eisenman RN, Weintraub H. Sequence specific DNA binding by the c–myc protein. *Science.* 1990;250:1149–1151.
20. Blackwood EM, Eisenman RN. Max: a helix–loop–helix zipper protein that forms a sequence–specific DNA–binding complex with Myc. *Science.* 1991;251:1211–1217.

CHAPTER 19

MECHANOPERCEPTION AND MECHANOTRANSDUCTION IN CARDIAC ADAPTATION: MECHANICAL AND MOLECULAR ASPECTS

Robert S. Reneman,[1] Theo Arts,[2] Marc van Bilsen,[1] Luc H.E.H. Snoeckx,[1] and Ger J. van der Vusse[1]

ABSTRACT

Cardiomyocytes grow in hypertrophy due to a net increase in the synthesis of proteins, especially contractile proteins, in the cell. There is abundant information about the molecular and biochemical changes involved in this process, but it is not completely understood how cells sense mechanical stimuli and how these stimuli are transferred into a biochemical signal inducing the growth response. This mechanotransduction most likely takes place at the cellular membrane. The resulting signal is transferred to the nucleus, where it can initiate alterations in gene expression.

INTRODUCTION

Cells adapt to new situations by changing their shape and function. A well-known adaptation is the hypertrophic response of the heart to an increase in workload, as in pressure- and/or volume-overload. Although this process has been studied intensively, most of the information presently available concerns the cellular response in terms of molecular and biochemical changes. Relatively little is known about the type of mechanical stimulus (e.g. strain or stretch) actually responsible for the response, and the way in which cells sense this stimulus (mechanoreception or mechanoperception) and the way in which the mechanical stimulus is transferred into a biochemical signal (mechanotransduction) inducing, for example, the growth response of cardiomyocytes.

[1]Departments of Physiology, and [2]Biophysics, Cardiovascular Research Institute Maastricht, University of Limburg, P.O. Box 616, 6200 MD Maastricht, the Netherlands.

Molecular and Subcellular Cardiology: Effects of Structure and Function
Edited by S. Sideman and R. Beyar, Plenum Press, New York, 1995

In this chapter we will focus on the cardiac hypertrophic response, and discuss the mechanical stimuli and the mechanisms of mechanotransduction which are possibly involved in this response. The discussion on the mechanical stimuli and mechanotransduction will be preceded by a short survey of the alterations in gene expression during myocardial hypertrophy.

GENE EXPRESSION IN HEARTS SUBJECTED TO INCREASED WORKLOADS

In the hypertrophic response cardiac myocytes increase their size, practically without changing their number. The growth of cardiomyocytes results from an increase in protein content, especially contractile proteins, per cell. Although differences between stimuli have to be appreciated, a general pattern of gene expression can be recognized upon cellular activation by stimuli like growth factors, angiotensin II, α-adrenergic agonists, endothelin-1 and stretch [1-4]. These stimuli induce expression of immediate early gene products, like proto-oncogenes and stress proteins, and of embryonic active genes, and enhance the expression of constitutively active genes, like myosin light chain (MLC)-2 and α-cardiac actin. The most important cardiac proto-oncogenes expressed are c-*fos*, c-*jun*, c-*myc*, *egr*-1 and *ras*. The rapid expression (i.e within hours) of these genes is likely to be functional, because the expression of c-*fos* and c-*myc* is followed by oncoprotein translation [5]. Although most of the heat shock proteins (HSP's) are constitutively present, some members of this family, like HSP-28 and HSP-72, are inducible early gene products when cardiac cells are stressed. HSP's play an important role in the folding and translocation processes of proteins and have shown to be expressed during heat shock, a measure to protect the hypertrophic heart against ischemia [6]. Important embryonic active genes expressed in the hypertrophic response are α-skeletal actin, β-myosin heavy chain (MHC) and atrial natriuretic factor (ANF). The expression of α-skeletal actin is significantly faster than that of β-MHC. The dominance of the (enhanced) expression of contractile proteins is essential for the formation of new sarcomeres which are probably brought in register with the existing sarcomeres through the cytoskeletal protein desmin [7]. During embryonic development ANF is expressed in both atrial and ventricular myocardium [8], but ANF expression is down-regulated in the ventricle in the adult myocardium and the primary site of ANF synthesis is in the atrium. The reexpression of ANF in the ventricle during cardiac hypertrophy [9] may play a role in regulating circulatory ANF levels and, hence, in controlling blood pressure and natriuresis in cardiac hypertrophy [1]. In relation to the expression of contractile proteins it is important to note that in (compensated) cardiac hypertrophy, induced by pressure-overload, sarcoplasmic reticular (SR) function and SR-Ca^{2+} ATPase activity are reduced [10, 11]. This results from a less pronounced increase in the total content of the biologically active protein, as compared with the contractile proteins, rather than a decrease in activity per mol of the protein. The velocity of Ca^{2+}-transport within SR is likely to be reduced [11].

The cardiac hypertrophic response also includes changes in the cytoskeletal [7] and extracellular matrix (ECM) proteins. In pressure-overload cardiac hypertrophy the content of both collagen and fibronectin increases, the expression of fibronectin occurring significantly earlier than that of collagen. The concentration (mg/g) of collagen does not necessarily change and may even decrease. It has also been shown that the different types of collagen are not coordinately expressed in the myocardium of hypertrophic hearts [see [4] for review]. These observations impose the question as to whether the functional consequences of the changes in extracellular collagen have to be ascribed to an increase in collagen content or to functional differences between the various types of collagen. The

possibility that the total collagen content is functionally of less importance is emphasized by the observation that the collagen concentrations did not change in volume-overload hypertrophy but that the extractable amount of type I and III collagen was reduced [12, 13]. The latter modification, suggesting increased cross-linking of these types of collagen, was associated with increased diastolic stiffness of the left ventricle.

The molecular changes in the hypertrophic response described above following pressure-, and occasionally volume-overload, are not necessarily the same in other forms of hypertrophy. For example, pressure-overload in rats leads to hypertrophy characterized by a reduction in SR-Ca^{2+} ATPase activity [10, 11] and a shift from α-MHC to β-MHC isoform expression [14, 15]. In contrast in the same species thyroid hormone-induced hypertrophy is associated with increased SR-Ca^{2+} ATPase activity [16], while α-MHC isoform expression is enhanced in exercise induced hypertrophy [17]. Even so there is increasing evidence that stimulation of α- and β-adrenoceptors leads to a different type of response and that the results obtained are different *in vitro* and *in vivo* [see [18] for review].

MECHANICAL STIMULUS RESPONSIBLE FOR INDUCTION OF THE HYPERTROPHIC RESPONSE

It is still incompletely understood which of the mechanical stimuli are sensed by the cardiac cells and induce the hypertrophic response to an increase in workload. It is often assumed that stress is the determinant factor, but in a recent model study we have shown that feedback through fiber stress is not a compelling condition for the control of cardiac growth [19]. The results of this study indicate that stable transmural distribution of fiber direction and physiological adaptation of wall mass and cavity volume to hemodynamic loading can be obtained by a feedback control system sensing changes in fiber shortening (or strain) and sarcomere stretching in the close vicinity of the cardiomyocytes (e.g. the extracellular matrix), and global contractility, defined as the factor by which the reference value of fiber stress has to be multiplied to obtain the required left ventricular systolic pressure. The observation that these mechanical stimuli are involved in myocardial growth is in keeping with the findings in *in vitro* studies on isolated cardiomyocytes. (Cyclic) stretching of cardiomyocytes leads to immediate expression of proto-oncogenes [20, 21] followed by an increase in amino acid incorporation into proteins, these changes being dependent on the degree and duration of stretching [20]. That the expression of proto-oncogenes may indeed be followed by cell growth is indicated by the finding that myocyte stretching results in increases in nuclear RNA labeling and cytoplasmic protein translation [22]. Contractile activity of cardiomyocytes also accelerates growth of these cells [23], indicating that contractility in itself or fiber shortening may also be sensed by the cardiomyocytes as inductors of the hypertrophic response. At present it is our believe that fiber shortening (or strain), cellular stretching and global contractility are the most important determinants of cell growth in cardiac loading and that these stimuli need to act together to obtain stable cardiac growth. However, it remains to be seen how cardiomyocytes control their growth and how they set the reference for starting it.

Although experiments on isolated cardiomyocytes suggest that mechanical stimuli may be a direct regulator of cellular growth, this is not necessarily the only mechanism involved, because it has been shown that cyclic straining of endothelial cells leads to the production of endothelin-1 [24] and cyclic stretching of cardiomyocytes to that of angiotensin II [25]. Since both these substances are known to be potent stimulators of

cardiomyocyte growth, paracrine and autocrine mechanisms are likely to be also involved in load–induced growth of these cells.

MECHANISMS OF MECHANOPERCEPTION AND MECHANOTRANSDUCTION

The mechanisms involved in mechanoperception and mechanotransduction in the cardiac growth response are still incompletely understood. In principle the mechanical information sensed by the cell can be transmitted to the genome directly via the cytoskeleton or indirectly following mechanotransduction, for example, at the site of the cellular membrane. In the former option, the mechanotransduction has to take place at the site of the nucleus. The nuclear membrane might be the site of transduction, but the evidence to support this hypothesis is lacking. Besides, the role of the cytoskeleton in this process is subject to debate, because it has been shown that neither disruption of microtubules nor that of actin microfilaments prevents stretch–induced proto–oncogene expression and increased protein synthesis in cardiomyocytes [26]. It should be kept in mind that sensing of the mechanical stimulus does not necessarily have to occur in the cell. The mechanical stimulus may also be sensed in the ECM and from there transferred into the cell. The most likely site of mechanotransduction is the cellular membrane, deforming under the influence of mechanical stimuli. The mechanisms possibly involved in mechanotransduction at the cellular membrane are schematically depicted in Fig. 1.

Activation of adenylate cyclase, leading to an increase in intracellular cyclic AMP (cAMP) and cAMP–protein kinase, has been proposed as a cause of increased cardiac protein synthesis due to enhanced workload [see [27] for review]. The evidence for this mechanism has been obtained in *in vitro* perfused rat hearts exposed to increased aortic

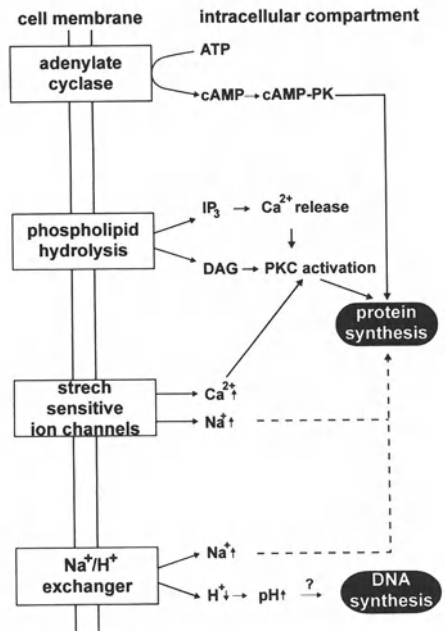

Figure 1. Possible candidates for mechanotransduction at the cellular membrane in cardiomyocytes. Solid arrows refer to "result in" and dashed arrows to "association". cAMP, cyclic AMP; cAMP–PK, cyclic AMP–protein kinase; IP_3, inositol triphosphate; DAG, diacylglycerol; PKC, protein kinase C.

pressure. In isolated cardiomyocytes, however, cyclic stretching of the cells resulted in only a minimal increase in intracellular cAMP, while inhibition of adenylate cyclase activity did not prevent stretch-induced proto-oncogene expression [21]. These contradictory observations may result from the difference in experimental models used and/or mechanical stimulus applied.

A very likely mechanism of mechanotransduction is the enhanced activation of membrane bound phospholipase C (PLC), resulting in increased hydrolysis of phosphatidylinositol phosphates and the formation of diacylglycerol, an endogenous activator of protein kinase C (PKC), and inositol phosphates, which in turn induce Ca^{2+}-release from the SR which also leads to PKC activation. It has indeed been shown that the production of inositol monophosphate, inositol biphosphate as well as inositol triphosphate is increased in cardiac muscle cells subjected to stretch [21, 28, 29], demonstrating the involvement of PLC-mediated phosphatidylinositol phosphates hydrolysis. The stretch-induced increased activation of PLC seems to be essential, because inhibition of this enzyme significantly suppresses the stretch-induced expression of proto-oncogenes [2]. The important role of PKC is demonstrated by the finding that proto-oncogene expression is suppressed by PKC inhibitors and is inhibited substantially by PKC down-regulation [29]. Moreover, nuclear PKC activity was found to be increased in cardiomyocytes during growth stimulation [30]. It is unknown whether the nuclear PKC is activated locally or that activated PKC is translocated to the nucleus from the cytosol. The way in which PKC exerts its action is still incompletely elucidated. It has been proposed that PKC acts through regulating gene expression via phosphorylation of transcription factors or other regulators [3]. It should be kept in mind that different isoforms of PKC, even Ca^{2+}-independent ones, and other kinases may be involved in this signal transduction.

The presence of mechanosensitive ion channels has been demonstrated in a variety of cell types [31]. It has been proposed that stretch-activated channels play a role in translating mechanical load into alterations in protein synthesis [32]. This possible mechanism is still subject to debate. Although activation of stretch-dependent channels results in Na^+-and Ca^{2+}-influx into the cell accompanied by protein synthesis [see [3] for review], blocking of stretch-activated cation channels with gadolinium failed to affect stretch-induced expression of proto-oncogenes and protein synthesis enhancement in neonatal cardiomyocytes [3, 26]. It cannot be excluded, however, that gadolinium-insensitive stretch-activated cation channels are involved in the growth response. An alternative possibility is that isolated neonatal cardiomyocytes behave differently from adult intact cardiomyocytes *in vivo*, because the experiments demonstrating Na^+-uptake and protein synthesis following stretch were performed on isolated papillary muscles [33]. The causal relation between Na^+-influx and protein synthesis is still incompletely understood. One possibility is that Na^+-influx results in increased intracellular Ca^{2+}-concentrations, via the Na^+/Ca^{2+} exchanger, activating PKC (Fig. 1). Alternatively Na^+-influx leads to activation of Na^+, K^+-ATPase, resulting in increased intracellular K^+ concentrations which enhances the elongation process of polypeptide synthesis [33].

Cellular growth and/or proliferation, as induced by a variety of stimuli, including mechanical ones, is associated with an increase in intracellular pH. There are indications that in several cell types, including endothelial cells, activation of the Na^+/H^+ exchanger is involved in this process of intracellular alkalinization, the latter being accompanied by an increase in intracellular Na^+-concentration and DNA synthesis [27]. Whether activation of the Na^+/H^+ exchanger also plays a role in the hypertrophic response of cardiac cells is as yet unknown.

More recently it has been proposed that cells obtain their stimulus to grow from the ECM [34, 35]. In this concept the information is transferred from the ECM into the cell

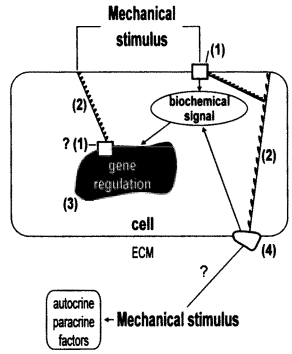

Figure 2. Possible mechanisms involved in mechanoperception, mechanotransmission and mechanotransduction. At the cellular membrane the mechanical stimulus may be directly transferred into a biochemical signal and from there, via the cytoskeleton, transmitted to the nuclear membrane for mechanotransduction. At the focal adhesion site the mechanical stimulus may be transmitted to the mechanotransducer and/or transferred directly into a biochemical stimulus. The latter mechanism has been described for various cell types, but it is unknown whether it plays a role in cardiomyocyte growth. (1) – mechanotransducer; (2) – cytoskeleton; (3) – nucleus; (4) – focal adhesion site; ECM, extracellular matrix.

at focal adhesion points. At this site ECM proteins are via adhesion proteins connected to transmembrane integrins, which in turn are connected to actin filaments in the cell via linker proteins [34, 36]. In integrin-mediated signaling two different mechanisms may play a role, combined or independently. In the first one integrins transmit signals to the mechanotransduction sites in the cell through the cytoskeleton [35] and in the second one integrins act as true receptors giving rise to biochemical stimuli [34, 37]. The ability to sense growth stimuli via the ECM has been described for endothelial cells and fibroblasts. Although it cannot be excluded that cardiomyocytes receive their growth stimulus from the ECM through integrins, at the present state of the art there is no evidence for this mechanism in the growth response of cardiomyocytes. The observation that in cardiomyocytes stretch-induced proto-oncogene expression and increased protein content are not influenced by disruption of the cytoskeleton argues against the integrin-cytoskeleton concept in these cells [26].

Autocrine (angiotensin II) or paracrine (endothelin-1) stimulation might be an alternative mechanistic explanation for the cardiac hypertrophic response upon increased workload of the heart [25 and 24, respectively]. The angiotensin II release from stretched cardiomyocytes and the endothelin-1 released from cyclically strained endothelial cells may indeed exhibit a hypertrophic response similar to that induced by mechanical stimuli [1]. Autocrine or paracrine stimulation, however, merely rephrases the problem definition because the mechanism responsible for the synthesis and release of these substances upon mechanical stimulation is not well understood.

CONCLUSIONS

Despite the abundant information presently available about the molecular and bio-chemical changes accompanying the cardiac growth response, the mechanisms involved in mechanoperception and mechanotransduction are still incompletely understood. The

possible mechanisms are summarized schematically in Fig. 2. The most likely possibility is that mechanotransduction takes place at the site of the cellular membrane whereupon the biochemical stimulus is transferred to the nucleus for transcription. The mechanical stimulus is likely to be sensed directly by the cellular membrane. Indirect sensing via the ECM through transmembrane integrins and the cytoskeleton may be an alternative possibility. Although the evidence is circumstantial, it cannot be excluded that transduction occurs at the site of the nuclear membrane, the mechanical stimulus being transferred to this site via the cytoskeleton. An alternative explanation is autocrine or paracrine stimulation through the release of growth stimulators by cardiomyocytes and endothelial cells, respectively. In a recent model study we have shown that fiber shortening (strain), cellular stretching and global contractility are important determinants of cell growth in cardiac loading and that these stimuli need to act together to obtain stable cardiac growth. However, it remains to be seen how cardiomyocytes control their growth and how they set the reference for starting it.

Acknowledgements

The authors are indebted to Jos Heemskerk, Karin van Brussel and Emmy van Roosmalen for typing the manuscript.

DISCUSSION

Dr. D. Burkhoff: You relate to three things: stretch, stress and global contractility. What do you mean by contractility?

Dr. R. Reneman: Stretch is quantified by the maximum value of sarcomere length during the cardiac cycle. Strain, defined as systolic shortening, is quantified as the decrease in sarcomere length during the ejection phase. Contractility is considered to be a global stimulus to the heart, and is expressed as the factor by which the reference value of fiber stress has to be multiplied to obtain the required left ventricular systolic pressure. When you leave one of these three mechanical stimuli out, you do not get a stable growth situation.

Dr. J. Bassingthwaighte: Oncologists looking at thymidine incorporation in the tumors use C11 labeled ryanodine or PET cycling. While looking at the thymonus, they observe a large uptake of thymidine by the normal unstretched myocardium. I wonder if this has any implications on how you look at these growth processes since thynadine is supposed to be only incorporated into the body.

Dr. R. Reneman: In quiet cells, or a quiet papillary muscle, there is still protein synthesis present, albeit at a fairly low level.

Dr. J. Bassingthwaighte: But this is not protein; it is DNA.

Dr. R. Reneman: I know, but I am referring to proteins because of the available information. To my best knowledge no such information is available for DNA.

Dr. H.E.D.J. ter Keurs: I would like to continue with the question about contractility by asking the definition. As soon as you define it for us, we may judge better whether you can do without stress development and therefore have to use contractility, or alternatively, you might do away with contractility and use stress as the input of your system. Contractility can have a multitude of definitions. Force development at any given length will go up with a change in sensitivity of the

contractile filaments for calcium, or it may go up with calcium without a change, or it may go up as a result of both; all confuse the issue of contractility. Therefore, the use of contractility as a physical or physicochemical input into this system is difficult to grasp.

Dr. R. Reneman: In the model, contractility is considered to be a very global stimulus to increase cardiac work. Feedback through regionally sensed fiber stress is not a compelling factor.

Dr. H.E.D.J. ter Keurs: That is equivalent, given a particular initial length, to the slope of the end systolic force–length / pressure–volume relation and that would be equivalent to stress.

Dr. T. Arts: The mechanism related to contractility is not acknowledged. In a model a signal equivalent to calcium concentration can be used. The signal may change in response to, for instance, catecholamine concentration. Such a signal is not of a regional character, but globally applied to the heart.

Dr. R. Reneman: Again, in my opinion, changes in fiber stress as feedback control are not compelling to obtain stable growth.

Dr. B. O'Rourke: Has anyone done the experiment of looking at the growth response in response to passive stretch in the presence of BDM so as to eliminate the contractility component?

Dr. R. Reneman: Not that I am aware of.

Dr. M. Parmacek: I have never seen the map kinase pathway mentioned in the overview of hypertrophy and signal transduction. The reason that I bring that up is that map kinase is known to activate SRF and SRF is known to be imperative to turn on c-*fos* and skeletal actin. It has also been demonstrated in cardiac myocytes that map kinase can be activated at the cell surface by the ras–raf signal G protein signal transduction pathway. Do you have any data?

Dr. R. Reneman: We have not looked into this ourselves, but in a recent review by Sadoshima and Izumo [*EMBO J* 1993;12:1681–1692], it was indicated that mitogen activated protein (MAP) kinases and others are indeed involved in signal transduction in stretch–activated cardiomyocytes.

Dr. M. Lab: We have to be careful about the mechanotransduction system at the membrane. Stretch activated channels look as if they are regular ion channels. There is not only one. Sadoshima [Sadoshima and Izumo. *J Receptor Res.* 1993;13:777–794] showed that gadolinium did not affect cascades from stretch to hypertrophy. Gadolinium is quite a dirty drug and there may also be several different kinds of stretch activated channels. The fact that he used gadolinium may mean nothing.

Dr. R. Reneman: I fully agree. One cannot exclude the involvement of stretch–sensitive channels based upon the gadolinium experiments. Firstly, they are performed on neonatal cardiomyocytes, which may behave differently from adult cardiomyocytes. Secondly, in these studies, stretch was applied alone. It may quite well be that different results are obtained when other, alone or combined, mechanical stimuli are applied. Thirdly, gadolinium–insensitive stretch–sensitive channels may be involved. Taking into consideration the TTX experiments, I am inclined to say that the Na^+–channels are not involved, at least under these experimental circumstances.

REFERENCES

1. Chien KR, Knowlton KU, Zhu H, Chien S. Regulation of cardiac gene expression during myocardial growth and hypertrophy: molecular studies of an adaptive physiologic response. *Faseb J.* 1991;5:3037–3046.

2. Parker TG, Schneider MD. Growth factors, proto-oncogenes, and plasticity of the cardiac phenotype. *Annu Rev Physiol.* 1991;53:179-200.
3. Komuro I , Yazaki Y. Control of cardiac gene expression by mechanical stress. *Annu Rev Physiol.* 1993;55:55-75.
4. Reneman RS, Arts T, Van Bilsen M, Snoeckx LHEH, Van der Vusse GJ. Adaptation of the left ventricular wall under pathological circumstances - Molecular and mechanical aspects. In: Hori M, Maryama Y, Reneman RS, eds. *Cardiac adaptation and failure.* Tokyo: Springer Verlag, 1994.
5. Snoeckx LHEH, Contard F, Samuel J-L, Marotte F, Rappaport L. Expression and cellular distribution of heat-shock and nuclear oncogene proteins in rat hearts. *Am J Physiol.* 1991;261:H1443-H1451.
6. Cornelussen R, Spiering W, Webers JHG, De Bruin L, Reneman RS, Van der Vusse GJ, Snoeckx LHEH. Heat-shock improves the ischemia tolerance of the hypertrophied rat heart. *Am J Physiol.* 1994;267:H1941-H1947.
7. Watkins SC, Samuel J-L, Marottte F, Bertier-Savalle B, Rappaport L. Microtubules and desmin filaments during onset of heart hypertrophy in rat: a double immunoelectron microscope study. *Circ Res.* 1987;60:327-336.
8. Bloch KD, Seidman JG, Naftilan JD, Fallon JT, Seidman CE. Neonatal atria and ventricles secrete atrial natriuretic factor via tissue-specific secretory pathways. *Cell.* 1986;47:695-702.
9. Gutkowska J, Horky K, Lachance C, Racz K, Garcia R, Thibault G, Kuchel O, Genest J, Cantin M. Atrial natriuretic factor in spontaneously hypertensive rats. *Hypertension (suppl. 1)* . 1986;8:137-140.
10. De la Bastie D, Levitsky S, Rappaport L, Mercadier J-J, Marotte F, Wisnewsky C, Brovkovich V, Schartz K, Lompré A-M. Function of the sarcoplasmic reticulum and expression of its Ca^{2+}-ATPase gene in pressure overload-induced cardiac hypertrophy in the rat. *Circ Res.* 1990;66:554-564.
11. Levitsky D, De la Bastie D, Schwartz K, Lompré A-M. Ca^{2+} ATPase and function of sarcoplasmic reticulum during cardiac hypertrophy. *Am J Physiol.* 1991;261:23-26.
12. Iimoto DS, Covell JW, Harper E. Increase in cross-linking of type I and type III collagens associated with volume-overload hypertrophy. *Circ Res.* 1988;63:399-408.
13. Harper J, Harper E, Covell JW. Collagen characterization in volume-overload- and pressure-overload-induced cardiac hypertrophy in minipigs. *Am J Physiol.* 1993; 265: H434-H438.
14. Mercadier J-J, Lompré A-M, Wisnewsky C, Samuel J-L, Bercovici J, Swynghedauw B, Schwartz K. Myosin isoenzymic changes in several models of rat cardiac hypertrophy. *Circ Res.* 1981;49:525-532.
15. Izumo S, Lompré A-M, Matsuoka R, Koren G, Schwartz K, Nadal-Ginard B, Mahdavi V. Myosin heavy chain messenger RNA and protein isoform transition during cardiac hypertrophy. *J Clin Invest.* 1987;79:970-977.
16. Sayen MR, Rohrer DK, Dillmann WH. Thyroid hormone response of slow and fast sarcoplasmic reticulum Ca^{2+} ATPase mRNA in striated muscle. *Mol Cell Endocrinol.* 1992;87:87-93.
17. Scheur J, Buttrick P. The cardiac hypertrophic responses to pathologic and physiologic loads. *Circulation (suppl. 1).* 1987;75:63-68.
18. Van Bilsen M, Chien KR. Growth and hypertrophy of the heart: towards an understanding of cardiac specific and inducible gene expression. *Cardiovasc Res.* 1993;27:1140-1149.
19. Arts T, Prinzen FW, Snoeckx LHEH, Rijcken JM, Reneman RS. Adaptation of cardiac structure by mechanical feedback in the environment of the cell, a model study. *Biophys J.* 1994;66:953-961.
20. Komuro I, Kaida T, Shibazaki Y, Kurabayashi M, Katoh Y, Hoh E, Takaku F, Yazaki Y. Stretching cardiac myocytes stimulates protooncogene expression. *J Biol Chem.* 1990;265:3595-3598.
21. Sadoshima J, Izumo S. Mechanical stretch rapidly activates multiple signal transduction pathways in cardiac myocytes: potential involvement of an autocrine/paracrine mechanism. *EMBO J.* 1993;12:1681-1692.
22. Mann DL, Kent RL, Cooper IV G. Load regulation of the properties of adult feline cardiocytes: growth induction by cellular deformation. *Circ Res.* 1989;64:1079-1090.
23. McDermott PJ, Rothblum LI, Smith SD, Morgan HE. Accelerated rates of ribosomal RNA synthesis during growth of contracting heart cells in culture. *J Biol Chem.* 1989;264:18220-18227.
24. Carosi JA, Eskin SG, McIntire LV. Cyclical strain effects on production of vasoactive materials in cultured endothelial cells. *J Cell Physiol.* 1992;151:29-36.
25. Sadoshima J, Yuhui X, Slayter HS, Izumo S. Autocrine release of angiotensin II mediates stretch-induced hypertrophy of cardiac myocytes in vitro. *Cell.* 1993;75:977-984.

26. Sadoshima J, Takahashi T, Jahn L, Izumo S. Roles of mechano-sensitive ion channels, cytoskeleton, and contractile activity in stretch-induced immediate-early gene expression and hypertrophy of cardiac myocytes. *Proc Natl Acad Sci.* 1992;89:9905-9909.
27. Watson PA. Function follows form: generation of intracellular signals by cell deformation. *Faseb J.* 1991;5:2013-2019.
28. Von Harsdorf R, Lang RE, Fullerton M, Woodcock EA. Myocardial stretch stimulates phosphatidylinositol turnover. *Circ Res.* 1989;65:494-501.
29. Kumoro I, Katoh Y, Kaida T, Shibazaki Y, Kurabayashi M, Hoh E, Takaku F, Yazaki Y. Mechanical loading stimulates cell hypertrophy and specific gene expression in cultured rat cardiac myocytes. *J Biol Chem.* 1991;266:1265-1268.
30. Allo SN, Carr LL, Morgan HE. Acceleration of growth of cultured cardiomyocytes and translocation of protein kinase C. *Am J Physiol.* 1992;263:C319-C325.
31. Morris CE. Mechanosensitive ion channels. *J Membr Biol.* 1990;113:93-107.
32. Bustamante JO, Ruknudin A, Sachs F. Stretch-activated channels in heart cells: relevance to cardiac hypertrophy. *J Cardiovasc Pharmacol (suppl. 2).* 1991;17:S110-S113.
33. Kent RL, Hoober JK, Cooper IV G. Load responsiveness of protein synthesis in adult mammalian myocardium: role of cardiac deformation linked to sodium influx. *Circ Res.* 1989;64:74-85.
34. Juliano RL, Haskill S. Signal transduction from the extracellular matrix. *J Cell Biol.* 1993;120:577-585.
35. Wang N, Butler JP, Ingber DE. Mechanotransduction across the cell surface and through the cytoskeleton. *Science.* 1993;260:1124-1127.
36. Davies PF, Barbee KA. Endothelial cell surface imaging: insights into hemodynamic force transduction. *NIPS.* 1994;9:153-157.
37. Hynes RO. Integrins: versatility, modulation, and signaling in cell adhesion. *Cell.* 1992;69:11-25.

CHAPTER 20

MOLECULAR MANIFESTATIONS OF CARDIAC HYPERTROPHY IN THE SPONTANEOUSLY HYPERTENSIVE RAT EFFECTS OF ANTIHYPERTENSIVE TREATMENTS

Gania Kessler-Icekson,[1] Yael Barhum,[1] Hadassa Schlesinger,[1] Joseph Shohat,[2] Hari Sharma,[3] and Wolfgang Schaper[3]

ABSTRACT

Antihypertensive treatments were given to young and adult SHRs, to prevent and reverse hypertension, respectively. Cardiac hypertrophy and the steady state level of the "fetal" genes, ANP, α-skeletal actin (α-skA), and β myosin heavy chain (β-MHC) mRNAs were assessed. Our findings show that the reduction of blood pressure does not consistently result in a similar regression of the "fetal gene program".

INTRODUCTION

Primary hypertension is a complex, multifactorial, disease of the cardiovascular system with eventual adverse effects on many end-organs. The sustained increase in hemodynamic load stimulates left ventricular (LV) hypertrophy, during which cardiac musculature increases in mass and undergoes functional adaptation by changing its protein profile [1, 6].

The spontaneously hypertensive rat (SHR) is a widely used animal model for the investigation of primary hypertension. SHR offsprings are normotensive at birth and develop hypertension with ontogeny. Elevated blood pressure (BP) is already detected by the second month of age increasing rapidly during the third month. A slow progressive augmentation of blood pressure is maintained for at least 12 months of age. Concurrent with the elevation of BP, LV hypertrophy appears [2, 3].

In experimentally induced workload, the increased weight of the hypertrophied LV reverses to normal after removal of the inciting stimulus [4]. However, the reduction of BP

[1]The Basil and Gerald Felsenstein Medical Research Center and [2]Department of Nephrology, Beilinson Medical Campus, Petah-Tikva, Israel, and [3]The Max Planck Institute, Bad-Nauheim, FRG.

Molecular and Subcellular Cardiology: Effects of Structure and Function
Edited by S. Sideman and R. Beyar, Plenum Press, New York, 1995

with various drugs that diminish its values by the same degree in genetically inherited hypertension, does not consistently result in a similar regression of LV hypertrophy. Such a discrepancy has been observed between hydralazine, a directly acting vasorelaxant, and captopril, an angiotensin converting enzyme (ACE) inhibitor. The two drugs proved equally effective for the reversal of hypertension but only the ACE inhibitor was efficient in regressing hypertrophy. These and other studies established our notion that humoral, non-hemodynamic factors are active in the regulation of LV hypertrophy in primary hypertension [1, 5, 21].

The enlarged myocardial cells of the hypertrophied LV undergo phenotypic alterations characterized as the reactivation of "fetal gene program", and considered beneficial for cardiac performance under elevated work demands [6, 7]. Observations made in adult SHR heart, revealed increased expression of ANP, β-MHC and collagens [8-10]. We have recently completed a study of the developmental changes in gene expression in the ventricles of SHR heart, comparing them to age matched normotensive Wistar Kyoto and Wistar rats (WKY, WR). In the three rat strains we have found that mRNAs of ANP, α-skA, β-MHC, and β-actin are highly abundant at birth and decline rapidly during the first two months. In SHR, the expression of ANP, α-skA and β-MHC, re-increases during the third month, remaining elevated thereafter. WKY, the genetic control for SHR, displays mild hypertension (130-150 mmHg) when young, which reverses to normal BP with age. ANP mRNA is moderately but persistently elevated in WKY whereas α-skA and β-MHC stay low with age. Although not yet proven, it is thought that ANP may contribute to the control of BP in WKY. In the normotensive WR, all the mRNAs listed exhibit low abundance. The expression of the non muscle β-actin declines progressively from birth, in the three rat strains, irrespective of BP or hypertrophy [11].

We were interested to find out how would the control of BP, in SHR, influence gene expression, and would it be co-regulated with hypertrophy. For this purpose, we treated male SHRs with hydralazine and captopril and quantified the relative abundance of ANP, α-skA, β-MHC, and β-actin mRNAs.

METHODS

Animals

Male SHRs, obtained from the Sackler School of Medicine, Tel-Aviv University, were housed 2-3 in a cage in climatized rooms at a 14/10h light/dark cycle, with free access to food and water. Antihypertensive drugs were given in the drinking water, from 1 to 3, or from 6 to 9 months of age. Each age group was divided into 3 subgroups (3-7 rats each) which received: 1. Hydralazine, 120 (1-to-3 mo), or 150 (6-to-9 mo) mg/L; 2. Captopril, 50 (1-to-3 mo), or 100 (6-to-9 mo) mg/Kg/day; 3. Tap water. Systolic BP was measured using the tail-cuff method. At the end of treatments, the rats were weighed, anesthetized with ether, and the heart, while beating, was rapidly removed. The atria and great vessels were excised and the biventricular weight measured. The tissues were quickly frozen in liquid nitrogen, and stored at -70°C until used.

Analysis of RNA

Total mRNA was isolated as described in [12], size fractionated on 1% agarose-formaldehyde gels, transferred to nitrocellulose membranes and UV-immobilized [13]. The membranes were subjected to multiple Northern blot analyses by hybridization with

[^{32}P]-labeled probes specific for: (1) rat ANP mRNA [14]; (2) rat α-skA mRNA [15]; (3) rat β-MHC mRNA (oligoprobe) [16]; (4) rat brain β-actin mRNA [17]; (5) rat 18S rRNA (oligoprobe) [18]. The hybridized membranes were exposed to Kodak X-OMAT film [13], and band intensity was measured by soft laser scanning densitometry. Variations between lanes were corrected by normalization to 18S rRNA [18]. Between consecutive hybridizations, the membranes were dehybridized and exposed to x-ray film to assure removal of residual radioactivity. Every membrane always contained 3 samples of newborn ventricular RNA, each being a pool of 5 hearts. The mRNA scores obtained with each probe were expressed in arbitrary units relative to the calculated mean of the scores obtained with the newborn RNAs.

RESULTS

Blood Pressure and Cardiac Hypertrophy

Effects of two antihypertensive drugs are presented, the vasodilator hydralazine, and the ACE inhibitor captopril. Initiation of antihypertensive therapy at 1 month of age aimed at preventing the development of hypertension, hypertrophy, and reprogrammed gene expression. Treatments starting at 6 months of age were designed to reverse hypertension, hypertrophy, and altered protein profile which had prevailed for at least 3 months. While 1 month old SHR are still normotensive (≈120 mmHg), their 3 month old counterparts have already developed hypertension (≈200 mmHg) (Fig. 1). At these ages, a 2-month antihypertensive treatment restricted BP to values as low as high-normotensive (hydralazine) and mild-hypertensive (captopril) [19]. The mean BP at 6 and 9 months of age ranges between 200-220 mmHg. At 9 months, following a 3-month treatment, the two drugs reduced the systolic BP to high-normotensive values (Fig. 1).

The biventricular weight to body weight ratio (BVW/BW) served as a measure for relative cardiac mass. In adult normotensive rats of either WKY or WR, the mean BVW/BW ratio has been found to be ≈2.6, whereas in adult SHR it is higher than 3 [11, 20]. Treatment with hydralazine had no effect on the relative cardiac mass, a result

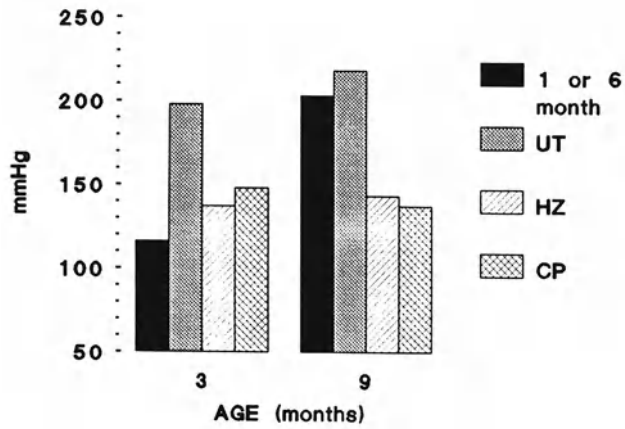

Figure 1. Bar graph showing systolic BP of male SHRs at 3 and 9 months of age of untreated rats (UT) and the effects of hydralazine (HZ) and captopril (CP) administered from 1-to-3 and 6-to-9 months. Solid bars represent the mean BP of 1 and 6 months old SHRs, at which ages the treatments were started.

complying with previous reports [5, 21]. While captopril treatment of young SHRs reduced the BVW/BW ratio to values still higher than 3, its administration to adult SHR corrected the BVW/BW ratio to normotensive values. This discrepancy may be related to differences in captopril doses, 50 versus 100 mg/Kg/day in young and adult rats, respectively.

Gene Expression

It is generally accepted that the abundance of mRNA species reflects the actual capacity of the tissue to synthesize the protein encoded by it. We assessed the expression of ANP, α-skA, β-MHC and β-actin by quantifying the steady state levels of their mRNAs using Northern blot hybridization.

Figures 2 and 3 depict the cumulative results of mRNA scores in untreated 1 and 6 months old, and in treated and untreated 3 and 9 month old SHRs, respectively. The abundance of the "fetal" ANP, α-skA, and β-MHC mRNAs increases from 1 to 3 months of age, whereas that of β-actin decreases (Fig. 2). At 6 months, the steady state levels of the "fetal" mRNAs are elevated and do not much differ from those in the 9 month old rats (Fig. 3).

The two drugs, when given to young SHRs, prevented the increase of ANP and α-skA mRNAs, retaining their steady state levels comparable with those of age matched normotensive WR [11]. β-MHC mRNA was not affected by hydralazine, and was only partially attenuated by captopril. We conclude that at this age, prevention of hypertension is sufficient to inhibit the increase in ANP and α-skA mRNAs but has only a limited effect on β-MHC. From 1 to 3 months of age, β-Actin mRNA decreased by the same degree in both, untreated and treated rats.

In the older SHRs, hydralazine treatment, moderately reduced the abundance of ANP mRNA and only slightly diminished the abundance of α-skA or β-MHC mRNAs (Fig. 3). On the other hand, captopril corrected to normal the levels of ANP and α-skA mRNA and markedly reduced that of β-MHC mRNA. β-Actin mRNA decreased from 6 to 9 months of age, in the treated as much as in the untreated rats.

Preliminary results of treatments with the Ca^{+2} channel antagonist nifedipine, have shown that it elicits only a small decrease in BP and no change in the BVW/BW ratio. Nevertheless, it seems to prevent the up-regulation of ANP and α-skA mRNAs in the

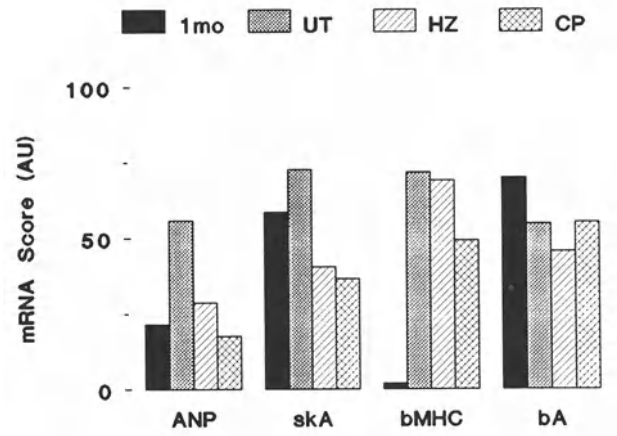

Figure 2. Bar graph summarizing the mRNA scores at 1 (1 mo) and 3 (UT) months of age and in 2 months old treated (HZ, CP) rats.

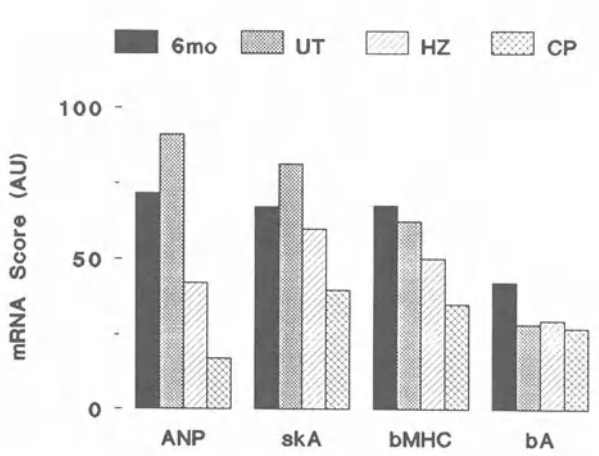

Figure 3. Bar graph summarizing the mRNA scores at 6 (6 mo) and 9 (UT) months of age, and in treated (HZ, CP) 9 months old SHRs.

young, and reduce them in the adult SHR. By contrast, β–MHC mRNA seems not to be affected by nifedipine. The expression of β–actin is not influenced by nifedipine.

DISCUSSION

Our studies show that the control of BP in primary hypertension can be dissociated from the regulation of both cardiac hypertrophy and the pattern of gene expression. In accordance with previous reports [1, 5, 21], we have found that in SHR, hydralazine and captopril are equally efficient in controlling BP but vary in their effect on cardiac hypertrophy. While hydralazine seems totally ineffective, captopril also reduces hypertrophy. We have shown earlier that in SHR, the development of hypertension is accompanied with enhanced expression of mRNAs for ANP, α–skA, and β–MHC. The resumption of ANP and α–skA expression was totally suppressed by both hydralazine and captopril, when given prior to the rise in BP. In the adult SHR, however, hydralazine reduced the abundance of ANP mRNA showing only a slight effect on α–skA. Captopril reversed to normal the relative amounts of both, ANP and α–skA mRNAs. It appears as if at younger ages, the increasing BP is a major determinant in the regulation of ANP and α–skA expression, whereas in the adult, BP seems to influence ANP more than α–skA. The expression of β–MHC was practically unaffected by hydralazine in the young, and only slightly affected in the adult SHR. Yet, captopril attenuated β–MHC expression in the two age groups. The difference observed between α–skA and β–MHC expression in young SHRs suggests that these two contractile protein isogenes respond, in part, to different signals or vary in their sensitivity to the same signals. It is proposed that the regulation of β–MHC expression may be less sensitive to the hemodynamic effects of systolic BP, and is more responsive to signals generated by the renin–angiotensin system. The regulation of the non–muscle β–actin gene is not influenced by changes in BP or hypertrophy, during either ontogeny or antihypertensive therapy.

In vitro studies have shown that expression of cardiac "fetal" isogenes is independently signaled by various vasoactive hormones and peptide growth factors, as well as mechanical stretch. Part of these factors also regulate the hypertrophic growth of

myocardial cells [7, 22, 23]. Even though the mechanical stress is greatly abolished when BP is normalized by hydralazine, the humoral factors, in all or in part, may be present, supporting the hypertrophic state and modified gene expression. In contrast, the efficacy of captopril treatment emphasizes the importance of ACE inhibition in antihypertensive therapy.

ACE is an enzyme of dual action, catalyzing both, the production of AII and the degradation of bradykinin (kininase). Inhibition of ACE reduces the levels of circulating and tissue AII, and increases those of bradykinin. In addition to regulating systemic BP and sodium handling, AII elicits direct cardiac responses including potentiation of local sympathetic action, positive inotropic and arrhythmogenic effects, stimulation of hypertrophy, fibrosis, and transitions in cardiac isoproteins [24]. Bradykinin actions seem to antagonize AII by enhancing coronary vasodilation, antiarrhythmogenic response, glucose uptake by myocytes, and reduction of fibrosis [25].

CONCLUSION

This study, conducted in the SHR model for primary hypertension, offers additional support of the pivotal role of ACE in controlling quantitative and qualitative alterations in the hypertensive heart.

Acknowledgement

This work was supported by the German–Israeli Foundation for Scientific Research and Development.

DISCUSSION

Dr. S. Vatner: Most surprising to me were the modest hypertrophies you saw with doubling BP in your SHR, and the lack of reduction in BP with nifedipine yet with marked reduction in hypertrophy. Is it at all possible that what you are looking at is not on the cardiac myocytes but either changes in body weight or changes in other components of the heart, such as fibrous tissue. Have you looked at any way to document the amount of myocyte hypertrophy?

Dr. G. Kessler–Icekson: Body weight was not affected whatsoever. As for the fibrous tissue, we are studying it now and I do not have any definitive results. We did not do morphometric studies of the sizes of the cells of the heart because it is a lot of work that has already been done. The ratio of the biventricular weight to body weight is the ratio seen in these animals. It is not like an experimental aortic banding that you can double the weight of the LV.

Dr. S. Vatner: I guess the question is whether the nifedipine is affecting the development of the fibrosis as opposed to affecting the size of the heart cells, because it is known in this model that there is a considerable increase in fibrous tissue.

Dr. G. Kessler–Icekson: Yes. I checked the literature for this because I was also amazed. The degree of reduction of BP by nifedipine was about 10–15%. If you start from 200 or 220 mmHg, taking 10–15% off does not reduce it much.

Dr. S. Vatner: It is not surprising that you may not have had enough of an effect to affect BP. The surprising thing is that with such a minimal effect on the hemodynamic stimulus you have such a marked effect on hypertrophy.

Dr. G. Kessler-Icekson: This is apparently because of the direct effect on calcium entry into the cells. We have another project on cultured myocytes and we have started to look at the direct effect of nifedipine and verapamil on the cells.

Dr. R. Reneman: In all the models, not only in SHR, the volume load in heart, you see the early expression of ANF. Do you want to speculate on the functional consequences, or what the functional meaning is of the expression of ANF?

Dr. G. Kessler-Icekson: I know of several reports in the literature on the effect of overexpression of ANP in the myocardium. For instance, there is a transgenic mouse overexpressing ANP and the authors [Barbee *et al.* Hemodynamics in transgenic mice with overexpression of atrial natriuretic factor. *Circ Res.* 1994;74:747-751] showed that it has an hypotensive effect with no effect on cardiac function; only an hemodynamic effect, with no effect on contractility. In the WKY there was an elevation of ANP and a reduction of BP with age. After making this finding regarding ANP, I tend to speculate that it is one of the participants in this control of BP. But since I didn't have direct measurements of serum ANP, or other kinds of relevant measurements, it is only a speculation at the moment.

Dr. R. Reneman: I know that ANP may play a role in volume regulation and therefore in BP but the challenging finding is that ANP comes up fairly early and stays there while it barely effects BP in the early days, so there is a discrepancy. In other words, we can say that ANF or ANP might play a role in regulating volume and therefore BP in the long term and in the knock outs, or in the overexpression that has been shown. But in your model, and also in ours, there is very early ANF expression without any effect on BP.

Dr. G. Kessler-Icekson: ANP seems to be very sensitive to all kinds of changes in BP, on the tissue, or on some other cardiac myocardial dysfunctions. Sometimes investigators studying hypertrophy choose ANP as the marker for hypertrophy and I think this might be wrong, because, as you see, this is not always a true representative of the hypertrophic state of the cell.

Dr. J. Janicki: I too share Dr. Vatner's concerns about the hypertrophy you saw. But I do not think we can blame fibrosis for this hypertrophy. We have made calculations based on density of collagen and how much it increases. If you double the amount of collagen in the myocardium, it adds very little to the overall increase in weight of the ventricle. So collagen would not be a factor here in the hypertrophy index.

Dr. G. Kessler-Icekson: This is a very rough measure. You measure the ventricles, or the LV or bi-ventricular weight, and then you measure body weight. So this may not be so accurate.

Dr. H.E.D.J. ter Keurs: ANP in particular showed secondary rise of message between approximately 9 and 12 months. I wonder what that might be. Is that early sign of failure, could it be that the secondary rise also in skeletal actin although less outspoken. Therefore, is also a sign of failure?

Dr. G. Kessler-Icekson: We have not looked at any signs of failure. We just scored mRNA. This is for future studies because you have to pursue your studies to older animals.

Dr. H.E.D.J. ter Keurs: With respect to α-skeletal-actin, can you speculate about the differences between your observation and the observation of the Paris group.

Dr. G. Kessler–Icekson: α–skeletal–actin is very similar to the cardiac actin. It differs only in four amino acids, which are in the region of the binding site to myosin. There is no very clear information as to the role of this isoform of actin. Only in the BALB/C mouse, there is a naturally occurring high abundance of this product. You find it in the human heart at about 50% or so. The people who studied this mouse [Hewett et al. *Circ Res.* 1994;74:740–746] suggest that it somehow increases contractility or the interaction between actin and myosin. But it is not yet clear. As for speculation, it has been suggested by Ketty Schwartz and her colleagues that in the aortic banding model, α–skeletal actin increases with the hypertrophy until it is compensated. Once it is compensated, for some reason, there is no more need for the α–skeletal–actin. If this is really the interpretation, then in the SHR it is not compensated, but of course there is no experimental data.

Dr. J. Solaro: Is there any evidence that the protein level change with the α–actin? One has to be careful about speculating about what is going on. Also, with the anomalous heavy change in the α–myosin, is there any change in thyroid state that occurs in these animals. Is that something that you monitor? You didn't have any evidence on the protein levels.

Dr. G. Kessler–Icekson: No, because with the α–skeletal–actin, as you know, there is no means to measure the protein. There is no antibody, so it is very difficult. Only molecular measurements. We did not do direct measurements, it is only relative measurement by Northern blot analysis. It is nothing like primer extension, which is more accurate. As for the myosin heavy change, it was not the α. It was the β that was unregulated.

Dr. J. Solaro: Even so, the thyroid state might change..

Dr. G. Kessler–Icekson: We did not test it. The thyroid state might change, but generally it is considered that the SHR is euthyroid. So it is something stronger than the thyroid. Let me comment that I saw upregulation of the β–myosin heavy chain by Angiotensin II in cell cultures where we studied expression of the β–myosin heavy chain with direct administration of Angiotensin II. But if I pretreat the cells with thyroid hormone, then remove the thyroid hormone and rinse the cells, and after a couple of days administer the AII, the AII could not compete. The β–myosin heavy chain remained low.

REFERENCES

1. Frohlich ED. Cardiac hypertrophy in hypertension. *N Eng J Med.* 1987;317:831–833.
2. Sen S, Tarazi RC, Khairallah PA, Bumpus FM. Cardiac hypertrophy in spontaneously hypertensive rats. *Circ Res.* 1974;35:775–781.
3. Adams MA, Bobik A, Korner PI. Differential development of vascular and cardiac hypertrophy in genetic hypertension, relation to sympathetic function. *Hypertension.* 189;14:191– 202.
4. Beznak M, Korecky B, Thomas G. Regression of cardiac hypertrophies of various origin. *Can J Physiol Pharmacol.* 1969;47:579–586.
5. Sen S, Tarazi RC, Bumpus FM. Effect of converting enzyme inhibitor (SQ14, 225) on myocardial hypertrophy in spontaneously hypertensive rats. *Hypertension.* 1980;2:169–176.
6. Samuel JL, Dubus F, Contard K, Schwartz K, Rappaport L. Biological signals of cardiac hypertrophy. *Eur Heart J.* 1990;11G:1–7.
7. van Bilsen M, Chien KR. Growth and hypertrophy of the heart: towards an understanding of cardiac specific and inducible gene expression. *Cardiovasc Res.* 1993;27:1140–1149.
8. Arai H, Nakao K, Saito Y, Morii N, Sugawara A, Yamada T, Itoh H, Shiono S, Mukoyama M, Ohkubo H, Nakanishi S, Imura H. Augmented expression of atrial natriuretic polypeptide (ANP) gene in ventricles of spontaneously hypertensive rats (SHR) and SHR stroke–prone. *Circ Res.* 1988;62:926–930.
9. Morano I, Lengsfeld M, Ganten U, Ganten D, Ruegg JC. Chronic hypertension changes myosin isoenzymes pattern and decreases myosin phosphorylation in the rat heart. *J Mol Cell Cardiol.* 1988;20:875–886.

10. Weber KT. Cardiac interstitium in health and in disease: The fibrillar collagen network. *J Am Coll Cardiol.* 1989;13:1637–1652.
11. Kessler–Icekson G, Barhum Y, Shohat J, Sharma H, Schaper W. Altered gene expression in the heart of spontaneously hypertensive rats (SHR). *J Mol Cell Cardiol.* 1993;25(Supll I):S.30(abs).
12. Auffray C, Nageotte R, Chambraund B, Rougeon F. Mouse immunoglobulin genes: a bacterial plasmid containing the entire coding sequence for a pre–gamma 2α heavy chain. *Nucleic Acids Res.* 1980;8:1231–1241.
13. Sammbrook J, Fritsch EF, Maniatis T. *Molecular Cloning*. 2nd ed. New York: Cold Spring Harbor Laboratory, Cold Spring Harbor, 1989.
14. Kamanaka M, Greenberg B, Johnson L, Seilhamer J, Brewer M, Friedmann T, Miller J, Atlas S, Laragh J, Lewicki J, Fiddes J. Cloning and sequence analysis of the cDNA for the rat atrial natriuretic factor precursor. *Nature.* 1984;309:719–722.
15. Shani M, Nudel U, Zevin–Sonkin D, Zakut R, Givol D, Katcoff D, Carmon Y, Rieter J, Frischauf AM, Yaffe D. Skeletal muscle actin mRNA. Characterization of the 3' untranslated region. *Nucleic Acids Res.* 1981;9:579–589.
16. Mahdavi V, Periasamy M, Nadal–Ginard B. Molecular characterization of two myosin heavy chain genes expressed in the adult heart. *Nature.* 1982;297:659–664.
17. Ginzburg I, De Baetselier A, Walker MD, Behar L, Lehrach H, Frischauf AM, Littauer UZ. Brain tubulin and actin cDNA sequences: isolation of recombinant plasmids. *Nucleic Acids Res.* 1980;8: 3553–3564.
18. Mendez RE, Pfeffer JM, Ortola FV, Bloch KD, Anderson JG. Atrial natriuretic peptide transcription, storage, and release in rats with myocardial infarction. *Am J Physiol.* 1987;253:H1449–H1455.
19. The fifth report of The Joint National Committee on Detection, evaluation, and treatment of high blood pressure (JNC V). *Arch Intern Med.* 1993;153:154–183.
20. Kessler–Icekson G, Barhum Y, Shohat J, Schaper W. Effects of captopril, hydralazine and nifedipine on cardiac hypertrophy and gene expression in SHR. *J Mol Cell Cardiol.* 1994; 26(6):504(abs).
21. Sen S. Regression of cardiac hypertrophy, experimental animal model. *Am J Med.* 1983;75(3A):87–93.
22. Chien KR, Zhu H, Knowlton KU, Miller–Hance V, van–Bilsen M, O'Brien TX, Evans S. Transcriptional regulation during cardiac growth and development. *Annu Rev Physiol.* 1993;55:77–95.
23. Komuro I, Yazaki Y. Control of cardiac gene expression by mechanical stress. *Annu Rev Physiol.* 1993;55:55–75.
24. Baker KM, Booze GW, Dostal DE. Cardiac actions of angiotensin II: role of an intracardiac renin–angiotensin system. *Annu Rev Physiol.* 1992;54:227–241.
25. Gavras H. Angiotensin–converting enzyme inhibition and the heart. *Hypertension.* 1994;23(Pt 2): 813–818.

CHAPTER 21

REGULATION OF ADENOSINE RECEPTORS IN CULTURED HEART CELLS

Dalia El-Ani,[1] Kenneth A. Jacobson,[2] and Asher Shainberg[1]

ABSTRACT

A_1 adenosine receptors were studied on heart cells grown in cultures by the radioligand binding technique. Treatments with agents that accelerated heart rate for 3–4 days, caused an increase in the level of adenosine receptors. Treatments that attenuated heart rate, reduced the level of the receptors. Thus, the cardiac cells respond to environmental conditions affecting heart contraction so as to restore the basal rate of heart activity.

INTRODUCTION

Adenosine produces a combination of negative inotropic, chronotropic and dromotropic effects on the heart and thereby modulates a variety of its physiological functions. These effects are mediated by cell surface adenosine receptors, which have been classified into A_1 and A_2 subtypes based upon ligand potency and on inhibition (A_1), or stimulation (A_2) of adenylate cyclase activity [1, 2]. Activation of A_2 receptors produces coronary and systemic vasodilation, resulting in hypotension, whereas the effects of adenosine on cardiac rate and contractility are thought to be mediated by A_1 adenosine receptors [3]. Recently, a third class of adenosine receptors, A_3, was described based on their pharmacological and functional properties [4, 5]. These receptors are linked to inhibition of adenylate cyclase activity and stimulation of phospholipase C leading to Ca^{2+} mobilization. These A_3 receptors facilitate release of mediators from mast cells.

It has been reported that adenosine concentration can rise dramatically in the extracellular fluid of the heart in stress conditions like hypoxia or ischemia [2], mainly

[1]The Otto Meyerhoff Drug Receptor Center, Department of Life Sciences, Bar-Ilan University, Ramat Gan 52900 Israel. [2]Molecular Recognition Section, Laboratory of Bioorganic Chemistry, NIH, NIDDK, Bethesda, MD 20892, USA.

Molecular and Subcellular Cardiology: Effects of Structure and Function
Edited by S. Sideman and R. Beyar, Plenum Press, New York, 1995

through the breakdown of ATP. The release of adenosine by the myocardium appears to be governed by the oxygen supply/demand ratio. With a decrease in this ratio, the enhanced adenosine formation and release elicit coronary vasodilation [6]. In stress conditions intense activity of the heart occurs and the high local concentration of adenosine acts to suppress the over activity. Moreover, adenosine causes hyperpolarization by activation of K^+ channels, which are the same channels that acetylcholine stimulates in the heart [7, 8].

The radioligand binding technique is used here to study the possible mechanisms involved in up- or down-regulation of A_1-adenosine receptor level, as a result of treatment with agents affecting contractile activity. We have used intact cardiac cells rather than tissue homogenates or membrane preparations for binding assays because of the similarity to physiological conditions. We show that treatments which accelerate heart contractility, such as norepinephrine (NE), electrical stimulation (ES), theophylline (Theo) or dibutyryl-cAMP (cAMPdB), cause up-regulation in the density of the A_1 receptors, whereas treatments that decrease heart rate, such as carbamylcholine (Carb) or lower temperature, down-regulate the level of the receptors. Our data thus show that contractile activity plays a major role in regulating the level of adenosine receptors in the heart.

METHODS

Preparation of cell cultures: Rat hearts (1–2 days old) were removed under sterile conditions and washed three times in phosphate buffered saline (PBS) to remove excess blood cells. The hearts were minced to small fragments and then gently agitated in a solution of proteolytic enzyme-RDB (Ness-Ziona, Israel) prepared from a fig tree extract. The RDB was diluted 1:50 in PBS, at 25°C for a few cycles of 10 min each, as described previously [9, 10].

Measurement of contractility: Changes in the contractile state of individual cells in the monolayer cardiocytes were performed by using an optical video system. The cells were viewed with a 20x objective and the image monitored by a television camera connected to a video motion detector that followed cell movements.

Radioligand binding: Intact cells were incubated at room temperature (23–25°C) for 60 min, with various concentrations of [^{3}H]-8-cyclopentyl-1,3-dipropylxanthine ([^{3}H]CPX), 1 μM dipyridamole and 2 U/mL adenosine deaminase in PBS, pH 7.4. Incubation was stopped by quick rinsing the cells five times with cold (4–8°C) PBS. The cells were solubilized with 0.2 mL 0.5 N NaOH and neutralized upon addition of 0.1 mL 2 N Tris-HCl, pH 3.7. After addition of 3 mL of scintillation liquid, radioactivity was determined using a β counter. Non-specific binding of [^{3}H]CPX was defined as the amount of radioactivity remaining after incubation with theophylline (5 mM). Specific [^{3}H]CPX binding was calculated as the total radioactivity bound minus the non-specific binding, which was less than 20% of total.

Electrical stimulation (ES): Cardiomyocytes grown for four days in culture at 37°C were transferred to a temperature of 25°C, to reduce the rate of spontaneous contractions, for three days before ES was applied. ES of heart cells was achieved by placing a pair of platinum electrodes in the culture medium and fastening them to a cover glass on the 35 mm dish, 25 mm apart [11]. The frequency of the pulses was 4 Hz, the duration time 1 msec and the voltage, 20 V. After ES, the level of the A_1 adenosine receptors was determined by binding experiments.

Protein content: Protein determination was performed according to the method of Bradford [12], using bovine serum albumin as a standard.

Materials: Triiodothyronine (T_3) was dissolved in 0.1 N NaOH and applied to the heart culture dishes at final concentration of 10 nM. Norepinephrine hydrochloride was dissolved in 0.1 mM of ascorbic acid. Dipyridamole was dissolved in 10% ethanol. Drugs and chemicals used were from Sigma Chemical Co. (St. Louis, MO, U.S.A.). [^{3}H]CPX (sp. act. 108.3 Ci/mmol) was purchased from NEN (Boston, MA, USA).

RESULTS

Characterization of Adenosine Receptors

Saturability of [^{3}H]CPX binding: To define the saturability of the ligand, intact cardiocytes (6-days-old) were incubated at room temperature with various concentrations of [^{3}H]CPX. For determination of non-specific binding the cardiocytes were also incubated with theophylline. Figure 1 shows the relationship between the radioligand concentration and the number of specific binding sites in the cultured cardiocytes. Maximal saturation of the antagonist occurred at a concentration of 0.2 nM. Scatchard analysis [13] indicates that the maximum number of binding sites is 23 ± 2.9 fmol/dish (21 fmol/mg protein) and the K_d for [^{3}H]CPX is 0.13 ± 0.07 nM (Fig. 1, inset). The data fit a straight line, indicating that there is only one binding site on the receptor.

Kinetics of [^{3}H]CPX binding: The time-course of specific [^{3}H]CPX binding to intact cardiocytes grown in culture is illustrated in Fig. 2. The binding reached equilibrium within 7 min of incubation at room temperature and was maintained for an additional 70 min. The non-specific binding was less than 20% of the total binding. The rate constant for the pseudo first order association reaction (k_{ob}), was calculated to be 0.337/min (Fig. 2, inset).

The dissociation of [^{3}H]CPX from the receptor binding sites was reversible and temperature dependent. At 25°C, 50% of the ligand were dissociated from the receptors within 8 min (data not shown). Equilibrium was achieved after 20 min of dissociation. The dissociation rate constant (k_{off}) was calculated to be 0.099/min.

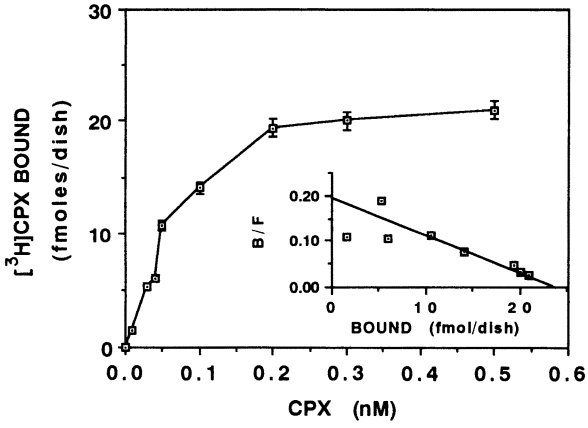

Figure 1. Specific binding of [^{3}H]CPX to heart cells. Six-day-old cardiocytes were exposed to the indicated concentrations of the radioligand. Specific binding was determined as the [^{3}H]CPX binding displaceable by 5 mM theophylline. Each value is the mean ± SE of triplicate determinations from a representative experiment of sister cultures. Inset: Scatchard plot of specific [^{3}H]CPX binding of Fig. 1. B, bound ligand (fmol/dish); F, free ligand (nM).

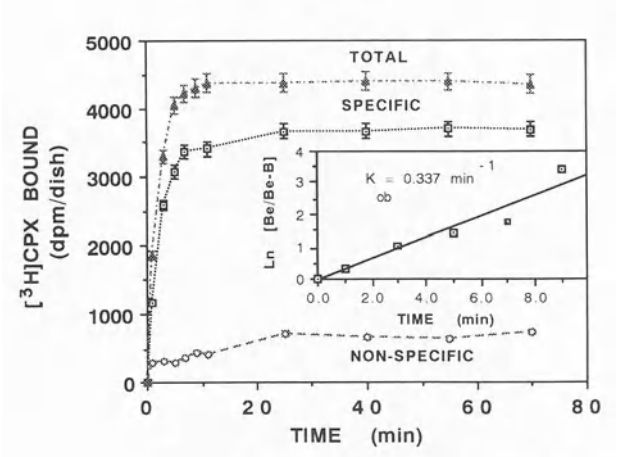

Figure 2. Time-course of [^{3}H]CPX binding to heart cells. Six-day-old cardiocytes were incubated in the presence of 0.6 nM [^{3}H]CPX at 25°C. Specific binding was determined as the [^{3}H]CPX binding displaceable by theophylline. Each value is the mean ± SE of triplicate determinations. Inset: Pseudo first order kinetic equilibrium.

The association constant (k_1) was calculated according to Cheng and Prusoff [14], from the equation $k_1 = k_{ob} - k_{off}$ / ([^{3}H]CPX) and was found to be 0.397/min/nM. Thus, the equilibrium dissociation constant determined kinetically from the ratio k_{off}/k_1 was estimated to be 0.25 nM, which is in adequate agreement with the K_d value obtained in Scatchard analysis of Fig. 1.

Relationship between Heart Rate and Receptor Level

Effect of various drugs on [^{3}H]CPX binding. Since NE, T_3, Theo and cAMP stimulate the contractions of cardiocytes (Table 1), we have investigated whether this increase in the rate of heart contractions is associated with a change in the level of adenosine receptors. Thus, treatment with NE for four days caused an increase to 270% of control [^{3}H]CPX binding (Table 1). Scatchard analysis showed [15] that the affinity of the receptor for its ligand remained almost unchanged. There was no significant difference in protein content between control and NE-treated cells (1.08 ± 0.14 mg/dish and 1.18 ± 0.18 mg/dish, respectively). However, lactate dehydrogenase (LDH) and creatine kinase (CK) activity increased in NE-treated cardiocytes by 22% and 34%, respectively [15]. The effect of catecholamines was time and dose-dependent [15]. This elevation in adenosine receptors is probably a result of increased receptor synthesis, since the protein synthesis inhibitor cycloheximide (5 μg/mL) and actinomycin D (2 μg/mL) prevented NE stimulation (Fig. 3). Although NE treatment also caused an elevation in CK and LDH activities, the relative increase in [^{3}H]CPX binding was 7-8-fold higher than the elevation of these cytoplasmic enzymes. Similar results were achieved with isoprenaline treatments (data not shown).

Thyroid hormones like catecholamines stimulate the contraction of cardiocytes [9]. Therefore, the effect of excess T_3 on [^{3}H]CPX binding was studied. It was found that treatment with T_3 for 3 days increased the density of adenosine receptors by 56% (Table 1). As Theo also stimulates the contractions of the heart, cardiocytes were treated with Theo, and heart rate and the receptor level were measured. A non-linear correlation was achieved between the increased level of A_1 adenosine receptors and the heart rate at various

Table 1. The Effect of Various Drugs on [^{3}H]CPX Binding

Treatment		[^{3}H]CPX Binding B_{max} (fmol/dish)		Heart Rate % of Control
		C	T	
NE	(20 μM)	21.5 ± 2.2	58.0 ± 4.0	212 ± 7.3
T_3	(10 nM)*	3.2 ± 0.1	5.0 ± 0.2	245 ± 11.9
Theo	(50 μM)	20.5 ± 1.7	28.0 ± 1.6	157 ± 9.8**
cAMP	(100 μM)	24.5 ± 2.1	36.0 ± 2.7	210 ± 18
ES	(4 Hz)#	3.5 ± 0.2	7.8 ± 1.1	
Carb	(5 μM)	25.5 ± 1.9	18.7 ± 1.1	11 ± 5

Four or five-day-old cardiocytes were treated with the indicated drugs for 4, 3, 5, 4, 1.5 and 3 days for NE, T_3, Theo, cAMPdB, ES, and Carb, respectively. Then, [^{3}H]CPX binding was measured in control (C) and treated (T) cells. Heart rate was measured following 48 hrs of treatment. *Binding of T_3-treated cells was carried out in multi-well dishes. #The cultures were incubated at 25°C. **100 μM Theo.

Theo concentrations (Fig. 4). Increases of 80–235% in A_1 adenosine receptor levels were obtained and the increase of heart rate was 60–130%, following 5 days of treatment with 0.1–1000 μM Theo (Fig. 4).

Direct application of dibutyryl-cyclic-AMP (cAMPdB) induced significant increase in heart rate. Therefore, cardiocytes which received this nucleotide were analyzed for contractility and [^{3}H]CPX binding. As shown in Fig. 5, 100 μM of cAMPdB increased heart rate by 90–130%, while the levels of A_1 adenosine receptors were increased by 28% and 47% following 3 and 4 days of treatment, respectively.

In order to study whether the increased rate of activity caused the elevation in A_1 adenosine receptors, the cardiocytes were stimulated electrically to contract. To increase the efficiency of ES, the temperature of the cells (4 days old) was reduced from 37°C to

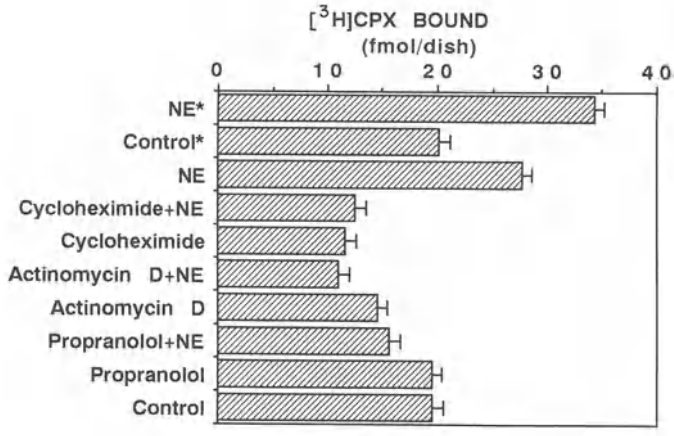

Figure 3. The effect of NE, propranolol, actinomycin D and cycloheximide on [^{3}H]CPX binding. Five-day-old cardiocytes were treated with, NE (20 μM), propranolol (100 μM), actinomycin D (2 μg/mL) and cycloheximide (5 μg/mL) for 2 days and with NE also for 4 days(*). Specific [^{3}H]CPX binding was determined. Heart rate measured was 35 ± 22 and 102 ± 42 (beats/min) in control and NE-treatment following 2 days and 18 ± 5 and 54 ± 15 respectively following 4 days of drug application. The experiment was carried out in chemically defined medium. The results are expressed as means ± SE of triplicate determinations.

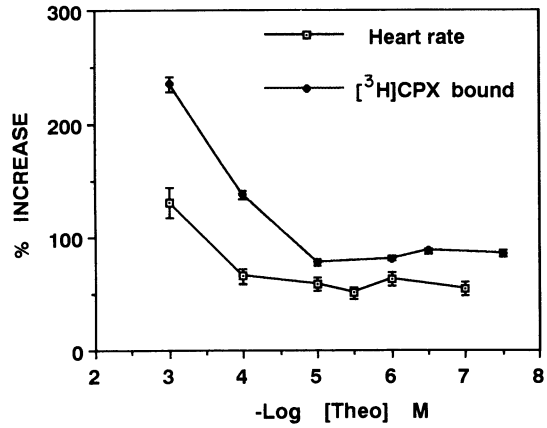

Figure 4. Dose response of theophylline (Theo) on [^{3}H]CPX binding and heart rate. Four-day-old cardiocytes were treated with the indicated concentrations of Theo for 5 days. Then, specific binding of [^{3}H]CPX and heart rate (beats/min) were determined. The results are expressed as means ± SE of at least triplicate [^{3}H]CPX binding or 5 determinations of the heart rate.

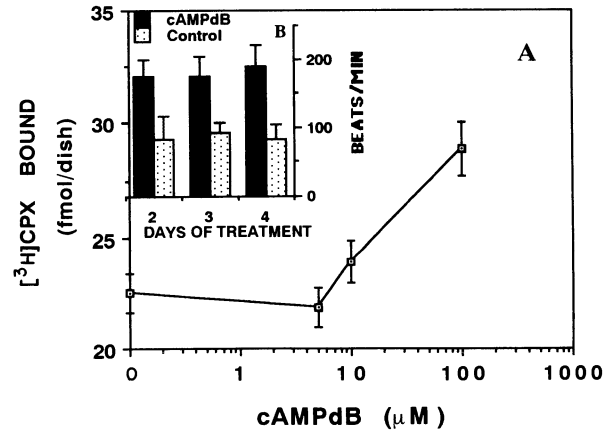

Figure 5. Dose response of cAMP on [^{3}H]CPX binding and heart rate. Five-day-old cardiocytes were treated with the indicated concentrations of dibutyryl-cAMP for 3 days. **A:** Specific binding of [^{3}H]CPX after 3 days of treatment; **B (insert):** heart rate following 2-4 days treatment with 100 μM cAMPdB.

25°C during the ES. This reduced temperature attenuated the spontaneous rate of contractions from 96 ± 8 to 36 ± 6 beats/min (Fig. 6). Scatchard analysis shows that ES for 36 hrs caused 122% increase in A_1 adenosine receptor (B_{max}) without a significant change in the K_d. Whereas ES caused an elevation in A_1 adenosine receptors, CK and LDH activities did not change significantly (data not shown).

We examined the influence of Carb, which is known as an inhibitor of contractile force and heart rate, on A_1 adenosine receptors. It was found that [^{3}H]CPX binding was decreased by 27% following 72 hrs of Carb treatment, without a significant change in the affinity of the receptor (Table 1, the saturation and Scatchard curves are not shown). Protein content in the drug treated cells was similar to that of the control (1.1-1.0 mg/dish).

Since low temperatures decrease heart rate, we investigated the effect of temperature on [^{3}H]CPX specific binding. Four day old cardiocytes were transferred from 37° to 30° and 25°C for 4 days. It was found that [^{3}H]CPX bound was reduced from 23 to 7.6 and 3.5 fmol/dish at temperatures of 30 and 25°C, respectively (Fig. 6).

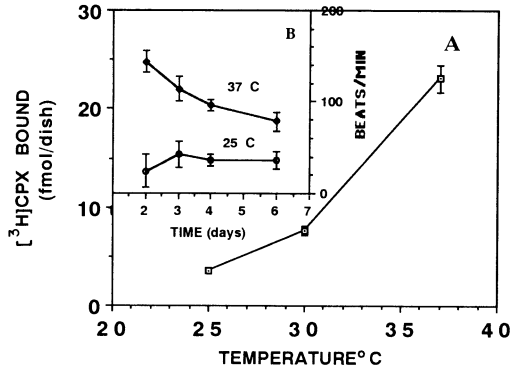

Figure 6. The effect of temperature on [^{3}H]CPX binding and heart rate. Four-day-old cardiocytes were transferred into 25°C or 30°C. **A:** Specific binding of [^{3}H]CPX after 4 days; **B (insert):** heart rate at the indicated times.

DISCUSSION

We have characterized and quantified the surface A_1 adenosine receptors in intact cardiomyocytes grown in culture, using the antagonist [^{3}H]CPX. The binding of [^{3}H]CPX is saturable, reversible and of high affinity. The dissociation constant of this ligand is K_d = 0.13 nM (Fig. 1). This value is lower than that obtained by Liang [16], who found K_d in the membranes of chick atrial cultured cardiomyocytes to be 2.1 nM. The difference may be related to species differences, or due to differences in experimental conditions: intact cells versus a membrane preparation. A value closer to our results was obtained by Martens *et al.* [17], who measured adenosine receptors on intact rat cultured ventricular cells, in which the K_d was 0.48 nM. A recent study using [^{3}H]CPX binding to bovine cardiac membranes [18] reported a K_d of 0.12 nM, which is similar to our study.

The B_{max} value in chick atrial myocytes was 26.2 fmol/mg protein [16]. Considering that this value was obtained in membrane preparations, it is higher than our B_{max} (20–30 fmol/mg protein). We have calculated the number of receptors per cell, assuming that the receptor distribution is uniform among the cells, to be $14–15 \cdot 10^3$ receptors/cardiomyocyte. This number is lower than the number of adenosine receptors obtained by Martens *et al.* [17] in adult heart cells ($40 \cdot 10^3$). This difference may reflect age dependence, since, as shown previously [15], the receptor level continues to increase with time during the development of cardiac cells in cultures. The number of adenosine receptors is about 10–20 times lower than the muscarinic acetylcholine receptors on the same cells [10], or in cardiac atrium [19]. The number of adenosine A_1 receptors is similar to the number of β-adrenoreceptors, e.g. 24,000 [20].

The present study shows an increase in the [^{3}H]CPX binding (B_{max}) with no significant change in the K_d upon exposure of the cardiomyocytes to NE, T_3, ES, cAMPdB, or Theo (Table 1). All these treatments that increased heart rate were accompanied by an increase in the level of adenosine receptors. The increase in the level of adenosine receptors

is probably reflected by increased sensitivity of the cardiocytes to adenosine-linked functional responses. These responses include negative chronotropic, dromotropic and ionotropic effects on the heart [21]. A_1 adenosine receptors in the heart also appear to mediate the attenuation of the positive inotropic effects of catecholamine [22–24]. Thus, the increased level of adenosine receptors following the above treatments (Table 1) acts as an inhibitory feedback to protect heart cells from excessive contractions. Further support for the therapeutic mechanism on the heart is demonstrated in the experiments with Carb and with a lower temperature (Table 1, Fig. 6). These treatments, like adenosine which attenuates the heart rate, caused a reduction in the level of adenosine receptors.

Our results agree with earlier studies that have demonstrated that the levels of adenosine receptors in fat, brain and other tissues are up- or down-regulated. The adenosine receptor density increased with chronic blockade by antagonists [25–27] and decreased with chronic stimulation by agonists [28]. Liang and Donovan [29] measured a 33–51% decrease in the receptor density as demonstrated by competition experiments of [^{3}H]CPX binding with R-PIA. They also found an increase in R-PIA inhibition of adenylate cyclase activity and contractility in Theo-treated chick cardiocytes. In these experiments A_1 adenosine receptor level was up-regulated from 20 to 33 fmol/mg protein, similar to our results. However, the radioligand binding assay in the Liang and Donovan study [29] was performed on atrial chick membranes and not on intact rat cultures as our work. Similar results were obtained in chick atrial myocytes treated with 30 μM 8-PST for 24 hrs [30]. In contrast, Shryock *et al.* [31] found that administration of 2 μM Theo to 15-day-old chick embryos for 44 hrs did not lead to a significant change in either the number or affinity of cardiac A_1 adenosine receptors in membrane preparations. Similar results were obtained with 0.5 μM of CPX [31]. Thus, contradicting results were obtained by different groups on the effects of ligands on the level of adenosine receptors. These differences could be due to the different concentrations of the ligands, time of treatments, species differences and *in vivo* versus *in vitro* experiments.

It is possible that the changes obtained in the level of the A_1 receptors are related to changes in concentrations of cAMP and not to cardiac contractions, since extracellular cAMP caused an increase of A_1 receptors (Table 1, Fig. 5). However, an increase in adenosine receptors was obtained with Theo at 100 μM or below. At these concentrations Theo exerts minimal inhibitory effects, less than 5%, on phosphodiesterase [32]. Hence, the increased heart rate and [^{3}H]CPX binding in 0.1–10 μM Theo (Fig. 4), is probably not a result of elevation in intracellular cAMP through phosphodiesterase inhibition. Moreover, when direct measurements of cAMP level were performed following isoprenaline treatment, it caused an elevation of the level of cAMP during the first 30 min. However, the values of cAMP returned to normal in the cardiomyocytes after 24 and 48 hrs [20]. Furthermore, when the cardiocytes were treated with T_3 for 48 hrs, the basal level of cAMP was 10–12% higher than the control, an insignificant difference [20]. These results support our hypothesis that contractile activity plays a major role in regulation of adenosine receptor density, although the possibility that cAMP influences this process is not excluded.

CONCLUSION

We have previously demonstrated that any treatment which stimulates or inhibits heart contractions causes a reduction in the level of muscarinic acetylcholine receptors [10]. We reasoned that we could not get up-regulation in the muscarinic receptor level, either because we did not find the required experimental conditions for the induction process, or because the cardiac cells used were saturated with these receptors and no further up-

regulation was possible [10]. Now, when comparing between these two receptors which have similar functions on the heart, we find that: 1) the ratio of muscarinic to A_1 receptors is 10:1. 2) Under the same experimental conditions, such as T_3 treatment, the muscarinic receptors are down-regulated [10], whereas A_1 adenosine receptors are up-regulated (Table 1). Thus, a different mechanism probably regulates the levels of these two receptors, but only the A_1 receptors respond to stress conditions so as to restore the basal rate of heart contractions.

Acknowledgements

We are indebted to Ms. T. Zinman and Ms. A. Isaac for their valuable technical assistance. This work was partially supported by funds from Binational Science Foundation, Israel-USA (BSF) and the Otto Meyerhoff Drug Receptor Center at Bar-Ilan University.

DISCUSSION

Dr. J. Solaro: Have you tried to uncouple contraction from excitation, perhaps by using BDM or KCl arrest?

Dr. A. Shainberg: We have not yet tried it. In *in vitro* experiments, we have shown that thyroid hormone increases the heart rate, and changes the level of receptors. We are now trying to see whether it has the same effects *in vivo*. But we have not tried to separate the effects by high potassium or by other local treatments.

Dr. H.E.D.J. ter Keurs: You suggest that contractility may be involved in determining how many receptors you have. However, you show us that the beating rate is predominantly involved in a number of receptors. How does the mechanism of converting heart rate into receptor number work?

Dr. A. Shainberg: All I can say is that when we apply cyclohexamide, a protein synthesis inhibitor, we no longer get the effect. This shows that the changes in the receptor are not caused by an unmasking of receptors, but rather by the synthesis of receptors. The mechanism probably involves calcium, but we do not know that for sure.

Dr. H.E.D.J. ter Keurs: One should experiment in the absence of calcium or at low calcium levels in the medium.

Dr. A. Shainberg: We have not done it because at these conditions the cells will not contract, but it is interesting to apply norepinephrine in low calcium and to see how this will affect the level of the receptors.

Dr. H.E.D.J. ter Keurs: They may not contract, but they will make action potentials.

Dr. A. Shainberg: Maybe.

Dr. W. Barry: You can certainly vary the amplitude of the fraction over quite a wide range just by varying the calcium concentration in these cells, so you could work at a calcium concentration where you can still see some contractile activity but it would be markedly reduced from control. Does adenosine slow contraction in these cells?

Dr. A. Shainberg: Yes. Adenosine reduces calcium uptake by the cells whereas catecholamine stimulates calcium uptake by the cells. We measured the functional response but we plan to expand it further for electrophysiological measurements.

Dr. G. Kessler-Icekson: You mention that upregulation of these receptors would be beneficial for the myocardium under certain changing environmental conditions. How fast did these changes occur in the heart? Also, are you using neonatal cells? How similar or dissimilar are these cells to the adult myocardial cells.

Dr. A. Shainberg: We have not grown adult cardiac cells in culture. With regard to the rate of these changes, we have a time course of response to norepinephrine treatment, which shows that after 48 hrs you get an increase in the level of adenosine receptors. These changes, even if they require a long time, 2–3 days, can be meaningful if there are stress conditions that sustain for a long period of time.

REFERENCES

1. Van Calker D, Muller M, Hamprecht B. Adenosine regulates via two different types of receptors, the accumulation of cyclic AMP in cultured brain cells. *J Neurochem.* 1979;33:999–1005.
2. Londos C, Cooper DMF, Wolff J. Subclasses of external adenosine receptors. *Proc Natl Acad Sci USA.* 1980;77:2551–2554.
3. Collis MG. Evidence for an A_1–adenosine receptor. Br J Pharmacol. 1983;78:207–212.
4. Carruthers AM, Fozard JR. Adenosine A_3 receptors: two into one won't go. *TIPS.* 1993;14:290–291.
5. Zhou QY, Li C, Olah ME, Johnson RA, Stiles GL, Civelli O. Molecular cloning and characterization of an adenosine receptor– The A_3 adenosine receptor. *Proc Natl Acad Sci USA.* 1992;89:74332–74336.
6. Cassis LA, Loeb AL, Peach MJ. *Topics and Prospective in Adenosine Research.* In: Gerlach, Becker BF, eds. New York: Springer Verlag, 1986; 486–496.
7. Jochem G, Nawrath H. Adenosine activates a potassium conductance in guinea–pig atrial heart muscle. *Experientia.* 1983;39:1347–1349.
8. Kurachi Y, Nakajima T, Sugimoto T. On the mechanism of activation of muscarinic K^+ channels by adenosine in isolated atrial cells: Involvement of GTP–binding proteins. *Pflugers Arch.* 1986;407:264–274.
9. Brik H, Shainberg A. Thyroxine induces transition of red towards white muscle in cultured heart cells. *Basic Res Cardiol.* 1990;85: 237–246.
10. Waisberg M, Shainberg A. Characterization of muscarinic cholinergic receptors in intact myocardial cells *in vitro. Biochem Pharmacol.* 1992;43:2327–2334.
11. Shainberg A, Burstein M. Decrease of acetylcholine receptor synthesis in muscle cultures by electrical stimulation. *Nature.* 1976;264:368–369.
12. Bradford MM. A rapid and sensitive method for the quantitation of microgram quantities of protein utilizing the principle of protein dye binding. *Anal Biochem.* 1976;72:248–254.
13. Scatchard G. The attraction of proteins for small molecules and ions. *Ann NY Acad Sci.* 1949;51:660–672.
14. Cheng YC, Prusoff WH. Relationship between the inhibition constant Ki and the concentration of inhibition which caused 50% inhibition of an enzymatic reaction. *Biochem Pharmacol.* 1973;22:3099–3108.
15. El–Ani D, Jacobson KA, Shainberg A. Characterization of adenosine receptors in intact cultured heart cells. *Biochem Pharmacol.* 1994;48:727–735.
16. Liang BT. Characterization of the adenosine receptor in cultured embryonic chick atrial myocytes: coupling to modulation of contractility and adenylate cyclase activity and identification by direct radioligand binding. *J Pharm Exp Therap.* 1989;249:775–785.
17. Martens D, Lohse MJ, Schwabe U. [^{3}H]–8–Cyclopentyl–1,3–dipropylxanthine binding to A_1 adenosine receptors of intact rat ventricular myocytes. *Circ Res.* 1988;63:613–620.

18. Leung E, Jacobson KA, Green RD. Apparent heterogeneity of cardiac A_1 adenosine receptors as revealed by radioligand binding experiments on N-ethylmaleimide-treated membranes. *Naunyn-Schmiedebergs Arch Pharmacol.* 1991;344:639-644.
19. Linden J, Hollen CE Patel A. The mechanism by which adenosine and cholinergic agents reduce contractility in rat myocardium: Correlation with cyclic adenosine monophosphates and receptor densities. *Circ Res.* 1985;56:728-735.
20. Disatnik MH, Shainberg A. Regulation of β-adrenoceptors by thyroid hormones and amiodarone in rat myocardiac cells in culture. *Biochem Pharmacol.* 1991;41:1039-1044.
21. Belardinelli L, Wu SN, Visentin S. Adenosine regulation of cardiac electrical activity. In: Zipes DP, Jalife J (eds), *Cardiac Electrophysiology: From Cell to Bedside.* WB Saunders:Philadelphia, PA, 1990, pp 284-290.
22. Dobson JG JR. Mechanism of adenosine inhibition of catecholamine-induced responses in heart. *Circ Res.* 1983;52:151-160.
23. Rardon DP, Bailey JC. Adenosine attenuation of the electrophysiological effects of isoproterenol on canine Purkinje fibers. *J Pharmacol Exp Ther.* 1984;228:792-798.
24. Belardinelli L, Isenberg G. Actions of adenosine and isoproterenol on isolated mammalian ventricular myocytes. *Circ Res.* 1983;53:287-297.
25. Fastbom J, Fredholm BB. Effect of long-term theophylline treatment on adenosine A_1 receptors in rat brain: autoradiographic evidence for increased receptor number and altered coupling to G-proteins. *Brain Res.* 1990;507:195-199.
26. Wu SN, Linden J, Visentin S, Boykin M, Belardinelli L. Enhanced sensitivity of heart cells to adenosine and up regulation of receptor number after treatment of guinea pigs with theophylline. *Circ Res.* 1989;65:1066-1077.
27. Ramkumar V, Bumgarner JR, Jacobson KA, Stiles L. Multiple components of the A_1 adenosine receptor-adenylate cyclase system are regulated in rat cerebral cortex by chronic caffeine ingestion. *J Clin Invest.* 1988;82:242-247.
28. Longabaugh JP, Didsbury J, Spiegel A, Stiles GL. Modification of the rat adipocyte A_1 adenosine receptor adenylate cyclase system during chronic exposure to an A_1 adenosine receptor agonist: alterations in the quantity of Gsa and Gia are not associated with changes in their mRNAs. *Mol Pharmacol.* 1989;36:681-688.
29. Liang BT, Donovan LA. Sensitization of cardiac A_1 adenosine receptor-linked physiologic responses (abstract). *Circulation.* 1989;80:II-444.
30. Liang BT, Hirsch AJ. Homologous sensitization of embryonic chick atrial myocytes to adenosine: mediation by adenosine A_1 receptor and guanine nucleotide binding protein. *Cardiovasc Res.* 1993;27:102-110.
31. Shryock JA, Patel A, Belardinelli L, Linden J. Down regulation and desensitization of A_1-adenosine receptors in embryonic chicken heart. *Am J Physiol.* 1989;256:H321-H327.
32. Fredholm BB. On the mechanism of action of theophylline and caffeine. *Acta Med Scand.* 1985;217:149-153.
33. Kukovetz WR, Poch G, Wurm A. Quantitative relations between cyclic AMP and contraction as affected by stimulators of adenylate cyclase and inhibitors of phosphodiesterase. *Adv Cyclic Nucleotide Protein Phosphorylation Res.* 1975;5:395-414.

CHAPTER 22

A MODEL APPROACH TO THE ADAPTATION OF CARDIAC STRUCTURE BY MECHANICAL FEEDBACK IN THE ENVIRONMENT OF THE CELL

Theo Arts,[1] Frits W. Prinzen,[2] Luc H.E.H. Snoeckx,[2] Robert S. Reneman[2]

ABSTRACT

The uniformity of the mechanical load of the cardiac fibers in the wall is maintained by continuous remodeling. In this proposed model the myocyte changes direction in optimizing systolic sarcomere shortening. Early systolic stretch and contractility increases the mass of contractile proteins. Cyclic strain of the myocardial tissue diminishes passive stiffness, resulting in the control of ventricular end-diastolic volume. Utilizing these rules of remodeling in our mathematical model yields that the natural helical pathways of the myocardial fibers in the wall are formed automatically.

INTRODUCTION

The contractile work of the myocardial fibers is converted into pump work during ejection of blood from the cardiac left ventricle (LV). Under normal loading conditions, all myocardial fibers contribute equally to the total pump function [1, 2]. It is, however, yet unclear how this uniformity is preserved, and under what circumstances. Clearly, chronic changes in hemodynamic load affect the structure and shape of the heart [3]. For instance, an increase in aortic pressure causes predominantly an increase in wall mass. An increase in stroke volume is followed by an increase of both wall mass and cavity volume. After return to the original load level, the adaptations are reversible to a large extent. The complicated helical organization of the muscle fibers [4, 5] is maintained throughout these changes of the cardiac mass.

[1]Departments of Biophysics and [2]Physiology, Cardiovascular Research Institute Maastricht, University of Limburg, P.O.B. 616, 6200MD Maastricht, The Netherlands.

Molecular and Subcellular Cardiology: Effects of Structure and Function
Edited by S. Sideman and R. Beyar, Plenum Press, New York, 1995

Here we discuss the mechanism of preservation of the cardiac structure. Obviously, the global cardiac structure may be maintained by a permanent comparison of the current structure with the structure as defined by a reference design. Adaptations of the global structure will be carried out if deviations from the reference are detected. However, such a hypothesis is not attractive, as no biological mechanism is known that senses the global structure of the heart and changes selected parts of the structure.

Alternatively, the mass and shape of the heart may be controlled as an entity by the summed action of many regional control units. Cells can sense mechanical signals. Within their small sphere of influence the various cells may respond by adapting their mass, shape and intra- and extra-cellular structure. The characteristics of the controlling units within the myocardium may be similar everywhere. The summation of controlling actions of the numerous cardiac cells should guarantee preservation of the macroscopic anatomical structure. An attractive aspect of this hypothesis is that the cell is likely to have the tools for such individual cellular controlling actions. Cells can respond to various physical stimuli related to mechanics. Cells have messengers that control the growth and formation of various intra- and extra-cellular structures according to a stored program determined by the type of the cell. The question remains to be solved if a multitude of regional controlling mechanisms can yield stable control of the global structure of the heart.

UNIFORMITY OF REGIONAL MECHANICAL LOAD

Evidence is growing that the systolic mechanical load of the healthy LV is evenly distributed over all myocytes in the heart. In investigating the relation between the mechanics of the LV and the coronary perfusion, mechanical stresses within the LV were estimated [6, 7]. In this mathematical model, the equatorial region was simulated by a thick-walled cylinder, having helical structures of myocardial fibers inside. Mechanical load of the myocardium was assumed to be uniformly distributed. Consequently the relation between the torsional motion and volume decrease of the LV was predicted to be unique. This predicted relation was found to be in close agreement with the data in the open chest dog [8] and in the closed chest dog under normal hemodynamic load [9].

More recently it was investigated whether this relation may also hold under a wide variety of hemodynamic load conditions. Radiopaque markers were attached to the LV free wall and septal wall in an open chest dog preparation [10]. Preload, afterload and contractility were varied over a wide range. The relation between torsion and the logarithm of cavity volume was almost linear in each experiment. The slope of this relation (-0.173 ± 0.028; mean $\pm$ sd; $n = 38$) was close to the model prediction, as based on the mechanics of a cylindrical LV wall segment (-0.194 ± 0.026).

The LV transmural differences in coronary perfusion, metabolic activity, and mechanical load are likely to be small [2]. The reported vulnerability of the subendocardial layers to coronary artery stenosis can be fully attributed to the fact that the decrease of coronary perfusion in the subendocardial layers is more prominent than in the subepicardial layers. In the normal LV, the differences in coronary perfusion are small between the subendocardial and subepicardial layers, as well as between different regions of the LV wall [11, 12]. Coronary flow may become more inhomogeneous on a smaller scale because of the fractal character of the flow distribution [13].

The mechanical load appears to be maintained by adaptation of the cardiac structures. After a chronic increase of hemodynamic load, the mass of the myocardium increases. An increase in aortic pressure causes an increase in wall mass, while cavity volume remains practically the same (concentric hypertrophy) [14-16]. An increase in

aortic flow with constant systolic aortic pressure causes an increase of both wall mass and cavity volume (eccentric hypertrophy). Fiber stress (σ_f) and natural fiber shortening (ε_f=ln[l/l_{ref}]) in the LV wall may be calculated from the LV pressure (P_{lv}), cavity volume (V_{lv}) and wall volume (V_{wall}) by the following relations [17]:

$$\sigma_f = P_{lv}(1 + 3V_{lv} / V_{wall}) \qquad \varepsilon_f = 1/3\ \Delta\ln(1 + 3V_{lv} / V_{wall}) \qquad (1)$$

After chronic adaptation, the calculated peak fiber stress and systolic fiber shortening appear to be similar (≈37 kPa and 0.15, respectively) for different states of the hemodynamic load. The adaptations to changes in hemodynamic load are reversible to a large extent [18]. Cardiac mass returns to about normal after surgical repair of cardiac valve defects [19, 20]. The complicated helical organization of the muscle fibers [4, 5] is maintained during these changes in cardiac mass.

HYPOTHESIS ON REGIONAL CONTROL OF MECHANICAL LOAD

It is commonly accepted that the mechanical load is similar in the various regions of the normal heart. Furthermore, adaptations to chronic changes in hemodynamic load are aimed to maintain this situation. The question is how this uniformity of load is maintained. Several conditions should be satisfied when formulating a hypothesis on the control mechanism. The proposed mechanism should have a physiological basis. Cells are the basis of the cardiac structure. After a change in hemodynamic load the structure of the heart adapts. This adaptation is the summed effect of many changes on the small scale of the individual cells. Each cell acquires signals from the regional sphere of influence. They process these signals, and take appropriate action, resulting in regional adaptations. The summed effect of these adaptations should result in a stable control of the structure of the whole heart.

Because the main function of the myocardium is mechanical, feedback is postulated to be mediated by mechanical parameters too. The cardiac myocyte perceives a cardiac contraction as a sequence of events and actions (Fig. 1). The myocyte is stretched in diastole. Electrical depolarization is the first signal of an upcoming contraction. The cell develops force. This phase is critical. If the myocyte is activated relatively late or is not contracting as strongly as the cells in the environment, the myocyte will be stretched before contraction [21]. The myocyte shortens during the ejection phase. Note that the amount of

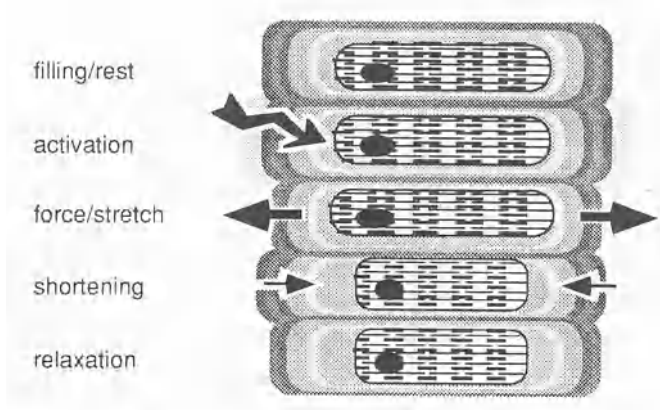

Figure 1. Sequence of events and actions as sensed by the cardiac myocyte.

shortening is mainly determined by the gross deformation of the tissue, because the force of a single cell is insufficient to significantly affect gross deformation of the tissue. During relaxation, force may decline asynchronously, causing transients in deformation. For instance, in the presence of ischemia, severe deformations may occur around the ischemic region.

The most relevant mechano-feedback signals are likely to be related to deformation (see also the contribution by Dr. Reneman in this Volume). In this respect, stress is likely to be of less importance [3]. Stretch is quantified by the maximum value of sarcomere length that occurs during the cardiac cycle. Stretch is likely to be involved in the control of cellular growth [22, 23]. Stretching of cardiac myocytes causes immediate expression of the proto-oncogene c-fos, the amount of which depends on the degree and duration of stretching [24]. Besides, other transcription factors, like c-jun and c-myc, are also induced rapidly [25]. The expression of proto-oncogenes may induce cell growth, as indicated by the finding that stretch enhances nuclear RNA labeling and translation of genes, such as skeletal α-actin, atrial natriuretic factor, and β-myosin heavy chain [25, 26]. Stretch induces ion transport through the cell membrane [27], but the role of this pathway in growth is subject to discussion [28]. Contractile activity also accelerates growth of cardiac myocytes [29], indicating that in addition to stretch, fiber shortening (strain) and/or contractility may also regulate cardiac growth. The fibroblast is also affected by stretch, causing enhancement of collagen expression [30]. The expression of collagen [31-34] and fibronectin [32, 35] is enhanced inn the early phase of adaptation to pressure overload.

Many indications can be found for the presence of control mechanisms acting in the cellular environment, in which mechanical load is involved. For instance, sarcomere length which is defined as the repetition length of the cross-striations of cardiac muscle, is controlled to approximately 1.95 μm for the unstressed LV [36, 37]. The regional character of adaptation of the cardiac tissue mass to mechanical load is also indicated during asynchronous electrical activation of the ventricle caused by pacing or conduction blockade of the left bundle branch, when regional differences in mechanical load and coronary perfusion are found [11, 38]. Tissue mass decreases selectively in those regions where load is relatively low [39].

DESIGN OF THE MODEL

The above mentioned cellular abilities for sensing of mechanical signals have been used to design a model for the regional feedback system (Fig. 2). The myocytes form the force generating structure. Orientation and mass of the myocytes are controlled by myocyte shortening, early systolic stretch, and more global signals related to contractility. The passive elastic structures are extremely important for the diastolic filling of the LV. The extra-cellular matrix of collagen fibers is formed and controlled by fibroblasts. The cooperation of both the active and the passive controlling structures is responsible for regional control of the mechanical structures. The input and output signals for control are active in the sphere of influence of the separate cardiac cells.

Fiber direction is controlled by the amount of sarcomere shortening during the ejection phase. In our model, the myocyte "looks" for an optimum shortening of 15% by trial and error. The frequency of trials for new directions increases the further the myocyte operates from the optimum. The mass of the myocyte is controlled by stretch and global contractility. Generally, stretch occurs in the early phase of systole. Large early systolic stretch is a strong stimulus for mass increase of the myocyte. Another stimulus to growth is related to contractility. If the mass of the LV is too low for a given stroke volume, blood

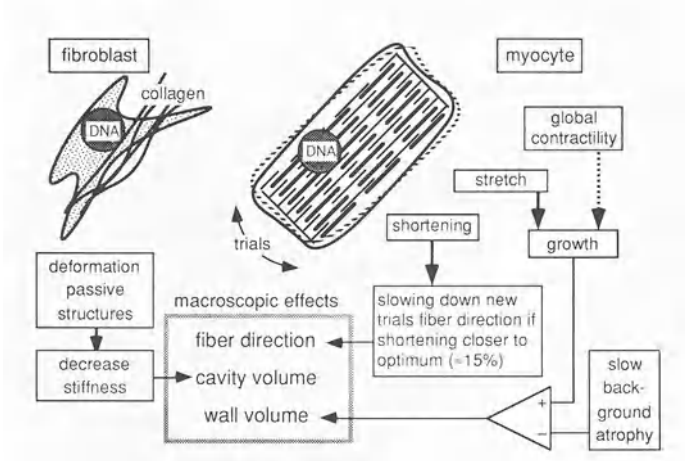

Figure 2. Model of the controlling system for adaptation of the mechanical structures to mechanical load, acting in the cellular sphere of influence. The myocyte controls mass and fiber direction on the basis of the input signals systolic sarcomere shortening, early systolic sarcomere stretch and global stimuli to increase contractility. The passive collagen structures are expected to become more compliant when the amount of cyclic deformation is above normal.

pressure is maintained by the control system for systemic blood pressure. The heart receives various physiological stimuli to increase work. Sympatic stimuli may increase the heart rate and contractility. Also, hormonal stimuli may be of importance. The point is that the heart is subjected to a chronic stimulus to increase its pump work. This stimulus is thought to have a relatively small but important mass increasing effect.

The collagen structure of the myocardial wall is subject to continuous deformation. If the span of cyclic deformation increases, the collagen structure is assumed to weaken. Thus, on the small scale of the cellular environment, the passive structures are thought to be more compliant in regions of large deformation like in the subendocardial layers. On the global scale, a large ejection fraction is a stimulus to make the ventricle more compliant. Given a fixed stroke volume, the resulting ventricular dilatation causes a decrease of the ejection fraction.

IMPLEMENTATION IN A MODEL OF CARDIAC MECHANICS

The myocardial elements defined in Fig. 2 were incorporated in a model of the mechanics of the equatorial region of the LV. This part of the LV was assumed to be cylindrical [1, 3]. The thick-walled cylinder was composed of 10–1500 concentric cylinders. Fiber orientation varied across the wall. Deformation was determined by equilibria of forces and torques acting on the short axis cross-section of the LV wall. Calculated deformation was converted to the input signals for regional load control. Mass and direction of the myocytes, and compliance of the passive structures, were adapted according to the proposed control mechanism. Deformation of the thus remodeled LV equatorial region has been calculated again, and a new calculation cycle has been performed.

Required LV pump load was defined by a given stroke volume and systolic cavity pressure. Initially, the transmural course of fiber orientation was simplified to two layers. The fibers in the subendocardial half were arranged according to a right handed helix with

a pitch angle of 40°. A left handed helix arrangement was used in the subepicardial half with the same, but opposite, pitch angle.

RESULTS

Using the model of LV remodeling, a natural [4] transmural course of fiber orientation automatically formed after about 200 calculation cycles (Fig. 3). The final solution appeared to be practically independent of the initially chosen distribution of fiber direction, as long as the primary helix structures could be recognized. Sarcomere shortening approached, but did not quite reach, the target value as set by the control mechanism related to myocyte direction. The solution oscillated around this value in a relatively narrow range. The variations in sarcomere length are followed by similar variations in fiber stress.

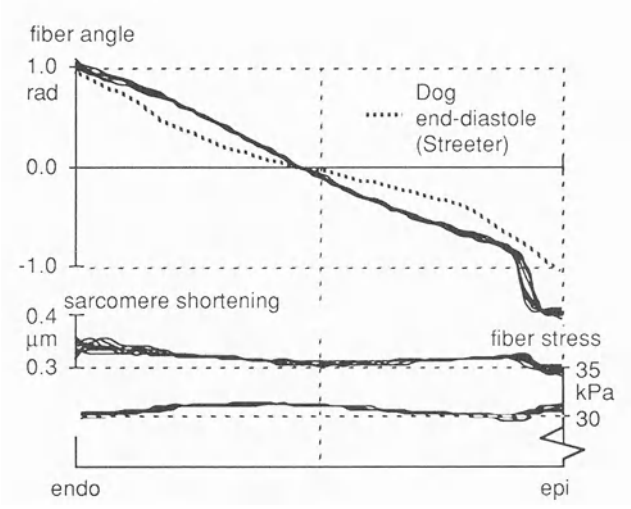

Figure 3. Transmural course of fiber direction, sarcomere shortening and fiber stress in a cylindrical model of LV mechanics. The distributions were obtained using the adaptation mechanism shown in Fig. 2. Changes in sarcomere length are to be referred to an end-diastolic length of 2.1 µm. The broken line indicates experimental results [4].

Adaptation to an Increase in Stroke Volume

Starting from the control state, stroke volume was doubled in the simulation (Fig. 4). The ejection fraction increased because the heart had to pump a larger stroke volume. The related larger deformation caused an immediate stimulus for dilatation of the cavity. Also, because of a mismatch of sarcomere shortening, more trials were performed to find a more optimal fiber direction. Contractility was above normal because the weight of the LV was low for the delivered stroke work. As a result, there was a stimulus to increase wall volume by growth. During this increase, part of the dilatation effect was reverted. Both weight and cavity volume were increased proportionally after stabilization to the new state.

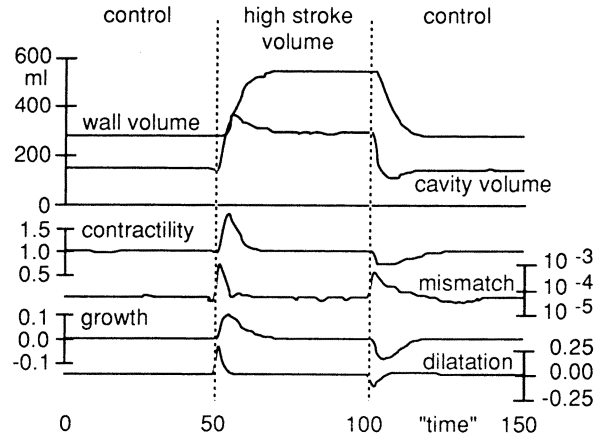

Figure 4. Time course of LV adaptation to an increase in volume load, followed by reversion to original loading condition. After the invoked change in stroke volume signals appear of dilatation and of increased mismatch with optimum shortening. Both stroke volume and contractility increase. Consequently wall mass increases steadily. After reversion of the load, most signal changes are approximately opposite.

DISCUSSION

The present study investigated whether the global structure of the heart could be controlled by a mechanism of distributed controlling actions. In a thick-walled cylinder, each shell represented such a control unit. The myocyte (Fig. 2) changed direction to optimize the amount of sarcomere shortening during the ejection phase. Early systolic stretch of the myocyte, and to a lesser extent stimuli for enhanced contractility, were assumed to increase the mass of the contractile proteins. Apart from the active myocytes, the passive elastic structures were also controlled by deformation signals. A large deformation was considered to weaken the strength of these structures.

Applying the program of regional control to the cylindrical shells in the model, a stable global fiber structure formed automatically. This rather complicated structure of helical fiber pathways is close to what is found in anatomical studies (Fig. 3). Furthermore, mass and geometry of the LV changed after a change in hemodynamic load. These changes were so that mechanical load of the myocytes was preserved in all regions. The observed changes of the geometry of the cavity and wall agreed with physiological findings on cardiac hypertrophy.

The proposed mechanism of control is attractive because several of its characteristics (Fig. 2) were indeed found to exist. The importance of stretch and contractility as stimuli to growth is consistent with molecular biological findings. So, stretch and contraction of cardiomyocytes are clearly involved in mechanical signaling and protein synthesis. The possibility to use trials as a tool to optimize fiber direction is indicated by a dispersion of myocyte direction of a few degrees. Furthermore, the limited length of the cardiac myocytes ($\approx$120 μm) allows the cell to change its direction. Such optimization of cellular orientation can also be understood as slowing down continuous search if conditions are more optimal. Statistically, each myocyte spends most time in the more optimal direction.

As suggested by Janicki [40], adaptation to an increase in the volume load involves a temporary phase of enhanced collagenase. This finding is consistent with our simulation

shown in Fig. 4. The increase of volume load is followed by a stimulus to decrease passive ventricular stiffness, as evident by the positive peak in the dilatation signal. This signal parallels collagenase. It represents the average decrease in stiffness, as shown in Fig. 2. After adaptation to the new loading state, the LV is scaled up to a larger size, while regional cyclic deformation is returned to normal. Because the mechanical properties of the tissue are mainly controlled by deformation, the tissue composition also returns to normal after reaching steady state. It has been reported [41] that the ventricular cavity becomes smaller during cardiac assist by volume unloading. According to the simulation in Fig. 4, the decrease of volume load is followed immediately by a decrease of end-diastolic cavity volume, before mass of the LV decreases significantly. This decrease is accompanied by a stimulus to increase ventricular passive stiffness. Using our hypothesis on remodeling, a cardiac assist procedure should preferably be directed to unload pressure rather than volume. Larger volume changes keep the ventricle more compliant. The end-diastolic pressure is then expected to stay at a lower level.

Interestingly, feedback through regionally sensed fiber stress is not a compelling condition. At a closer look, this is not surprising. No stress sensors are presently known. Generally, force or stress is detected by measuring deformation of a compliant structure. Another indication is given by the development of the chicken embryonic heart. The heart starts beating very early in the phase of development, and then LV systolic pressure is as low as a few mmHg [42], because the density of contractile proteins in the tissue is still very low. Evidently, cardiac structures are already forming in this phase. Deformation seems to be the most likely candidate for control of structure formation, because the level of cyclic deformation of this heart is already quite close to normal.

Indirectly, stress affects cardiac growth. For instance, if afterload increases, wall stress increases to above normal. Unless some precautions are taken, the stroke volume would diminish, causing systemic perfusion to be inadequate. As a result, systemic blood pressure control stimulates the heart to do more work. This physiological stimulus, or the related effects, are likely to be a factor in stimulating the synthesis of contractile proteins.

CONCLUSIONS

Adaptation of the tissue to mechanical load is postulated to be invoked by various deformation parameters. Using a thick-walled cylindrical model of LV mechanics yields that fiber direction changes to optimize sarcomere shortening. Early systolic stretch, and the physiological stimulus to increase cardiac work, increase cardiac mass. The stiffness of the passive structures diminishes with deformation. Beginning with a primitive design of the helical fiber structures in the LV, the distributed control system arranges the fibers automatically to a macroscopic structure, resembling the fiber structure of the true LV. Also, mechanical load is quite evenly distributed over the myocardial structures. The assumptions used for the properties of the regional mechano-feedback are in compliance with studies on mechano-transduction.

DISCUSSION

Dr. H.E.D.J. ter Keurs: When the heart and cardiac cells hypertrophy there are two different modalities: concentric hypertrophy and volumetric hypertrophy in response to volume overload. Various studies, including among others Cooper's group [Mann *et al. Circ Res.* 1989;64:1079-1090], have shown that you get two different kinds of responses of the cardiac myocyte. During concentric hypertrophy the myocytes show a large increase in cross sectional diameter and a much

smaller increase in length. This is in contrast to the eccentric hypertrophy where the cardiac cell adds more sarcomeres in series and thereby grows longer, leading to an increase of volume of the heart. It seems to me that in order to describe that you need the information so as to choose between adding more myofibrils in parallel or adding more sarcomeres in series within the myofibrils. I did not see how your model could do that.

Dr. T. Arts: We defined hypertrophy as an increase in wall mass. We did not distinguish between different kinds of hypertrophy. The findings of Cooper's group indicate that the design of the model needs more details. Maybe feedback signals should be introduced which can distinguish between elevated volume load and elevated pressure load. Such distinctions can be made locally. At increased volume load the cells are subject to more stretch and more shortening. At increased pressure load, shortening may diminish due to dilatation. So, the cell can locally obtain information about the type of external load.

Dr. H.E.D.J. ter Keurs: I would like to make a suggestion with respect to that, based on observations that we made. If you transplant a heart from one rat heterotopically into an identical recipient, which means that the heart now is not sensitive to hemodynamic conditions, and you test whether sympathetic drive causes hypertrophy, then you find that isoproterenol injections in the recipient of that transplant cause substantial hypertrophy in the recipient's heart but not in the donor heart. That means that calling the sympathetic system into action may be correct but may also be incorrect. An alternative hypothesis for what you have called contractility may be that the heart senses stress development by the contractile filaments and may use that to tell the local "factory" to build more myofilaments in parallel.

Dr. T. Arts: Maybe I did not emphasize clearly that stress itself is not a factor which induces hypertrophy. The present model is based on sensing deformation. I am not so sure if there is a stress sensor active in the heart. I do not know how it would be built. From the chicken embryo it is known that the heart starts beating when systolic pressure is only 2.5 mmHg, and remodeling seems to be already active. The structure of the chicken embryo heart is already present in a very early stage. In a later stage, the cells become more densely filled with myofilaments, causing the pressure to increase. I cannot easily understand how a stress sensor would change its sensitivity by a factor of 100. However, if deformation is sensed, this embryo development can be understood. Also, if we measure force or stress, we always convert stress to deformation, and we measure this deformation. So, deformation is more likely to be the primary sensed signal.

Dr. H.E.D.J. ter Keurs: Stressing cardiac muscle costs – ATP. So if you measure ATP fluxes you can convert that into a drive for hypertrophy [Meerson and Pomoinstsky. *J Mol Cell Cardiol.* 1972;4:571].

Dr. T. Arts: I agree.

Dr. P. Hunter: Your adapted fiber orientation had an interesting blip at the epicardial end, a sudden dive. I wonder whether that indicates that you should be putting into the model a distribution of more collagen content which adds an extra strengthening effect at the epicardial layer. A second question is: the fiber distribution in the septum is substantially different from the free wall and I think that your model is describing the behavior of the free wall. But it is an interesting study to explain why the septum develops as it does.

Dr. T. Arts: Both questions are strongly related. We have made a huge simplification in using a cylindrical model. The real heart is asymmetric due to the attachment of the right ventricle. This right ventricle normally counteracts torsion. Thus, the real deformation pattern is not rotational symmetric as it is in the model. The dip of the transmural course of the fiber angle just below the epicardium is caused by the presence of a forbidden zone, where optimum shortening cannot be reached. If you add more dispersion of the fiber angle or change values of the feedback parameters,

this dip may become less distinct or even disappear. I have to add that changing parameter values is not critical. The results may change somewhat, but not essentially. Stability of the structure is maintained even if you change the feedback parameter values over a range of a factor of 100.

Dr. Y. Lanir: Do you assume that the collagen becomes weaker when the LV expands?

Dr. T. Arts: In our opinion the LV undergoes a large cyclic deformation, if the range of strain is about 30%.

Dr. Y. Lanir: We have learned from Dr. Janicki that this is perhaps true in a short time scale, but after a while there is new synthesis of collagen which actually tends to increase the concentration of collagen. This may be a problem here.

Dr. T. Arts: No. In the case of volume hypertrophy there is no problem. If the heart is too light then it will adapt first. After stabilization the pressure is back to normal, and deformation is also back to normal. The remodeling signals are back to normal, and the structure may also be back to normal. Both the cavity and the wall volume are scaled up by the same factor. We should note, however, that this statement is not perfectly true. Back to normal should be interpreted to occur only approximately.

Dr. Y. Lanir: You had torsion in your model, so your model must distinguish between collagen that is parallel to the fibers and the one that is transverse to it. Do you include them as one compartment in your feedback mechanism, or do you distinguish between them?

Dr. T. Arts: We did not go into these details. If you really want to know the effects of cross deformation and stiffness, you should work with a model description in three dimensions. Then you also need big computational power.

Dr. J. Bassingthwaighte: I have a question on your modeling strategy. In your model you had reference points, and I know that there are no real reference points. You do not have feedback relative to some magic reference anywhere in the body. Those things do not exist. But you have reference points in your model.

Dr. T. Arts: I put in a reference setting of shortening of 12%, but it may not be correct.

Dr. J. Bassingthwaighte: So let me assume it is not correct. What will you do to replace that reference and what kind of strategy would you go about using to get rid of this obnoxious reference? Most reference points are more or less present in nature and they are defined by a multitude of nonlinear equations. They behave like reference, but not completely so. It is a cooperation of a complicated system which goes down to the cells. This would be a way to describe such a behavior macroscopically.

Dr. R. Beyar: When you have hypertrophy adapted to pressure overload, you have a thicker wall and you may need more twist to equilibrate between endocardium and epicardium strains. Do you get more twist in your model results? It has not been observed, to my knowledge, that hypertrophied hearts twist more. With MRI, we have looked at patients with hypertrophic cardiomyopathy. There was noise there but we could not say whether it increases, does not increase, or stays the same. That is one way to check the model experimentally and it might be that the heart can not adapt to an increase in the twist.

Dr. T. Arts: That might be true in a cardiomyopathic heart. In the hearts of different dogs under many different loading conditions we found a similar relation between torsion and normalized volume. We did not include hypertrophic hearts in our study. For those hearts there may be a difference.

REFERENCES

1. Arts T, Reneman RS. Dynamics of left ventricular wall and mitral valve mechanics: a model study. *J Biomech.* 1989;22:261–271.
2. Van der Vusse GJ, Arts T, Glatz JFC, Reneman RS. Transmural differences in energy metabolism in the left ventricular myocardium: Fact or fiction. *J Mol Cell Cardiol.* 1990;22:23–27.
3. Arts T, Prinzen FW, Snoeckx LHEH, Rijcken JM, Reneman RS. Adaptation of cardiac structure by mechanical feedback in the environment of the cell, a model study. *Biophys J.* 1994;66:953–961.
4. Streeter DD. Gross morphology and fiber geometry of the heart. In: R. M. Berne, eds. *The cardiovascular system, the heart.* Bethesda, Maryland, USA: Am Physiol Soc, 1979, 61–112.
5. Torrent-Guasp F. *An Experimental Approach on Heart Dynamics.* Madrid: Aguirre Torre, 1959.
6. Arts T, Veenstra PC, Reneman RS. A model of the mechanics of the left ventricle. *Ann Biomed Eng.* 1979;7:299–318.
7. Chadwick RS. Mechanics of the left ventricle. *Biophys J.* 1982;39:279–288.
8. Arts T, Veenstra PC, Reneman RS. Epicardial deformation and left ventricular wall mechanics during ejection in the dog. *Am J Physiol.* 1982;243:H379–H390.
9. Arts T, Meerbaum S, Reneman RS, Corday E. Torsion of the canine left ventricle during the ejection phase in the intact dog. *Cardiovasc Res.* 1984;18:183–193.
10. Arts T, Hunter WC, Douglas AS, Muijtjens AMM, Corsel JW, Reneman RS. Macroscopic three-dimensional motion patterns of the left ventricle. In: Sideman S, Beyar R, eds. *Interactive Phenomena in the Cardiac System.* New York: Plenum Press, 1993, 383–392.
11. Delhaas T, Arts T, Prinzen FW, Reneman RS. Regional fibre stress – fibre strain area as estimate of blood flow and regional oxygen demand in the canine heart. *J Physiol London.* 1994;477:481–496.
12. Prinzen FW, Arts T, Van der Vusse GJ, Coumans WA, Reneman RS. Gradients in fiber shortening and metabolism across the ischemic left ventricular wall. *Am J Physiol.* 1986;250:H255–H264.
13. Bassingthwaighte JB, Liebovitch LS, West B. *Fractal Physiology.* New York: Oxford University Press, 1994.
14. Aoyagi T, Mirsky I, Flanagan MF, Currier JJ, Colan SD, Fujii AM. Myocardial function in immature and mature sheep with pressure-overload hypertrophy. *Am J Physiol.* 1992;262:H1036–H1048.
15. Gelpi RJ, Pasipoularides A, Lader AS, Patrick TA, Chase N, Hittinger L, Shannon RP, Bishop SP, Vatner SF. Changes in diastolic cardiac function in developing and stable perinephritic hypertension in conscious dogs. *Circ Res.* 1991;68:555–567.
16. Sasayama S, Ross J, Franklin D. Adaptations of the left ventricle to chronic pressure overload. *Circ Res.* 1976;38:172–178.
17. Arts T, Bovendeerd PHM, Prinzen FW, Reneman RS. Relation between left ventricular cavity pressure and volume and systolic fiber stress and strain in the wall. *Biophys J.* 1991;59:93–103.
18. Shigematsu S, Hiromatsu K, Aizawa T, Yamada T, Takasu N, Niwa A, Miyahara Y, Tsujino M, Schimizu Z. Regression of left ventricular hypertrophy in patients with essential hypertension: Outcome of 12 years antihypertensive treatment. *Cardiology.* 1990;77:280–286.
19. Gaasch WH, Andrias CW, Levine HJ. Chronic aortic regurgitation: the effect of aortic valve replacement on left ventricular volume, mass and function. *Circulation.* 1978;58:825–836.
20. Monrad ES, Hess OM, Murakami T, Nonogi H, Coriu WJ, Krayenbühl HP. Time course of regression of left ventricular hypertrophy after aortic valve replacement. *Circulation.* 1988;77:1345–1355.
21. Delhaas T, Arts T, Prinzen FW, Reneman RS. Relation between regional electrical activation time and subepicardial fiber strain in the canine left ventricle. *Eur J Physiol.* 1993;423:78–87.
22. Watson PA. Function follows form: generation of intracellular signals by cell deformation. *FASEB J.* 1991;5:2013–2019.
23. Yazaki Y, Komuro I, Yamazaki T, Tobe K, Maemura K, Kadowaki T, Nagai R. Role of protein kinase system in the signal transduction of stretch-mediated protooncogene expression and hypertrophy of cardiac myocytes. *Mol Cell Biochem.* 1993;119:11–16.
24. Komuro I, Kaida T, Shibazaki Y, Kurabayashi M, Katoh Y, Hoh E, Takaku F, Yazaki Y. Stretching cardiac myocytes stimulates proto-oncogene expression. *J Biol Chem.* 1990;265:3595–3598.
25. Sadoshima JI, Jahn L, Takahashi T, Kulik TJ, Izumo S. Molecular characterization of stretch-induced adaptation of cultured cardiac cells. *J Biol Chem.* 1992;267:10551–10560.
26. Mann DL, Kent RL, Cooper G, IV. Load regulation of the properties of adult feline cardiocytes: growth induction by cellular deformation. *Circ Res.* 1989;64:1079–1090.

27. Sigurdson W, Ruknudin A, Sachs F. Calcium imaging of mechanically induced fluxes in tissue cultured chick heart: role of stretch-activated ion channels. *Am J Physiol*. 1992;262:H1110-H1115.
28. Sadoshima JI, Takahashi T, Jahn L, Izumo S. Roles of mechano-sensitive ion channels, cytoskeleton, contractile activity in stretch-induced immediate-early gene expression and hypertrophy of cardiac myocytes. *Proc Natl Acad Sci USA Cell Biol*. 1992;89:9905-9909.
29. McDermott PJ, Rothblum LI, Smith SD, Morgan HE. Accelerated rates of ribosomal RNA synthesis during growth of contracting heart cells in culture. *J Biol Chem*. 1989;264:18220-18227.
30. Carver W, Nagpal ML, Nachtigal M, Borg TK, Terracio L. Collagen expression in mechanically stimulated cardiac fibroblasts. *Circ Res*. 1991;69:116-122.
31. Chapman D, Weber KT, Eghbali M. Regulation of fibrillar collagen types I and III and basement membrane type IV collagen gene expression in pressure overloaded rat myocardium. *Circ Res*. 1990; 67:787-794.
32. Contard FC, Koteliansky V, Marotte F, Dubus I, Rappaport L, Samuel JL. Specific alterations in the distribution of extracellular matrix components within rat myocardium during development of pressure overload. *Lab Invest*. 1991;64:65-75.
33. Mukherjee D, Sen S. Collagen phenotype during development and regression of myocardial hypertrophy in spontaneously hypertensive rats. *Circ Res*. 1990;67:1474-1480.
34. Weber KT, Janicki JS, Shroff SG, Pick R, Chen RM, Bashey RI. Collagen remodeling of the pressure overloaded, hypertrophied nonhuman primate myocardium. *Circ Res*. 1988;62:757-765.
35. Samuel JL, Barrieux A, Dufour S, Dubus I, Contard F, Kotelianski V, Farhadian F, Marotte F, Thiéry J-P, Rappaport L. Accumulation of fetal fibronectin mRNA's during the development of rat cardiac hypertrophy induced by pressure overload. *J Clin Invest*. 1991;88:1737-1746.
36. Grimm AF, Lin HL, Grimm BR. Left ventricular free wall and intraventricular pressure sarcomere length distributions. *Am J Physiol*. 1980;239:H101-H107.
37. Yoran C, Covell JW, Ross J. Structural basis for the ascending limb of left ventricular function. *Circ Res*. 1973;32:297-303.
38. Prinzen FW, Augustijn CH, Arts T, Allessie MA, Reneman RS. Redistribution of myocardial fiber strain and bloodflow by asynchronous activation. *Am J Physiol*. 1990;259:H300-H308.
39. Prinzen FW, Delhaas T, Arts T, Reneman RS. Asymmetrical changes in ventricular wall mass by asynchronous electrical activation of the heart. In: S. Sideman and R. Beyar, eds. *Interactive Phenomena in the cardiac system*. New York: Plenum Press, 1993, 257-264.
40. Janicki JS, Brower GL, Henegar JR, Wang L. Ventricular remodeling in heart failure: the role of myocardial collagen. In: Sideman S, Beyar R, eds, *Molecular and Subcellular Cardiology*, Proc. of the 9th Henry Goldberg Workshop, Haifa, Israel. New York: Plenum Publishing Corp., 1995; in press.
41. Levin HR, Burkhoff D, Chen JM, Packer M, Rose EA. Restoration of cardiac structure in end-stage cardiomyopathy by marked, prolonged mechanical loading of the left ventricle: evidence for reverse cardiac remodeling. *Circulation*. 1994;90:I-111.
42. Taber LA, Hu N, Pexieder T, Clark EB, Keller BB. Residual strain in the ventricle of the stage 16-24 chick embryo. *Circ Res*. 1993;72:455-462.

CHAPTER 23

THE EFFECT OF CYTOTOXIC LYMPHOCYTES ON CONTRACTION, ACTION POTENTIAL AND CALCIUM HANDLING IN CULTURED MYOCARDIAL CELLS

Yonathan Hasin, Yael Eilam, David Hassin, and Ruhama Fixler[1]

ABSTRACT

Cytotoxic T lymphocytes are important in the pathogenesis of several disease states, yet the pathophysiology of the lymphocyte–myocyte interaction is not well known. We have developed *in vitro* viral and autoimmune models to study the physiological phenomena associated with this interaction. To produce these models, lymphocytes were obtained from adult rats injected either with mengo virus or autologous cardiac myocytes. Cardiac myocytes from neonatal rats were then exposed to these lymphocytes. In both models, reversible physiologic changes in myocytes preceded irreversible cell damage. The physiologic changes included reduced amplitude of myocyte contraction, impairment of relaxation and prolongation of the duration of contraction and action potential. In addition, oscillations were noted in the plateau phase of the action potentials. These physiologic changes were accompanied by an early elevation in the cytosolic free calcium concentration, a late elevation in the total exchangeable calcium pool, and attenuation of the $[Ca^{2+}]_i$ transient signals. Verapamil inhibited the late elevation in the total exchangeable calcium pool, but failed to inhibit the early elevation in the cytosolic free calcium concentration. These phenomena may explain transient cardiac functional abnormalities that may appear during myocarditis prior to cell destruction.

INTRODUCTION

Myocarditis, in its acute, subacute or chronic forms may be caused by several infections agents [1]. Rhythm disturbances, electrocardiographic changes and contractile

[1]Cardiology Department, Hadassah Medical Organization, Kiryat Hadassah, P.O.B. 12000, Jerusalem, 91120, Israel.

Molecular and Subcellular Cardiology: Effects of Structure and Function
Edited by S. Sideman and R. Beyar, Plenum Press, New York, 1995

abnormalities appear during the active phase of the disease [2]. While myocarditis may completely resolve with restoration of normal cardiac function, in some cases it results in destruction of myocardial fibers, fibrosis and a permanent decrement in cardiac function [3]. The precise mechanism responsible for the transient electrical and mechanical alteration during active myocarditis is not clear. Cytotoxic T lymphocytes are important in the pathogenesis of this disease, but the pathophysiology of the lymphocyte – myocyte interaction is not well known. We have developed an *in vitro* viral model and an autoimmune model for the study of myocarditis. This model demonstrates the physiologic changes occurring in cardiac myocytes during their interaction with cytotoxic lymphocytes [4, 5].

MATERIALS AND METHODS

Experimental Models

Viral model. The model has been described previously [4]. Briefly, mengo virus was injected into adult rats. After 14 days splenic lymphocytes were isolated from the injected animals. The lymphocytes were then cultured in the presence of inactivated virus for 5 days for further *in vitro* stimulation. Cultured myocytes obtained from newborn rats, prepared as described in [6], were exposed to the same virus. After exposure to the virus, these myocytes were exposed to the lymphocytes.

Autoimmune model. This model has been described previously [5]. Briefly, autologous cardiac myocytes were repeatedly injected into adult rats. Following 3 months of injections, splenic lymphocytes were isolated from the immunized animals. The lymphocytes were cultured in the presence of cardiac myocytes for 5 days to stimulate a secondary response. Cultured myocytes obtained from newborn rats were exposed to these lymphocytes.

In some experiments, supernatant was removed from the dishes with myocytes and lymphocytes. This supernatant was then centrifuged in order to remove the lymphocytes. The cultured myocytes were then exposed to the lymphocyte–free supernatant.

Measurements

Cell wall motion was measured using a video motion analyzer [4]. Transmembrane action potentials were obtained using intracellular microelectrodes [4].

Total exchangeable calcium content was determined from ^{45}Ca tracer measurements after loading the myocytes with ^{45}Ca and then exposing them to CTL [4]. Free cytosolic Ca^{2+} was measured by fluorescence measurement after loading the myocytes with quin 2/AM or fura 2/AM. This procedure is described in detail in Hallaq *et al.* [7].

Calcium transients were measured by a fluorescence system after exposing myocytes to indo 1/AM. This procedure is described in detail in [8].

RESULTS

The viral model of virus–infected cardiac myocytes interacting with virus–sensitized lymphocytes demonstrated prominent but reversible physiologic changes. Initial changes in myocyte contractions included a slowed rate of relaxation. Later changes included a reduced amplitude of contraction and a slowed spontaneous beating rate (Fig. 1). Action potential duration showed a gradual lengthening with oscillations appearing in the plateau

phase (Fig. 2). Resting membrane potential, upstroke magnitude and upstroke velocity were not affected.

Similar results obtained in the autoimmune model included impaired myocyte relaxation with prolonged contractions and prolongation and oscillations in the plateau of the action potential (Fig. 3). These effects induced in both models were reversible by washout or by 10^{-6} M verapamil (Figs. 3 and 4) but not by tetrodotoxin (10^{-5} g/ml).

Supernatant collected in the autoimmune model had the same effect on myocyte contractility as that observed following exposure of myocytes to cytotoxic lymphocytes (Fig. 5).

Since these phenomena may be associated with cellular changes in calcium handling, we examined total exchangeable Ca^{2+} pool, average free cytosolic Ca^{2+} ($[Ca^{2+}]_i$ and $[Ca^{2+}]_i$ transients. Total exchangeable Ca^{2+} pool was measured in the viral model. Fourteen percent increase was observed (Fig. 6) following 90 min and 120 min of exposure to lymphocytes. This was prevented by pretreatment with verapamil (Fig. 7).

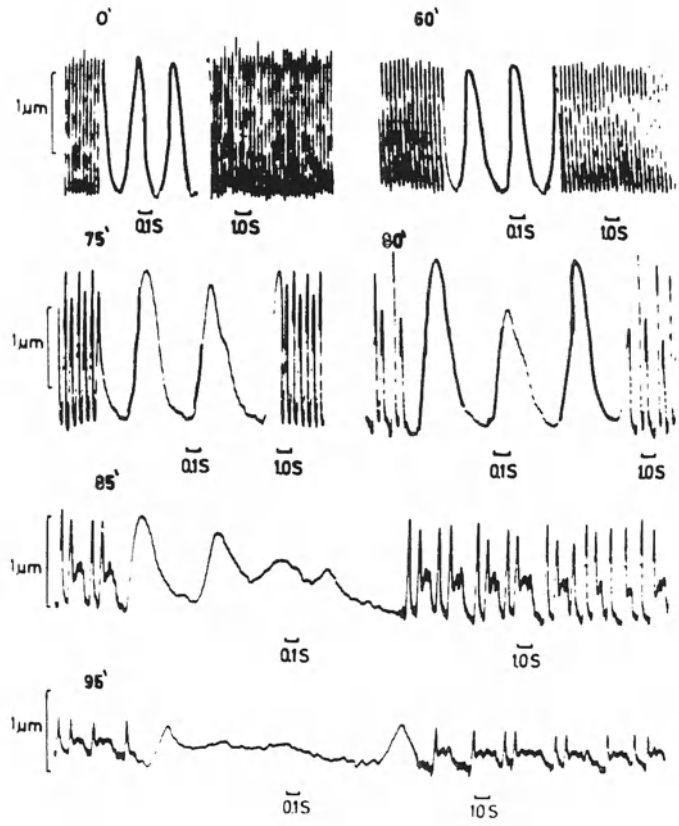

Figure 1. Effect of mengo virus-sensitized cytotoxic T lymphocytes (CTL) on the spontaneous contractions of mengo virus-infected myocytes. Motion traces are shown at different times after exposure of myocytes to CTL. After a 60 min lag period, shape of twitches starts to change with a prolongation of relaxation. Later, mechanical alternans of twitch amplitude and of relaxation rate appear. Eventually, contractions become very prolonged and oscillatory. Finally, amplitude and rate decrease until cellular arrest (reprinted with permission [4]).

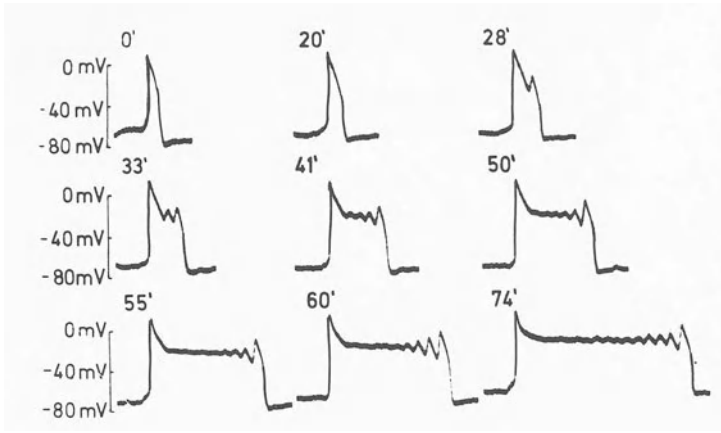

Figure 2. Effects of mengo virus-sensitized cytotoxic T lymphocytes (CTL) on action potentials recorded from mengo virus-infected myocytes. Times following exposure to CTL are noted. Action potentials show a gradual lengthening with oscillations appearing in the plateau phase. Resting, or maximal diastolic potential, was unaltered during all these changes (reprinted with permission [4]).

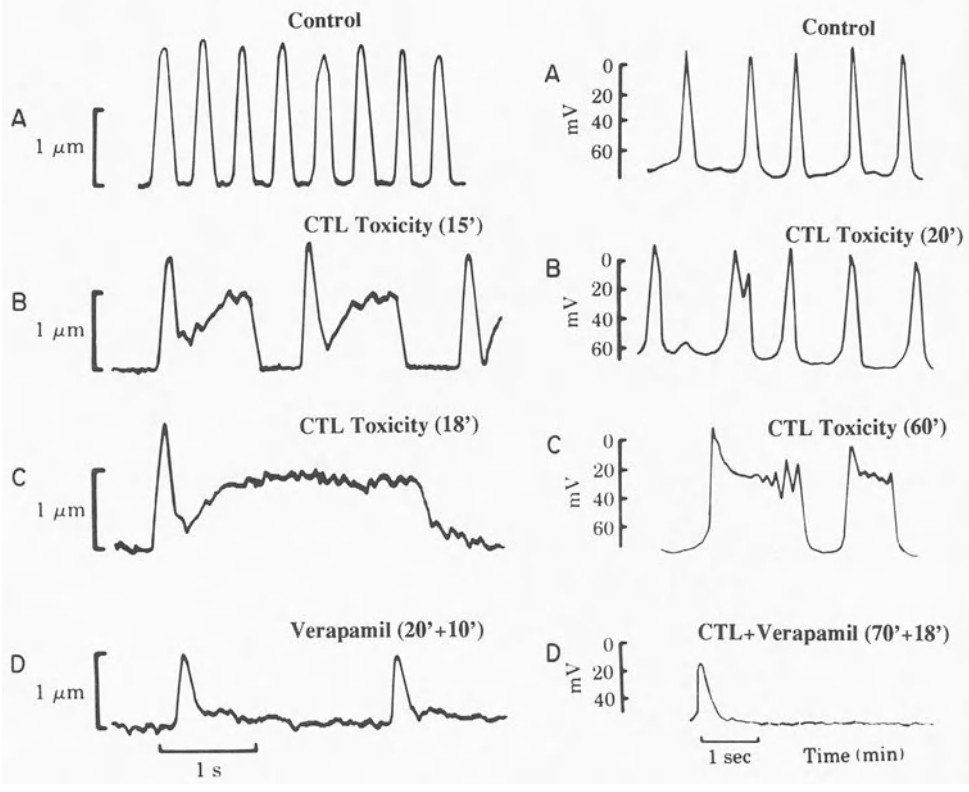

Figure 3. Effect of autoimmune-sensitized cytotoxic T lymphocyte (CTL). **Left:** Effect on the spontaneous contractions of cardiac myocytes. Motion traces are shown at different times after exposure to CTL. After a lag period of 15 min, the shape of twitches starts to change with a prolongation of relaxation with oscillations. A direct application of verapamil (10^{-6} M) to the bath blocks the effects (D). **Right:** Effect on action potentials recorded from cardiac myocytes. Times (min) following exposure to CTL are noted. Action potentials show a gradual lengthening with oscillations appearing in the plateau phase. Resting, or maximal diastolic potential, was unaltered. A direct application of verapamil (10^{-6} M) to the bath blocks the effect (reprinted with permission [5]).

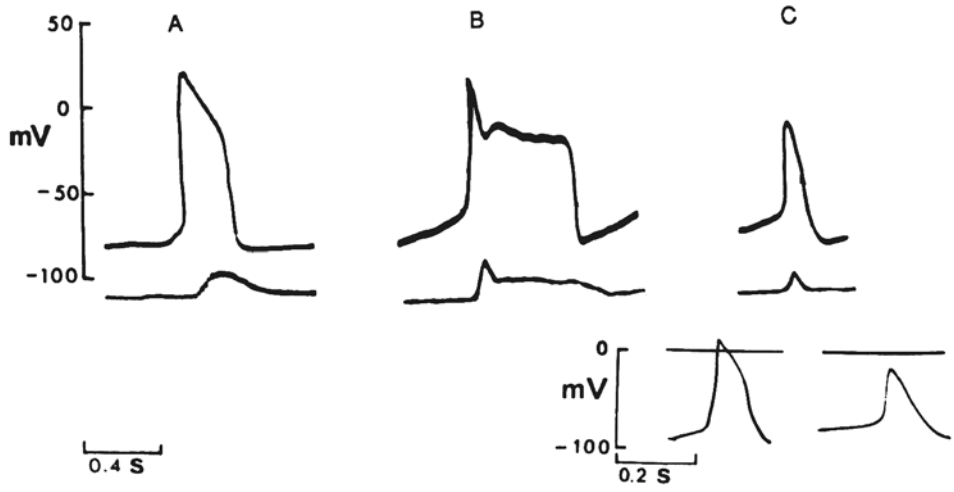

Figure 4. Effect of verapamil on action of cytotoxic T lymphocytes (CTL) on mengo virus-infected cultured myocytes. **A:** intracellularly recorded action potential and accompanying contraction of myocytes recorded during control period. **B:** action potential and contraction of these myocytes 65 min after CTL were added to bath. Plateau of action potential is lengthened and shows oscillations of membrane potential. Accompanying twitch is also longer and oscillatory. **C:** A direct application of verapamil (10^{-6} M) to the bath blocks the effect. (There is an accompanying negative inotropic effect and reduction in action potential amplitude characteristic of verapamil). **Inset** on bottom right shows a typical action potential in these cells, before (left) and after (right) the addition of 10^{-6} M verapamil.

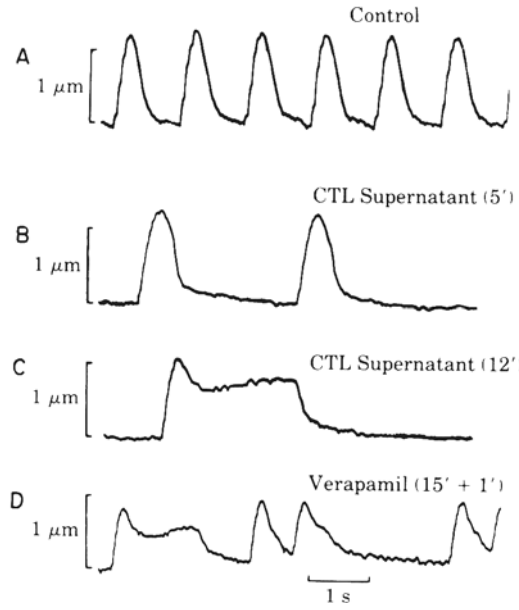

Figure 5. Effect of supernatant on myocyte contractility. When the toxic effect of the lymphocytes on the myocytes was observed, the medium in the chamber was collected and centrifuged in order to remove the lymphocytes. **A:** Myocyte contractility in control medium. **B:** Myocyte contractility after changing the control medium to the lymphocyte-myocyte supernatant. Note that spontaneous but impaired cellular contractions appeared 5 min after an immediate arrest of contractions. **C:** Contractions became very prolonged and oscillatory. **D:** This effect was only partially blocked by 10^{-6} M verapamil.

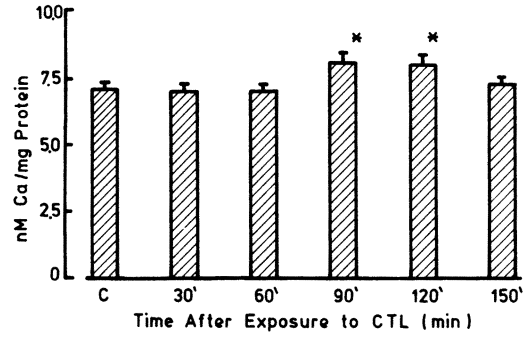

Figure 6. Time after exposure to cytotoxic T lymphocytes (CTL). Note significant increases in total exchangeable calcium after 90 and 120 minutes of exposure to CTL ($p<0.05$).

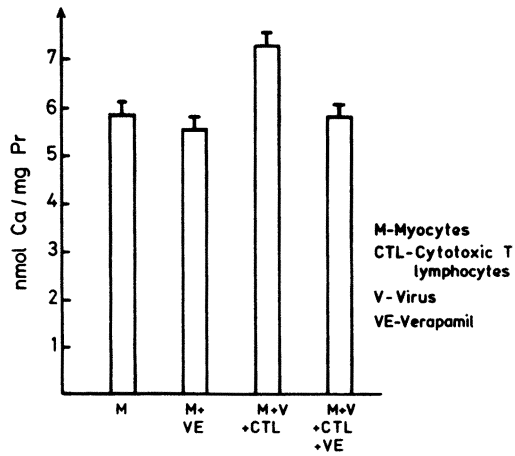

Figure 7. Effect of verapamil on total exchangeable calcium pool: M – Control myocytes. M+VE – Myocytes in the presence of 10^{-6} M verapamil. M+V+CTL – Virus-infected myocytes exposed to sensitized cytotoxic lymphocytes. M+V+CTL+VE denotes M+V+CTL in the presence of 10^{-6} M verapamil. Note that the increase in calcium content of M+V+CTL was prevented by verapamil.

Free cytosolic Ca^{2+} showed an increase of 300% in $[Ca^{2+}]_i$ within 5 min of exposure to CTL (Fig. 8). Verapamil (10^{-6} M) did not prevent this elevation either by pretreatment, or when given after exposure to CTL. Comparison between total exchangeable Ca^{2+} and $[Ca^{2+}]_i$ concentration in the viral model showed a difference in the time of appearance and the relative change observed. The increase in $[Ca^{2+}]_i$ appeared earlier and was much more prominent in comparison to the changes in total exchangeable Ca^{2+}.

The changes observed in $[Ca^{2+}]_i$ transients in all models were:

1. A significant increase in time to peak of $[Ca^{2+}]_i$ transients in all models ($p<0.02$). *Viral model:* from 166±35 msec to 248±40 msec. *Autoimmune model:* from 151±20 msec to 184±20 msec. *Active supernatant:* from 168±16 msec to 366±116 msec (M±SE, n=6).
2. A decrease in amplitude of $[Ca^{2+}]_i$ transients in all models ($p<0.02$). *Viral model:* to 100% to 79%±9%. *Autoimmune model:* to 86%±12%. *Active supernatant:* to 57%±3.3% (M±SE, n=6).

3. An increase in interval between onset of $[Ca^{2+}]_i$ transient and onset of contraction. *Viral model:* from 74±20 msec to 160±40 msec. *Autoimmune model:* from 50±12 msec to 79±19 msec. *Active supernatant:* from 60±9 to 280±150 msec.
4. Prolongation of $[Ca^{2+}]_i$ transient decay. Time to 2/3 relaxation increased: *Viral model:* from 412±60 msec to 633±109 msec. *Autoimmune model:* from 415±50 msec to 576±195 msec. *Active supernatant:* from 400±30 msec to 794±155 msec.

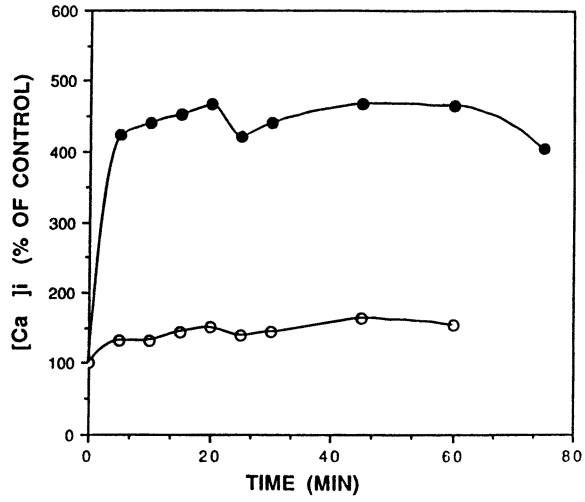

Figure 8. Free cytosolic calcium measured by quin 2 fluorescence using spectrophotometer after exposure to sensitized lymphocytes (●————●) or to control lymphocytes (o————o).

DISCUSSION

Reversible physiologic changes in myocytes preceded irreversible cell damage in our *in vitro* study of lymphocyte - myocyte interaction. Changes in both models included reduction in the amplitude of cell contraction, impairment of relaxation and prolongation of contraction. Action potential duration was also prolonged, with the appearance of oscillations noted during the plateau phase. All these changes were reversible upon washout. These phenomena may explain transient cardiac functional abnormalities occurring in clinical myocarditis without cell destruction.

Normal myocytes are able to maintain a 10,000 fold Ca^{2+} concentration gradient across the sarcolemma. Our experimental results demonstrate abnormal myocyte calcium metabolism after exposure to immunized lymphocytes and their products. The inability to maintain an adequate calcium concentration gradient may cause the observed myocyte dysfunction following immune attack.

Dysfunction of calcium handling at any of the multiple sites of calcium action in the cardiac cell can result in abnormal contraction and action potential. Our results suggest a combined defect of $[Ca^{2+}]_i$ handling by the sarcolemma and sarcoplasmic reticulum (SR).

The effect of verapamil indicates that there is either an increased or maintained transsarcolemmal calcium influx. The increase in cytosolic free Ca^{2+} was not blocked by 10^{-6} M verapamil (presumably blocking both L type Ca^{2+} channels and Na^{+}-Ca^{2+}

exchanger). This may suggest that changes in calcium homeostatic mechanisms may not be exclusively related to the sarcolemma.

The increased diastolic level of calcium in the cytosol can explain the relaxation abnormalities and may reflect changes occurring in the SR apparatus. The slowed decline in $[Ca^{2+}]_i$ during relaxation can be a result of a reduced Ca^{2+} sequestration rate by the SR. Furthermore, prolongation of action potential can lead to reduction of Ca^{2+} efflux, or even Ca^{2+} influx through the Na^+–Ca^{2+} exchange system. The prolonged time of depolarization may be an additional reason for the changes in the diastolic decay of $[Ca^{2+}]_i$.

Prolongation of the action potential was shown in other models of heart failure as well. Examples include muscle strips obtained from human hearts with dilated or ischemic cardiomyopathy [9]. This can be related to alterations in Ca^{2+} and K^+ currents. Similar alterations in membrane function and intracellular $[Ca^{2+}]_i$ handling may be a feature common to different causes of heart failure.

Another possibility is the involvement of cytotoxic T lymphocytes in other physiologic processes not directly involving myocarditis per se. Activation of lymphocytes was indicated in humans with angina pectoris or following coronary angioplasty (PTCA) [10]. Activation of cardiac specific cytotoxic lymphocytes was also demonstrated following coronary ligation in a rat model [11].

CONCLUSION

The following hypothesis may explain the clinical manifestations of active myocarditis: cytotoxic lymphocytes interact with cardiac myocytes. This results in secretion of an active soluble factor which causes transient dysfunction of the cell membrane and sarcoplasmic reticulum. The changes in action potential configurations cause electrocardiographic changes and induce rhythm disturbances. Elevation of diastolic $[Ca^{2+}]_i$ results in impaired relaxation of cardiac myocytes. Similarly, reduction in the peak of the calcium transients corresponds with a reduced amplitude of contraction in affected heart cells. This explains the impaired diastolic and systolic ventricular function of acute myocarditis.

Acknowledgements

This study was supported by the grant from the Ministry of Health – Chief Scientist's Office, Jerusalem, Israel.

DISCUSSION

Dr. G. Kessler-Icekson: What is the cytotoxic cell mediator? Would it be perforin? How do you explain the specificity of the block by verapamil?

Dr. Y. Hasin: I doubt very much whether it is perforin, since perforin, according to what we have learned, is introduced into the membrane, polymerized and creates an irreversible hole. I do not know what it is, but it is certainly solubilized, it is circulated into the medium, since only the medium can cause the same effect.

Dr. M. Morad: I am a bit puzzled. You showed electrophysiological data that the plateau dropped from around +20 to around −20 mV. The low plateau of the action potential is consistent with the idea that you blocked the Ca^{2+} channel and perhaps you have done something to the sodium and

K^+ currents. Then you put verapamil, and presumably it blocks calcium channels alone, and you reverse the effect. How much verapamil did you use? Is it possible that the verapamil was also blocking the sodium current and that is why you were really shortening back the action potential and reversing the effect?

Dr. Y. Hasin: Yes, but the TTX did not cause the effect. We have put 10^{-6} molar verapamil. That is a good dose and probably not specific. But when we use TTX it did not block the effect.

Dr. H.E.D.J. ter Keurs: Did you do studies of potassium currents? It looks like reactivation of calcium current can be inhibited by verapamil.

Dr. Y. Hasin: No. It is a good question.

Dr. H.C. Strauss: I just wonder if stimulation of NO synthase might be a mediator since the nitric oxide released will effect the K channels and possibly other channels as well. This might be another signal pathway that might be worthy of exploration.

Dr. S. Marom: Voltage clamp experiments are called upon here.

Dr. E. Marban: Is the supernatant activity heat stable? Do you have any idea whether this might be a peptide, or something else?

Dr. Y. Hasin: No. I can only tell you from observation of calcium and motion that the effect is not stable. The effect goes very fast into arrest of beating with a sudden increase in calcium level. It stays there for as long as the supernatant is there. Early on we see this prolonged contraction accompanied with prolonged calcium transient and eventually the cells just stay in contracture with elevated calcium, cytosolic calcium, until washout.

Dr. E. Marban: If you keep the supernatant, if you store it for a long period, or if you try to destroy the activity with heat, does it still work or is it labile?

Dr. Y. Hasin: We have not worked further on the supernatant as yet.

REFERENCES

1. Weinstein C, Fenoglio J. Myocarditis. *Hum Pathol.* 1987;18:613–618.
2. Matsumori A, Kawai C. An experimental model for congestive heart failure after encephalomyocarditis in mice. *Circulation.* 1982;56:1230–1235.
3. Matsumori A, Kawai C. An animal model of congestive dilated cardiomyopathy: Dilatation and hypertrophy of the heart in chronic stage in DB1/2 mice with myocarditis caused by encephalomyocarditis virus. *Circulation.* 1982;56:355–360.
4. Hasin D, Fixler R, Shimoni Y, Rubinstein E, Raz S, Gotsman S, Hasin Y. Physiological changes induced in cardiac myocytes by cytotoxic T lymphocytes. *Am J Physiol.* 1987;252:(*Cell Physiol* 21) C10–C16.
5. Fixler R, Shimoni Y, Hasin D, Admon D, Raz S, Yarom Y, Hasin Y. Physiological changes induced in cardiac myocytes by cytotoxic lymphocytes. An autoimmune model. *J Moll Cell Cardiol.* 1994;26:351–360.
6. Yageve S, Heller M, Pinson A. Changes in cytoplasmic and lysosomal enzyme activities in cultured rat heart cells: the relationship to cell differentiation and cell population in culture. *In Vitro* 1984;20:893–898.
7. Hallaq H, Hasin Y, Fixler R, Eilam Y. Effect of ouabain on the concentration of free cytosolic Ca^{++} and on contractility in cultured rat cardiac myocytes. *J Pharmacol Exp Ther.* 1989;248:716–721.
8. Ela C, Hasin Y, Eilam Y. Opioid effects on contractility, Ca^{2+} transients and intracellular pH in cultured cardiac myocytes. *J Moll Cell Cardiol.* 1993;26:599–613.

9. Perreault CL, Williams CP, Morgan JP. Cytoplasmic calcium modulation and systolic versus diastolic dysfunction in myocardial hypertrophy and failure. *Circulation.* 1993;87:VII31–VII37.
10. Blum A, Sclarovsky S, Shohat B. T lymphocyte activation in stable angina pectoris and after percutaneous transluminal coronary angioplasty. *Circulation.* 1995;91:20–22.
11. Varda-Bloom N, Leor J, Ohad D, Kaminer R, Battler A, Eldar M, Hassin D. Cytotoxic T lymphocytes are stimulated after myocardial infraction and are able to recognize and kill healthy myocyte *in vitro*. *Circulation.* 1994;90: I–522.

CHAPTER 24

VENTRICULAR REMODELING IN HEART FAILURE: THE ROLE OF MYOCARDIAL COLLAGEN

Joseph S. Janicki, Gregory L. Brower, Jeffrey R. Henegar, and Lizhen Wang[1]

ABSTRACT

Collagen which is present in the myocardium in relatively small amounts is the most abundant structural protein of the connective tissue network. Its structural organization consists of a complex weave of collagen fibers that surrounds and interconnects myocytes, groups of myocytes, muscle fibers and muscle bundles. The conformation of interstitial fibrillar collagen makes it highly resistant to degradation by all proteinases other than specific collagenases. In hearts with myocardial damage secondary to myocardial infarction, chronic ischemia, inflammation, or cardiomyopathy, a complex sequence of compensatory events occur that eventually result in an adverse left ventricular remodeling. This continual state of remodeling is characterized by persistent collagenase activity, fibrillar collagen degradation, and progressive myocyte loss. The net effect is a shift in the balance between collagen synthesis and degradation which leads to an inadequate fibrillar collagen matrix, progressive ventricular dilatation and sphericalization with wall thinning and eventual congestive heart failure.

INTRODUCTION

Cardiac or ventricular remodeling represents the structural changes that occur in ventricular chamber size, wall thickness and composition that typify the heart failure state. Specifically the definition of adverse remodeling includes progressive left ventricular (LV) dilatation, wall thinning and sphericalization which occur in chronic myocardial failure. Regardless of the underlying cause of heart failure, there is a preclinical heart failure phase where ventricular dysfunction due to myocardial damage exists with no signs or symptoms

[1]Department of Internal Medicine, Dalton Cardiovascular Research Center, University of Missouri, Columbia, Missouri 65212, USA.

Molecular and Subcellular Cardiology: Effects of Structure and Function
Edited by S. Sideman and R. Beyar, Plenum Press, New York, 1995

of congestive heart failure. It is during this phase that ventricular remodeling begins as a compensatory process. Compensatory myocardial adaptations included in this process are activation of the renin–angiotensin–aldosterone and sympathetic nervous systems, elevations in circulating blood volume and ventricular preload, cardiac myocyte hypertrophy and progressive ventricular enlargement. Eventually, however, this remodeling results in an inefficient, spherical ventricle that is markedly dilated with an inappropriate chamber diameter to wall thickness ratio.

The marked LV dilatation which develops weeks to months following myocardial infarction occurs with little change in LV filling pressure [1]. This observation indicates that injury–related dilatation is the result of structural remodeling of the muscular and interstitial components of the myocardium. Myocardial fibrillar collagens maintain muscle fiber and cardiac myocyte alignment. They also impart a tensile strength to the myocardium that governs tissue stiffness and maintains ventricular shape and size. Therefore, it is our belief that an anatomic requisite for ventricular remodeling is a disruption and degradation of collagen fibers. Accordingly, the purpose of this communication is to provide evidence in support of this contention.

MYOCARDIAL COLLAGENASE

Collagen is present in the myocardium in small amounts (i.e., 2 to 4% of total myocardial volume). Its structural organization consists of a complex weave of collagen fibers that surrounds and interconnects myocytes, groups of myocytes, muscle fibers and muscle bundles [2, 3]. Secreted in fibrillar form and subsequently crosslinked, extracellular collagen is exceptionally stable. It consists of three peptide chains which entwine to form a right–handed super–helix. This conformation makes interstitial fibrillar collagen highly resistant to degradation by all proteinases except specific collagenases [4]. Collagenase is a member of a class of neutral proteinases known collectively as the matrix metalloproteinases (MMPs). Metalloproteinases are secreted as proenzymes or zymogens which are activated by other proteinases or by organomercurials. MMP activity can be inhibited by tissue inhibitors of metalloproteinases (TIMP). Once activated, their ability to catalyze collagen cleavage is dependent on the presence of zinc at the active site [4, 5].

Substrates which interstitial collagenase (MMP–1) will degrade are collagen types I–III, VII, X and gelatins. Neutrophil collagenase (MMP–8) will degrade collagen types I–III [5]. These enzymes cleave all three α chains of native collagen types I, II, and III at a single, specific locus [6, 7]. At physiologic temperatures the cleaved fragments spontaneously denature into nonhelical gelatin derivatives [8] which are digested by gelatinase or MMP–2 into smaller peptides that are further cleaved by nonspecific proteases [5].

The myocardial collagenase system was first identified by Montfort and Pérez–Tamayo in 1975 [9]. Using an antibody to collagenase and immunohistochemical methods, abundant amounts of collagenase were found to be present in interstitial spaces between myocardial fiber bundles. When the distributions of collagen and collagenase in the myocardium are compared, the two are found to be closely associated. While collagenase in the normal heart is plentiful, the majority is in a proenzyme or latent form. Recently, Tyagi *et al.* [10] estimated the activated collagenase component in rat myocardium to be between 1 to 2% of total myocardial collagenase. In vitro activation with trypsin and plasmin increased the amount of active enzyme to between 60 and 80% of total collagenase [11]. They also presented evidence for the existence of myocardial TIMP.

Interstitial or extracellular degradation of collagen in the normal heart is relatively slow. The synthesis rate of collagen for the right and left ventricles in dogs is 0.56% of total ventricular collagen per day [12]. If an equilibrium is assumed between collagen synthesis and degradation, then the degradation and synthesis rates would have to be similar and the half life of collagen would be between 80 and 120 days [12, 13]. Such a slow turnover rate is in agreement with the small amount of active myocardial collagenase estimated by Tyagi *et al.* [10, 11]. Because an unabated secretion or activation of proteinases is capable of destroying an organism's supportive framework, the collagenase system is normally highly regulated. This is accomplished as follows: an increased proenzyme secretion occurs only when needed; there are multistep processes required for activation of the zymogens; and there are multiple inhibitors of collagenase in tissue and blood.

COLLAGEN DEGRADATION AND VENTRICULAR DILATATION

Experimentally induced collagen degradation in normal myocardium has been reported to cause ventricular enlargement and increased chamber compliance [14, 15]. Also, an acutely induced but sustained increase in ventricular volume secondary to the creation of an infra-renal abdominal aorta-vena cava fistula is associated with a significant activation of the myocardial collagenase system [16]. Within 12 hrs of initiating the volume overload condition, collagenase activity was significantly elevated by 54% relative to the control activity level. Over the next 5 days of volume overload, collagenase activity was further increased to levels that were 86% greater than control levels and there was a consequent significant reduction (40%) in ventricular collagen concentration. Subsequently, collagenase activity declined to a level which was 33% above control collagenase activity and remained at this value for the remainder of the study period (i.e., 8 weeks). The reduction in collagen concentration was accompanied by a significant dilatation of the LV as evidenced by a significant shift to the right of the LV diastolic pressure-size relationship. That is, for any given diastolic pressure, LV volume was significantly greater than that in aged-matched controls. Preliminary data from our laboratory also indicate that activation of LV collagenase occurs in pregnant rats following a much smaller and more gradual chronic increase in circulating blood volume.

A similar ventricular remodeling that is preceded by an increase in collagenase activity occurs in diseased or injured myocardium. Within 3 hrs after an experimental infarction there is a two-to threefold increase in collagenase activity and a 50% reduction in collagen content in the infarcted region. Also, the infarcted myocardium had an inadequate collagen network and thinned considerably [17, 18]. Similarly in stunned myocardium there is a rapid loss of ultrastructural collagen [19, 20] which is preceded by a 74% increase in collagenase activity [20]. Recently Reddy *et al.* [21] compared collagenase activity in endomyocardial biopsy tissue obtained from patients with end-stage dilated cardiomyopathy and from post-transplant patients with presumably normal hearts. Collagenase activity in the cardiomyopathic hearts was increased eight-fold above that in the normal hearts. Evidence of collagen degradation in dilated cardiomyopathic hearts was provided in another report by Weber *et al.* [22]. Thick coiled perimysial fibers were rare and numerous widened interstitial spaces were present with conspicuous reduction or disruption of lateral collagen connections between muscle fibers. As expected, the cardiomyopathic LVs were significantly dilated and the LV walls were thinner than normal. Also, LV shape of the diseased heart was more spherical than normal [21].

The above results, while indicating a role for enhanced collagenase activity in the progressive dilatation associated with cardiomyopathy, represent data after the fact and

provide no insight into the temporal relation between collagenolysis and ventricular dilatation in diseased or injured hearts. For such information we have utilized the cardiomyopathic Syrian hamster. This animal model of dilated cardiomyopathy has the advantages of a predictable pathophysiologic course which includes progressive ventricular enlargement and heart failure. The disease process occurs in four histological and clinical phases: prenecrotic, necrotic, hypertrophic and terminal [22]. During the first phase (i.e., < 45 days of age) the hamster's myocardium is normal. The necrotic phase lasts until 120 days of age and is characterized by the occurrence of multiple areas of focal myocytolytic necrosis in the myocardium. Towards the end of the necrotic phase, healing of the necrotic areas is essentially complete. The hypertrophic compensated phase continues until the heart begins to fail due to progressive dilatation and wall thinning around 250 days of age. In the terminal stage, congestive heart failure is clinically evident.

The temporal relationship between myocardial collagenase activity, collagen concentration and ventricular dilatation was recently examined in cardiomyopathic hamsters of several ages and compared to age-matched golden Syrian hamsters [15]. In contrast to an age-invariant collagenase activity in the control group, collagenase activity in the cardiomyopathic hamster was found to progressively increase with age, and at all ages greater than 150 days, this activity was significantly greater than the control value. A significant progressive decline in collagen volume fraction (CVF) and ultrastructural collagen occurred at ages greater than 210 days. At 240 and 300 days, the LV wall became notably thinner. Thus, in the cardiomyopathic hamster, there is a continual increase in collagenase activity with age such that a point is reached where collagen degradation exceeds collagen synthesis resulting in an inadequate supportive interstitial collagen matrix. The fact that this occurs close to the age where significant ventricular dilatation and wall thinning occur is indicative of a strong causal relationship between collagenase activity and ventricular remodeling.

It is not known whether the increase in collagenase activity and the ensuing ventricular remodeling is preventable. However, it should be noted that chronic therapy with an angiotensin converting enzyme (ACE) inhibitor has been shown to attenuate progressive ventricular enlargement following experimental myocardial infarction [23]. In addition, administration of quinapril to cardiomyopathic hamsters from 180 to 300 days of age prevented ventricular dilatation and prolonged survival time by 33% [24]. Similar efficacious results were obtained in human clinical trials with chronic ACE inhibitor treatment [25, 26]. Patients receiving ACE inhibitors experienced less ventricular enlargement and fewer deaths attributed to heart failure. Furthermore, LV shape of the patients at greatest risk for enlargement remained normal with ACE inhibition while patients receiving placebo had ventricles which became progressively more spherical [27]. The influence of ACE inhibitors on collagenase activity, be it direct or indirect, remains to be determined.

CONCLUSION

Abnormally increased myocardial collagenase activity, either experimental or as a result of cardiac disease, is strongly correlated with collagen degradation and ventricular wall thinning with dilatation and sphericalization.

Acknowledgements

This work was supported in part by Grants from NHLBI (# RO1-HL-46461), American Heart Association (# 901397) and American Heart Association, Missouri Affiliate (# 93-GS-016).

DISCUSSION

Dr. P.J. Hunter: In your SEM measurements of ultrastructural collagen, are you able to distinguish between the relative degradation of endomysial and perimysial collagen? This seems to be important in view of the fact that they have very different functional roles in the mechanical behavior of the ventricle.

Dr. J.S. Janicki: At a magnification of x4000 we are primarily looking at that portion of the collagen matrix which surrounds myocytes, as well as the collagen struts which connect myocytes to neighboring myocytes and capillaries. That is, we are focused in our SEM analysis on the endomysial components of the myocardial fibrillar collagen matrix which we feel are very important determinants of the mechanical behavior of the ventricle.

Dr. B. Rabinowitz: Your cardiomyopathic human and Syrian hamster results are the result of a chronic or slow remodeling process, and tell us something about end stage heart failure. In contrast, the effect of angiotensin converting enzyme (ACE) inhibitors on remodeling after infarction are related to an acute and rapid type of remodeling. Are there differences between these two types of remodeling? Are there data on the collagen matrix post infarction, either in experimental models or in human studies?

Dr. J.S. Janicki: There are two phases of remodeling which occur following myocardial infarction. There is an acute phase where dilatation and hypertrophy are observed, and there is a chronic phase where the ventricle continues to dilate beyond that seen in the acute phase and wall thinning occurs. The study I refer to focused on the long term remodeling phase [Pouleur H, *et al. Circulation.* 1993:88;481–491]. The data were obtained shortly after infarction (baseline) and one year after therapy. As far as what happens to collagen immediately after infarction, it has been shown that in the area that has been infarcted, a major portion of that collagen disappears. In the border zone there is also evidence of collagen degradation. In the remote, non–infarcted myocardium, the collagen remains normal.

Dr. G. Kessler–Icekson: In your model of volume overload, when you have activation of collagenase, is it newly formed collagenase or preexisting collagenase? The second question concerns the beneficial effects of ACE inhibitor on the diastolic pressure–volume relationship. Cell culture studies indicate that angiotensin II promotes collagen synthesis and reduces collagenase synthesis. Accordingly, one would expect ACE inhibition to decrease collagen synthesis and perhaps increase collagenase synthesis. Is this what happens *in vivo*?

Dr. J.S. Janicki: The results of Pouleur *et al.* [*ibid*] regarding long–term ACE inhibitor therapy indicated a tendency for ACE inhibition to prevent ventricular dilatation and a decrease in ventricular stiffness. From these observations one could hypothesize that ACE inhibition prevented collagen from being degraded. As I pointed out in the proposed model of progressive ventricular dilatation following injury, this could be related to the ability of ACE inhibitors to lower preload and thereby prevent a stretch–related increase in collagenase activity. Thus, in this case, it does not appear that one can extrapolate cell culture findings to the *in vivo* situation. Regarding your first question, the increase in collagenase activity appears to be the result of activation of existing latent collagenase as opposed to the synthesis of new collagenase. This statement is based on the fact that there is a generous amount of latent collagenase normally present in the myocardium and that, in the fistula model of ventricular volume overload, a significant increase in collagenase activity was observed as early as 12 hours after initiation of the overload condition. Another interesting observation in the fistula model concerned the collagenase activity in the right ventricle. No change in collagenase activity was observed here, even though the right ventricle was also markedly distended in this biventricular volume overload model. This indicates that perhaps the end diastolic pressure and not the end diastolic volume is responsible for the activation of myocardial collagenase.

Dr. T. Arts: There is a large gradient in deformation across the wall, i.e, deformation in the endocardium is much greater than deformation in the epicardium. Were you able to find transmural gradients in collagenase activity?

Dr. J.S. Janicki: We have not looked at that. However, it occurred to me that this is something we should do. It would not be possible to look at collagenase activity transmurally, but instead we could assess whether there is a trend for collagen degradation to be greater in the endocardial region.

Dr. W. Barry: In your biopsy specimens from the patients with dilated cardiomyopathy, did you assess them with your ultrastructural grading technique?

Dr. J.S. Janicki: No. We have tried to assess collagen concentration in endomyocardial biopsies, but in general the results were too variable. From this experience we concluded that the biopsy tissue samples are too small to accurately determine collagen concentration that is representative of the rest of the myocardium. Furthermore, since we only received one sample of biopsy tissue per patient for research purposes, we decided to use it solely for the collagenase activity determination.

REFERENCES

1. Ertl G, Gaudron P, Hu K. Ventricular remodeling after myocardial infarction; experimental and clinical studies. *Basic Res Cardiol.* 1993;88:(Suppl. 1)125–137.
2. Caulfield JB, Borg TK. The collagen network of the heart. *Lab Invest.* 1979;40:364–372.
3. Robinson TF, Cohen–Gould L, Factor SM. The skeletal framework of mammalian heart muscle: arrangement of inter– and pericellular connective tissue structures. *Lab Invest.* 1983;49:482–487.
4. Woolley DE. Mammalian collagenases. In: Piez K, Reddi AH, eds. *Extracellular Matrix Biochemistry*, New York: Elsevier, 1984; 119–158.
5. Woessner JF Jr. Matrix metalloproteinases and their inhibitors in connective tissue remodeling. *FASEB J.*. 1991;131:2145–2154.
6. Miller EJ, Harris ED Jr, Chung E, Finch JE, McCroskery PA, Butler WT. Cleavage of types II and III collagens with mammalian collagenase: site of cleavage and primary structure at the NH_2–terminal portion of the smaller fragment released from both collagens. *Biochem.* 1976;15:787–792.
7. Hofmann H, Fietzek PP, Kühn K. The role of polar and hydrophobic interactions for the molecular packing of type I collagen. *J Mol Biol.* 1978;125:137–165.
8. Sakai T, Gross J. Some properties of the products of reaction of tadpole collagenase with collagen. *Biochemistry.* 1967;6:518–528.
9. Montfort I, Pérez–Tamayo R. The distribution of collagenase in normal rat tissues. *J Histochem Cytochem.* 1975;23:910–920.
10. Tyagi SC, Matsubara L, Weber KT. Direct extraction and estimation of collagenase(s) activity by zymography in microquantities of rat myocardium and uterus. *Clin Biochem.* 1993; 26:191–198.
11. Tyagi SC, Ratajska A, Weber KT. Myocardial matrix metalloproteinase(s): localization and activation. *Mol Cell Biochem.* 1993;126:49–59.
12. Bonnin CM, Sparrow MP, Taylor RR. Collagen synthesis and content in right ventricular hypertrophy in the dog. *Am J Physiol.* 1981;241:H708–H713.
13. Laurent GJ, Sparrow MP, Bates PC, Millward DJ. Turnover of muscle protein in the fowl: collagen content and turnover in cardiac and skeletal muscles of the adult fowl and the changes during stretch–induced growth. *Biochem J.* 1978;176:419–47.
14. Caulfield JB, Norton P, Weaver RD. Cardiac dilatation associated with collagen alterations. *Mol Cell Biochem.* 1992;118:171–179.
15. Janicki JS, Tyagi SC, Matsubara BB, Campbell SE. Structural and functional consequences of myocardial collagen remodeling. In: Hori M, Maruyama Y, Reneman RS (eds). *Cardiac Adaptation and Failure.* Tokyo: Springer–Verlag, 1994; 279–289.
16. Henegar JR, Janicki JS. Temporal response of collagenase activity during chronic ventricular volume overload in the rat. *Circulation.* 1994;90:I–262.

17. Takahashi S, Barry AC, Factor SM. Collagen degradation in ischemic rat hearts. *Biochem J.* 1990;265:233–241.
18. Sato S, Ashraf M, Millard RW, Fujiwara H, Schwartz A. Connective tissue changes in early ischemia of porcine myocardium: an ultrastructural study. *J Mol Cell Cardiol.* 1983;15:261–267.
19. Zhao M, Zhang H, Robinson TF, Factor SM, Sonnenblick EH, Eng C. Profound structural alterations of the extracellular collagen matrix in postischemic dysfunctional ("stunned") but viable myocardium. *J Am Col Cardiol.* 1987;10:1322–1334.
20. Charney RH, Takahashi S, Zhao M, Sonnenblick EH, Eng C. Collagen loss in the stunned myocardium. *Circulation.* 1992;85:1483–1490.
21. Reddy HK, Tyagi SC, Tjahja IE, Voelker DJ, Campbell SE, Weber KT. Enhanced endomyocardial collagenase activity in dilated cardiomyopathy: a marker of dilatation and architectural remodeling. *Circulation.* 1993; 88:I–407.
22. Gertz EW. Cardiomyopathic Syrian hamster: a possible model of human disease. *Prog Exp Tumor Res.* 1972;16:242–260.
23. Pfeffer MA, Pfeffer JM, Lamas GA. Development and prevention of congestive heart failure following myocardial infarction. *Circulation.* 1993;87:IV120–IV125.
24. Haleen SJ, Weishaar RE, Overhiser RW, Bousley RF, Keiser JA, Rapundalo SR, Taylor DG. Effects of quinapril, a new angiotensin converting enzyme inhibitor, on left ventricular failure and survival in the cardiomyopathic hamster. *Circ Res.* 1991;68:1302–1312.
25. The SOLVD Investigators. Effect of enalapril on mortality and the development of heart failure in asymptomatic patients with reduced left ventricular ejection fractions. *New Engl J Med.* 1992;327:685–691.
26. Pfeffer MA, Braunwald E, Moye LA, Basta L, Brown EJ Jr, Cuddy TE, Davis BR, Geltman EM, Goldman S, Flaker GC, *et al.* Effect of captopril on mortality in patients with left ventricular dysfunction after myocardial infarction: results of the survival and ventricular enlargement trial. *New Eng J Med.* 1992;327:669–677.
27. Lamas GA, Pfeffer MA. Left ventricular remodeling after acute myocardial infarction: clinical course and beneficial effects of angiotensin–converting enzyme inhibition. *Am Heart J.* 1991;121:1194–1202.

Analysis and Modeling:

From Microstructure to Macro-Performance

CHAPTER 25

MECHANISMS OF ENDOCARDIAL ENDOTHELIUM MODULATION OF MYOCARDIAL PERFORMANCE

Puneet Mohan, Stanislas U. Sys, and Dirk L. Brutsaert[1]

ABSTRACT

The endocardial endothelium (EE) modulates the performance of the subjacent myocardium and plays an important role in regulation of cardiac function. This modulation has been confirmed in a number of different species and in both *in vitro* and *in vivo* conditions. The mechanisms of EE modulation of myocardial performance are still under investigation and the possibilities include the role of EE as a transendothelial physico-chemical barrier and/or the release of various chemical messengers by the EE.

INTRODUCTION

Modulation of the cardiac pump function *in vivo* is a complex phenomenon. It is regulated by both intrinsic and extrinsic factors viz. loading condition and the Frank-Starling mechanism, coronary perfusion and the neurohumoral system. There is now compelling evidence to suggest that the endothelium, both endocardial and coronary vascular, also plays an important role in regulation of cardiac function. The endocardial endothelium (EE), which lines the inner wall of the heart, was for the first time shown by Brutsaert *et al.* to modulate the peak contractile performance and relaxation of the subjacent myocardium in isolated papillary muscles [1]. Selective destruction of the EE in isolated papillary muscles, with no morphological or functional evidence of myocardial damage, resulted in an immediate and irreversible abbreviation of twitch duration associated with concomitant decrease in peak force and twitch shortening with no significant changes in the early phase of the twitch. In other words, presence of an intact EE has a twitch prolonging and a positive inotropic effect in terms of contractile performance. This pattern of change in

[1]Department of Physiology and Medicine, University of Antwerp, Groenenborgerlaan 171, B-2020 Antwerp, Belgium.

Molecular and Subcellular Cardiology: Effects of Structure and Function
Edited by S. Sideman and R. Beyar, Plenum Press, New York, 1995

performance of myocardium is different from other known positive inotropic conditions (sympathetic stimulation, increased $[Ca^{2+}]_0$, frequency and post-extrasystolic potentiation), while it resembles the increased isometric twitch performance induced by increasing resting muscle length along the ascending limb of the length tension relationship [2, 3]. This unique endocardial modulation of myocardial contraction has been subsequently confirmed by other investigators in a number of different species and conditions [4–9]. These observations were further extended to *in vivo* conditions where selective EE damage by intracavitary ultrasound irradiation of the ventricle in a dog resulted in a decreased ventricular ejection duration and earlier fall of isovolumic pressure during ventricular relaxation [10]. Similar results have been observed in Langendorff-perfused ferret hearts with selective endocardial removal by brief detergent treatment [11]. Several substances including atrial natriuretic peptides [12], alpha 1 agonists [13], vasopressin [14], serotonin [5-HT] [14], and aggregating platelets [15] exert their inotropic action on the myocardium through the EE. Recently, coronary vascular endothelium has also been shown to similarly modulate the contraction of cardiac muscles and the two effects may be complimentary [16].

The present body of evidence thus suggests that all endothelial cells, irrespective of origin, endocardial or coronary (micro)vascular, directly contribute to control or modulation of the contractile state of subjacent cardiomyocytes. Therefore, existence of an endothelium-mediated regulation of cardiac performance may be postulated. The EE occupies a large surface area due to prominent trabeculations of the cavitary side of the ventricular wall as well as the presence of numerous microvilli and invaginations in EE cells. The EE, by virtue of its unique position, comes in contact with all the circulating blood at least once every 2 min, and this contact may increase by a factor of 4–5 during exercise. This intimate contact between the circulating blood and the EE may help in accomplishing the postulated autoregulation of cardiac performance through the EE by feedback and direct interaction with the superfusing blood.

MECHANISMS OF EE MODULATION OF MYOCARDIAL PERFORMANCE

The presence of an intact EE increases the contractile state of the subjacent myocardium by prolonging the isometric twitch with concomitant increase in peak twitch tension [17]. As mentioned earlier, this pattern of contraction induced by the EE is different from other positive inotropic interventions. The endocardial effects do resemble the increased isometric twitch performance induced by increasing resting muscle length along the ascending limb of the length-tension relationship [2, 3]. Because of this similarity between changes in resting muscle length and those induced by the EE, it was postulated that EE-dependent changes in contraction pattern might also be mediated through increased sensitivity of the myofilaments to the intracellular Ca^{2+} concentration ($[Ca^{2+}]_i$) [2, 3]. This hypothesis was supported by experiments where simultaneous measurements of aequorin-induced light signals and isometric twitch force were performed in isolated cardiac muscles from ferret hearts [9]. The results demonstrated that EE removal decreased peak developed tension with early onset of relaxation without corresponding changes in the intracellular Ca^{2+} transient. This suggested that the intact EE does indeed enhance myocardial performance by increasing myofilament Ca^{2+} sensitivity. The different steps involved in the EE-mediated events linking function of the EE cells to the myofilaments are, as yet, only at a speculative stage.

The role of EE acting as a physical barrier to inhibit penetration of certain agents into the myocardium cannot explain the modulation of inotropic effects of various substances by the EE. However, analogous to the vascular endothelial regulation of smooth

muscle tone, the EE could influence the myocardial contraction either by the establishment of transendothelial physicochemical control, by release of various chemical messengers, or by a combination of both [17].

Presence of long intercellular clefts and numerous tight and gap junctions in the EE suggest that EE may act as a selective physico-chemical barrier and regulate the homeostasis of certain ions in the interstitial fluid around the myocyte. Changes in the transendothelial permeability will cause changes in the concentration of ions and substances in the interstitial fluid. A transendothelial electrochemical potential would require a strong electrochemical gradient for certain ions as well as a selective boundary barrier. The basement membrane of the subendocardium has a large number of charged (mainly anionic) sites and may thus limit permeability to certain ions [17, 18]. Although there is some data regarding selective permeability to certain ions, like the K^+ ions in vascular endothelium, information about permeability of the EE is still unclear. In a pioneering study of electrophysiological properties of cultured pig endocardial cells, Fransen *et al.* [19] described inwardly and outwardly rectifying K^+ currents, similar to those described in vascular endothelial cells. In addition, an outwardly rectifying Cl-current, ATP-dependent and volume-activated, was observed in endocardial cells. The authors suggested that volume-activated Cl-channels in the endocardial cells may be involved in cellular volume or stretch activation.

It is, however, unclear how a transendothelial electrochemical potential would lead to a series of EE-derived events leading to changes in myofilament $[Ca^{2+}]_i$ sensitivity. It has also been suggested that abbreviation of contraction due to damaging of EE is not associated with significant changes in action potential duration of subjacent myocardium [20]. These observations do not preclude, however, the existence of functional electrical coupling between the EE and subjacent myocardium [18]. In vascular endothelial cells, transmembrane potentials and various Ca^{2+} and K^+ channels and K^+ currents have been demonstrated. If EE cell have similar electrophysiological properties, it still has to be established if the individual EE cells would establish a transcellular electrical potential difference across the whole EE. In spite of the presence of numerous gap junctions between EE cells [18], direct junctions between EE cells and subjacent cardiomyocytes have not been detected.

In the early experiments, where EE modified the inotropic response to various substances and cells, it was hypothesized that the EE may release myocardial contraction (MCF) and relaxation (MRF) factor(s) in response to different inotropic stimuli. The EE-dependent positive inotropic effect of low concentration of phenylephrine [13] would be due to the release of MCF from the EE, whereas the EE-dependent atrial natriuretic peptide-induced early relaxation and fall in peak twitch tension [12] would result from release of MRF from the EE. The responses to other substances like serotonin [15], vasopressin [14], angiotensin [21] and endothelin [5] may be thus explained by alterations in the release and/or balance of MCF and MRF in the EE. Recently, a change in contractility of isolated trabecula by superfusion with coronary venous effluent from an isolated perfused heart was observed which depended on the degree of oxygen saturation of the effluent and the rate of coronary flow [6]. The response was altered when the EE was damaged and was completely eliminated when the endothelial cells in both the perfusing heart and the superfused trabecula were damaged. The results, thus, suggested that the effluent contained "pre-endothelial factors" which signal the EE cells on the trabecula to release "endothelial factors" which alter the contractility of the trabecula. This would also suggest the existence of a sensory role for the EE for various substances or cells and maybe even for changes in cavitatory volume. The presence of several types of receptors in EE, e.g., receptors for atrial natriuretic peptide, supports this hypothesis. Thus the EE can be

postulated to play an important role in signal transduction in the subjacent myocyte and thereby regulate its contractile performance.

There is now experimental evidence, especially from bioassay experiments, that EE cells release chemical mediators which determine the myocyte inotropic response. Effluent from superfused cultured porcine EE cells was bioassayed with endothelium-denuded pig coronary artery rings or with EE-denuded ferret papillary muscles [22, 28]. The effluent caused vasodilation of the de-endothelized coronary artery. This response could be potentiated in the presence of super oxide dismutase and catalase while it was blocked by hemoglobin and inhibitors of nitric oxide (NO) synthase. Thus cultured endocardial cells released an endothelial-derived relaxing factor (EDRF) like substance. The demonstration of Ca^{2+}-dependent NO synthase in EE cells [23] supports the contribution of NO/EDRF in EE modulation. Release of prostacyclin from the EE may also play an important role in the modulation of myocardial function. Recently production of both prostacyclin and prostaglandin E_2 from cultured bovine right and left ventricular EE cells was reported. The EE cells also express the mRNA for endothelin and have been shown to release endothelin in bioperfusion experiments. In addition, release of a unique "myofilament desensitizing factor" from cultured EE cells has also been reported [24]. Thus, tonic release of these biochemical modulators from the EE may account for its regulation of myocardial performance.

ROLE OF NO-cGMP IN EE MODULATION

Evidence for a role of NO in EE modulation came initially from experiments utilizing substance P, a known stimulant of NO release from vascular endothelium. In isolated ferret papillary muscles with intact EE, substance P induced an abbreviation of twitch contraction and decrease in peak performance that was similar in pattern to EE removal [22]. This effect required the presence of intact EE and was inhibited by hemoglobin, an inhibitor of NO activity, thus suggesting that it was mediated by the release of NO from the EE. Continuous basal release of EDRF by EE cells from isolated cardiac valves has also been demonstrated [25]. In the isolated papillary muscle with intact EE, a variety of agents that elevate intracellular cGMP either directly, like atrial natriuretic peptide [12], or through release of NO like sodium nitroprusside [12, 22], induce similar effects on myocardial performance as substance P. An analogue of cGMP, 8-bromo cGMP, at relatively high concentrations also causes a similar abbreviation of twitch associated with some decrease in contractile performance [26, 27]. These early experiments focused on the similarity of the pattern of twitch abbreviation and concomitant decrease in twitch tension observed with selective damaging of EE, and on measures that elevated myocardial cGMP concentration. There was, however, no evidence as to how the EE regulated the myocardial cGMP concentration. Furthermore, the inotropic effects of NO-cGMP, as described in the literature, could not fully explain how their basal release would account for the unique positive inotropic effect associated with prolongation of the twitch duration, imparted by the presence of intact EE.

Recently, in a preliminary report, we reported for the first time, a novel concentration-dependent positive inotropic effect of NO-releasing nitrovasodilators in muscles with damaged EE which contrasted with their negative inotropic effect in muscles with intact EE; both of these opposite responses were mediated by cGMP [28]. Administration of 8-bromo cGMP, a cGMP analogue, induced a biphasic effect on myocardial performance; addition of low concentrations of 8-bromo cGMP induced a positive inotropic effect while subsequent higher concentrations had a negative inotropic effect. Damaging

the EE shifted the exogenous cGMP concentration–tension curve to the right. These results suggest that the inotropic response to NO and cGMP is modulated by the status of the EE. Although the precise evidence for the nature and magnitude of myocardial cGMP regulation by EE is lacking, we have hypothesized from these observations that an intact EE would induce higher cGMP level in the underlying cardiomyocytes due to basal NO release while damaging the EE would lower the cGMP level. Thus, in the presence of an intact EE, nitrovasodilators or exogenous nitric oxide would cause a further elevation in already high baseline myocardial cGMP levels, leading to a negative inotropic response. A similar increase in the myocardial cGMP by exogenous nitric oxide donors from a lower baseline myocardial cGMP level, in the case of damaged or dysfunction EE, would result in a positive inotropic response. Accordingly, response to exogenous cGMP or agents causing elevation in cGMP may depend on the basal cGMP levels which in turn may be determined by the state of the overlying EE. In blood vessels, tissue cGMP levels have been frequently reported to be significantly higher in endothelium–intact than in denuded vessels (for references see [29]), although this feature has not yet been confirmed in the cardiac tissue [22].

The positive inotropic effect associated with relatively smaller elevations in cGMP levels was further confirmed by a study examining the effects of a cGMP analogue in *in vivo* conditions [30]. In acutely instrumented cats, administration of dibutyryl cGMP, a cGMP analogue, in the absence of changes in ventricular loading conditions, caused a positive inotropic, effect with no effect on the parameters of relaxation. cGMP was also suggested to account for at least part of the positive inotropic effect induced by acetylcholine in isolated papillary muscles [31]. On the basis of these results, we suggest that basal release of NO from the EE, and the consequent elevation in cGMP in the cardiomyocyte confers a positive inotropic effect. This would also suggest that an NO synthase inhibitor–induced cardiac depression seen in animals [32–35] and in human volunteers [36] could be due to a significant reduction in myocardial cGMP.

We can only speculate as to how cGMP mediates the positive inotropic effect. Based on current knowledge, the response to cGMP could be mediated by cyclic ADP ribose (cADPR), a recently described new second messenger which stimulates release of Ca^{2+} from intracellular stores through the ryanodine receptor in sea urchin eggs [37–40]. It has also been reported that cADPR increase the open probability of cardiac ryanodine–sensitive Ca^{2+} channels and thus cADPR can trigger the release of Ca^{2+} from the sarcoplasmic reticulum in cardiac cells [41]. In sea urchin eggs, cGMP–induced Ca^{2+} transient was mediated through ryanodine receptors by stimulation of cADP–ribosyl cyclase [42]. Stimulation of guanylate cyclase by NO causes elevated cGMP which stimulates cGMP–protein kinase (PKG). PKG phosphorylates ADP–ribosyl cyclase, enhancing the synthesis of cADPR from NAD^+, which would release calcium from the sarcoplasmic reticulum through ryanodine receptors [38]. The overall result would thus be an increase in cytosolic calcium concentration that could explain the positive inotropic effect of basal NO and cGMP.

Another possible mechanism underlying the inotropic effects of NO and cGMP could involve modulation of cGMP–dependent cAMP phosphodiesterase by cGMP. The evidence for this mechanism comes from electrophysiology studies on isolated cardiomyocytes. In isolated guinea pig ventricular myocytes, a stimulatory effect of relatively low concentrations of cGMP (0.1 to 10 fmol/L) on cAMP–elevated L–type calcium channel current (I_{Ca}) has been reported [43], leading to an increase in Ca^{2+} availability. Higher concentrations of cGMP, 8–bromo–cGMP, or cGMP–dependent protein kinase (cGMP–PK) had either no effect or reduced I_{Ca}. It was suggested that this stimulation of cAMP–elevated I_{Ca} by low concentrations of cGMP was due to participation of cGMP–inhibitable cAMP–phosphodiesterase, whose presence in the heart has been well documented [44, 45].

The higher concentrations of cGMP have been reported to inhibit cAMP-elevated I_{Ca} via cGMP-PK in mammalian myocytes [46]. Intracellular perfusion of cGMP-PK fragment caused a similar inhibition of I_{Ca} [47]. In addition to its direct effects on Ca^{2+} channel, cGMP-PK may also decrease the Ca^{2+} sensitivity of the myofilaments through phosphorylation of the inhibitory subunits of troponin [48]. In isolated cardiac myocytes, administration of relatively high concentrations of 8-bromo cGMP (50 fmol/L) was associated with a negative inotropic effect which was mediated by cGMP-PK-induced decreased Ca^{2+} sensitivity of the myofilament [27]. Recently, a NO-mediated biphasic response on stimulated I_{Ca} was reported in frog ventricular myocytes with administration of increasing concentrations of SIN-1 [49]. All the responses to SIN-1 were inhibited by methylene blue and LY83583, another inhibitor of the guanylate cyclase. The authors suggested that the stimulatory effect of NO donors on I_{Ca} resulted from an inhibition of the cGMP-inhibitable cAMP-phosphodiesterase while the inhibitory response was due to activation of the cGMP-stimulated cAMP-phosphodiesterase, both linked to the activation of guanylate cyclase. A similar stimulatory and inhibitory effect of SIN-1 on I_{Ca} was also reported by another group [50] and both effects were said to be mediated by cGMP-PK.

To summarize, EE probably regulates basal intracellular cGMP concentration in cardiomyocytes by basal release of NO. Tonic or basal release of NO from the EE and consequent elevation in cardiomyocyte cGMP concentration, by virtue of its positive inotropic response, will thus be important in preserving cardiac function in physiological states. However, excess cGMP stimulation due to large amount of NO released from nitrovasodilators or from inducible NO-synthase in pathological states would cause a negative inotropic effect and contribute to the deterioration of cardiac function.

ROLE OF PROSTAGLANDINS IN EE MODULATION

As in vascular endothelium, release of prostacyclin (PGI2) from the EE may also play an important role in the modulation of myocardial function. Tissue cyclo-oxygenase has been found to be twice as high in the endocardium as compared to the myocardium and is located specifically in the endothelial fraction [51]. EE from isolated cardiac valves [25], as well as valvular EE cells in culture [52] produce significant amounts of prostacyclin. Production of both prostacyclin and prostaglandin E_2 from cultured bovine right and left ventricular EE cells were reported with prostacyclin production 10 times greater than prostaglandin E_2 [53]. It is also of interest that EE cells have been reported to produce far larger amounts of prostacyclin than vascular endothelial cells [54].

The role of endogenous prostaglandins, released from the EE in large amounts, has been difficult to explain in the past. Previous studies utilizing exogenous prostaglandins to examine their direct myocardial actions and the underlying mechanisms, mainly cAMP-mediated, were unclear; the responses ranged from increased contractility with prostacyclin and prostaglandin E_2 in isolated atria, to no effect or negative inotropic effect in isolated papillary muscles.

We recently postulated that although endogenous NO and prostaglandins released from the EE may significantly contribute to the endothelial modulation of myocardial function, their mutual interaction may be at least as important. In isolated papillary muscles, we have demonstrated that the stimulation of endogenous NO and prostaglandin (prostacyclin and prostaglandin E_2) production results in a qualitatively different contractile response to one factor, depending on the stimulation or inhibition of the release of the other factor from the EE. While stimulation of endogenous NO release by substance P caused a negative inotropic effect with reduction of twitch duration, this effect of substance P was

not observed in the presence of arachidonic acid. The negative inotropic effect of substance P was preserved in presence of the cyclo-oxygenase inhibitor, indomethacin. Stimulation of endogenous prostaglandin release thus counteracted effects of endogenous NO stimulation. On inhibition of the basal release of NO by incubation with L-NOARG, administration of arachidonic acid in presence of L-NOARG had a positive inotropic effect with prolongation of twitch duration, while indomethacin had an opposite effect. The basal release of prostaglandins from the EE thus appears to prolong the twitch duration and may increase peak twitch tension, particularly when the concomitant release of NO is suppressed or diminished. Thus, basal release of NO and prostaglandins, similar to the regulation of vascular tone in blood vessels, may also maintain myocardial performance in basal conditions and the net balance of NO and prostaglandin effects may determine the basal state of myocardium, reflecting the interaction of the different second messenger systems in regulation of myocardial function.

ROLE OF ENDOTHELIN IN EE MODULATION

The demonstration of mRNA for endothelin-1 in the EE [56] and its release from EE [56, 57] suggests an important role for endothelin-1 in the positive inotropic effect of intact EE. Administration of exogenous endothelin-1 has been associated with a large positive inotropic effect in various myocardial preparations. This, however, is generally not associated with prolongation of the twitch duration at low concentrations of endothelin. Thus, endothelin would be an important contributor to the positive inotropic effect but probably not to the twitch prolonging effect of intact EE. It has been suggested recently that endothelin may account for as much as 50% of the positive inotropic effect of EE [57].

We thus propose that the unique positive inotropic effect imparted by an intact EE associated with twitch prolongation may be explained, at least partly, by the net effects of basal release of endogenous NO, prostaglandins and endothelin and their mutual interactions. The relative contribution and release of these mediators from the EE may vary according to the circumstances. EE apparently also functions as a sensory organ and could thereby regulate the release of these mediators individually in order to maintain homeostasis. There is also some emerging evidence from our lab that EE may also mediate its effect through regulation of ionic currents (mainly Cl-) in the cardiomyocyte. This mechanism may independently, or synergistically with release of biochemical mediators, also play a significant role in modulation of myocardial performance by EE.

CONCLUSION

The mechanisms underlying the EE modulation of myocardial performance do not, as yet, fully explain the unique positive inotropic effect induced by the presence of an intact EE. While there is morphological evidence of an epithelial-like organization of EE in the form of long intercellular clefts, numerous gap and tight junctions, existence of transendothelial physicochemical barrier would also require a strong transcellular electrochemical gradient for certain ions. Direct junctions between EE cells and subjacent cardiomyocytes have also not been detected. The EE has also been shown to be capable of releasing NO, prostaglandins and endothelin. The myocardial effects of basal release of endogenous NO, prostaglandins and endothelin may partly explain the EE modulation. The

EE may thus maintain homeostasis by regulating the release of these biochemical mediators.

DISCUSSION

Dr. E.L. Ritman: All these magic things happen at the endothelium, but that is only a very small proportion of the cardiac wall and rather distant from much of the myocardium. You show a tremendous surface area of the endothelium, but also a rather intimate relationship with the underlying myocardium to some depth into the myocardium. What do you think is most important, the fact that this gives it a big surface area, or is it because of its intimate relation to some inner fraction of the myocardium? Is it the intimacy or is it the surface area that is important here?

Dr. D. Brutsaert: Both. The EE cells have many structural features of intense cell–to–cell communication, as, e.g., numerous gap junctions, emphasizing that activation of some endothelial cells may be quickly transmitted over large surface areas. On the other hand, the proximity to the subjacent myocytes also propagates local control. Moreover, we should keep in mind that the heart is unique by the fact that the entire circulating blood mass circulates through that cavity at least once every 2 min, whereas only 5% of this goes through the coronary circulation. The endocardium, with its tremendous surface, is probably involved in overall performance and overall coordination of performance as well as local control whereas the role of the endothelium in the myocardial microvasculature may be more local.

Dr. W. Barry: As you know, many substances which induce NO synthesis in isolated ventricular myocytes have been shown to not necessarily cause a direct negative inotropic effect but to blunt the positive inotropic effect of catecholamines, for example. I wonder if you have investigated whether there could be some basal catecholamine release in your intact muscles, the effects of which are being blunted by NO, perhaps produced by the EE. The second question is, since endothelin probably induces most of its inotropic effect by stimulation of sodium–hydrogen exchange, do sodium–hydrogen exchange inhibitors have any effect on the inotropic effects of the removal of the EE in your papillary muscle preparations.

Dr. D. Brutsaert: With respect to NO in isolated myocytes, most of these studies have used very high concentrations of NO or cGMP, where both agents become negative inotropic instead of positive inotropic as suggested by our observations at lower concentrations. With respect to possible interactions of NO with catecholamines, all our observations have also been confirmed in control groups under β–blockade. The interesting hypothesis concerning the contribution of sodium–proton exchanger is presently under investigation.

Dr. J. Janicki: We know that elevated levels of circulating angiotensin II will cause damage to arterial endothelial cells. Is this also the case for EE cells?

Dr. D. Brutsaert: Yes, if isolated papillary muscles are exposed for, say, 30 min to high concentrations of angiotensin II (10^{-4} M) followed by wash, the endocardium is damaged. It is not as intensively damaged as after exposure to serotonin for example. Serotonin fully destroys the endocardium very selectively after 10–15 min exposure at much lower concentrations.

Dr. J. Janicki: I wonder about angiotensin converting enzyme (ACE) inhibitors which are known to increase bradykinin and prostacyclin levels. Do you think that the mechanism that you described would partly explain the efficacious aspects of ACE inhibition?

Dr. D. Brutsaert: Possibly yes. We have previously reported that there is an intimate functional interaction between angiotensin at the level of the endocardium and the action of prostacyclin.

More recent data on the inotropic action of prostacyclin have now shown that both systems are indeed intimately connected to one another. Previously, we have not been able to show an inotropic response to prostaglandins, the data from literature being highly conflicting going from positive to nothing to negative inotropic responses. In order to unmask a positive inotropic effect by prostacyclin one must first inhibit the NO system, whereafter prostacyclin is manifested as a positive inotrope that closely interacts with the angiotensin system.

Dr. J. Bassingthwaighte: The question of the mechanism is evading me. Your hypothesis was that there is a connection between the EE and, through the subendocardial and vascular network, connections to the myocytes. Yet, in the dog heart, where you have made these observations, and in other hearts, the vascular endothelial connections to the EE are very rare. There are about 12 Thebesian veins per heart in the dog's left ventricle, quite different from the right ventricle, and the trabeculation is minor, relatively smooth left ventricular endocardium. So there has to be some other way. You can consider a number of other ways. One would be exudation or release of some substance from the endocardial endocardium, that is then delivered through the coronaries to the vascular endothelium. Or, alternatively, there are antidroml neural connections via the sympathetic system that permeates the whole heart and is parallel to every capillary. Alternatively, there is some mechanical connection, whereby you compromise the subendocardial myocardium and it inhibits contraction throughout the whole ventricle. But there has got to be some other way.

Dr. D. Brutsaert: Of course there may be additional ways. Yet, it is always appropriate to look at these questions from a phylogenetic or developmental point of view. For example, it would be interesting to see how the EE control system has developed from frog and fish heart and early embryonic mammalian hearts to large adult mammals and to see what is more important—the coronary system, which develops only late, or the EE system— and to what extent both may be complementary. Cardiac nerves are, embryonically speaking, late contributors to cardiac function; they follow the development of the coronary circulation. Hence, at first we just have myocardium merely covered by EE. Only subsequently do we see the development of the coronary circulation and the concomitant nerves. The Purkinje fiber network comes in last and lies immediately subjacent to the EE cells.

Coming back to the question as to how the substances—i.e., NO, PgI_2, Et—are being released from the endocardium and how they would affect the inotropic state of the myocytes, we know that these substances are being released both luminally and abluminally. The way of their inotropic action will of course largely depend on the half-life of the substances. For example, as NO has a half-life of only a couple of seconds, that substance will act predominantly through abluminal release. Prostacyclin is probably also active mainly through abluminal release, given its short half-life. As for endothelin, it may reach the myocardium both ways.

Dr. J. Bassingthwaighte: Have you tried this in autotransplanted hearts or otherwise denervated hearts or reserpine treated?

Dr. D. Brutsaert: Not yet.

Dr. J. Solaro: On the NO effects. You dwelled on the PDE as the mechanism through the cyclic G dependent PDE. Have you found some species variation in the effect which might give some clues as to mechanism and if you have thought about the role of kinase?

Dr. D. Brutsaert: Our observations were virtually the same in cats, rats and rabbits.

Dr. J. Solaro: If you inhibit PDE, I guess it depends on the types of PDE and their localization, but that might provide some clue as to what's going on here. There has been recent work by Fischmeister (Méry *et al.* [49]) on SIN-1 that has a positive and negative effect on calcium channels.

Dr. D. Brutsaert: Right. The interpretation given by Fischmeister [49] would be one possibility, i.e. that through either inhibition or activation of cyclic GMP-dependable-phosphodiesterase, inhibition or activation of cyclic AMP could either increase or decrease $[Ca^{2+}]_i$ through L-type calcium channels. Another possible explanation could be that the recently discovered C-ADP-ribose would act as second messenger. This novel pathway has been used recently to explain many of the NO activities in vascular endothelial cells. A c-ADP-ribose dependent mechanism has been invoked to explain why, e.g., NO contracts smooth muscle in the colon for example, and, by contrast, relaxes smooth muscle in vasculature.

Dr. H.E.D.J. ter Keurs: Basically, your quantification of the effects of the cyclic GMP shows a series of experiments. For example, in the study of acetylcholine, there is about an 80% increase of force development. That results in two questions. First, did you quantify the *in vivo* cat data and was there only a leftward shift or was there substantial increase in E_{max} of the left ventricle of the cat? The second question is, if there is such a large effect on papillary muscle properties in response to acetylcholine, what would be the cholinergic pathway in the daily life of that ventricle?

Dr. D. Brutsaert: With respect to the *in vivo* cat data, we were interested in the mere qualitative confirmation of the positive inotropic response to low concentrations of cGMP, sufficiently low in order for the loading conditions, i.e., ventricles, peak pressures, not to be affected. All the data were, therefore, obtained before peak pressure either dropped or end diastolic pressure went up. These *in vivo* data were rather difficult to quantify in terms of concentration response curves, as we did not know the exact tissue concentration and molarity. Hence, we were merely interested in the qualitative confirmation of the positive inotropic response of cGMP in *in vivo* conditions, where loading conditions were strictly controlled.

With respect to acetylcholine, we are still puzzled by the results. As can be seen from the data, the response is very complex. It is muscarinic, it is completely blocked after atropine, NO is not involved, and cyclic GMP is only partly involved. The latter observation is at present not well understood. Cyclic GMP is undoubtedly partly involved, as may e.g. prostacyclin.

Dr. H.E.D.J. ter Keurs: With respect to acetylcholine, which is the nerve fiber doing the trick in the ventricle?

Dr. D. Brutsaert: There are scarce parasympathetic nerves distributed in the ventricle. These nerves may perhaps be more important than we have thought so far. But how and to what extent acetylcholine release would participate in the interaction between the endothelial cells and the myocardium is indeed still an open question.

Dr. T. Arts: One of the points of discussion is how the signal comes to the myocardium. One hypothesis is based on a uniform activation of the whole cardiac muscle. The other one is that activation starts from the inside through some kind of diffusion from the endocardium and gradually reaches the outer side. A trick which you might use is to have a tool to determine transmural gradients in mechanics, which are related to torsional deformation and can be measured with MRI. You can perhaps separate a few mechanisms by just looking into transmural differences in mechanics.

REFERENCES

1. Brutsaert DL, Meulemans AL, Sipido KR, Sys SU. Effects of damaging the endocardial surface on the mechanical performance of isolated cardiac muscle. *Circ Res.* 1988;62:357-366.
2. Allen DG, Kentish JC. The cellular basis of the length-tension relation in cardiac muscle. *J Mol Cell Cardiol.* 1985;17:821-840.
3. Hibberd MG, Jewell BR. Calcium and length-dependent force production in rat ventricular muscle. *J Physiol Lond.* 1982;329:527-540.

4. Li K, Rouleau JL, Calderone A, Andries JL, Brutsaert DL. Endocardial function in pacing-induced heart failure in the dog. *J Mol Cell Cardiol.* 1993;25:529-540.
5. Li K, Stewart DJ, Rouleau J-L. Myocardial contractile actions of endothelin-1 in rat and rabbit papillary muscles. Role of endocardial endothelium. *Circ Res.* 1991; 69:301-312.
6. Ramaciotti C, McClellan G, Sharkey A, Rose D, Weisberg A, Winegrad S. Cardiac endothelial cells modulate contractility of rat heart in response to oxygen tension and coronary flow. *Circ Res.* 1993;72:1044-1064.
7. Ramaciotti C, Sharkey A, Mcclellan G, Winegrad S. Endothelial cells regulate cardiac contractility. *Proc Nat Acad Sci USA.* 1992; 89:4033-4036.
8. Shah AM, Smith JA, Lewis MJ. The role of endocardium in the modulation of contraction of isolated papillary muscles of the ferret. *J Cardiovasc Pharmacol.* 1991; 17(S3):S251-S257.
9. Wang JX, Morgan JP. Endocardial endothelium modulates myofilament Ca^{++} responsiveness in aequorin-loaded ferret myocardium. *Circ Res.* 1992; 70:754-760.
10. Gillebert TC, De Hert SG, Andries LJ, Jageneau AH, Brutsaert DL. Intracavitary ultrasound impairs left ventricular performance: presumed role of endocardial endothelium. *Am J Physiol.* 1992; 263:H857-H865.
11. Fort S, Lewis MJ, Shah AM. The role of endocardial endothelium in the modulation of myocardial contraction in the isolated heart. *Cardioscience.* 1993:4;217-223.
12. Meulemans AL, Sipido KR, Sys SU, Brutsaert DL. Atriopeptin III induces early relaxation of isolated mammalian papillary muscle. *Circ Res.* 1988; 62:1171-1174.
13. Meulemans AL, Andries LJ, Brutsaert DL. Endocardial endothelium mediates positive inotropic response to alpha1-adrenoreceptor agonist in mammalian heart. *J Mol Cell Cardiol.* 1990; 22:667-685.
14. Schoemaker IE, Meulemans AL, Andries LJ, Brutsaert DL. Role of the endocardial endothelium in the positive inotropic action of vasopressin. *Am J Physiol.* 1990; 259:H1148-1151.
15. Shah AM, Andries LJ, Meulemans AL, Brutsaert DL. Endocardium modulates inotropic response to 5-hydroxytryptamine. *Am J Physiol.* 1989; 257:H1790-H1797.
16. Li K, Rouleau JL, Andries LJ, Brutsaert DL. Effect of dysfunctional vascular endothelium on myocardial performance in isolated papillary muscles. *Circ Res.* 1993; 72:768-777.
17. Brutsaert DL, Andries LJ. The endocardial endothelium *Am J Physiol.* 1992; 263:H985-H1002.
18. Brutsaert DL. The endocardium. *Annu Rev Physiol.* 1989; 51:263-273.
19. Fransen PF, Demolder MJM, Brutsaert DL. Whole-cell membrane currents in cultured pig endocardial cells. *Am J Physiol.* 1994; in press.
20. Shah AM, Shattock MJ, Lewis MJ. Action potential duration and endocardial modulation of myocardial contraction. *Cardiovasc Res.* 1992;26:376-378.
21. Meulemans AL, Andries LJ, Brutsaert DL. Does endocardial endothelium mediate positive inotropic response to angiotensin I and angiotensin II? *Circ Res.* 1990; 66:1591-1601.
22. Smith JA, Shah AM, Lewis MJ. Factors released from endocardium of the ferret and pig modulate myocardial contraction. *J Physiol.* 1991; 439:1-14.
23. Schulz R, Smith JA, Lewis MJ, Moncada S. Nitric oxide synthase in cultured endocardial cells of the pig. *Br J Pharmacol.* 1991;104:21-24.
24. Shah AM, Mebazaa A, Wetzel RC, Lakatta EG. Novel cardiac myofilament desensitizing factor released by endocardial and vascular endothelial cells. *Circulation.* 1994;89:2492-2497.
25. Ku DD, Nelson JM, Caulfield JB, Winn MJ. Release of endothelium-derived relaxing factors from canine cardiac valves. *J Cardiovasc Pharmacol.* 1990;16:212-218.
26. Shah AM, Lewis MJ, Henderson AH. Effects of 8-bromo-cyclic GMP on contraction and on inotropic response of ferret cardiac muscle. *J Mol Cell Cardiol.* 1991;23:55-64.
27. Shah AM, Spurgeon HA, Sollot SJ, Talo A, Lakatta EG. 8-bromo-cGMP reduces the myofilament response to Ca^{2+} in intact cardiac myocytes. *Circ Res.* 1994;74:970-978.
28. Mohan P, Sys SU, Brutsaert DL. Nitric oxide donors induce a positive inotropic effect mediated by cGMP in isolated cardiac muscle without endothelium. *Eur Heart J.* 1994;15:145.
29. Ignarro LJ. Biological actions and properties of endothelium-derived nitric oxide formed and released from artery and vein. *Circ Res.* 1989;65:1-21.
30. Leite-Moreira AF, Mohan P, Sys SU, Brutsaert DL. Myocardial positive inotropic effect of dibutyryl-cyclic GMP *in vivo*. *Eur Heart J.* 1994;15:114.
31. Mohan P, Brutsaert DL, Sys SU. Inotropic effect of acetylcholine: role of endocardial endothelium. *Eur Heart J.* 1994;15:283.
32. Klabunde RE, Ritger RC, Helgren MC. Cardiovascular actions of inhibitors of endothelium-derived relaxing factor (nitric oxide) formation/ release in anesthetized dogs. *Eur J Pharmacol.* 1991;199:51-59.

33. Klabunde RE, Ritger RC. NG-Monomethyl-L-arginine (NMA) restores arterial blood pressure but reduces cardiac output in a canine model of endotoxic shock. *Biochem Biophys Res Commun* 1991;178:1135-1140.
34. Richard V, Berdeaux A, la Rochelle CD, Guidicelli J-F. Regional coronary hemodynamic effects of two inhibitors of nitric oxide synthesis in anesthetized, open chest dogs. *Br J Pharmacol.* 1991;104:59-64.
35. Hasebe N, Shen YT, Vatner SF. Inhibition of endothelium-derived relaxing factor enhances myocardial stunning in conscious dogs. *Circulation.* 1993;88:2862-2871.
36. Stamler JS, Loh E, Roddy MA, Currie, Creager MA. Nitric oxide regulates basal systemic and pulmonary vascular resistance in healthy humans. *Circulation.* 1994;89:2035-2040.
37. Berridge MJ. Cell signalling: a tale of two messengers. *Nature.* 1993;365:388-389.
38. Cheung Lee H. A signalling pathway involving cyclic ADP-ribose, cGMP, and nitric oxide. *News in Physiol Sci.* 1994;9:134-137.
39. Galione A, Cheung Lee H, Busa WB. Ca^{2+}-induced Ca^{2+} release in sea urchin egg homogenates: modulation by cyyclic ADP-ribose. *Science.* 1991;253:1143-1146.
40. Galione A. Cyclic ADP-ribose: a new way to control calcium. *Science.* 1993;259:325-326.
41. Mészáros LG, Bak J, Chu A. Cyclic ADP-ribose as an endogenous regulator of the non-skeletal type ryanodine receptor Ca^{2+} channel. *Nature.* 1993;364:76-79.
42. Galione A, White A, Willmott N, Turner M, Potter BVL, Watson SP. cGMP mobilizes intracellular Ca^{2+} in sea urchin eggs by stimulating cyclic ADP-ribose synthesis. *Nature.* 1993;365:456-459.
43. Ono K, Trautwein W. Potentiation by cyclic GMP of a-adrenergic effect on Ca^{2+} current in guinea-pig ventricular cells. *J Physiol (Lond).* 1991;443:387-404.
44. Beavo JA, Reifsnyder DH. Primary sequence of cyclic nucleotide phosphodiesterase isozymes and the design of selective inhibitors. *Trends Pharmacol Sci.* 1990;11:150-155.
45. Walter U. Physiological role of cGMP and cGMP-dependent protein kinase in the cardiovascular system. *Rev Physiol Biochem Pharmacol.* 1989;113:42-48.
46. Levi RC, Alloatti G, Fischmeister R. Cyclic GMP regulates the Ca-channel current in guinea pig ventricular myocytes. *Pflugers Arch.* 1989;413:685-687.
47. Méry P-F, Lohmann SM, Walter U, Fischmeister R. Ca^{2+} current is regulated by cyclic GMP-dependent protein kinase in mammalian cardiac myocytes. *Proc Natl Acad Sci USA.* 1991;88:1197-1201.
48. Pfitzer G, Ruegg JC, Flockerzi V, Hofmann F. cGMP protein kinase decreases calcium sensitivity of skinned cardiac fibres. *FEBS Lett.* 1982;149:171-175.
49. Méry P-F, Pavoine C, Belhassen L, Pecker F, Fischmeister R. Nitric oxide regulates cardiac Ca^{2+} current. Involvement of cGMP-inhibited and cGMP-stimulated phosphodiesterases through guanyl cyclase activation. *J Biol Chem.* 1993;268:26286-26295.
50. Dollinger SJ, Wahler GM. A nitric oxide donor has stimulatory and inhibitory effects on the cardiac calcium current, both of which are inhibited by a G-kinase blocker. *Biophysical J.* 1994;66:A238.
51. Brandt R, Nowak J, Sonnenfeld T. Prostaglandin formation from exogenous precursor in homogenates of human cardiac tissue. *Basic Res Cardiol.* 1984;79:135-141.
52. Manduteanu I, Popov D, Radu A, Simionescu M. Calf cardiac valvular endothelial cells in culture: production of glycosaminoglycans, prostacyclin and fibronectin. *J Mol Cell Cardiol.* 1988; 20:103-118.
53. Mebazaa A, Martin LD, Robotham JL, Maeda K, Gabrielson W, Wetzel RC. Right and left ventricular cultured endocardial endothelium produces prostacyclin and PGE_2. *J Mol Cell Cardiol.* 1993;25(3):245-248.
54. Mebazaa A, Cherian M, Abraham M, Dodd-o J, Martin L, Wetzel R. Endocardial endothelial prostanoid release responds to flow and hypoxia with response greater than that of the vascular endothelium. *Circulation.* 1993;88:185.
55. Mohan P, Brutsaert DL, Sys SU. Myocardial performance is modulated by interaction of cardiac endothelium-derived nitric oxide and prostaglandins. *Cardiovasc Res.* 1995; in press.
56. Mebazaa A, Mayoux E. Maeda K, Martin LD, Lakatta EG, Robotham JL, Shah AM. Paracrine effects of endocardial endothelial cells on myocyte contraction mediated via endothelin. *Am J Physiol.* 1993;265(*Heart Circ Physiol.* 34):H1841-H1846.
57. McClellan G, Weisberg A, Rose D, Winegrad S. Endothelial cell storage and release of endothelin as a cardioregulatory mechanism. *Circ Res.* 1994;75:8.

CHAPTER 26

MYOCARDIAL MICROCIRCULATION AS EVALUATED WITH CT

Xue-si Wu,[1] Robert C. Bahn,[2] and Erik L. Ritman[3]

ABSTRACT

This study explores use of whole-body CT imaging to separately quantitate the physiological behavior of the nonrecruitable (e.g., arterioles) and recruitable (mostly capillary) components of the intramyocardial microcirculation. In two groups of dogs, one with microembolization and one with epicardial artery stenosis, we demonstrate that intramyocardial blood volume (ρ) and blood flow (F) follow the relationship $\rho = AF + BF^{1/2}$ where A represents the transit time of the recruitable and $BF^{-1/2}$ is the transit time of the nonrecruitable components. These transit times are shown to change in different, but characteristic, patterns.

INTRODUCTION

For indicator dilution curve analysis of vascular transport function, fast CT imaging methods have several advantages over the use of catheter-sampled and projection imaging methods. These include:

1) Concentration of indicator can be sampled without a catheter—hence vessels and parenchyma not readily accessible to catheters can be sampled.

2) The site of sampling, anywhere in the heart wall, can be retrospectively chosen and repeated in response to the information (e.g. anatomy of vascular tree, tissue characteristics etc.) acquired after completion of the CT scans.

3) The problem of superposition of spatially heterogeneously perfused tissues or of feeder vessels is reduced because small "tissue" volumes can be sampled in three-dimensional space.

---

[1]Department of Beijing Heart, Lung and Blood Vessel Medical Center, Beijing Anzhem Hospital, Beijing, China, and [2]Departments of Laboratory Medicine and Pathology, and [3]Physiology and Biophysics, Mayo Clinic, 200 First Street SW, Rochester, MN 55905, USA.

Molecular and Subcellular Cardiology: Effects of Structure and Function
Edited by S. Sideman and R. Beyar, Plenum Press, New York, 1995

4) Frequent scan repetition and brief scan duration reduce "blurring" of the indicator dilution curve, a feature of catheter sampling.

5) Exact location of the indicator's injection (e.g., right heart) is not critical because the input function can be evaluated at a site that is more difficult (e.g., coronary artery) to achieve with a direct catheter delivery system.

Whole-body CT is limited, however, to approximately 1 mm^3 spatial resolution. This means that most of the intramyocardial coronary circulation is not resolvable and hence the nonrecruitable (arteries, arterioles, veins <0.5 mm diameter) and recruitable (mostly capillaries), vessels cannot be evaluated separately. However, because the recruitable and nonrecruitable microcirculation behave differently in response to various stimuli, we hypothesize that we can separately quantitate these components by virtue of their characteristic blood volume-to-flow relationships. We have evaluated this technique by comparing the results obtained in dogs with controlled alterations of their recruitable and nonrecruitable coronary circulation.

METHODS

The CT Scanner

The dynamic spatial reconstructor (DSR) scanner [1] was used to perform these studies. It has 14 x-ray tubes arranged in a semicircular array around the subject which are activated sequentially at 750-microsec intervals, thereby effectively moving a single x-ray tube around the subject in 11 msec. This scan can be repeated 60 times/sec for up to 1,200 sequential scans and thus generates a movie-sequence of the multislice CT image data. Fourteen digital-recording television cameras provide the information for computing a stack of up to 240 parallel, 0.8 mm-thick, slices that describe a cylindrical volume of 18.5 cm axial height and up to 40 cm in transverse diameter.

Animal Preparation

Group I - Selective coronary artery embolization with 16μm microspheres. Mongrel dogs were anesthetized and intravascular catheters positioned via cutdown in the neck and femoral regions. A balloon catheter in the descending aorta maintained aortic blood pressure at control levels as the embolization process proceeded, and contrast agent was injected through a catheter in the aortic root. A #4 catheter was positioned in either the left anterior descending (LAD), left circumflex (LCX) or left main (LM) coronary artery for injection of microspheres.

Group II - Mild lumen stenosis of selected coronary arteries. Mongrel dogs were anesthetized and catheterized as for Group I and a hollow Delrin cylinder was embolized into a left coronary artery [2].

Diameter stenosis was calculated as: (%) stenosis = (OD-ID)/OD) x 100, with OD the outer diameter and ID the cylinder's lumen diameter in mm. The range of percent coronary stenoses produced by these cylinders was 25% to 55%.

Scanning Procedure

All dogs were scanned in the supine position with the ventilator stopped at end-expiration. Four sec after the commencement of the DSR scan sequence, a bolus of 30 ml

of nonionic iohexol contrast medium was injected into the aortic root over 2 sec. With the heart paced at 112.5 bpm, the coronary arteries were opacified throughout four or five consecutive cardiac cycles. Total scan duration was 18.5 sec.

Experimental Protocols

Group I – DSR scans were performed under 1) Control, 2) Adenosine (1 $mg \cdot kg^{-1} \cdot min^{-1}$) infusion into the right atrium, and 3) a series of microsphere injections selectively into the LAD or LCX coronary artery. For the adenosine scans the intra-aortic balloon was inflated to an extent necessary to maintain left ventricular (LV) pressure at the Control level. After the adenosine scan was completed, the adenosine infusion was stopped and the balloon catheter deflated. In all dogs, 16.5 μm microspheres were injected over a period of approx. 1 min following which the DSR scan was performed. This process was repeated at 30–45 min intervals until the heart arrested. A 1 g sample of myocardium was taken from the middle of each perfusion territory and adjacent areas. Microspheres were recovered by digestion of the tissue samples for direct counting of microspheres.

Group II – Four study sets were performed: under control, elevated aortic pressure (inflated aortic balloon), decreased inferior vena caval inflow (inflated balloon in inferior vena cava) and adenosine infusion conditions.

Image Data Analysis

After each scan was completed the digitized DSR projection image data were processed using a filtered backprojection algorithm to obtain images of approximately 3 mm thick short-axis cross sections of the heart. These tomographic images were reconstructed for every diastolic phase occurring in the 18 sec scan sequence. Images of slices through the aortic root and mid-level of the LV were transferred to an image analysis workstation. The operator defined the endocardial and epicardial surfaces of the LV myocardium in the CT images. The free wall portion of the LV was divided roughly in half – defining the nominal LAD and LCX perfusion territories. Each region of interest (aortic root, LAD, LCX) outlined in the images was sampled to obtain its indicator dilution curves by measuring its average brightness (above background) for each of the approximately 33 images in the scan sequence. The intramyocardial blood volume and flow were estimated from these curves by the procedures described elsewhere [3,4].

RESULTS

Group I – Figure 1 summarizes the relationship of intramyocardial blood volume to flow. Note that for each embolization state the relationship is well fitted with the curve given by:

$$\rho = AF + BF^{0.5} \quad (1)$$

where ρ is the intramyocardial blood volume, F denotes the blood flow, and A and B are constants representing the transit times of the recruitable and non-recruitable components of the intramyocardial microcirculation. Note that the A value increases progressively with increasing embolization. Table 1 lists the values of the coefficients.

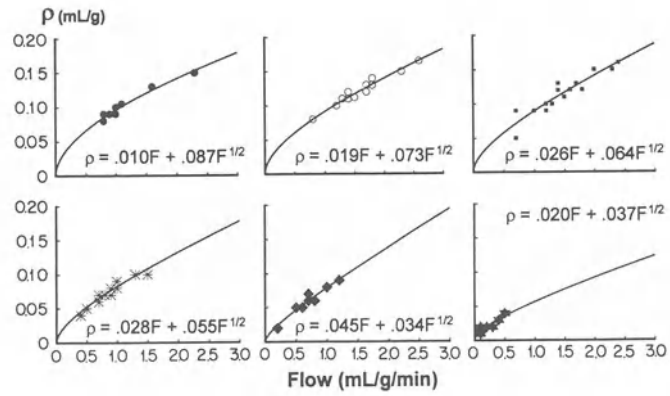

Figure 1. Impact of progressive embolization of coronary microcirculation on myocardial blood volume–to–perfusion relationship. Left upper to right lower panels are successively, 0%, 1–25%, 26–50%, 51–75%, 76–99% and 100% of fatal dose of microspheres. Solid line is the fitted volume vs flow curve (Eq. (1)). Note the increasing "straightening" of the relationship, i.e., increasing A and decreasing B, with increasing embolization.

Table 1. Microembolism of Coronary Circulation. Transit Time Coefficients of Myocardial Blood Volume to Flow Relationship (in minutes).

% Fatal Dose	0	1–25	26–50	51–75	76–99	100
A	0.010	0.019	0.026	0.028	0.045	0.020
B	0.087	0.073	0.064	0.055	0.034	0.037

Group II – Figure 2 summarizes the relationship of intramyocardial blood volume to blood flow in the epicardial coronary artery stenosis group. Table 2 indicates the coefficients under these conditions. Note that with increasing stenosis that the A value increases progressively with increased stenosis.

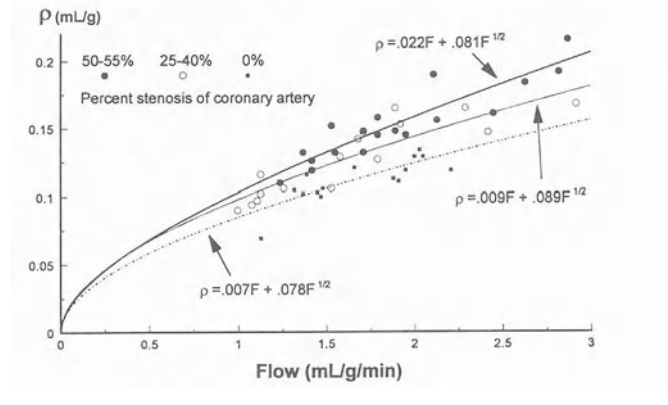

Figure 2. Effect of coronary artery stenosis on myocardial blood volume and perfusion. A single stenosis of either 0%, 25–40%, 50–55% stenosis in a proximal epicardial coronary artery results in a characteristic intramyocardial volume vs flow (Eq. (1)) relationship. Note the increase in A, while B changes little, with increasing stenosis.

Table 2. Epicardial coronary artery stenosis. Transit Time Coefficients of Myocardial Blood Volume to Flow Relationship (in minutes).

% Stenosis	0	25–43	50–55
A	0.007	0.009	0.022
B	0.078	0.089	0.081

DISCUSSION

The results in these studies are quite reproducible and, as discussed below, consistent with published information about the in situ myocardial microvasculature. This model shows that the nonrecruitable vessel volume changes as the square root of the flow. This is consistent with Poiseuille's Law linking flow to the vessel lumen radius [4].

To the extent that A is the transit time through the capillary vessels, the value range of 0.007 through 0.045 min (i.e., 0.42 to 2.7 sec, with a "normal" value of 1 sec) is consistent with values in the literature [5]. Similarly, the transit time through the non recruitable vessels ranges from 2.04 to 5.34 sec. Thus, a total transit time of 2.5 to 8 sec would be predicted. These values are also quite consistent with values derived by direct measurement of the aorta to coronary sinus transit time values [6,7]. The intramyocardial blood volume estimates are also consistent with values in the literature [8]. Thus a maximum capillary volume of 9.6% at 6 $ml \cdot g^{-1} \cdot min^{-1}$ perfusion is consistent with a volume predicted if there are 3600 capillaries per mm^3 of myocardium and each capillary segment is 20 square micrometers in cross-sectional area and 1 mm long. The total intramyocardial blood volume of 9% at 1 $ml \cdot g^{-1} \cdot min^{-1}$ and 20 to 25% under extreme vasodilation conditions is also consistent with the literature values.

The capability to independently quantitate the two components of the microvascular system would be useful in estimation of several interesting physiological variables. For instance, we can estimate the permeability surface area product [10] of the microcirculation (primarily in the recruitable component) so that with the knowledge of the recruitable volume, which allows us to estimate the capillary surface area (ρ_r), we can estimate an index of the permeability itself with PS/ρ_r. In addition, the knowledge of the transit time through the capillaries will allow us to assess the differential impact on flow-limited and diffusion-limited solute transport. Another possible application might be the analysis of the role of the intravascular blood content on the mechanical properties of the myocardium [11]. It is conceivable that the capillaries and the conductive vessels have different impacts on myocardial stiffness for a given change in their respective volumes.

CONCLUSIONS

The data suggest that we can quantitate the recruitable and nonrecruitable (i.e., dilatable) components of the intramyocardial microvasculature from the behavior of the intramyocardial blood volume relative to the flow. If the conducting vessels dilate or contract in response to the flow through them, then whatever happens to the recruitable component won't affect the nonrecruitable vessels unless the flow changes, or alternatively, the same influence (e.g., sympathetic nerve stimulation) affects both components directly. The recruitable component presumably changes in response to the local humoral milieu such as the adenosine concentration, which increases or decreases depending on whether

the oxygenation is adequate. Thus, there should be more recruitment in the capillaries just to keep the flow constant in the case of the stenosis. By recruiting more vessels than warranted by the flow, the pressure at the downstream end of the connecting vessels drops and the flow returns to normal. In case of embolization, the recruitment should compensate for the flow but we would actually expect a greater capillary volume for the flow because there needs to be more recruitment than just replacement [9].

Acknowledgements

This work was supported in part by National Institutes of Health Grant HL-43025. We thank Don Erdman and colleagues for technical assistance with the scans and animal preparation and thank Drs. D. L. Ewert and W.J.T. Spyra for use of some of their scan data for the present analysis.

DISCUSSION

Dr. R. Beyar: Conceptually, what you presented here depends on the idea that most of the flow increase is associated with the recruitment of capillaries. Is that correct?

Dr. E.L. Ritman: No, I do not make that assumption. I do say that recruitable component is probably mostly capillaries. Flow then increases as a consequence of the fact that there are more parallel channels to flow through. The two would follow, but I do not have that as a basic assumption.

Dr. R. Beyar: An increase of the diameter of vessels would be part of the explanation of increased flow. It would still not invalidate the measurements that you have presented in terms of analysis of the relations of volume and flow.

Dr. E.L. Ritman: The model is simple in the sense that it assumes that the capillaries have a constant fixed transit time. That is almost certainly not true. There is probably some variation, so you might want to tweak the model some. But even with this very simplistic assumption, it seems to behave correctly.

Dr. S. Sideman: How did you define the coefficient B?

Dr. E.L. Ritman: The coefficient B has units of $\text{min} \cdot F^{-0.5}$. Consequently, $B \times F^{-0.5}$ is the transit time of the nonrecruitable component. It means that the non-recruitable vessels have a transit time that is somewhat proportional to flow.

Dr. S. Vatner: How does this affect coronary venous oxygen in your experiments? How would a change in perfusion pressure or any other change in oxygen determinants affect your model?

Dr. E.L. Ritman: We kept the pressures constant, as best we could, by blowing up a balloon in the aorta. But once you get beyond a certain point of embolization, nothing you can do can keep that pressure up, so that is a variable that we have poor control of. We did not measure the oxygen content in these studies.

Dr. T. Arts: What was the influence of viscosity, or hematocrit, on the number of capillaries with the same flow? Was your method sensitive to this variable?

Dr. E.L. Ritman: I do not know. We measure the hematocrit. In the pig it is somewhat less than in the dog, but I have not looked at that systematically.

Dr. S. Akselrod: There must be some assumption about the recruitable and nonrecruitable elements being in series or in parallel. I am surprised that such a simple formula fits something that must be much more complex than just assuming that they are in series.

Dr. E.L. Ritman: We make the assumption that the nonrecruitable components can be represented by one pipe and that the recruitable components are in series with that. However, there must be parallel sets of these. It is important to realize that this is a steady state analysis. Maybe these parallel "sets" interact for a while and then settle down to a representative state that can be well represented by one bulk model. In the transient state, and it might take 5–10 min after a change, such as embolization in this case. There may be changes that can best be explained by having a parallel set of these elements, each of which behave somewhat differently. That is possible.

Dr. R. Reneman: To follow up on that, when you look at Kajiya's (unpublished) data in the endocardium and Tillmann's (unpublished) data in the epicardium, the capillaries are always perfused in the heart and blood flow is changed by measuring or decreasing blood flow velocity in the capillaries. Dr. Beyar asked about the diameter change. I would like to ask the same question in terms of velocity changes. If recruitment is defined as an increase in velocity in the capillaries rather than an increase in the number of capillaries perfused, how does that affect your model?

Dr. E.L. Ritman: I have not thought about that. It is obviously a concern if there is no such thing as recruitment in the coronary microcirculation. It might turn out that the change in velocity behaves as though there is recruitment.

Dr. M. Lab: Your lines go through the origin. But must they?

Dr. E.L. Ritman: I can not be sure. My model says they should, therefore I fit the model through the origin. Statistically you could make a good case that you have a non-zero intercept. I do not know what that would mean physiologically. That is not really explained in a simple physiological model. But you are right. That is why there is a confidence "ellipse" drawn around the A to B relationship derived from the blood volume to flow relationship.

Dr. J. Bassingthwaighte: Wouldn't that be equivalent to zero flow pressure? Do you have a remaining volume while the flow goes to zero?

Dr. E.L. Ritman: Yes.

Dr. M. Lab: One physiological way of getting that would be if the critical closing pressure would operate here.

Dr. R. Reneman: Critical closing pressure does not exist; one should call it flow cessation pressure because microvessels do not close when lowering arterial pressure.

Dr. Y. Lanir: Is there any way of directly validating your assumption about the division between recruitable and not recruitable and attributing one to the microcirculation and the other to...??

Dr. E.L. Ritman: Both are microcirculation to the extent that you cannot individually resolve the vessels in the imaged wall.

Dr. Y. Lanir: Can you make the division between capillaries and other components?

Dr. E.L. Ritman: I do not like to call them capillaries. I call them recruitable vessels and nonrecruitable.

Dr. Y. Lanir: Is there a way to validate this basic assumption?

Dr. E.L. Ritman: I hope so. The microspheres would affect most directly the recruitable components, or the capillaries. Perhaps there are more clever ways of doing it, and perhaps you have to do this at the same time as a video fiber looking at the endocardium or epicardium. Maybe these things have to be done in parallel to get a better handle on this problem.

Dr. H.E.D.J. ter Keurs: With 50% microembolization, I would assume that a number of cardiac cells are shut off, do not contract anymore, therefore their oxygen demand will be lowered. Does that come into your flow embolization chart under the heading of ischemia?

Dr. E.L. Ritman: In our simplistic scheme, I call those ischemic. I do not knwo for sure whether it is true or not.

REFERENCES

1. Jorgensen SM, Whitlock SV, Thomas PJ, Roessler RW, Ritman EL: The dynamic spatial reconstructor: A high speed, stop action, 3-D, digital radiographic imager of moving internal organs and blood. *Proc SPIE, Ultrahigh- and High-speed Photography, Videography, Photonics, and Velocimetry '90.* 1990;1346:180-191.
2. Spyra WJT, Bell MR, Bahn RC, Zinsmeister AR, Ritman EL, Bove AA: Detection of mild coronary stenoses using the Dynamic Spatial Reconstructor. *Invest Radiol.* 1990;25:472-479.
3. Wang T, Wu X, Chung N, Ritman EL: Myocardial blood flow estimated by synchronous, multislice, high-speed computed tomography. *IEEE Trans Med Imaging.* 1989;8:70-77.
4. Wu X, Ewert DL, Liu Y-H, Ritman EL: *In vivo* relation of intramyocardial blood volume to myocardial perfusion: Evidence supporting microvascular site for autoregulation. *Circulation.* 1992;85:730-737.
5. Honig CR, Odoroff CL, Frierson JL: Capillary recruitment in exercise: rate, extent, uniformity and relation to blood flow. *Am J Physiol* 238 (*Heart, Circ Physiol*) 1980;7:H31-H42.
6. Spiller P, Schmiel FK, Pölitz B, Block M, Fermor U, Hackbarth W, Jehle J, Kärfer R, Pannek H: Measurement of systolic and diastolic flow rates in the coronary artery system by x-ray densitometry. *Circulation.* 1983;68:337-347.
7. Knopp TJ, Dobbs WA, Greenleaf JF, Bassingthwaighte JB: Transcoronary transport functions obtained via a stable deconvolution technique. *Ann Biomed Eng.* 1976;4:44-59.
8. VanderPloeg CPB, Dankelman J, Spaan JAE: Functional distribution of coronary vascular volume in beating goat hearts. *Am J Physiol (Heart Circ Physiol).* 1993;33:H770-H776.
9. Hori M, Inoue M, Kitakaze M, Koretsune Y, Iwai K, Tamai J, Ito H, Kitakatake A, Sato T, Kamada T: Role of adenosine in hyperemic response to coronary blood flow in microembolization. *Am J Physiol* 250 (*Heart Circ Physiol*). 1986;19:H509-H518.
10. Ritman EL: Myocardial capillary permeability to iohexol: evaluation with fast x-ray computed tomography. *Invest Radiol.* 1994;29:612-617.
11. Pao YC, Simari RD, Ritman EL: Finite-element assessment of change in regional ventricular wall muscle stiffness due to coronary occlusion. *Adv in Bioeng, ASME Pub.* 1993;#H00863:567-570.

CHAPTER 27

VASCULAR GENE THERAPY

Moshe Y. Flugelman[1]

ABSTRACT

Gene therapy is emerging as a new and exciting therapeutic modality for cardiovascular pathology. The work reported here was carried out in the National Heart, Lung and Blood Institute (NHLBI) in Bethesda, MD, USA, where genetically engineered endothelial cells were used to seed endovascular prostheses and cell adhesion to the prostheses was tested both *in vitro* and *in vivo*. Two catheter based systems were used to deliver genes to the arterial wall cells *in vivo*, employing retroviral and adenoviral vectors. Efficient gene transfer to vascular cells *in vivo* was achieved with adenoviral vectors.

INTRODUCTION

Gene therapy refers to the replacement or correction of an abnormal gene in somatic cells [1, 2]. This term describes a new therapeutic modality and has been expanded to include control of various genes expression in somatic cells. Suppression or over-expression of various genes may induce a therapeutic effect on the treated organ or person [3, 4]. The use of gene therapy to cure cardiovascular diseases is a rational step in the application of gene therapy in clinical medicine; modification of gene expression or introduction of exogenous gene into a specific group of cells of the blood vessel walls appears to be an ideal mode of therapy for segmental vascular pathology.

The two methods of gene transfer employed in cardiovascular targeted therapy are: 1) *ex vivo* gene transfer into cells and re-introduction of the cells into the blood vessels and, 2) direct *in vivo* gene transfer into the blood vessel cells. The concept of *ex vivo* gene transfer was pioneered by Nabel *et al.* [5] who reported the transfer of a marker gene into endothelial cells in the laboratory and the introduction of these genetically modified cells back into a blood vessel. This concept was expanded by the NHLBI group who had used

[1]Department of Cardiology, and the Technion Medical School, Lady Davis Carmel Medical Center, 7 Michal Street, Haifa, 34362, Israel.

Molecular and Subcellular Cardiology: Effects of Structure and Function
Edited by S. Sideman and R. Beyar, Plenum Press, New York, 1995

genetically engineered endothelial cells to cover endovascular prostheses and deployed the covered prostheses in blood vessels [6–8]. Effective direct *in vivo* gene transfer has evolved with recent advances in vector technology. The use of liposomes mediated gene transfer and the use of retroviral vectors is limited by low efficiency of gene transfer. Thus, effective *in vivo* gene transfer is feasible only with the use of adenoviral vectors [9].

The syndromes that are the objectives of cardiovascular gene therapy are post-angioplasty restenosis, artificial and venous grafts occlusion and unstable angina pectoris. All these syndromes have a common pathophysiology: smooth muscle cells proliferation and luminal thrombosis [10, 11].

The NHLBI experience is described here to exemplify a group effort directed to enhance the use of gene therapy in cardiovascular diseases. The obstacles that are yet to overcome and the recent advances in the field will be discussed.

METHODS

Ex Vivo Gene Transfer

This set of experiments exercised the use of genetically engineered endothelial cells to improve the surface of a metallic endovascular prosthesis known as *stent*. The stainless steel slotted prosthesis was mounted on a balloon catheter and deployed in arterial narrowing by balloon inflation. After inflation the balloon was deflated and withdrawn and the expanded stent was left to support the arterial walls. Since active thrombosis occurs in the site of the stent deployment, the patients treated with stents receive large doses of anticoagulant drugs [12, 13]. The stents were seeded with genetically engineered endothelial cells. These cells were transduced with one of two retroviral vectors that transferred the neomycin phosphotransferase gene and either the human t-PA gene (B2NSt) or the bacterial beta-galactosidase marker gene (LBgSN). Neomycin phosphotransferase gene is a selectable marker that confers resistance to the antibiotic neomycin and to its analog G418. The B2NSt vector expressing human t-PA was used to produce large amounts of t-PA and thus obviate the need for systemic anti-coagulation to prevent stent thrombosis. The stents were seeded with sheep saphenous vein endothelial cells. The saphenous veins were extracted from the hind legs of three adult sheep using conventional surgical techniques for vein stripping. The cells were grown in the laboratory and transduced with the retroviral vectors.

Cell adherence to the stent was tested by three methods: **a)** scanning electron microscopy, **b)** histochemical staining with X-gal chromogen of the seeded stents and examination under dissecting microscope and, **c)** recovery of the cells from the seeded stent and counting and re-plating of the recovered cells. The three methods were used to determine cells adherence to balloon mounted stents, to stents deployed by balloon inflation in plastic tubing and, to expanded stents that were exposed for 2 hrs to pulsatile flow.

After completion of the *in vitro* experiments (see Results) we deployed seeded stents in the femoral arteries of the three donor sheep (autologous re-implantation) [8]. Three seeded stents and one unseeded stent, as a control, were deployed in each sheep. Ten days after deployment we assessed flow via the stents with color doppler mapping, and then harvested the seeded and unseeded stents and studied half of each stent for endothelial cell coverage. We extracted DNA from the arterial segment in which the other half of the stents was deployed. Polymerase chain reaction (PCR) was used to identify the neomycin phosphotransferase gene sequence as an evidence of the presence of the genetically engineered cells in the relevant arterial segment. Amplifications from each segment were

repeated three times to avoid errors related to the sensitivity of PCR and the presence of low number of relevant DNA copies.

In Vivo Gene Transfer

For *in vivo* direct gene transfer we used: **a)** perfusion, or porous, balloons with multiple microscopic holes that allowed infusion of the solution, used for balloon inflation, into the arterial wall and, **b)** double balloon catheters which created an isolated compartment within the arterial lumen once the two balloons were inflated. A solution of various vectors could be infused inside the compartment via a small hole in the catheter shaft which was centered between the two balloons.

To deliver genes directly to rabbit aortas we used perfusion balloons and various retroviral vectors encoding the neomycin phosphotransferase gene as well as other genes [14]. Controls were rabbit aortas that were not treated or aortas perfused with the vector vehicle but no retroviral vectors. All rabbits were sacrificed 5–14 days after exposure to the retroviral or control solutions and the aortas were extracted. Since histochemistry, using the X-gal chromogen, failed to discriminate control from study aortas due to false positive staining of the control aortas, we used PCR for the neomycin phosphotransferase gene sequence to detect gene transfer to aortic cells. Again, DNA was extracted from the aortas and samples from each aorta was amplified three times. Gene transfer efficiency was assessed by the comparison of the amplification product to the amplifications of a known number of copies of the neomycin phosphotransferase gene (semi-quantitative PCR).

Double balloon catheters were used to deliver various inert particles to sheep carotid artery [9]. Sized particles were chosen to find out whether there were size-related barriers in the vessel wall that limited viral and liposomal vectors' penetration into the media. The dynamics of vessel wall penetration was indicative of the viral vectors penetration of vessel walls. The medial layer contains the smooth muscle cells that are a major target of gene therapy. Inhibition of smooth muscle cells proliferation may prevent neo-intima formation after balloon angioplasty. India ink (120–500 nm) and fluorescent latex spheres (93 nm) were used, and the penetration of these particles was compared to the penetration of horse radish peroxidase (2–6 nm). These particles were chosen as their size was similar to the size of viral and liposomal particles. The particles were dissolved in a solution. The two balloons were inflated and the solution was infused into the compartment created by the two balloons and the arterial walls and was allowed to fill the compartment for 30 min. A pressure of 100–400 mmHg was maintained during the 30 min inside the compartment by adding particle solution. The sheep were sacrificed on the day of the experiments and, after fixation, sequential arterial sections were studied for the presence of the various particles. Histology and electron microscopy (India ink) were used for the larger particles, and fluorescence microscopy for the latex spheres. Arteries exposed to horse radish peroxidase were processed for detection of this enzyme.

Finally, both the double balloon and the perfusion balloon catheters were used with adenoviral vector expressing a nuclear-targeted beta-galactosidase gene (a kind gift from Dr. Bruce Trapnell, Genetic Therapy Inc., Gaithersburg, MD, USA) in the carotid and femoral arteries of sheep. Using the nuclear-targeted beta galactosidase gene, it was possible to determine the efficiency of gene transfer and to locate the transduced cells with no false positive staining. The sheep were sacrificed 3 days after the experiments, and the arteries fixed and stained with X-gal chromogen.

RESULTS

Ex Vivo Gene Transfer

Endothelial cells were harvested successfully from the veins of the three sheep with no morbidity. The three primary cell lines were transduced in the laboratory and after G418 (a neomycin analog) selection a homogenous population of transduced cells was at hand. Four catheter mounted stents were seeded with transduced cells. Complete coverage of the stent surface was demonstrated in all four stents with the two methods of microscopy (electron and dissecting). After deployment in plastic tubing and exposure to pulsatile flow, cell coverage was predominant on the lateral aspects of the stents. By microscopy it was estimated to be as high as 80% of the lateral surface area. When cells were recovered from the stents we counted 8,100 ± 2,400 cells from the unexpanded stents (n = 5), 7,600 ± 1,900 cells from the expanded stents (n = 4), and 5,700 ± 2,600 cells from the stents that were expanded and exposed to flow for 2 hrs (n = 3). The recovered cells were re-plated in tissue culture dishes and retained their proliferative capacity and typical morphology [7].

Seeded stents deployed in the donor animal demonstrated, by using Doppler flow mapping, laminar flow in the seeded and control stents. Using PCR, we detected the presence of the neomycin phosphotransferase gene sequence in six out of nine arteries with seeded stents and in none of the control arteries with unseeded stents. Seeded stents coverage, estimated from electron micrographs by three independent observers, was 59 ± 39% of surface area, as compared to 41 ± 8% in the unseeded control stents [8].

In Vivo Gene Transfer

Using the perfusion balloon and retroviral vector infusion into the rabbits aortic walls we detected, with PCR, the neomycin phosphotransferase gene sequence in 6/12 vector infused rabbits aortas and in 1/13 control rabbits. However, using this semi quantitative PCR amplification, we estimated the number of transduced cells to be as low as 100 cells in a 2 cm long arterial segment. The number of transduced cells was even lower [14] in most animals, and no physiological effect could be expected with such a low number of transduced cells.

The double balloon catheters demonstrated that the India ink and latex spheres were mostly concentrated in the intima (69–98% of sections showing the particles), both in intact arteries and in arteries that underwent balloon angioplasty prior to double balloon treatment. Particles were also detected in the adventitia (19–55% of sections showing particles). Very few particles were detected in the media (0–5% of sections showing particles); 227 sections from 18 arteries were studied. Arteries infused with horse radish peroxidase showed a high level of penetration of the enzyme to all arterial layers: 83–100% of sections showed intimal staining, 83–100% of sections in the media, and 67–100% of sections in the adventitia (a total of 87 sections from nine arteries).

Nuclear targeted beta galactosidase was detected in intimal and adventitial cells after the infusion of adenoviral solution via a double balloon. The distribution of transduced cells observed after X-gal staining corresponded the distribution of the larger inert particles. Transduced medial smooth muscle cells were detected with the perfusion balloon and a high infusion pressure (5 ATM). Multiple regions of cell necrosis and complete loss of endothelial cells were found in these regions. This experiment confirmed the observation that viral sized particles did not penetrate the vessel wall beyond the intima unless the endothelial cells were denuded and the particles were injected using high pressures [9].

Medial necrosis and endothelial cells denudation (with both retro- and adeno-viral vectors) were found in all the perfusion balloon experiments.

DISCUSSION

Experimental vascular gene therapy is the subject of major research effort by academical institutions and commercial enterprises [15]. The potential advantages of gene therapy in cardiovascular medicine are numerous. Two examples are: 1) Local pathologies can be treated locally by gene transfer or gene modulation with no systemic distribution and no systemic side-effects. 2) Some of the major cellular events in the arterial wall occur within two weeks of arterial injury [16] and can be treated with vectors expressing various genes for only 2 weeks. However, many problem still exist in this field.

Both *ex vivo* and *in vivo* approaches are legitimate methods for gene transfer [6–9, 14], but both need be perfected before being used in humans. We need to improve cells' adhesion to the stents *in vivo* and to test whether these cells exert a physiological effect. We have isolated human endothelial cells from saphenous veins and transduced these cells in the laboratory with viral vectors. We are presently developing methods to detect cell adherence to the stents *in vivo* and to test physiological effects of these cells.

Our *in vivo* direct gene therapy experiments have demonstrated that adenoviral vectors are far more effective than retroviral vectors for *in vivo* gene transfer [9, 14]. Viral sized particles do not penetrate intact arterial wall beyond the intima. These particles reach the adventitia via the vasa vasorum. As retroviral vectors will transduce only proliferating cells [1], its use for stable chronic vascular pathology is limited. It can be used when prolonged periods of expression are sought as the transferred genes are integrated into the host genomic DNA. Adenoviral vectors are highly efficient when non-selective, high level expression for short periods is needed [4, 17]. The adeno viral vectors were expressed in the medial layer of rats' carotid arteries after endothelial cells denudation and over-stretching of the artery [17]. With both viral vectors, cytotoxic effects can be seen both *in vitro* and *in vivo* [9, 14, 17]. A therapeutic window, referring to optimal adenoviral concentrations for efficient gene transfer, was described by Schulick *et al.* [18]. Little or no gene transfer was observed with low vector concentrations, while a higher dose produced effective gene transfer; an even higher dose caused a cytotoxic effect with no gene transfer.

The two catheter based systems are being used by most groups experimenting vascular gene therapy [19]. The perfusion balloon is effective in transferring vectors to the medial layer but causes some degree of mechanical damage to the arterial wall [20]. The damage is related to the perfusion pressure. The double balloon is less effective with regard to arterial wall penetration, but is effective in transferring small size molecules as well as gene transfer to the endothelial cells and adventitial layer. The efficiency of gene transfer to atherosclerotic arteries is reduced when compared to transfer efficiency in normal arteries [21].

Many genes were suggested as potential genes that will prevent luminal thrombosis and smooth muscle cells proliferation. Genes that modulate the clotting system, such as t-PA gene and hirudin, may play a role in clinical trials of gene therapy. Other genes that enhance endothelial cell growth, such as vascular endothelial growth factor, or genes that suppress smooth muscle cell proliferation are potential candidates for vascular gene therapy [22, 23]. Other genes or antisense oligonucleotides that either render smooth muscle cells sensitive to anti-viral drugs or arrests cell proliferation are also possible candidates for gene therapy [24, 25].

CONCLUSIONS

Gene therapy can be applied to clinical medicine if appropriate genes are identified and the local delivery systems perfected. Our experiments have shown that both *ex vivo* and *in vivo* gene transfer systems are legitimate, although some modifications are required to increase gene transfer to the arterial medial layer and to secure cells adherence to the stents. Advances in molecular biology, vascular biology and interventional cardiology may provide the needed solutions. Premature clinical trials, with no gain to patients, may jeopardize the major scientific effort invested in vascular gene therapy.

Acknowledgements

I am in debt to Dr. David A. Dichek who introduced and guided me in this exciting field and to my other colleagues, Drs. Renu Virmani, Ward Casscells, Kurt D. Newman, Jack J. Rome, Andrew Farb, Vafa Shayani, Michael T. Jaklitsch, and Martin B. Leon, for the help and friendship given so generously.

The experiments and results presented here are the result of the efforts of the team made up of these scientists, and many others, at the NHLBI.

DISCUSSION

Dr. M. Parmacek: One of the theories on why smooth muscle cells proliferate following balloon angioplasty is that endothelial cells serve as both a physical and potentially chemical barrier to smooth muscle cell proliferation; they express inhibitory substances. Do you still see smooth muscle proliferation when you use coated stents with endothelial cells and look at those histologically? You should see some, obviously. Did you compare the coated stents to the non-coated stent where you got a great deal of smooth muscle cell proliferation?

Dr. M. Flugelman: It is difficult to answer those questions as our experiments were not set to look at smooth muscle proliferation. Smooth muscle cell proliferation leading to restenosis occured within weeks to 6 months at the site of deployment. We looked at the stents 10 days after deployment, thus this information was not available to us. The only information related to this issue is that there was a tendency to more rapid endothelialization of the seeded stents when compared to the unseeded stents. We know that once the stents are covered by endothelial cells their surface is less thrombogenic. We therefore believe that we can prevent thrombosis and its sequela, smooth muscle cell proliferation and restenosis by rapid endothelialization.

Dr. B. O'Rourke: Is any of the necrosis related to an immune response? Have you tried to induce immunosuppression?

Dr. M. Flugelman: The necrosis we observed in our direct gene transfer experiments may be related in some extent to the immunologic reaction to the viral vehicle and mostly to viral transduction of the vessel wall cells. We did not use immunosuppression in our experiments as we looked specifically at gene transfer efficiency. An abstract reports the use of ciclosporine to prolong expression of adenoviral mediated gene transfer to the myocardium [Duboc *et al. Circulation* 1994;90:I-517.]

Dr. M. Parmacek: It is now very clear that the immune response to adenovirus depends upon two factors. First is the dose dependency of the adenovirus in that there is a window. It can go on a per cell basis, in culture, or on a per artery basis *in vivo*. If you go per cell, to keep it simple, with less

than 10 pfu/cell (and the equivalent dose *in vivo*), you do not elicit an immune response. If you use a dose greater than that *in vivo*, you elicit a tremendous immune response and a lytic response in the vessel wall. So you have to keep your dosage low. The second aspect is that there are great disparities in the preparations of viruses that different groups use. In particular, many cardiologist use crude viral lysates, which are produced in 293 cells and are not purified before being injected *in vivo*; they are loaded up with a host of immunogenic antigens which will undoubtedly solicit a tremendous immune response. Purified viral preparations in low dosages, in our experience at the University of Chicago, clearly do not exhibit immune response. Using those preparations, and contrary to some of the data that Drs. Dichek and Flugelman saw, we have been able (and this will come out in *Science* in some weeks), to efficiently affect injured vessel walls. Approximately 70% of the smooth muscle cells when we immunocytochemically stained for protein, that is an HA tagged protein epitope. Another advance, which is again in unpublished data, is that there are now new vectors which can be complexed with liposomes which supposedly, are 10–20 times more efficient than any of the previously used liposome mediated mechanism. We have not tested this ourselves. That may be tremendous advantage because obviously we would rather get around using viruses *in vivo*.

Dr. M. Flugelman: Liposomes are relatively large in size and therefore will not penetrate vessel wall. Only if vessel wall integrity is disrupted, like after angioplasty, than large particles will come in contact with medial smooth muscle cells.

Dr. W. Barry: The endothelial cells express Class–II antigens fairly strongly and could be a target for an immune response. Were those endothelial cells in your sheep experiments from the same animal that you implanted the stent in? If not, do you think an immune response to the endothelial cells on the stent could be one factor which would limit the survival of the endothelial cells on the stent.

Dr. M. Flugelman: It was an autologous implantation. This is how we planned to avoid such an immune response. We did not specifically looked whether cells grown in the laboratory induce immune response when re–implanted in the donor animal, although this is possible.

Dr. H.E.J. ter Keurs: Endothelial cells transport materials in general, and quite often by endocytosis, through the endothelial cells and exocytosis. Are there gene transfer techniques that use that pathway in the intact endothelium to reach the underlying layers?

Dr. M. Flugelman: I am not aware of such techniques. As far as I know, viral vectors attach to receptors on the endothelial cells membrane before penetrating the cell. Small molecules, like small proteins, do enter the vessel wall via the endothelial cells and for this reason I believe that stent seeded with endothelial cells that secrete therapeutic proteins, may be a good way to transfer proteins into vessel wall.

Dr. M. Lab: There are great technical difficulties that are too big to surmount in taking the patients own endothelium from a vessel and using that on a stent and back into coronary arteries.

Dr. M. Flugelman: What we anticipate is that the patient will come to the outpatient clinic. It takes 15 minutes or so for an experienced surgeon to get a 5 cm long vein from the leg, using local anesthesia. Cell harvesting, transduction, selection and stent seeding take about 2–3 weeks. Than we will be ready for stent deployment. It is self evident that this procedure is not suitable for unplanned, emergency stent deployment. There are many clinical circumstances in which one can wait a month before stent deployment, such as stent deployment in the peripheral vasculature or in coronary vein grafts. A seeded stent may be needed to treat otherwise untreatable disease in some patients. The seeded cells will secrete substances as NO and will induce continuous local therapeutic effect. This all may sound like science fiction but advances in molecular biology and vascular

biology are made every day. Progress in the biology and pathobiology of the vessel wall is crucial for the implantation of vascular gene therapy in humans.

Dr. R. Reneman: You were discussing stents with a slow release of heparin. Have they used stents with heparin coating? They are making tremendous progress in open-heart surgery with heparin coated auxiliaries, probably avoiding the need for intravenous heparinization during short perfusions.

Dr. M. Flugelman: There are some technological breakthroughs. There are reports of gel coated balloon and stents. Multiple drugs were used with these devices but all have been tried in a relatively small numbers. Experiments in both vascular biology and vascular gene therapy are very tricky as some animal models will not yield the same results as other models and all animal models do not predict response in humans. Therefore, I will be extremely cautious before using the new techniques in humans. For the time being, vascular gene therapy should be looked at mainly as a research tool.

Dr. R. Reneman: What one wants is a natural membrane on the stents. In our neighboring institute on biomaterials, they are trying to mimic vessel walls by incorporating phospholipids in membranes and coating them with heparin.

Dr. R. Beyar: There are clinical trials with coated stents, either covalently bonded heparin, or even albumin, which have shown high efficiency in the pig model. They are doing it in patients. The major question is whether those stents are efficient in preventing thrombosis, and maybe restenosis. The balance between the role of molecular biology vs regular coating will have to depend on how much more efficient you get from molecular biology relative to other coatings.

REFERENCES

1. Mulligan RC. The basic science of gene therapy. *Science*. 1993;260:926–932.
2. Anderson WF. Human gene therapy. *Science*. 1992;256:808–813.
3. Swain JL. Gene therapy; anew approach to the treatment of cardiovascular disease. *Circulation*. 1989;80:1495–1496.
4. Schneider M, French BA. The advent of Adenovirus – Gene therapy for cardiovascular disease. *Circulation*. 1993;88:1937–1942.
5. Nabel EG, Plautz G, Boyce FM, Stanley JC, Nabel GJ. Recombinant gene expression *in vivo* within endothelial cells of the arterial wall. *Science*. 1989;244:1342–1344.
6. Flugelman MY, Leon MB, Bowman RL, Virmani R, Anderson WF, Dichek DA. Retention of seeded cells on balloon expanded stents under flow conditions. *Circulation*. 1990;82(Supl. III):72.
7. Flugelman MY, Virmani R, Leon MB, Bowman RL, Dichek DA. Genetically engineered endothelial cells remain adherent and viable after stent deployment and exposure to flow *in vitro*. *Circ Res*. 1992;70:348–354.
8. Flugelman MY, Rome JJ, Virmani R, Newman KD, Dichek DA. Detection of genetically engineered endothelial cells seeded on endovascular prosthesis ten days after *in vivo* deployment. *J Mol Cell Cardiol*. 1993;25 (supp I):S.38.
9. Rome JJ, Shayani V, Flugelman MY, Newman KD, Farb A, Virmani R, Dichek DA. Anatomic barriers determine the distribution of *in vivo* gene transfer into the arterial wall: modeling with microscopic tracer particles and verification with a recombinant adenoviral vector. *Atherosclerosis & Thrombosis* 1994;14:148–161.
10. Ross R. The pathogenesis of atherosclerosis: a perspective for the 1990s. *Nature*. 1993;362:801–809.
11. Flugelman MY, Virmani R, Correa R, Yu Z-X, Farb A, Leon BM, Fu YM, Casscells W, Epstein SE. Smooth muscle cell abundance and fibroblast growth factors in coronary lesions of patients with non fatal unstable angina: a clue to the mechanism of transformation from the stable to the unstable clinical state. *Circulation*. 1993;88:2493–2500.
12. Serruys PW, de Jaegere P, Kiemeneij, *et al.* A comparison of balloon expandable-stent implantation with balloon angioplasty in patients with coronary artery disease. *N Engl J Med*. 1994;331:489–495.

13. Fischman DL, Leon MB, Baim DS, *et al.* A randomized comparison of coronary-stent placement and balloon angioplasty in the treatment of coronary artery disease. *N Engl J Med.* 1994;331:496-501.
14. Flugelman MY, Jaklitsch MT, Newman KD, Casscells SW, Bratthuaer GL, Dichek DA. Low levels *in vivo* gene transfer into the arterial wall through a perforated balloon catheter. *Circulation.* 1992;85:1110-1117.
15. Coghlan A. Gene superclub signs up top players. *New Scientist.* 1994;1952:4.
16. Banai S, Shou M, Correa R, Jaklitsch MT, Douek PC, Booner RF, Epstein SE, Unger EF. Rabit ear model of injury induced arterial smooth muscle cell proliferation. *Circ Res.* 1991;69:748-756.
17. Lee SW, Trapnell BC, Rade JJ, Virmani R, Dichek DA. *in vivo* adenoviral vector-mediated gene transfer into balloon-injured rat carotid arteries. *Circ Res.* 1993;73:797-807.
18. Schulick AH, newman KD, Dichek DA. A therapeutic window for *in vivo* adenoviral vector mediated gene transfer. *Circulation* 1994;90(Supl 4):I-516.
19. Reissen R, Isner JM. Prospects for site-specific delivery of pharmacologic and molecular therapies. *J Am Coll Cardiol.* 1994;23:1234-1244.
20. Plante S, Dupuis G, Mongeau CJ, Durand P. Porous balloon catheters for local delivery: assessment of vascular damage in a rabbit iliac angioplasty model. *J Am Coll Cardiol.* 1994;24:820-824.
21. Feldman LJ, Steg PG, Zheng LP, Kearney M,Barry JJ, Perricaudet M, Isner JM. Percutaneous adeno-mediated gene delivery to normal and atherosclerotic arteries *in vivo*: a comparative study. *Circulation.* 1994;90(Supl 4):I-517.
22. Shweiki D, Itin A, soffer D, Keshet E. Vascular endothelial growth factor induced by hypoxia may mediate hypoxia-initiated angiogenesis. *Nature.* 1992;359:843-845.
23. Ferrara N, Houck K A, Jakeman L B, Winer J, Leung DW. The vascular endothelial growth factor family of polypeptides. *J Cell Biochem.* 1991;47:211-218.
24. Ohno T, Gordon D, San H, Pompili VJ, Imperiale MJ, Nabel GJ, Nabel EG. Gene therapy for vascular smooth muscle cell proliferation after arterial injury. *Science.* 1994;265:781-84.
25. Morishita R, Gibbons GH, Ellison KE, Nakajima Masatoshi, von der Leyen H, Zhang L, Kaneda Y, Ogihara T, Dzau VJ. Intimal hyperplasia after vascular injury is inhibited by antisense cdk 2 kinase oligonucleotides. *J Clin Invest.* 1994;93:1458-1464.

CHAPTER 28

INTEGRATION OF STRUCTURE, FUNCTION AND MASS TRANSPORT IN THE MYOCARDIUM

Daniel Zinemanas, Rafael Beyar, and Samuel Sideman[1]

ABSTRACT

A left ventricular (LV) model that integrates muscle mechanics, coronary flow, and fluid transport, and accounts for the three-phase (fiber-blood-interstitium) myocardial structure and composition, is used to study the interactions between the mechanics, coronary flow and fluid and mass transport in the myocardium. Theoretical simulations elucidate the effects of ventricular load, coronary perfusion pressure, and fluid and mass transport on ventricular performance and coronary dynamics. The analysis yields a direct relation between cardiac function and structure to cardiac mechanics, coronary flow, and intramyocardial fluid (and mass) transport, and allows to study the interactions between coronary flow, ventricular and myocardial mechanics and intramyocardial fluid shifts.

INTRODUCTION

Cardiac performance has been a central topic in cardiovascular research over the last decades and has usually involved some aspects of myocardial mechanics, coronary flow and intramyocardial fluid transport. Although these and other phenomena interact, and altogether determine the overall myocardial performance, most of the experimental and theoretical studies have been focused on the study of a single aspect of myocardial function. The basic limitation of such isolated approaches is that the multilateral effects between the various parameters that affect myocardial function have not been elucidated. For example, while it is known that LV mechanics affects the coronary flow and the interstitial fluid transport [1, 2], and that, conversely, coronary pressure and flow [3–5] and fluid transport [6] affect LV mechanics, none of the present approaches and theories of

[1]Heart System Research Center, The Julius Silver Institute, Department of Biomedical Engineering, Technion-IIT, Haifa, 32000, Israel.

Molecular and Subcellular Cardiology: Effects of Structure and Function
Edited by S. Sideman and R. Beyar, Plenum Press, New York, 1995

myocardial mechanics [7–13] and coronary flow [14–17] allow for an analytical evaluation of these bidirectional interacting effects. A typical example is the failure of present models of coronary flow (e.g. waterfall [18], intramyocardial pump [19], or varying elastance [20, 21] models) to relate the coronary flow impediment to myocardial mechanics under a wide range of operating conditions [22].

While earlier theoretical studies have contributed considerably to the understanding of LV function and performance, a more comprehensive approach that integrates the inter-related phenomena and permits to study their interactions is obviously greatly desired. McCulloch *et al.* [5], who studied the mechanical effects of the coronary perfusion in the passive canine LV, showed that the large effect of the coronary perfusion on the passive LV cannot be explained solely by changes in the volume of the coronary vessels. Anderson and Johnson [6] have shown that a change in blood osmolarity can change the tissue fluid pressure and the myocardial volume, and hence the LV performance. Similarly, Rubboli *et al.* [23] showed that acute edema has an important effect on the LV mechanics and the coronary flow. Obviously, "the myocardium has to be viewed as a structure composed of connective tissue and contractile elements (myocytes) vessel attachments, interposed by an interstitial fluid gel-like matrix," [2].

Here, we describe a new approach to LV performance which is based on a structural description of the myocardium, accounts for its three phase (fiber–blood–interstitium) composition and activity, and involves the simultaneous interactions between myocardial mechanics, coronary flow and the capillary to interstitial fluid transport. The inclusion of fluid (mass) transport considerations is emphasized by the observed bilateral effects between coronary flow and myocardial mechanics as well as by the functional relationship between these phenomena and the interstitial fluid transport.

Like all man made models, the integrated model presented here is but an approximation aimed to study trends and gain understanding of the interactions between the major parameters affecting the LV characteristics and the overall LV performance in normal and pathological operating conditions. For the sake of clarity, we review some of our earlier work [22, 24–26] and present some new data which further confirms the validity of the proposed model.

THEORY

Physiological Background

Myocardial composition. As is well known, the myocardium is a complex structural matrix, made of muscle fibers and connective collagen fibers, which contains the blood vessels and the interstitial fluid. The total volume V_{wall} of this three-phase (fiber–blood–interstitium) composite (Fig. 1) is given by the sum of the individual components:

$$V_{wall} = V_{blood} + V_{int} + V_{fib} \tag{1}$$

Under normal conditions the vascular blood volume, V_{blood}, and the interstitial fluid volume, V_{int}, occupy some 15% (each) of the total LV wall volume [27] while the muscle fiber volume occupies the remaining 70% of the total LV wall volume. The volumes of the blood, interstitial fluid and fibers are affected by the fluid transport between the compartments and may change according to the operating conditions of the heart, thus affecting the overall LV performance. As a first approximation we assume that the fiber volume, which includes the muscle fiber and the extracellular collagen, remains constant,

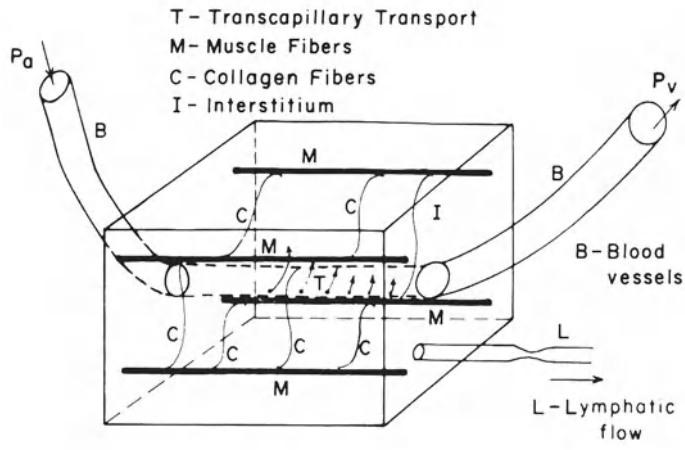

Figure 1. Schematic of the myocardial tissue emphasizing the three major components: fibers, vessels and interstitium.

and consequently, neglect the fluid and mass exchange between the interstitium and the myocardial cells. The blood and interstitial fluid volumes are evaluated by the corresponding mass conservation balances and follow the changes in LV operating conditions.

Myocardial mechanics. Viewing the myocardium as a fluid–fiber structure, and neglecting the shear stresses in the interstitial fluid phase, the myocardial stress tensor, $\boldsymbol{\sigma}$, is given by [13]:

$$\boldsymbol{\sigma} = \boldsymbol{\sigma}_a + \boldsymbol{\sigma}_p - P\,\boldsymbol{I} \tag{2}$$

where P denotes the interstitial fluid pressure, i.e. the IMP; $\boldsymbol{I}$ is the unit tensor and the subscripts a and p denote the active (myocytes) and passive (collagen) stress components, respectively. This myocardial stress tensor is used in combination with the myocardial volume in the myocardial force balance to calculate the stresses, the IMP and the fibers deformation during the heart cycle. Note that while earlier models [7, 8, 10–13] assume *a priori* knowledge of the diastolic IMP and the total LV wall volume, the present integrative LV approach solves for these parameters as dependent variables with Eq. (1) substituting the generally used incompressibility condition.

Coronary flow. The coronary flow and the blood volume depend on the cross-sectional area, A, of the intramyocardial blood vessels submerged in the interstitial compartment, and is therefore determined by the difference between the vascular and the extravascular pressure [17, 28]. Thus, the flow resistance R, the capacitance C, and the volume of the vessels are functions of the pressure dependent cross-sectional area, i.e.:

$$R = R(A)\,, \qquad C = C(A)\,, \qquad V_{blood} = V_{blood}(A)\,, \qquad A = A(P_{vas} - IMP) \tag{3}$$

Equation (3) states that the coronary flow and myocardial blood volume depend on myocardial mechanics which determines the IMP, and thus changes in the myocardial mechanics will affect the coronary circulation through changes in IMP. Consequently, these mechanical effects which affect the blood and total intramyocardial volume also affect the myocardial mechanics. As shown below, these parameters also depend on the fluid and mass transport since the IMP is a function of the myocardial fluid content. The suggested

[2] "direct" mechanical effect between the myocardial fibers and the coronary vessels is not well established and is not considered here.

Fluid transport. The myocardial interstitial fluid content is determined by the interstitial fluid mass balance:

$$\frac{dV_{int}}{dt} = J_w S_{cap} - F_{lymph} \tag{4}$$

where S_{cap} is the total capillary wall area and J_w is the transcapillary fluid flux. Assuming an ideal semipermeable capillary wall, the fluid flux is given by [29]:

$$J_w = L_p (\Delta P - \nu \Delta \pi) \tag{5}$$

where L_p denotes the hydraulic conductivity of the capillary wall, $\Delta P \equiv (P_{cap} - IMP)$ and $\Delta\pi$ is the osmotic pressure gradient across the capillary wall. Note that the lymphatic flow, F_{lymph}, is also a function of the IMP. Clearly, J_w and the interstitial volume depend on the IMP and the vascular pressures, i.e. on the LV mechanics and the coronary circulation.

Model Description

The basic relationships coupling the phenomena under study are schematically described in Fig. 2, demonstrating that the overall LV performance and function is determined by the interactions between cardiac mechanics, coronary blood flow and fluid and mass transport. As seen in Fig. 2, the interstitial intramyocardial fluid pressure, the IMP, links these three phenomena. Changes in one of these basic processes will affect the other two and influence the overall LV performance.

A number of simplifying assumptions are made here to reduce the mathematical and computational complexity of the system while preserving the major and basic physiological characteristics of the phenomena involved. Briefly, the model is based on the following basic assumptions:

1) The LV is represented by a thin wall cylindrical geometry.
2) The (muscle and collagen) fiber volume is constant.

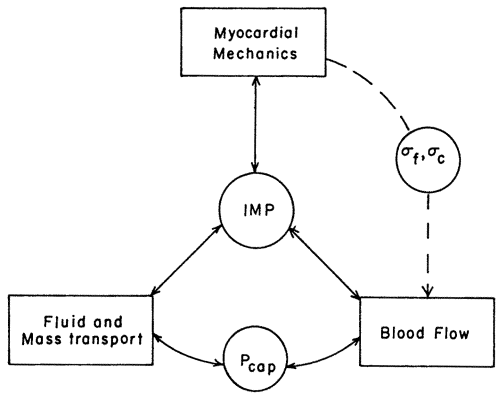

Figure 2. Schematic representation of the basic myocardial relationships among myocardial mechanics, coronary flow (Q), and fluid and mass transport. IMP, intramyocardial pressure; σ_f and σ_c, muscle and collagen stresses, respectively; P_{cap}, capillary pressure. (Reproduced from [26] with permission.)

3) Stress components are evaluated based on the active (muscle) and passive (collagen) constitutive equations for the fibers, accounting for the fiber's spatial architecture and the total myocardial and LV cavity volumes. Stresses are averaged transmurally and used in the analysis as a single parameter representing the midwall; the thin wall stress analysis used here takes into account the circumferential, longitudinal and an additional radial myocardial force balance components.
4) Active muscle stresses are calculated based on the sarcomere stress–length relationship, the force velocity relationship (stress–strain rate) and a non-symmetric mechanical activation function.
5) The coronary flow is described by an artery to vein series of resistive-capacitive components which depend on the instantaneous vessel transmural pressures.
6) The interstitium is modeled as a fluid compartment representing the extracellular and extravascular space; the pressure of that fluid is defined as the IMP.
7) The capillary walls are ideal semipermeable membranes of the Kedem–Katchalsky type.

The details of the physiological and mathematical models, the numerical solution, the constitutive equations and parametric data involved in the model are described elsewhere [25]. Briefly, the numerical procedure consists of solving simultaneously and interactively the mechanical, flow and fluid transport equations. Clearly, accounting for the fluid and mass transport balances provides an additional linkage between the mechanical and blood flow variables. This allows to determine the total myocardial interstitial fluid and blood content as well as the diastolic IMP [22, 24–26], determine the flow–mechanics relationship uniquely and study the bidirectional interactions between the coronary blood flow and LV mechanics. Calculations were performed to evaluate steady state and transient conditions for the interacting processes.

RESULTS

The Normal Beating Heart

Typical results for the LV mechanics and coronary flow for a canine heart under normal beating conditions, i.e. coronary perfusion pressure taken as the aortic pressure and normal afterload and preload conditions, are shown in Fig. 3. The LV cavity pressure (LVP), the IMP and the aortic pressure (AOP) are presented in Fig. 3A, and the corresponding coronary flow (Q), is depicted in Fig. 3B. The preload, or filling pressure, is assumed constant and the afterload is described by a three-element Windkessel model. These results correspond to a steady state conditions under maximum vasodilatation. Inspection of Fig. 3A shows that the peak IMP does not coincide with the peak LV pressure. Also, the slope of the LV pressure, and particularly that of the IMP, change with the opening of the aortic valve, i.e. end of the isovolumic contraction. These dynamic features of the LV wall predicted IMP are in excellent agreement with experimental observations and IMP measurements [30–34].

The coronary flow rate depicted in Fig. 3B reflects the dynamics of the IMP (dIMP/dt) which is determined by the mechanical muscle activity and the LV wall volume. As seen, the heart cycle starts with a rapid decrease in the coronary flow due to myocardial contraction and a consequent rapid rise in IMP. This is followed by a flow increase due to

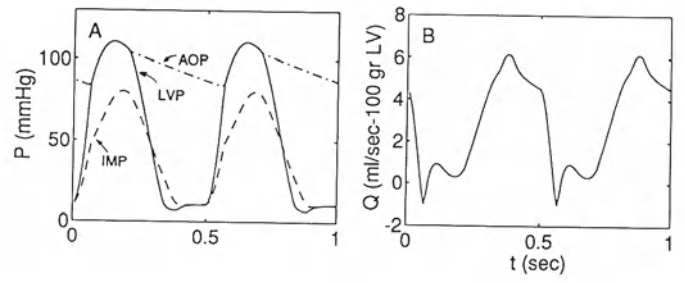

Figure 3. Mechanics and flow in a normal beating heart. **A:** Left ventricular pressure (LVP), IMP, and aortic pressure (AOP). P – pressure. **B:** Flow rate per 100 gr myocardial weight (Q).

the increase in the aortic pressure at the beginning of ejection. Towards end–systole the flow decreases again due to the continuous increase in the IMP and the decrease of the aortic pressure. Thus, the first coronary flow minimum corresponds to the beginning of ejection, while the second minimum reflects a combination between IMP and aortic pressure. The flow increases again at the beginning of relaxation and reaches a maximum near the end of isovolumic relaxation. The late diastolic decrease of the coronary flow corresponds to the decrease in the aortic pressure. The predicted coronary flow dynamics is in very good agreement with well known experimental observations [25, 26].

Effects of Sarcomere Contractile State and LV Loading Conditions on Coronary Flow

Experimental observations by Krams *et al.* [35] and Doucette *et al.* [36] of the coronary flow under different contractile and LV loading conditions are simulated in Figs. 4 and 5. The oscillatory flow amplitude (OFA) was calculated for an isovolumic contracting heart with a constant coronary perfusion pressure for two conditions: a) different LV cavity volumes while the sarcomere contractile state is kept constant (Fig. 4A), and b) various contractility levels while the LV cavity volume is kept constant (Fig. 4B). Perfusion pressure was taken as 100 mmHg and sarcomere contractile state was changed by assuming different values of the maximum isometric stress, σ_0, of a fully activated sarcomere. Figures 4C and 4D depict Krams *et al.* [35] OFA data obtained in a constant perfusion pressure and maximal vasodilation for isovolumic contracting feline heart. The contractility was decreased by infusing EGTA, a free calcium binding factor that reduces myocardial activity. An excellent qualitative and a good quantitative match between the experimental and theoretical results is evident. As observed, the model predicts a weak dependence of the OFA on the LVP but a large effect of the myocardial contractile state on the OFA. This is due to the fact that the IMP, which plays a mayor role in determining the flow characteristics, remains almost unchanged despite large differences in the LVP in the contractions at different cavity volumes but is significantly affected by the changes in sarcomere activity at the same cavity volume.

The effects of preload induced LVP changes on the normalized OFA in the normal and passive myocardium are depicted in Figs. 5A and 5B, respectively. Preload changes were also used by Doucette *et al.* [36] to study the effect of cardiac contraction and cavity pressure on coronary blood flow in open–chest coronary perfused and maximum vasodilated dog hearts. Under normal contractile conditions, changes in the preload conditions, and consequently changes of the LVP, did not affect the oscillatory flow amplitude. However,

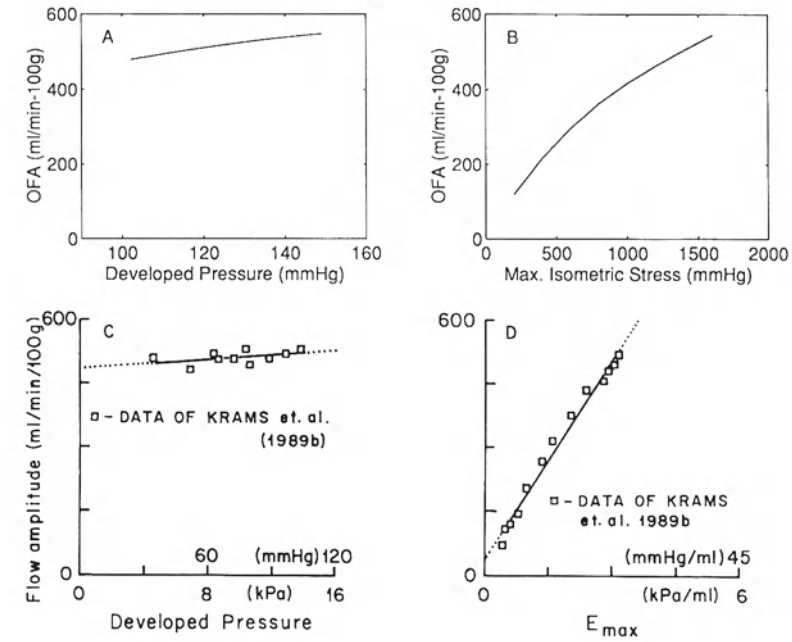

Figure 4. **A:** OFA as a function of developed pressure. **B:** OFA as a function of maximal sarcomere isometric tension. **C and D:** Experimental data of Krams *et al.* [35] (with permission of the American Physiological Society). Note that both E_{max} and the maximal isometric tension of the sarcomere are directly related to myocardial contractility.

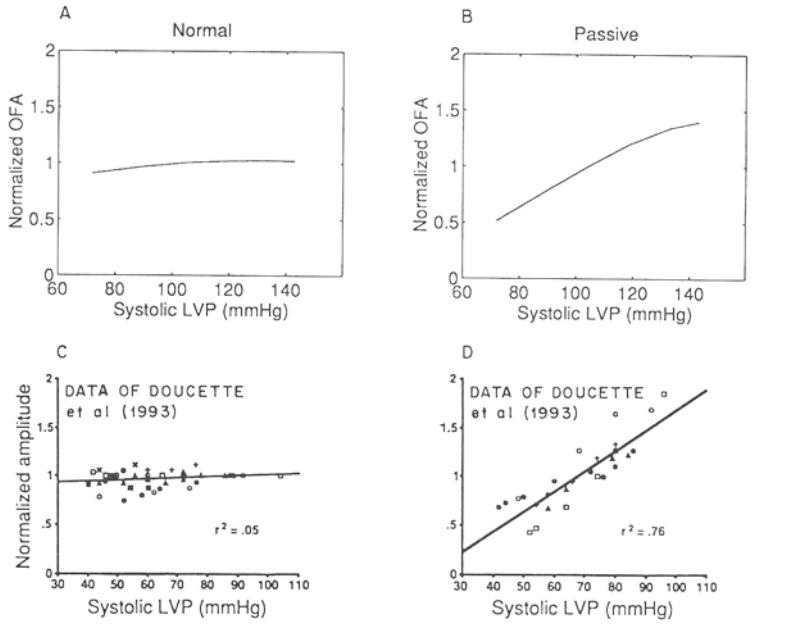

Figure 5. Normalized coronary flow amplitude as a function of peak LVP. **A:** Normal. **B:** Noncontracting myocardium. **C and D:** Experimental data of Doucette *et al.* [36] (with permission of the American Physiological Society).

when contraction was locally abolished by infusing Lidocaine into one of the coronary arteries, the changes in the preload had marked effects on the OFA in the affected region.

As seen in Fig. 5, the calculated results are in good agreement with the corresponding experimental data of Doucette *et al.* [36] (Figs. 5C and 5D) and they predict that, in the normal case, the coronary flow and OFA are very similar despite the large differences in the LVP. This is due to the fact that the IMP does not depend on the LVP when the latter is modified by preload manipulations. However, the effect of the LVP on the IMP, and consequently on the coronary flow in the passive myocardium, is much stronger. Moreover, our analysis correctly predicts that unlike the normally contracting myocardium, the passive LV wall becomes thinner during systole and its thickness decreases as the LVP increases [22].

Fluid Transport Effects

As previously shown [24, 26], the model correctly predicts changes in LV performance due to various manipulations of the myocardial fluid transport and mass balance. These include the effects of a transient cardiac arrest (reducing the myocardial forces acting on the interstitium and vessels) [24], lymphatic outflow blockage [24], changes in blood osmolarity [26], and coronary perfusion pressure [26]. Here, we show the effect of changes in the coronary perfusion pressure. The model simulations depicted in Fig. 6 (left) are in agreement with the data of Rubboli *et al.* [23] (right) who studied the effect of acute edema on flow and LV function in isolated isovolumic rat hearts. They found that following a step increase in the coronary perfusion pressure, the coronary flow increases rapidly and later gradually decreases, with a time constant of about 1 hr. These experiments were simulated here by imposing a step change in the perfusion pressure and then following the response of the coronary flow along a time interval long enough to match the experimental range; the much slower fluid transport which follows the rapid vascular changes is thus observed. The decrease in coronary flow on the long time scale is explained by the accumulation of

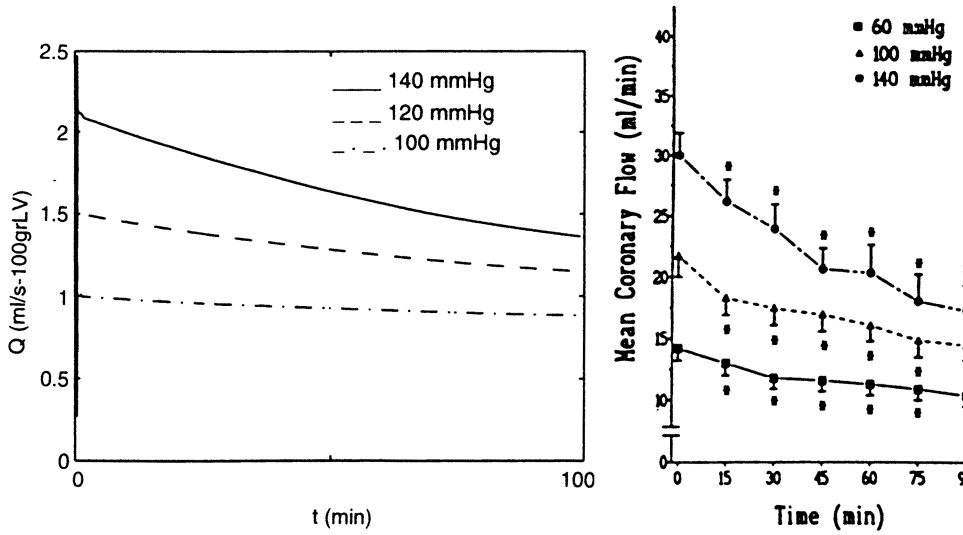

Figure 6. Left: Simulation of coronary flow response to a step change in the coronary perfusion pressure. **Right:** Q, flow. Experimental data of Rubboli et al. [23] (with permission of the American Physiological Society).

fluid in the myocardium. Simultaneous with the increase in perfusion pressure, the flow increases due to the increase in the pressure drop along the coronary tree and due to the change in the blood vessel cross section area. However, as the capillary pressure increases, the transcapillary fluid transport also increases, and the myocardial fluid content and IMP gradually increase, thus causing the observed decline in coronary flow.

DISCUSSION

Integration between structure, function and mass transport in the myocardium, which allows for the multilateral interactions between the related phenomena, is an important step in the study and analysis of the LV performance. This is evident from the ability of the model to simulate a wide variety of experimental data which were hitherto unsatisfactorily explained. Undoubtedly, the LV operating conditions are determined by the interactions between various phenomena and these change according to the changes in the myocardial function, structure and composition and the LV loading conditions. For example, the change in the coronary perfusion pressure shown above does not only affect the coronary flow by changing the pressure drop along the coronary tree and the vessel cross sectional area, but also affects the myocardial composition and fluid content which consequently affects the myocardial mechanics and the coronary flow. While the mechanical and flow dynamics and characteristics are clearly observed in Fig. 3 the role of fluid transport in determining these features is not so evident. Clearly, fluid transport affects the total LV wall volume which affects both the LV mechanics, coronary flow and blood volume and is consequently affected by them. The results are therefore the outcome of the interaction between the three phenomena. Clearly, changes in the coronary perfusion pressure, the contractility and other parameters will affect the mass balance as well as the LV mechanics and coronary flow thus lead to new operating conditions with different values of the LV wall volume, IMP, etc. [22, 24–26].

Another important outcome of the model is the possibility to predict the coronary flow characteristics under different myocardial mechanical conditions, such as the effects of changing myocardial contractility or LV loading conditions, with very good accuracy. It must be noted that while present theories of coronary flow based on the waterfall [18] and intramyocardial pump [19] effects do not explain certain important experimental observations, such as the peculiar relation between the coronary flow impediment and the LV pressure, the present model provides a good prediction of the experimental findings. This is shown in Figs. 4 and 5. Thus, the model correctly predicts the small dependence of the flow impediment on the LV pressure when the latter is changed by altering the preload or the afterload at a constant perfusion pressure [22, 26]. It is noted that the IMP does not change significantly with great changes in the LV loading conditions and the different contraction modes. The flow impediment is, however, predicted to be significantly affected by changes in the myocardial contractility. This behavior, as well as the LV loading effects, is due to the fact that the IMP in the contracting myocardium is principally determined by the stresses that develop in the myocardium rather than by the boundary condition at the endocardial surface, i.e. the LV cavity pressure. These stresses, which develop in the myocardium, are mainly determined by the contraction of the sarcomere matrix but do also depend on the passive fiber matrix and the total wall fluid content. However, the IMP in the passive myocardium is affected in a greater manner by the LV pressure since, in this case, the endocardial boundary condition has a larger effect on the myocardial stresses. Figure 5 shows the good agreement between the prediction of the model and the experi-

mental findings. The model also correctly predicts [24–26] the coronary flow, oscillatory flow amplitude and IMP dependence on the coronary perfusion pressure.

A most important feature of the model is that it allows to analyze the effects of fluid transport on the LV performance within a comprehensive framework. As observed in various experimental studies [6, 23], changes in the fluid transport conditions which alter the intramyocardial fluid content affect both the coronary flow and the LV mechanics. These effects are closely reproduced in our model simulations in Fig. 6, as well as in our previous studies [24–26].

The ability of the model to describe such a wide range of normal and pathological conditions, as compared to some of the earlier models, attests to the importance of maintaining a mass balance in the system under study. The obvious advantages of the present integrated model are:

1) The myocardial composition, volume and volume shifts are evaluated using physical principles (e.g., mass conservations balances) rather than *a priori* estimates.
2) The overall LV performance characteristics (mechanics, blood flow, and fluid and mass transport) are directly related to the mechanical sarcomere activity, spatial structure and physiological composition (fiber–blood–interstitium) of the myocardium rather than to the commonly used dependent variables, such as the IMP, LVP or others variables which are derivatives of the myocardial activity.
3) Pathological changes in LV performance, which are characterized by changes in the myocardial mechanical activity, the coronary flow and/or the fluid and mass transport, can now be directly and simultaneously studied.

In agreement with experimental observations, the model predicts that: 1) Coronary flow impediment and mechanics are not significantly affected by changes in the afterload and preload. 2) An increase in coronary perfusion pressure increases the intramyocardial pressure (IMP) as well as the mean flow and oscillatory flow amplitude. 3) Changes in the coronary perfusion pressure, and other effects altering the balance of the intramyocardial fluid, affect both ventricular mechanics and coronary flow. 4) Contractility has a direct and significant effect on the IMP and coronary flow impediment.

The satisfactory agreement of the model's predictions with a wide range of experimental data, shown here and in previous studies [22, 24–26], strongly suggests that the present model includes the major parameters needed to describe the LV performance and provide insight into the characteristics of the mechanical–flow–fluid transport interactions. It is obviously expected that more accurate quantitative results could be obtained by employing a more realistic LV geometry, a better description of the transmural heterogeneities and a better description of the muscle and collagen fiber–blood vessel interactions. However, this additional information, or otherwise improved LV assumptions, will most probably not significantly change the conclusions of the study.

CONCLUSION

The LV model presented here is based on a three–phase (fiber–blood–interstitium) myocardial model and integrates three important related phenomena: myocardial mechanics, coronary flow and interstitial fluid transport. It thus provides a better description of the myocardial activity and the relationships between the various myocardial parameters. Moreover, it allows the direct relation between cause (myocardial force generation, given the structure and physiological composition) and effect (LV mechanical performance,

coronary flow and fluid and mass transport). The model describes the LV performance under a wide range of normal and pathological conditions affecting myocardial mechanics, coronary flow and fluid and mass transport and their interactions. Although some simplifying assumptions were needed in order to obtain a coherent manageable picture of the complex intramyocardial interaction, the analysis provides insight into the myocardial performance and its operating characteristics under a wide range of constraints.

Acknowledgments

This study was sponsored by the Women's Division of the American Technion Society, USA, and supported in part by grants from the N. Seideman Family, Greatneck, NY, USA, the Anna and George Ury Endowment Fund, Chicago, USA, and the Technion Fund for the Promotion of Science.

DISCUSSION

Dr. T. Arts: Your integrated model fits a wide range of variables, maybe the widest range I have ever seen in describing the coronary arterial flow. What I do not clearly understand is the exact relation between the force in fibers, the stress in the fibers and the intramyocardial pressure (IMP), and what parameters did you use?

Dr. R. Beyar: We are looking at average properties across the wall. We did not look at transmural properties because this complexity would introduce a lot of problems. The major assumption is the biphasic approach. The total stress is the sum of the active stress (which is generated in our model only in the muscle fiber direction), and the passive stress (which is the stress in the collagen, both in the fiber direction and perpendicular to the fiber direction), minus the IMP, the pressure in the interstitial fluid. At steady state conditions this pressure is determined by the balance of forces and is subject to the balance between the fluid influx into the interstitial space by the fluid transport condition, and the outflow from the interstitial space (which is determined by the lymphatic flow conductivity). The biphasic approach was proposed by Chadwick [10] and others. The new concept in this model is that the IMP is defined by the fluid balance and the other interacting mechanical and coronary flow parameters.

Dr. H.E.D.J. ter Keurs: You interpret the data of Kresh [16] that intramyocardial pressure rose as a result of a shift in fluid balance. An alternative hypothesis is that as a result of the barbiturate intervention, which caused the active pressure development to drop, and then the washout of barbiturate, it is quite possible that a substantial calcium overload of cells in the area infused with barbiturates occurred, and therefore stress development by those cells rose as a DC signal, and that caused the decrease in IMP, and not the other way around.

Dr. R. Beyar: That is an interesting alternative, which can only be resolved by the right experiments.

Dr. H.E.D.J. ter Keurs: An experiment that looks a bit like it is one of creating ischemia in the myocardium, followed by reperfusion. In that case we know that calcium rises in the muscle cells, contracture develops, and, according to this scheme, that should cause a rise in intramyocardial pressure.

Dr. R. Beyar: Another way might be to measure the volume of the myocardium accurately during that 1 min transient. You could maybe infer how much fluid has been accumulated. One of the

things which is missing in the literature is the rate of the transport process under these conditions. It seems like the literature is very inconclusive on this point.

Dr. J. Bassingthwaighte: There is actually a lot of experimental data on osmotic transients.

Dr. Y. Lanir: How does contractility affect the intramyocardial pressure?

Dr. R. Beyar: For isovolumic contractions, if you decrease contractility, both the left ventricular pressure and the IMP fall down. If it is not isovolumic then you have a more complex situation: there is an interaction between the generated left ventricular pressure, which is the afterload constraint, and the deformation. Deformation is stretching the collagen fibers in the radial direction, across the wall thickening. This added stretching complicates the stresses in the fibers in the radial direction and this will modify the fluid pressure.

Dr. Y. Lanir: I understand that under isovolumic conditions the left ventricular pressure goes down. But the group of Westerhof showed that contractility affects the flow, independent of the left ventricular pressure. I thought this was the main issue here.

Dr. R. Beyar: If you do not change contractility, the pressure in the interstitial fluid does not decrease even if you decrease the afterload and the LVP decreases. This is due to a significant IMP build-up due to deformation of the passive elements, leading to a large increase in σ_p, the passive stress element. There is an interplay between the active stress σ_a, σ_p and the IMP. You have higher deformation under a low afterload, increasing σ_p. As a result, you have an almost independence of IMP on the preloading condition at constant contractility.

Dr. R. Reneman: When I gave up working on the IMP in the 1960s, I had a simple concept that the contractile forces that are generating the pressures in the left ventricle are basically the same forces generating pressure in the fluid compartments in the intermyocardial wall and are the same contractile forces that are generating the pressure. The key question is: How much fluid is trapped in the fluid pockets in the wall and how much is leaking out? This concept explains everything, because you can have a high intramyocardial pressure and an empty left ventricle. It is as simple as that. But the key question is, and I think you have not solved it either, how much fluid is leaking from the fluid compartments in the wall during systolic contraction. The lymph flow is part of the story because it can be squeezed out in other directions too.

Dr. R. Beyar: The volume of the interstitial space does not change much during a cycle. However, if you wait over many beats, after a step change in loading or perfusion conditions, then you may observe a change in fluid content. Our analysis considers only gross changes and total lymphatic flow.

Dr. R. Reneman: The simplest experiment to demonstrate that, and we measured it 24 years ago, is on coronary bypass grafts. When you have an empty beating left ventricle and the patients are still in bypass and the heart starts to contract, you get a beautiful squeeze of blood flow back into the aorta at a pressure of 70 mmHg.

REFERENCES

1. Kouwenhoven E, Vergroesem Y, Spaan JAE. Retrograde coronary flow is limited by time-varying elastance. *Am J Physiol.* 1992;263:H484-H490.
2. Kresh JY. Myocardial modulation of coronary circulation (letter). *Am J Physiol.* 1989;257: H1934-H1935.
3. Fukui A, Yamaguchi S, Tamada Y, Miyawaki H, Baniya G, Shirakabe M. Different effects of coronary perfusion pressure on diastolic properties of left and right ventricles (Abstract). *Circulation* 1991; 84:II-45.

4. Kresh JY, Frash F, McVey M, Brockman SK, Noordergraaf A. Mechanical coupling of the myocardium with coronary circulation in the beating and arrested heart (Abstract). *Circulation.* 1990; 84:II–45.
5. McCulloch AD, Hunter PJ, Smaill BH. Mechanical effects of coronary perfusion in the passive canine left ventricle. *Am J Physiol.* 1992;262:H523–H530.
6. Anderson SE, Johnson JA. Tissue–fluid pressure measured in perfused rabbit hearts during osmotic transients. *Am J Physiol.* 1987;252:H1127–H1137.
7. Arts T, Veenstra PC, Reneman RS. Transmural course of stress and sarcomere length in the left ventricle under normal hemodynamic circumstances. In: Baan J, Arntsenius AC, Yellin EL, eds, *Cardiac Dynamics*. The Hague: Martinus Nijhoff, 1980; 115–122.
8. Beyar R, Sideman S. A computer study of the left ventricular performance based on fiber structure, sarcomere dynamics and transmural electrical propagation velocity. *Circ Res.* 1984;55:358–375.
9. Beyar R, Ben–Ari R, Gibbons–Kroeker CA, Tyberg JV, Sideman S. The effect of interconnecting collagen fibers on LV function and intramyocardial compression. *Cardiovasc Res.* 1993;27(12): 2254–2263.
10. Chadwick RS. Mechanics of the left ventricle. *Biophys J.* 1980;39:279–288.
11. Huyghe JM, Arts T, van Campen DH, Reneman RS. Porous medium finite element model of the beating left ventricle. *Am J Physiol.* 1992;262:H1256–H1267.
12. Nevo E, Lanir Y. Structural finite deformation model of the left ventricle during diastole and systole. *J Biomech Eng Trans ASME.* 1989;111:342–349.
13. Ohayon J, Chadwick RS. Effects of collagen microstructure in the mechanics of the left ventricle. *Biophys J.* 1988;54:1077–1088.
14. Beyar R, Sideman S. Time dependent coronary blood flow distribution in the left ventricular wall. *Am J Physiol.* 1987;252:H417–H433.
15. Chadwick RS, Tedgui A, Michel JB, Ohayon J, Levy BI. Phasic regional myocardial inflow and outflow: comparison of theory and experiments. *Am J Physiol.* 1990;258:H1687–H1698.
16. Kresh JY, Fox M, Brockman SK, Noordergraaf A. Model–based analysis of transmural vessel impedance and myocardial circulation dynamics. *Am J Physiol.* 1990;258:H262–H276.
17. Bruinsma P, Arts T, Dankelman J, Spaan JAE. Model of the coronary circulation based on pressure dependence of coronary resistance and compliance. *Bas Res Card.* 1988;83:510–524.
18. Downey JM, Kirk ES. Inhibition of coronary flow by vascular waterfall mechanism. *Circ Res.* 1975;36:753–760.
19. Spaan JAE, Breuls N, Laired J. Diastolic systolic coronary flow differences are caused by intramyocardial pump action in the anesthetized dog. *Circ Res.* 1981;49:584–593.
20. Krams R, Sipkema P, Westerhof N. Coronary oscillatory flow amplitude is more affected by perfusion pressure than ventricular pressure. *Am J Physiol.* 1990;258:H1889–H1898.
21. Krams R, Sipkema P, Westerhof N. Varying elastance concept may explain coronary systolic flow impediment. *Am J Physiol.* 1989;257:H1471–H1479.
22. Zinemanas D, Beyar R, Sideman S. Effects of myocardial contraction on coronary blood flow: an integrated model, transport. *Annals Biomed Eng.* 1994;22(6):638–652.
23 Rubboli A, Sobotka PA, Euler DE. Effect of acute edema on left ventricular function and coronary vascular resistance in the isolated rat heart. *Am J Physiol.* 1994;267:H1054–H1061.
24. Zinemanas D, Beyar R, Sideman S. Intramyocardial fluid transport effects on coronary flow and LV mechanics. In: Sideman S, Beyar R, eds, *Interactive Phenomena in the Cardiac System*. New York: Plenum Press, 1993; 219–231.
25. Zinemanas D, Beyar R, Sideman S. Relating muscle mechanics, blood flow and mass transport interactions in the LV wall. *Int J Heat & Mass Trans.* 1994;37:191–205.
26. Zinemanas D, Beyar R, Sideman S. An integrated model of LV muscle mechanics, coronary flow and fluid and mass transport. *Am J Physiol.* 1995;268: (in press).
27. Gonzalez F, Bassingthwaigthe JB. Heterogeneities in regional volumes of distribution and flows in rabbit heart. *Am J Physiol.* 1990;258:H1012–H1024.
28. Beyar R, Caminker R, Manor D, Sideman S. Coronary flow patterns in normal and ischemic hearts: Transmyocardial and artery to vein distribution. *Annals Biomed Eng.* 1993;21:435–458.
29. Kedem O, Katchalsky A. Thermodynamic analysis of the permeability of biological membranes to non–electrolytes. *Biochim Biophys Acta.* 1958;27:229–246.
30. Baird RJ, Manktelow RT, Shah PA, Ameli FM. Intramyocardial pressure. A study of its regional variations and its relationship to intraventricular pressure. *J Thor Card Surg.* 1970;59:810–823.
31. Cantin B, Rouleau JR. Myocardial tissue pressure and blood flow during coronary sinus pressure modulation in anesthetized dogs. *J Appl Physiol.* 1992;73:2184–2191.
32. Rabbany SY, Kresh JY, Noordergraaf A. Intramyocardial pressure: interaction of myocardial fluid pressure and fiber stress. *Am J Physiol.* 1989;257:H357–H364.

33. Stein PD, Sabbah HN, Marzili M. Intramyocardial pressure and coronary extravascular resistance. *J Biomech Eng Trans ASME.* 1985;107:46–50.
34. Stein PD, Marzili M, Sabbah HN, Lee T. Systolic and diastolic pressure gradients within the left ventricular wall. *Am J Physiol.* 1980;238:H625–H630.
35. Krams R, Sipkema P, Zegers J, Westerhof N. Contractility is the main determinant of coronary systolic flow impediment. *Am J Physiol.* 1989;257:H1936–H1944.
36. Doucette JW, Goto M, Flynn AE, Austin RE Jr, Husseini W, Hoffmian JIE. Effects of cardiac contraction and cavity pressure on myocardial blood flow. *Am J Physiol.* 1993;265:H1342–H1352.

CHAPTER 29

HYPERTROPHIC CARDIOMYOPATHY: FUNCTIONAL ASPECTS BY TAGGED MAGNETIC RESONANCE IMAGING

Rafael Beyar[1]

ABSTRACT

Studies addressing the issue of regional function in hypertrophic cardiomyopathy patients (HCM) are reviewed. The relationship between regional wall thickness and function in these patients was studied by three dimensional (3D) tagged magnetic resonance imaging (MRI) utilizing the volume-element approach. Regional function was indexed by myocardial thickening and circumferential shortening and related to the local thickness and wall stress index. An inverse relationship was found between wall thickening and thickness as well as between circumferential shortening and wall thickness. Lower stresses were obtained for thicker myocardial segments. Function of the normal-thickness regions was enhanced in the HCM patients relative to the normal subjects. Thicker segments in patients with HCM are thus characterized by reduced systolic function, which occurs at segments with relatively low stress levels. This pattern is consistent with the hypothesis that the thick myocardial segments have reduced contractile activity, probably due to recently identified mutations in the gene responsible for production of β heavy chain myosin as well as other contractile proteins.

INTRODUCTION

Regional performance in hypertrophic cardiomyopathy (HCM) is still incompletely characterized, with studies variably reporting that the hypertrophied myocardium has reduced [1–4] or normal function [5–6]. In general, nonuniform myocardial performance throughout the different regions have been reported [7, 8]. Such heterogeneities in HCM

[1]Heart System Research Center, Julius Silver Institute of Biomedical Engineering, Technion-IIT, Haifa 32000, Israel.

Molecular and Subcellular Cardiology: Effects of Structure and Function
Edited by S. Sideman and R. Beyar, Plenum Press, New York, 1995

are greater and may therefore be associated with greater variation in regional myocardial performance.

Past studies have used somewhat limited imaging modalities to study HCM patients; these one or two dimensional echocardiography [1, 3, 5] or radionuclide ventriculography [9], and methods of analysis (fixed or floating frame of reference for wall motion analysis) are probably the reason for the inconsistency of the reported results.

Myocardial tagging is a method of magnetic resonance imaging (MRI) by which specific myocardial points can be traced from end-diastole to end-systole, allowing direct measurement of strains [10, 11]. Some recent studies have used MRI modalities to study patients with HCM [4, 12]. The use of 3D reconstruction of tagged MRI data [12–15] correct for possible "translation errors" and provide the best noninvasive method to measure regional function. Here, we discuss the recent observations of the anatomical and physiological features in patients with HCM obtained by novel methods of MRI tagging, concentrating on regional functional aspects of the disease and its clinical applications. Specifically, an hypothesis that while global ventricular function is maintained in HCM patients, regions of "abnormally" functioning hypertrophied myocardium exist is presented and supported by experimental data.

MRI Tagging Using Spatial Modulation of Magnetization (SPAMM)

Maier *et al.* [4], using MRI with the SPAMM technique, found that the wall motion, as assessed by radial displacement of the hypertrophied septum, was significantly reduced with marked heterogeneity between regions and a reduced motion in the inferior and septal zones. A trend towards reduced torsion was also reported. Other studies using the same imaging technique have also found reduced shortening in these patients, reporting different degrees of heterogeneities between regions [12, 15]. Interestingly, Young *et al.* [15] have recently reported increased torsion in spite of reduced shortening.

All these studies have clearly shown the heterogeneity of reduced function in HCM patients. Specifically, they looked into this heterogeneity based on the anatomical division, but none of these studied have specifically addressed the relationship between local thickness, function and load.

Functional MRI Analysis Using Radial Tagging Method

MRI with radial tagging was first described by Zerhouni *et al.* [10]. Typically, a series of cross sectional images is taken at end diastole and end systole. Four to six pre-saturation long axis planes rotated at equal angles around the long axis of the LV, are placed as close to end-diastole as possible (Fig. 1). These planes result in 8–12 black lines (tags) on the images that persist for 400–600 ms and move with the muscle. Similarly, long axis images with parallel short axis tagged planes can be obtained. When the two sets of images are combined [13, 14], a complete 3D representation of the set of intersection points between the tags, endocardium and epicardium can be obtained (Fig. 2). This allows accurate description (within the resolution limits of the image) of the deformation field of each volume element, defined by four adjacent endocardial and epicardial intersection points.

While one can calculate the deformation field in detail for each cube, as done by Azhari *et al.* [14], we are interested in the parameter which will represent regional function in a global manner. Regional thickening by the volume element approach suggested by Beyar *et al.* [16] has been proven as a superior index of regional function [17]. In addition, circumferential shortening is another index frequently used to characterize ventricular function. This index can be easily extracted from the MRI data.

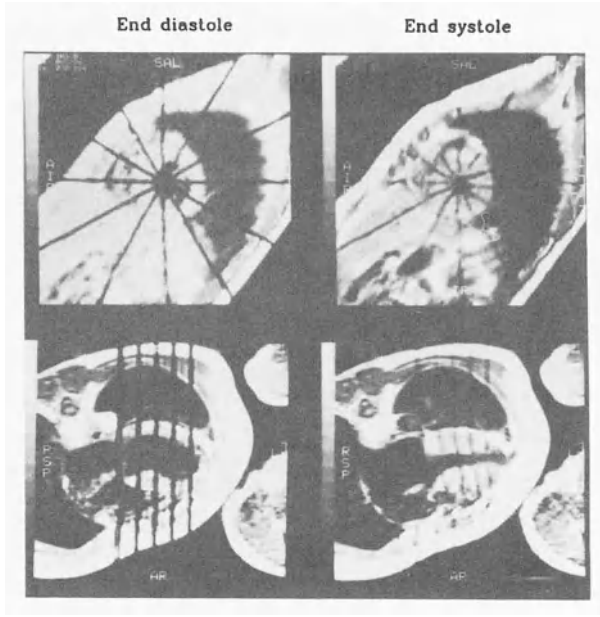

Figure 1. Short axis images with six pre-saturation long axis planes and long axis images with parallel short axis tagged planes (graph reproduced from Dong *et al.* [13] by permission).

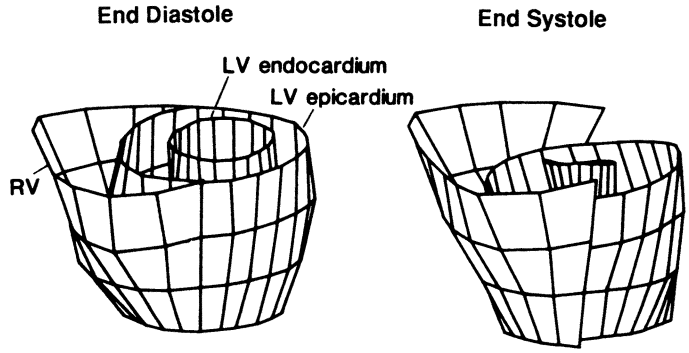

Figure 2. Representation of the 3D image of the LV. Note that the RV is uncorrected for longitudinal displacement (reproduced from Dong *et al.* [13] by permission).

RESULTS

Using the 3D set of data mentioned above, we have developed a method to estimate regional load [18, 19]. The longitudinal and circumferential radii of curvature were calculated regionally for each point by a special fitting algorithm [19]. These, combined with the local thickness, yielded an index of stress, normalized to pressure [18]. Stress mapping for the entire LV was thus feasible and could be used to characterize diseases with marked heterogeneities such as LV aneurysms [18].

Regional function was assessed in terms of systolic wall thickening and segment shortening in a series of patients with HCM. Particular attention was paid to study the relationship between regional functional parameters and the end-diastolic wall thickness, and the relationship between regional function and load.

Relation between Function to Thickness

Figure 3 shows the relationship between regional function, as determined by wall thickening and regional thickness for 17 patients with HCM and 6 normal volunteers. While each point represents one volume element, the complete set of data points from all the dogs are plotted in Fig. 3. A clear, significant inverse correlation between regional function and local thickness is observed. The thicker the segment the lower is its function, with almost no thickening for segments thicker than 20 mm. A similar relationship is also observed between circumferential shortening and thickness. Therefore, independent of the method to index regional function, the pattern of inverse correlation between function and thickness is maintained.

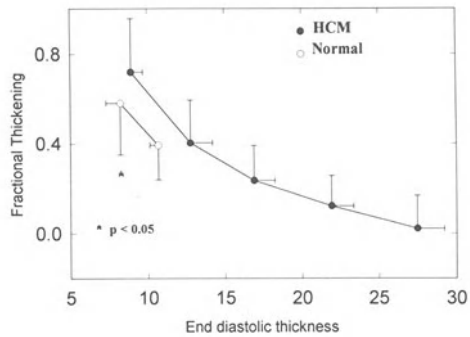

Figure 3. The relationship between regional function as measured by wall thickening and regional thickness (reproduced from Dong *et al.* [13] by permission).

Relation between Function to Load

Regional load normalized by pressure can be indexed by the equation proposed by Janz [20] and modified for application to 3D reconstructed hearts by MRI [19] or computed cine tomography [18]. To obtain the regional stress/pressure index it is required that, in addition to the thickness, the curvatures in the circumferential and longitudinal directions are known. To obtain the curvature from the digitized 3D reconstructed heart, an averaging algorithm which accounts for the immediate neighboring segments around the region of interest was used. A schematic presentation of the regional curvatures obtained from the 3D surface is shown in Fig. 4. The stress/pressure was calculated for each segment from the thickness and curvature data.

The relationship between regional stress/pressure and thickness is shown in Fig. 5. Note that, similar to the function–thickness relationships, the stress–thickness relationship are also inversely related. This relationship, which is not unexpected, indicates lower stresses for the thicker segments and suggests that regional function is reduced for these segments in spite of the low regional load.

CONCLUSION

Recent studies that employ MRI tagging to analyze regional function in HCM patients yield the following conclusions:

1) The myocardium in HCM is heterogeneously thickened and the fractional thickening and circumferential shortening of the abnormally thickened myocardium is reduced compared to the normals while global LV function is preserved.
2) Local function, manifested by the decrease in fractional thickening and shortening (local function) is inversely related to the local thickness.
3) Regions of reduced function are also subjected to reduced load.

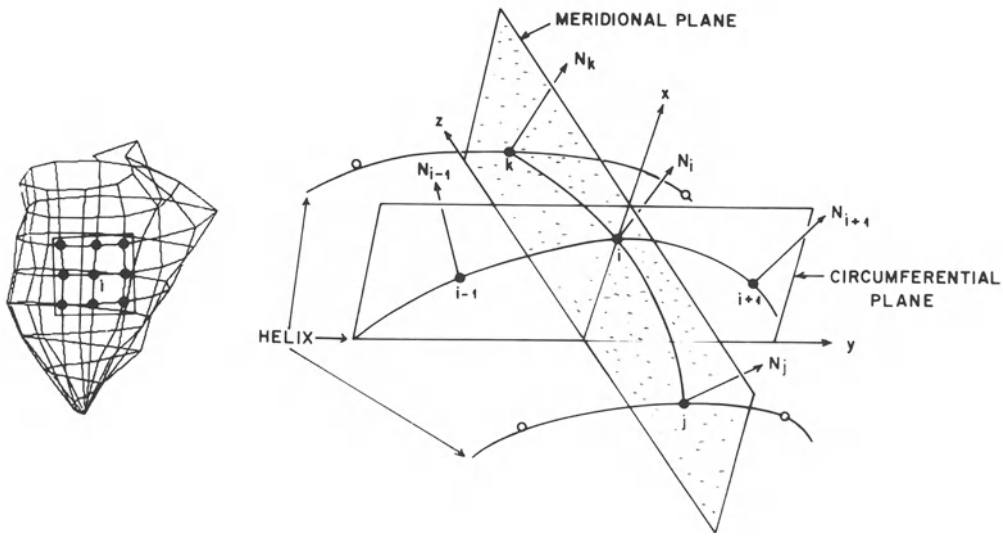

Figure 4. The method to calculate regional curvature (reproduced from Lessick *et al.* [19] with permission).

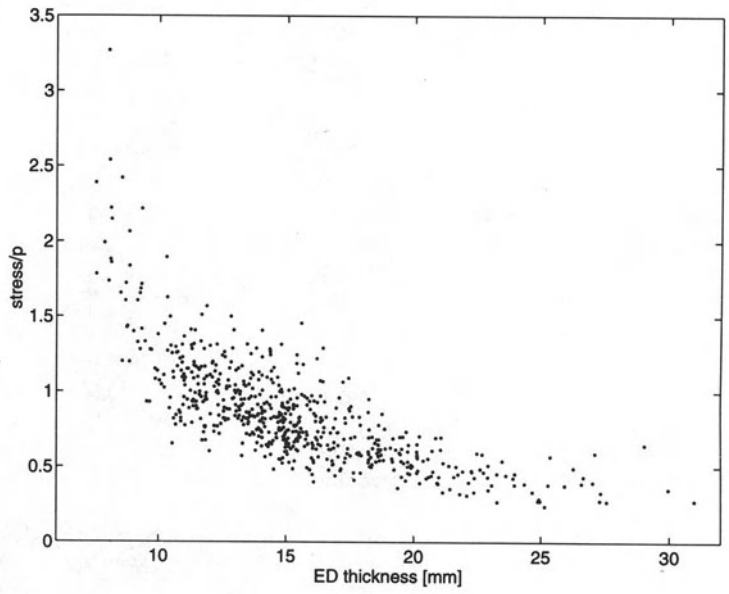

Figure 5. The relationship between regional load index (end-diastolic meridional stress/pressure) vs. end diastolic local thickness.

These observations are purely mechanical, but they can be interpreted either with respect to geometry, or related to known abnormalities of the contractile proteins in these patients [25–27]. One possible explanation of these observations is that the thicker portions of the myocardium are restricted in motion due to partial or complete cavity obliteration. Indeed, both reduced motion [4, 12] and reduced thickening or shortening [13, 15] are reported in HCM patients. However, this typical inverse relationship between function and thickness is observed even in cases without cavity obliteration in the absence of an intraventricular gradient. Consequently, we suggest that mechanical restraining factors do not play a significant role in the observed relationship.

Increased connective-tissue content that limits myocardial shortening and wall thickening might be another contributing factor. Connective tissue within the myocardium is arranged around and between cells and cell groups [21]. These connective structures deform and store energy as myocardial cells contract and tend to keep the structures in their original shape and limit deformation; excessive connective tissue might also limit myocardial contraction. In HCM, there is a significant increase in the amount of connective tissue [22, 23]. A recent study [24] has demonstrated that there is a marked increase in both pericellular weave fibers and strut connection fibers. We suspect that the increased connective tissue may also limit active systolic longitudinal shortening and lateral thickening of the cells, in addition to the well-recognized limitation of passive diastolic filling.

Classical muscle physiology predicts that increased shortening occurs with reduced afterload. The observation that the afterload is regionally reduced for thick, abnormally functioning, segments suggests that changes in regional load cannot explain the observed heterogeneity in function. However, these can possibly be explained by genetic defects in the contractile or structural proteins in patients with HCM. Several mutations that cause defects in the β cardiac myosin heavy chain [25], as well as alpha tropomyosin and cardiac troponin T genes [26] have been reported. Therefore, either a biochemical abnormalities in the contraction of the myocardium, which is associated with abnormalities in the contractile proteins, or a structural abnormalities in the direction of the fibers recognized as "myocardial disarray" [27, 28] may cause the abnormal heterogeneity in function. Both these factors are possibly related to genetic defects in the contractile or structural proteins in the myocardium.

Acknowledgement

This study was supported in part by the Anna and George Ury Endowment Fund, Chicago, IL, USA, and the Joseph and Edythe Jackier Endowment Fund, Detroit, MI, USA. Particular thanks are due to Professor S. Sideman for his constructive support.

DISCUSSION

Dr. H.E.D.J. ter Keurs: I like your results. In your comparison between cardiomyopathy and normal subjects, it strikes me that the thickness of normals is so narrowly distributed that you cannot make statements about the relation between function and thickness. Maybe it would be wise to add people who are normal but have hypertension in order to study the thickness.

Dr. R. Beyar: I agree. We did not study patients with essential hypertension as a cause for hypertrophy. Such a patient group will certainly increase the range of thickness over the normal range.

Dr. H.E.D.J. ter Keurs: In relation to the regional character of the disease of this type of cardiomyopathy, you describe decreased function while the area is hypertrophied. There might be a speculation from your side, and from Dr. Parmacek, as to whether the genetic abnormality that has been shown in patients who have this disease may be regionally distributed.

Dr. R. Beyar: I ask the same question: is the abnormal protein that is known to be present in HCM only confined to the hypertrophied regions? Is it just a matter of time until the other regions also undergo failure and hypertrophy?.

Dr. E. Ritman: Did you see any consistent differences between the occurrence within the cardiac cycle of peak thickness in the normals vs the hypertrophied ones?

Dr. R. Beyar: We did not look at that. We looked at end diastole and end systole and we did not as yet analyze the mid systolic points. In general, just looking at the images, my impression is that maximum thickening did happen at end systole, as defined in these patients by the closure of the aortic valve. However, I can not state conclusively whether different regions reach maximum thickness at different times.

Dr. P. Hunter: I am a bit concerned about the transmural lumping that you are doing with the volume element technique. You are essentially taking a volume element that smooths out any transmural variation that may exist in strain. Particularly if you use a very simple index of stress to determine regional function with these very large thick walled hearts. Because, it may be that the transmural gradients of stress may mean that in these patients there is a different load being carried by the subepicardial region vs the subendocardial region. There has been some work by Young *et al.* [15] that uses a technique which looks transmurally at these hypertrophic cardiomyopathy patients. Can you comment on whether there is a danger in this lumping process?

Dr. R. Beyar: One of the limitations of the current tagging technique at this stage is that you can only look at the complete thickness of the wall. It is clear that there is a transmural distribution of load. We calculate an average of the entire wall, which obviously may be incomplete or inaccurate. It is interesting to see the transmural variation of strains across the myocardium. I am not sure if Young *et al.* [15] addressed that. I do not recall seeing the transmural gradient in this particular group of patients in hypertrophic cardiomyopathy. One of the major limitations of this technique is the problem of resolution. The thickness of the wall is about 10 pixels. You make a mistake of 1 pixel and you have huge error. When you break the wall into layers, you amplify this error several-fold and then you run into major problems. We could not calculate with this method anything regarding transmural distribution. It is something to look at in the future.

Dr. P. Hunter: Did you find constant volume in your elements and how closely?

Dr. R. Beyar: Yes. The variations in end-diastolic to end-systolic muscle volume values were between 5-10%.

Dr. D. Burkhoff: Bill Gaasch [Shimizu et al., *Circulation.* 1991;83:1676-1684] has published a study with hypertensive hypertrophy using echocardiography to calculate midwall circumferential shortening, showing that even though global ejection fraction is normal in that patient population, there is a reduction in midwall circumferential shortening. That would extend the scope of your findings. It may not necessarily relate to genetic changes in myosin but something more intrinsic to hypertrophy that may not be related to the myocyte.

Dr. R. Beyar: If you take a normal ventricle with the same end-diastolic and end-systolic volume, and one with homogenous hypertrophy you will get less shortening and thickening for the

hypertrophic ventricle, just based on mass conservation. No sophisticated mechanical principles should be used. The issue in this study is regional parameters.

Dr. W. Parmacek: Regarding genetics and hypertrophic cardiomyopathy. As everyone is aware, approximately 50% of the patients with familial hypertrophic cardiomyopathy have a defect in the β-myosin heavy chain. Recent data which came out in Selno about 3–4 months ago by John and Cricket Siman also show that defects in other contractile proteins, troponin and tropomyosin, also result in familial hypertrophic cardiomyopathy phenotype. The concept which is emerging is that hypertrophic cardiomyopathy is not a defect of the myosin heavy chain *per se*, but that of the sarcomeric or contractile proteins. Getting back to Dr. ter Keurs question as to whether there is abnormal gene expression in specific regions of the heart which would account for regional variations in function, that data is not known at this point for the simple reason that every cell has the same genetic defect. There is no question about that. To measure gene expression within particular regions, you would obviously have to have large quantities of biopsy samples from those regions and that study has not been done to date. Perhaps when autopsy data are available from these patients we can make that assessment. Obviously, the old data from the NIH lab has shown that myofibrillar disarray does not always correlate with the areas of dysfunction and/or the areas of hypertrophy so it is hard to know what that will show.

Dr. M. Flugelman: Does your finding explain why some patients with hypertrophy do better with ventricular pacing?

Dr. R. Beyar: It is very difficult to reach such a conclusion based on available data.

Dr. J. Janicki: As was mentioned, there is a lot of muscle fiber disarray in hypertrophic cardiomyopathy. Was this fact reflected in any of the parameters that you measured?

Dr. R. Beyar: The two parameters that we measured were radial thickening, and endocardial and epicardial shortening. It is just an observation of what this volume element is doing. What is exactly happening in terms of micro-mechanics inside this cube is beyond the scope of this method.

REFERENCES

1. Cohen MV, Cooperman LB, Rosenblum R. Regional myocardial function in idiopathic hypertrophic subaortic stenosis: An echocardiographic study. *Circulation*. 1975;53:842–847.
2. tenCate FJ, Hugenholtz PG, Van Dorp WG, Roelandt. Prevalence of diagnostic abnormalities in patients with genetically transmitted asymmetric septal hypertrophy. *Am J Cardiol*. 1979;43:731–737.
3. Silverman KJ, Hutchins GM, Weiss JL, Moore GW. Catenoid shape of the interventricular septum in idiopathic subaortic stenosis: Two-dimensional echocardiographic confirmation. *Am J Cardiol*. 1982;49:27–32.
4. Maier SE, Fischer SE, McKinnon GC, Hess OM, Krayenbuehl H-P, Boesiger P. Evaluation of left ventricular segment wall motion in hypertrophic cardiomyopathy with myocardial tagging. *Circulation*. 1992;86:1919–1928.
5. Kaul S, Tei C, Shah PM. Interventricular septal and free wall dynamics in hypertrophic cardiomyopathy. *J Am Coll Cardiol*. 1983;4:1024–1030.
6. Betocchi S, Hess OM, Losi MA, Nonogi H, Krayenbuehl HP. Regional left ventricular mechanics in hypertrophic cardiomyopathy. *Circulation*. 1993;88[part I]:2206–2214.
7. Gallagher KP, Osakada G, Matsuzaki M, Miller M, Kemper WC, Ross J Jr. Nonuniformity of inner and outer systolic wall thickening in conscious dogs. *Am J Physiol*. 1985;249:H241–H248.
8. Clark NR, Reichek N, Bergey P, Hoffman EA, Brownson D, Palmon L, Axel L. Circumferential myocardial shortening in the normal human left ventricle. Assessment by Magnetic Resonance Imaging using spatial modulation of magnetization. *Circulation*. 1991;84:67–74.

9. Mochizuki T, Murase K, Fijiwara Y, Tanada S, Hamamoto K, Tauxe WN. Assessment of systolic thickening with thallium-201 ECG-gated single-photon emission computed tomography: A parameter for local left ventricular function. *J Nucl Med.* 1991;32:1496-1500.
10. Zerhouni EA, Parish DM, Rogers WJ, Yang A, Shapiro EP. Human heart tagging with MR imaging: A method for noninvasive assessment of myocardial motion. *Radiology.* 1988;169:59-63.
11. Axel L, Dougherty L. MR imaging of motion with spatial modulation of magnetization. *Radiology.* 1989;171:841-845.
12. Kramer CM;Reichek N;Ferrari VA;Theobald T;Dawson J;Axel L. Regional heterogeneity of function in hypertrophic cardiomyopathy. *Circulation.* 1994;90:96-94.
13. Dong SJ, MacGregor JH, Crawley AP, McVeigh E, Belenkie I, Smith ER, Tyberg JV, Beyar R. Left ventricular wall thickness and regional systolic function in patients with hypertrophic cardiomyopathy: A three-dimensional tagged magnetic resonance imaging study. *Circulation.* 1994;in press.
14. Azhari H, Weiss JL, Rogers WJ, Siu CO, Zerhouni EA, Shapiro EP. Noninvasive quantification of principal strains in normal canine hearts using tagged MRI images in 3D. *Am J Physiol.* 1993;264:H205-H216.
15. Young AA, Kramer CM, Ferrari VA, Axel L, Reichek N. Three-dimensional left ventricular deformation in hypertrophic cardiomyopathy. *Circulation.* 1994;90:854-67.
16. Beyar R, Shapiro EP, Graves WL, Rogers WJ, Guyer W, Zerhouni EA, Soulen R, Weisfeldt ML, Weiss JL. Quantification and validation of left ventricular wall thickening by a three-dimensional volume element magnetic resonance imaging approach. *Circulation.* 1990;81:297-307.
17. Azhari H, Sideman S, Weiss JL, Shapiro EP, Weisfeldt ML, Graves WL, Rogers WJ, Beyar R. Three dimensional mapping of acute ischemic regions from magnetic resonance images: Wall thickening versus motion analysis. *Am J Physiol* 259 (*Heart Circ Physiol*) 1990;28:H1492-H1503.
18. Lessick J, Sideman S, Azhari H, Marcus M, Grenadier E, Beyar R. Regional 3D geometry and function of left ventricles with fibrous aneurysms: a Cine-CT study. *Circulation.* 1991;84:1072-1086.
19. Lessick J, Sideman S, Azhari H, Shapiro EP, Weiss JL, Beyar R. Evaluation of regional load in acute ischemia by three-dimensional curvature analysis of the left ventricle. *Annals Biomed Eng.* 1993;21(2):147-161.
20. Janz RF, Waldron RJ. Predicted effect of chronic apical aneurysms on the passive stiffness of the human left ventricle. *Circ Res.* 1978;42:255-263.
21. Caulfield JB, Borg TK. The collagen network of the heart. *Lab Invest.* 1979;40:364-372.
22. Roberts CS, Roberts WC. Morphologic feature. *Prog Cardiol.* 1989;2(Pt 2):3-32.
23. Tanada M, Fijiwara H, Onodera T, Wu D-J, Hamashima Y, Kawai C. Quantitative analysis of myocardial fibrosis in normals, hypertensive hearts, and hypertrophic cardiomyopathy. *Br Heart J.* 1986;55:575-581.
24. Factor SM, Butany J, Sole MJ, Wigle ED, Williams WC, Rojkind M. Pathologic fibrosis and matrix connective tissue in the subaortic myocardium of patients with hypertrophic cardiomyopathy. *J Am Coll Cardiol.* 1991;17:1343-1351.
25. Jarcho JA, McKenna W, Pare JAP, Solomon SD, Holcombe RF, Dickies S, Levi T, Donis-Keller H, Seidman JG, Seidman CE. Mapping a gene for familial hypertrophic cardiomyopathy to chromosome 15q1. *N Engl J Med.* 1989;321:1372-1378.
26. Thierfelder L, Watkins H, MacRae C, Lamas R, McKenna W, Vosberg HP, Seidman JG, Seidman CE. Alpha-tropomyosin and cardiac troponin T mutations cause familial hypertrophic cardiomyopathy: a disease of the sarcomere. *Cell,* 1994;77:701-712.
27. Roberts CS, Roberts WC. Morphologic feature. *Prog Cardiol.* 1989;2(Pt 2):3-32.
28. Kuribayashi T, Roberts WC. Myocardial disarray at junction of ventricular septum and left and right ventricular free walls in hypertrophic cardiomyopathy. *Am J Cardiol.* 1992;70:1333-1340.

CHAPTER 30

MYOCARDIAL CONSTITUTIVE LAWS FOR CONTINUUM MECHANICS MODELS OF THE HEART

Peter J. Hunter[1]

ABSTRACT

Myocardial constitutive laws, for use in anatomically accurate finite element models of the heart, are presented for the passive and active mechanical properties of cardiac muscle. Biaxial testing of tissue sheets together with observations of tissue microstructure are used to define a "pole–zero" strain energy function for passive myocardium. A "fading memory" model of actively developed tension is based here on published work on the active properties of cardiac trabeculae.

INTRODUCTION

The heart is primarily a mechanical pump and many studies of cardiac function depend upon a thorough understanding of the mechanics of ventricular contraction and filling. The heart's electrical activation, coronary blood supply, chemical energetics and the highly complex system of local and global control are all influenced by the stresses and strains in the contracting myocardium. Considerable progress has been made in the analysis of ventricular mechanics over the last five years: ventricular geometry and the fibrous-sheet structure of myocardium have been measured and modelled with three-dimensional finite element models [1, 2]. The equations of motion based on large deformation elasticity theory are well understood and the computer models can solve these equations in reasonable time on an engineering workstation [3]. However, the most crucial component of these models is also the most poorly developed: the formulation of constitutive laws describing the stress–strain properties of cardiac muscle. The challenge is to find mathematical descriptions of stress–strain relations for both the passive and active muscle which accurately represent *in vitro* experimental measurements, are computationally efficient when

[1]School of Engineering, The University of Auckland, Private Bag 92019, Auckland, New Zealand.

Molecular and Subcellular Cardiology: Effects of Structure and Function
Edited by S. Sideman and R. Beyar, Plenum Press, New York, 1995

used in the continuum whole heart models, and which permit successful material parameter estimation when the models are used with clinical data. The difficulty is that myocardial tissue is highly nonlinear, inhomogeneous and anisotropic in the passive state and has time-varying active properties. Two stress-strain models are presented in this paper: one for passive muscle, based on our own studies of cardiac microstructure and biaxial testing of myocardial sheets, and one for active muscle, based on recently published uniaxial testing of cardiac trabeculae.

ORTHOTROPIC CONSTITUTIVE LAW FOR PASSIVE MUSCLE

Recent studies of the microstructure of myocardial tissue [4] have shown that the myocardium consists of layers of interconnected sheets of tissue separated by "cleavage planes". The muscle fibers lie in the plane of a sheet and adjacent fibers are coupled more strongly in the plane of the sheet than transverse to it. Three micro-structural axes are therefore evident: one along the fiber direction, the *fiber axis*, one orthogonal to the fiber axis but also in the plane of the sheet, the *sheet axis*, and a third, orthogonal to these two, directed across the cleavage planes, the *sheet normal*. The uniaxial stress-strain properties are quite different in the three orthogonal directions, reflecting in part the organization of collagen relative to these three axes.

The most striking difference in material behavior along the three axes is the limiting strain for an elastic response (Fig. 1). If the tissue is stretched along the fiber direction, the limiting stretch ratio is about 1.3 and along the sheet axis the limiting stretch ratio is 1.5. In the direction of the sheet normal very little tension is developed below a stretch ratio of 1.5 but tension increases rapidly above this and cannot be stretched beyond 1.7 without irreversible damage. Another characteristic feature of the biaxial tests is that the stress-strain curve along one axis is very nearly independent of the degree of lateral stretch [5]. A fundamental feature of the stress strain curves is the very steep rise in stress as the limiting elastic strain along each axis is approached.

For incompressible materials the components of the second Piola-Kirchhoff stress tensor referred to material coordinates and measured per unit area of the undeformed material, are given by

$$T^{MN} = -p\delta^{MN} + \frac{1}{2}\left(\frac{\partial W}{\partial e_{MN}} + \frac{\partial W}{\partial e_{NM}}\right) \tag{1}$$

where W is an elastic strain energy function and p is the hydrostatic pressure [6]. To accommodate the microstructural observations and biaxial test results we have proposed a strain energy function, called the *pole-zero law* [4], of the form

$$W = k_1 \frac{e_{11}^2}{(a_1 - |e_{11}|)^{\beta_1}} + k_2 \frac{e_{22}^2}{(a_2 - |e_{22}|)^{\beta_2}} + k_3 \frac{e_{33}^2}{(a_3 - |e_{33}|)^{\beta_3}} + k_4 \frac{e_{12}^2}{(a_4 - |e_{12}|)^{\beta_4}} + k_5 \frac{e_{23}^2}{(a_5 - |e_{23}|)^{\beta_5}} + k_6 \frac{e_{31}^2}{(a_6 - |e_{31}|)^{\beta_6}} \tag{2}$$

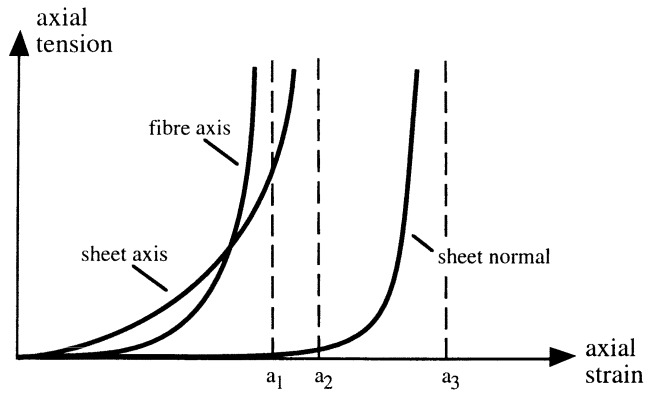

Figure 1. Uniaxial stress–strain relations along the three micro–structurally defined axes. The solid lines show the 'pole–zero' curves approaching the elastic strain limits in each direction at the respective pole positions a_1, a_2, and a_3.

where e_{MN} are the components of the Green strain tensor referred to material coordinates aligned with the structurally defined axes of the tissue (the e^2_{MN} numerator terms are necessary to ensure non–zero stiffness at zero strain); a_1 .. a_6 are parameters expressing the limiting strain for a particular type of deformation (i.e., the strain energy becomes very large as e_{11} approaches a_1, etc.) and $a_1 > e_{11}$, $a_2 > e_{22}$, $a_3 > e_{33}$, $a_4 > e_{12}$, $a_5 > e_{23}$, $a_6 > e_{31}$; β_1 .. β_6 are parameters expressing the curvature of the uniaxial stress–strain curves (partly a reflection of the distribution of unextended fiber lengths as more collagen fibers are recruited); k_1 .. k_6 are parameters giving the relative contribution of each strain energy term and k_1, k_2, k_3 are defined to be zero if e_{11}, e_{22} or e_{33}, respectively, are negative.

Using a separate pole for each microstructurally defined axis accommodates the different strain limiting behavior seen along each axis without the need for the (numerically unstable) large exponents found necessary for exponential or power law expressions. This strain energy function can be considered as the first part of a polynomial expansion in the pole–zero terms (i.e., terms of the form $W(e) = k(e^2/(a-e)^{\beta})$). A higher order expansion including cross–product terms may be justified by further experimental testing, particularly of shear behavior. As it stands there are 18 free parameters in equation (2) but some of these parameters must be strongly correlated because some tensile and shearing deformations are likely to involve the same underlying collagen microstructure. To elucidate these parameter correlations we have developed a biophysical model of muscle elasticity in which the strain energy arises from the stretching of several families of collagen fibers, whose distributions are based on observations of tissue microstructure.

The strain energy function, Eq. (2), is designed to model the tensile behavior of myocardial tissue but does include a compressive stiffness indirectly through the incompressibility of the tissue, as we now show. Consider the axial compression ($\lambda_1<1$) of a cylindrical segment of muscle under the assumption that the material properties in the plane orthogonal to the axis are isotropic (i.e. the muscle is transversely isotropic). To maintain incompressibility ($\lambda_1\lambda_2\lambda_3 = 1$), $\lambda_2 = \lambda_3 = 1/\sqrt{\lambda_1}$, giving

$$e_{11} = \frac{1}{2}(\lambda_1^2-1),\ e_{22} = e_{33} = \frac{1}{2}(\lambda_2^2-1) = \frac{1}{2}\left(\frac{1}{\lambda_1}-1\right) \quad \text{and} \quad W = 2k_2\frac{e_{22}^2}{(a_2-e_{22})^{\beta_2}} \ .$$

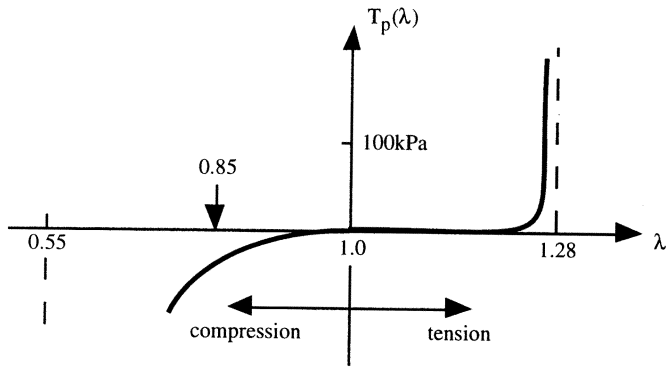

Figure 2. Passive stress–strain relation in uniaxial tension and compression. The dashed lines on the right and left show the pole positions in tension at $\lambda_1 = (1+2a_1)^{0.5} = 1.28$ (a sarcomere length of about 2.4 μm) and in compression at $\lambda_1 = (1 + 2a_2)^{-1} = 0.55$, respectively. The point marked at $\lambda = 0.85$ corresponds to the minimum attainable sarcomere length of 1.6 μm (see next section).

Then, using $T^{22} = (dW/de_{22}) - p = 0$ to give $p = dW/de_{22}$, the axial second Piola–Kirchhoff stress is:

$$T^{11} = \frac{dW}{de_{11}} - p = \frac{dW}{de_{11}} - \frac{dW}{de_{22}} = \frac{-2k_2e_{22}}{(a_2 - e_{22})^{\beta_2}} \left[2 - \frac{\beta_2 e_{22}}{(a_2 - e_{22}} \right] \left[\frac{1}{2\lambda_1^3} + 1\right] \quad , \quad (3)$$

This relation (for $\lambda_1<1$) is shown in Fig. 2, along with the uniaxial stretch behavior ($\lambda_1>1$). Note that the pole at $e_{22} = a_2$ (with $a_2 = 0.41$) occurs when $1/2\ [(1/\lambda_1)-1] = a_2$ or $\lambda_1 = 1/(1 + 2a_2) = 0.55$.

A CONSTITUTIVE LAW FOR ACTIVELY CONTRACTING MUSCLE

Experimental Procedure

The mechanical properties of active cardiac muscle are obtained primarily from experiments on small papillary muscles or trabeculae. The muscle fibers in these prepara–

Table 1. Passive Muscle Parameters

Parameters	Epicardial	Midwall
k_1 (kPa)	2.842	1.469
k_2 (kPa)	0.063	0.028
k_3 (kPa)	0.310	0.074
a_1	0.318	0.268
a_2	0.429	0.681
a_3	1.037	1.177
β_1	0.624	0.591
β_2	2.480	5.991
β_3	0.398	1.460

tions are aligned with the longitudinal axis and, provided muscles with a sufficiently large aspect ratio are used, sarcomere lengths are reasonably constant throughout the muscle cross-section. Measurement artifacts associated with unavoidable damage to the clamped ends of the preparation can be minimized by measuring the length changes of a central undamaged region (usually with laser diffraction techniques).

Mechanical Properties

The mechanical properties of cardiac muscle are summarized below under (i) steady state properties, and (ii) dynamic properties at a constant level of activation. Muscle length at time t is measured by the muscle fiber extension ratio $\lambda(t)$ and the actively developed tension in the muscle fiber is denoted by T. The extension ratio λ is the current sarcomere length divided by the *resting length*, the sarcomere length to which the unloaded muscle returns (1.85–1.90 μm for rat and cat cardiac muscle). Here we assume $\lambda = 1$ at a sarcomere length of 1.9 μm. The *level of activation* of a cardiac muscle cell is taken to mean the internal myoplasmic Ca^{2+} concentration $[Ca^{2+}]_i$. (Note: some authors use the Ca^{2+} bound to troponin-C as the measure of activation).

Since the active tension T is developed along the muscle fiber direction (taken as the first material coordinate here) the constitutive law, Eq. (1), with the strain energy given by Eq. (2), is now extended for T^{11} only:

$$T^{MN} = -p\delta^{MN} + \frac{1}{2}\left(\frac{\partial W}{\partial e_{MN}} + \frac{\partial W}{\partial e_{NM}}\right) + T.\delta_1^M\delta_1^N \quad , \tag{4}$$

where $T = T(\lambda, [Ca^{2+}]_i)$ and $\lambda = \left(1 + 2e_{11}\right)\cdot 0.5$.

Steady State Properties

At a constant level of activation the steady state muscle tension is an increasing function of muscle length – characterized by the extension ratio λ – as shown by the solid lines in Fig. 3a for various Ca^{2+} levels [7–9]. When the passive tension $T_p(\lambda)$, as given by Eq. (3) and shown in Fig. 2, is subtracted from the measured total tension (for $[Ca^{2+}]_o = 2.5$ Mm), the maximally activated *isometric* tension $T_0(\lambda)$ is found to be a linear function of λ with a slope $dT_0/d\lambda = 145$ kPa or a nondimensional slope $\beta = [(dT_0)/(T_0\, d\lambda)]_{\lambda=1} = 1.45$. If the increase in tension with length came about solely as a result of changing myofilament overlap, this parameter would be $\beta = 1$. Thus, $\beta > 1$ is evidence for length-dependent binding of Ca^{2+}. At $\lambda = 1$, $T_0 = 100$kPa, and the $T_0(\lambda)$ relation is therefore $T_0(\lambda) = T_{ref}\,[1 + \beta(\lambda-1)]$, where $T_{ref} = 100$ kPa is the isometric, actively developed tension at $\lambda = 1$ and saturating $[Ca^{2+}]_i$. The change in T_{ref} with $[Ca^{2+}]_i$ below saturation, under steady state conditions and constant λ, is described by a sigmoidal Hill relation. Note that $[Ca^{2+}]_i$ is also length-dependent, since the release of Ca^{2+} from the sarcoplasmic reticulum is influenced by stretch [7].

Dynamic Properties at a Constant Level of Activation

The most notable feature of the dynamic properties of cardiac (and skeletal) muscle is the fact that very small dynamic length changes are associated with large changes in tension. For example, shortening the muscle by less than 1% of its length in 1 ms produces a 100% drop in tension. Three types of experiment are often used to characterize the dynamic properties under a constant level of activation.

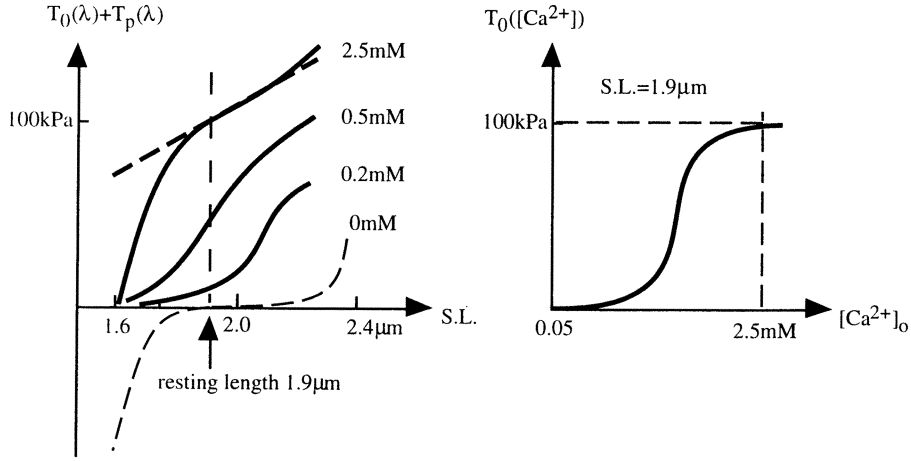

Figure 3. Left: Solid lines show total tension as a function of sarcomere length (S.L.) for different $[Ca^{2+}]_0$. The thin curved dotted line shows the passive tension. Also indicated (thick dotted line) is the resting length (1.9 μm, corresponding to $\lambda = 1$) and the $T_0(\lambda)$ relation obtained by subtracting the passive tension from the total tension. **Right:** Isometric tension, at a sarcomere length of 1.9 μm, as a function of $[Ca^{2+}]_o$.

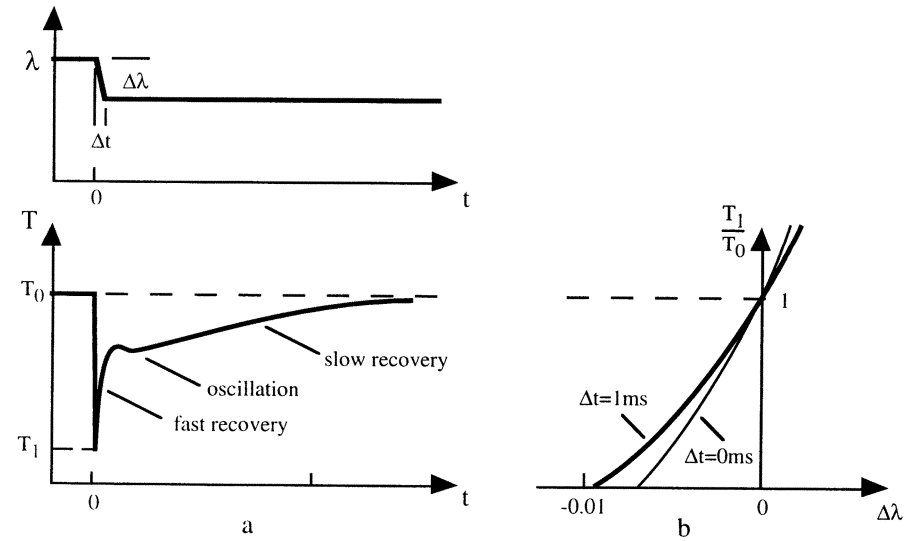

Figure 4. a: Tension recovery (lower panel) following a length step of Δλ in time Δt (upper panel). Notice the different phases of the tension recovery. **b:** Tension T_1 reached at the end of the length step, divided by isometric tension T_0, plotted against the magnitude of the length step Δλ. One curve is for a length step of 1 ms duration and the other for an idealized instantaneous step.

EXPERIMENTAL STUDIES

Length Step Experiments

Length step experiments in which the tension changes following a rapid length step are recorded. Fig. 4a shows a typical result. Notice (a) the drop in tension concomitant with

the length change $\Delta\lambda$; the lowest tension reached is labelled T_1, (b) the rapid recovery of tension, often with a slight oscillation before, and (c) a slower recovery to equilibrium. When the experiment is performed from a different initial value of T_0 (e.g. from a different point on the isometric tension–length curve) the entire response is found to scale with T_0. As shown in Fig. 4b, the magnitude of T_1 shows a nonlinear dependence on $\Delta\lambda$.

Constant Velocity Experiments

Constant velocity experiments in which the muscle is controlled to shorten at a constant rate, or shorten at a constant rate (following an initial transient), in response to a reduction in tension, to a constant value less than T_0. The plot of velocity against tension, the *force–velocity curve*, is shown in Fig. 5a. These curves are typically hyperbolic and are accurately described for the tetanized (maximally activated) muscle by the equation first proposed by Hill [10]:

$$\frac{-V}{aV_0} = \frac{\dot{\lambda}}{aV_0} = \frac{T/T_0 - 1}{T/T_0 + a} \tag{5}$$

where V_0 is the maximum velocity obtained when T = 0, and **a** is a parameter which controls the curvature of the force–velocity relation (the parameter **a** is chosen here to be non-dimensional: the '**a**' in Hill's original equation is represented here by aT_0). As with force recovery following a length step, the force–velocity curves scale with isometric tension T_0.

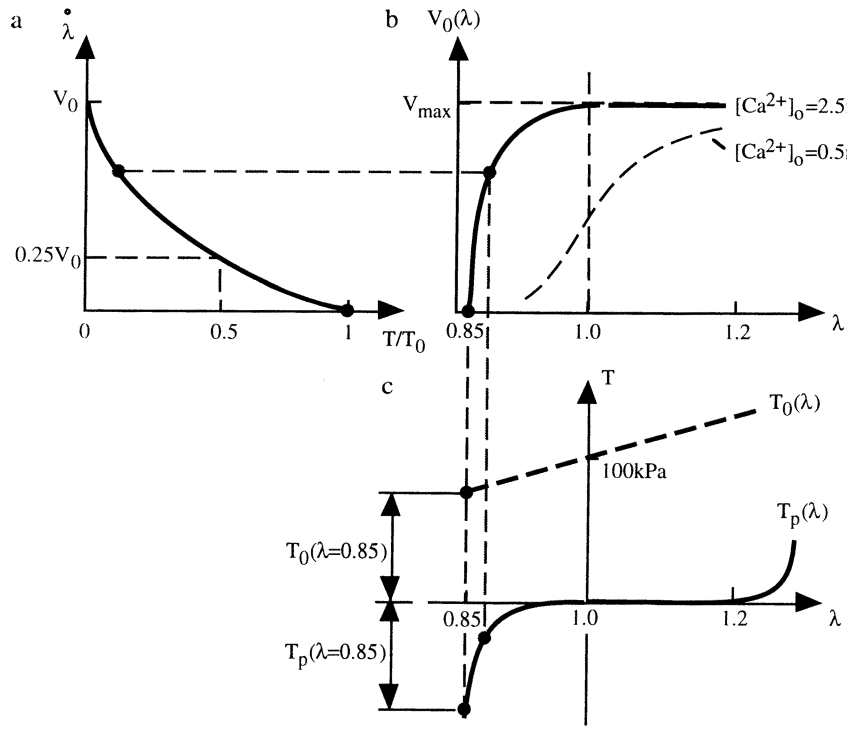

Figure 5. a: Shortening velocity at resting length as a function of relative tension. V_0 is the velocity when shortening against zero external load. **b:** V_0 as a function of λ. The decline of V_0 for $\lambda<1$ is a result of the increasing internal compressive load as shown in (**c**). See text for details.

The unloaded shortening velocity V_0 has had a special significance for muscle physiologists because it appeared to be independent of length and level of activation, at least for lengths greater than resting length ($\lambda>1$). For $\lambda<1$ the passive muscle structures are in compression and the 'unloaded' shortening is now in fact shortening against an internal load (Fig. 5).

An external Ca^{2+} concentration of 2.5 mM (or a lower concentration but with paired pulse stimulation) is sufficient to saturate the troponin Ca^{2+} binding sites. For $\lambda>1$ V_0 is independent of length (see Fig. 5b), but for $\lambda<1$ the internal load from the passive elasticity of the muscle, as shown in Fig. 5c, effectively drops the operating point down the velocity–tension curve and V_0 is therefore reduced at these shorter lengths. When the muscle shortens to the point ($\lambda = 0.85$) where the passive compressive stress T_p equals the actively developed stress T_0, V_0 is zero. At lower Ca^{2+} concentrations the unloaded shortening velocity V_0 is no longer independent of length for $\lambda>1$ (see the dashed line in Fig. 5b for $[Ca^{2+}]_o = 0.5$ mM). The most likely explanation for this is an internal viscous load [11].

Frequency Response Experiments

Frequency response experiments in which a small sinusoidal length perturbation is applied to the muscle while it is otherwise isometric or shortening at constant velocity, i.e., against a constant load. Dividing the recorded sinusoidal tension changes by the applied length changes gives a dynamic stiffness. This too scales directly with T_0 and is therefore plotted in Fig. 6 as relative stiffness against relative tension. An interesting feature of the relationship is the non-zero stiffness (typically 12% of isometric) at zero tension. This relative stiffness versus relative tension relation is found to be independent of the perturbation frequency.

To model these observations of cardiac muscle mechanics we have proposed [12] a model – called the *fading memory* model – in which a nonlinear function of tension $Q(T,T_0)$ is written as a linear superposition of dynamic length changes:

$$Q(T,T_0) = \int_{-\infty}^{t} \phi(t-\tau)\dot{\lambda}(\tau)\,d\tau \qquad (6)$$

where $\dot{\lambda} \equiv d\lambda/dt$, $\phi(t)$ is a material response function, and $T_0(\lambda, [Ca^{2+}]_i)$ is the isometric tension–length–Ca^{2+} relation for cardiac muscle discussed above. The justification for this

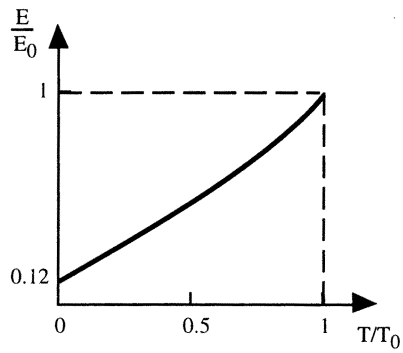

Figure 6. Relative dynamic stiffness in constant velocity release experiments, plotted against relative tension. The relative stiffness at zero tension is 0.12.

separation of the linear dynamic length changes from the static nonlinear function of tension is simply the experimental observation that dynamic length changes are small in comparison to the corresponding changes in tension. Under steady state conditions the RHS of Eq. (6) is zero and the as yet unspecified function $Q(T,T_0)$ must be defined such that $Q(T_0,T_0) = 0$. Note that a system defined by Eq. (6) is known in the system identification literature as a "Wiener cascade model" – a linear dynamic system followed by a static nonlinearity.

ADDITIONAL EXPERIMENTAL OBSERVATIONS

Tension Measurements

Two further experimental observations are now used. The first is that all tension measurements on cardiac muscle scale with the isometric tension and therefore $Q(T,T_0) = Q(T/T_0)$. The second is that the current tension is influenced more by recent length changes than earlier length changes, i.e., the fading memory assumption. This latter assumption allows the material response function to be written as a sum of exponentials:

$$\phi(t) = \sum_{i=1}^{N} A_i e^{-\alpha_i t} \tag{7}$$

where α_i and A_i, i = 1..N, are the exponential rate constants and associated weighting coefficients, respectively.

In fact the tension recovery curves in Fig. 4a show evidence of two distinct physical processes: the initial fast recovery with a slight oscillation is indicative of a second order process (e.g. myosin head rotation in the Huxley and Simmons model [13]) and the subsequent slow recovery phase is evidence of a first order process: the crossbridge detachment–attachment cycle in the Huxley [14] model with the rate limiting step being detachment. We therefore limit the number of rate constants N in Eq. (7) to 3, and Eq. (6) becomes

$$Q(T/T_0) = \sum_{i=1}^{3} A_i \int_{-\infty}^{t} e^{-\alpha_i(t-\tau)} \mathring{\lambda}(\tau)\, d\tau \tag{8}$$

where we let α_1 be the rate constant associated with the first order slow tension recovery, and α_2 and α_3 be the rate constants for the second order fast recovery process in Fig. 4a.

A parameterized form of the function $Q(T/T_0)$ can be determined from the constant velocity experiments described above. Ignoring the two rate constants α_2 and α_3 associated with the initial transient following the tension step (since this has decayed by the time the force–velocity measurements are made) and putting $\mathring{\lambda} = -V$ (the constant velocity of shortening), Eq. (8) reduces to $Q(T/T_0) = -(A_1/\alpha_1) V$. An exact match to Hill's force–velocity relation Eq. (5) is then obtained by choosing $Q(T/T_0) = [(T/T_0)-1] / [(T/T_0)+a]$ and $V_0 = \alpha_1/aA_1$, giving,

$$\mathring{\lambda} = -V = \frac{\alpha_1}{A_1} \frac{T/T_0 - 1}{T/T_0 + a} \tag{9}$$

Experimental results from cardiac muscle [7–9] give a relative velocity (V/V_0) of about 25% at a relative tension (T/T_0) of 50%. Putting $T/T_0 = 1/2$ in Eq. (9) gives $V/V_0 = (1/2)\mathbf{a} / (1/2 + \mathbf{a})$ and hence $\mathbf{a} = 1/2$.

The fading memory model of active muscle mechanics is now given by

$$\frac{T/T_0 - 1}{T/T_0 + \mathbf{a}} = \sum_{i=1}^{3} A_i \int_{-\infty}^{t} e^{-\alpha_i(t-\tau)} \dot{\lambda}(\tau)\, d\tau \qquad (10)$$

The response to a rapid length change is found by putting $\dot{\lambda} = \begin{cases} 0 & t<0 \\ \dfrac{\Delta\lambda}{\Delta t} & 0<t<\Delta t \\ 0 & t>\Delta t \end{cases}$ in Eq. (10) (see Fig. 4a top) and integrating to give

$$\frac{T/T_0 - 1}{T/T_0 + \mathbf{a}} = \frac{\Delta\lambda}{\Delta t} \cdot \sum_{i=1}^{3} \frac{A_i}{\alpha_i} e^{-\alpha_i t}(e^{\alpha_i \Delta t} - 1) \qquad (11)$$

The maximum velocity of *sarcomere shortening* in the force–velocity experiments is found [11] to be 14.3 μm/s at a slack length of 1.9 μm. In terms of the nondimensional velocity V_0, therefore, $V_0 = \alpha_1/\mathbf{a}A_1 = 7.53\ s^{-1}$. An estimate for the rate constant α_1, found by fitting the tension recovery from Eq. (11) to the slow recovery phase following a length step, is $\alpha_1 = 32\ s^{-1}$. With $\mathbf{a} = 1/2$, this gives $A_1 = 32/(1/2 \times 7.53) = 8.5$. The remaining parameters α_2, α_3, A_2 and A_3 are found by matching Eq. (11) to the fast tension recovery phase. Table 2 gives the fitted parameter values (using skeletal muscle experiments for the fast time constant parameters α_2 and α_3 [12]). Note that the tension recovery obtained from Eq. (11) closely matches experimental measurements for rapid length changes up to 0.5%. For larger length steps the assumption of linear superposition breaks down [12].

Table 2. Active Muscle Parameters

Parameters	Trabeculae
a	0.5
A_1	8.5
A_2	91
A_3	151
α_1 (s^{-1})	32
α_2 (s^{-1})	1000
α_3 (s^{-1})	5000

The tension T_1 immediately after the step is found from Eq. (11) by putting $t=\Delta t$ and $T=T_1$. Thus,

$$\frac{T_1/T_0 - 1}{T_1/T_0 + \mathbf{a}} = \frac{\Delta\lambda}{\Delta t} \cdot \sum_{i=1}^{3} \frac{A_i}{\alpha_i} (1 - e^{-\alpha_i \Delta t}) \qquad (12)$$

Equation (12) gives the plot of (T_1/T_0) against $\Delta\lambda$ shown in Fig. 4b. The response to an idealized instantaneous length step (inertial effects prevent it from being achievable)

is found from Eq. (12) by putting $\Delta t = 0$. The instantaneous length step required to drop the tension to zero is $\Delta\lambda = -1/\mathbf{a}\Sigma A_i = -0.008$ or 0.8% of fiber length.

It should be emphasized that a unique relationship between shortening velocity and tension in a tension–step experiment can only exist when the isometric tension does not vary with length and then only when the initial velocity transients have decayed. To find the relationship between velocity, tension and length in a tension–step experiment conducted on the ascending limb of the isometric tension–length curve, consider the single rate constant version of Eq. (10), which is applicable once the transient velocity fluctuations have decayed:

$$\frac{T/T_0 - 1}{T/T_0 + \mathbf{a}} = A_1 \int_{-\infty}^{t} e^{-\alpha_i(t-\tau)} \mathring{\lambda}(\tau)\, d\tau \quad . \tag{13}$$

Differentiating Eq. (13) with respect to time, with T constant, gives

$$\mathring{\lambda} = \frac{\alpha_1 \dfrac{T/T_0 - 1}{T/T_0 + \mathbf{a}}}{A_1 + \dfrac{1 + \mathbf{a}}{(T/T_0 + \mathbf{a})^2} \cdot \dfrac{T}{T_0^2} \cdot \dfrac{dT_0}{d\lambda}} \tag{14}$$

when $dT_0/d\lambda = 0$, Eq. (14) reduces to the previous expression, Eq. (9).

Frequency Response

The other type of experiment mentioned above is the frequency response test. To determine the predicted dynamic stiffness during constant velocity (V) shortening, let

$$\lambda = \lambda_0 - V.t + \Delta\lambda.e^{j\omega t} \; ; \qquad (j = \sqrt{-1}\,)$$

where $\Delta\lambda$ and ω are the amplitude and frequency of the applied length perturbation. Substituting $\mathring{\lambda} = -V + j\omega\Delta\lambda.e^{jwt}$ into the RHS of Eq. (10), extracting the corresponding tension perturbation from the LHS, using a Taylor series expansion [12], and putting $\Delta\tilde{\lambda} = \Delta\lambda.e^{j\omega t}$ and $\Delta\tilde{T} = \Delta T.e^{j(\omega t+\phi)}$ gives $\Delta\tilde{T} = E.\Delta\tilde{\lambda}$, where $E(T,T_0,\omega)$ is the dynamic stiffness:

$$E(T,T_0,\omega) = \frac{T}{T_0} \cdot \frac{dT_0}{d\lambda} + \frac{T_0(T/T_0 + \mathbf{a})^2}{1 + \mathbf{a}} \cdot \sum_{i=1}^{3} A_i \frac{j\omega}{\alpha_i + j\omega} \quad . \tag{15}$$

If $dT_0/d\lambda = 0$, equation (15) becomes

$$E(T,T_0,\omega) = \frac{T_0(T/T_0 + \mathbf{a})^2}{1 + \mathbf{a}} \cdot \sum_{i=1}^{3} A_i \frac{j\omega}{\alpha + j\omega} \quad . \tag{16}$$

and the stiffness relative to isometric is

$$\frac{E(T,T_0,\omega)}{E(T_0,T_0,\omega)} = \left(\frac{T/T_0 + \mathbf{a}}{1 + \mathbf{a}}\right)^2 \quad . \tag{17}$$

Note that Eq. (17) is independent of frequency, as observed experimentally, and yields a plot of relative stiffness versus relative tension as shown in Fig. 6, in excellent agreement with experimental measurements. The predicted stiffness ratio at zero tension (with **a** = 1/2) is $(\mathbf{a}/1+\mathbf{a})^2 = 1/9 = 0.11$, which compares with the experimental value of 0.12. The phase of the dynamic stiffness with $dT_0/d\lambda = 0$ is, from Eq. (16),

$$\phi = \tan^{-1}\left\{\sum_{i=1}^{3} \frac{A_i \omega/\alpha_i}{1+(\omega/\alpha_i)^2} \Big/ \sum_{i=1}^{3} \frac{A_i(\omega/\alpha_i)^2}{1+(\omega/\alpha_i)^2}\right\} \quad , \tag{18}$$

which is independent of tension, in agreement with the experimental findings of de Tombe and ter Keurs [11]. The predicted phase shift at 500Hz is 35° which compares with their experimental value of 51.8°.

CONCLUSION

The active properties of cardiac muscle appear to be very nearly independent of the passive elastic structures for an axial extension ratio λ in the range $1<\lambda<1.2$ (ignoring the visco-elastic effects seen at low levels of activation). But below the resting length ($\lambda<1$) the internal compressive load faced by a contracting sarcomere substantially affects the externally measured tension and shortening velocity. Quantification of this passive elasticity cannot be achieved by uniaxial experiments alone, because then the only way to put the muscle into compression is by active contraction. Rather, biaxial (or, ideally, triaxial) experiments are needed. This paper has shown how the 3D passive elastic behavior of myocardial tissue, obtained from biaxial experiments and observations of tissue micro-structure, can be combined with the 1D active behavior of cardiac trabeculae in the formulation of computationally efficient constitutive laws. These laws may be used with 3D finite element models to link sarcomere dynamics to the mechanics of the intact heart.

DISCUSSION

Dr. S. Sideman: I am in awe of your tenacity and patience to work with finite elements. I started my career in cardiology with a finite elements study and after a year or so gave it up. It was years back and it took a long time on the computer. The computer is faster today, but I am uncertain whether the finite elements really give an advantage in learning the phenomena. There are many basic phenomena that we can study without elaborating too much on the real geometry. Do you feel that this hard work is worth it? Are you gaining something that we cannot gain by doing some simpler models?

Dr. P. Hunter: There are things that you can answer without this sort of detailed modeling. But there are also questions, particularly relating to regional inhomogeneity, which do require it. If you have an infarct in one part of the heart and you are to understand how that infarct affects the performance of the intact heart, or you clinically want to identify where reentrant pathways occur in relation to an infarct, for example, you have no option but to model the anatomical reality of the heart. I am proposing what I really believe, that it is computationally feasible to put in anatomical detail into a model which is computationally efficient and can provide the link between the cellular properties and the integrated function of the heart. Modern work stations are fast enough, providing the models really do address the problem of computational efficiency and are not just black box models that have a huge number of parameters. You have to put in a lot of *a priori* knowledge

about the structure and use methods which mean that you can solve these equations in a reasonable time on work stations, and I think you can.

Dr. H. Fozzard: Given the anatomical complexity, if we assume conduction of the action potential in the axial direction in individual cells, does it make sense that there would be a constant conduction velocity to make the system work, or would you imagine that we would be better off if there were variable conduction velocities depending on the orientation and situation of the cells?

Dr. P. Hunter: I would not want to make an *a priori* assumption that conduction velocities are constant everywhere on the heart. That has to come out of the physiological measurement of membrane properties from tissue in different places. I can not see any particular reason why the heart would "want" to have different conduction velocities in different regions, but there is no reason to make that assumption in a model such as this. In other words, if you can measure it, the spatial variation can go into the mathematical description. We know, for example, that we can measure the ratio of the shortest path length through the various branching in the sheets to the direct length and thereby what the transverse conduction velocity would be. That is definitely different in different places around the heart. There is a parabolic change in the path length as you go across the wall, much longer path length in the center, shorter path length in the subendocardium and subepicardium and that is important information to include in these models because that certainly will affect the potential for reentry, for example.

Dr. H. Fozzard: In the human heart it takes the order of 100 ms to complete the electrical activation. That is a substantial fraction of the whole contractile cycle, so there has to be some phasing of these electrical and mechanical processes to make things work right.

Dr. P. Hunter: There are lots of unanswered questions as to the mechanical–electrical coupling that we do not know about yet, which is an extremely rich field for future work. I am sure the structure of the heart is partly a compromise between the requirements of the electrical system and the requirements of the mechanical system.

Dr. J.B. Bassingthwaighte: You have a marvelous *tour de force* in showing relationships between fiber direction and potential for strain. Have you measured strain and stress in all of these areas? I have sets of data in my lab where we have myocardial flow distributions with very high resolution. In some of these we also have the regional capacity for the uptake for fatty acid across the endothelial cells. Can I use your data for getting at an overall hypothesis of the relationship between local work and local metabolism and flow? Is one heart sufficiently close to the next one so that I could take one of your hearts and relate it to my data in a spatial sense? Or do we have to get all of these data from one heart, the fiber directions, the sheets, the deformation as well as the metabolic and flow information? What generality do you see in your fiber directions?

Dr. P.J. Hunter: We have studied about 30 dogs now, in terms of fiber orientation and geometry, and a smaller number in terms of sheet structure. I am convinced that there is a standard description of the fibrous structure which can be applied, once it is understood in relation to the geometry. It is really important to do those measurements or understand the structure in relation to the particular geometry of that heart. But, for a given geometry, we may only require a reasonably small number of parameters to define. Once you have that basic description of the geometry, the fiber sheet structure follows, and it must follow for very good reasons. No doubt Dr. Arts could comment on that relationship between the growth of the structures and the loads they are supporting, which are comparable in all these hearts so that the structure is going to be similar. In terms of your question, we must put in a flow system in these models. We must have a definition of the coronary tree right down to the capillary level in order to be able to use these stress–strain predictions in terms of the things that you want to ask.

Dr. J.B. Bassingthwaighte: It sounds like we are in trouble. In our studies on a variety of different hearts, we do not see a consistent relationship between the spatial localization and the flow from heart to heart. They are different in each heart. Dr. Reneman has had the same experience over the years of looking at many hearts with micro-shear flow distributions with high resolution. It appears that there is something beyond the anatomic structuring that we have to take into account. It is probably the roots of excitation and therefore force-development.

Dr. H.E.D.J. ter Keurs: I have always wondered whether studying linear trabeculae that I could accidentally find in the right ventricle was relevant at all. Seeing your results, I am a little more confident that it might be. In the course of the past years, we have done a number of experiments trying to quantify opposing forces. Those are the forces that you derived from your orthotropic stress-strain measurements and the modeling. We have tried to get information about opposing forces in single linear muscles, which is not too easy because it is not too easy to compress a muscle and only the contractile proteins can do that. We had to devise a number of awkward, sometimes ugly, tricks to do it. But, I was quite happy to see that the result of these tricks was that the shape of the passive force-length relation, including the opposing forces and the extension forces, is very similar to the one that you have presented. What you show is that the sheets are not simple linear structures, but they are warped domains. That means that there must be a complicated third dimension. My question is how do you combine the third dimension in the case that the muscle bifurcates or takes off in a slightly different direction. How do you model that in terms of force development? Do you only need the intersheet connections or intercellular connections or do you need more?

Dr. P. Hunter: These models are continuum mechanics models. That is, when you describe the properties at a point, you are describing it for a continuous material where you have a constitutive relation that represents the average behavior, which is anisotropic so that it is related to the orthotropic axes at that point in the tissue. But the passive properties are very much three dimensional and are based on the fiber sheet structure. Once you have measured those and put them into the model, and those properties are appropriately related to the orthotropic axes which are varying everywhere, you have taken care of the three dimensionality of the passive properties. Now the sort of work that you have done on the active properties can be included in terms of an active force generated just along the fiber direction. So it is a one dimensional description embedded within this three dimensional context. That has always seemed to me one of the beautiful things about the heart: the fact that force is generated in one dimension and that the connection with the other dimensions comes through the three dimensional passive elasticity of the muscle. It is not that we are modeling individual collagen struts connecting sheets. We are using that structural information and the biaxial test to come up with a 3D constitutive law into which we then embed a one dimensional active force development model based on your data.

Dr. T. Arts: You have a beautiful but complicated model. You show what is going on at the microscopic and the macroscopic levels, and you try to obtain knowledge about the microscopic tissue properties, by calculating backward from macroscopic measurements. When you have a complicated model and you are estimating parameters, then you have to worry about the sensitivity of parameters to, say, the accuracy of the estimate. You know that you have uncertainties. You make preassumptions and you know they are not correct because, as Dr. Bassingthwaighte has said, models are never correct. Do you have an idea about the accuracy of the material properties you estimate? What are they in reality, and what is the tolerance of your estimates?

Dr. P. Hunter: I do not think of this as a complicated model. There is a big difference between this model and having a large number of free parameters which are thrown into a model and then you tune all these parameters to fit experimental data.

Dr. T. Arts: But you have some 100 parameters...

Dr. P. Hunter: I disagree. The anatomical description is something that is totally separate from the description of material properties, so those anatomical descriptions of the geometry and the fiber–sheet architecture are based directly on measurements and there are no free parameters. Once you have fitted those measurements, you have an efficient description of the anatomical structure. As to the mechanical properties, we spent a lot of time trying to find ways of defining 3D material properties in a way that lends itself to material parameter estimation. What we do is to define what we call the "pole–zero" law, where we essentially define the elastic limit along a given axis because that is something that can be observed microscopically. For example, the number of free parameters that we have in fitting MRI data for the mechanical parameters is about 6, at the most, and we have a good idea of the sensitivity of those parameters from biaxial experiments. We do not yet have a good idea of what the spatial variation of those parameters is likely to be in the heart and there is a lot more work to do on that.

Dr. M. Lab: My comment is related to what we are doing, and is also related to spatial variation in electrophysiology. The The endpoint is ventricular fibrillation. When you electrically stimulate the heart as a 2D plane you create a vortex, but the vortex moves and leaves the plane. You have to have three dimensions before you can support a vortex that leads to ventricular fibrillation. So the complexity that you are studying is in the right direction. My question: What validity is there in using simpler models, using nonlinear dynamics, and paring down the equations to be able to tackle more complex interactions.

Dr. P. Hunter: An interesting question, I do not know the answer. It seems to me there are two alternatives. You regard the ionic current models almost like an experimental test bed and you fit the simple models to that and then come up with a very simple description to define the models that you use in this 3D context. There is an enormous danger in that, particularly in view of the wonderful work we have seen here in terms of defining channel behavior, very specific actions of drugs on individual channels and so on. The only way to incorporate that information into the 3D intact heart model is to use the models that Dr. Rudy or Dr. Noble are developing. Otherwise you do not have the proper connection between the channel behavior and the intact behavior. I do not think the simplified models are going to tell us very much in terms of electrophysiology of the intact heart.

Dr. R. Beyar: About the branching of the fibers which is sometimes askew from the average direction that you are using for your fiber direction. That would mean that even 10° skewedness, in active force direction between layers, will generate huge difference in your modeling results in terms of what happens in the interstitial spaces. That is something to think about. I do not know what implication this kind of observation might have on our own modeling because if we are modeling the average force only in the fiber direction, in terms of active force, then this is a point we need to think about. My question is with regard to your cleavage planes. I am still uncertain that it is not fixation artifacts. But if it is not, then at least my interpretation would be that it is like a region of loose tissue cleavage between layers in 3D. Might it be that this plane of cleavage relates to planes where slippage of fibers and rearrangement might happen during contraction? If that is true then maybe strain analysis will show that the plane where you have maximum shear is proportional to the cleavage planes that you see.

Dr. P. Hunter: We have looked at that. Ian LeGrice and Jim Covell [LeGrice IJ, Tarayama Y, Covell JW. Transverse shear along myocardial cleavage planes provides a mechanism for normal systolic wall thickening. *Am J Physiol*, submitted, 1994] implanted beads in the subendocardium of the free wall and the septum and there happens to be a change in the orientation of the sheets between the free wall and septum, a very substantial change as you move around the heart. They looked at the maximum shear behavior in relation to those sheet orientations and found a very consistent story between this shearing action. You are quite right that the major shear is occurring by slipping or shearing of those planes and when you look in the different parts of the heart and see the changed sheet orientation it does relate very closely to the change in measured shear behavior from the bead studies.

Dr. J. Bassingthwaighte: A comment in response to Dr. Lab's question. Three dimensional vortices and spiral waves shown by Jalife's group [Perstov AM, Davidenko J, Salomonsz R, Baxter WT, Jalife J. *Circ Res.* 1993;72:631–650] do require this 3D kind of structuring that Dr. Hunter has demonstrated, and that is the route they have to take. They have already decided they have to incorporate that into better models of fiber structure.

REFERENCES

1. Hunter PJ, Smaill BH. The analysis of cardiac function – a continuum approach. *Prog Biophys Molec Biol.* 1989;52:101–164.
2. Nielsen PMF, LeGrice IJ, Smaill BH, Hunter PJ. A mathematical model of the geometry and fibrous structure of the heart. *Am J Physiol.* 1991;29(4):H1365–H1378.
3. McCulloch AD, Guccione J, Waldman LK, Rogers JM. Large scale finite element analysis of the beating heart. In: Pilkington TC, Loftis B, Thompson JF, Woo SL–Y, Palmer TC, Budinger TF, eds. *High Performance Computing in Biomedical Research*, Florida: CRC Press, 1993; 27–49.
4. Smaill BH, Hunter PJ. Structure and function of the diastolic heart: Material properties of passive myocardium. In: Glass L, Hunter PJ, McCulloch AD, eds. *Theory of Heart: Biomechanics, Biophysics and Nonlinear Dynamics of Cardiac Function.* New York: Springer–Verlag, 1991; 1–29.
5. Nielsen PMF, Hunter PJ, Smaill BH. Biaxial testing of biomaterials: Testing equipment and procedures. *ASME J Biomech Eng.* 1991;113:295–300.
6. Eringen AC. *Mechanics of Continua.* New York:Krieger, 1980.
7. ter Keurs HEDJ, Rijnsburger WH, van Heuningen R, Nagelsmit MJ. Tension development and sarcomere length in rat cardiac trabeculae. Evidence of length–dependent activation. *Circ Res.* 1980;46:703–714.
8. de Tombe PP, ter Keurs HEDJ. Force and velocity of sarcomere shortening in trabeculae from rat heart. Effects of temperature. *Circ Res.* 1990;66:1239–1254.
9. de Tombe PP, ter Keurs HEDJ. Sarcomere dynamics in cat cardiac trabeculae. *Circ Res.* 1991;68:588–596.
10. Hill AV. Heat of shortening and the dynamic constants of muscle. *Proc Roy Soc B.* 1938;126:136–195.
11. de Tombe PP, ter Keurs HEDJ. An internal viscous element limits unloaded velocity of sarcomere shortening in rat myocardium. *J Physiol.* 1992;454:619–642.
12. Bergel DH, Hunter PJ. The mechanics of the heart. Chapt. 4. In: Hwang HHC, Gross DR, Patel DJ, eds. *Quantitative Cardiovascular Studies, Clinical and Research Applications of Engineering Principles.* Baltimore: University Park Press, 1979; 151–213.
13. Huxley AF, Simmons RM. Proposed mechanism of force generation in striated muscle. *Nature* 1971;233:533–538.
14. Huxley AF. Muscle structure and theories of contraction. *Prog Biophys Chem.* 1957;7:255–318.

CHAPTER 31

DISTRIBUTION OF MYOCARDIAL STRAINS: AN MRI STUDY

Haim Azhari,[1] James L. Weiss,[2] and Edward P. Shapiro[2]

ABSTRACT

Quantification of myocardial strains is essential for understanding cardiac mechanics. Previous techniques for assessing regional myocardial strains have been mainly limited to invasive procedures. A technique by which tagging can be added to magnetic resonance images (MRI) has recently been introduced and allows for noninvasive measurement of myocardial deformations. We have applied MRI tagging to two sets of orthogonal planes and have obtained three dimensional (3D) reconstructions of 24 myocardial cuboids at end-diastole (ED) and at end-systole (ES). Applying finite strain analysis to these cuboids we were able to study the longitudinal distribution of the endocardial and epicardial principal strains (PS) in the normal canine heart. In addition we have calculated the longitudinal distribution of the left ventricular (LV) transmural thickening using a 3D approach. Our results show similarity in the longitudinal distribution of endocardial PS and transmural thickening. These results imply that endocardial strains are determined not only by endocardial fiber deformations but mainly by geometrical coupling through transmural thickening.

INTRODUCTION

Numerous techniques for studying regional myocardial deformations have been suggested. For example, Prinzen *et al.* [1] employed needles which were inserted into the LV wall and measured shortening of the inner myocardial layers. Dieudonne [2] and others sewed strain gauges to the myocardium and used them to evaluate regional strains. Hawthorne *et al.* [3] sewed mercury filled rubber tubes to the myocardium and by studying

[1]Julius Silver Institute, Department of Biomedical Engineering, Technion-IIT, Haifa 32000, Israel, and [2]Johns Hopkins University, School of Medicine, Baltimore MD, USA.

Molecular and Subcellular Cardiology: Effects of Structure and Function
Edited by S. Sideman and R. Beyar, Plenum Press, New York, 1995

the changes in their electrical resistance, they evaluated the corresponding myocardial elongation and contraction.

Waldman *et al.* [4] and others implanted many small metal beads into the myocardium of canine hearts. By using biplanar angiographic studies, they determined the changes in the beads 3D coordinates throughout systole and calculated the corresponding regional myocardial strains. Using a somewhat similar approach Yun *et al.* [5] and others inserted many small metal screws into the myocardium of human hearts. The corresponding myocardial deformations were also evaluated by tracking the 3D coordinates of each metal screw, using biplanar angiography.

Freeman *et al.* [6], Villarell *et al.* [7] and many others inserted pairs of miniature ultrasonic transducers into the myocardium and by measuring the systolic changes of distances between them calculated the corresponding myocardial strains. Other techniques involved the use of small optical markers which were glued to the epicardium (e.g. Prinzen *et al.* [8]) and tracked by a video camera, while some have employed special tripodal strain gauge devices attached by suction to the epicardium (e.g. Lab *et al.* [9]) to study epicardial strains.

All the above mentioned techniques suffer from the same disadvantage: they are invasive in nature and require a surgical procedure which may affect the studied tissue. The introduction of MRI tagging by Zerhouni *et al.* [10] in 1988 and the SPAMM by Axel *et al.* [11] a year later marked the beginning of a new era. For the first time one could tag a specific tissue region at ED and follow it through systole in a totally harmless and noninvasive manner. The tags which appear as dark lines in the MRI image and deform with the myocardium enable one to literally visualize patterns of myocardial deformations.

However, even two-dimensional (2D) tagged MRI analysis is insufficient to provide the true myocardial strains. As shown in many studies, the LV deforms in the longitudinal direction as well as in the radial direction, and twists substantially. On the other hand, typical MRI scans are performed along 2D planes fixed in space. As a result of the substantial through-plane motion of the myocardium, it is likely that images acquired at different cardiac phases correspond to different tissue segments. Hence, only techniques which account for the 3D nature of LV deformation can accurately assess the patterns of myocardial strains.

Recently reported studies by Azhari *et al.* [12, 13] introduced a method by which the technique of MRI tagging is implemented to track many small myocardial cuboids from ED to ES. Combined with 3D analysis, this enables measurement of endocardial and epicardial strains. Here, we demonstrate how this method is utilized to study the longitudinal distribution of myocardial principal strains (PS) and transmural thickening in the normal canine LV.

METHODS

Canine Preparation

Seven healthy mongrel dogs were studied. The dogs were anesthetized by intravenous injection of 25–35 mg/Kg of Pentobarbital and 0.05 mg/Kg of Fentanyl and administered additional doses when needed. The dogs were then artificially ventilated using a Harvard respirator (model 710A). The chest was opened by applying left thoracotomy at the fifth intercostal space. The heart was supported on a pericardial cradle and the chest was re-closed. A pace-maker wire was inserted through the jugular vein to the right atrium and the heart was paced. The natural heart rate was monitored and reduced below the

pacing rate, if needed, by additional intravenous injection of Fentanyl. Using a Gould phonotransducer the heart sounds were registered. The first high frequency component of the second heart sound was used to determine end systole. Using a Hewlett-Packard transmitter (model 78100A) the ECG signal was monitored. The dog was then placed in the MRI scanner for image acquisition.

Imaging

A Resonex RX4000 resistive core MRI system with a main magnetic field of 0.38 Tesla was used. Images were acquired using the spin-echo technique with a time to echo of 30 msec and Tr = twice the cardiac cycle. Following several scout images the spatial orientation of the LV long axis (LAX) was determined. Two sets of planes were then selected: The first set comprised of four long axis planes rotated about the LAX (using it as a pivot) with an angel of 45° apart. The second set comprised of four short axis parallel planes covering the LV from apex to base with and an inter slice distance of about 1 cm.

Radial tagging was produced in the first phase of the imaging protocol by applying RF pulses to the set of long axis planes and imaging along the short axis planes. As a result, a set of short-axis radially tagged images, such as the one depicted in Fig. 1, were obtained. Note that the tag lines correspond to the intersection lines between the long axis planes and the imaged short axis plane. Long axis tagging was obtained in the second phase of the imaging protocol, by applying RF pulses to the short axis planes and imaging along the long axis planes. As a result, a set of four long axis images with tags which corresponded to the short axis planes were obtained. The images were then traced manually using a PC based computer station. The coordinates of the endocardial and epicardial intersection points of each tag line were registered. Using the computer algorithm described in [12], 3D reconstructions of 24 myocardial cuboids were obtained at ED and ES.

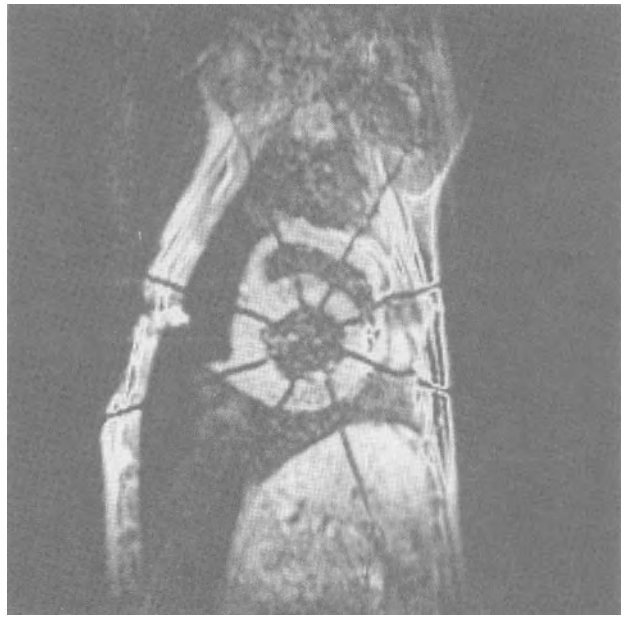

Figure 1. A typical radially tagged short axis MRI image of a canine heart. Note the dark tag lines which deform with the myocardium.

Strain Analysis

Strains were calculated for the epicardial and endocardial surfaces. Using three endocardial or epicardial nodal points at a time, a triangular tile was attached to the face of each reconstructed myocardial cuboid. Following the ED to ES deformations of that triangular tile, the 2D strain tensor was calculated using the finite strain approach as suggested by Waldman *et al.* [4]. With this approach the strain tensor E_{ij} is calculated from the set of 3x3 algebraic equations derived by applying the following relation to each of the triangle edges:

$$\Delta S^2 - \Delta S_0^2 = \sum_{i=1}^{2} \sum_{j=1}^{2} 2E_{ij} \Delta a_i \Delta a_j \qquad (1)$$

where (ΔS_0) and (ΔS) are the initial and deformed distances, respectively, between the two points defining the edge, and Δa_j are the projections of the edge into the regional coordinate system.

The three independent components of the strain tensor (i.e. circumferential E_{11}, longitudinal E_{22}, and in plane shear E_{12} strains) were obtained by solving this set of equations. By solving the corresponding eigenvalue problem, the magnitudes and directions of the two PS, E1 and E2, were determined. Here, we chose to focus on the major PS which designates the maximal in plane deformation.

As four different triangular tiles can be defined for each face of the studied myocardial cuboid, we have obtained four PS values for the endocardial and four for the epicardial surfaces. The average of these four PS values was used here to characterize the endocardial or epicardial PS of the myocardial cuboid.

Transmural Thickening

The endocardial and epicardial strains characterize the deformations tangential to the LV walls. In order to complete the picture we chose to characterize the radial deformations by studying the regional transmural thickening. For that purpose we employed the formulae suggested by Beyar *et al.* [14]:

$$T = \frac{2 \cdot V}{\left(A_{endo} + A_{epi}\right)} \qquad (2)$$

where T is the wall thickness, V is the volume of the studied myocardial cuboid, A_{endo} and A_{epi} are the endocardial and epicardial surface areas of the studied cuboid. This formulae utilizes the 3D data and accounts for the conical shape of the LV (see [14] for details).

Transmural thickening is consequently derived by calculating the ED to ES change in T. Thickening data is presented here in percent change relative to the ED wall thickness.

RESULTS

Principal Strains (PS)

In order to study the longitudinal distribution of the PS, the LV was divided into three levels: (i) basal (ii) middle and (iii) apical. For each level the average and standard

deviation were calculated. The results obtained for the PS are summarized in Table 1 and depicted graphically in Figs. 2 and 3. It should be noted that each PS value outlined in the table represents the average of 224 triangles (8 cuboids in each level X 4 triangular tiles per cuboid X 7 dogs).

As can be noted in Table 1, there was no change in the average epicardial PS value from apex to base. However, apical PS exceeded significantly the basal PS (by almost 20%) at the endocardium. This difference was tested for statistical significance by applying repeated measures analysis of variance (ANOVA), accounting for variations in both dog and location. The difference was found statistically significant ($P<0.05$).

Table 1. Average (±s.d.) Magnitudes of Principal Strains and Transmural Wall Thickening (Longitudinal Distribution)

	Principal Strain		Transmural Thickening
Level	Endocardium	Epicardium	
Basal	−0.215 ± 0.077	−0.117 ± 0.061	29.8% ± 15.7
Mid	−0.247 ± 0.064	−0.101 ± 0.043	38.4% ± 16.2
Apical	−0.258 ± 0.062	−0.105 ± 0.062	37.4% ± 23.0

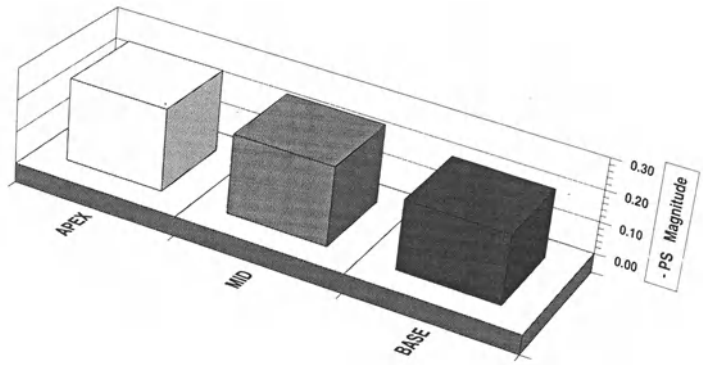

Figure 2. Longitudinal distribution of average endocardial principal strain (PS) magnitude. Note the reduced basal strains as compared to the apical ones.

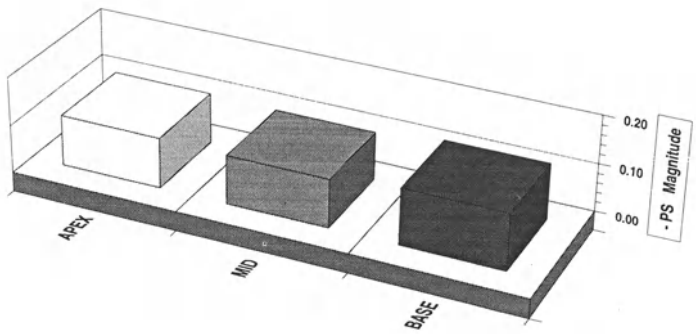

Figure 3. Longitudinal distribution of average epicardial principal strain (PS) magnitude. Note the relatively uniform distribution of these epicardial PS values.

Transmural Thickening

The results obtained for transmural thickening are also summarized in Table.1 and depicted graphically in Fig. 4. As can be observed, while average ED to ES thickening at the basal level was about 30%, thickening at the middle and apical levels was almost 40%. However, thickening values were too scattered particularly at the apical level (apical s.d. was 23%) to produce a clear statistical significance. Nevertheless, the trend observed in Fig. 2 and Fig. 4 indicates that the transmural thickening is very much related to the endocardial strains.

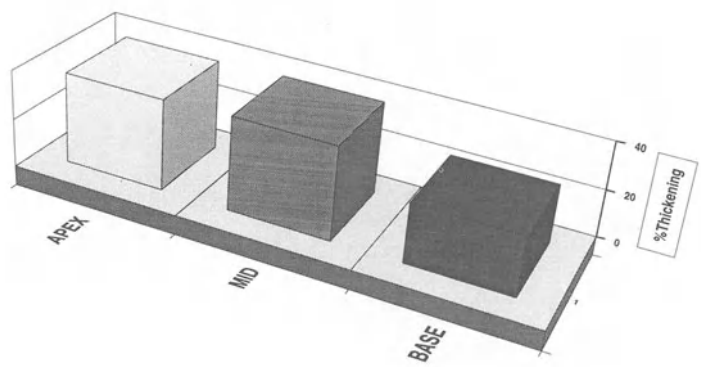

Figure 4. Longitudinal distribution of the average transmural thickening. Note the reduced basal thickening and the similarity to the endocardial PS distribution.

CONCLUSION

MRI tagging provides a unique tool for studying the deformation field within the *in vivo* heart. With MRI tagging one can select and tag specific regions of the myocardium and study their deformations in a noninvasive manner. In our recently published studies [12, 13] we have shown that many small myocardial cuboids can be marked and reconstructed in 3D by combining long axis and short axis tagged MRI images. Studying the systolic spatial deformations of these cuboids, endocardial and epicardial strains can be studied for the first time noninvasively *in situ* and simultaneously in many sites.

Recalling our previously published data for the normal canine heart [12], the following findings are worth noting: First we have found that the endocardial PS magnitudes exceeds the epicardial PS by approximately two-fold (-0.24 ± 0.07 vs. -0.11 ± 0.05, respectively). Second, we have found that while the average epicardial PS direction ($59° \pm 32$) aligned with the expected fiber direction, an average endocardial PS direction ($26° \pm 30$) was perpendicular to it. This finding is consistent with earlier reports by others (e.g. Waldman *et al.* [4]).

Another finding reported in [12] was that the anterior-posterior (A-P) pair of walls contracted differently from the septal-lateral (S-L) pair. At the endocardium the average PS magnitude for the S-L pair exceeded significantly the average PS magnitude for the A-P pair. On the other hand, the average PS magnitude for the A-P pair at the epicardium significantly exceeded the average PS magnitude for the S-L pair.

The findings reported here indicate that the pattern of longitudinal distribution for the endocardial PS magnitudes, is similar in nature to that of transmural thickening (Table 1 and Figs. 2 and 4). This pattern similarity implies that endocardial strains are not

only determined by endocardial fiber deformations but mainly by geometrical coupling through transmural thickening. This argument is further enhanced by the above cited observations that the average endocardial PS direction is perpendicular to the expected fiber orientation. This can also explain why endocardial PS magnitudes are significantly larger than the epicardial ones.

Our suggested method which combines tagged MRI with 3D analysis has great potential in studying the spatial distribution of myocardial strains. The consistency of our findings with results reported by others implies that MRI-obtained strain measurements are reliable. As this method is noninvasive and hazardless it can be implemented to study human hearts (e.g. McGowan *et al.* [15]) and can potentially serve as a clinical tool for mapping ischemic regions (e.g. Azhari *et al.* [16]).

Acknowledgement

The study was supported in part by NHLBI Ischemic heart Disease SCOR grant HL-17655-16, RO1-HL-43722 (Dr. JL. Weiss), AHA grant 891230 (Dr. EP. Shapiro) and the Chesapeake Education/Research Trust. Dr. H. Azhari was initially supported by the US-Israel Educational Fund (Fulbright) and later by the NIH Fogarty Grant Num. 5-FO5-TW04415-02 ICP(5).

DISCUSSION

Dr. E. Ritman: This is potentially a very potent technique, so I want to be sure about the method. These tag lines that you generate in the volume of the chest are read off time-sequentially, is that correct?

Dr. H. Azhari: Yes; first we study the radial tags and then the long axis tags.

Dr. E. Ritman: Therefore when you are reading it out, you are, in a sense, sampling the heart time sequentially. Is there less beat to beat variation in those measurements than there is in the position that you read off the black lines in an image?

Dr. H. Azhari: Beat-to-beat variability was reduced by pacing the hearts at a constant rate and artificially ventilating the dogs. Furthermore, with the spin echo technique that we have used, each image was acquired by sampling data from 256 heart beats. Thus, beat-to-beat variability was probably averaged out.

Dr. E. Ritman: Lets assume that you get the spatial location of the horizontal, the transverse and the sagittal, or whatever planes they are, absolutely correctly. Is there a unique solution to the cube or the cubic type element that you generate? Is that a unique solution or is it a pretty good guess?

Dr. H. Azhari: As the endocardial and epicardial surfaces can not be imaged directly, we had to interpolate between images in order to track the nodal points. The accuracy, therefore, is determined by the quality of our interpolation procedure.

Dr. E. Ritman: And the interpolation assumes that the volume of that myocardium is invariant?

Dr. H. Azhari: We did not assume that the volume is constant. In fact, we have found that the volume of the myocardial cuboids increased in systole. This finding is consistent with the results reported by you and Dr. Eric Hoffman [17]. Using DSR, you have found an increase of about 12%

in the myocardial volume. My belief is that this increase is an artifact caused by the endocardial trabeculae. At ED the "bays" in the endocardial trabeculae are filled with blood and the wall appears thinner. At ES the "bays" can disappear; the blood is squeezed out and the wall appears thicker.

Dr. R. Beyar: I must comment that at Calgary, using a different MRI machine, we did not get a significant change in myocardial mass between end-diastole and end-systole. So it is not inherent to the technique.

Dr. E. Ritman: Leon Axel does show a change in his little cubes *[Verbal Communication]*, so maybe there is something about the technique that you need to look at.

Dr. M. Lab: Can your technique be used for volume calculation and ejection fraction as well?

Dr. H. Azhari: Yes, we can also measure LV volume and ejection fraction. However, the purpose of this study was to measure the deformations of small myocardial cuboids about 1 cc in size. In a study by Shapiro *et al.* [18], the accuracy of determining LV mass by MRI was determined and they reported a very good correlation with PM studies.

Dr. P. Hunter: As you probably know, your finding that the principle strain aligns with the fiber direction of the epicardium but is substantially different on the endocardium, is very consistent with the bead studies of Waldman *et al.* [4] and others. What I would like to ask is whether the principle strain is the right index to be used in these studies. A lot of the shearing action that is occurring in the subendocardium, which has to do with the sheet orientation there, partly explains this divergence of the principle strains from the fiber direction and means that you are not really getting at the function of the myocardium by looking at principle strains. You will do better to look at behavior in relation to the local microstructure. I can not see that there is any particular validity in using principle strain.

Dr. H. Azhari: Let me explain why we chose to use the principle strains. As you probably know, all strain calculations are axis dependent, meaning that if you select a slightly different coordinate system you get different results for the lateral and longitudinal strains. Principle strains, on the other hand, are axis invariant. This enables us to compare our strain results to results reported by others. Secondly, we assumed that since the fibers contract only along their axis, we would find better correlation between fiber directions and principle strains, and therefore obtain a more sensitive functional index.

Dr. P. Hunter: I agree with you completely that principle strain gives you invariance from the coordinate systems. But the alternative is that you look at the strain in relation to a local axis which is based on the fiber sheet orientation and then it is easier to interpret what is functionally going on. Then you are invariant in terms of large motions of the heart but you are interpreting the strain fields in terms of something that means something physiologically, namely the local material coordinate systems.

Dr. H. Azhari: This approach was adopted by Guy McGowan, my successor at Johns Hopkins. He has done fiber oriented strain calculations using the same MRI technique. [19].

Dr. H.E.D.J. ter Keurs: I was intrigued by the concordance of the behavior of the anterior and posterior wall and the different behavior of the septum and the lateral wall. It is obvious that the LV is embraced by the right ventricle and that the action of the right ventricle might confer that concordance on the two walls. In that case you might expect that interventions that changed pulmonary artery pressure or right ventricular pressure may also change the degree of concordance and discordance between the two pairs.

Dr. H. Azhari: This is an interesting point. This hypothesis can be best tested on an isolated heart model.

Dr. R. Beyar: I think that Jing-Dong, now at Johns Hopkins, is trying to do this.

Dr. T. Arts: You have used end diastole as a reference for your stress calculation. But as Dr. Beyar has shown, there is a very fast motion between end diastole and the beginning of systole.

Dr. H. Azhari: Yes, I know what you mean. There is a rapid change in the isovolumic phase. That is why we have paced the dogs and defined our reference point 30 msec prior to the ECG r-wave. This way our reference preceded the isovolumic phase.

Dr. T. Arts: It would be very interesting to watch the strain from the beginning of ejection. Can you get it from your data?

Dr. H. Azhari: With this technique you can study the isovolumic phase as well. We have imaged about five time points during systole. However, post processing (i.e., tracing the images) is a very tedious and time consuming procedure, so we did not analyze the entire data set.

REFERENCES

1. Prinzen FW, Arts T, Van Der Vus GJ, Reneman RS. Fiber shortening in the inner layers of the ventricular wall as assessed from epicardial deformation during normoxia and ischemia. *J Biomech.* 1984;17:801-811.
2. Dieudonne JM. Gradients de directions et la deformations principales dans la paroi ventriculaire gauch normale. *J Physiol (Paris).* 1969;61:305-330.
3. Hawthorne EW. Dynamic geometry of the left ventricle. *Am J Cardiol.* 1966;18:566-573.
4. Waldman LK, Fung YC, Covell JW. Transmural myocardial deformation in the canine left ventricle. Normal *in vivo* three-dimensional finite strains. *Circ Res.* 1985;57:152-163.
5. Yun KL, Niczyporuk MA, Daughters GT, Ingels NB, Stinson EB, Alderman EL, Hansen DE, Miller DC. Alterations in left ventricular diastolic twist mechanics during acute human cardiac allograft rejection. *Circulation.* 1991;83:962-973.
6. Freeman GL, LeWinter MM, Engler RL, Covell JW. Relationship between myocardial fiber direction and segment shortening in the midwall of the canine left ventricle. *Circ Res.* 1985;56:31-39.
7. Villarreal FJ, Lew WY. Finite strain in the anterior and posterior wall of canine left ventricle. *Am J Physiol. (Heart Circ Physiol.* 28): 1990;259:H1409-1418.
8. Prinzen FW, Augustijn CH, Arts T, Allessie MA, Reneman RS. Redistribution of myocardial fiber strain and blood flow by asynchronous activation. *Am J Physiol. (Heart Circ Physiol.)* 1990;259:H300-308.
9. Lab MJ, Woollard KV. Monophasic action potential, electrocardiograms and mechanical performance in normal and ischemic epicardial segments of the pig ventricle in situ. *Cardiovascular Res.* 1978;12:555-565.
10. Zerhouni EA, Parish DM, Rogers WJ, Yang A, Shapiro EP. Human heart: Tagging with MR imaging- A method for noninvasive assessment of myocardial motion. *Radiology.* 1988;169:59-63.
11. Axel L, Dougherty L. MR imaging of motion with spatial modulation of magnetization. *Radiology.* 1989;171:841-845.
12. Azhari, H., J. L. Weiss, W. J. Rogers, C. O. Siu, E. A. Zerhouni, E. P. Shapiro. Non-invasive quantification of principal strains in normal canine hearts using tagged MRI images in 3D. Am. J. Physiol 264: (Heart Circ. Physiol. 33): H205-H216, 1993.
13. Azhari H, Weiss JL, Rogers WJ, Siu C, Shapiro EP. A Non-invasive comparative study of myocardial strains in ischemic canine hearts using tagged MRI in 3D. *Am J Physiol.* 1994;in press.
14. Beyar R, Shapiro EP, Graves WL, Rogers WJ, Guier WH, Carey GA, Soulen RL, Zerhouni EA, Weisfeldt ML, Weiss JL. Quantification and validation of left ventricular wall thickening by a three dimensional volume element magnetic resonance imaging approach. *Circulation.* 1990;81:297-307.

15. MacGowan GA, Azhari H, Rademakers FE, Rogers WJ, Perry LV, Hutchins GM, Weiss JL, Shapiro EP. Quantification of principal strains in the normal human left ventricles using tagged magnetic resonance imaging in 3D. 65th Scientific Sessions of the American Heart Association, New Orleans, LA, Nov. 16–19. *Circulation*. 1992;86(4)(Supp. I):166.
16. Azhari H, Oliker S, Rogers WJ, Weiss JL, Shapiro EP. Three dimensional mapping of acute ischemic regions using Artificial neural networks and Tagged MRI. *IEEE Trans on Biomed. Eng.* 1995; in press.
17. Iwasaki T, Sinak LJ, Hoffman EA, Robb RA, Harris LD, Bahn RC, Ritman EL. Mass of left ventricular myocardium estimated with dynamic spatial reconstructor. *Am J Physiol* 246 (*Heart Circ Physiol.*) 1984;15:H138–H142.
18. Shapiro EP, Rogers WJ, Beyar R, Soulen RL, Zerhouni EA, Lima JAC, Weiss JL. Determination of left ventricular mass by magnetic resonance imaging in hearts deformed by acute infarction. *Circulation*. 1989;79:706–711.
19. MacGowan GA, Shapiro EP, Salvado RD, Azhari H, Rogers WJ, Guier WH, Hutchins G, Lima JAC, Weiss JL, Rademakers FE. Cross-fiber shortening is preserved in human idiopathic dilated cardiomyopathy (abstract). *Circulation*. 1993;88(4):I–346.

CLOSURE

TOWARD MODELING THE HUMAN PHYSIONOME

James B. Bassingthwaighte[1]

ABSTRACT

The physionome is the description of the physiological dynamics of the normal intact organism. The march of science brings us now into the era where integration of the various facets of the knowledge of biology and medicine has become a major issue. Modeling is a vehicle for the combining of information from molecular biology, biophysics, and medical biology, but must be combined with strategies for databasing the raw data with greater efficiency than is currently possible. The lessons from the genome project can be applied to the next level major projects, the morphonome and the physionome, the objective being to put integrated forms of the data into the hands of physicians and medical scientists.

INTRODUCTION

The physionome is the description of the physiological dynamics of the normal intact organism. The root, "physio", concerns nature. Physiology is defined as the study of nature, or the study of natural or normal function. The root, "nome", means a part, as in binome, trinome, or means a name, as in nomenclature or classification. The "physionome" therefore means: a part of nature, and more particularly naming and describing of normal function.

Without stretching our imagination very far, one can nowadays classify biological science into a few broad categories that capture the essence of the fields of study. The inspiration for this comes with the success that followed the defining of the genome as a structure that contains the essence of life, the code that captures the phylogeny, and directs the ontogeny of animate organisms. Although regarded as a romantic notion when it was embarked upon two decades ago by a handful of scientists, it really represented a new paradigm for biological research: the large scale collaborative project designed to achieve

[1]Center for Bioengineering, University of Washington, WD-12, Seattle, WA 98195, USA.

Molecular and Subcellular Cardiology: Effects of Structure and Function
Edited by S. Sideman and R. Beyar, Plenum Press, New York, 1995

a specific goal. Others whose titles mimic that of the genome will benefit from its strategies and from the realization that magnificent objectives are realizable.

Here are our "nomes":

Genome: the sequence of bases in DNA and the locations of genes.

Morphonome: the structures of molecules, cells, tissues, organs, and organisms.

Physionome: the functions, kinetics, and regulation of the morphonome.

Psychonome: the state of mind, feelings of well being, fitness, and energy.

Socionome: the individual's and the group's relationships to others.

Long range strategies for the physionome need to be developed now. Given the magnitude of the set of knowledge that must be organized this won't be at all simple; currently this type of project is simply ignored. It is enormously larger than any of the so-called grand challenges which have been forwarded to the scientific community over the past several years. The tendency to see it as impossibly large must be overcome, and the goals clarified so that the "impossible" can be expressed as a set of perhaps very difficult but achievable goals. This is where there must inevitably be some hierarchical structuring.

Envisaging some of the pieces of the physionome is not a problem. Thinking of the heart, we could try to define the "cardionome", building a "theory of heart" (following the title of the text edited by Glass and Hunter [1]) that would provide a comprehensive picture of the behavior of the heart under a variety of physiological conditions. This would represent the integrated physiology of this organ, and even if not linked to the other parts of the body would still serve as a useful stepping stone. Other organs could be likewise used as "pieces of the physionome".

Structuring the physionome along organ system lines is inadequate from the point of view of the regulatory influences to which each organ is subjected, even though it might work in describing an isolated organ's *in vitro* or *in perfuso* state. Missing are the humoral, neural, psychological, and sociological linkages. By using the terms psychological and sociological in this context I mean to keep us aware of how the heart responds to complex internal feelings which are not mediated solely through neural influences directly on the heart, but through a complex mixture of neural, humoral, mechanical, and emotional influences. That these differ widely among individuals is well recognized. What are the causes of blushing in a psychopath compared to a normal sensitive person? Why do exercise, versus self neglect, induce such different levels of feeling of well being? How does being fit and healthy influence the normal responses to injury, healing repair, resistance to foreign substances and bacterial or viral invaders?

This kind of structure is like a huge pyramid, very broad, but not necessarily very high. At the lowest levels many of the pieces are the same for many tissues and organs; there are not very many different types of building blocks, but the same types of blocks are used at many sites. Even so, the number of blocks is large, and even a simple channel, a sodium channel, has different isoforms in different tissues, and may function a little differently in each setting. If there are 200,000 genes, each for a different protein, then the breadth of the pyramid is evident. But one can't start at the bottom and work upward rapidly for not all of the proteins and their reactions are yet known. In any case functional descriptions of organisms and organs did not and need not await knowledge of all of the details. So the question turns toward priorities and practicalities. Are there components of the physionome (Table 1) on which we have enough good data and which we can describe well enough to build realistic models of them, and can we structure such models in a modular fashion so that as our knowledge improves, the models can be corrected and augmented (Table 2)?

Table 1. Hierarchical Structure of the Physionome

1. The overall physiologic state of the organism: healthy or impaired, resting or stressed, conditioned, aged, overall functional adequacy.
2. Organ level function: Blood flow, oxygen consumption, utilization of substrates and production of metabolites, hormones, etc., energy balance, adequacy to maintain normal function over a range of conditions of the organism. For the heart this level would include stroke output, heart rate, pressure output, work, energy consumption, substrate consumption. flows. Relation to organism: neural humoral, mechanical feedback.
3. Intraorgan regional variations: Differences in functions such as regional flows, substrate uptake, metabolism, work (internal, external) For the heart: atria versus ventricles, contractility, heart rhythm and rate, contractile tension, myocardial deformation and relaxation, propagation of excitation
4. Tissue and cells: cellular physiologic and biochemical functions, mechanical and physicochemical features, composition and anatomic measures, blood–tissue exchange, metabolic fluxes, intercellular communication, traffic along biochemical pathways, all of which contribute to stabilizing the volumes and the concentrations in cells and in intercellular spaces.
5. Subcellular constituent and protein level, the basic biophysical, biochemical levels of subcellular function: Pumps, channels, enzymes, receptors: activation, inhibition, rates, competition, regulation.
6. Molecular behavioral level: Protein conformational states: site accessibility, channeling, sensitivity to pH, etc., molecular abnormalities.

Table 2. Reasons for Undertaking the Physionome Project

1. Databasing and modeling produce integrated knowledge for practical understanding.
2. Groups of related hypotheses, based up until now on small separate sets of observations, can be put together and tested for contradictions. This results in increasingly strong and more general hypotheses which have been cleared of internal contradictions, and which represent larger and more comprehensive sets of data.
3. The existence of "accepted", standard, comprehensive models aids refuting incomplete and incorrect hypotheses. It also enlarges the risk that investigators will be attracted to build only on the "party–line" model, so attention should be paid to the development of competing models of large systems, with the natural and explicit goal of determining which one, if either, is correct. This aids in experiment design: experiments should be designed to distinguish between alternative hypotheses, so that one is doomed to learn something from the results which should prove at least one of the models wrong.
4. Increased efficiency in experiment design helps to minimize the numbers of animals studied.
5. Teaching and training can make use of integrated model systems in both basic sciences and in medical practice situations. Such usage illustrates that quantitative approaches to biology are worthwhile.
6. The physionome and its many components would provide not only comprehensive databases which are not currently existent, but also integrated, analytical approaches to the study of medicine and physiology.
7. The establishment of a defined broad umbrella for many focussed yet integrated targets generates foci of interdisciplinary collaborative activity, and provides a means of bringing the efforts of many laboratories into a single self–consistent framework.

MODELS OF THE CARDIONOME

How simply could the modeling of a single organ be accomplished so that the result is both useful and reasonably accurate? What are the major features of myocardial structure and function that need to be brought together, and to what level of detail? Certainly many features can be omitted in the interests of obtaining a description of contraction and ejection of blood. A minimal model should contain a representation of the relationships between inflow pressures, ventricular pressures and outflow pressures. An example is the cyclical elastance model of the heart [2], a remarkably simple model adequate to give reasonable approximations to the pressure waveforms in the ventricle and aorta, and reasonable stroke volumes, and even reasonable durations of transients in response to changes in state.

There are many models or working concepts or data sets that serve as simple descriptors at this most primitive level. They are for the most part unrelated to each other: models for the spread of excitation over a layer of epicardium [3], models for purine metabolism and high energy phosphates [4, 5], models for flow distribution throughout the heart [6], models for the action potential [7], models for fatty acid metabolism [8, 9], models of excitation–contraction coupling at the cellular level [10–12], models for calcium release from the SR [13], models for vasoregulation in the heart [14] and in skeletal muscle [15].

Table 3. The Cardionome: A One-organ Component of the Physionome

Molecules	*Structure:*	of proteins for channels, pumps, receptors, enzymes, junctions, contractile apparatus, binding sites.
	State:	conformational state, receptor occupancy.
	Kinetics:	activation energies for changes of state, diffusion, reaction, aggregation.
	Function:	transport, catalysis, signalling, energy transduction, regulation.
Organelle	*Structure:*	mitochondria, SR, Golgi, nucleus, gap junctions, T-system.
	State:	electrochemical potential, pH, pCa.
	Kinetics:	substrate and O_2 usage, ATP production.
	Functions:	sequestration reactions, microenvironment creation.
Cell	*Structure:*	cell, shape, size, arrangements of organelles.
	State:	membrane potassium, energy stores.
	Kinetics:	cellular function, rate of output of product.
	Functions:	ionic balance, action potential generation, calcium regulation, tension development, response to stretch.
Tissue	*Structure:*	cell arrangements, interstitial matrix, capillarity, fiber direction and cross connectivity, mechanical linkages (collagen to cytoskeleton), vascular arrangement.
	State:	material composition, mechanical properties.
	Kinetics:	blood–tissue exchange, deformation, excitatory spread.
	Functions:	solute exchanges between cells, blood–tissue exchanges, propagation of excitation, generating shortening stresses and strains.
Organ	*Structure:*	fiber arrangements, anisotropy, directed spread-of-excitation.
	State:	contraction, relaxation, inflow, outflow, innervation.
	Kinetics:	rate of deformation, ejection velocity, cardiac output, pressures (Coupling with body, e.g., output impedance).
	Function:	coordinated spread of excitation, cardiac contraction, volume ejection, responses to humoral agents and autonomic outflow, ANF production.

Models for various aspects of the cardionome can be expressed by using only parts of the extensive possibilities listed in Table 3. Models for an ionic channel, enzyme, or transporter would be at the molecular level and also require local feedback of information on concentrations of substrates, reaction products, and regulators at the subcellular level. Models for excitation–contraction coupling could be developed so that they are mainly at the cellular level, but would have to be modified by information available at the tissue level to account for influences such as the stretch dependency of channel conductances and ionic currents. Models for oxygen exchange and pH regulation would be at the tissue level with respect to solute exchanges, but at the cellular level for the binding, buffering, and chemical reaction. Models of cardiac mechanics would be mainly at the tissue and organ level. Models for coronary blood flow and its distribution require primary information at the organ level of intraorgan and intramural pressures, but with added information on perfusion pressures which are influenced by the state of vasoregulation throughout the body. Since one influences the other, body resistances influencing the pressures available for coronary perfusion and coronary perfusion influencing force generation and cardiac output such models should be considered in the same fashion as transcendental equations, namely that they are solved by allowing them to run to steady state. (They will not run to equilibrium, a state which exists only after death. In fact almost no intracellular reaction is at equilibrium, but many run at near–equilibrium states with net fluxes that are much less than unidirectional fluxes.)

Modeling is clearly a part of the integrating character of the physionome project. In theory, the ultimate model of the cardionome would be one in which the blood flowing through the cavities and the tissues of the heart could be defined in terms of its composition and its pressures at the various inflow points, including the concentrations of regulatory hormones, and the autonomic outflow, and the fully detailed model would give the appropriate response. The current state of the art is that the cardionome's subsidiary models have only a relatively few variables, and can usefully represent very circumscribed states. Nevertheless, given that a useful long range goal is the full "cardionome" model, these limited models provide steps in the right direction.

The problems are that now we have neither good databases, nor good standard models, both of which should be publicly available. By that I imply that it will not be even possible to develop comprehensive models until very extensive databases are available in well organized fashion so that their information can be used when integrated via the model. What will inevitably occur when such archived data are used in comprehensive models is that either the model will be proven wrong (as they all are, in the sense of being either incomplete or incorrect), or some parts of the database will be found to be contradictory to others (which is bound to occur when not all the data have been obtained simultaneously from a single animal). The best model cannot be a perfect representation of any particular model, but is merely a representation of an average state of an average organism of a particular species.

This raises the question of what should be the prime target species, the focus of the data gathering and modeling: a particular animal species or a human? If the dog, should a particular breed be chosen for parsimony in building the database? Can the database be constructed in a fashion that is not race–blind or species–blind, for the distinctions are important in understanding the functional physiological behavior of the individual, but so as to accommodate the wide variety of species and subspecies on which data are naturally gathered in our laboratories? If there is to be a focus on human data, are we in a position to gather it in this day and age of serious political and social encumbrances to data acquisition? Is it possible to find any species on which all types of data can be gathered

or must we continue to make, and be misled by, the inference that one species is much like another?

STRATEGIES FOR THE PHYSIONOME PROJECT

The overall strategies involve the science and the politics of supporting and integrating the science. The social compact, the covenant between scientific workers and their supporting agencies representing the people and the state, by which scholarly effort offers benefits to society so that the society will invest in the effort, is currently being challenged by those who feel that research is no longer needed. Such views will have to be overcome. At this point it is evident that even the funding agencies have difficulty in being a force for integration, and this is left to the scholarly community and to the writers of science fiction.

Nevertheless, beginnings can be made, for much has been learned from the Genome Project [16] and more will be learned before it is complete. We can begin with the simpler and more obvious and more practical aspects of the physionome project, perhaps as follows.

1. Promote Extensions of the Scientific Method

A hypothesis cannot be proven, only disproven, and disproof is usually quantitative rather than qualitative. Make the hypothesis quantitative. Give equations, and formulate the model. Use it in experiment design. Define the most critical test of the idea. Devise an alternative hypothesis, and treat it likewise. From this, devise the single experiment or the set of experiments which clearly test the distinction between the two hypotheses. (The result is new knowledge, a real advance and not merely acceptance of the status quo: One hypothesis must die! Maybe both!) At the same time, at a less formal level, encourage the recording of the unexpected observation that does not fit in with previous notions, for these may be the most precious ones of all.

2. Build Hierarchical Sets of Models

This is a variant of what has been termed the reductionist approach. Start with the lowest level blocks, e.g., the detailed kinetic behavior of a purine transporter or a channel. Include the influences of competitors, blockers, pH, potential, etc. At the next hierarchical level, e.g., in an excitation–contraction coupling model, use a reduced version of the channel model, one which provides the correct fluxes under the given circumstances, as a limited but efficient representation. Instead of using the general flexible channel model, use one of a set of distinct reduced models. Repeat this strategy at the next level, e.g., in building models for force–velocity relationships at different heart rates.

3. Target Subsets, and Organize a Cooperative

Gather experts, and meet to define targets and assign tasks. Develop multimedia network connections for conferencing in reviewing data and models by staff of several institutions simultaneously via Internet. Develop database configurations and standards. Write model code under a "source code control system" so that it is testable and reviewable by staff at several institutions. Code for clarity and portability in accord with code standards and modeling standards. Obtain funding for focussed central resources to archive

and maintain model code and its support packages, parameter databases, exemplary experimental data, targeted facets of morphonome and genome data for each target area. (These should be narrowly enough focussed that resource personnel are expert in the particular areas of study.)

4. Organize the Task Force

Establish resource facilities for special fields. Each one could serve as a large integrating center for a target such as hypertension, diabetes, atherogenesis, etc., that is, have clinical disease focus. Others could have a focus on an organ system: heart, lung, liver, brain, bones, etc. Still others would be centers for tissue studies: autonomic nerves, interstitium. Resources for cellular functions (RBC, neutrophils, myocytes, etc.) would still be comprised of fairly large groups. Yet others might be biophysical or biochemical resources concentrating on transporters, channels, pumps, enzymes, molecular dynamics, and biochemical subsystems. These latter would necessarily build upon the genome and morphonome. Within each resource one would attempt to devise small model systems that can be linked to those of other resources. By having such foci of expertise and open lines of communication one may hope to integrate (models and scientists) early in the development of the physionome, and thereby obtain some understanding of how both the physionome and the scientific system works.

5. Develop an International Infrastructure

Develop support of research at an integrative level. Organize symposia at each society's national meetings. Define and develop the required technologies: a database such as Physbank with linkages to Genebank, on-line reference libraries to detailed information (Enzyme Handbook), and establish at each center directories available via ftp for model code with test routines. Organize workshops, Gordon conferences, and symposia on particular topics. Establish training programs at pre-and postdoctoral levels. Establish consultation services at each center.

SUMMARY

The physionome is proposed as an integrating concept describing the function of an organism. The concept serves as a vehicle for defining a "Physionome Project" around which one can establish lines for collecting, reviewing and retrieving data, and using the data to formulate an understanding of physiological function in an intact organism where multiple interactions between systems is the norm. The Physionome Project would be a huge enterprise, and so can only be undertaken via a long series of steps, with scientists of many labs and many nations working in concert to test each others' ideas and approaches. At each stage of the development there would be rewards in the form of improved understanding of how the body works and of how it can malfunction.

DISCUSSION

Dr. E. Ritman: I am left with a feeling of "what do I do now?" You have presented too much. But there is an area where you might elaborate a little bit even though you've given us too much already to think about. In the physionome, if you took a liver and ground it up so that the cells stay intact,

that bucket of cells would behave very much like the liver in many respects. You could do molecular and genetic medicine and biology and come up with answers as we do now for organs that we grind up.

Dr. J.B. Bassingthwaighte: You do not really believe that!

Dr. E. Ritman: That is the point I'm getting to! The one thing you might emphasize is the basic functional unit. There is the hepatic lobule, for instance, or the nephron in the kidney, or the haversian canal system in the bone, or the terminal bronchiole with its alveoli. These are sort of morphological units, certainly basic functional units that have the function that is multiplied to give the total organ function. But if you had even one basic functional unit, it will behave like the organ and just looking at the major cell components of that basic functional unit, you will not duplicate the organ function. This is something that we should pay more attention to. I am not sure what the basic functional unit of the heart is, for instance, but one beginning is to identify one arteriole with its capillaries and the associated muscle cells that are perfused by that. It may be something different, but once you have that, then you have a structure that the people from the molecular domain can aim at and other people can aim at in terms of the given functional unit, i.e., how does that impact on the macroscopic structure and function of the organ.

Dr. J.B. Bassingthwaighte: That is a good point. If we took a small piece of the heart and determined its biochemical and ionic regulatory functions and how they related to sarcomere shortening, we would then face the next problem on how to arrange that set of units so they would be connected appropriately to each other. One has the hypothesis, for example, that there is a sort of an impedance matching relationship between flow, transport capacity of membranes and enzymes, metabolic energy utilization, and work locally. Then one would have to arrange those units so that the work units have the correlation structure that allows the ventricle to contract appropriately and for this, one has to have an appropriate representation of velocities of propagation and the direction along the excitation pathways. There are these multiple levels of integration that are occurring through the set of tissues. The liver certainly needs its arrangement along the sinusoid. The enzymes are different at the upstream end of the sinusoid from the downstream end of the sinusoid. Some enzymes only exist at just a few terminal cells along the sinusoid toward the hepatic vein. There is this heterogeneity within a functional unit, usually axially related to inflow and outflow in a metabolic organ like the liver, and in other ways in the heart. So it is rather complicated. Where should we start? Maybe we have already started. We are each looking at pieces and putting them together in broader and broader ways. Some of the following chapters will present ways of putting the whole organ together.

REFERENCES

1. Glass L, Hunter P. There is a theory of heart. *Physica D.* 1990;43:1–16.
2. Westerhof N. Physiological hypotheses—intramyocardial pressure. A new concept, suggestions for measurement. *Basic Res Cardiol.* 1990;85:105–119.
3. Jalife J. *Mathematical Approaches to Cardiac Arrhythmias.* New York, NY: New York Acad. Sci.; 1990.
4. Kohn MC, Garfinkel D. Computer simulation of ischemic rat heart purine metabolism: I. Model construction. *Am J Physiol.* 1977;232 (*Heart Circ Physiol.* 1):H386–H393.
5. Kohn MC, Garfinkel D. Computer simulation of ischemic rat heart purine metabolism: II. Model behavior. *Am J Physiol.* 1977;232 (*Heart Circ Physiol.* 1):H394–H399.
6. Beard D, Bassingthwaighte JB. Fractal nature of myocardial blood flow described by whole organ model of arterial network. *Ann Biomed Eng.* 1994;22(Suppl.1):20.
7. Luo CH, Rudy Y. A dynamic model of the cardiac ventricular action potential: II: Afterdepolarizations, triggered activity, and potentiation. *Circ Res.* 1994;74:1097–1113.
8. Kohn MC, Garfinkel D. Computer simulation of metabolism in palmitate-perfused rat heart: I. Palmitate oxidation. *Ann Biomed Eng.* 1983;11:361–384.

9. Kohn MC, Garfinkel D. Computer simulation of metabolism in palmitate-perfused rat heart: II. Behavior of complete model. *Ann Biomed Eng*. 1983;11:511-531.
10. Johnson EA, Shepherd N. Models of the force-frequency relationship of rabbit papillary muscle. *Cardiovasc Res*. 1971;Supplement.1:101-108.
11. Bassingthwaighte JB, Reuter H. Calcium movements and excitation-contraction coupling in cardiac cells. In: DeMello WC, ed. *Electrical Phenomena in the Heart*. New York: Academic Press, Inc.; 1972:353-395.
12. Varghese A, Winslow RL. Dynamics of the calcium subsystem in cardiac Purkinje fibers. *Physica D*. 1993;68:364-386.
13. Wong AYK, Fabiato A, Bassingthwaighte JB. Model of calcium-induced calcium release mechanism in cardiac cells. *Bull Math Biol*. 1992;54:95-116.
14. Wong AYK. A kinetic model of coronary reactive hyperemic response to transient ischemia. *Bull Math Biol*. 1995;57:137-156.
15. Greene AS, Tonellato PJ, Lombard J, Cowley AW Jr.. The contribution of microvascular rarefaction to tissue oxygen delivery in hypertension. *Am J Physiol*. 1992;31 (*Heart Circ Physiol*.):H1486-H1493.
16. Cook-Deegan RM. *The Gene Wars: Science, Politics, and the Human Genome*. New York, NY: W. W. Norton; 1994.

THE EDITORS

Samuel Sideman, D.Sc., R.J. Matas/Winnipeg Professor of Biomedical Engineering, is Chairman of the Department of Biomedical Engineering, Director of the Julius Silver Institute of Biomedical Engineering, and Head of the Cardiac System Research Center of the Technion–Israel Institute of Technology.

Born in Israel (1929), he received his B.Sc. and D.Sc. from the Technion and his M.Ch.E. from the Polytechnical Institute of Brooklyn. On the faculty of the Technion since 1957, he served as Dean of Faculty, Dean of Students, and Chairman of the Department of Chemical Engineering. He was a Visiting Professor at the University of Houston and CCNY, a Distinguished Visiting Professor at Rutgers University, NJ, and is a Visiting Professor of Surgery (Bioengineering) at the University of Medicine and Dentistry, New Jersey (UMDNJ), USA.

His interests include transport phenomena, with particular emphasis on the analysis and simulation of the cardiac system. He has authored and co–authored over 250 scientific publications and co–edited 12 books. He received of a number of professional awards and citations, President of the Assembly for International Heat Transfer Conferences, and is on the editorial board of some major scientific journals. He is a Senior Member of a number of professional societies, Fellow of the American Institute of Chemical Engineering and the New York Academy of Science.

Rafael Beyar, M.D., D.Sc., is a Professor in the Department of Biomedical Engineering and is Associate Head of the Cardiac Research Center at the Technion.

Born in Israel (1952), he received his M.D. from Tel Aviv University and obtained his D.Sc. in Biomedical Engineering from the Technion–Israel Institute of Technology. In the Julius Silver Institute, Department of Biomedical Engineering, Technion–IIT since 1984, he was (1985 to 1987) at the Division of Cardiology, Johns Hopkins University Hospital, Baltimore. He was a Visiting Professor of Medicine and a Visiting Scientist to Alberta at the University of Calgary (1991–1992).

His interests include modeling, simulation of the cardiovascular system, 3D analysis of ventricular function, MRI, coronary flow, interventional cardiology, CPR and cardiac assist. He is a member of medical and engineering societies, and a recipient of a number of institutional and national excellence awards. He has authored and co–authored over 100 scientific publications and is editor of nine volumes dealing with imaging, analysis, simulation and control of the cardiac system.

List of Contributors

Dan Adam, Ph.D., Heart System Research Center, The Julius Silver Institute, Department of Biomedical Engineering, Technion–IIT, Haifa, 32000, Israel

Giora Amitzur, Ph.D., Neufeld Cardiac Reserach Institute, Sackler Faculty of Medicine, Chaim Sheba Medical Center, Tel Hashomer, Israel

Theo Arts, Ph.D., Department of Biophysics, Cardiovascular Research Institute Maastricht, University of Limburg, P.O. Box 616, 6200 MD Maastricht, the Netherlands

Haim Azhari, D.Sc., Heart System Research Center, The Julius Silver Institute, Department of Biomedical Engineering, Technion–IIT, Haifa, 32000, Israel

Robert C. Bahn, M.D., Ph.D., Department of Laboratory Medicine and Pathology, Mayo Medical School, Rochester, MN 55905, USA

Yael Barhum, M.Sc., The Basil and Gerald Felsenstein Medical Research Center Beilinson Medical Campus, Petah–Tikva, Israel

William H. Barry, M.D., Division of Cardiology, University of Utah Medical School, Salt Lake City, UT 84132, USA

James B. Bassingthwaighte, M.D., Ph.D., Center for Bioengineering, University of Washington, WD–12, Seattle, WA 98195, USA

Rafael Beyar, M.D., D.Sc., Heart System Research Center, The Julius Silver Institute, Department of Biomedical Engineering, Technion–IIT, Haifa, 32000, Israel

Erez Braun, D.Sc., Faculty of Physics, Technion–IIT, Haifa 32000, Israel

John H.B. Bridge, Ph.D., Division of Cardiology, and The Nora Eccles Harrison Cardiovascular Research Training Inst., University of Utah Medical School, Salt Lake City, UT 84132, USA

Gregory L. Brower, D.V.M., Department of Internal Medicine, Dalton Cardiovascular Research Center, University of Missouri, Columbia, Missouri 65212, USA

Dirk L. Brutsaert, M.D., Ph.D., Department of Physiology and Medicine, University of Antwerp, Groenenborgeriaan 171, B–2020 Antwerp, Belgium

Daniel Burkhoff, M.D., Ph.D., Department of Medicine Columbia University, 630 W. 168th Street, New York, NY, USA

Donald L. Campbell, Ph.D., Department of Pharmacology, Duke University, Durham, NC 27710, USA

Robert C. Castellino, M.S., Department of Cell Biology, Duke University, Durham, NC 27710, USA

Nipavan Chiamvimonvat, M.D., Division of Cardiology, Department of Medicine, The Johns Hopkins University, Baltimore, Maryland 21205 USA

William M. Chilian, Ph.D., Texas A&M University, Health Science Center, College Station, TX 77843, USA

Mary B. Comer, Ph.D., Department of Pharmacology, Duke University, Durham, NC 27710, USA

Yael Eilam, Ph.D., Cardiology Department, Hadassah Medical Organization, Kiryat Hadassah, P.O.B. 12000, Jerusalem, 91120, Israel

Dalia El–Ani, M.Sc., The Otto Meyerhoff Drug Receptor Center, Department of Life Sciences, Bar–Ilan University, Ramat Gan, 52900, Israel

Ruhama Fixler, M.S., Cardiology Department, Hadassah Medical Organization, Kiryat Hadassah, P.O.B. 12000, Jerusalem, 91120, Israel

Moshe Y. Flugelman, M.D., Faculty of Medicine, Technion–IIT, and Department of Cardiology, Lady Davis Carmel Medical Center, 7 Michal Street, Haifa 33333, Israel

Harry A. Fozzard, M.D., Departments of Pharmacological and Physiological Sciences and Medicine, The University of Chicago, MC6094, 5841 S. Maryland Ave., Chicago, IL 60637, USA

Arkady Glukhovsky, D.Sc., Heart System Research Center, The Julius Silver Institute, Department of Biomedical Engineering, Technion–IIT, Haifa, 32000, Israel

Yonathan Hasin, M.D., Cardiology Department, Hadassah Medical Organization, Kiryat Hadassah, P.O.B. 12000, Jerusalem, 91120, Israel

David Hassin, M.D., Cardiology Department, Hadassah Medical Organization, Kiryat Hadassah, P.O.B. 12000, Jerusalem, 91120, Israel

Markku Heikinheimo, M.D., Departments of Pediatrics and Molecular Biology and Pharmacology, Washington University School of Medicine, St. Louis, MO, 63110, USA

Jeffrey R. Henegar, M.S., Department of Internal Medicine, Dalton Cardiovascular Research Center, University of Missouri, Columbia, Missouri 65212, USA

Simon Horner, M.D., British Heart Foundation Cardiac Arrhythmia Research Group, Department of Physiology, Charing Cross and Westminster Medical School, London W6 8RF, United Kingdom

Peter J. Hunter, D.Sc., School of Engineering, The University of Auckland, Private Bag 92019, Auckland, New Zealand

Hon S. Ip, Ph.D., Department of Medicine, University of Chicago, MC 6088, Room G–611, 5841 S. Maryland Ave., Chicago, IL 60637, USA

Kenneth A. Jacobson, Ph.D., Molecular Recognition Section, Laboratory of Bioorganic Chemistry, National Institutes of Health, NIDDK, Bethesda, MD, 20892, USA

Joseph S. Janicki, Ph.D., Department of Internal Medicine, Dalton Cardiovascular Research Center, University of Missouri, Columbia, Missouri 65212, USA

David C. Johns, B.A., Division of Cardiology, Department of Medicine, The Johns Hopkins University, Baltimore, Maryland 21205 USA

Gania Kessler–Icekson, Ph.D., The Basil and Gerald Felsenstein Medical Research Center Beilinson Medical Campus, Petah–Tikva, Israel

Ralph Knöll, M.Sc., Max–Planck–Institute, Department of Experimental Cardiology, Benekestrasse 2, D–61231 Bad Nauheim, F.R. Germany

Max J. Lab, M.D., Ph.D., British Heart Foundation Cardiac Arrhythmia Research Group, Department of Physiology, Charing Cross and Westminster Medical School, London W6 8RF, United Kingdom

Amir Landesberg, M.D., D.Sc., Heart System Research Center, Department of Biomedical Engineering, Technion–IIT, Haifa, 32000, Israel

John H. Lawrence, M.D., Division of Cardiology, Department of Medicine, The Johns Hopkins University, Baltimore, Maryland 21205 USA

Jeffrey M. Leiden, M.D., Ph.D., Departments of Medicine and Pathology, University of Chicago, MC 6088, Room G–611, 5841 S. Maryland Ave., Chicago, IL 60637, USA

David Lichtstein, Ph.D., Department of Physiology, Hebrew University – Hadassah Medical School, Jerusalem, Israel

Gregory Lipkind, Ph.D., Department of Biochemistry and Molecular Biology, The University of Chicago, MC6094, 5841 S. Maryland Ave., Chicago, IL 60637, USA

Shuguang Liu, M.D., Ph.D., Department of Medicine Duke University, Durham, NC 27710, USA

Eduardo Marban, M.D., Ph.D., Division of Cardiology, Department of Medicine, The Johns Hopkins University, Baltimore, Maryland 21205 USA

Shimon Marom, M.D., D.Sc., Faculty of Medicine, Dept. of Physiology, Rappaport Institute, Technion–IIT, Bat Galim, Haifa 31096, Israel

Hiroshi Matsui, M.D., Division of Cardiology, University of Utah Medical School, Salt Lake City, UT 84132, USA

Puneet Mohan, M.D., Department of Physiology and Medicine, University of Antwerp, Groenenborgeriaan 171, B–2020 Antwerp, Belgium

Martin Morad, Ph.D., Georgetown University School of Medicine, 3900 Reservoir Road, NW, Washington, DC 20007, USA

Michael J. Morales, Ph.D., Department of Pharmacology, Duke University, Durham, NC 27710, USA

H. Bradley Nuss, Ph.D., Division of Cardiology, Department of Medicine, The Johns Hopkins University, Baltimore, Maryland 21205 USA

Kazuhide Ogino, M.D., Department of Medicine Columbia University, 630 W. 168th Street, New York, NY, USA

Brian O'Rourke, Ph.D., The Johns Hopkins University, Department of Medicine, Division of Cardiology, 844 Ross Building, 720 N. Rutland Avenue, Baltimore, MD 21205, USA

Michael S. Parmacek, M.D., Department of Medicine, University of Chicago, MC 6088, Room G–611, 5841 S. Maryland Ave., Chicago, IL 60637, USA

Frits W. Prinzen, Ph.D., Department of Physiology, Cardiovascular Research Institute Maastricht, University of Limburg, PO. Box 616, 6200MD Maastricht, The Netherlands

Brian M. Ramza, M.D., Ph.D., The Johns Hopkins University, Department of Medicine, Division of Cardiology, 844 Ross Building, 720 N. Rutland Avenue, Baltimore, MD 21205, USA

Randall L. Rasmusson, Ph.D., Department of Biomedical Engineering, Duke University, Durham, NC 27710, USA

Robert S. Reneman, M.D., Ph.D., Department of Physiology, Cardiovascular Research Institute Maastricht, University of Limburg, PO. Box 616, 6200MD Maastricht, The Netherlands

Erik L. Ritman, M.D., Ph.D., Mayo Clinic, 200 First Street SW, Rochester, MN 55905 USA

Dmitry N. Romashko, Ph.D., The Johns Hopkins University, Department of Medicine, Division of Cardiology, 844 Ross Building, 720 N. Rutland Avenue, Baltimore, MD 21205, USA

Yoram Rudy, Ph.D., The Cardiac Bioelectricity Research and Training Center, Department of Biomedical Engineering, Case Western Reserve University, Cleveland, Ohio 44106–7207, USA

Wolfgang Schaper, M.D., Ph.D., Max–Planck–Institute, Department of Experimental Cardiology, Benekestrasse 2, D–61231 Bad Nauheim, F.R. Germany

Hadassa Schlesinger, M.Sc., The Basil and Gerald Felsenstein Medical Research Center Beilinson Medical Campus, Petah–Tikva, Israel

Asher Shainberg, Ph.D., The Otto Meyerhoff Drug Receptor Center, Department of Life Sciences, Bar–Ilan University, Ramat Gan, 52900, Israel

Edward P. Shapiro, M.D., Johns Hopkins University School of Medicine, Division of Cardiology, Francis Scott Key Medical Center, 4940 Eastern Ave., Baltimore, MD 21224, USA

Hari Sharma, Ph.D., The Max Planck Institute, Bad–Nauheim, Germany

Joseph Shohat, M.D., Department of Nephrology, Beilinson Medical Campus, Petah–Tikva, Israel

Samuel Sideman, D.Sc., Heart System Research Center, The Julius Silver Institute, Department of Biomedical Engineering, Technion–IIT, Haifa, 32000, Israel

Luc H.E.H. Snoeckx, Ph.D., Department of Physiology, Cardiovascular Research Institute Maastricht, University of Limburg, P.O. Box 616, 6200 MD Maastricht, the Netherlands

R. John Solaro, Ph.D., Department of Physiology & Biophysics, College of Medicine (M/C 901), University of Illinois–Chicago, 901 South Wolcott, Chicago, IL 60612–7342, USA

Kenneth W. Spitzer, Ph.D., The Nora Eccles Harrison Cardiovascular Research Training Inst., University of Utah Medical School, Salt Lake City, UT 84132, USA

Harold C. Strauss, M.D., Department of Medicine, Duke University, Durham, NC 27710, USA

Richard A. Stennett, M.D., Department of Anesthesiology Columbia University, 630 W. 168th Street, New York, NY, USA

Stanislas U. Sys, M.D., Ph.D., Department of Physiology and Medicine, University of Antwerp, Groenenborgeriaan 171, B–2020 Antwerp, Belgium

Henk E.D.J. ter Keurs, M.D., Ph.D., Departments of Medicine and Medical Physiology, the Faculty of Medicine, University of Calgary, Canada

Amir Toib, M.Sc., Faculty of Medicine, Dept. of Physiology, Rappaport Institute, Technion–IIT, Bat Galim, Haifa 31096, Israel

Marc van Bilsen, Ph.D., Department of Physiology, Cardiovascular Research Institute Maastricht, University of Limburg, P.O. Box 616, 6200 MD Maastricht, the Netherlands

Ger J. van der Vusse, Ph.D., Department of Physiology, Cardiovascular Research Institute Maastricht, University of Limburg, P.O. Box 616, 6200 MD Maastricht, the Netherlands

Lizhen Wang, M.S., Department of Internal Medicine, Dalton Cardiovascular Research Center, University of Missouri, Columbia, Missouri 65212, USA

James L. Weiss, M.D., Johns Hopkins University School of Medicine, Division of Cardiology, Francis Scott Key Medical Center, 4940 Eastern Ave., Baltimore, MD 21224, USA

Withrow Gil Wier, Ph.D., Department of Physiology, University of Maryland at Baltimore, 655 West Baltimore St., Baltimore, MD 21201, USA

David B. Wilson, M.D., Ph.D., Departments of Pediatrics and Molecular Biology and Pharmacology, Washington University School of Medicine, St. Louis, MO, 63110, USA

Xue–si Wu, M.D., Department of Beijing Heart, Lung and Blood Vessel Medical Center, Beijing Anzhem Hospital, Beijing, China

Ying Zhang, M.S., Department of Pharmacology, Duke University, Durham, NC 27710, USA

René Zimmermann, Ph.D., Max–Planck–Institute, Department of Experimental Cardiology, Benekestrasse 2, D–61231 Bad Nauheim, F.R. Germany

Daniel Zinemanas, D.Sc., Heart System Research Center, The Julius Silver Institute, Department of Biomedical Engineering, Technion–IIT, Haifa, 32000, Israel

INDEX